Decision Scaling Evaluation of Climate Risks to the State Water Project

Final Report

A Collaborative Study of the Hydrosystems Research Group, University of Massachusetts, Amherst and the California Department of Water Resources

"Snow White Mountains and Blue Watershed," Dr. Qinqin Liu, DWR Climate Change Program, 2017

May 2019

Acknowledgments

Lead authors
Andrew Schwarz[1]
Patrick Ray[2]
Wyatt Arnold

Contributors
Casey Brown[3]
Sungwook Wi[4]
Jordi Vasquez

Editors
Frank Keeley
William O'Daly

Climate Change Program Management
Elissa Lynn
John Andrew

[1] Delta Stewardship Council (formerly at California Department of Water Resources)
[2] University of Cincinnati (formerly at University of Massachusetts, Amherst)
[3] University of Massachusetts, Amherst
[4] University of Massachusetts, Amherst

Contents

Figures

Tables

Abbreviations and Acronyms

AD	accretion/depletion parameters within CalLite
ARMA	auto-regressive moving average model
WARM	Wavelet ARMA model
CalLite	a simplified, faster version of CalSim
CalSim	the DWR and Reclamation California water resources simulation model
CALVIN	CALifornia Value Integrated Network, a hydro-economic optimization model of California's statewide water supply system
cdf	cumulative distribution function
CMIP	Coupled Model Intercomparison Project
CVP	Central Valley Project
CVS	California Central Valley Water System
CWP	California Water Plan
DWR	California Department of Water Resources
ENSO	El Niño Southern Oscillation
GCM	General Circulation Model
IPCC	Intergovernmental Panel on Climate Change
maf	million acre-feet
NDO	Net Delta Outflow
NOAA	National Oceanic and Atmospheric Administration
NWS	National Weather Service
pdf	probability density function
PDO	Pacific Decadal Oscillation
RCP	Representative Concentration Pathways
SAC-SMA-DS	a distributed version of the Sacramento Soil Moisture Accounting hydrologic model
SLW	Supercooled liquid water
SWE	Snow water equivalent
SWP	State Water Project
USBR	United States Bureau of Reclamation
WRIMS	Water Resource Integrated Modeling System

Executive Summary

This Final Decision Scaling Vulnerability Assessment Report updates and describes a joint endeavor of the California Department of Water Resources (DWR) and the University of Massachusetts, Amherst (UMass) to improve planning for the uncertain effects of climate change on the California Central Valley Water System (CVS)[1] by integrating vulnerability-based analysis with traditional risk-based assessment methods. This report summarizes the research goals, analytical approach, workflow of modeling tools, evaluation of alternative experimental designs, refined strategy for data visualization, and assessment of the vulnerability of the CVS to climate change.

This report begins with a review of historical and projected climate change in California, which includes descriptions of several DWR-UMass team investigations of historical records, observed climate trends, and many climate projections for the CVS, specifically. The next section of this report summarizes the work previously accomplished by the academic community, the government, and the community of water resources practitioners evaluating climate change-related risks to the CVS.

With that background in place, this report explains the methodology developed for this study (illustrated in Figure ES1) and provides details on each sub-step of the process. Whereas previous studies have tested the response of some aspect of the California water system to ahistorical climate traces, the decision scaling approach adopted for this study allows systematic assessment of the vulnerability of the entire (interconnected and complex) CVS to a wide range of potential future climate conditions, and quantification of the significance of climate shift relative to natural (and climate-change-amplified) variability. The climate response function that results from the decision scaling approach depicts expected water system performance relative to historical performance across a range of climate changes. An important benefit of this approach is the ability to use a variety of climate information sources to assess the level of concern to assign to the vulnerabilities that are identified. Consequently, climate information, including climate change projections and formal probability estimates, can be used as a sensitivity factor when assessing risk, rather than the driver of the analysis. This allows discussion of risk and opportunity (each a function of impact and likelihood) in water system investment.

This assessment of long-term and persistent hydrologic impacts of climate change focuses on the effects to the operation of the State Water Project (SWP), including ecological conditions that dictate operating rules. DWR owns and operates the SWP for flood control, maintenance of environmental and water quality conditions, water supply, hydropower, and recreation. Consequently, analysis of SWP performance under climate-changed conditions yields an array of impact metrics across these areas of concern. The analysis focuses on persistent medium- and long-term conditions evaluated at a monthly time-step. Short-duration extreme precipitation events that cause flooding may also stress water resource management but are beyond the scope of this study.

This study has adopted CalLite 3.0 to simulate the coordinated operations of the Central Valley Project (CVP) and SWP under a wide range of climate possibilities. Climate traces are developed through coupling historical daily temperature and precipitation (1950–2013) (Livneh et al. 2013) to the paleo-dendrochronological reconstructed streamflow record of the Sacramento-4-river annual streamflow (900–2013) (Meko et al. 2014). An advanced hydrologic model, the Sacramento Soil Moisture Accounting

[1] For the purposes of this study, the CVS is considered as the interconnected system of natural river channels and man-made facilities that comprise the Central Valley Project (CVP) and the State Water Project (SWP). See Figure 3 for a map of the CVS.

distributed hydrologic model (SAC-SMA-DS), translates the hydroclimatic traces into streamflow, which are the key inputs to the water system model.

Figure ES1 Modeling Workflow for Climate Change Vulnerability Assessment

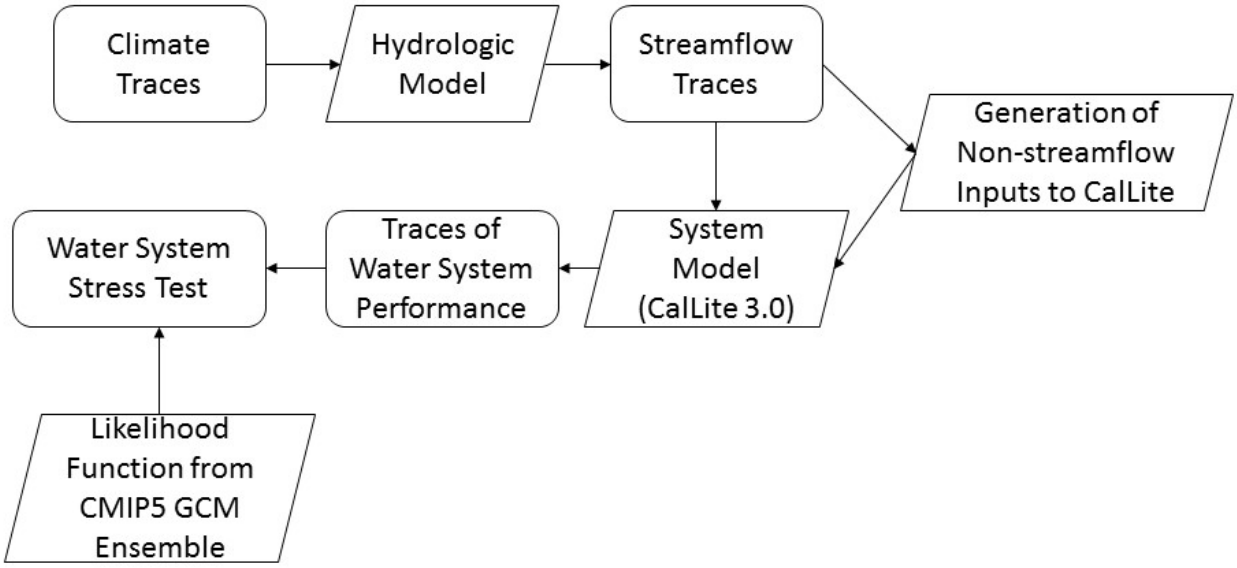

When simulated repeatedly, the resulting workflow (Figure ES1) allows the exploration of climate change impact in response to a wide range of meteorological input. Table ES1 lists the decision-relevant metrics used for the DWR climate vulnerability assessment.

Table ES1 Decision-Relevant Metrics

1	**Oroville Storage levels**
	April 30
	September 30
2	**Net Delta Outflow**
	Winter (Dec, Jan, Feb)
	Spring (Mar, Apr, May)
	Summer (Jun, Jul, Aug)
	Fall (Sep, Oct, Nov)
3	**SWP Deliveries**
	Average Annual
4	**System Shortages**
	Average Annual

Despite substantial uncertainty, results of the analysis show that increasing temperatures cause a significant downward shift in mid-century system performance and that the temperature increases of concern are consistent with the consensus of climate model projections. By 2050, the majority of climate outcomes that might reasonably be expected to occur lead to decreased system performance in each of the Table ES1 metrics (see Table ES2). While the results of this study are influenced by incorporation of 1,000 years of annual climate variability contained in the paleo reconstructed streamflow record, this

study does not account for projected increases in climate variability (intensification of precipitation events and extended duration of droughts) which could lead to additional performance impacts.

Table ES2 Probability that Mid-Century Long-Term Average Performance Will be Inferior to Current Average Performance

Performance Metric	Probability that Mid-Century Performance Will be Inferior to Current Performance
Oroville April Storage	76%
Oroville Carryover Storage	95%
Winter Net Delta Outflow	65%
Spring Net Delta Outflow	65%
Summer Net Delta Outflow	21%
Fall Net Delta Outflow	56%
SWP Deliveries	93%
System Shortages	87%

Improved system performance is possible if temperature increases are offset by precipitation increases, but this combination of climate changes is relatively rare across the climate projection archive, and thus considered relatively unlikely. This situation is especially acute for average Oroville September storage, SWP deliveries, and spring net Sacramento-San Joaquin Delta (Delta) outflows, in which substantial downward shifts are identified under a warmer climate.

The United States Bureau of Reclamation (Reclamation) Sacramento and San Joaquin Basin Study from 2016 provides a useful point of comparison for this study, though the climate conditions evaluated spanned a limited range of model scenarios, the possible changes were not sampled comprehensively, and the total number of evaluated changes was relatively small. Reclamation simulations showed an average decrease in 2015–2099 end-of-September reservoir storage of 9 percent relative to the Reference-No-Climate-Change scenario (where "reservoir storage" includes all system reservoirs), and an average decrease in Delta outflows of 3 percent. This study, by contrast, finds a 98 percent likelihood that September 1 Oroville storage will be lower by mid-century than it has been historically, and highlights the risk of decreases (by 25–30 percent) in Oroville storage. Regarding Net Delta Outflow (NDO), this study found a 65 percent likelihood of performance loss in spring, winter, and fall, and an 88 percent likelihood in summer. Spring NDO in low-flow years was found to decrease 25–30 percent, in median years 25–30 percent, and in high-flow years 15–20 percent. The downward shift in fall NDO was concentrated in already-at-risk low-flow years (decreasing by 25–30 percent relative to historical).

Recommendations for Future Applications of Decision Scaling

The analysis suggests that SWP performance will very likely deteriorate over the coming decades if no action is taken to adapt to climate change; however, there are opportunities for improved climate change planning. Applications of decision scaling (1-9 identified below) within three major categories are recommended for future study to support adaptation planning.

Resource Management Strategies

Among 37 resource management strategies (RMS) identified in the California Water Plan Update 2013 (Water Plan), there are several which address vulnerabilities described in this report, are technically feasible, and for which DWR has the capacity as well as the authority to implement (see Annex C: Resource Management Strategy Screening). As a next step, DWR's Climate Change Program will use the decision scaling platform built for this study to conduct a systematic evaluation of a sample of proposed climate change adaptation strategies drawn from the 37 RMS including, but not limited to:

- (1) The effect of monthly reservoir inflow forecasting ability on system operation (Annex D: Adaptation Strategies — Seasonal Forecasting).
- (2) Weather modification or "cloud-seeding" (Annex E: Adaptation Strategies – Enhanced Precipitation).
- (3) Incorporation of improved multi-objective upper watershed management (Annex F: Adaptation Strategies — Upper Watershed Management)

Supplemental Analysis

The decision scaling platform built for this study establishes a probabilistic framework and set of tools that allow evaluation of a much larger range of historical and potential future changes in inter-annual variability and drought length and severity (4). The platform, through its use of the system operations model CalLite 3.0, also reduces concerns related to accuracy of modelling regulations and institutional constraints thus enabling an exploration of the sensitivity of water indexing methods to climate change and potential ways of adapting water year typing methods to support water management decisions (5) (see Annex G: Water Year Typing). Although considered to some extent in this report, further investigation into the presence and causes of trends in seasonal and elevation-dependent warming would help prioritize adaptive strategies that are evaluated in studies using this platform (6).

Groundwater

While climate change risks to the groundwater component of water supply have not been evaluated here, DWR's Flood Managed Aquifer Recharge program (California Department of Water Resources 2018) has adopted the decision scaling platform to evaluate using flood waters to recharge groundwater aquifers (7). In addition, DWR's Climate Change Program has drafted a simplified strategy for evaluating the potential benefits of increased groundwater storage north and/or south of Delta (see Annex H: Groundwater) using CalLite 3.0 (8). If simplified modeling of groundwater in CalLite 3.0 is found infeasible, shifting the operations model used in this study from CalLite 3.0 to CalSim-III, which features a dynamic link to the California Central Valley Groundwater-Surface Water Model (C2VSIM), would enable exploration of climate change risks and adaptation strategies based on modelling of the integrated surface-groundwater system (9) (see Annex I: Move From CalLite 3.0 to CalSim-III Operations Modeling).

Introduction

Developing adaptation plans to address future climate changes is hindered by the uncertainty associated with the magnitude and character of those changes. Vulnerability-based assessments are promising for identifying where climate uncertainties are most problematic but can yield a litany of vulnerabilities with little means for prioritizing action or justifying the expenses required to address them. Given the financial constraints of the typical government water agency or municipality, vulnerabilities with unknown probabilities of occurrence can be treated as low priorities, and long-term preparedness to climate change yields to the pressing concerns of the present.

The goal of this project is to improve planning for the uncertain effects of climate change by integrating vulnerability-based analysis with traditional risk-based assessment methods. Risk-based approaches are typical for engineering water resources but are problematic under climate change because of their dependence on estimating the probability distributions of possible climate futures. The process adopted here preserves the risk-based planning framework but reserves estimation of probabilities until the assessment of adaptation alternatives, where the consequences of any assumption are quickly realized in terms of effects on decisions.

Water managers struggle to prioritize responses to the predicted hazards of climate change because of the uncertainty associated with projections of those hazards. This struggle is not without cause. At present, decision-makers face the unsavory choice of relying on trusted, traditional approaches that depend on statistics from the past, and thus may be ill-suited for the future, or adopting uncertain projections of the future known to have the least capacity for the most critical design variables (Hirsch 2011). The prevailing wisdom of "no regrets" approaches offered in response to this dilemma (Intergovernmental Panel on Climate Change 2012) is hardly a rallying cry for increasing long-term preparedness for climate change.

This effort is designed to directly address this challenge. The methodology outlined in this report enables planning for future changes that is *informed* by the best available science on climate change while not being dependent on precise prediction of future values. Instead, the process focuses on incorporating credible information on future changes within traditional risk-based planning approaches and through merging historical trends with future expectations. Those effects are delineated through a "climate stress test" that is independent of projections of future climate. Where the effects are significant compared to other factors, the concern associated with the possible occurrence of those effects is described in accordance with the best available climate science.

Previous studies that have used a robust decision-making approach (Lempert et al. 2006), including California Water Plan Update 2013 (Update 2013) (California Department of Water Resources 2013), have identified potential adaptations through stakeholder consultation and systems analysis but have not systematically assessed the alternatives. They have also not evaluated the impacts of possible changes in climate extremes such as droughts and floods. This study uses previous planning efforts, in particular Update 2013, as a foundation for illustrating the planning procedure for the climate uncertainty described here.

Climate Change in California

It has long been anticipated that anthropogenic climate change would alter the water resources of California (Gleick 1987). Recent observations indicate that changes to the hydro-climatology of California have begun and that further substantial change is likely to occur throughout this century (Pierce et al. 2018).

Observed Trends

Mean temperature has increased 0.6 to 1.1 degrees Celsius (°C) since 1900 (California Department of Water Resources 2015a), and temperature change is accelerating (LaDochy et al. 2011), with the greatest rate of change occurring in temperature minimums (California Department of Water Resources 2015a). Rising temperatures in the Sierra Nevada and Northern California have triggered decreasing snowpack and earlier snowmelt (Cayan et al. 2010; Dettinger & Anderson 2015; Mote et al., 2005). Warmer temperatures also cause sea level rise, with 0.2 meters of rise recorded in San Francisco Bay in the past century (National Oceanic and Atmospheric Administration 2016). Rates of rise are now accelerating (Kopp et al. 2016), threatening the sustainability of the Sacramento-San Joaquin Delta, the heart of the California water supply system and the source of water for millions of Californians and millions of acres of farmland.

Since 1970, California has become wetter in its north and drier in its south (Killam et al., 2014), though the large historical variability of precipitation in California makes it difficult to separate trends from natural variability. Higgins et al. (2007) found that the 1976–2004 period was substantially wetter in the western U.S. than the 1948–1975 period, though the large increase in total precipitation might be partially explainable by the occurrence of the warm phase of the Pacific Decadal Oscillation (PDO). It may be that the warm phase of the PDO during the last quarter of the 20th century was an exceptional period (as suggested by the 1000-year tree-ring record [Swetnam & Betancourt 1998]) and that the last 15 years marks a return to normal, pre-1977 conditions (Pavia et al. 2016). Regionally, the central and northern regions show increases in both annual totals and number of rainfall days, while southern regions show either no significant trend or some decreases since the early 1900s. A shift from light rains to heavy rains has occurred in Northern California regions (Killam et al. 2014).

It is not yet clear that the trend observed in the past century will continue into the coming century, nor is the behavior of the PDO well-enough understood that confident forecasts can be made of its oscillations far into the future. The global climate models do not indicate a clearly wetter or drier expectation for the region (discussed later). Caution should be exercised when looking for conclusions attached to expectations of future precipitation in the region.

Projections

Figure 1 shows the shift in average annual precipitation and temperature for the ensemble of general circulation models (GCMs) driven with Intergovernmental Panel on Climate Change (IPCC) Representative Concentration Pathways (RCP) scenarios 2.6, 4.5, 6.0, and 8.5 (van Vuuren et al. 2011) in the region contributing flow to the Central Valley Water System (CVS)[2] for the 2036–2065 period relative to the 1971–2000 period. The probability density cloud identifies the bivariate normal distribution

[2] The CVS is considered as the interconnected system of natural river channels and man-made facilities that comprise the Central Valley Project (CVP) and the State Water Project (SWP). See Figure 3 for a map of CVS.

on the full ensemble of the Fifth Coupled Model Intercomparison Project (CMIP5) GCMs (see Annex A: GCM Likelihood Function for detailed steps on GCM probability density function). As can be seen, there is no agreement on the direction of precipitation change (positive or negative), with some GCM runs indicating increases in precipitation of over 20 percent and some indicating decreases in precipitation of over 20 percent. Temperature increases range from almost 1°C to almost 4°C.

Figure 1 Mid-Century Conditional Climate Probability Density

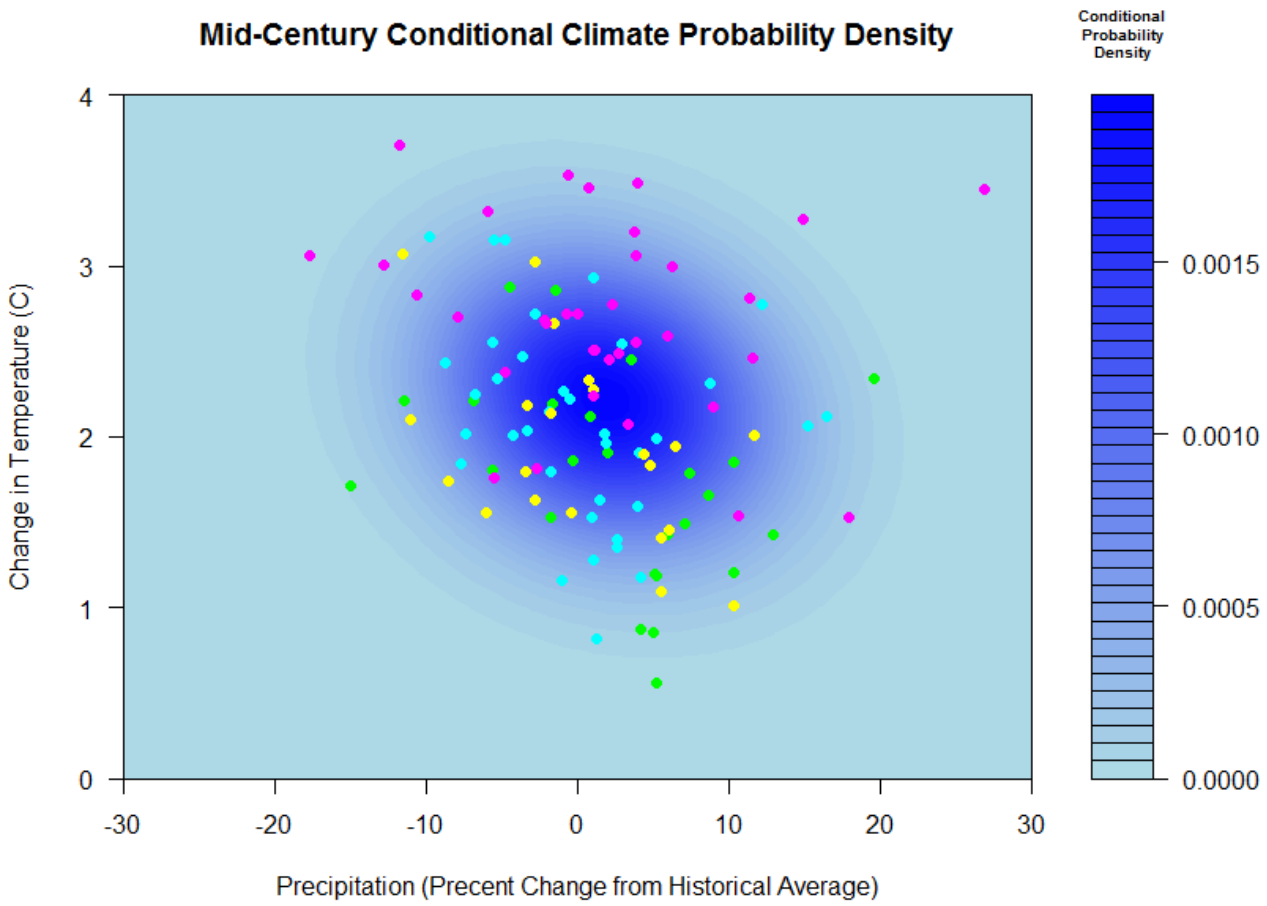

Note: Cyan dots represent GCMs run with RCP 8.5; yellow dots represent GCMs runs with RCP 6.0; turquoise dots represent GCMs run with RCP 4.5; Green dots represent GCMs runs with RCP 2.5.

The projected changes in California weather patterns could exacerbate both drought and flood risks and increase challenges for water supply management. Projections of future temperatures across California suggest greater increases in summer temperatures than in winter temperatures (California Department of Water Resources 2015a) and intensification of hot extremes (Diffenbaugh & Ashfaq 2010). By the end of this century, the Sierra snowpack is projected to experience a 48–65 percent loss relative to the historical April 1st average on which water supply throughout the summer and fall depends (D Cayan et al. 2013; California Department of Water Resources 2015a).

Most climate model precipitation projections for the state anticipate drier conditions in Southern California, heavier and warmer winter precipitation in Northern California, and greater proportions of

winter precipitation falling as rain instead of snow (Yoon et al. 2015). Decrease in snowpack storage and the concentration of streamflow in winter months would increase dry season deficits during periods of high irrigation-water demand.

Atmospheric Rivers

The effect of climate change on atmospheric rivers, the source of 30–50 percent of all precipitation for the west coast and the principal cause of winter floods (Dettinger 2014), is not yet well understood (Steinschneider & Lall 2015). But several simulation experiments using climate models have indicated that projected changes are mostly at the extremes (Dettinger 2011), with California's atmospheric rivers becoming longer and more intense, but not more frequent (Shields & Kiehl 2016), carrying warmer water vapor more likely to fall at high altitudes as rain than snow (Dettinger 2011). The net effect being exacerbated winter floods but not reduced water stress, despite increases in winter mean precipitation (Warner et al. 2015). While the evaluation of the effect of potentially increasing climate variability is outside of the scope of this analysis, California's high precipitation variability creates challenges for General Circulation Models (GCMs) and results in a particularly wide spread of projections (relative to ranges throughout the rest of the United States) of future precipitation values in the region (Zhang & Stanley 1999; Roy et al. 2010).

Drought

California's most significant droughts of the past century (by hydrologic dryness) were: 1929–1934, 1976–1977, and 1987–1992. The 2012–2014 water years were California's driest three consecutive years in terms of statewide precipitation, and the drought conditions (a combination of record high temperatures and near-record low precipitation) faced by California may be the worst in the last millennium (AghaKouchak et al., 2014; Griffin & Anchukaitis 2014). Even so, the impact of the 2012–2015 drought would be far worse if not for the slightly wet 2010 and significantly wet 2011 preceding the start of the drought (California Department of Water Resources 2015b).

Drought conditions in California are increasing in intensity and length (Diffenbaugh et al. 2015). Climate change is expected to amplify droughts in California, both because of rising temperatures (Cayan et al. 2010) and because of an intensification of ENSO activity, the warm/cold phases of which together with the transitions between phases modulate climate variability in California (Yoon et al. 2015). The rise in global temperatures has amplified naturally occurring drought conditions in California and has increased the chance of severe droughts in the future (Williams et al. 2015), though the main cause of intensification of California droughts so far has been natural precipitation variability, not warming (Mao et al., 2015; Seager et al., 2015). Sea-surface temperature (SST)-forcing, for example (a combination of a La Niña event in 2012/2013 and a warm west - cool east tropical Pacific SST pattern from 2012–2014), sustained a high pressure ridge over the West Coast that suppressed precipitation during the three winters from 2012–2014 (Wang & Schubert 2014; Seager et al. 2015). This recent event indicates that better understanding of the climatological causes of persistent North Pacific ridging events might be crucial in anticipating future severe drought in California (Swain et al. 2014).

California's most recent drought began in winter 2011–2012, and intensified in winter 2013–2014, a period marked by very low winter precipitation, mountain snowpack, and spring runoff (California Department of Water Resources 2014b; U.S. Geological Survey 2014; United States Drought Monitor 2014). The drought drew down reservoir storage in the state to low levels and threatened the state's

agricultural production, drinking water supply, and fisheries (California Department of Fish and Wildlife 2014; California Department of Water Resources 2014a; U.S. Department of Agriculture 2014). The drought has included:

1. Lowest three-year statewide precipitation total on record (2012–2014);
2. Most severe values of NOAA's National Climatic Data Center drought indicators (D4, or exceptional drought, first noted across the Salinas Valley and western San Joaquin Valley in January 2014, and extending over almost 60 percent of the state by July 2014) (National Oceanic and Atmospheric Administration 2014);
3. Lowest calendar-year precipitation in the history of much of the state, including San Francisco, Sacramento, and Los Angeles (2013);
4. Warmest calendar-year temperatures on record (2014);
5. Warmest winter on record (2015);
6. Highest one-year (water year 2014, 9–12 percent above average) and three-year (water year 2012–2014, 7–9 percent above average[3]) potential evapotranspiration on record (Williams et al. 2015);
7. Lowest Palmer Modified Drought Index (PMDI) on record (July 2014, approximately -3) (Diffenbaugh et al., 2015);
8. Lowest recorded April 1st snowpack (2015, 5 percent of normal) (Dettinger & Anderson, 2015);
9. Record-low water allocations for State Water Project and federal Central Valley Project contractors (California Department of Water Resources, 2015a).

The drought was responsible for an estimated $2.2 billion in economic loss from 2013–2014 alone (Howitt et al., 2014), and $2.7 billion from 2014–2015 (Howitt et al., 2015), and took a heavy toll on people and ecosystems (Swain 2015). Snowpack was well below normal for each of the four years of the drought. Year 2015 snowpack was significantly less across all elevations and shifted to higher elevations. This shift is likely driven in part by the significantly warmer temperatures, which "would lead to less snowfall and more rainfall at lower elevations, and increased accumulation season melt across all elevations (with more melt at lower elevations)" (Margulis et al. 2016).

Relevant Studies

Recent global (Intergovernmental Panel on Climate Change), National (National Climate Assessment), regional (National Climate Assessment for the Southwest Region), and Statewide (4th California Climate Change Assessment) climate change assessments have all highlighted climate-change-driven impacts to water supply, water demand, increased flooding and drought, and changes to hydrologic processes. Climate change impacts on California has been the focus of many studies conducted by DWR and others, a selection of which include:

[3] Potential evapotranspiration was calculated using gridded data from the Global Precipitation Climatology Centre (GPCC) (Schneider et al., 2014); for some grids, potential evapotranspiration for water year 2012–2014 was second highest behind water year 2007–2009. But it should be noted that statewide temperatures in 2015 were the second-highest on record, behind only temperatures for 2014. The year 2015 was not included in Williams (2015) and would likely result in record three-year potential evapotranspiration for the period 2013–2015.

- Progress on Incorporating Climate Change into Management of California's Water Resources (March 2008)
  Published in the March 2008 special issue of Climatic Change — *California at a Crossroads: Climate Change Science Informing Policy*. This is an 18-page condensed version of the original 350-page 2006 report of the same name. Coauthored by DWR staff.

- Managing an Uncertain Future; Climate Change Adaptation Strategies for California's Water (October 2008)
  Focuses discussion on the need for California's water managers to adapt to the effects of climate change, with a focus on the effects already affecting water supplies. This report proposes 10 adaptation strategies in four categories.

- Using Future Climate Projections to Support Water Resources Decision Making in California (May 2009)
  Evaluates how climate change could affect the reliability of California's water supply.

- Isolated and integrated effects of sea level rise, seasonal runoff shifts, and annual runoff volume on California's largest water supply (May 2011)
  A detailed analysis of climate change impacts on seasonal pattern shifts of inflow to reservoirs, annual inflow volume change, and sea level rise on water supply in the Central Valley of California.

- Hydrological Response to climate warming: the Upper Feather River Watershed (2012)
  The hydrological response and sensitivity to climate warming of the Upper Feather River Basin, a snow-dominated watershed in Northern California, were evaluated and quantified using observed changes, detrending, and specified temperature-based sensitivity simulations.

- Paleoclimate (Tree-Ring) Study (February 2014)
  New Hydroclimate Reconstructions have been released, using updated tree-ring chronologies for these California river basins; Klamath, San Joaquin, and Sacramento. The report, prepared by the University of Arizona, allows assessment of hydrologic variability over the course of centuries and millennia, gives historical context for assessing recent droughts, and can be used in climate change research.

- Estimating Historical California Precipitation Phase Trends Using Gridded Precipitation, Precipitation Phase, and Elevation Data, DWR Memorandum Report (July 2014)
  This exploratory study develops and describes a methodology that uses readily available research data sets to produce gridded estimates of historical rainfall as a fraction of total precipitation for areas comprising the major water-supply watersheds of California. Written by Aaron Cuthbertson (DWR), Elissa Lynn (DWR), Mike Anderson (DWR, California State Climatologist), and Kelly Redmond (Western Regional Climate Center).

- Reclamation Sacramento-San Joaquin Basin Study (2016)
  Assessment of potential climate change impacts to the basins' agriculture and urban water supplies and demands, flood control, hydroelectric power generation, recreation, fisheries, wildlife and wildlife habitats, water quality, and water-dependent ecological systems.

- California Climate Risk: Evaluation of Climate Risks for California Department of Water Resources (February 2017)
  This inception report introduces a joint endeavor of DWR and the University of Massachusetts, Amherst (UMass), to improve planning for the uncertain effects of climate change on DWR's system by integrating vulnerability-based analysis with traditional risk-based assessment methods. This report summarizes the progress made during approximately two years of informal partnership during which the team defined research goals, established an experimental approach, developed and validated a workflow of modeling tools, tried and abandoned a number of alternative experimental designs, refined the strategy for data visualization, and produced preliminary assessments of the vulnerability of the CVS to climate change using the decision scaling approach.

- Climate Change Risk Faced by The California Central Valley Water Resource System. California's Fourth Climate Change Assessment (September 2018)
  Released in September 2018, the Fourth Assessment includes 44 technical reports that address California-specific informational gaps about climate vulnerabilities. The technical report cited above assesses the future performance of key water resources management factors for the Central Valley water system using the same probability-based climate change risk assessment discussed here.

Academic Studies of Climate Change Impact on California Water Resources

In addition to the reports just described, an array of academic research has focused on specific aspects of climate change effects on California's water resources. Previous exercises in hydro-system modeling have provided substantial insights for policy-making and public discussion related to water resources management in California (Harou et al. 2010; Connell-Buck et al. 2011; Tanaka et al. 2011; Null et al. 2014;). Most of these studies have shown that California's water system, while not impervious, can stand up quite well to substantial climate disturbances without widespread catastrophic losses, if well managed.

Climate change impact assessment studies of the CVS using the CALifornia Value Integrated Network (CALVIN) (Tanaka et al. 2006; Medellin-Azuara et al. 2008; Harou et al. 2010; Connell-Buck et al. 2011), a hydro-economic optimization model of the water supply management of the intertied water supply system of California, "demonstrate that Delta export operations are often central for economic adaptation to climate change, and changes in hydrology lead to increased scarcity and costs as users adapt to reduced supplies and a seasonal shift in water availability" (Tanaka et al. 2011). Except for Tanaka et al. (2006), each of these studies provides estimates of the costs to adapt the California water system to no more than a few hypothesized futures that might be warmer, drier, more drought-prone, or some combination of the three. Tanaka et al. (2006) expand the set of considered climate futures to 12, including the possibility for a wetter future. Unfortunately, the snapshots of potential future conditions are limited and are provided without a sense for the relative likelihood of the occurrence of the conditions explored. Furthermore, the results from CALVIN, being optimized to maximize statewide net economic

benefits, are not constrained by administrative agreements governing water allocations in California in practice, and therefore (though of great value in imagining an improved future) are diminished in value to California water system planners who must operate within jurisdictional realities.

Reclamation (2016) used CalLite 3.0 to identify risks to water deliveries and water quality resulting primarily from seasonal shifts in runoff, sea level rise, and an altered state of the Delta requiring greater reservoir releases within an altered water delivery schedule. CalLite 3.0 is a simplified, faster version of the CalSim-II (Draper et al. 2004) water system model used by DWR and Reclamation to simulate the coordinated operations of the CVS. CalLite 3.0 represents reservoir operations, SWP and CVP operations and delivery allocation decisions, existing water-sharing agreements, and Delta salinity responses to river flow and export changes on a monthly time-step. It can also represent the effect on the water system of sea-level rise. Because it represents the mechanics of DWR and Reclamation allocation rules and water sharing agreements, the Reclamation (2016) study is better able to inform adaptation responses in water system planning and management than studies using CALVIN. But in the interest of computational efficiency, the Reclamation (2016) study evaluated only a limited set of five "representative" climate futures taken from the Intergovernmental Panel on Climate Change's (IPCC's) Coupled Model Intercomparison Project Phase 5 (CMIP5) ensemble of GCM runs (Taylor et al. 2012), plus an additional set of twelve GCM-simulated climate scenarios taken from the California Climate Change Technical Advisory Group (CCTAG). Though the evaluated range spanned a reasonably wide range of potential future climate conditions (1.5–5°C warming, and -15 percent to +35 percent average annual precipitation by 2100), the possible changes were not sampled comprehensively, and the total number of evaluated changes was relatively small.

Other water system modeling studies have indicated that the effects of climate change on water resources management in California may result in the need to: (1) increase electricity imports to the Sacramento region during hot, dry spells, when scarce water most constrains local power production (especially hydropower) (Dale et al. 2015); (2) carefully control hydropower generation and local electricity demand in an ongoing effort to balance the dual objectives of stabilizing reservoir levels and the reduction of greenhouse gas emissions (thermal power plants being used when hydropower is unavailable) (Tarroja et al. 2014); (3) give greater consideration to stream temperatures in order to protect fish habitat when developing reservoir operating rules (Null et al. 2013; Rheinheimer et al. 2015); and (4) improve conveyance between existing surface and groundwater storage (Null 2016). These studies provide important insights, but none use more than four climate change possibilities, and none use water system models that can holistically inform the vulnerability of the CVS water system to climate change.

Two studies have explored a wider range of possible climate futures on water system domains similar to those considered in this work: (1) Willis et al. (2011), a flood impact study showing the relative effects of temperature and precipitation changes on flood risk in the Sacramento River Basin (and the utility of dynamic reservoir rule curves to absorb flood flows); and (2) Groves and Bloom (2013), an analysis of water resource-management response packages for California's Central Valley showing the reduction in system vulnerabilities (and improvement in resilience) achievable through implementation of well-designed response packages. Both studies take climate input from downscaled GCMs run for selected emissions scenarios of the Coupled Model Intercomparison Project Phase 3 (CMIP3). The ensemble of GCM projections (11 GCMs in the case of Willis et al. (2011) and six in the case of Groves and Bloom (2013), each using CMIP3 scenarios A2 and B1) provides valuable perspective on a system response to a wider range of possible climate futures.

But the climate uncertainty space explored by these two studies is less than that included in either the CMIP3 or CMIP5 ensembles (themselves an underestimate of climate change uncertainty [Stainforth et al. 2007; DR Cayan et al. 2010; Steinschneider et al. 2015; Stouffer et al. 2017]), and is not investigated in a comprehensive, systematic fashion. Willis et al. (2011) consider temperature ranges of only 0.4–1.4°C and precipitation ranges of only -6.6 percent to 16.8 percent relative to the historical. The downscaled GCM runs used by Groves and Bloom (2013) spanned a "hot and dry" extreme marked by approximately 2–2.5°C warming and -5–10 percent average annual precipitation to a "cool and wet" extreme marked by approximately 0.5°C warming and +5 percent annual average precipitation. Only 12 discrete samples were taken, and almost no samples were taken representing "hot and wet" or "cool and dry," though those conditions are present in the CMIP5 ensemble of projections for California. Groves and Bloom (2013) identified conditions under which the Central Valley system and tributary watersheds consistently performed poorly, but the highlighted composite scenario (hot [$\Delta T > 0.67$°C increase relative to historical] and dry [$\Delta P > 25$ percent decrease]) addressed questions of climate change likelihood only subjectively, limiting the applicability of the results to risk-informed decision-making.

The findings of each of these studies, including the 2016 Reclamation study discussed earlier, are conditional on the fidelity of a downscaled set of GCM projections. These are likely not representative of the parameters of local climate variability most relevant to water management (Brown & Wilby 2012) and cannot present a direct comparison to historical performance. In terms of utility to decision-making at DWR, the Willis et al. (2011) study assesses flood risk, not water supply risk, and the Groves and Bloom (2013) study uses a Water Evaluation and Planning (WEAP) model that is a coarse approximation of Delta dynamics, which likely over-simplifies simulation of Delta water quality conditions essential to water system allocations in practice (Joyce et al. 2010).

In summary, despite a large number of studies that have evaluated the effects of climate change on the California water system, significant questions remain, such as:

- How much climate change can the system withstand?
- What are the critical thresholds of climate change which cause the system to fail to meet expectations?
- What are the specific climate changes that are problematic, and are they likely to occur?

No previous study was found presenting sensitivity of the water system to changes in climate in a comprehensive way and in connection with a quantitative assessment of the relative likelihood of possible climate change outcomes. For example, Reclamation (2016) calculated the future unmet demand that would occur in five selected climate change scenarios but provided no means by which to interpret the relative likelihoods of those five possible scenarios, limiting any meaningful quantification of risk based on the results. In response, this study presents a decision scaling (Brown et al., 2012) approach that allows systematic climate vulnerably assessment across a range of potential future climate conditions spanning a climate change uncertainty domain inclusive of (and extended beyond) the full CMIP5 ensemble, including quantification of the relative likelihood of potential future performance levels.

Methodology

DWR's vulnerability assessment for long-term and persistent hydrologic effects of climate change focuses on impacts to the operation of the State Water Project (SWP), including ecological conditions that dictate operating rules. DWR owns and operates the SWP for flood control, maintenance of environmental and water quality conditions, water supply, hydropower, and recreation. Consequently, analysis of SWP performance under climate-changed conditions yields an array of impact metrics across these areas of concern.

Water resources system models are essential tools for exploring the risks to water system performance of potential future hydro-climatological and socio-economic conditions (Brown et al. 2015). This section presents an overview of the modeling approach developed for this study, introducing the model workflow and key terms and concepts depicted in Figure 2. Each element of Figure 2 is explained in detail in its own dedicated section later in this report. The analysis focuses on persistent medium- and long-term conditions evaluated at a monthly time-step. Short-duration extreme precipitation events that cause flooding may also stress water resource management but are beyond the scope of this study.

To conduct a stress test that can meaningfully inform the vulnerability of the multifaceted CVS, a water system model that can rapidly simulate the coordinated operations of the Central Valley Project (CVP) and SWP is needed. This study has adopted CalLite 3.0, a simplified, faster version of the CalSim-II water system model used by DWR. DWR estimates that the trade-off for the faster speed of CalLite 3.0 is an approximate error of 1 percent when compared with a corresponding run of CalSim-II (Islam et al. 2014). CalLite 3.0 is loaded with all system-wide relational data, such as reservoir area-elevation-capacity, wetness-index dependent flow standards, and monthly flood control requirements. For each month of the simulation period, CalLite 3.0 employs a mixed integer program to maximize water deliveries and/or storage per specified priorities and system constraints. Output includes water supply indicators, environmental indicators, and water-use metrics (Draper et al. 2004; California Department of Water Resources & United States Bureau of Reclamation 2011).

CalLite 3.0 receives time series of streamflow as input; however, to inform the likelihood of climate-change-related water-system vulnerabilities, it is necessary to begin with the most fundamental factors available — those describing conditions of meteorological drought, i.e., precipitation and temperature. This study uses a paleo-drendrochronology reconstructed streamflow record (Meko et al. 2014) coupled with historical daily temperature and precipitation to develop 1,100-year climate traces of plausible alternative precipitation and temperature. A hydrologic model (SAC-SMA) translates descriptors of fundamental meteorological drought into measures of available water at Earth's surface. The estimates of available water from the hydrologic model become the key inputs to a water system model (CalLite 3.0) which simulates the complex interactions of water supply, water demand, regulatory compliance, and operational choices, producing metrics of water system performance such as water deliveries, reservoir storage, and river flow volume.

Figure 2 Modeling Workflow for Climate Change Vulnerability Assessment

Note: Page number indicates the location in this report where the description of the workflow element can be found.

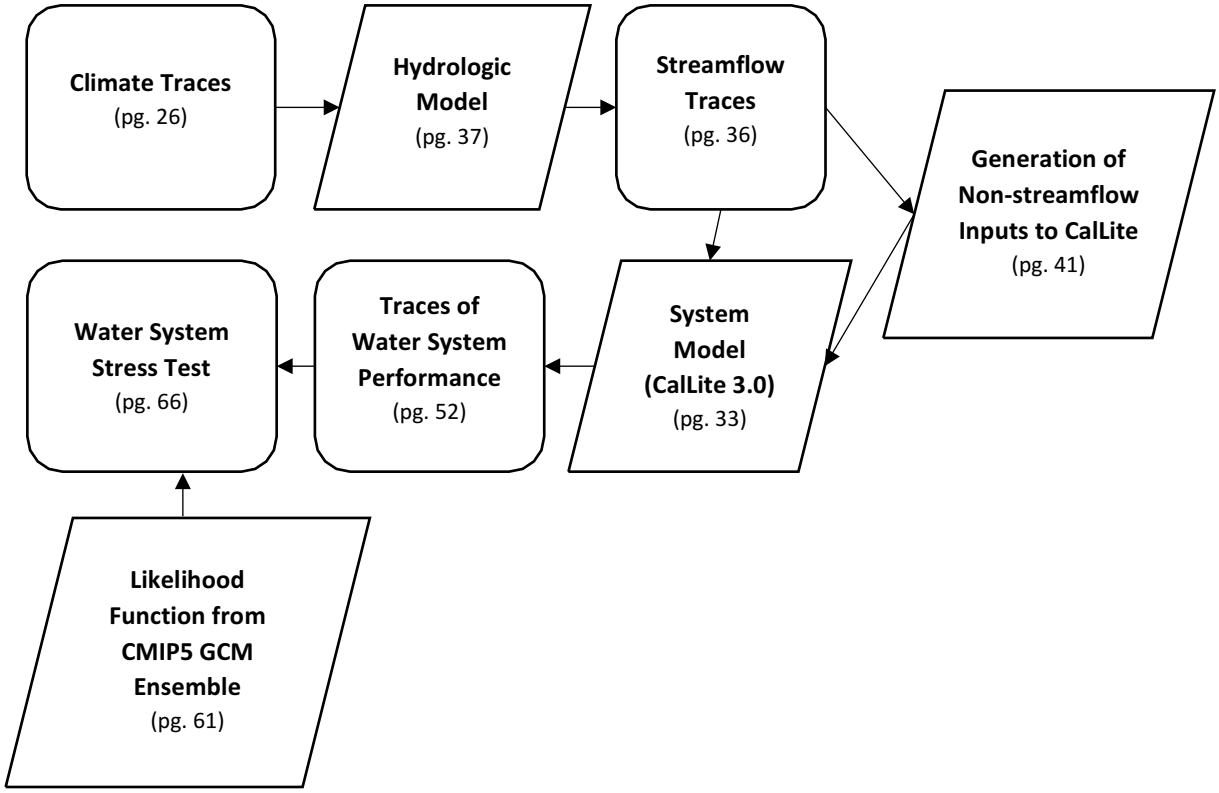

Structured, repeated simulation of the resulting workflow (Figure 2) – a "water system stress test" – allows the systematic exploration of climate change impact on the water system in response to a wide range of meteorological input. Table 1 lists the CVS metrics evaluated using this approach. The response of each performance metric to a systematically-explored climate space is presented relative to a performance threshold (in this case, historical performance).

Table 1 Decision-Relevant metrics

1	**Oroville Storage levels**
	April 30
	September 30
2	**Net Delta Outflow**
	Winter (Dec, Jan, Feb)
	Spring (Mar, Apr, May)
	Summer (Jun, Jul, Aug)
	Fall (Sep, Oct, Nov)
3	**SWP Deliveries**
	Average Annual
4	**System Shortages**
	Average Annual

Description of Study Area

The catchment area of the Sacramento and San Joaquin rivers (Figure 3) provides at least a portion of the water supply for about two-thirds of California's population. About half of California's average annual streamflow flows toward the Sacramento-San Joaquin Delta, and most of California's farmland depends on water tributary to it (Lund et al. 2010). The Delta is a web of channels and reclaimed islands at the confluence of the Sacramento and San Joaquin rivers. It forms the eastern portion of the wider San Francisco Estuary, which includes the San Francisco, San Pablo, and Suisun bays, and collects water from California's largest watershed, which encompasses roughly 45 percent of the state's surface area (Lund et al., 2010). The Delta is also a center for important components of California's civil infrastructure, such as electricity transmission lines, gas transmission pipes, underground storage of natural gas, and transportation lines, and provides crucial habitat for many California fish species that live in or migrate through it (especially four fish that are listed as "Endangered" or "Threatened" pursuant to the federal Endangered Species Act [Mount & Twiss 2005]). Not inconsequentially, the Delta is valued for its agricultural production, aesthetic appeal, and support of recreational activities (Lund et al. 2010). The usable water resources for the CVS can be approximated as the quantity of streamflow flowing into the Central Valley from the north-east upgradient regions. These regions are comprised of twelve large subbasins, referred to as the *rim subbasins* (Figure 3).

DWR and Reclamation oversee the operation of the Central Valley water systems that store and manage water supplies that flow through the Delta (see Figure 4). The California Central Valley Water System (CVS) is therefore defined as *the interconnected system of natural river channels and man-made facilities that comprise the CVP, owned and operated by the United States Bureau of Reclamation and the SWP, owned and operated by DWR*. The CVP includes more than 13 million acre-feet of storage capacity in 20 reservoirs. The CVP provides water to about 3,000,000 acres of irrigated agricultural fields, for municipal water uses, and for river and wetland water releases used to meet State and federal ecological standards. The SWP includes more than 30 storage facilities, namely reservoirs and lakes, and about 700 miles of open canals and pipelines that distribute water to approximately 25 million Californians and about 750,000 acres of irrigated farmland. The SWP is not the exclusive water supplier for those it serves, as many of its customers supplement the water provided by SWP with local or other imported sources. The SWP is designed to bolster local supplies and ensure greater supply reliability. Thus, demands on the project vary year to year.

Figure 3 California Central Valley System (CVS) and Rim Subbasins

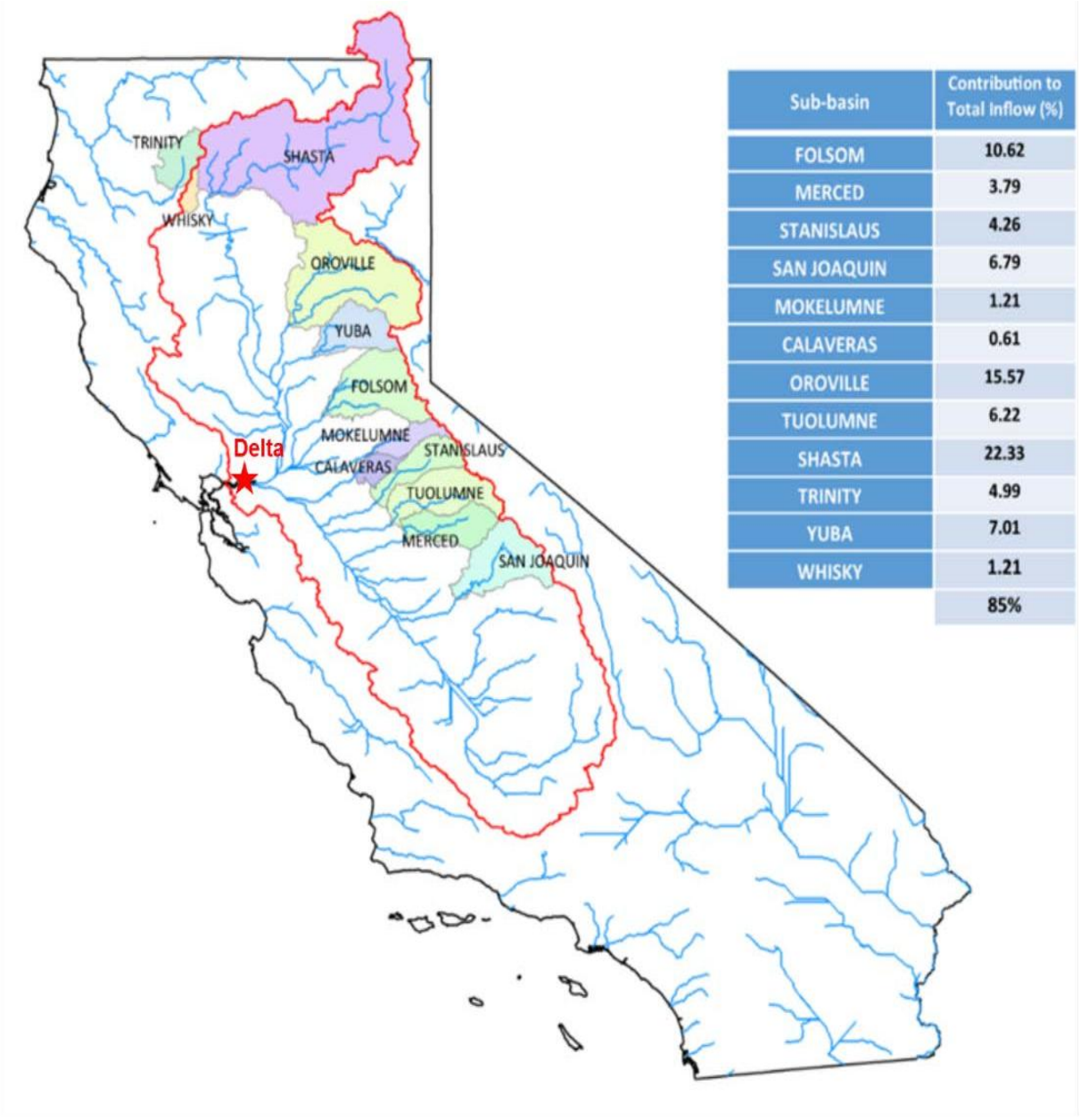

Sub-basin	Contribution to Total Inflow (%)
FOLSOM	10.62
MERCED	3.79
STANISLAUS	4.26
SAN JOAQUIN	6.79
MOKELUMNE	1.21
CALAVERAS	0.61
OROVILLE	15.57
TUOLUMNE	6.22
SHASTA	22.33
TRINITY	4.99
YUBA	7.01
WHISKY	1.21
	85%

Note: Table inset shows percent contribution of each of the 12 rim inflows to the total Delta outflow. Fifteen percent of the total Delta outflow is contributed by unshaded areas within the red outline.

Figure 4 State, Federal, and Local Water Infrastructure

Note: From Volume 3, Page 7-6 of the California Water Plan, Update 2013 (2013).

Generation of Climate Traces

In the original experimental design of this study (California Department of Water Resources 2017), a weather generator (Steinschneider and Brown 2013) produced 5000 unique climate realizations using a Wavelet Auto-Regressive Model (WARM) designed to maintain the 15-year low frequency variability of the precipitation signal visible in the latter half of the paleo record (Dettinger and Cayan 2014; Meko et al 2014). The initial sampling strategy required the establishment of a specific metric upon which to gauge the severity of the simulation (e.g., five-year precipitation). While this sampling strategy allowed exploration of system sensitivity to specific types of climatic characteristics of concern, the sampling of baseline traces was limited to within ±1 percent of the long-term mean to maintain fidelity to the historical observed interannual climate variability. This sampling strategy resulted in the omissions of traces with extended wet or dry periods. For this reason, the current iteration of this study has adopted an approach that utilizes the paleo-dendrochronological record to generate climate traces that are informed by a larger range of interannual variability than contained in the instrumental record alone.

The paleo-dendrochronology reconstructed record of Sacramento 4-river annual streamflow (900–2013) (Meko et al. 2014) was coupled with historical daily temperature and precipitation from 1950–2013 (Livneh et al. 2013) to generate a 1,100-year climate trace. The reconstructed Sacramento 4-river annual flow provides information about long-term inter-annual variability through a 1,100-year record of the wet and dry cycles that the CVS has endured. The daily temperature and precipitation provide information about the spatiotemporal distribution of weather that produced such annual streamflow. While not evaluated in this study, the 1,100-year record of wet and dry periods provides additional data to be used for the evaluation of future drought risk, which will be the focus of a future study.

The Sacramento 4-river annual streamflow is the aggregate annual water-year (October 1–September 30) streamflow of the Sacramento River at Bend Bridge, the American River inflow to Folsom Reservoir, the Yuba River at Smartsville, and Feather River inflow to Oroville Reservoir. The Sacramento 4-river annual streamflow covers the major inflow points to the CVS. Additional flows into the CVS not covered by the Sacramento 4-river annual streamflow are highly correlated to the Sacramento 4-river flow (Meko et. al. 2014).

The following steps were taken to link the 50-year daily temperature record to the 1,100-year paleo-dendrochronological record:

> **Step 1:** Prior to using the historical observed temperature data, it was necessary to remove the linear warming trend in the data. Temperature detrending was achieved by applying a linear trend to the data so that the detrended temperature time series had a trend line of slope zero and an average value equal to the average temperature from 1981 through 2010. This procedure was applied to each grid cell across the CVS watershed. The detrended historical temperature allows reference to current and recent historical conditions when developing the stress test as opposed to a more abstract reference to mid-20th-century temperatures at the mean of the historical time series. Furthermore, detrending was necessary to ensure the same average temperature reference is maintained across the 1,100-year coupled sequence. The observed historical precipitation data showed no trend, thus required no detrending.

Step 2: Using the historical (1950–2003) detrended temperature and precipitation data as input, the Sacramento Soil Moisture Accounting distributed hydrologic model (SAC-SMA-DS) (described in Section 2.2 *Hydrologic and Streamflow Traces*) was used to simulate streamflows in the Sacramento, Feather, Yuba, and American rivers of the Sacramento basin to generate the Sacramento 4-river annual streamflow.

Step 3: For each paleo-drendrochronology reconstructed Sacramento 4-river annual streamflow from 900 through 1949, the closest historical observed (1950–2003) analog flow was associated with it.

Step 4: The historical (1950–2003) detrended temperature and precipitation data for the water year of the analog historical observed flow was then copied into the historical reconstructed years.

This method of bootstrapping full years of temperature and precipitation ensures that spatial and temporal correlations are maintained and an exploration of a wider range of hydrologic inter-annual variability than is present in the observed meteorological record. There are several extended periods of below and above-average annual streamflows in the paleo reconstructed record which are greater in magnitude than found in the observed period of meteorological record (1950-2003) used in this study. For example, the maximum and minimum 10-year moving average annual streamflows calculated over the observed record are 21.7 maf (12% below the paleo maximum of 24.7 maf in the year 1606) and 16.2 maf (25% above the paleo minimum of 12.0 maf in 1929). Furthermore, periods of above and below-average flows persist for longer in the paleo record, up to 30 years (1126-1156) as shown in Figure 5.

The bootstrapped 1,100-year historical trace of daily temperature and precipitation was then perturbed systematically to explore the climate vulnerability domain of the CVS. The explored range for temperature and precipitation was informed by the range of changes projected for the CVS watershed area by the global climate models included in the Intergovernmental Panel on Climate Change's (IPCC's) Fifth Coupled Model Intercomparison Project (CMIP5) (Taylor et al. 2012). Figure 6 shows the range of average temperature and precipitation change projected (2036–2065 relative to 1981–2010) by 36 different models simulated at two different representative concentration pathways (RCP 4.5 and RCP 8.5). The scatter of the model projections indicates that the likely range of temperature and precipitation change that the CVS would experience ranges from -20 percent to +30 percent change in precipitation, and a temperature change of 0°C to +4°C (0 °F to 7.2 °F) relative to 1981-2010.

A total of 54 combinations of temperature shifts (+0°C to +4°C, by 0.5°C increments; +0 °F to +7.2 °F, by 0.9 °F increments) and precipitation shifts (-20 percent to +30 percent, by 10 percent increments) were imposed on each day of the 1,100-year historical climate record in each CVS grid cell using the Delta method described in the "Details on Approach to Climate Change Factors" section of this report. The result was 54 independent climate traces identical to the historical in internal variability but unique in average temperature and precipitation.

Figure 5 Sacramento 4-River Paleo Reconstructed Annual Streamflow

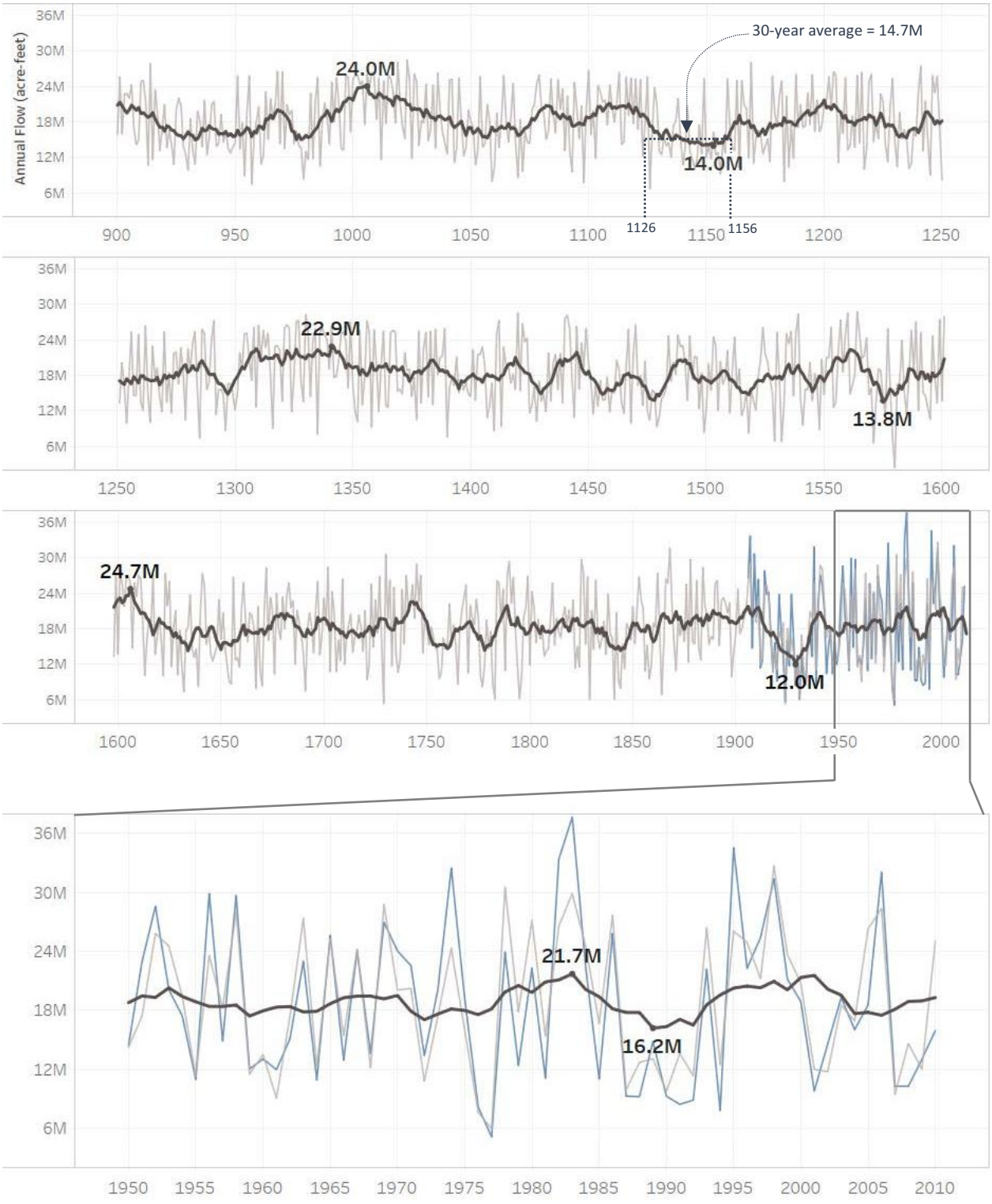

Note: The light grey line is paleo reconstructed Sacramento 4-River annual streamflow from 900 to 2010 and the blue line is observed Sacramento 4-River annual streamflow from 1906 to 2010. 10-year moving (centered) average annual paleo reconstructed flow is represented by the dark grey line with minimum and maximum values annotated for each time-window shown.

Figure 6 CMIP5 Ensemble of GCM Output Projecting Climate Changes by 2050 for the CVS

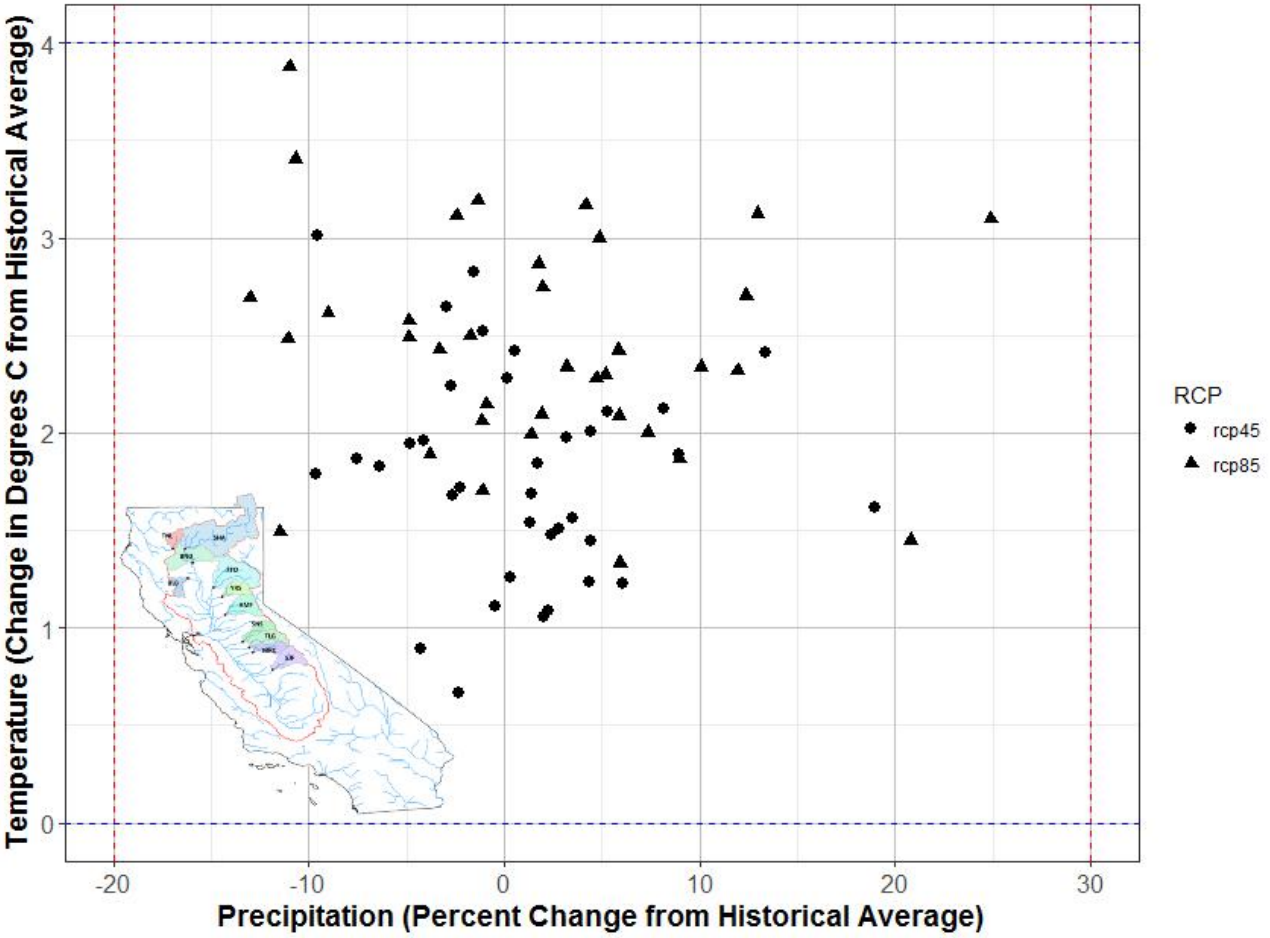

Note: Changes shown are average annual precipitation and temperature shifts: 2036–2065 relative to 1981–2010.

Details on Approach to Climate Change Factors

Because precipitation and temperature vary both spatially and temporally, the relationships of temperature and precipitation trends (for both observed and projected) with several geographical and timescale factors (including elevation, latitude, and season) should be investigated. In doing so, the levels of precipitation and temperature changes can be incorporated in more detail, which would help a realistic distribution of climate changes across the large study area as a function of space as well as time. This section presents an analysis conducted to analyze seasonal trends in temperature. See Annex B: Spatial and Temporal Climate Trends for further detail on spatial and seasonal trend analysis conducted for this study.

Relationship Between Temperature Trend and Season

This study uses daily climate data from the National Climate Data Center (NCDC) to identify relationships between temperature trends and season. Only the NCDC station data for which missing data rate is less than 20 percent was used. The winter dataset consists of the months of December, January, and February; spring with March, April, and May; summer with June, July, and August; and fall data with September, October, and November. Boxplots of trend slopes for five datasets (annual data, winter, spring, summer, and fall) are shown in Figure 7. The daily temperature data used to conduct this analysis went through quality checks based on two rates of missing station observations: Figure 7 results from 94

stations for which the missing data rate is less than 10 percent, while Figure 8 shows the results of trend analysis from 145 stations for which the missing rate is less than 20 percent.

In Figure 7 and Figure 8, red numbers represent medians of seasonal temperature trend, and black numbers are means of seasonal temperature trend. All trend slopes are positive, which implies that temperature tends to rise during 1950–2015. According to these box plots, seasonally distinct warming trends were observed. The seasonal warming patterns derived from this observed temperature analysis were applied to the new sequences of temperature reflecting 8 increase levels (i.e., 0.5, 1, 1.5, 2, 2.5, 3, 3.5, 4°C) as shown in Figure 9. Seasonal warming patterns define ratios among the four seasons. Then, these ratios are maintained in 8 increasing levels of temperature shift. In one season, increase levels are assumed to be the same across three months. The calculation processes are as follows:

Step 1: From the temperature data of each station during 1950–2015, Sen's slope is computed for four datasets of spring, summer, fall, and winter. Then, boxplots are calculated (Figures 7 and 8).

Step 2: From these boxplots, means of temperature trend slope (black numbers in boxplots) are attained from 94 stations (i.e., dataset with less than 10 percent missing data) and 145 stations (i.e., dataset with less than 20 percent missing data). These means are shown in Table 2 below.

Step 3: Finally, temperature increases reflecting the spring, summer, fall, and winter trends are calculated for eight scenarios (temperature increase of 0.5; 1; 1.5; 2; 2.5; 3; 3.5; 4°C). These patterns are shown in Figure 9.

Table 2 Means of Seasonal Warming Pattern

Season (Months)	Average Temperature Increase Per Decade (°C/decade)
Winter (DJF)	0.116
Spring (MAM)	0.265
Summer (JJA)	0.1915
Fall (SON)	0.0435

Figure 7 **Trend Slope of Temperature With Less Than 10 Percent Missing Data in 94 Stations**

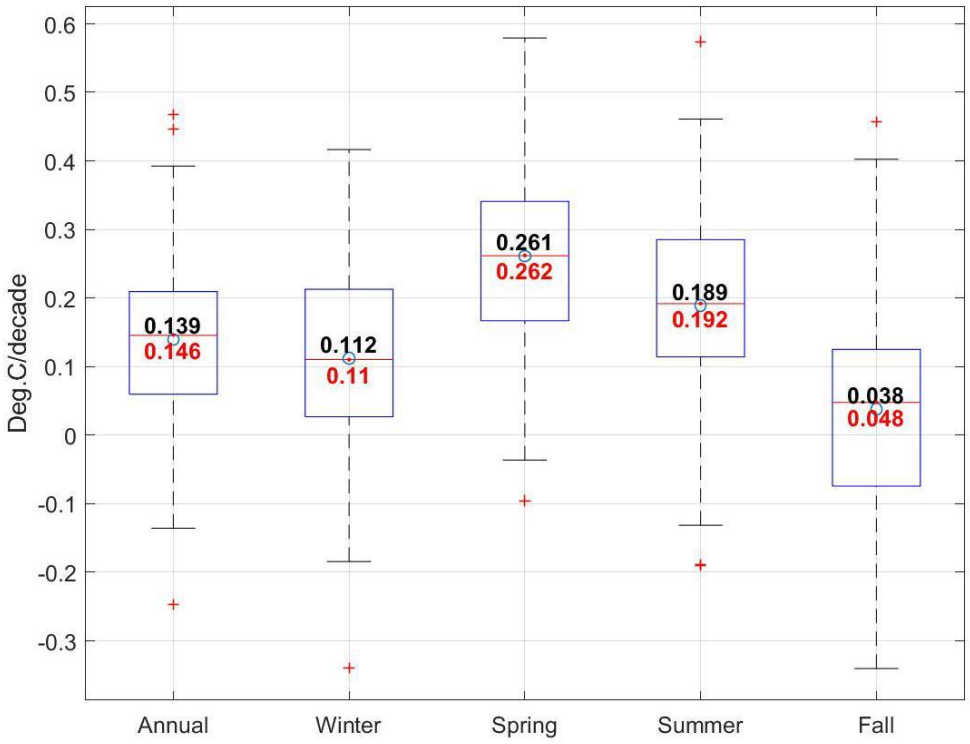

Figure 8 **Trend Slope of Temperature With Less Than 20 Percent Missing Data in 145 Stations**

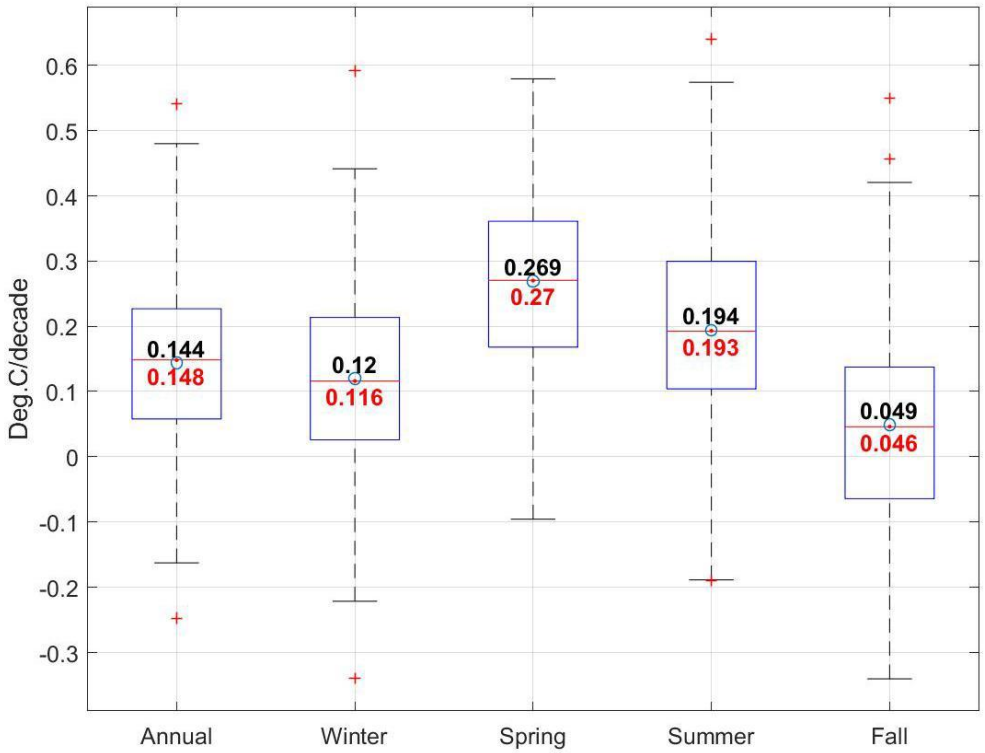

Figure 9 Seasonal Warming Patterns for Climate Projections

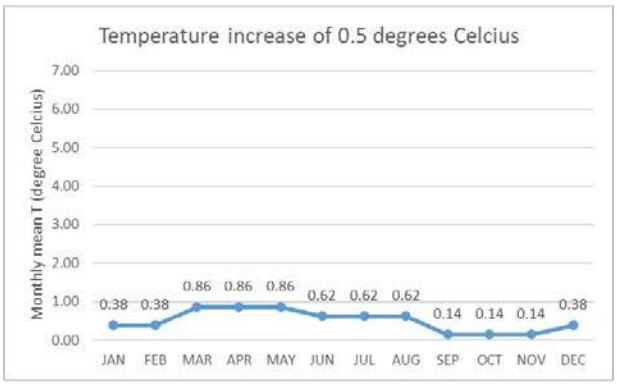

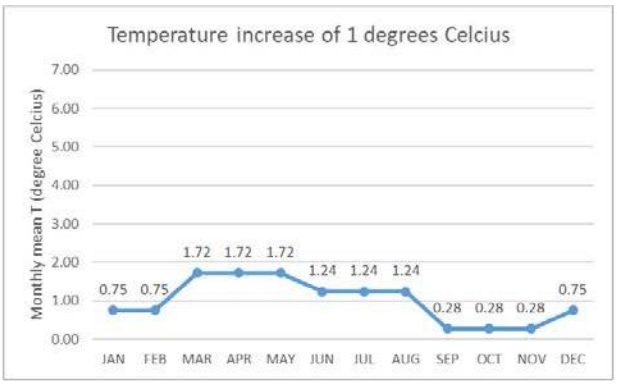

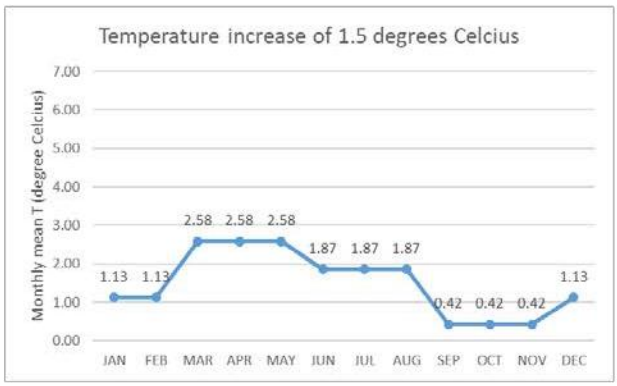

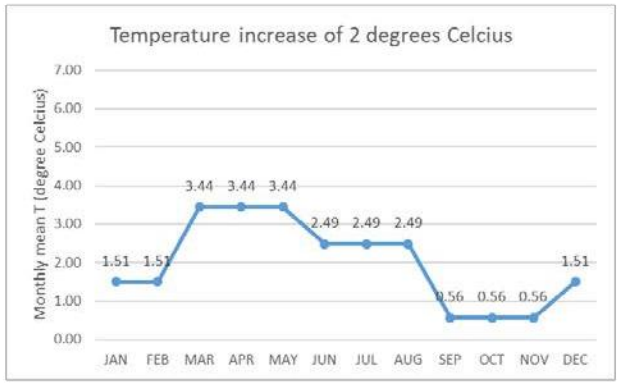

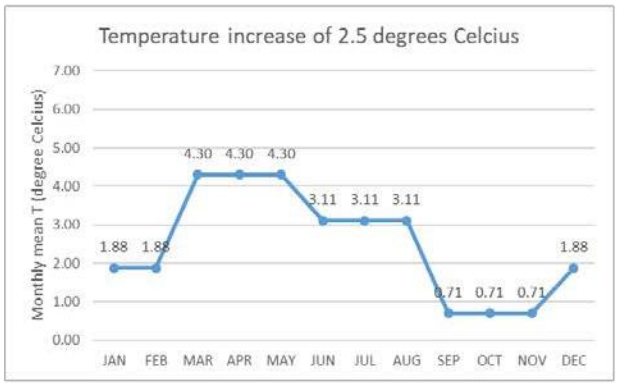

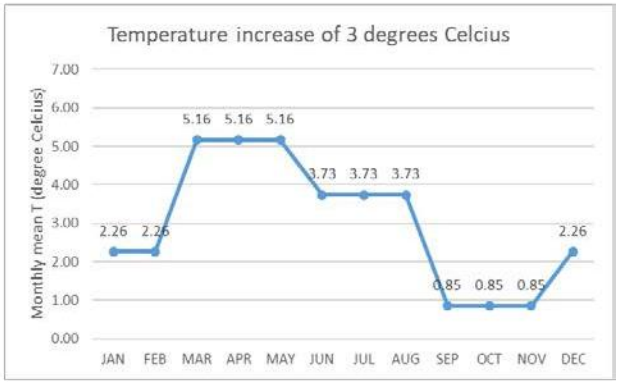

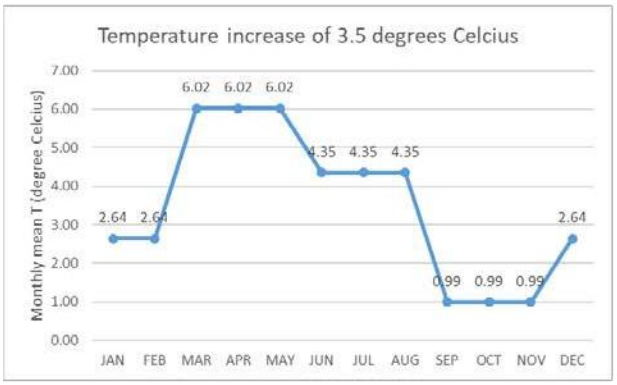

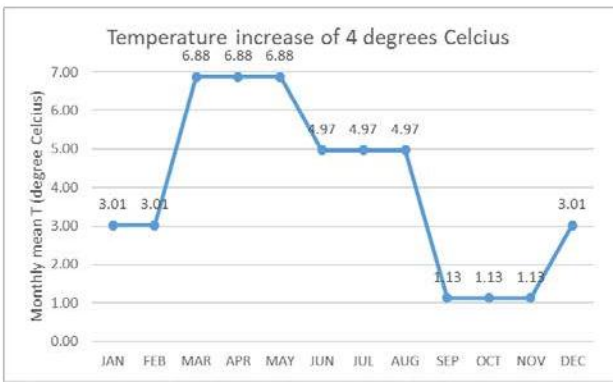

Conclusion

No significant correlations were found for either temperature or precipitation trends with elevation and latitude (see *Annex B: Spatial and Temporal Climate Trends* for further analysis). Consequently, mean annual precipitation changes were applied without considering season, elevation, or latitude factors. On average, temperatures in Spring and Summer were seen to warm more significantly than in Winter and Fall over the past 65 years; therefore, seasonal mean annual temperature changes were applied using the seasonal factors described above.

Although the results of this investigation enable us to account for seasonal warming effects, two major assumptions are made. First, ratios of seasonal warming to annual warming are assumed to be the same at any level of annual warming. This results in relatively large warming differentials such as at an annual warming of 4°C under which the spring is warmed to nearly 7°C compared to the winter at 3°C. Second, the seasonal warming effect is assumed to be uniform across the entire CVS area. However, as is evident in the distribution of seasonal warming trends observed in NCDC station data (see Figures 7 and 8), sub-selection of station locations in a given region of the CVS will likely result in different ratios of seasonal to annual warming. Future investigation into the presence and causes of trends in seasonal warming would improve understanding of how seasonal warming effects may persist or change in the future.

A version of this study which does not include an application of the seasonal warming effect was published in California's Fourth Climate Change Assessment (Schwarz 2018). Although the performance metrics selected for reporting in the Fourth Assessment version of this study differ from those selected here, the Fourth Assessment study is a reference point for comparing the effect of seasonal warming at the macro, system-wide scale since both studies were completed using the modeling workflow shown in Figure 2.

Water Resources System Model

CalLite 3.0 is the water resources system model used in this study to assess impacts. It is a screening level planning tool developed by DWR and Reclamation to simulate the coordinated operations of the intertied CVS. CalLite 3.0 is the faster, streamlined version of CalSim-II[4] (Draper et al. 2004), designed to be accessible to policy and stakeholder demands for rapid and interactive policy evaluations. CalLite's mixed integer linear program maximizes monthly water deliveries and/or storage per specified priorities and system constraints. The system constraints and weights (fully described in Draper et al. [2004] and California DWR and Reclamation [2011]) are specified using the Water Resources Engineering Simulation Language (WRESL) (California Department of Water Resources 2000): "The objective function in the [CalLite] model is a linear combination of decision variables and their associated priority weights. In addition, slack and surplus variables added to the objective function from 'soft' constraints are multiplied by their associated negative penalties."

[4] CalSim-II, driven by the Water Resource Integrated Modeling System (WRIMS model engine or WRIMS) is "a generalized water resources modeling system for evaluating operational alternatives of large, complex river basins [that] integrates a simulation language for flexible operational criteria specification, a [mixed integer] linear programming solver for efficient water allocation decisions, and graphics capabilities for ease of use" (California Department of Water Resources & United States Bureau of Reclamation 2011). As explained by Draper et al. (2004), "for each time period, the solver maximizes the objective function to determine a solution that delivers or stores water according to the specified priorities and satisfies system constraints. The sequence of solved [Mixed Integer Programming] problems represents the simulation of the system over the period of analysis… [CalSim-II] also allows the user to specify objectives using a weighted goal-programming technique pioneered by Charnes and Cooper (1961)."

CalLite's CVS-specific design and substantial intricacy enable better fidelity to the mechanics of DWR allocation rules and water sharing agreements. That being said, the model contains many approximations of site-specific values for which historical observations are scarce, and also includes poorly-understood empirically-based relationships that pose challenges related to water system simulation under wide-ranging conditions of climate uncertainty.

CalLite 3.0, a schematic of which is shown in Figure 10, represents reservoir operations, SWP and CVP operations and delivery allocation decisions, existing water sharing agreements, and Delta salinity responses to river flow and export changes on a monthly time-step. CalLite 3.0 can also represent the effect on the water system from land use changes and sea level rise, features of particular use to this study. CalLite 3.0, released in 2014, has 796 input parameters and approximately 240 additional data tables that store all relational data, such as reservoir area-elevation-capacity data, wetness-index dependent flow standards, and monthly flood control requirements (Draper et al. 2004; California Department of Water Resources & United States Bureau of Reclamation 2011). Output includes water supply indicators, environmental indicators, and water-use metrics.

CalLite 3.0 Configuration of Regulatory Environment

CalLite 3.0 allows users to specify and turn on or off regulatory flow requirements including various river flows, Delta outflows, export restrictions, and salinity objectives relating to the operation of the CVP and SWP. In this study, regulatory constraints are set to represent operating conditions as of the year 2015. Table 3 identifies base assumptions for the regulatory environment used in this study and contrasts it with a similar version of this study published in California's Fourth Climate Change Assessment (Schwarz et al. 2018).

Table 3 Base Assumptions Used for Regulatory Environment in CalLite 3.0

Regulatory Standard	Configuration for this Study	Configuration for Schwarz et al. 2018
Vernalis Adaptive Management Plan (VAMP)	– VAMP is turned OFF	– VAMP is turned ON
Delta Cross Channel	– D-1641 standard is turned ON – National Marine Fisheries Service Reasonable and Prudent Alternative Action 4.1.2 is turned ON	– Same
Export-Inflow Ratio	– D-1641 standard is turned ON – National Marine Fisheries Service Reasonable and Prudent Alternative Action 4.2.1 is turned OFF	– Same except Action 4.2.1 is turned ON
Delta Outflow and Rio Vista Requirements	– D-1641 standard is turned ON – U.S. Fish and Wildlife Service Reasonable and Prudent Alternative Action 4 X2[a] requirement is turned ON – Roe Island standard is turned ON	– Same
Salinity Requirements	– Emmaton, Jersey Point, Rock Slough, and Collinsville are turned ON	– Same

[a] X2 = location of the 2 parts per thousand salinity contour, one meter off the bottom of the estuary, as measured in kilometers upstream from the Golden Gate Bridge

Figure 10 **CalLite 3.0 Schematic**

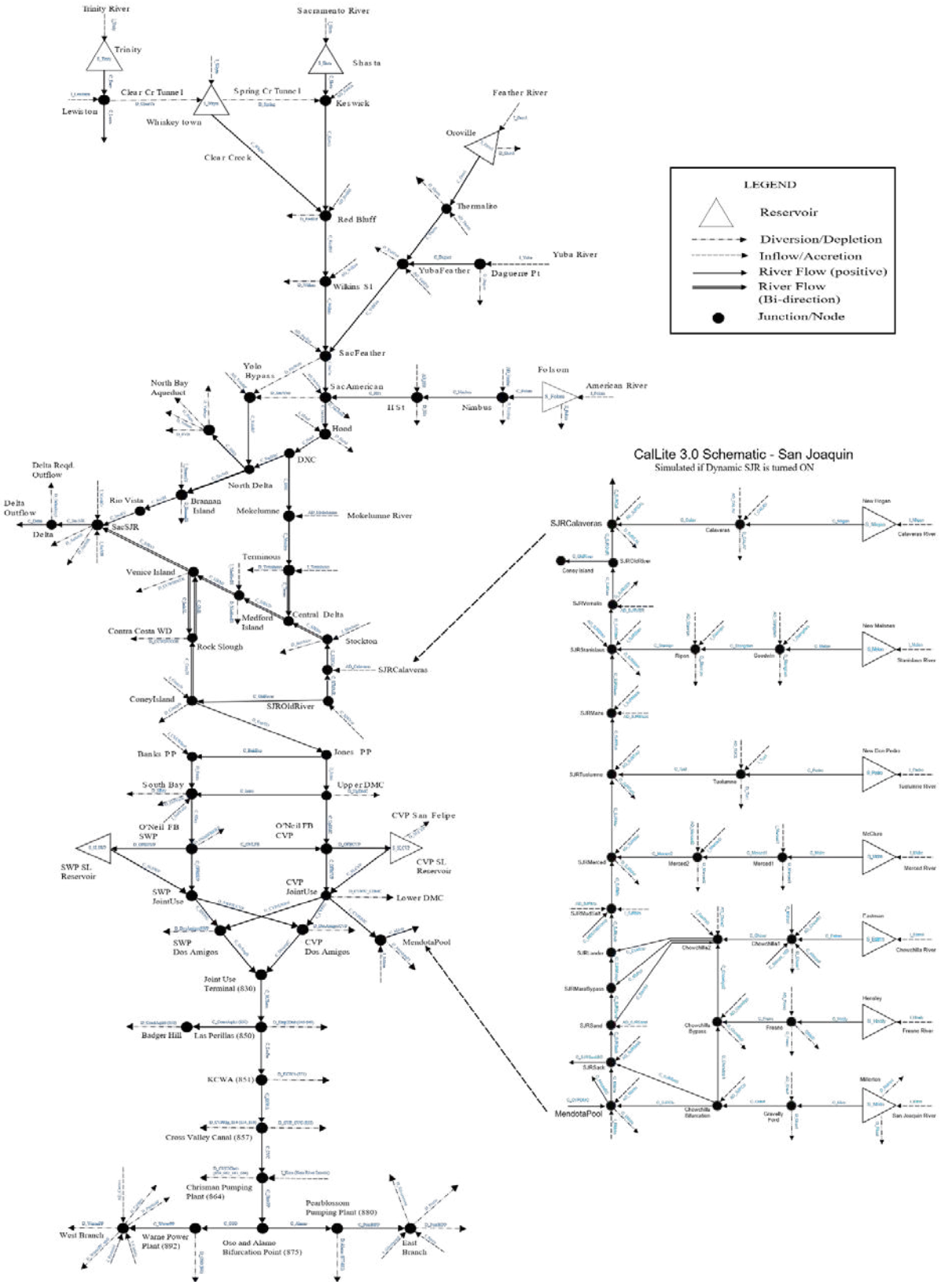

Generation of Streamflows

As illustrated in Figure 3, the coverage area of the hydrologic model includes all major tributaries to the northern CVS. The contributing flow is summarized in the Figure 3 table insert, showing the relative importance of the Shasta and Oroville subbasins. The SAC-SMA-DS hydrologic model is used to simulate streamflow at 32 locations throughout the CVS watershed. As shown in Figure 10, these 32 streamflow simulations include:

> **Calibration Set I:** 12 rim inflows to major reservoirs throughout the CVS.
>
> **Calibration Set II:** 11 gauging station streamflow points important for calculating water-year types used for regulatory constraints, management, and operational decision-making.
>
> **Calibration Set III:** 9 subbasin inflows that account for a substantial portion of the rain in the system and represent "unimpaired inflows," as they are the modeling results of estimating the runoff that would have occurred had water flow remained unaltered in rivers and streams instead of stored in reservoirs, imported, exported, or diverted (Bay-Delta Office 2007).

As shown in Figure 11, the locations of the 11 stream gages in Calibration Set II are nearly identical to the locations of the basin outlets for the 12 rim inflows in Calibration Set I. This is because the historical data for the CalLite 3.0 rim inflows are derived from the 11 physical stream gages described in Calibration Set II. To validate the workflow shown in Figure 2 relative to the baseline run of the CalLite 3.0 simulation model, the SAC-SMA-DS model was calibrated directly to the streamflow in the CalLite 3.0 package (Calibration Set I). This is different than calibrating to historical observations, as the streamflow pre-loaded in the CalLite 3.0 package is the output of previous hydrologic modeling (Variable Infiltration Capacity [VIC]) project performed for the CVS.

To evaluate the quality of the original VIC hydrologic model output used in CalLite 3.0, and to gain the confidence associated with validation relative to historical observations, it was necessary to calibrate the SAC-SMA-DS directly to the observations at the 11 physical gages of Calibration Set II. The results of Calibration Set II were not used as input to CalLite 3.0 but were used in the determination of water-year type classification as described below.

Calibration Set III was developed when it was realized that Calibration Set I and Calibration Set II failed to account for a substantial portion (especially south and west) of the total CVS basin area shown bounded in red in Figure 11. The nine unimpaired inflow basins of Calibration Set III add information on CVS subbasins that are rain-dominated (as opposed to many of the 12 rim inflows, which are largely snow-dominated), and accounts for a substantial portion of the rain that falls within the CVS system. The nine basins of Calibration Set III are referred to as "unimpaired inflows," as they are the result of a modeling project that estimated the runoff "that would have occurred had water flow remained unaltered in rivers and streams instead of stored in reservoirs, imported, exported, or diverted" for 24 Central Valley subbasins and the Sacramento-San Joaquin Delta for October 1920 through September 2003 (Bay-Delta Office 2007). Whereas Calibration Set I was used as direct input to CalLite 3.0 and Calibration Set II was used principally as a check on Calibration Set I and in the development of water year type classification, Calibration Set III was used principally to add information to the process for generating other, minor hydrologic and non-hydrologic inputs to CalLite 3.0.

Box 1 Description of the SAC-SMA-DS Hydrologic Model

The hydrologic model is required to be extremely robust because of its essential role in the quantification of the available water on which water allocations to all water sectors are based. Hydrologic model residuals propagate through the modeling chain and contribute to a cascade of uncertainty (Wilby & Dessai 2010). This box describes the development of a distributed, physically-based hydrologic model capable of supporting subsequent phases of the climate change vulnerability assessment workflow.

The amount of usable water for the CVS can be approximated as the quantity of streamflow in the 12 largest rivers flowing from the northeast into the Central Valley. These are referred to as the *rim inflows*. To estimate those 12 streamflows, a unique version of the Sacramento Soil Moisture Accounting (SAC-SMA) model was developed.

SAC-SMA (Burnash et al. 1973), is a lumped conceptual hydrological model employed by the National Weather Service (NWS) of the National Oceanic and Atmospheric Administration (NOAA) to produce river and flash flood forecasts for the United States (Burnash 1995; McEnery et al. 2005). It was coupled with a river routing model (Lohmann et al. 1998) for application to the large, distributed CVS watershed system (consisting of approximately one thousand 1/8th degree grid cells). The coupled model is hereafter referred to as SAC-SMA-DS (Wi & Brown 2013), distinguishing it from the distributed version of SAC-SMA previously developed by NWS. SAC-SMA-DS has been applied to a number of case studies (e.g., Koren et al. 2004; Smith et al. 2004). SAC-SMA-DS (Box 1 Figure (a)) is composed of hydrologic process modules that represent soil moisture accounting, potential evapotranspiration (Hamon 1961), snow processes (Anderson 1976), and flow routing, and operates in grid formulation on a daily time-step.

(a) Distributed Hydrologic Model

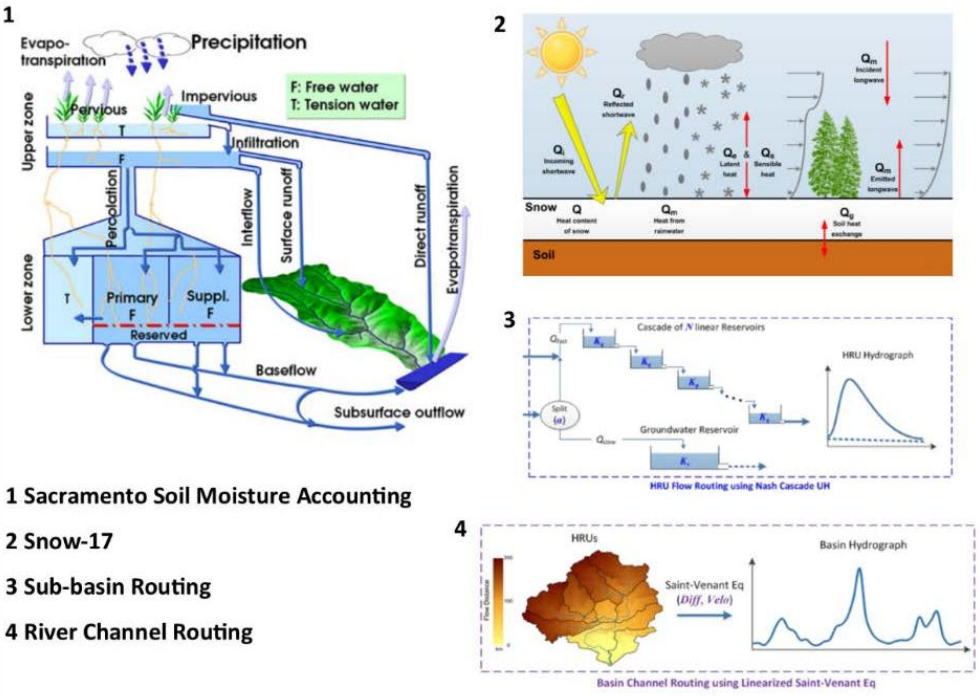

Box 1 Description of the SAC-SMA-DS Hydrologic Model (continued)

The overall model structure of SAC-SMA-DS is depicted in Box 1 Figure (a) above. More details on the model components are provided in the descriptions for the modules additionally introduced to develop the distributed version of SAC-SMA.

Hamon Evapotranspiration Calculation

The potential evapotranspiration (PET) is derived based on the Hamon method (Hamon 1961), in which daily PET in millimeters (mm) is computed as a function of daily mean temperature and hours of daylight:

$$\mathrm{PET} = \mathrm{Coeff} \cdot 29.8 \cdot \mathrm{L_d} \cdot \frac{0.611 \cdot \exp\left(17.27 \cdot \frac{\mathrm{T}}{(\mathrm{T}+273.3)}\right)}{\mathrm{T}+273.3} \qquad (2)$$

where L_d is the daylight hours per day, T is the daily mean air temperature (°C), and Coeff is a bias correction factor. The hours of daylight is calculated as a function of latitude and day of year based on the daylight length estimation model suggested by Forsythe et al. (1995).

In-grid Routing: Nash-Cascade Unit Hydrograph

The within-grid routing process for direct runoff is represented by an instantaneous unit hydrograph (IUH) (Nash 1957), in which a catchment is depicted as a series of N reservoirs each having a linear relationship between storage and outflow with the storage coefficient of Kq. Mathematically, the IUH is expressed by a gamma probability distribution:

$$\mathrm{u(t)} = \frac{\mathrm{K_q}}{\Gamma(\mathrm{N})}\left(\mathrm{K_q t}\right)^{\mathrm{N}-1}\exp\left(-\mathrm{K_q t}\right) \qquad (3)$$

where Γ is the gamma function. The within-grid groundwater routing process is simplified as a lumped linear reservoir with the storage recession coefficient of Ks.

River Channel Routing: Linearized Saint-Venant Equation

The transport of water in the channel system is described using the diffusive wave approximation of the Saint-Venant equation (Lohmann et al. 1998):

$$\frac{\partial \mathrm{Q}}{\partial \mathrm{t}} + \mathrm{C}\frac{\partial \mathrm{Q}}{\partial \mathrm{x}} - \mathrm{D}\frac{\partial^2 \mathrm{Q}}{\partial^2 \mathrm{x}^2} = 0 \qquad (4)$$

where C and D are parameters denoting wave velocity and diffusivity, respectively.

Figure 11 Maps of Three Calibration Sets For the Application of SAC-SMA-DS to the CVS

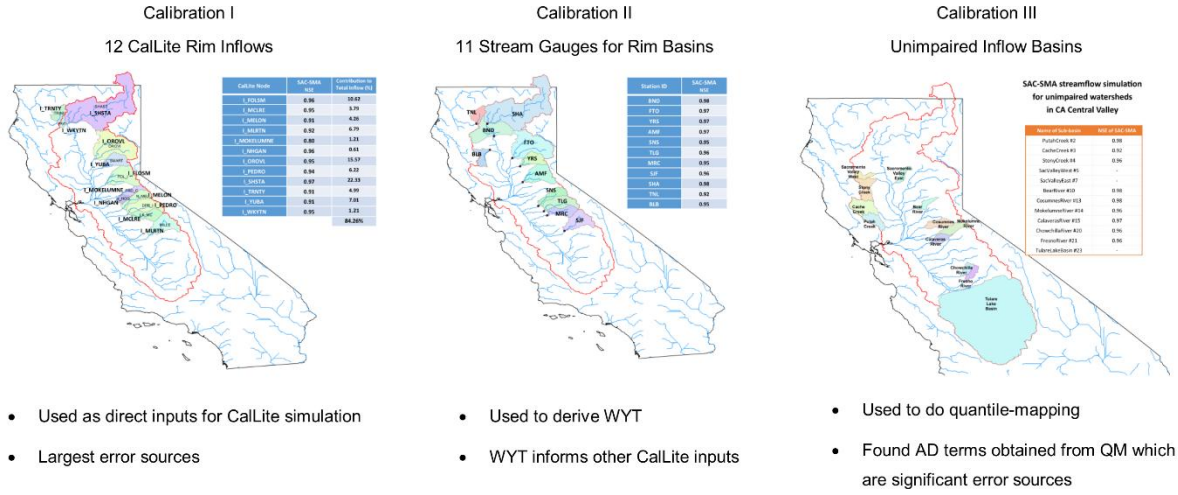

Generation of Hydrologic Inputs to CalLite 3.0

Of the 796 CalLite inputs, 39 are hydrologic inflows to the CVS. These 39 inflows consist of the 12 rim basin inflows (see Table 3), 9 "unimpaired" local inflows, and 18 "other" local inflows. Internal consistency in these hydrologic inflows can be maintained using the paleo-drendrochronology reconstructed climate traces in combination with the SAC-SMA-DS hydrologic model (see Box 1). Most of the input variables were found to have a relatively small impact on model output. Of the 796 inputs, only 20 (the 12 rim basins plus 8 of the 9 unimpaired local inflows) of the 39 inflow variables and 11 of 18 accretion/depletion (AD) terms[5] exerted a strong influence on model output (see Table 4).

Table 4 Twelve Major Rim Inflows to the CalLite 3.0 Model

American River (into Folsom Lake)
Merced River (into Lake McClure)
Stanislaus River (into New Melones Lake)
San Joaquin River (into Millerton Lake)
Mokelumne River
Calaveras River (into New Hogan Lake)
Feather River (into Lake Oroville)
Tuolumne River into (New Don Pedro Reservoir)
Sacramento River (into Shasta Reservoir)
Trinity River (into Trinity Reservoir)
Yuba River (into New Bullards Bar)
Clear Creek (into Whiskeytown Reservoir)

[5] Accretion/depletion terms are generated in CalLite 3.0 to account for differences between CalLite 3.0 and CalSim-II resulting from a less detailed schematic. Adjustments (addition and subtraction of CalSim-II terms) are made at each CalLite 3.0 node based on CalSim II outputs.

Table 5 R Squared Correlations For 31 CalLite 3.0 Input Parameters With Strong Influence on Model Output

CalLite 3.0 Input Parameter	Correlation Coefficient	Best Fit of Calibration Set I/II/III Outputs
I_NHGAN.FLOW.INFLOW	1	I_NHGAN
I_SHSTA.FLOW.INFLOW	1	I_SHSTA
I_FOLSM.FLOW.INFLOW	1	I_FOLSM
I_OROVL.FLOW.INFLOW	1	I_OROVL
I_MCLRE.FLOW.INFLOW	1	I_MCLRE
I_WKYTN.FLOW.INFLOW	1	I_WKYTN
I_PEDRO.FLOW.INFLOW	1	I_PEDRO
I_MLRTN.FLOW.INFLOW	1	I_MLRTN
I_LEWISTON.FLOW.INFLOW	1	I_TRNTY
I_TRNTY.FLOW.INFLOW	1	I_TRNTY
I_MELON.FLOW.INFLOW	1	I_MELON
I_YUBA.FLOW.INFLOW	1	I_YUBA
I_MOKELUMNE.FLOW.INFLOW	1	I_MOKELUMNE
I_ESTMN.FLOW.INFLOW	0.99	ChowchillaRiver
I_HNSLY.FLOW.INFLOW	0.99	FresnoRiver
AD_REDBLF.FLOW.ACCRDEPL	0.92	StonyCreek
AD_MOKELUMNE.FLOW.ACCRDEPL	0.9	CosumnesRiver
I_CALAV.FLOW.INFLOW	0.78	PutahCreek
AD_SACFEA.FLOW.ACCRDEPL	0.77	StonyCreek
AD_CALAVERAS.FLOW.ACCRDEPL	0.75	I_NHGAN
AD_YOLOBP.FLOW.ACCRDEPL	0.7	PutahCreek
AD_SJR_PULSE_V.FLOW.CHANNEL	0.65	I_MOKELUMNE
AD_SJR_V.FLOW.ACCRDEPL	0.65	I_MOKELUMNE
AD_SJR_VAMP_V.FLOW.CHANNEL	0.64	I_MOKELUMNE
AD_YUBFEA.FLOW.ACCRDEPL	0.46	CacheCreek
I_MDOTA.FLOW.INFLOW	0.39	I_MELON
I_TUOL.FLOW.INFLOW	0.27	CalaverasRiver
I_KELLYRIDGE.FLOW.INFLOW	0.26	SacWYT
I_KERN.FLOW.INFLOW	0.25	I_MLRTN
AD_WILKNS.FLOW.ACCRDEPL	0.24	SacWYT
AD_SACAME.FLOW.ACCRDEPL	0.1	SacWYT

27 local inflow inputs to CalLite 3.0, which make up the remaining portion of the system's total inflows apart from the 12 rim inflows, were not directly simulated because: (1) acquisition of unimpaired natural flow for those rivers was not straightforward; and (2) the increasing computational effort was not justified by the increase in model accuracy (given the small fraction of total flow contribution). The AD terms could not be simulated using a hydrologic model because they are aggregations of hydrologic, management, and other anthropogenic behaviors that cannot be approximated as unimpaired catchment inflows.

Generation of Non-Hydrologic Inputs to CalLite 3.0

The 757 non-hydrologic CalLite 3.0 input time series' fit into one of three categories: (1) constant value, (2) time series with several discrete steps or recurring values, (3) or continuously varying time series. In both the discrete recurring value time series and continuously varying time series, the values tended to vary as a function of hydrology (wetness or dryness of month), either directly (correlated to one of the 12 rim inflows of Calibration Set I or one of the 9 additional unimpaired inflows of Calibration Set III) or by way of one of two streamflow indices developed using Calibration Set II.

To evaluate the "goodness of fit" of each CalLite 3.0 input parameter to the Sacramento and San Joaquin water-year types, 60 water-year type values were computed (5 water-year types x 12 months) for each of the Sacramento and San Joaquin water-year-type indices. The average value of each CalLite 3.0 input parameter was calculated for each month of each water-year type. To explore correlation with the water-year types, the raw time series of each input parameter was then regressed against a discrete time series (with 60 unique values) representing the water-year-type average in each month of each year of the historical record.

719 of the CalLite 3.0 input parameters were better correlated to a water-year-type index than they were to one of the 21 inflows of Calibration Sets I and III. Those 719 input parameters were therefore associated with one of the two water-year-type indices and varied accordingly. 63 CalLite 3.0 input parameters were associated with an inflow of Calibration Set I or III and perturbed using a quantile mapping technique. Finally, the values of two CalLite 3.0 input parameters were generated by way of special processes unique to those inputs.

Creating Synthetic Time Series by Water-Year-Type Method

For those CalLite 3.0 input parameters that correlated most closely to one of the two water-year-type classifications (Sacramento or San Joaquin), a discrete, 60-value mapping procedure was then used. The 60 values for each input variable were calculated using the historical observed dataset. The historical dataset was sorted by historical water-year-type classification and an average value for each month-water-year combination was calculated.

To generate the synthetic input time series, the water-year type was calculated based on the synthetic hydrologic input time series (Calibration Set II) using the appropriate water-year calculation methodology (http://cdec.water.ca.gov/cgi-progs/iodir/WSIHIST), which is a combination of rim inflows. The historically calculated 60 values were then mapped into the synthetic time-series input variable according to the water-year type and month combination. Figure 12 shows three variables that have strong correlations with the San Joaquin water-year type classification.

Figure 12 Input Variables With Strong Correlation to San Joaquin Water Year Type Classification — Historical Observed Data Shown

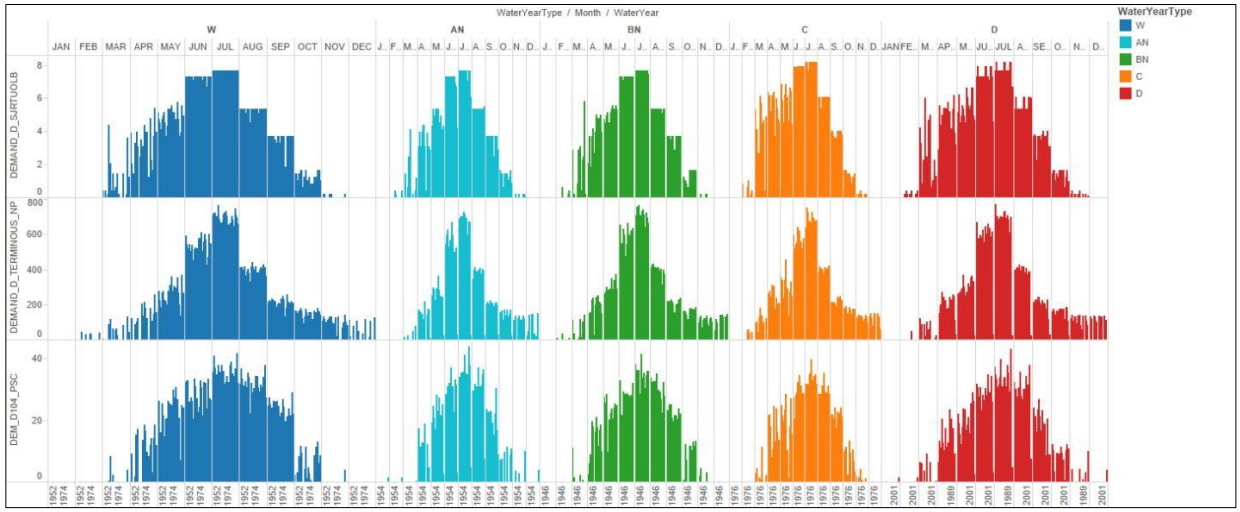

Creating Synthetic Time Series by Quantile Mapping Method

Sixty-three CalLite 3.0 input parameters were synthetically generated by quantile mapping the historical unimpaired-flow time series for each of the DWR 24 unimpaired flow basins (California Department of Water Resource Bay Delta Office 2007) to the historical values of each time series in the CalLite 3.0 input file.

The CalLite 3.0 input parameters that correlated most closely with one of the rim inflows were paired with that inflow. For example, Figure 13 shows the correlation that two historical local inflows (I_BRANANIS and I_MDOTA) have with the historical inflows of the 12 rim basins, and the rim inflows of I_NHGAN and I_MOKELUMNE are selected as the best pairs of I_BRANANIS and I_MDOTA, respectively. The pairs of local and rim inflows determined in this way are used in the quantile mapping procedure to generate new local inflows corresponding to new rim inflows. The quantile mapping procedure is described using an example in the following section. Table 5 shows pairs of local and rim inflows determined for all local inflows. Consequently, six of the rim inflows are selected based on which inflows are quantile-mapped.

Figure 13 Pearson Correlation Coefficients of Two Historical Local Inflows (I_BRANANIS and I_MDOTA) With 12 Historical Rim Inflows.

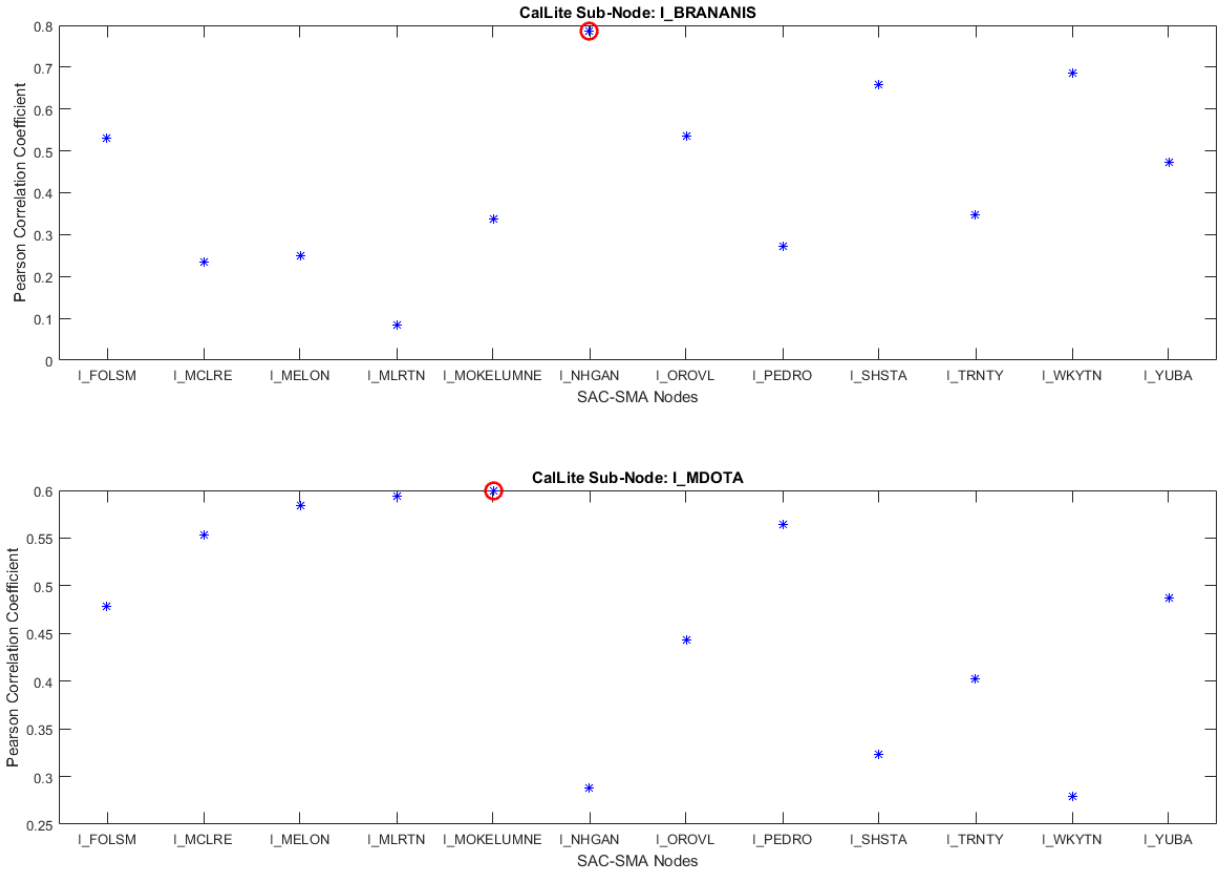

Table 6 Pairs of Rim Flows and Local Inflows Determined by Correlation

Rim Inflow Node	Local Inflow Node	Pearson correlation coefficient	Relative contribution to total system flows
	I_STANGDWN	0.99	0.01 percent
	I_NIMBUS	0.94	0.03 percent
	I_ESTMN	0.91	0.28 percent
	I_EASTBYP	0.90	0.76 percent
	I_CALAV	0.87	0.05 percent
	I_HNSLY	0.87	0.33 percent
	I_TERMINOUS	0.83	0.22 percent
	I_BRANANIS	0.79	0.32 percent
I_NHGAN	I_STOCKTON	0.77	0.06 percent
	I_MEDFORDIS	0.76	0.18 percent
	I_HOOD	0.72	0.05 percent
	I_SACSJR	0.72	0.02 percent
	I_CONEYIS	0.71	0.10 percent
	I_MARSHCR	0.61	0.13 percent
	I_SJRMS	0.57	0.09 percent
	I_SJRMSA	0.57	0.09 percent
	I_TUOL	0.42	0.79 percent
	I_SJRMAZE	0.58	1.45 percent
I_MELON	I_SJRSTAN	0.58	0.08 percent
	I_MERCED1B	0.51	0.33 percent
I_MLRTN	I_KERN	0.49	0.10 percent
	I_STANRIPN	0.32	0.40 percent
I_FOLSM	I_KELLYRIDGE	0.38	0.50 percent
I_MOKELUMNE	I_MDOTA	0.60	0.58 percent
I_TRNTY	I_LEWISTON	0.99	0.03 percent

Here, we provide a detailed description of the quantile mapping procedure with an example for the local inflow of I_NIMBUS. For the I_NIMBUS, the rim inflow of I_NHGAN is selected as the best-correlated inflow, with the correlation coefficient of 0.94. The quantile mapping procedure starts with fitting those two inflows to specific probability distributions. In this study, we employed two types of distributions: (1) empirical probability based on the Weibull plotting position, and (2) theoretical probability based on the 2-parameter gamma distribution. How the quantile mapping works for the I_NIMBUS with selected rim inflow I_NHGAN is illustrated in Figure 14. For those two inflows, both the empirical and theoretical distribution are fitted as shown in Figure 14; the red line with asterisk dots represents the fit by the Weibull plotting position and the blue line represents the fit by the Gamma distribution. The red continuous empirical probability line is formed by doing a linear interpolation between values of asterisk

dots. As shown in the figure, the new rim inflow leads to the new local inflow value through those two quantile plots of local and rim inflows. The quantile mapping procedure is simply summarized in two steps: (1) find a quantile (i.e., non-exceedance probability) for the new rim inflow, and (2) find the value of local inflow that corresponds to the quantile of the rim inflow. In our quantile mapping procedure, empirical distributions are used as long as new inflows are within the historically observed range. In case the new inflows are beyond the historical range, gamma distribution fit is used. This quantile mapping procedure is conducted monthly to take into account the seasonal variability of inflows.

Figure 14 Quantile Mapping Procedure Applied to Example California Sub-Basin

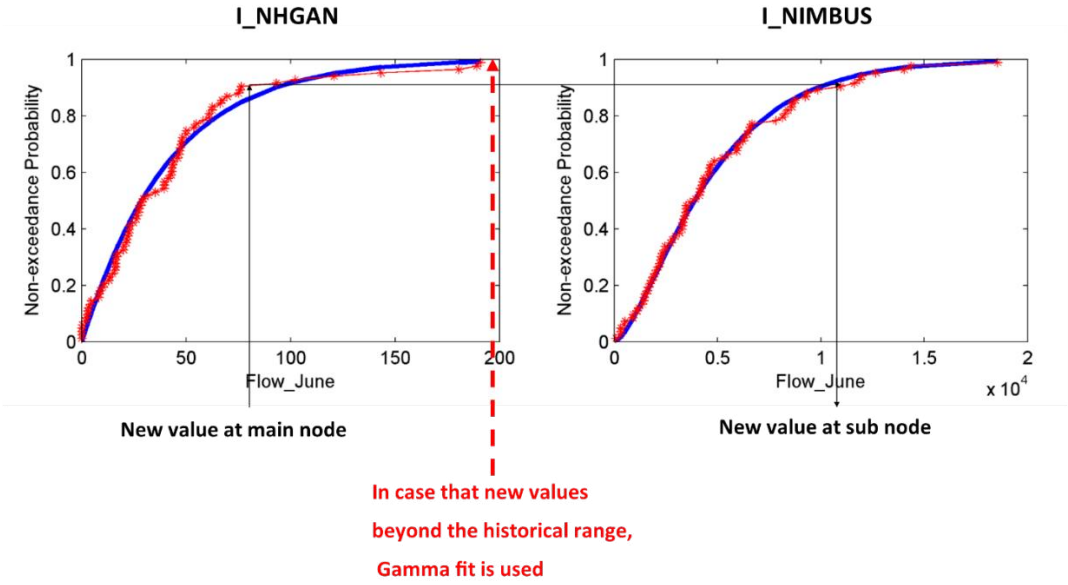

Parameter-Specific Generation of CalLite 3.0 Input (i.e., Special Cases)

Two AD terms, AD_Wilkins and AD_SACAME, had a large impact on model performance and did not correlate well to rim unimpaired inflow or water-year-type averages. Additional efforts were made to create new versions of these time series.

AD_Wilkins

CalLite's AD_Wilkins term was developed as a mass balance of CalSim-II terms along the Sacramento River from the Red Bluff Diversion Dam to Wilkins Slough in Colusa Basin. AD_Wilkins contained very large negative values. Through visual inspection of the CalSim-II schematic represented by the single lumped AD_Wilkins term, the time series was identified as containing Tisdale weir operations in the Butte basin. The design capacity of the Tisdale weir is 38,000 cubic feet per second (cfs)[6], which seems reasonable when compared to the largest negative values contained in the AD_Wilkins time series (Figure 15). AD_Wilkins correlated well to unimpaired flow from the Bay Delta Office's Shasta unimpaired flow basin. When flow from the Shasta Basin exceeds 13,300 cfs, it was assumed that water begins to exit the Sacramento River via a weir. Two linear equations were developed for AD_Wilkins: one for conditions in which Shasta flow is less than 13,300 cfs, and another when flow exceeds 13,300 cfs (Figure 15).

[6] http://cdec4gov.water.ca.gov/cgi-progs/products/Weir_Operations_Schematic.pdf

Figure 15 AD_Wilkins: Correlation With Shasta Flow

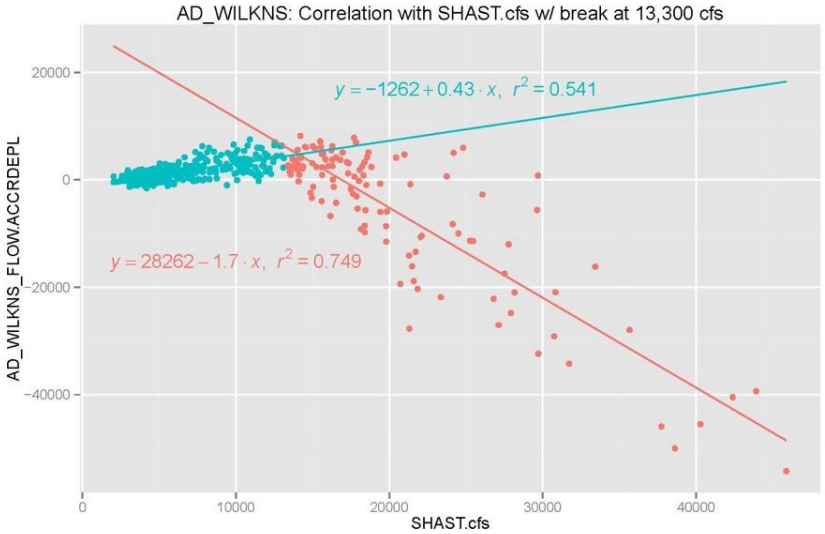

AD_SACAME

CalLite's AD_SACAME term represents the confluence of Sacramento and American rivers and was developed as a mass balance of CalSim-II terms along the Sacramento River from the Fremont Weir/Feather River confluence to Freeport. The term includes depletions in Yolo and Solano counties, agricultural and urban return flows, and water diverted from the Bear River. After an exhaustive search for a more adroit method of synthesizing the AD_SACAME variable, it was decided the best possible approximation was the Sacramento water-year-type classification average. It should be noted that the end of the AD_SACAME time series of historically observed values contains some extremely negative values (Figure 16) which call into question the assumptions used to create the CalSim-II terms on which the AD_SACAME time series is based.

Figure 16 **AD_SACAME Historical Behavior**

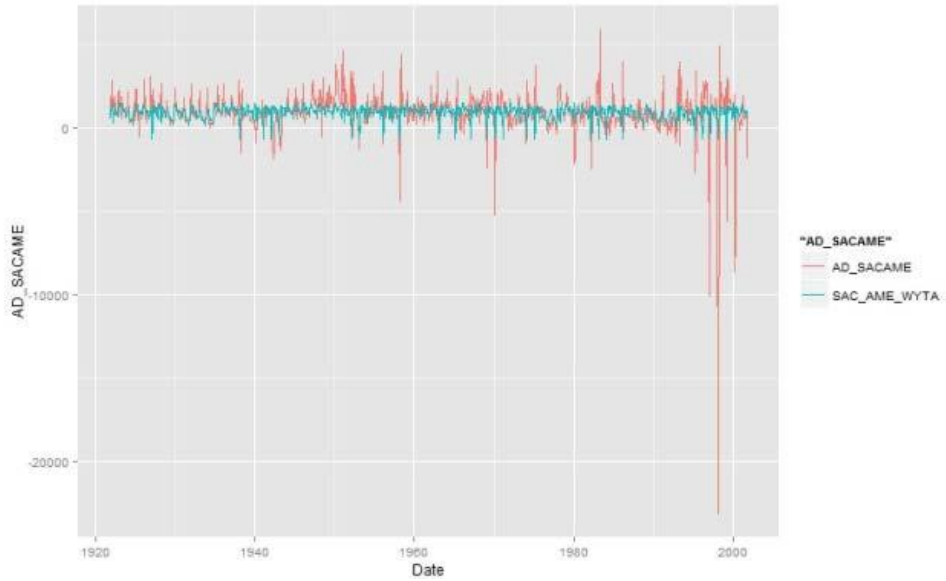

Sea Level Rise Assignment for CalLite 3.0

For operational purposes, it was important to estimate sea-level rise as a function of temperature and to associate the appropriate amount of sea-level rise with the temperature perturbation to which each CalLite 3.0 run was subjected. Sea-level rise increases saline intrusion into the Delta due to hydrostatic pressure from sea water head. During the spring and fall, DWR and Reclamation release additional water from reservoirs or reduce exports from the Delta to maintain regulatory compliance with maximum salinity limits and minimum outflow requirements.

At the start of this study, three sea-level rise scenarios were parameterized in CalLite 3.0: 0 centimeters (cm) (0 inches [in.]), 15 cm (6 in.), and 45 cm (18 in.). This coarse discretization of sea-level rise is a limitation of the model and may cause underestimation of impacts at higher temperatures (e.g., more than 2.5°C [4.5 degrees Fahrenheit (°F)], when sea-level rise would likely exceed 45 cm [18 in.]). Further, sea-level increases beyond 45 cm would likely cause significant changes in Delta hydrodynamics and would likely result in levee overtopping and additional inundation of lands that are currently protected by levees. Modeling such changes would require making assumptions about future levee investments and land uses, and those topics are beyond the scope of this project.

The National Research Council (2012) approximated the anticipated future rate of sea-level rise along the California coast, south of Cape Mendocino, for the years 2030, 2050, and 2100. These projections, in conjunction with values for projected global temperature increase by year from IPCC (2013), were used to estimate the amount of sea-level rise that should be expected along the California coast, south of Cape Mendocino, for each temperature band listed in Table 6 and shown in Figure 17. Recent guidance published by the California Ocean Protection Council Science Advisory Team Working Group projects the likely range (67% probability) of sea-level rise by 2050 to be 18.3-33.5 cm above the 1991-2009 mean (Griggs et al. 2017), placing estimates used in this study for the 2050 planning horizon within comparable limits.

Figure 17 Estimates of Sea-Level Rise by Degree C

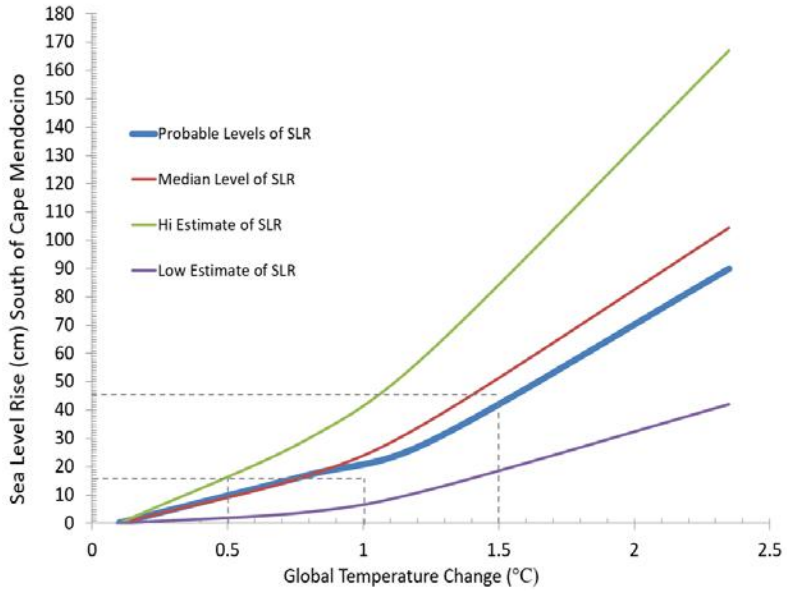

The sea-level rise assignment for CalLite 3.0 was made according to the logic shown in Table 6, which approximates and discretizes to the three sea-level rise steps available within the model and DWR's best understanding of the level of sea-level rise that would be expected at each increment of temperature change. Each time a climate trace was run through CalLite 3.0, the degree of temperature shift it received (as described in reference to Figure 9) was noted, and the corresponding sea-level rise function within the model was set according to Table 6.

Table 7 Sea-Level Rise Discretization Within CalLite 3.0

Temperature Change Relative to Recent Historical Average Temperature	Sea-Level Rise Relative to Recent Historical Average Sea Level
0°C (32 °F)	0 cm (0 in.)
0.5°C – 1.0°C (0.9 °F – 1.8 °F)	15 cm (6 in.)
≥ 1.5°C (2.7 °F)	45 cm (18 in.)

Notes:

°C = degrees Celsius
°F = degrees Fahrenheit
cm = centimeters
in. = inches

Model Verification

Hydrologic Model Performance

To calibrate the SAC-SMA-DS, a genetic optimization algorithm (Conn et al. 1991) was used to maximize the Nash-Sutcliffe efficiency (NSE) (Nash & Sutcliffe 1970). Table 7 summarizes the performance of the simulated historical inflows of the 12 rim subbasins for calibration (1951–1980) and validation (1981–2002) periods. NSEs evaluated on the monthly simulated streamflow show values of above 0.9 for all of them except for the Mokelumne subbasin. According to Moriasi et al. (2007), model simulation can be judged as satisfactory if NSE > 0.5.

Table 8 Hydrologic Model Performance by Subbasin

Subbasin	Nash Sutcliffe Efficiency	
	Calibration (1951–1980)	Validation (1981–2002)
American	0.96	0.94
Merced	0.95	0.93
Stanislaus	0.91	0.90
San Joaquin	0.92	0.90
Mokelumne	0.77	0.85
Calaveras	0.96	0.93
Feather	0.95	0.94
Tuolumne	0.94	0.93
Sacramento	0.97	0.97
Trinity	0.94	0.89
Yuba	0.91	0.95
Clear Creek	0.95	0.93

The second test of the hydrologic model concerned its ability to reproduce historical water-year type classifications based on the flow of rim-inflow rivers, using an algorithm designed to reproduce the water year classification system used by DWR. The combined hydrologic model and water-year-classification algorithm was shown to successfully match water-year type for every year of the historical record to the DWR method of water-year classification (http://cdec.water.ca.gov/cgi-progs/iodir_ss/wsihist).

System Model Performance

Figure 18 through Figure 20 show the sample output of a CalLite 3.0 validation run selected to demonstrate the ability of the model workflow (Figure 2) to reproduce historical CalLite 3.0 output for each of the decision-relevant metrics described in Table 1. Figure 18 presents the validation for Total North of Delta Storage, of which Oroville reservoir storage is a part. Figure 19 presents the validation for Delta outflow. Figure 20 presents the validation for SWP deliveries.

The validation is a perfect reproduction prior to 1950, as no reliable climate data were available for the development of climate traces before that time.

Figure 18 Validation of CalLite 3.0 Stress Test Modeling Workflow for Total North of Delta Storage

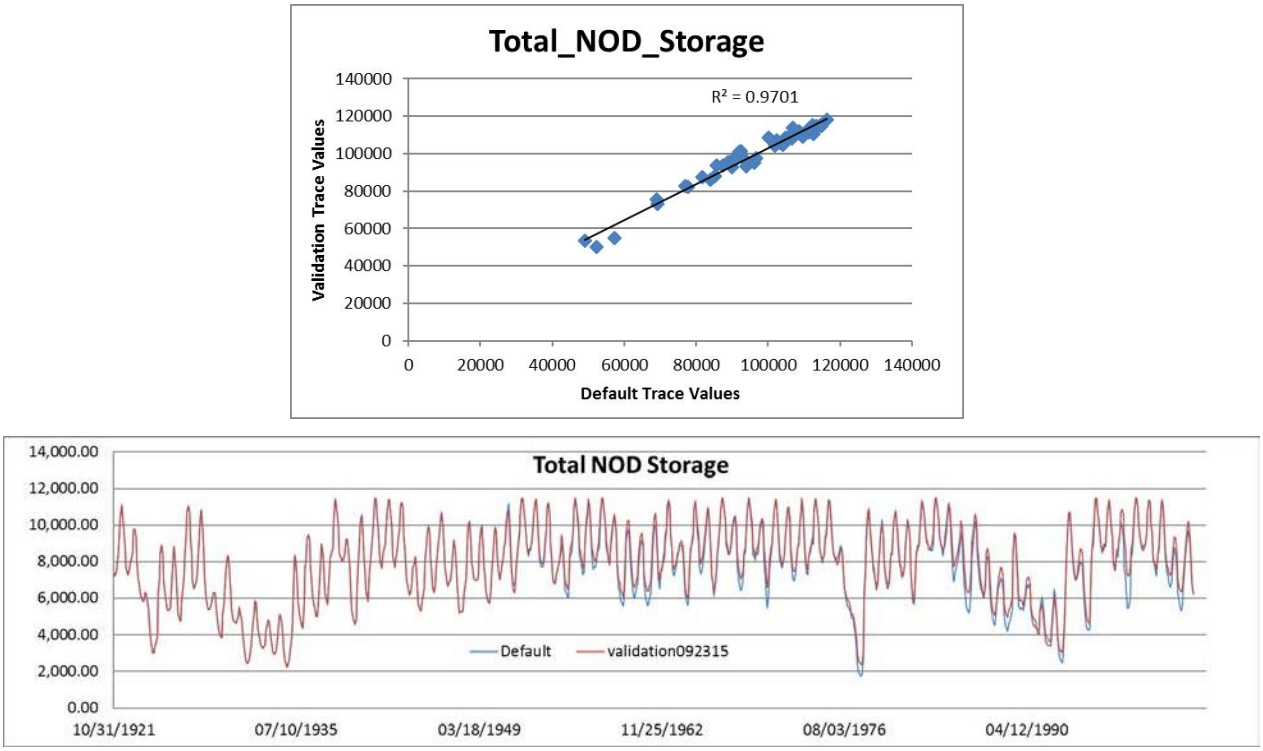

Note: Top: Scatterplot fit of annually averaged validation trace values to default trace values. Bottom: Default (blue) and validation (red) trace monthly Total North of Delta Storage showing perfect fit before 1950 and differences after 1950.

Figure 19 Validation of CalLite 3.0 Stress Test Modeling Workflow for Delta Outflow

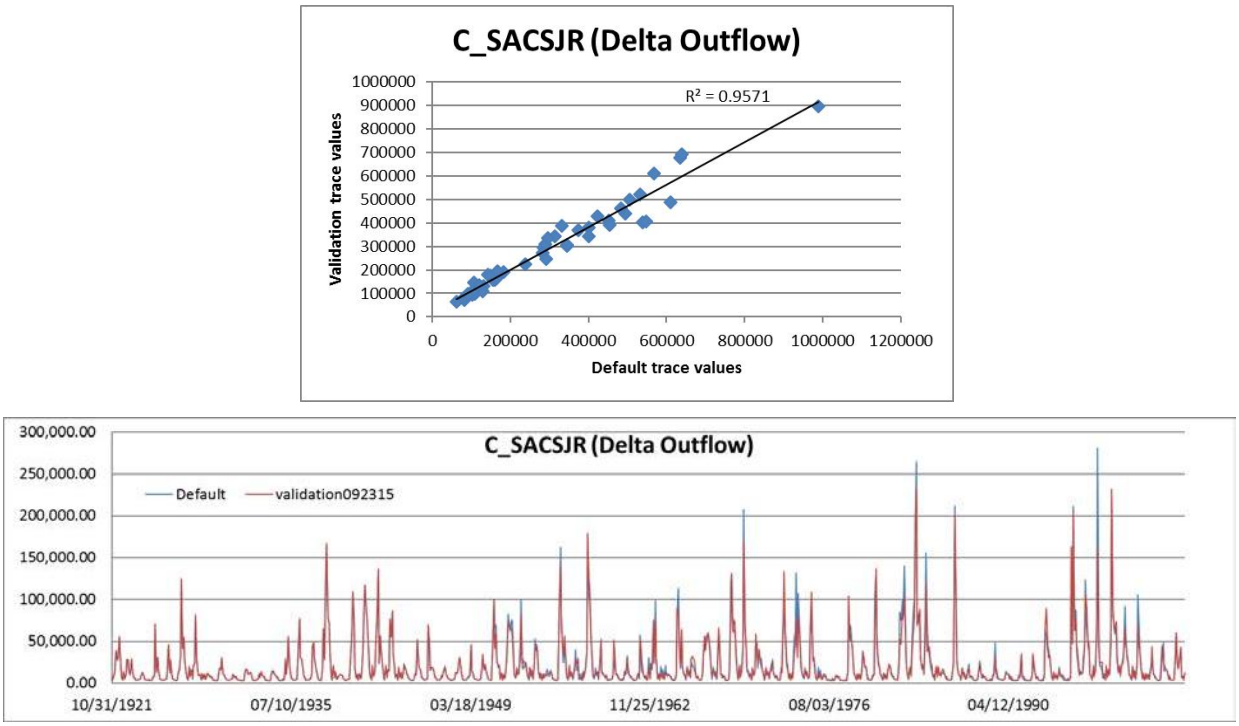

Note: Top: Scatterplot fit of annually averaged validation trace values to default trace values. Bottom: Default (blue) and validation (red) trace monthly Delta Outflow showing perfect fit before 1950 and differences after 1950.

Figure 20 Validation of CalLite 3.0 Stress Test Modeling Workflow for SWP Annual Deliveries

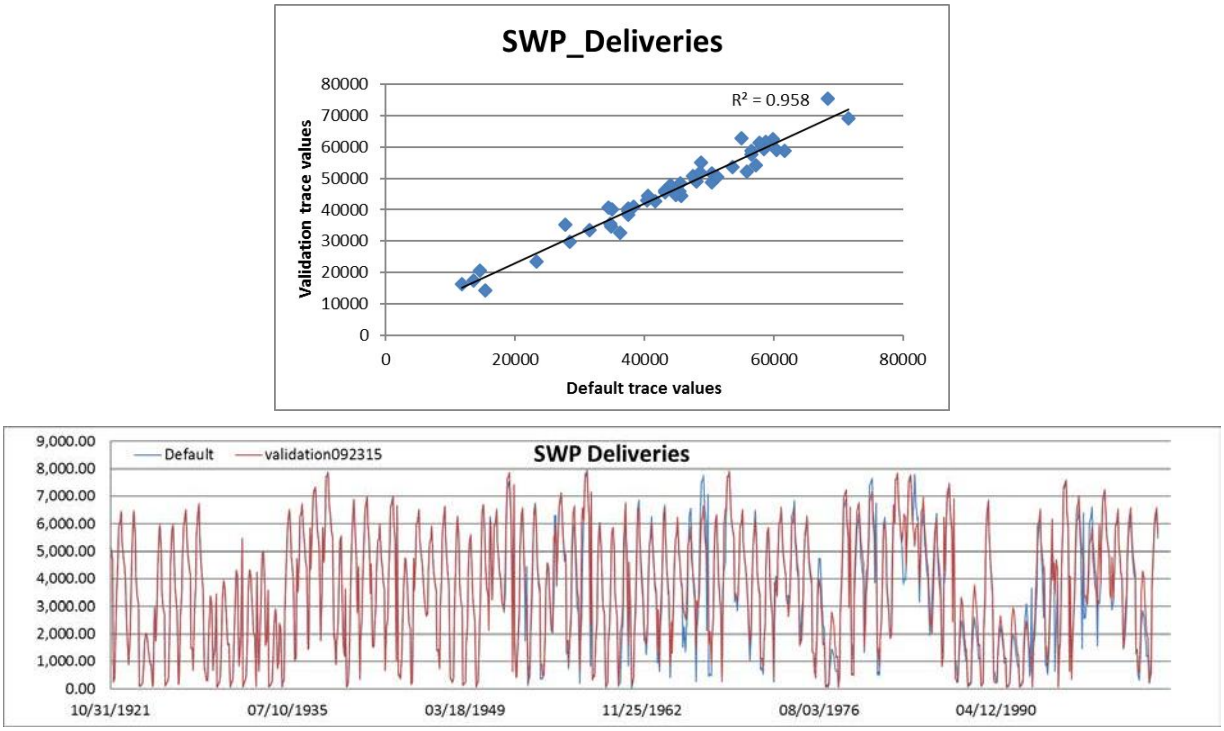

Note: Top: Scatterplot fit of annually averaged validation trace values to default trace values. Bottom: Default (blue) and validation (red) trace monthly SWP deliveries showing perfect fit before 1950 and differences after 1950.

Risk Assessment Results

Exposure

DWR's operation of the SWP is exposed to climate-changed conditions throughout the state. In the watersheds from which water supplies originate, higher temperatures and changes in precipitation are expected to change the availability of water. In the Sacramento-San Joaquin Delta, water supplies interact with the Delta's complex hydrology, which is influenced by sea level, tides, and flows from several rivers. Throughout the SWP's service areas, demand for SWP water supplies will be affected by higher temperatures and changing precipitation.

Climate change exposure for these areas has been estimated using data from an ensemble of projections derived from the CMIP5 to develop probabilistic climate information. While the ensemble of models indicates a range of future outcomes in temperature and precipitation, conditional probabilities for temperature and precipitation change can be inferred by plotting the bivariate normal distribution of the projected changes of the models. Figure 1 and Table 8 present the conditional climate probability density for climate changes at 2050. By expressing the range of climate changes in the future as probabilistic possibilities, a deeper understanding of the range of potential exposures is possible. In Figure 1, deeper blue colors represent higher agreement among the GCMs about future conditions, and lighter blue colors represent future conditions that are predicted by fewer models but still considered potential future outcomes.

Sensitivity

The decision scaling approach described in the preceding section "Methodology" was used to explore system performance for each of the metrics listed in Table 1. The system performance response surfaces describe how the system performs over the range of temperature and precipitation changes. See Box 2, *Understanding System Response Surfaces*, for additional information on interpreting the information in these graphics.

The response surface describes the sensitivity of the SWP system to changes in climate. On the response surface, the black line represents performance at historical levels; warm colors represent performance worse than historical levels while cool colors represent performance better than historical levels. Changes in color represent sensitivity to a change in climate.

Box 2 Understanding System Response Surfaces

For each performance metric, the response surface shows the performance that would be expected for various combinations of change in precipitation, warming, and sea level. In the example below, annual SWP deliveries are shown. The value at 0 degrees warming and 0 change in precipitation essentially represents current conditions (i.e., the long-term average of annual SWP deliveries that would be expected if climate conditions remained stable at today's levels). This level of performance is referred to as the "current conditions estimate" and represents the simulated long-term average system performance over the 1,100-year hydrological sequence with no climate warming beyond what has already occurred, and no change in precipitation from historical levels, i.e., 0 percent change. A black line extends up and to the right from 0 degrees warming and 0 percent change in precipitation. This line represents system performance at the same level as the current conditions estimate. In other words, current performance levels can be maintained for the given metric at these combinations of warming and precipitation change. For example, current Average Annual SWP Deliveries could be maintained at 2°C of warming coupled with about 13 percent higher precipitation rates or 4°C warming and about 19 percent higher precipitation rates.

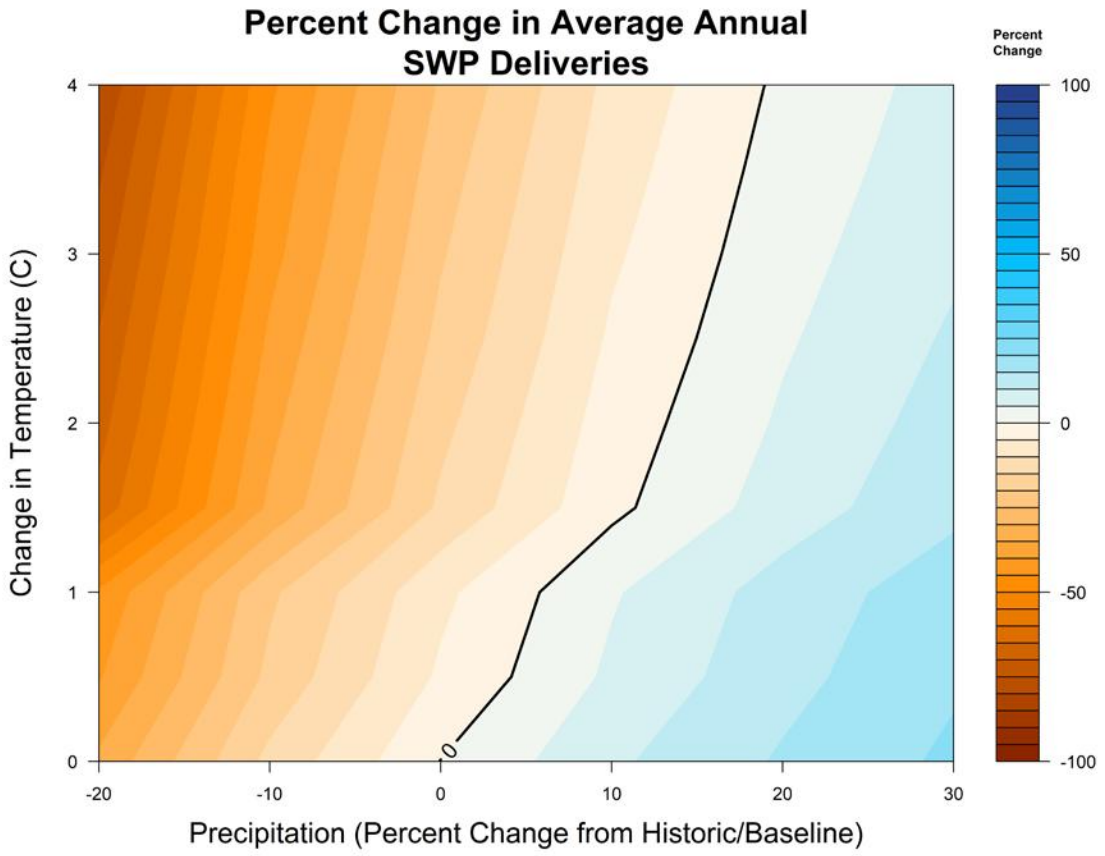

Each color band represents consistent system performance across a range of temperature and precipitation combinations. Bars that are more vertical indicate that the performance of the system is more sensitive to changes in average annual precipitation levels, while bars that are more horizontal indicate that the system performance is more sensitive to warming temperatures. Blue colors represent performance superior to current conditions and orange/red colors represent performance inferior to current conditions.

It is important to note that the response surface does not describe performance at any given time in the future. The response surface simply illustrates how the system performs, on average, over the 1,100-year hydrologic time sequence and across the range of precipitation and temperature. Also of importance is that the response surfaces presented in this report are for the current system infrastructure configuration, operations priorities, and regulations. The surfaces would change if any of these were to change in the future.

Performance Metric 1: Oroville End-of-April Storage

Historically simulated Oroville end-of-April storage levels are approximately 3.1 million acre-feet (maf). The response surface for Oroville end-of-April Storage (Figure 21) shows that this metric is moderately sensitive to changes in temperature, precipitation, and sea level. At a 2°C increase in temperature, a 10 percent increase in precipitation would be required to offset the storage losses resulting from the temperature increase. This metric is less sensitive to temperature increase than Oroville end-of-September storage (Figure 22) because it essentially measures accumulated runoff into the Oroville Reservoir during the winter rainy season. Higher temperatures are likely to result in less snowfall and faster melting rates of snow, resulting in more of the winter precipitation ending up in the reservoir and less being stored in higher watershed elevations as snow. As this additional water enters the reservoir it increases storage levels but leaves less water stored in the upper watershed to replenish the reservoir later in the season.

Figure 21 Oroville End-of-April Storage System Response Surface

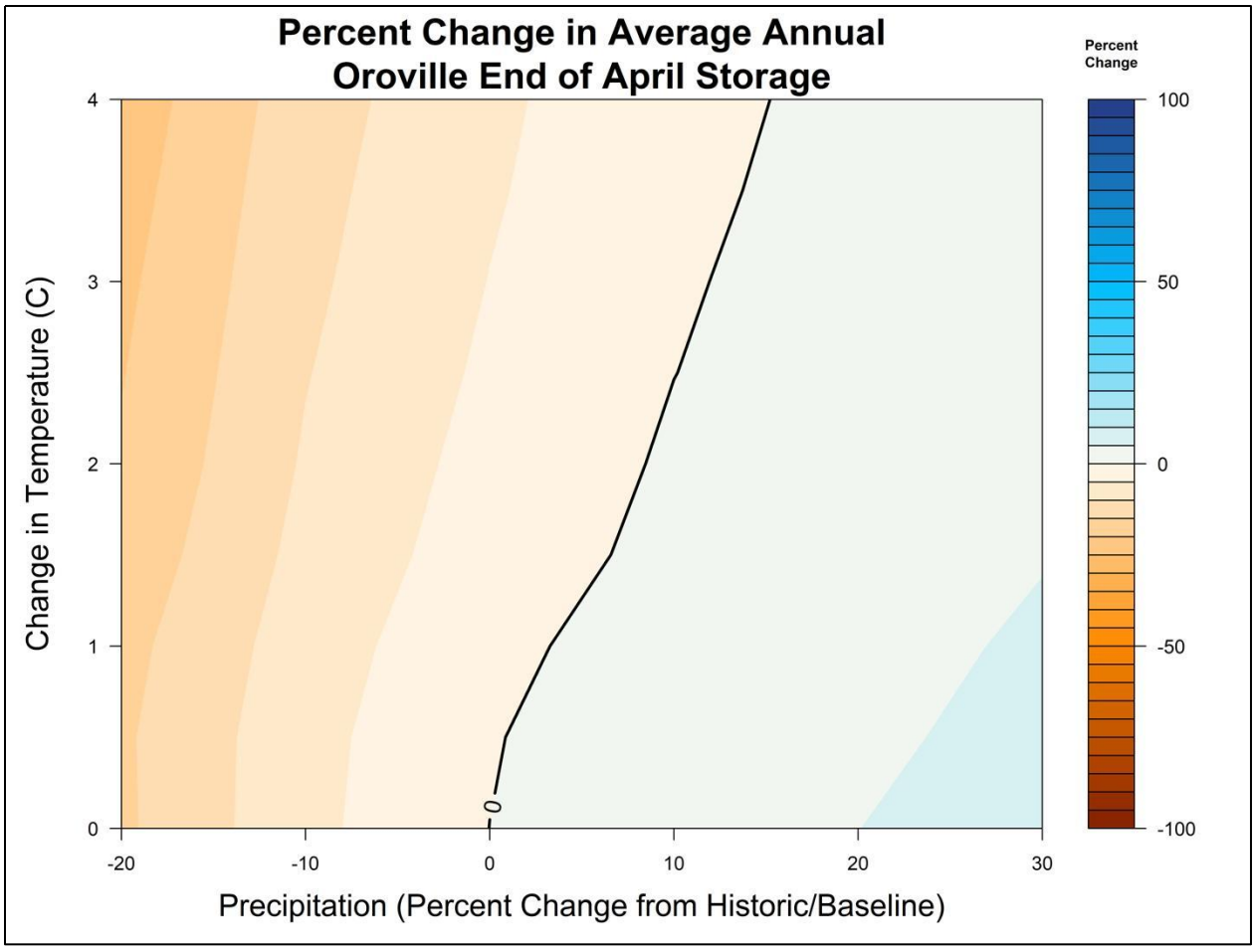

Performance Metric 2: Oroville Carryover Storage

Historically simulated end-of-September or carryover storage levels are approximately 2 maf. The response surface for Oroville carryover storage (Figure 22) shows that this metric is highly sensitive to changes in temperature, sea level, and precipitation. At temperature increases above 2°C, a greater than 20 percent increase in average annual precipitation would be needed to offset the loss in storage from increased temperatures. As described above for the end-of-April storage metric, higher temperatures result in more winter precipitation falling as rain instead of snow and the remaining snowpack melting and running off earlier. This leaves less snow in the upper watershed for later season replenishment and culminates in much lower storage levels at the end of the summer. This system response is also related to the higher sea levels assumed at higher temperature change levels. Above 1.5°C, 45 cm of sea-level rise is assumed, thus requiring more water to be released from storage (especially during the summer months) to repel seawater intrusion and meet Delta outflow and salinity requirements.

Figure 22 Oroville Carryover Storage System Response Surface

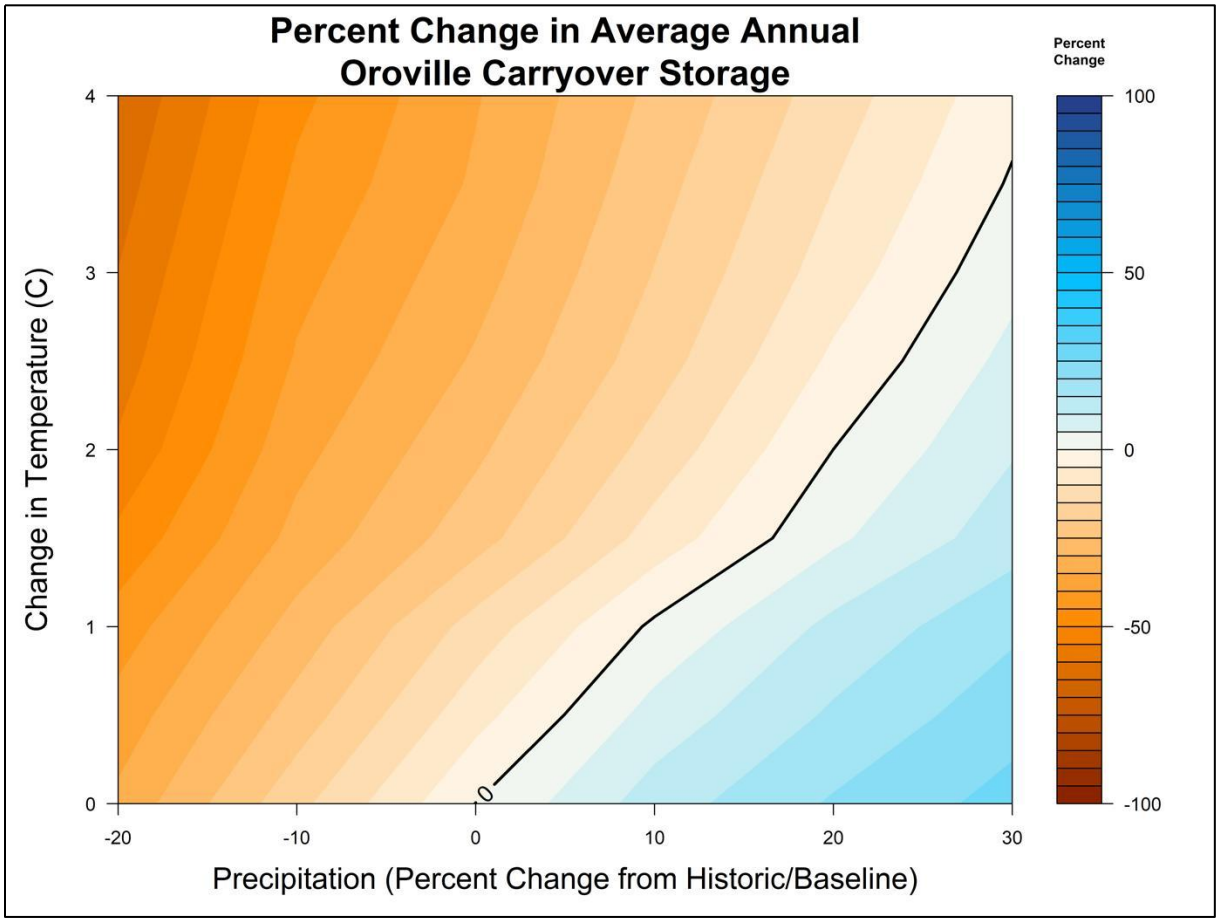

Performance Metric 3: Seasonal Net Delta Outflow

Delta conditions dictate SWP operations in summer and fall when maintenance of ecosystem conditions and water quality for Delta agricultural diverters is a critical aspect of CVS operations. While there are a

number of regulatory standards that must be met (and those standards change from month to month), net Delta outflow (NDO) provides a reasonable aggregate metric for Delta conditions.

Upstream conditions that influence NDO change throughout the year. Winter NDO is driven primarily by rainfall events and the resulting high flows in rivers flowing into the Delta. Spring NDO is driven by snowmelt and is sensitive to temperature changes that result in changes to spring snowpack conditions. Summer and fall NDO are driven primarily by regulatory and water quality requirements. Because these regulatory requirements are given high priority in real-world water operations decisions, the water distribution algorithm used by CalLite 3.0 also assigns them a very high priority. CalLite 3.0 attempts to meet all regulatory requirements first, at the expense of other system water demands. The impacts of climate changes on summer and fall NDO conditions should be understood in this context as described in more detail below.

The climate response surfaces for each seasonal NDO condition indicate that temperature changes have little effect on winter (Figure 23a) and fall NDO (Figure 24b) and relatively weak influence on spring NDO (Figure 23b). Summer NDO exhibits unique behavior, indicating that NDO would be likely to increase under future climate conditions. In the summer NDO response surface (Figure 24a) and, to a lesser extent, in the fall NDO response surface (Figure 5-9d), discontinuities in the system performance at 0.5°C, 1.0°C, and 1.5°C (0.9 °F, 1.8 °F, and 2.7 °F) are evident. These are caused by the implementation of sea-level increases (Table 5-4). The significant discontinuity between 1.0°C and 1.5°C is the result of the shift from the 15-cm sea-level rise parameterization of CalLite 3.0 to the 45-cm sea-level rise parameterization. Sea-level rise increases the hydrostatic pressure of seawater pushing into the Delta, requiring more fresh water to be released (resulting in more NDO) to repel the sea water and maintain the required salinity conditions in the Delta. In the case of summer NDO (Figure 24a), the sea-level increase results in NDO levels that exceed historical levels.

Sea-level rise is not the only influence on summer and fall NDO. The requirements for minimum NDO (as defined by California State Water Resources Control Board Decision 1641) and minimum average monthly Delta outflow at Chipps Island (as defined by California State Water Resources Control Board Decision 1485) both scale as a function of various wetness indices in the watersheds that feed the Delta. Under wetter future climate conditions, these indices would become wetter, resulting in increases in required Delta outflows, while drier future conditions result in these indices becoming drier, resulting in relaxation or reduction of Delta outflow conditions. This effect is evident in the slight left to right tilt of the performance (color) bands on the response surface.

The changes in summer and fall NDO shown in Figure 24 are largely a reflection of how the regulatory outflow requirements change, and consequently, how the operation of the system changes to meet those regulatory requirements. The shift to greater summer NDO to repel sea-level rise and maintain currently required Delta salinity and water quality conditions means that additional water is being released to achieve this higher NDO. Water releases to meet these requirements come at the expense of other important system functions, such as carryover storage, cold-water storage for aquatic resources, water deliveries, and instream flows later in the year. At the time of this study, 45 cm (18 in.) of sea-level rise was the highest parameterization available. At a temperature increase of more than 2.5°C (4.5 °F), higher sea-levels would be expected but were not modeled here. As a result, it would be expected that higher levels of NDO would be required during the summer if sea-levels rise more than 45 cm (18 in.).

Figure 23 a-b Winter and Spring Net Delta Outflow System Response Surfaces

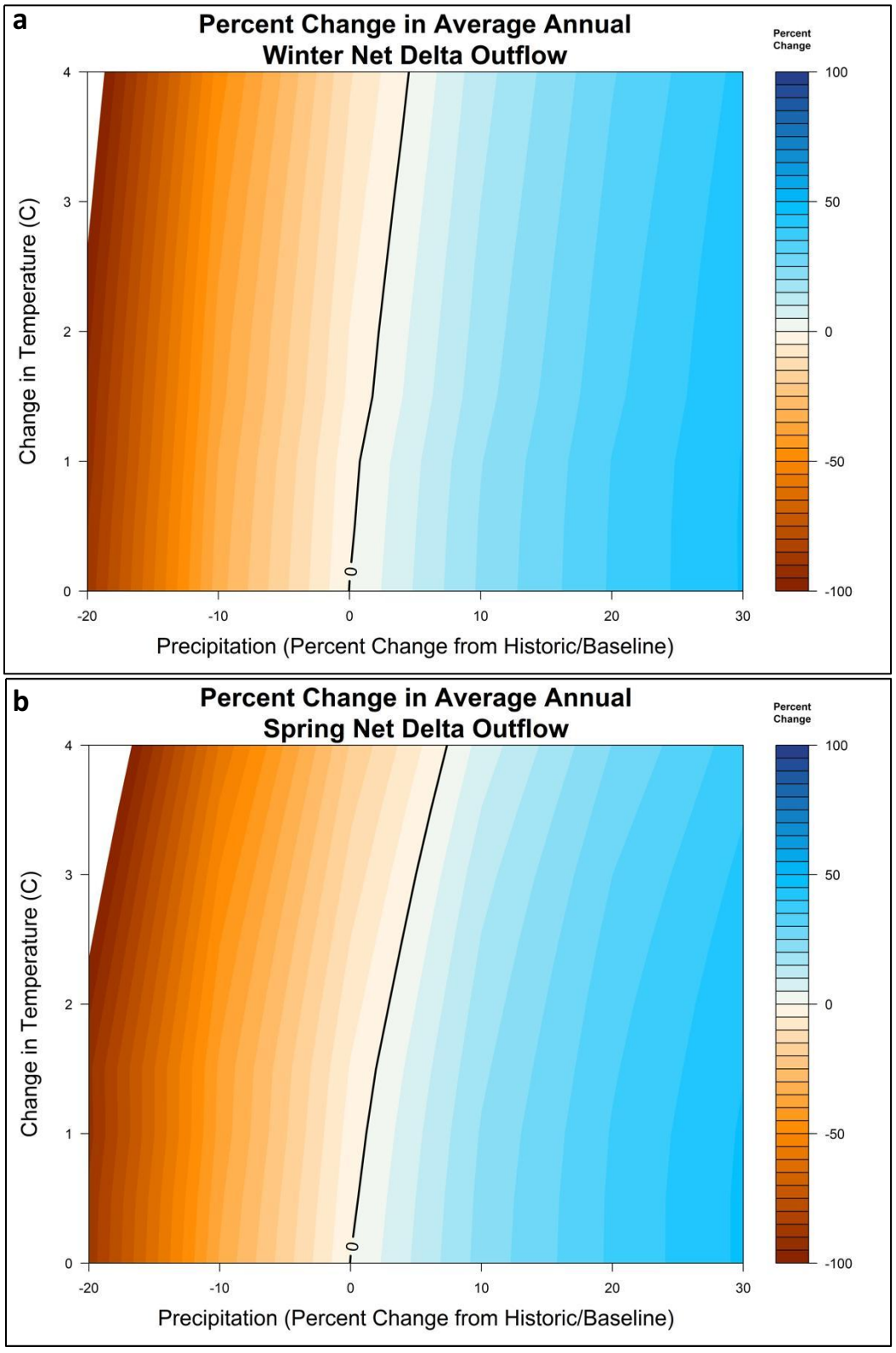

Figure 24 a-b Summer and Fall Net Delta Outflow System Response Surfaces

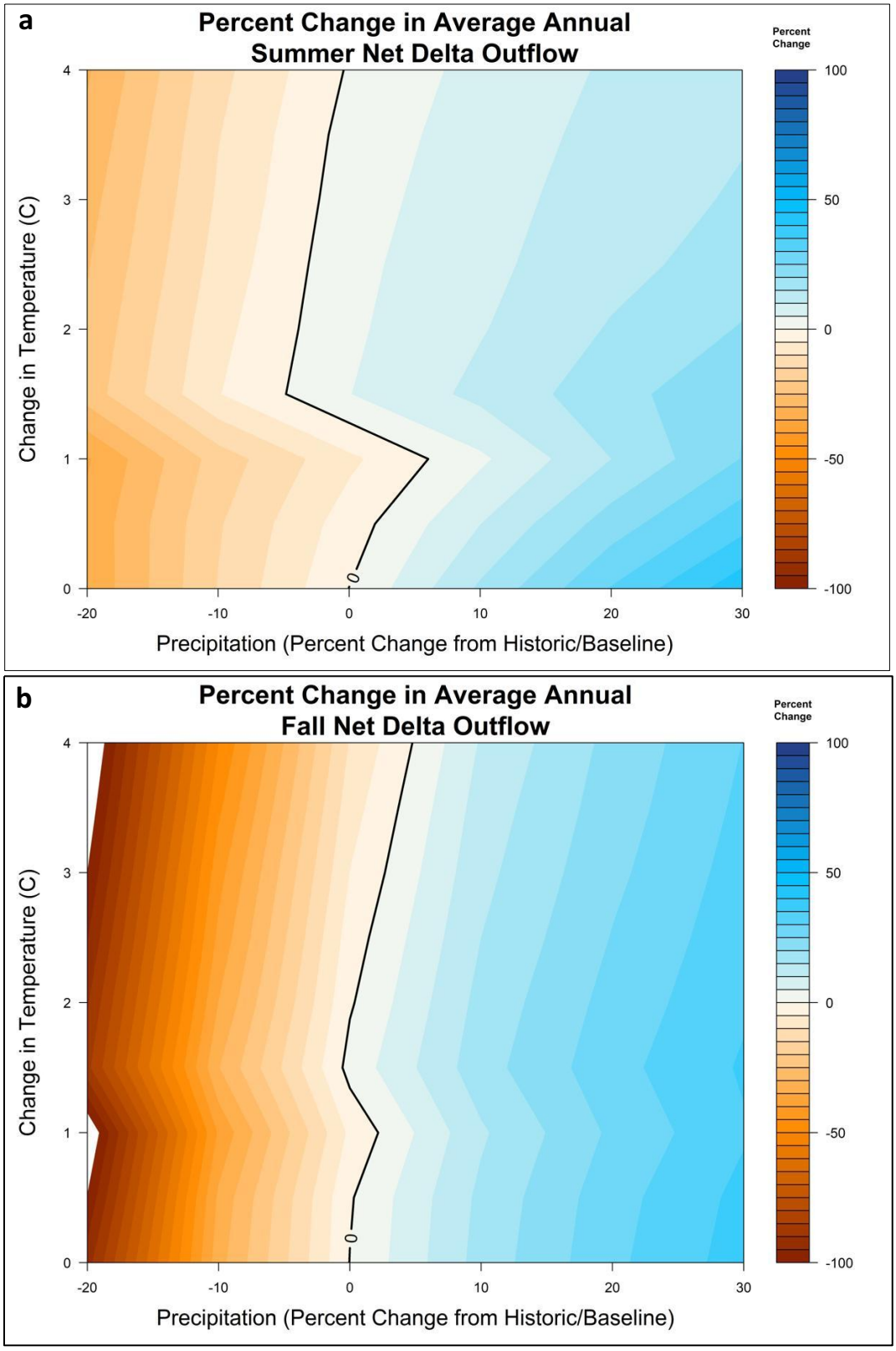

Performance Metric 4: Average Annual SWP Deliveries

The response surface for average annual SWP deliveries shows sensitivity to changes in temperature, precipitation, and sea-level rise (as would be expected). In the simulations, sea-level was implemented in three steps: (1) no sea-level rise at 0°C temperature change, (2) 15 cm of sea-level rise at 0.5 and 1.0°C temperature change, and (3) 45 cm of sea-level rise at 1.5°C and above temperature change (Table 5). These changes are evident in the response surface as inflection points where SWP deliveries decrease substantially (see Figure 25).

As noted above, each color band represents a change in system performance of 5 percent. For SWP deliveries, the performance bands become narrower to the left (less precipitation) and wider to the right (more precipitation), indicating that as precipitation decreases, SWP deliveries diminish faster than they improve as precipitation increases. Put another way, SWP deliveries are more sensitive to decreases in precipitation than increases in precipitation.

Figure 25 Average Annual SWP Deliveries System Response Surface

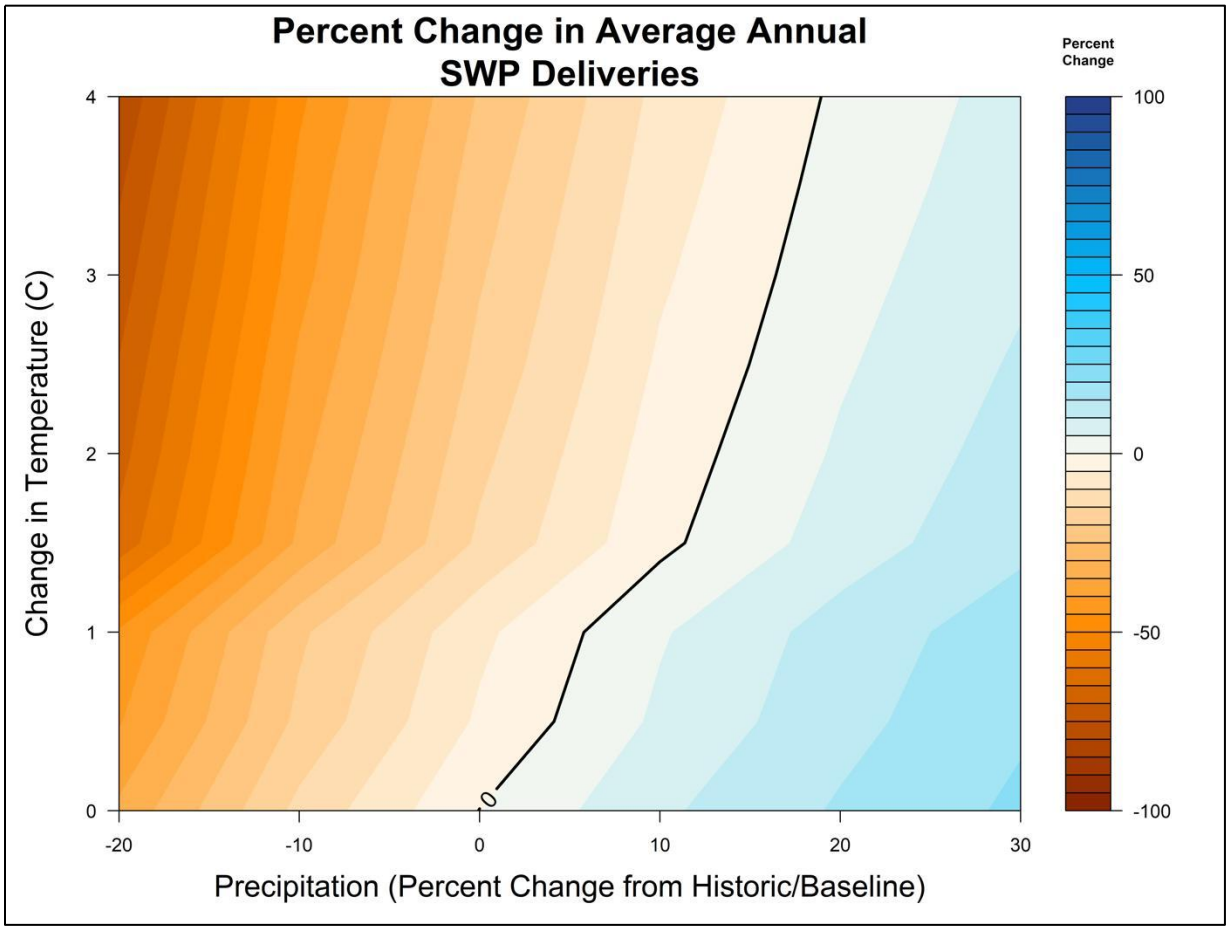

Performance Metric 5: Average Annual System Shortages

System shortages occur when there is not enough water in the system (precipitation, runoff, and storage) to meet all water demands, regulatory requirements, and health and safety required diversions. In the modeling simulations, these shortages typically result in the relaxation of Delta water quality or outflow requirements. The shortage amount is the amount of water that would be needed to meet all the requirements. Historically, these shortages have been rare but do occur periodically (i.e., 2014 and 2015).

The response surface for average annual system shortages (Figure 26) displays results in terms of absolute values of system shortages as opposed to percentage change since average annual system shortages cannot be smaller than zero and can become very large under extremely stressful conditions. Historically, average annual system shortages have been very low, averaging around 33,000 acre-feet per year, though some historical dry years have had much larger shortages and most years with normal or above normal precipitation have had no shortages at all. As the climate warms, system shortages increase by about 10,000 acre-feet per year per °C. Decreases in average annual precipitation will drive significant increases in system shortages.

Figure 26 **Average Annual System Shortages System Response Surface**

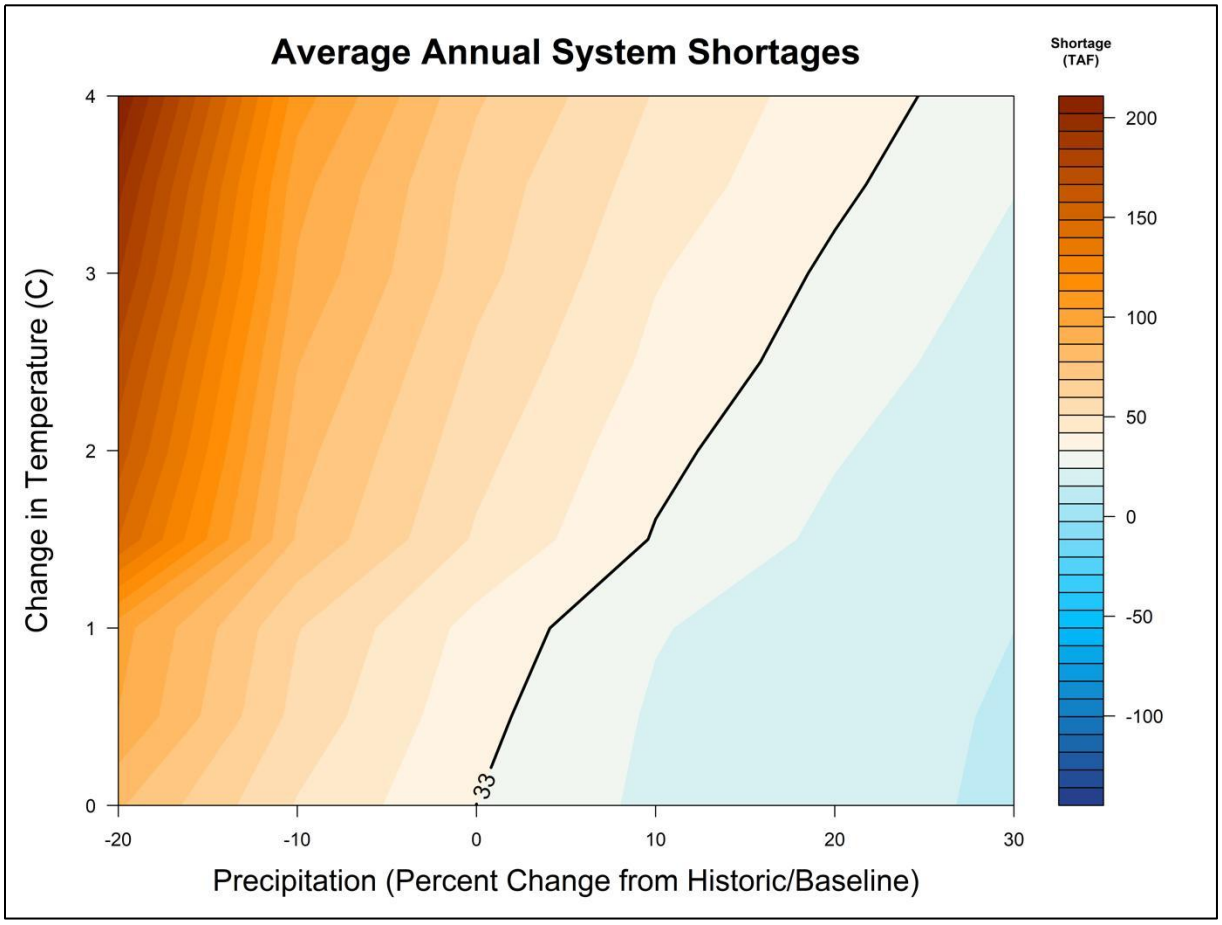

Risk

The sections above have described the SWP's exposure and sensitivity to climate change. By combining this information, probabilistic estimates of risk for each of the selected performance metrics can be developed. In this next step, the mid-century GCM-informed probability density function (pdf) of future Central Valley watershed climate conditions is superimposed on top of the response surface for each performance metric. This graphically illustrates the probabilistic range of future system performance.

The year 2050 conditional climate probability density is summarized in Table 8. Table 8 was developed by assigning a bivariate normal distribution to the shifts in mean annual temperature and precipitation of the ensemble of CMIP5 GCM output for the period of 2035–2065 relative to 1970–2000 (see Annex A: GCM Likelihood Function for the detailed steps for generating the GCM probability density function).

Table 9 Conditional Climate Probability Density of Each Climate Change Shift, 1970–2000 to 2035–2065

Temp. (C) Increase Over Historical	4	0.00000	0.00000	0.00001	0.00005	0.00007	0.00001	0.00000
	3.5	0.00000	0.00000	0.00017	0.00131	0.00145	0.00023	0.00001
	3	0.00000	0.00006	0.00244	0.01520	0.01370	0.00176	0.00003
	2.5	0.00000	0.00044	0.01540	0.07790	0.05670	0.00590	0.00009
	2	0.00001	0.00149	0.04260	0.17500	0.10300	0.00871	0.00011
	1.5	0.00001	0.00223	0.05180	0.17200	0.08230	0.00563	0.00006
	1	0.00001	0.00147	0.02760	0.07450	0.02880	0.00160	0.00001
	0.5	0.00000	0.00042	0.00646	0.01410	0.00443	0.00020	0.00000
	0	0.00000	0.00005	0.00066	0.00118	0.00030	0.00001	0.00000
		0.7	0.8	0.9	1	1.1	1.2	1.3
		Precipitation (relative to historical)						

Figure 27 through Figure 32 show the mid-century GCM-informed pdf for each of the performance metrics at 2050 conditions. As the circles in the climate probability space get lighter in color, the conditional probability density of that outcome falls. The mid-century climate probability density is roughly centered at no change in precipitation and about 2°C change in temperature, with significant uncertainties in both precipitation and temperature extending from about -20 percent to +26 percent change in precipitation and from +0.5°C to +3.5°C change in temperature. Despite this wide range of uncertainty, it is clear from this series of graphics that for all metrics except seasonal NDO, the majority of the GCM-informed pdf at 2050 overlays decreased SWP performance. At 2050, only a small portion of the GCM-informed pdf for each performance metric goes past the black line and into the blue areas of system performance (where performance would actually be better than historical). This situation is especially acute for average Oroville September storage, where only a tiny sliver of GCM-informed pdf at 2050 reaches into the blue area. For the seasonal NDO, Figure 29 and Figure 30, the GCM-informed pdf at 2050 is generally evenly distributed across higher and lower levels of NDO.

Figure 27 Average Annual Oroville End-of-April Storage System Response Surface With CMIP5 GCM pdf at 2050

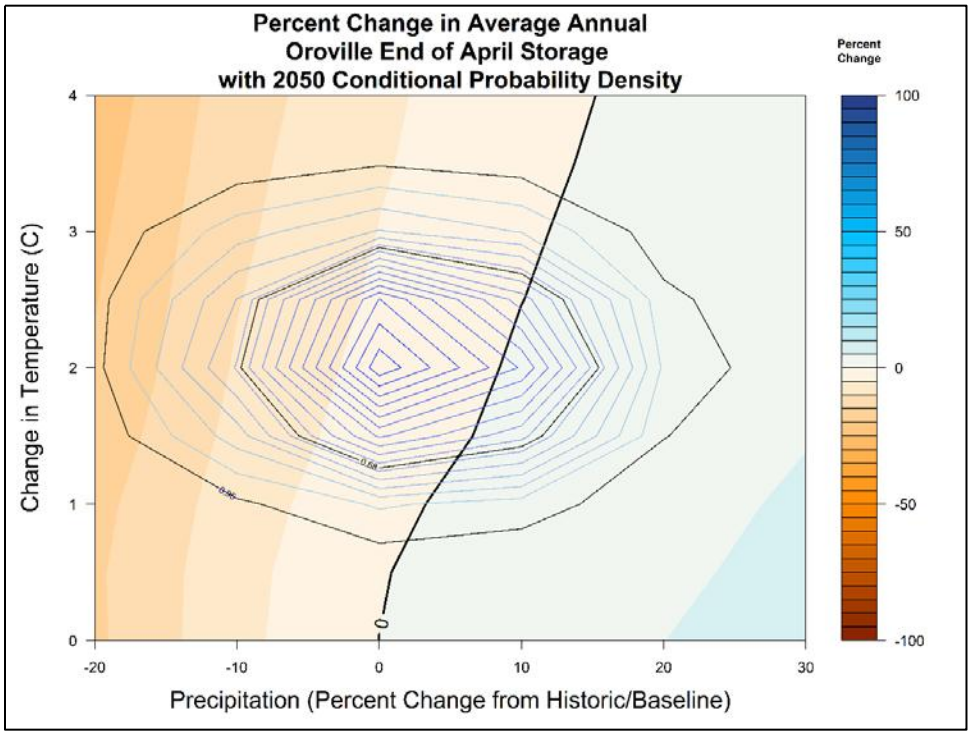

Figure 28 Average Annual Oroville Carryover Storage System Response Surface With CMIP5 GCM pdf at 2050

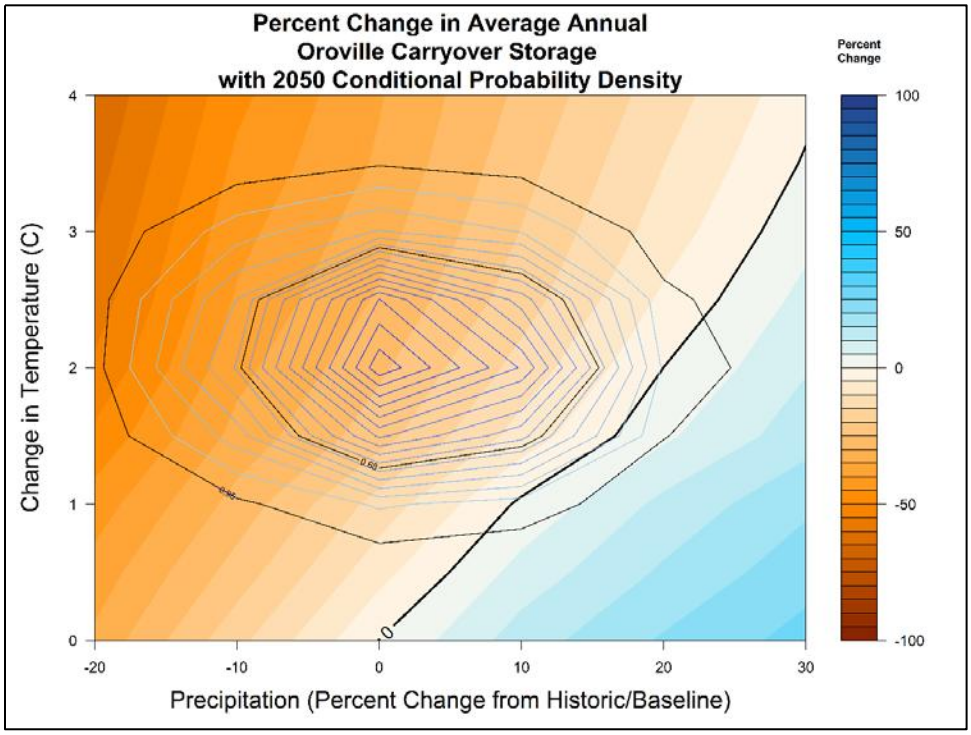

Figure 29 a-b Average Annual Winter and Spring Net Delta Outflow System Response Surface With CMIP5 GCM-Informed pdf at 2050

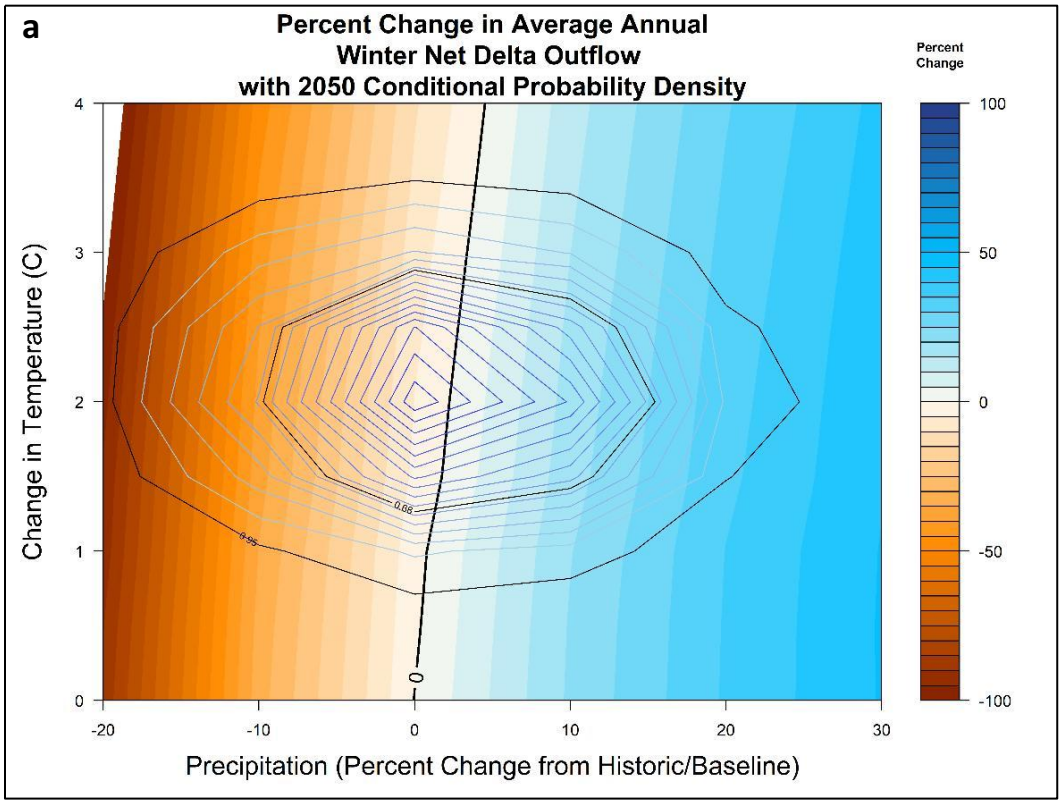

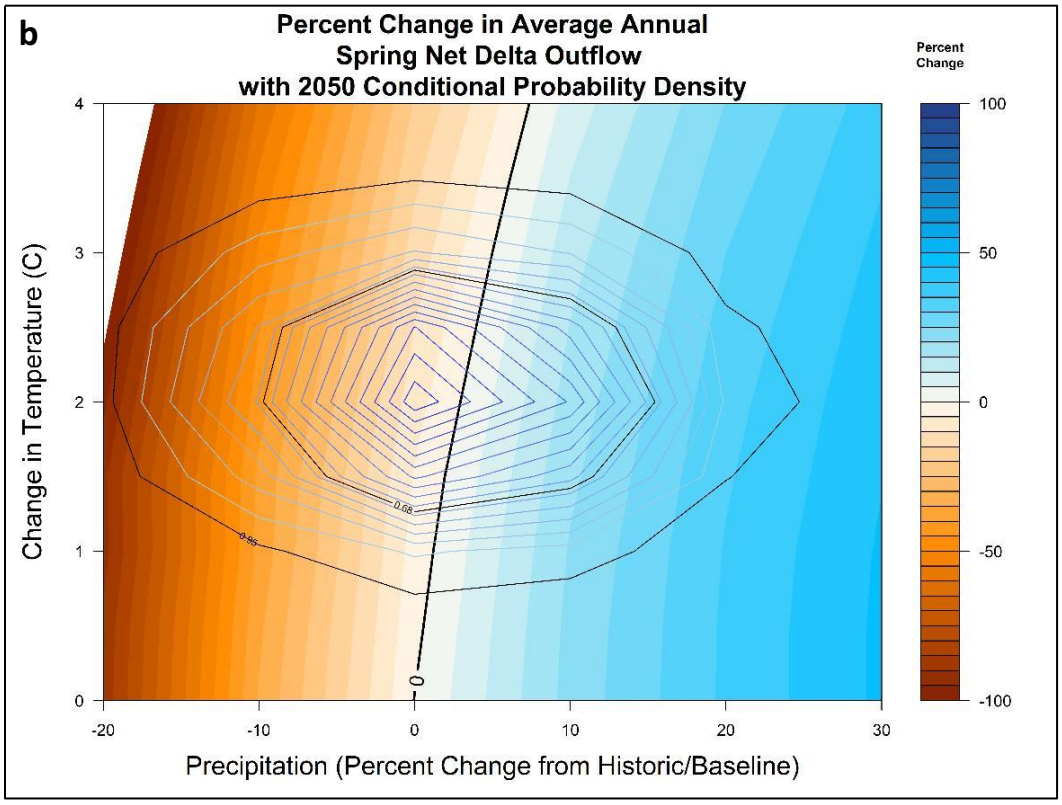

Figure 30 a-b Average Annual Summer and Fall Net Delta Outflow System Response Surfaces With CMIP5 GCM-Informed pdf at 2050

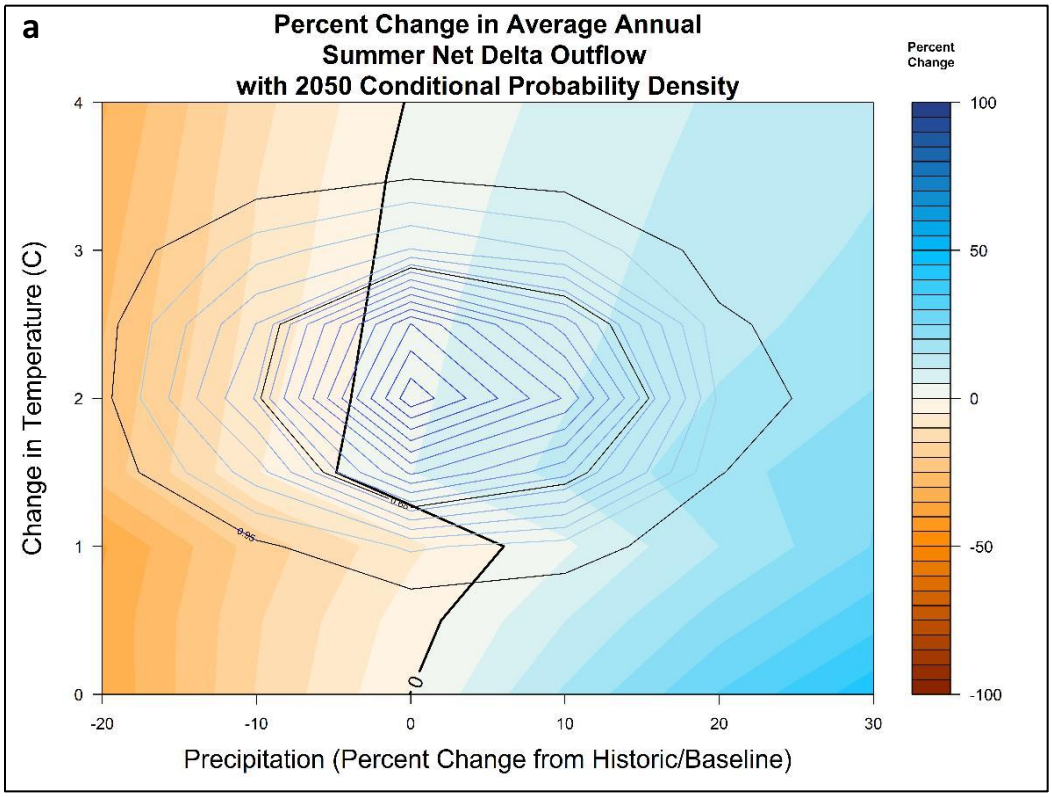

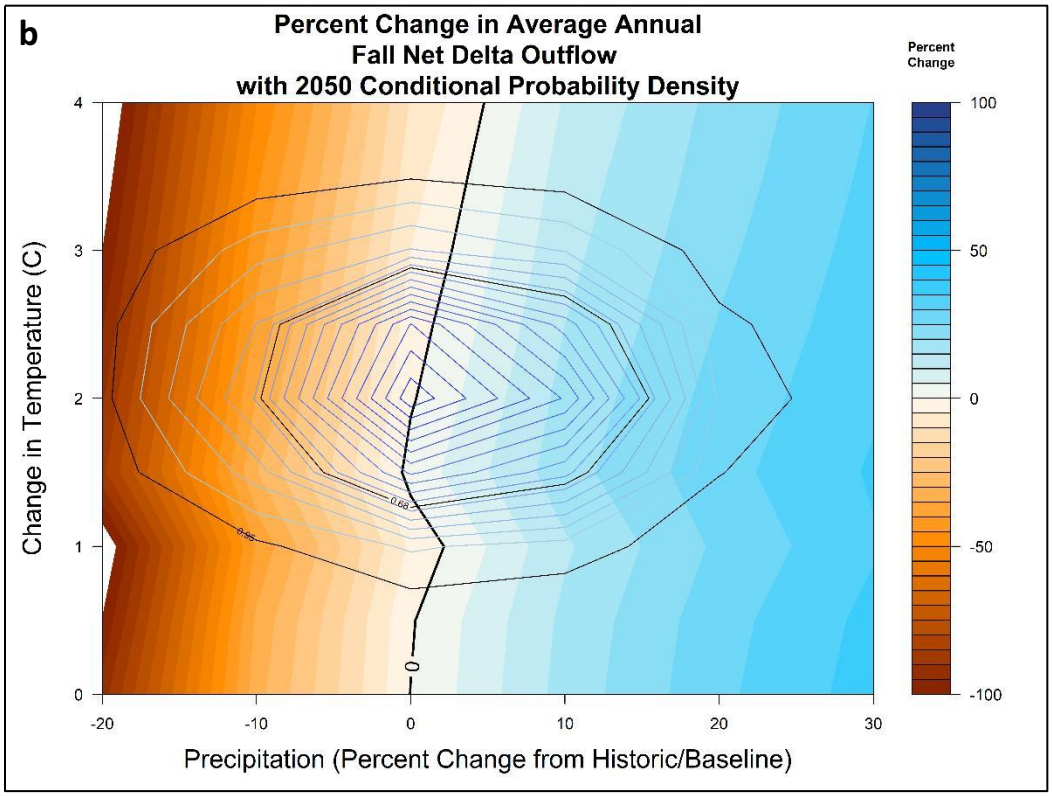

Figure 31 Average Annual SWP Deliveries Systems Response Surface With CMIP5 GCM-Informed pdf at 2050

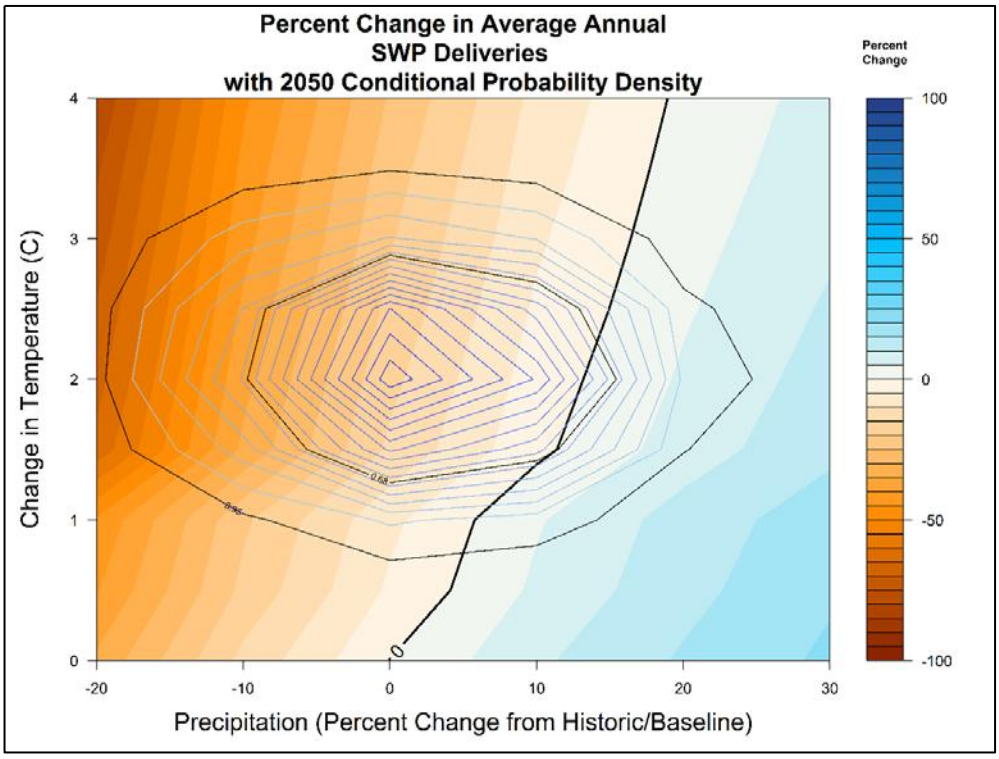

Figure 32 Average Annual System Shortage Response Surface With CMIP5 GCM-Informed pdf at 2050

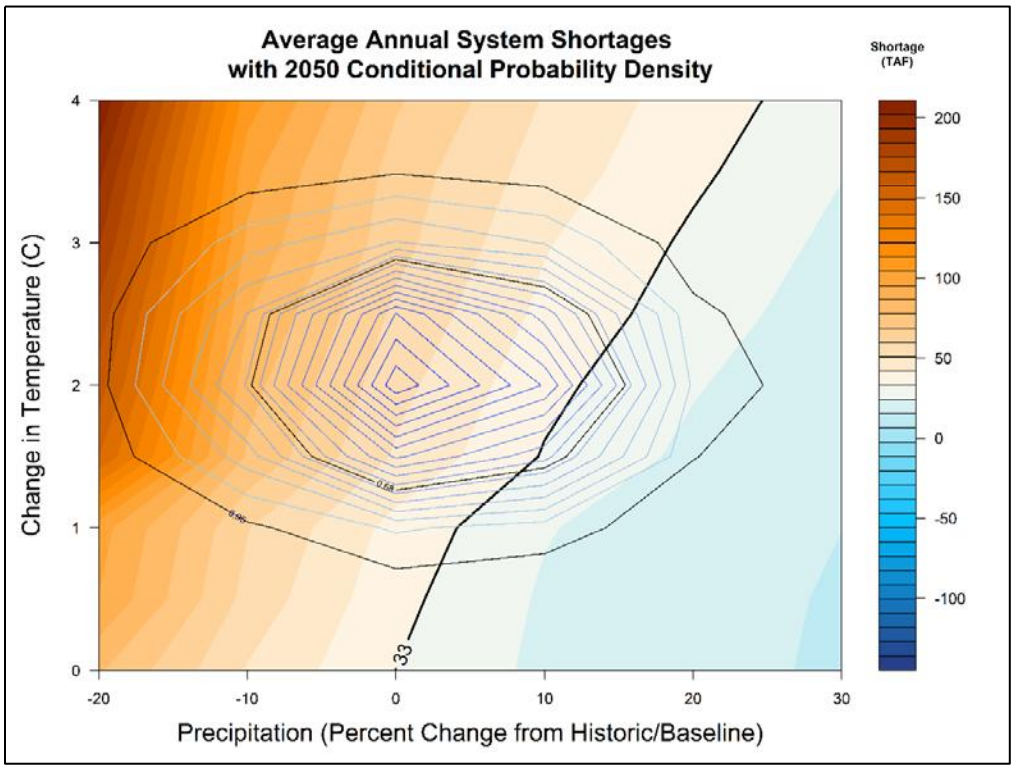

Table 10 Probability That Mid-Century Long-Term Average Performance Will Be Inferior to Current Average Performance

Performance Metric	Probability that Mid-Century Performance Will be Inferior to Current Performance
Oroville April Storage	76%
Oroville Carryover Storage	95%
Winter Net Delta Outflow	65%
Spring Net Delta Outflow	65%
Summer Net Delta Outflow	21%
Fall Net Delta Outflow	56%
SWP Deliveries	93%
System Shortages	87%

Long-term average system performance over a wide range of hydrologic conditions is summarized in Table 9 and depicted in Figures 33 through 38. While this is one important measure of changing risk, regulators, water managers, and SWP contractors are often focused on annual conditions and the risks associated with changing annual conditions, particularly conditions in the driest years. The analysis below provides information about the changing distribution of annual performance (i.e., how does system performance change across the entire distribution of hydrologic conditions from the wettest years to the driest years) for each of the performance metrics.

The cdf provides the probability that the system performance will be at or below any given value of system performance, while the pdf provides a measure of the relative likelihood of one level of performance over another or the probability that system performance will fall within a given range. The cdf and pdf take into account the yearly system performance data across all 54 different combinations of temperature and precipitation and weights them by the conditional GCM-informed probability density associated with the combination of temperature and precipitation change that produced the simulation. The cdf and pdf for each performance metric can be calculated at current conditions and at any future time period. Comparing the cdf and pdf for current conditions and mid-century conditions illustrates the shift in the distribution of annual performance.

For each performance metric, the 25th, 50th, and 75th percentile values of performance are calculated from the cdf and provided for both current conditions and 2050 conditions (notated as P25, P50, and P75 in the light blue table below cdf curves). The mode, or most likely level of system performance, is calculated from the pdf for both current conditions and 2050 conditions (light blue table below pdf curves). The 25th, 50th, and 75th percentile values help illustrate how system performance will change in dry years, median years, and wetter years, respectively, while the mode provides a measure of the expected value of system performance across the range of year types and climate uncertainty.

Vulnerability of Oroville April Storage

For Oroville end-of-April storage (Figure 33), the major shift in performance is during dry-to-median years. The 25th percentile performance falls by nearly 100,000 acre-feet and 50th percentile performance falls by 130,000 acre-feet. During wetter years (75th percentile and above), Oroville end-of-April storage is nearly identical at current and 2050 conditions. This is because Oroville is full in these years and any

additional inflow (resulting from earlier runoff of snowmelt) to the reservoir would not result in additional storage. Future conditions will almost certainly be warmer, resulting in an increasing amount of winter precipitation entering the reservoir by April and a decreasing amount remaining higher in the watershed until later in the spring and summer; however, it appears that climate change will still result in significant reductions to Oroville end-of-April storage. This is likely the result of lower carryover storage (September 30th storage) (i.e., starting out the winter with lower storage levels will result in lower end-of-winter storage conditions in all but the wettest years). Some of the reduction in April storage may also result from high temperatures leading to higher evapotranspiration rates, sublimation rates, and reduced soil moisture all contributing to reduced runoff and inflow to the reservoir.

The pdf shows that the most likely future outcome for end-of-April storage in Oroville is slightly reduced from current conditions to 2050 conditions with a loss of about 50,000 acre-feet (1.5 percent).

Figure 33 a) Cumulative Distribution and b) Probability Density for April Storage in Oroville

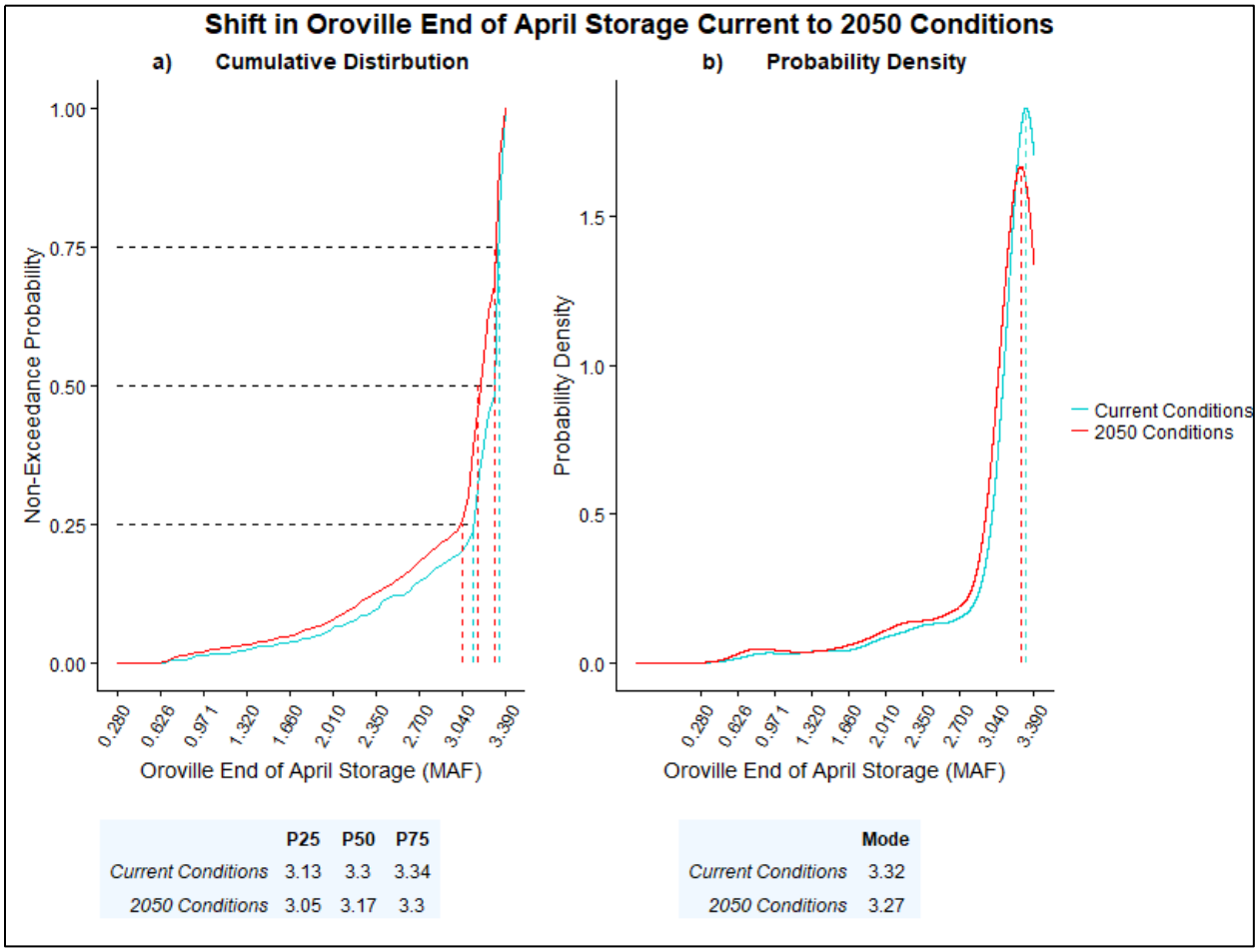

	P25	P50	P75
Current Conditions	3.13	3.3	3.34
2050 Conditions	3.05	3.17	3.3

	Mode
Current Conditions	3.32
2050 Conditions	3.27

Vulnerability of Oroville Carryover Storage

For Oroville carryover storage (Figure 34), the effect of climate change is exactly opposite from the effect on Oroville end-of-April storage. The impacts are felt more strongly toward the wetter end of the spectrum with 50th and 75th percentile 2050 performance around 350,000 and 450,000 acre-feet less than current conditions, respectively. To put it another way, even during the very wettest years (above 75th percentile) under 2050 conditions, Oroville is only slightly fuller (1.97 maf) than current levels during median years (1.88 maf). At the drier (25th percentile) end of the spectrum, where carryover storage at 2050 performance is 310,000 acre-feet less than current conditions, performance is driven by a management target simulated in the model that Oroville storage remain above at least 1 maf. Thus, when storage in Oroville nears this level, water allocations for other purposes are reduced to the extent possible to maintain this minimum target. At 2050 conditions, nearly 25 percent of years approach this minimum storage target versus approximately 12 percent of years under current conditions.

Figure 34 a-b Cumulative Distribution and Probability Density for September 1st Storage in Oroville

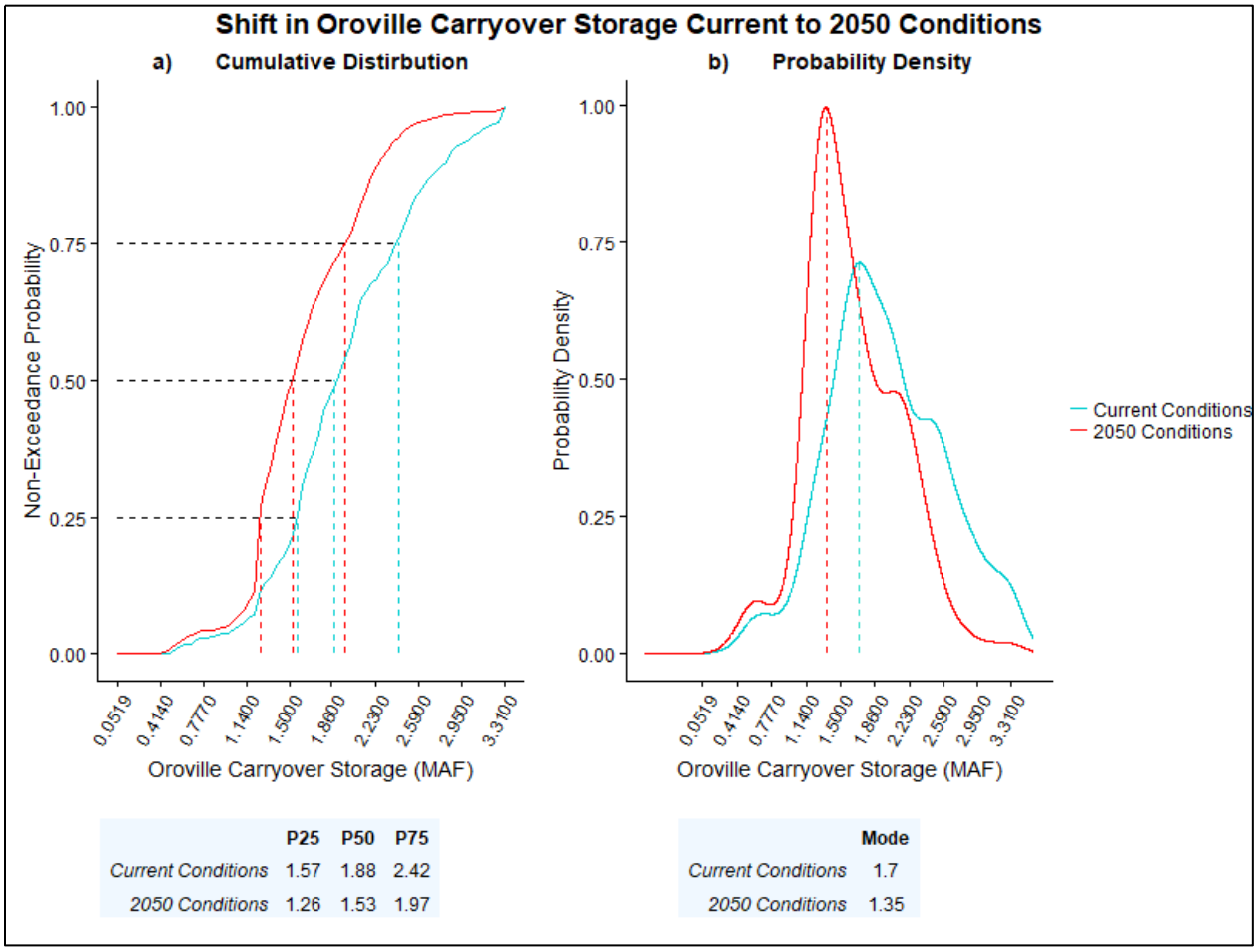

	P25	P50	P75
Current Conditions	1.57	1.88	2.42
2050 Conditions	1.26	1.53	1.97

	Mode
Current Conditions	1.7
2050 Conditions	1.35

The pdf shows very significant differences in the most likely levels of Oroville carryover storage, with the most likely future outcome falling from a current value of 1.7 maf to a 2050 storage level of 1.35 maf (a loss of 350,000 acre-feet). Despite the future climate uncertainty, the likelihood of ending September at much lower levels of storage in the future is actually higher than the likelihood under current conditions. Put another way, there is more certainty that carryover storage levels in Oroville will be around 1.39 maf by mid-century than there is certainty today that carryover storage levels in Oroville will be around 1.73 maf.

Vulnerability of Seasonal Net Delta Outflow

The annual cdf and pdf of seasonal net Delta outflow (Figure 35 and Figure 36) give a more nuanced picture than the response surfaces (Figure 29 and Figure 30) of how Delta outflows are likely to change because of climate change. The cdf and pdf show that changes in NDO are likely to be relatively small on an annual level. Slight shifts are seen in all seasons, with winter, spring, and fall NDO all increasing slightly above the 75th percentile, and summer NDO increasing slightly at all levels below the 80th percentile then decreasing above the 80th percentile. Increasing summer NDO, as noted above, is likely the result of increased outflow necessary to repel higher sea-levels and associated salinity intrusion into the Delta. The relatively small shifts in summer NDO indicated that DWR and Reclamation will continue to be able to meet Delta regulatory requirements, but there will be fewer years in which summer NDO exceeds required conditions.

Figure 35 **Winter and Spring Net Delta Outflow a) Cumulative Distribution and b) Probability Density**

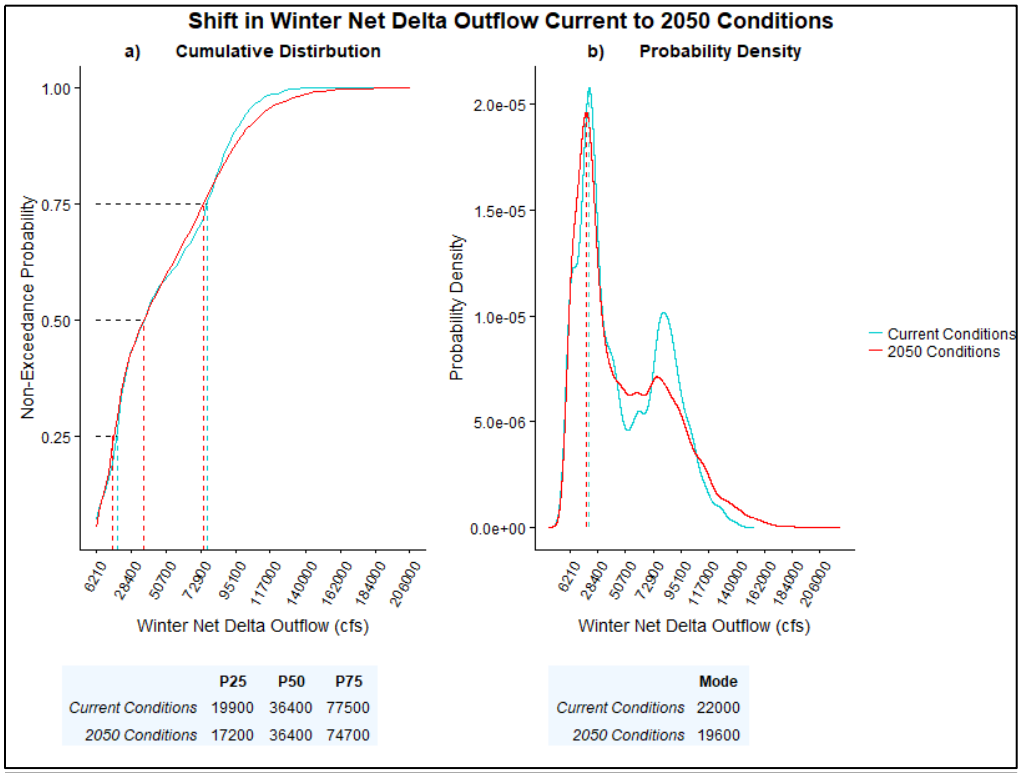

	P25	P50	P75
Current Conditions	19900	36400	77500
2050 Conditions	17200	36400	74700

	Mode
Current Conditions	22000
2050 Conditions	19600

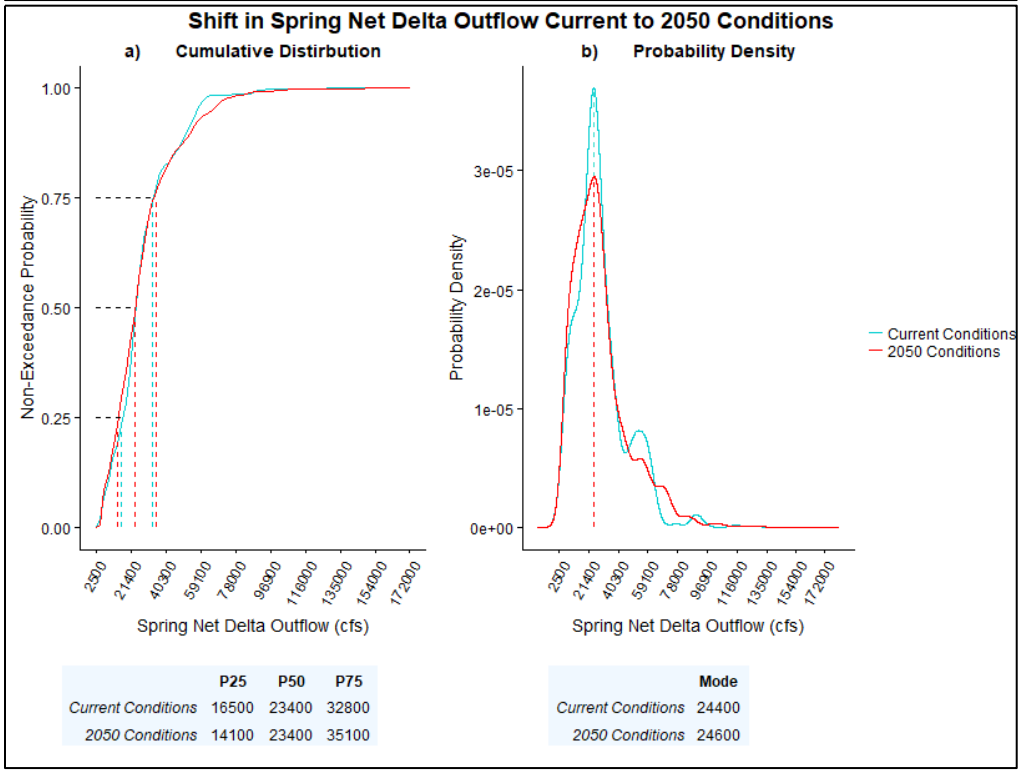

	P25	P50	P75
Current Conditions	16500	23400	32800
2050 Conditions	14100	23400	35100

	Mode
Current Conditions	24400
2050 Conditions	24600

Figure 36 a-b Summer and Fall Net Delta Outflow a) Cumulative Distribution and b) Probability Density

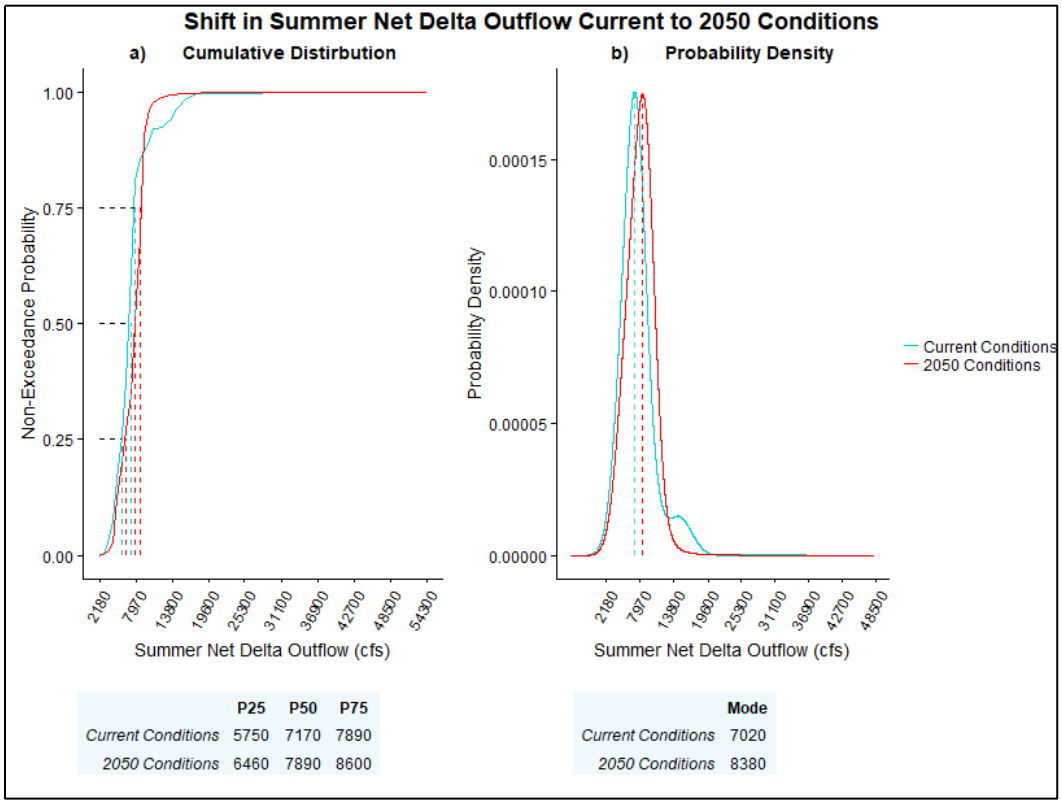

	P25	P50	P75
Current Conditions	5750	7170	7890
2050 Conditions	6460	7890	8600

	Mode
Current Conditions	7020
2050 Conditions	8380

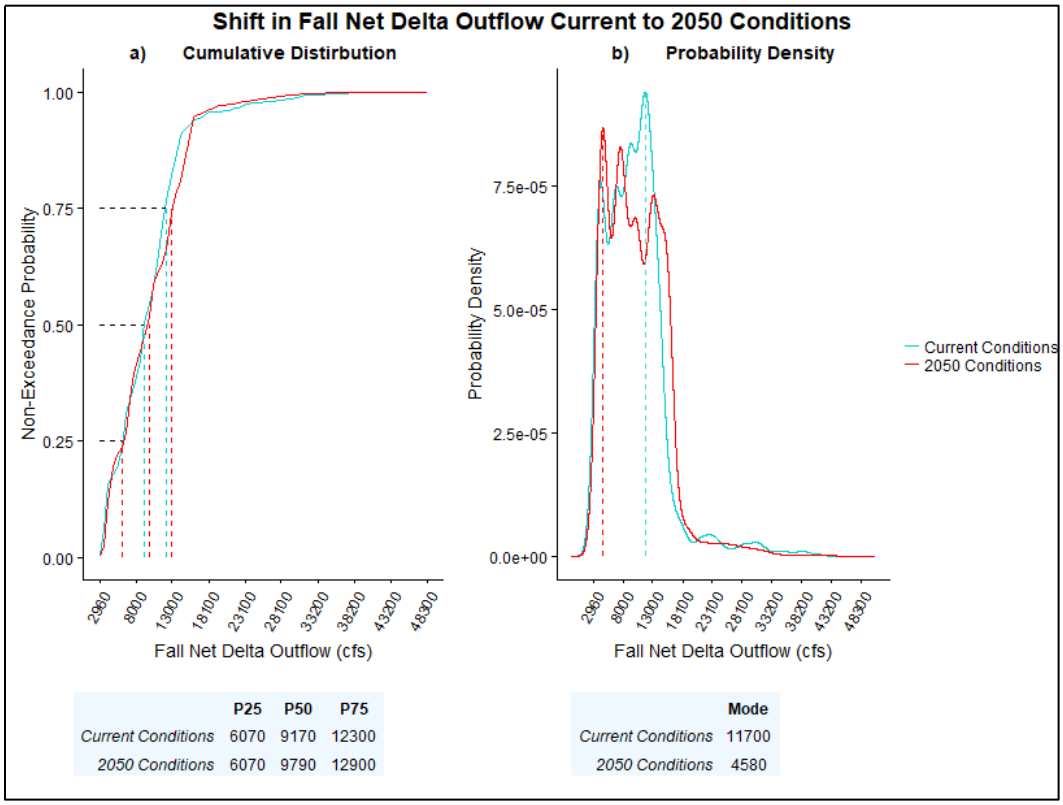

	P25	P50	P75
Current Conditions	6070	9170	12300
2050 Conditions	6070	9790	12900

	Mode
Current Conditions	11700
2050 Conditions	4580

Vulnerability of SWP Deliveries

SWP deliveries (Figure 37) show a significant loss in performance across the entire range of non-exceedance probabilities, with the most acute loss of performance coming at the drier end of the range. Twenty-fifth percentile deliveries fall by over 450,000 acre-feet between current conditions and 2050 conditions — a 17 percent reduction. Median performance falls by over 300,000 acre-feet (10 percent) and 75th percentile performance falls by 260,000 acre-feet (7 percent).

This is an important result, indicating that not only will SWP deliveries be less reliable in the future, but the largest reductions will occur in the driest years, placing additional stress on SWP water contractors.

The pdf shows that the most likely level of SWP deliveries in 2050 is about 300,000 acre-feet less than current conditions and is quite a bit less certain, with deliveries that are less than current levels being more likely and deliveries that are higher than current levels being less likely.

Figure 37 a-b Cumulative Distribution and Probability Density for Annual SWP Deliveries

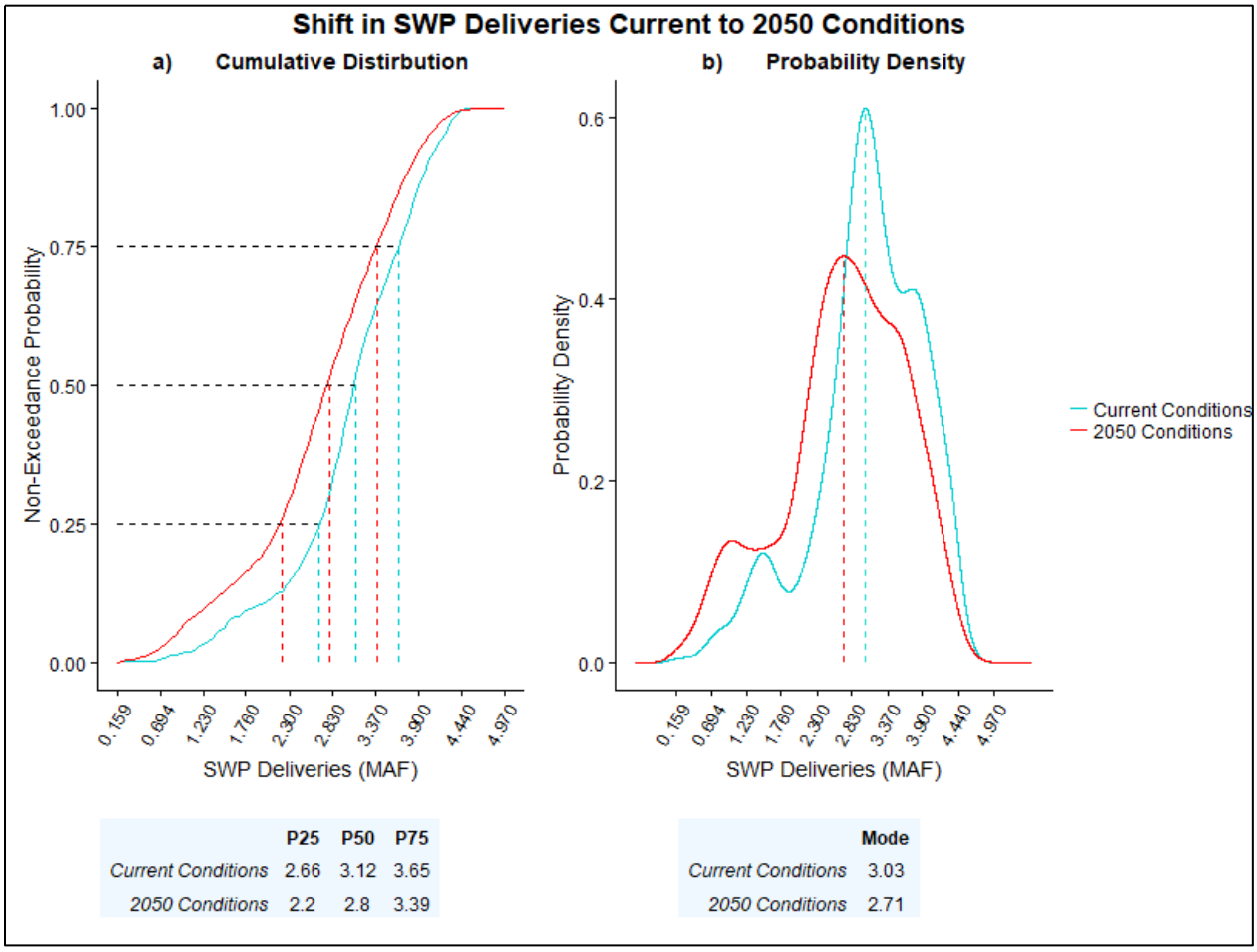

	P25	P50	P75
Current Conditions	2.66	3.12	3.65
2050 Conditions	2.2	2.8	3.39

	Mode
Current Conditions	3.03
2050 Conditions	2.71

Vulnerability of System Shortages

The cdf and pdf of system shortages (Figure 38) also provide a more nuanced picture of the likelihood of system shortages in the future than did the response surface of system shortages (Figure 32). The cdf and pdf illustrate that system shortages are rare under current conditions and will continue to be so under 2050 conditions. A small increase in magnitude and frequency of system shortages is likely to occur by 2050, but shortages of greater than a 1 maf would still be expected to occur in less than 1 percent of years.

Figure 38 a-b Cumulative Distribution and Probability Density for Annual System Shortages

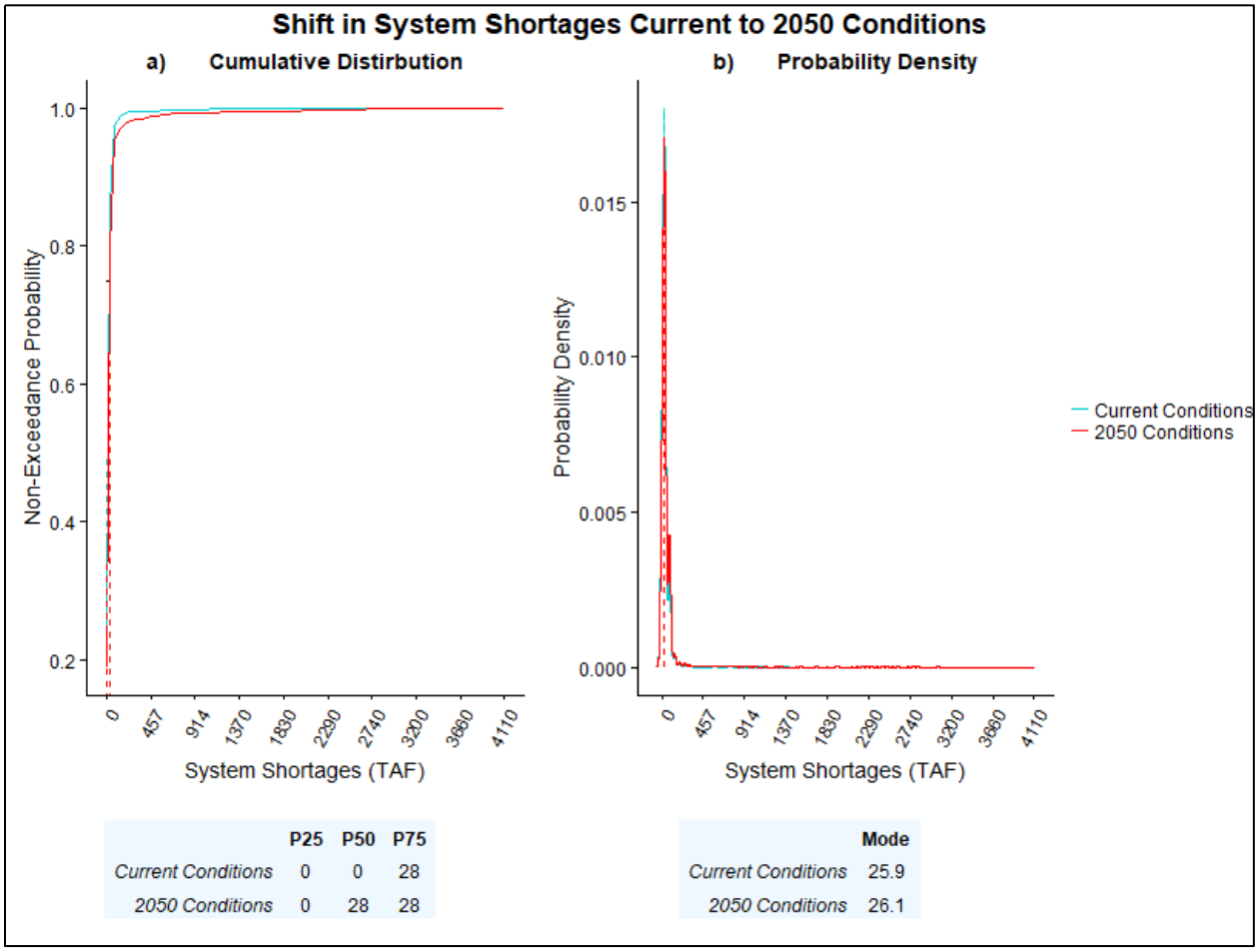

	P25	P50	P75
Current Conditions	0	0	28
2050 Conditions	0	28	28

	Mode
Current Conditions	25.9
2050 Conditions	26.1

Vulnerability

The analysis above suggests that there is a high likelihood that SWP storage and deliveries will diminish significantly in the future as the climate warms. Reductions in Oroville carryover storage mean that California will be vulnerable to future droughts, and these droughts will enter each winter with a smaller cushion if winter rains do not materialize. Lower storage levels in the future will also likely reduce the amount of hydroelectric generation from the Hyatt-Thermalito hydroelectric complex and will reduce recreational opportunities on Lake Oroville.

There is little evidence to suggest that climate change will impede DWR's ability to meet today's regulatory standards at mid-century as evidenced by the performance results for summer and fall NDO and system shortage. Overall, for the metrics analyzed in this vulnerability assessment, the SWP appears

to be relatively robust in its ability to continue to meet today's regulatory requirements at mid-century with only minimal loss of reliability. The same cannot be said about SWP deliveries. Since SWP deliveries are made only after regulatory standards are met, SWP deliveries show considerable vulnerability to changing climate. Without significant adaptation, SWP delivery reliability is likely to diminish as the climate warms.

Adaptive Capacity

It is still unclear to what extent SWP facilities and operations can be adapted to ameliorate these losses in performance. Several structural improvements, such as improved Delta conveyance; non-structural improvements, such as upper meadow restoration in the UFRW; and operational improvements, such as forecast-based operations of reservoirs, have been suggested. A full analysis of the efficacy of these types of adaptation strategies has yet to be completed; however, initial assessments of some strategies appear promising. Suggested adaptation strategies, such as those evaluated in California Water Plan 2013 and the Reclamation Sacramento-San Joaquin Basin Study, range in cost from a few million dollars to billions of dollars, with a range in social acceptability from "highly acceptable with nearly no social resistance" to "highly contentious." These issues will be evaluated further in DWR's Climate Change Adaptation Plan.

Other Considerations and Next Steps

The analysis shown here suggests that vulnerabilities to the SWP from persistent long-term changes in climate will be significant. It is very likely that the performance of the SWP will diminish over the coming decades if nothing is done to adapt to climate change; however, this new way of evaluating the system and assessing vulnerabilities provides opportunities to improve planning for climate change. Decision scaling allows planners to quantify the risks and costs associated with both the status quo and those of various adaptation strategies. Planners can then use this information to make informed decisions about which adaptation strategies will be most likely to improve conditions for various performance metrics. Unfortunately, the uncertainty associated with future climate conditions is here to stay and will likely not be substantially reduced in the near future. Therefore, our planning objectives need to acknowledge and accommodate this uncertainty. It is not feasible to plan for every possible climate outcome; however, with these quantitative assessments of future risk, quantitative adaptation objectives that address this uncertainty can be established.

An example quantitative climate adaptation objective might be: *For mid-century conditions, decision scaling analysis indicates that there is a 22 percent probability that long-term average annual SWP deliveries will fall below 2 maf. Implement adaptation strategies that reduce the probability of this condition to no more than 5 percent*.

Objectives like this acknowledge that we cannot plan for all "tail end" probabilities and there will always be a residual risk. This objective also acknowledges that climate adaptation is a moving target. Climate change will not stop at mid-century; indeed, the impacts are expected to become increasingly more severe toward the end of the century. Thus, adaptation objectives and the strategies we implement to achieve those objectives will need to be continually rolled out in the future to keep up with impacts.

Recommendations for Future Applications of Decision Scaling

The analysis suggests that SWP performance will very likely deteriorate over the coming decades if no action is taken to adapt to climate change; however, there are opportunities for improved climate change planning. Applications of decision scaling (1-9 identified below) within three major categories are recommended for future study to support adaptation planning.

Resource Management Strategies

Among 37 resource management strategies (RMS) identified in the California Water Plan Update 2013 (Water Plan), there are several which address vulnerabilities described in this report, are technically feasible, and for which DWR has the capacity as well as the authority to implement (see Annex C: Resource Management Strategy Screening). As a next step, DWR's Climate Change Program will use the decision scaling platform built for this study to conduct a systematic evaluation of a sample of proposed climate change adaptation strategies drawn from the 37 RMS including, but not limited to:

- (1) The effect of monthly reservoir inflow forecasting ability on system operation (Annex D: Adaptation Strategies — Seasonal Forecasting).
- (2) Weather modification or "cloud-seeding" (Annex E: Adaptation Strategies – Enhanced Precipitation).
- (3) Incorporation of improved multi-objective upper watershed management (Annex F: Adaptation Strategies — Upper Watershed Management)

Supplemental Analysis

The decision scaling platform built for this study establishes a probabilistic framework and set of tools that allow evaluation of a much larger range of historical and potential future changes in inter-annual variability and drought length and severity (4). The platform, through its use of the system operations model CalLite 3.0, also reduces concerns related to accuracy of modelling regulations and institutional constraints thus enabling an exploration of the sensitivity of water indexing methods to climate change and potential ways of adapting water year typing methods to support water management decisions (5) (see Annex G: Water Year Typing). Although considered to some extent in this report, further investigation into the presence and causes of trends in seasonal and elevation-dependent warming would help prioritize adaptive strategies that are evaluated in studies using this platform (6).

Groundwater

While climate change risks to the groundwater component of water supply have not been evaluated here, DWR's Flood Managed Aquifer Recharge program (California Department of Water Resources 2018) has adopted the decision scaling platform to evaluate using flood waters to recharge groundwater aquifers (7). In addition, DWR's Climate Change Program has drafted a simplified strategy for evaluating the potential benefits of increased groundwater storage north and/or south of Delta (see Annex H: Groundwater) using CalLite 3.0 (8). If simplified modeling of groundwater in CalLite 3.0 is found infeasible, shifting the operations model used in this study from CalLite 3.0 to CalSim-III, which features a dynamic link to the California Central Valley Groundwater-Surface Water Model (C2VSIM), would enable exploration of climate change risks and adaptation strategies based on modelling of the integrated surface-groundwater system (9) (see Annex I: Move From CalLite 3.0 to CalSim-III Operations Modeling).

References

AghaKouchak A, L Cheng, O Mazdiyasni, and A Farahmand. 2014, "Global warming and changes in risk of concurrent climate extremes: Insights from the 2014 California drought." Geophys. Res. Lett., 41, 8847-8852.

Anderson EA. 1976. "A point energy and mass balance model of a snow cover" *NOAA Tech. Rep.* NSW 19, Natl. Oceanic and Atmos. Admin., Silver Spring, MD., 1-150.

Bay-Delta Office. 2007. *California Central Valley Unimpaired Flow Data: 4th edition*. California Department of Water Resources, 1-53.

Brown C. and RL Wilby. 2012. "An alternate approach to assessing climate risks" EOS, Transactions, American Geophysical Union*, 92*, 401-412.

Brown CM, JR Lund, X Cai, PM Reed, EA Zagona, A Ostfeld, J Hall, GW Characklis, W. Yu, and L. Brekke. 2015. "The future of water resources systems analysis: Toward a scientific framework for sustainable water management" Water Resources Research. 51. 6110-6124.

Brown C, Y Ghile, M Laverty, and K Li. 2012. "Decision Scaling: Linking bottom-up vulnerability analysis with climate projections in the water sector." Water Resources Research. 48. W09537.

California Department of Fish and Wildlife. 2014 "CDFW moves to prevent fish loss, evacuates fish at American River and Nimbus Hatcheries" California Department of Fish and Wildlife, 16 June, hatcheries.

California Department of Water Resources. 2013. "California Water Plan 2013: Investing in Innovation and Infrastructure" Bulletin 160-13, 3 - Resource Management Strategies. 1-858.

California Department of Water Resources. 2014a. "Water year 2014 ends as 3rd driest in precipitation." California Department of Water Resources, Available at http://www.water.ca.gov/waterconditions/.

California Department of Water Resources. 2014b. Year's final snow survey comes up dry. California Department of Water Resources. 1 May. Available at: http://www.water.ca.gov/news/newsreleases/2014/050114.pdf.

California Department of Water Resources. 2015a. California Climate Science and Data for Water Resources Management. California Climate Science and Data, June 2015, 1-28.

California Department of Water Resources. 2015b. California's most significant droughts: comparing historical and recent conditions. California Department of Water Resources.

California Department of Water Resources. 2016. Precipitation Enhancement: A Resource Management Strategy of the California Water Plan. California Department of Water Resources.

California Department of Water Resources. 2017. California Climate Risk: Evaluation of Climate Risks for California Department of Water Resources. California Department of Water Resources. Available online at https://www.water.ca.gov/-/media/DWR-Website/Web-Pages/Programs/All-Programs/Climate-Change-Program/Files/California-Climate-Risk-Evaluation-of-Climate-Risks-for-California-Department-of-Water-Resources.pdf.

California Department of Water Resources. 2018. FLOOD-MAR: Using Flood Water for Managed Aquifer Recharge to Support Sustainable Water Resources. California Department of Water Resources. Available online at https://water.ca.gov/-/media/DWR-Website/Web-Pages/Programs/All-Programs/Flood-MAR/DWR_FloodMAR-White-Paper_06_2018_updated.pdf.

California Department of Water Resources and United States Bureau of Reclamation. 2011. *CalLite: Central Valley Water Management Screening Model (Version 2.0) Reference Manual*, vol. October 2011. 161 pp., California Department of Water Resources, Sacramento, California.

Cayan DR, T Das, DW Pierce, TP Barnett, M Tyree, and A Gershunov. 2010. "Future Dryness in the Southwest US and the Hydrology of the Early 21st Century Drought." Proceedings of the National Academy of Sciences of the United States of America, 107, 21271-21276.

Cayan D. et al. 2013. "Future climate: Projected average." in Assessment of Climate Change in the Southwest United States: A Report Prepared for the National Climate Assessment. A report by the Southwest Climate Alliance. edn., edited by G Garfin, A Jardine, R Merideth, M Black, and S LeRoy. pp. 101–125, Island Press, Washington, D.C., USA.

Charnes A and WW Cooper. 1961. *Management Models and Industrial Applications of Linear Programming*. Wiley. New York.

Connell-Buck CR, J Medellin-Azuara, JR Lund, and K Madani. 2011. "Adapting California's water system to warm vs. dry climates." Climate Change. 109, 133–149.

Dettinger, M. D. and M. L. Anderson (2015), Storage in California's Reservoirs and Snowpack in this Time of Drought*, San Francisco Estuary and Watershed Science, 13*, 1-5.

Dettinger, M. D. and D. R. Cayan (2014), Drought and the California Delta - A Matter of Extremes*, San Francisco Estuary and Watershed Science, 12*, 1-6.

Diffenbaugh, N. S. and M. Ashfaq (2010), Intensification of hot extremes in the United States*, Geophys. Res. Lett., 37*, L15701.

Diffenbaugh, N. S., D. L. Swain, and D. Touma (2015), Anthropogenic warming has increased drought risk in California*, Proc. Natl. Acad. Sci. U. S. A., 112*, 3931-3936.

Draper, A. J., A. Munevar, S. K. Arora, E. Reyes, N. L. Parker, F. I. Chung, and L. E. Peterson (2004), CalSim: Generalized model for reservoir system analysis*, Journal of Water Resources Planning and Management-ASCE, 130*, 480-489.

Forsythe, W. C., E. J. Rykiel Jr., R. S. Stahl, H. Wu, and R. M. Schoolfield (1995), A model comparison for daylength as a function of latitude and day of year, *Ecol. Model., 80*, 87-95.

Gleick, P. H. (1987), The Development and Testing of a Water-Balance Model for Climate Impact Assessment - Modeling the Sacramento Basin, *Water Resour. Res., 23*, 1049-1061.

Griffin, D. and K. J. Anchukaitis (2014), How unusual is the 2012-2014 California drought?, *Geophys. Res. Lett., 41*, 9017-9023.

Griffith D, Solak M, Almy R, Gibbs D. 2005. "The Santa Barbara Cloud Seeding Project in Coastal Southern California, Summary of Results and Their Implications." Journal of Weather Modification 37(April):21-27.

Griggs, G, Árvai, J, Cayan, D, DeConto, R, Fox, J, Fricker, HA, Kopp, RE, Tebaldi, C, Whiteman, EA (California Ocean Protection Council Science Advisory Team Working Group). Rising Seas in California: An Update on Sea-Level Rise Science. California Ocean Science Trust, April 2017.

Groves, D. G. and E. Bloom (2013), Robust Water-Management Strategies for the California: Water Plan Update 2013 Proof-of-Concept Analysis, *RAND Corporation, California Water Plan Update 2013*, 1-72.

Hallegatte, S., A. Shah, C. Lempert, C. Brown, and S. Gill (2012), Investment Decision Making under Deep Uncertainty: Application to Climate Change.

Hamon, W. R. (1961), Estimating potential evapotranspiration, *J. Hydr. Eng. Div. -ASCE, 87*, 107-120.

Harou, J. J., J. Medellin-Azuara, T. Zhu, S. K. Tanaka, J. R. Lund, S. Stine, M. A. Olivares, and M. W. Jenkins (2010), Economic consequences of optimized water management for a prolonged, severe drought in California, *Water Resour. Res., 46*, W05522.

Heim, R. R. (2002), A review of twentieth-century drought indices used in the United States, *Bull. Am. Meteorol. Soc., 83*, 1149-1165.

Higgins, R. W., V. B. S. Silva, W. Shi, and J. Larson (2007), Relationships between climate variability and fluctuations in daily precipitation over the United States, *J. Clim., 20*, 3561-3579.

Hirsch, R. M. (2011), A Perspective on Nonstationarity and Water Management, *J. Am. Water Resour. Assoc., 47*, 436-446.

Howitt, R. E., D. MacEwan, J. Medellin-Azuara, J. R. Lund, and D. A. Sumner (2015), Economic Analysis of the 2015 Drought for California Agriculture, *Center for Watershed Sciences, University of California – Davis, Davis, CA*, 1-16.

Howitt, R. E., J. Medellin-Azuara, D. MacEwan, J. R. Lund, and D. A. Sumner (2014), Economic Analysis of the 2014 Drought for California Agriculture, *Center for Watershed Sciences, University of California – Davis, Davis, CA*, 1-16.

IPCC (2012), *Managing the Risks of Extreme Events and Disasters to Advance Climate Change Adaptation: A Special Report of Working Groups I and II of the Intergovernmental Panel on Climate Change - Summary for Policymakers*, 1-19 pp., Cambridge University Press, Cambridge, UK, and New York, NY, USA.

IPCC (2013), *Climate Change 2013: The Physical Science Basis. Working Group I Contribution to the Fifth Assessment Report of the Intergovernmental Panel on Climate Change*, 1-1535 pp., Cambridge University Press, New York.

Islam, N. et al. (2014), Central Valley Water Management Screening Model for Water Management Alternatives, International Environmental Modelling and Software Society (iEMSs) 7th Intl. Congress on Env. Modeling and Software, June 15-19.

Joyce, B., D. Purkey, D. Yates, D. Groves, and A. Draper (2010), Integrated scenario analysis for the 2009 California water plan update, Vol. 4, *California Dept. of Water Resources, Vol. 4*, 1-112.

Killam, D., A. Bui, S. LaDochy, P. Ramirez, J. Willis, and W. C. Patzert (2014), California Getting Wetter to the North, Drier to the South: Natural Variability or Climate Change?, *Climate, 2*, 168-180.

Kopp, R. E., A. C. Kemp, K. Bittermann, B. P. Horton, J. P. Donnelly, W. R. Gehrels, C. C. Hay, J. X. Mitrovica, E. D. Morrow, and S. Rahmstorf (2016), Temperature-driven global sea-level variability in the Common Era, *Proc. Natl. Acad. Sci. U. S. A., 113*, E1441.

LaDochy, S., P. Ramirez, D. Killam, A. Bui, W. C. Patzert, and J. Willis (2011), California temperature and precipitation trends: climate variability or global warming, 91st Meeting of the American Meteorology Society 2011, Seattle, Washington, January 22-27.

Lempert, R. J., D. G. Groves, S. W. Popper, and S. C. Bankes (2006), A general, analytic method for generating robust strategies and narrative scenarios, *Management Science, 52*, 514-528.

Livneh, B., E. A. Rosenberg, C. Lin, B. Nijssen, V. Mishra, K. M. Andreadis, E. P. Maurer, and D. P. Lettenmaier (2013), A Long-Term Hydrologically Based Dataset of Land Surface Fluxes and States for the Conterminous United States: Update and Extensions, *J. Clim., 26*, 9384-9392.

Lohmann, D., R. Raschke, B. Nijssen, and D. P. Lettenmaier (1998), Regional scale hydrology: I. Formulation of the VIC-2L model coupled to a routing model, *Hydrolog. Sci. J., 43*, 131-141.

Lund, J. R., E. Hanak, W. E. Fleenor, W. A. Bennett, R. E. Howitt, J. F. Mount, and P. B. Moyle (2010), *Comparing Futures for the Sacramento-San Joaquin Delta*, Freshwater Ecology Series, vol. 3, 232 pp., Univ California Press, Berkeley; 2120 Berkeley Way, Berkeley, CA 94720 USA.

Mao, Y., B. Nijssen, and D. P. Lettenmaier (2015), Is climate change implicated in the 2013-2014 California drought? A hydrologic perspective, *Geophys. Res. Lett., 42*, 2805-2813.

Margulis, S. A., G. Cortes, M. Girotto, L. S. Huning, D. Li, and M. Durand (2016), Characterizing the extreme 2015 snowpack deficit in the Sierra Nevada (USA) and the implications for drought recovery, *Geophys. Res. Lett., 43*, 6341-6349.

McEnery, J., J. Ingram, Q. Duan, T. Adams, and L. Anderson (2005), NOAA'S Advanced Hydrologic Prediction Service – Building pathways for Better Science in Water Forecasting, *Bulletin of the American Meteorological Society, March*, 375-385.

Meko, D. M., C. A. Woodhouse, and R. Touchan (2014), Klamath/San Joaquin/Sacramento Hydroclimatic Reconstructions from Tree Rings, *Draft Final Report to California Department of Water Resources, Agreement 4600008850*.

Moriasi, D. N., J. G. Arnold, M. W. Van Liew, R. L. Bingner, R. D. Harmel, and T. L. Veith (2007), Model evaluation guidelines for systematic quantification of accuracy in watershed simulations, *Trans. ASABE, 50*, 885-900.

Mote, P. W., A. F. Hamlet, M. P. Clark, and D. P. Lettenmaier (2005), Declining mountain snowpack in western north America, *Bull. Am. Meteorol. Soc., 86*, 39-49.

Mount, J. and R. Twiss (2005), Subsidence, sea level rise, and seismicity in the Sacramento-SanJoaquin Delta, *San Francisco Estuary and Watershed Science, 3*.

Nash, J. E. (1957), The form of the instantaneous unit hydrograph, *International Association of Science and Hydrology, 3*, 114-121.

National Research Council (2012), Sea-Level Rise for the Coasts of California, Oregon, and Washington: Past, Present, and Future, 1-217.

NOAA (2014), California Drought: 2014 Service Assessment, *U. S. Department of Commerce and National Oceanic and Atmospheric Administration*, 1-72.

NOAA (2016), Mean Sea Level Trend 9414290 San Francisco, California, *NOAA Tides and Currents,* https://tidesandcurrents.noaa.gov/sltrends/sltrends_station.shtml?stnid=9414290.

Null, S. E. and J. R. Lund (2006), Re-Assembling Hetch Hetchy: Water Supply Implications of Removing O'Shaughnessy Dam, *Journal of the American Water Resources Association, 42*, 395-408.

Null, S. E., J. Medellin-Azuara, A. Escriva-Bou, M. Lent, and J. R. Lund (2014), Optimizing the dammed: Water supply losses and fish habitat gains from dam removal in California, *J. Environ. Manage., 136*, 121-131.

Null, S. E. and J. H. Viers (2013), In bad waters: Water year classification in nonstationary climates, *Water Resour. Res., 49*, 1137-1148.

Olivares, M. A., J. Haas, R. Palma-Behnke, and C. Benavides (2015), A framework to identify Pareto-efficient subdaily environmental flow constraints on hydropower reservoirs using a grid-wide power dispatch model, *Water Resour. Res., 51*, 3664-3680.

Pavia, E. G., F. Graef, and R. Fuentes-Franco (2016), Recent ENSO-PDO precipitation relationships in the Mediterranean California border region, *Atmos. Sci. Lett., 17*, 280-285.

Pierce, D. W., J. F. Kalansky, and D. R. Cayan, (Scripps Institution of Oceanography). 2018. Climate, Drought, and Sea Level Rise Scenarios for the Fourth California Climate Assessment. California's Fourth Climate Change Assessment, California Energy Commission. Publication Number: CNRA-CEC-2018-006.

Quiring, S. M. (2009), Developing Objective Operational Definitions for Monitoring Drought, *J. Appl. Meteorol. Climatol., 48*, 1217-1229.

Rheinheimer, D. E., S. E. Null, and J. R. Lund (2015), Optimizing Selective Withdrawal from Reservoirs to Manage Downstream Temperatures with Climate Warming, *J. Water Resour. Plann. Manage., 141*, 04014063.

Richter, B. D., J. V. Baumgartner, R. Wigington, and D. P. Braun (1997), How much water does a river need?, *Freshwat. Biol., 37*, 231-249.

Schneider, U., A. Becker, P. Finger, A. Meyer-Christoffer, M. Ziese, and B. Rudolf (2014), GPCC's new land surface precipitation climatology based on quality-controlled in situ data and its role in quantifying the global water cycle, *Theor. Appl. Climatol., 115*, 15-40.

Schwarz, Andrew, Patrick Ray, Sungwook Wi, Casey Brown, Minxue He, Matthew Correa. (California Department of Water Resources). 2018. Climate Change Risks Faced by the California Central Valley Water Resource System. California's Fourth Climate Change Assessment. Publication number: CCCA4-EXT-2018-001.

Seager, R., M. Hoerling, S. Schubert, H. Wang, B. Lyon, A. Kumar, J. Nakamura, and N. Henderson (2015), Causes of the 2011-14 California Drought*, *J. Clim., 28*, 6997-7024.

Steinschneider, S. and C. Brown (2013), A semiparametric multivariate, multisite weather generator with low-frequency variability for use in climate risk assessments, *Water Resour. Res., 49*, 7205-7220.

Swain, D. L. (2015), A tale of two California droughts: Lessons amidst record warmth and dryness in a region of complex physical and human geography, *Geophysical Research Letters*.

Swain, D. L., M. Tsiang, M. Haugen, D. Singh, A. Charland, B. Rajaratnam, and N. S. Diffenbaugh (2014), The Extraordinary California Drought of 2013/2014: Character, Context, and the Role of Climate Change, *Bull. Am. Meteorol. Soc., 95*, S7.

Swetnam, T. W. and J. L. Betancourt (1998), Mesoscale disturbance and ecological response to decadal climatic variability in the American Southwest, *J. Clim., 11*, 3128-3147.

SWRCB (State Water Resources Control Board). 2000. Revised Water Right Decision 1641: Implementation of Water Quality Objectives for the San Francisco Bay/Sacramento-San Joaquin Delta Estuary. California EPA. Available at: http://www.waterboards.ca.gov/waterrights/board_decisions/adopted_orders/decisions/d1600_d1649/wrd1641_1999dec29.pdf

Tanaka, S. K., C. Buck, K. Madani, J. Medellin-Azuara, J. Lund, and E. Hanak (2011), Economic Costs and Adaptations for Alternative Regulations of California's Sacramento-San Joaquin Delta, *San Francisco Estuary and Watershed Science, 9*, 28.

U.S. Department of Agriculture (2014), California drought 2014: Farm and food impacts, *United States Department of Agriculture*, impacts.aspx.

U.S. Geological Survey (2014), California Water Science Center, Available online at http://ca.water.usgs.gov/data/drought/surfacewater.html.

United States Drought Monitor (2014), California drought intensifies and U.S. drought spreads, *United States Drought Monitor, 6 Feb*, Available online at http://droughtmonitor.unl.edu/USDMNews/NewsArchive.aspx.

van Vuuren, D.P., Edmonds, J., Kainuma, M. et al. (2011), The representative concentration pathways: an overview, *Climatic Change 109: 5*. https://doi.org/10.1007/s10584-011-0148-z

Wang, H. and S. Schubert (2014), Causes of the Extreme Dry Conditions Over California during Early 2013, *Bull. Am. Meteorol. Soc., 95*, S11.

Whateley, S., S. Steinschneider, and C. Brown (2016), Selecting stochastic climate realizations to efficiently explore a wide range of climate risk to water resouces systems, *Journal of Water Resources Planning and Management, submitted*.

Wilby, R. L. and S. Dessai (2010), Robust adaptation to climate change, *Weather, 65*, 180-185.

Williams, A. P., R. Seager, J. T. Abatzoglou, B. I. Cook, J. E. Smerdon, and E. R. Cook (2015), Contribution of anthropogenic warming to California drought during 2012-2014, *Geophys. Res. Lett., 42*, 6819-6828.

Willis, A. D., J. R. Lund, E. S. Townsley, and B. Faber (2011), Climate Change and Flood Operations in the Sacramento Basin, California, *San Francisco Estuary and Watershed Science, 9*, 18.

Yoon, J., S. S. Wang, R. R. Gillies, B. Kravitz, L. Hipps, and P. J. Rasch (2015), Increasing water cycle extremes in California and in relation to ENSO cycle under global warming, *Nat. Commun*.

Zhang, Q. and S. J. Stanley (1999), Real-time water treatment process control with artificial neural networks, *Journal of Environmental Engineering-ASCE, 125*(2), 153-160, doi: 2(153).

Annex A: GCM Likelihood Function

Using Intergovernmental Panel on Climate Change (IPCC) Representative Concentration Pathways (RCP) scenarios of 4.5 and 8.5 of the CMIP5 ensemble in the region contributing flow to the CVS, the relative weights assigned to the climate states were obtained in five steps.

1) The vector of future mean annual precipitation and temperature changes was calculated from all climate projections.

2) The computed mean changes from the full ensemble of GCMs were reduced to 14 data points to account for the potential sampling biases because of the structural similarities in GCMs (Knutti et al. 2013). In so doing, all model runs were weighted equally and combined by arithmetic averaging within each model group.

3) The computed 14 data points were used to define a probability distribution function (pdf) for the domain of climate change. In this case, a bivariate Gaussian distribution was fit to the data (Whateley et al. 2014).

4) The Gaussian pdf was used to obtain the contingent normalized probability weights of the 54-plausible mean temperature and precipitation changes hereafter referred to as the GCM-informed pdf. Similar approaches have been taken by others (Borgomeo et al. 2015; Steinschneider et al. 2015; Tebaldi et al. 2005).

5) GCM-informed probabilities were applied to individual years in the development of cumulative density functions (cdf) of future system performance. Although each climate trace (i.e. "scenario") has a likelihood based upon its shift in precipitation and temperature from the historical, each year within a given climate trace was treated as equally likely. Probability notions were thus extended from "scenario" (shift in precipitation and temperature) to the realization of any given year within a scenario.

Annex B: Spatial and Temporal Climate Trends

Because precipitation and temperature changes vary both spatially and temporally, the relationships of temperature and precipitation (for both observed and projected) with several geographical and time-scale factors, including elevation, latitude, and season, should be investigated. In doing so, the levels of precipitation and temperature changes can be incorporated in more detail, which would provide a more realistic distribution of climate changes across the large study area as a function of space as well as time. This study uses daily climate data from the National Climate Data Center (NCDC) to identify these relations.

Relationship of Observed Temperature, Precipitation With Elevation, Latitude, and Season

Relationship of Temperature with Elevation and Latitude

This study uses the correlation coefficient (R) to define the relationship between seasonal temperature (fall [September–November], winter [December–February], spring [March–May], summer [June–August]) and elevations in various latitude ranges. According to Ratner (2009): R = 0 defines no linear relationship, R = -1 or +1 represents perfect negative or positive linear relationship, R = (-0.3,0) or (0,0.3) reveals weak negative or positive linear relationship, R = (-0.7,-0.3) or (0.3,0.7) indicates negative or positive moderate linear correlation, and R = (-1,-0.7) or (0.7,1) identifies negative or positive strong linear correlation. Negative R is expected since temperature tends to decrease with increases in elevation. These coefficients are summarized in Table 10.

Table 11 Relationship Between Seasonal Temperatures and Elevations

Data package	Trend	Correlation coefficient (R)
Missing data less than 10 percent	Fall temperature and elevation	-0.35
	Winter temperature and elevation	-0.32
	Spring temperature and elevation	-0.15
	Summer temperature and elevation	-0.05
Missing data less than 20 percent	Fall temperature and elevation	-0.28
	Winter temperature and elevation	-0.27
	Spring temperature and elevation	-0.07
	Summer temperature and elevation	0

According to Table 11, it was found that correlation coefficients (R) for relationships between temperatures and elevations in each latitude range are very weak, demonstrating that temperature does not have a clear linear relationship with elevations and latitudes. Most of the correlation coefficients are negative, showing negative correlations of temperatures with elevations and latitudes. The scatter plots used to derive these R coefficients are provided in the "Supplemental Figures" section below.

Table 12 Relationship Between Seasonal Temperatures and Elevations, Latitudes

Data package	Trend	Latitude Range	Correlation Coefficient (R)	Number of Samples
Missing data less than 10 percent	Fall temperature and elevation	(32 34]	-0.48	17
		(34 36]	-0.3	27
		(36 38]	-0.36	39
		(38 40]	-0.16	29
		(40 42]	-0.39	16
	Winter temperature and elevation	(32 34]	-0.53	17
		(34 36]	-0.46	27
		(36 38]	-0.3	39
		(38 40]	-0.15	29
		(40 42]	-0.25	16
	Spring temperature and elevation	(32 34]	0	17
		(34 36]	-0.07	27
		(36 38]	-0.14	39
		(38 40]	-0.01	29
		(40 42]	-0.29	16
	Summer temperature and elevation	(32 34]	0.16	17
		(34 36]	0.19	27
		(36 38]	-0.19	39
		(38 40]	0.04	29
		(40 42]	-0.08	16
Missing data less than 20 percent	Fall temperature and elevation	(32 34]	-0.29	30
		(34 36]	-0.23	39
		(36 38]	-0.25	52
		(38 40]	-0.2	45
		(40 42]	-0.24	25
	Winter temperature and elevation	(32 34]	-0.31	30
		(34 36]	-0.3	39
		(36 38]	-0.3	52
		(38 40]	-0.14	45
		(40 42]	-0.25	25
	Spring temperature and elevation	(32 34]	0.05	30
		(34 36]	0.02	39
		(36 38]	-0.01	52
		(38 40]	0.04	45
		(40 42]	-0.02	25
	Summer temperature and elevation	(32 34]	0.05	30
		(34 36]	0.11	39
		(36 38]	-0.04	52
		(38 40]	0.07	45
		(40 42]	0.14	25

Relationship Between Temperature and Season

This study divides temperature data into four seasons: winter (December, January, and February), spring (March, April, and May), summer (June, July, and August), and fall (September, October, and November) as well as an annual dataset that includes all data. Thiel Sen slopes are computed for each station in these five datasets, boxplots of which are shown in Figure 39. The daily temperature data used to conduct this analysis went through quality checks for two missing rates; Figure 39 results from 94 stations for which missing data rate is less than 10 percent, while Figure 40 shows the results of trend analysis from 145 stations for which missing rate is less than 20 percent. In Figure 39 and Figure 40, red numbers represent medians of seasonal/temperature trend; black numbers are means of seasonal temperature trend. According to these box plots, it was found that the warming trend is stronger in spring and summer than in winter and fall. The calculation processes are shown as follows:

Step 1: From temperature data of each station during 1950–2015, Sen's slope is computed for 4 datasets of spring, summer, fall, and winter. Then, boxplots are calculated as above (Figure 39 and Figure 40).

Step 2: From these boxplots, means of temperature trend slope (black numbers in boxplots) are attained (shown in the last column of Table 12 below).

Step 3: Finally, temperature increases reflecting the spring, summer, fall and winter trends are calculated for 8 increasing temperature shifts (temperature increase of 0.5; 1; 1.5; 2; 2.5; 3; 3.5; 4°C).

Table 13 Means of Seasonal Warming Pattern (Average Increase Per Decade)

SEASON	Mean T1 (10%) Black (Deg.C/decade)	Mean T2 (20%) Black (Deg.C/decade)	AVG increase per decade
Winter	0.112	0.12	0.116
Spring	0.261	0.269	0.265
Summer	0.189	0.194	0.1915
Fall	0.038	0.049	0.0435

The average annual temperature increase per decade across all stations was found to be 0.154°C per decade. Thus, as an example, winter months will have an increase of 0.38°C when the total annual temperature increase is 0.5°C, (0.5°C * 0.116°C per decade [winter trend] / 0.154°C per decade [annual trend] = 0.38°C). Likewise, seasonal warming is applied to other seasons (shown in Table 13 below) and incorporated into new sequences of temperature. All seasonal warming patterns are shown in Figure 41.

Table 14 Seasonal Warming Pattern Application for Eight Increase Levels

JAN	FEB	MAR	APR	MAY	JUN	JUL	AUG	SEP	OCT	NOV	DEC	T increase	
0.116	0.116	0.265	0.265	0.265	0.1915	0.1915	0.1915	0.0435	0.0435	0.0435	0.116	**0.154**	
0.38	0.38	0.86	0.86	0.86	0.62	0.62	0.62	0.14	0.14	0.14	0.38	0.5	Temperature increase of 0.5 degrees Celcius
0.75	0.75	1.72	1.72	1.72	1.24	1.24	1.24	0.28	0.28	0.28	0.75	1	Temperature increase of 1 degrees Celcius
1.13	1.13	2.58	2.58	2.58	1.87	1.87	1.87	0.42	0.42	0.42	1.13	1.5	Temperature increase of 1.5 degrees Celcius
1.51	1.51	3.44	3.44	3.44	2.49	2.49	2.49	0.56	0.56	0.56	1.51	2	Temperature increase of 2 degrees Celcius
1.88	1.88	4.30	4.30	4.30	3.11	3.11	3.11	0.71	0.71	0.71	1.88	2.5	Temperature increase of 2.5 degrees Celcius
2.26	2.26	5.16	5.16	5.16	3.73	3.73	3.73	0.85	0.85	0.85	2.26	3	Temperature increase of 3 degrees Celcius
2.64	2.64	6.02	6.02	6.02	4.35	4.35	4.35	0.99	0.99	0.99	2.64	3.5	Temperature increase of 3.5 degrees Celcius
3.01	3.01	6.88	6.88	6.88	4.97	4.97	4.97	1.13	1.13	1.13	3.01	4	Temperature increase of 4 degrees Celcius
Winter	Spring	Summer	Fall										
0.116	0.265	0.1915	0.0435										
Dec-Feb	Mar-May	Jun-Aug	Sep-Nov										

Figure 39 Trend Slope of Temperature With Less Than 10 Percent Missing Data in 94 Stations

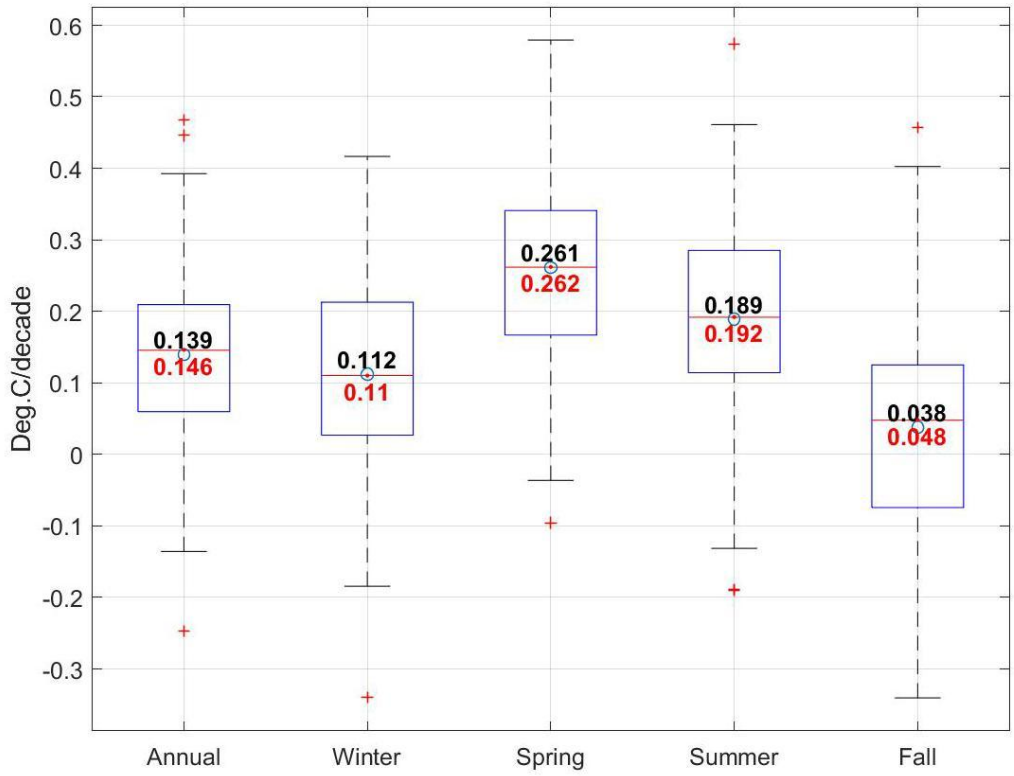

Figure 40 Trend Slope of Temperature With Less Than 20 Percent Missing Data in 145 Stations

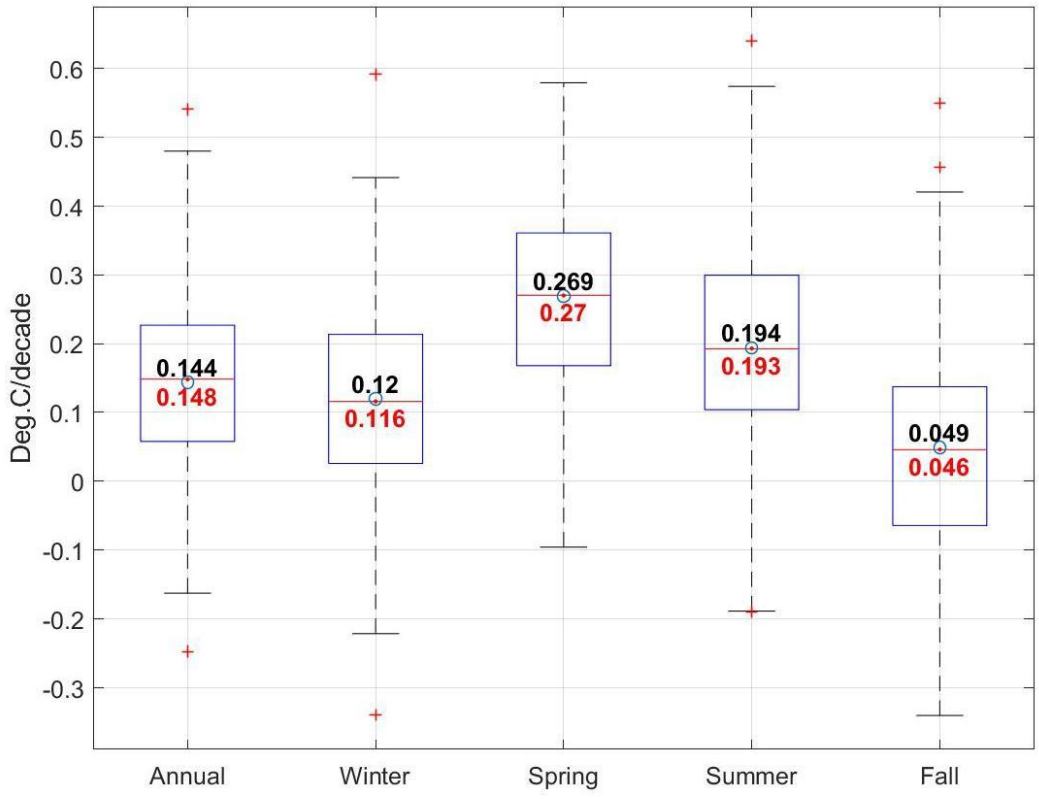

Figure 41 Seasonal Warming Patterns for Climate Projections

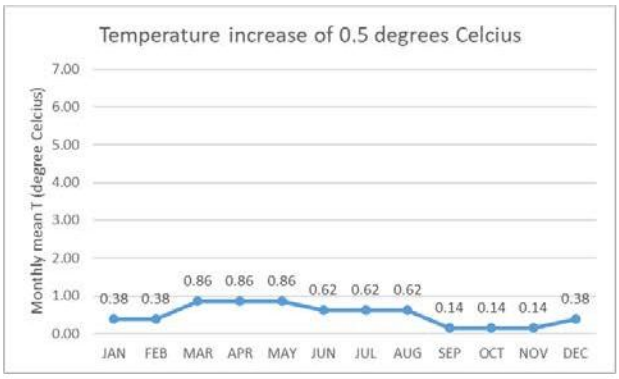

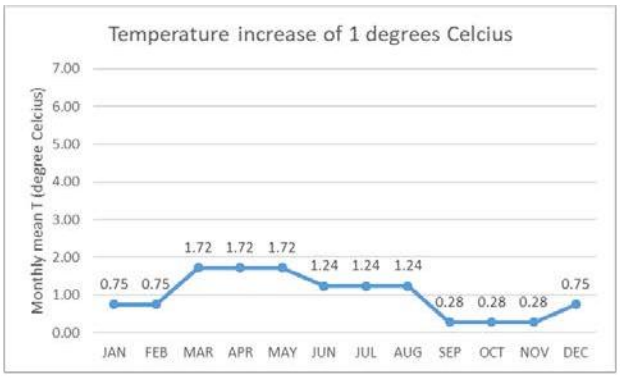

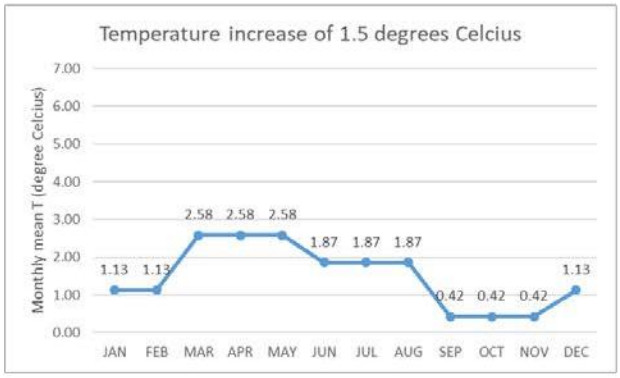

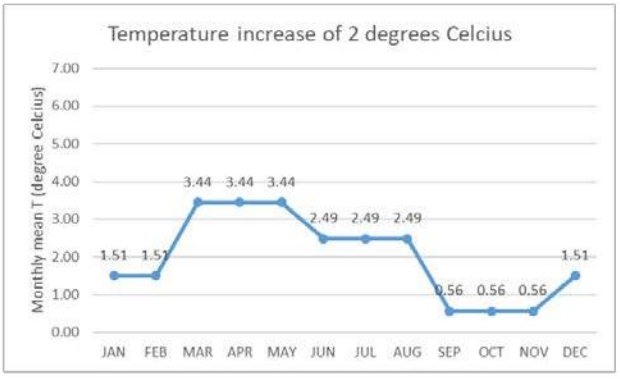

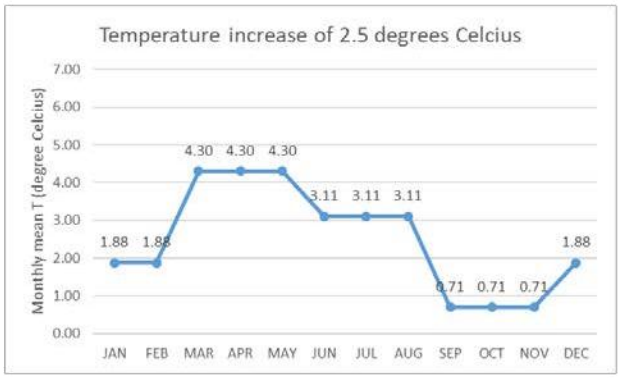

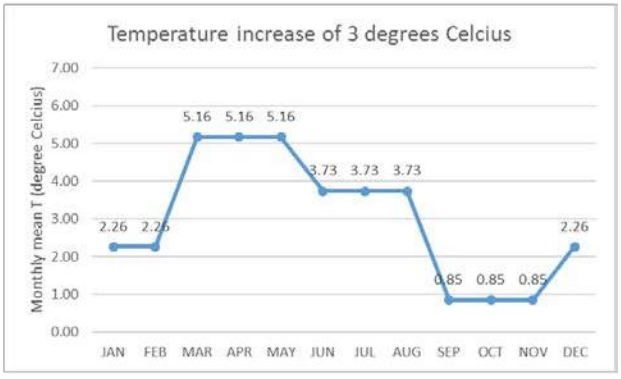

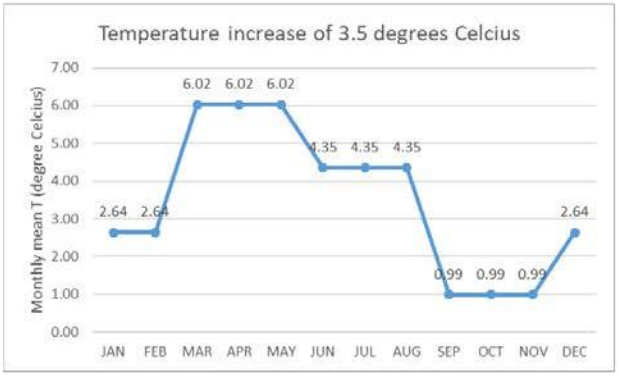

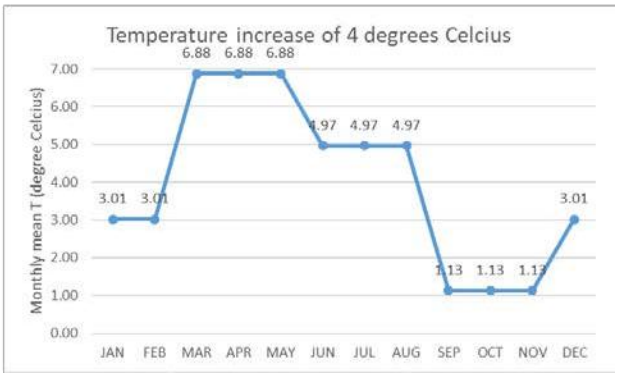

Relationship Between Precipitation and Elevation

In Figure 42, hollow triangles represent precipitation changes in high-elevation areas, while solid dots refer to low-elevation regions. High-elevation locations are considered as higher than 2000 m, and low-elevation locations lower than 2000 m. Ratios of differences between hollow triangles and solid dots vary from month to month which suggests that there is no trend of precipitation changes with elevation.

Figure 42 Differential Rate of Change in Precipitation Between Early Mid-20th Century (1920–1960) and Recent Past (1980–2011)

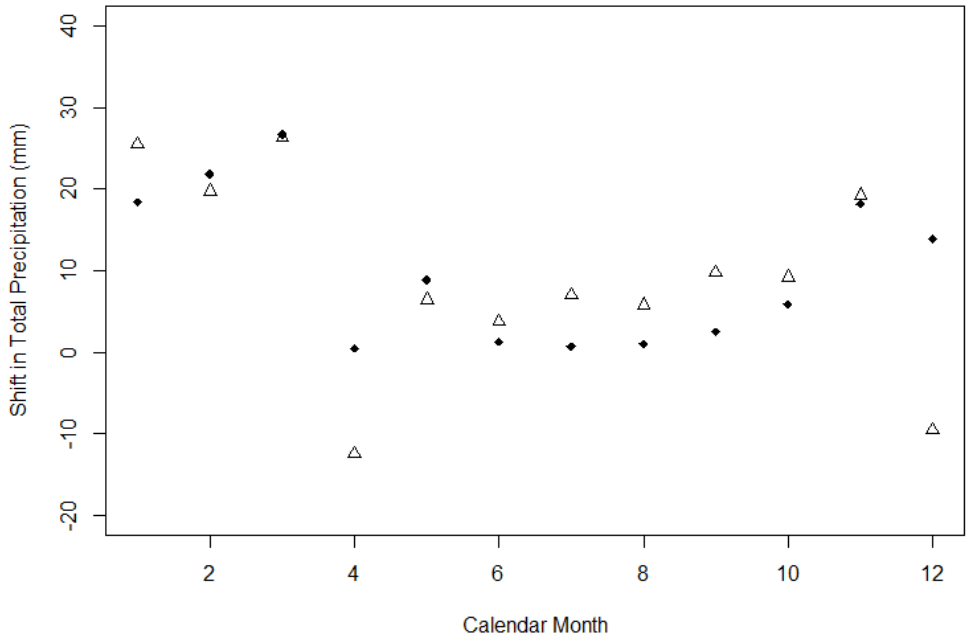

Note: Hollow triangles show changes in high-elevation (> 2000 m) grid cells of the Maurer et al. [2002] dataset, and solid dots show changes in low-elevation (< 2000 m) grid cells.

References

Gilbert RO. 1987. *Statistical Methods for Environmental Pollution Monitoring*. Wiley, NY.

Kendall MG. 1975. *Rank Correlation Methods*, 4th edition. Charles Griffin, London.

Mann HB. 1945. "Non-parametric tests against trend." Econometrica 13:163-171.

Maurer, E. P., A. W. Wood, J. C. Adam, D. P. Lettenmaier, and B. Nijssen (2002), A long-term hydrologically based dataset of land surface fluxes and states for the conterminous United States, *J. Clim., 15*, 3237-3251.

Ratner B. 2009. "A Closer Look: The correlation coefficient: Its values range between +1/-1, or do they?" Journal of Targeting, Measurement and Analysis for Marketing 17, 139 – 142. doi: 10.1057/jt.2009.5; https://link.springer.com/content/pdf/10.1057 percent2Fjt.2009.5.pdf.

Supplemental Figures

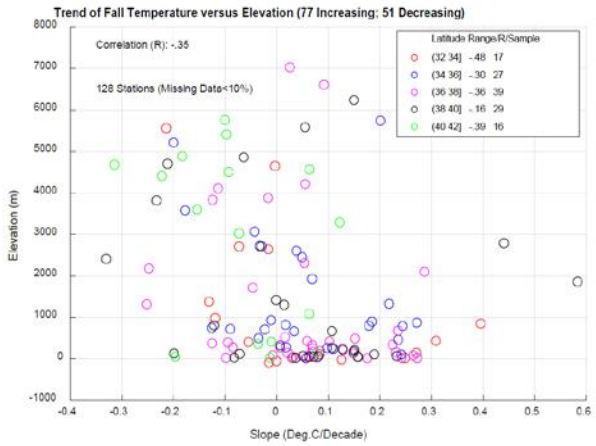

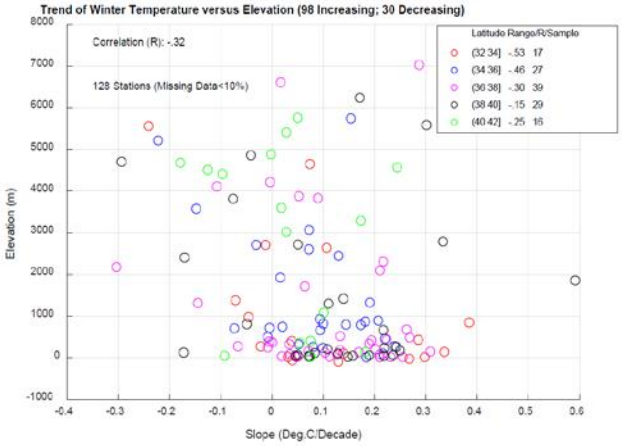

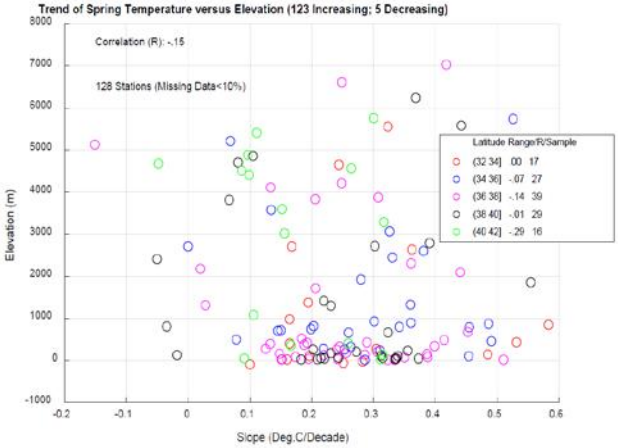

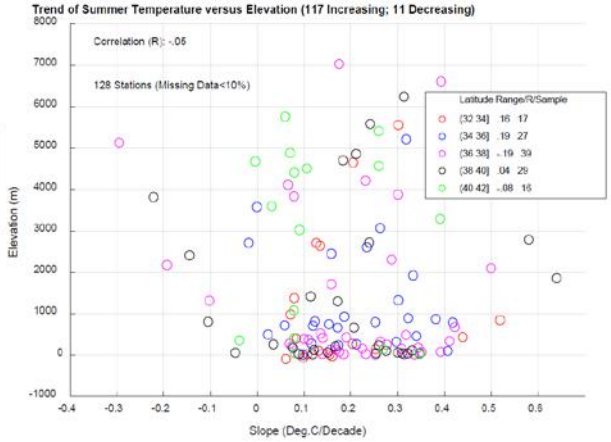

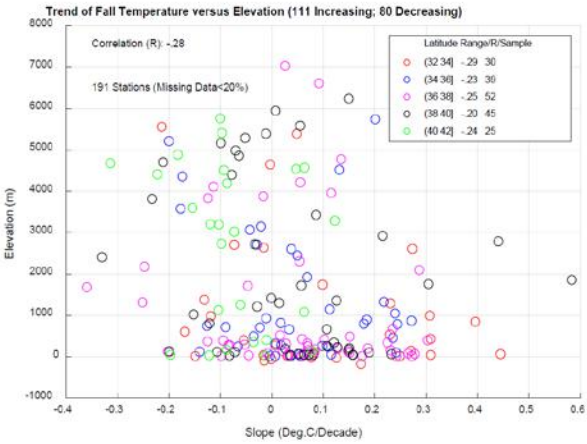
Trend of Fall Temperature versus Elevation (111 Increasing; 80 Decreasing)
Correlation (R): -.28
191 Stations (Missing Data<20%)
Latitude Range/R/Sample
(32 34] -.29 30
(34 36] -.23 39
(36 38] -.25 52
(38 40] -.20 45
(40 42] -.24 25
Elevation (m)
Slope (Deg.C/Decade)

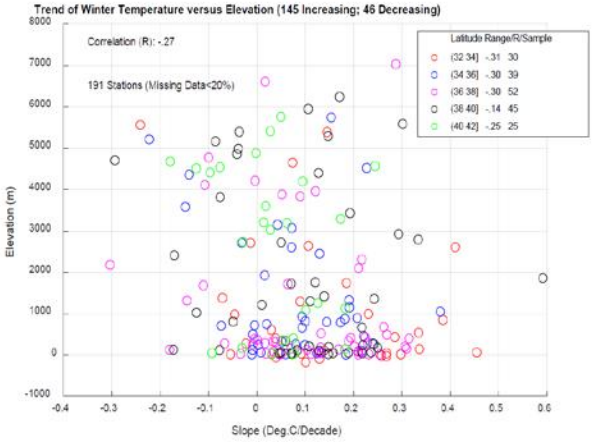
Trend of Winter Temperature versus Elevation (145 Increasing; 46 Decreasing)
Correlation (R): -.27
191 Stations (Missing Data<20%)
Latitude Range/R/Sample
(32 34] -.31 30
(34 36] -.30 39
(36 38] -.30 52
(38 40] -.14 45
(40 42] -.25 25
Elevation (m)
Slope (Deg.C/Decade)

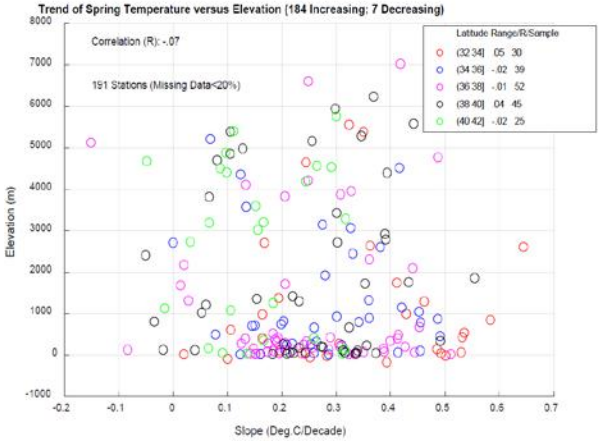
Trend of Spring Temperature versus Elevation (184 Increasing; 7 Decreasing)
Correlation (R): -.07
191 Stations (Missing Data<20%)
Latitude Range/R/Sample
(32 34] 05 30
(34 36] -.02 39
(36 38] -.01 52
(38 40] 04 45
(40 42] -.02 25
Elevation (m)
Slope (Deg.C/Decade)

Annex C: Resource Management Strategies Screening

As an initial step toward adapting to long term hydrologic shifts due to a changing climate, DWR is developing an Adaptation Plan (AP) as part of Phase III of its Climate Action Plan (CAP). Potential adaption strategies explored in the forthcoming AP are drawn from the 37 resource management strategies (RMS)[7] detailed in the California Water Plan Update 2013 (California Department of Water Resources 2013). The Climate Change Program has used four factors to drill down to a subset of screened RMS strategies that could address vulnerabilities of DWR's activities to climate change.

Factors Used to Screen RMS

Applicability

RMSs are considered in the context of their relationship to vulnerabilities identified in DWR's Vulnerability Assessment (VA). If the proposed actions do not address a specific vulnerability to DWR's activities identified within the VA, then they would be screened out from further consideration in the AP.

Authority

For the RMS to be a viable option for the immediate future, DWR would need decision-making authority to affect its implementation. A distinction is made between direct actions DWR can take and indirect actions taken to influence others to act. Direct actions would include such things as improved Delta conveyance, where DWR would be the project lead in terms of planning and implementation. Indirect actions could include topics such as outreach, education, and guidance, but also programs in which DWR is administering a public investment (e.g. implementation grants) in local or regional projects. Both direct and indirect actions are considered potential strategies for adaptation, but the distinction between them may influence applicability or feasibility in subsequent analyses.

Technical Feasibility

Some actions may meet the first two factors but are considered unlikely to be implemented for other reasons. If an action is deemed technically infeasible given current resources and technologies, it would be screened out from further consideration.

Capacity

Some actions may meet all three other factors, yet DWR does not possess the capacity to implement the action. For example, DWR may lack the expertise, tools, technology, or stakeholder relationships that would ensure full implementation. Otherwise, an action may prove cost-prohibitive even though the technical capacity is met, thus eliminating it from further evaluation in the AP.

[7] A full listing of California Water Plan resource management strategies is provided on DWR's website at https://water.ca.gov/Programs/California-Water-Plan/Water-Resource-Management-Strategies

Annex D: Adaptation Strategies – Seasonal Forecasting Skill

Plan of Study

As a possible adaptation strategy, improving seasonal forecast skill (or reducing the residual error in runoff forecasts) would provide operators with better information about how much additional runoff they could depend on for the rest of the water year. This information would allow operators to more optimally release water to meet downstream demands while always leaving sufficient water in the reservoir to meet end-of-year minimum storage targets.

The decision scaling platform can be used to test whether investments in improved seasonal forecasting results in improved system performance. CalLite 3.0 calls three table files that simulate the information provided to operators for the monthly forecasts of inflow to Folsom, Oroville, and Shasta reservoirs. These table files ("sacramento_runoff_forecast.table," "american_runoff_forecast.table," and "feather_runoff_forecast.table") provide the amount of runoff that remains in the watershed and is expected to arrive at the reservoir during the rest of the water year. Table 14 below shows the forecasts that are made for each of the reservoirs and the non-exceedance probabilities for runoff that are given in each month of the year.

Table 15 Non-Exceedance Runoff Values Given in Runoff Forecast Tables

	Folsom	Shasta	Oroville
January	NA	NA	99 percent
February	99 percent	99 percent	99 percent
March	90 percent	90 percent	90 percent
April	75 percent	75 percent	75 percent
May	50 percent	50 percent	50 percent
June	50 percent	NA	NA
July	50 percent	NA	NA
August	50 percent	NA	NA
September	50 percent	NA	NA

In the pre-processing routine that is used to create the input files to CalLite 3.0, these three tables are synthetically generated by taking a perfect runoff forecast for the year and then adding an stochastic error factor to that forecast so that the distribution of error in the forecasts mimics the distribution of errors that has been observed in the historical forecasts published in DWR's Bulletin 120. A random normal distribution number generator was used to generate a factor within the mean and standard deviation of the error distribution to apply to each perfect forecast in the simulations. A comprehensive study was conducted to develop the error values for these historical forecasts. All monthly runoff forecasts produced by DWR from 1996–2015 were compiled and compared to actual runoff values. Table 15 below provides the mean and standard deviation used in each forecast.

Table 16 Mean and Standard Deviation of Historical Runoff Forecasts

	Folsom		Shasta		Oroville	
	Mean	**Std**	**Mean**	**Std**	**Mean**	**Std**
January	NA	NA	NA	NA	0.51	0.2674
February	0.64	0.1619	0.50	0.1746	0.58	0.1912
March	0.43	0.3159	0.28	0.2173	0.39	0.2804
April	0.165	0.2915	0.118	0.2080	0.147	0.2436
May	0.014	0.1929	0.02	0.1844	0.012	0.1611

To evaluate the efficacy of improving seasonal runoff forecasts, an analysis could be done to reduce the mean and standard deviation of the error distribution that has historically been observed so that the new error distribution would reflect the level of improvement that might be possible if more monitoring, research, and tools were devoted to improving the forecasts. California State Climatologist, Dr. Michael Anderson, suggests mean error could be reduced to 0.05 for the April forecasts and to 0.15–0.25 for months earlier in the year; likewise, standard deviation could potentially be reduced to 0.10–0.15. Such seasonal forecast skill improvements could be realized through hydrologic modeling that leverages high-resolution (50 meter) maps of snow water equivalent derived from modern observation techniques such as the NASA's Airborne Snow Observatory project (ASO)[8,9].

Note: When developing this analysis, special attention should be given to how CalLite 3.0 uses the forecast information. CalLite 3.0 has two different methods for generating water supply forecasts (Water Supply Index/Delivery Index [WSI/DI] and Forecast Allocation Model [FAM]), which may be affected by the runoff forecasts. All current and past CalLite 3.0 runs have used a WSI/DI approach.

[8] Behrangi, A., Bormann, K. J., & Painter, T. H. (2018). Using the Airborne Snow Observatory to assess remotely sensed snowfall products in the California Sierra Nevada. Water Resources Research, 54.

[9] NASA Airborne Snow Observatory Factsheet for the San Joaquin River Restoration Program. Available online at http://www.restoresjr.net/?wpfb_dl=2127

Annex E: Adaptation Strategies – Enhanced Precipitation

Plan of Study

Precipitation enhancement, or "cloud seeding," is identified in the California Water Plan 2013 Update as a resource management strategy to help manage water shortages. Cloud seeding has been identified as a candidate for evaluation with the decision scaling platform due to its technical feasibility, DWR's capacity and authority to implement the strategy, and its applicability to the vulnerabilities to climate change discussed in this report (see Annex C: Resource Management Strategy Screening).

Winter orographic cloud seeding (seeding of colder clouds formed by wind uplift over mountain ranges) has been practiced by many entities throughout California since the early 1950s. Weather modification projects currently operate in mostly southern Sierra watersheds (see Figure 43). Winter orographic cloud seeding projects disperse silver iodide or liquid propane into clouds to artificially initiate ice nucleation and freezing of supercooled liquid water (SLW), thereby augmenting precipitation falling as rain or snow.

Studies of cloud seeding projects in California have found statistically significant water-year total streamflow increases ranging from 2-24% in several major watersheds in the Sierra Nevada mountains (Silverman, 2010). DWR estimates that an additional 400,000 acre-feet could be realized from the expansion of cloud seeding projects in California, particularly in the Pit River-McCloud River Basin (California Department of Water Resources 2016).

The best estimates of expected increases in runoff from cloud seeding projects can be made through dynamical weather modeling, which provides information on the average temperature and frequency of occurrence of clouds and weather systems with SLW, a key driver of winter orographic cloud seeding effectiveness for a given area. As dynamical modeling would require extensive computing resources and data collection, the could seeding adaptation strategy would be evaluated based on more simplified estimates of expected streamflow increases derived from a literature review of studies conducted to date for watersheds in California and other western states.

Using the decision scaling platform, simulated monthly streamflows in expanded cloud seeding operation candidate watersheds would be augmented based on expected annual runoff increases and applied equally for all incremental climate perturbations. With the modified streamflows as input, the water system operations model, CalLite 3.0, would simulate effects of these augmented flows on storage and other performance metrics. A method to adjust the amount of monthly flow augmentation according to the average temperature and rainfall of the simulated climate could be developed with further research to more accurately represent the effectiveness of cloud seeding operations in warmer and drier climates.

Figure 43 Weather Modification Projects in California during 2016

Annex F: Adaptation Strategies – Upper Watershed Management

Plan of Study

Land cover plays a key role in watershed management since it can absorb and navigate water in watersheds. Moreover, it affects the micro and macro climate in watersheds, which should be considered in management plans. To improve watershed management, it is necessary to assess the impacts of land cover change on the watershed. Thus, a hydrological model which can cope with land cover change assessment is proposed.

In its current configuration, the Sacramento Soil Moisture Accounting (SAC-SMA) is not capable of accounting for changes in land cover. SAC-SMA has no controls of water movement to satisfy evaporation. In this model, if the potential evaporation rate is not satisfied from the upper layer, it will withdraw water directly from the lower layer without considering the interaction between these two layers. Indeed, the model has a single evapotranspiration component and reduces the water content of each zone based on a residual of the potential evaporation from the upper to the lower zones. In dry basins, there is no water moving from the lower layer to the upper layer. Consequently, soil moisture in SAC-SMA's lower zone is underestimated. In addition, SAC-SMA does not consider the effects of vegetation, which absorbs water from the soil as a function of root depth, root distribution, and water demand. Under severely dry conditions, the upper and lower soil moisture can be further underestimated since vegetation resistance and transpiration withdrawals are not considered.

This proposal aims to build an evapotranspiration component into SAC-SMA that is explicitly connected to land cover, thus providing information which may help manage the Upper Feather River watershed. This plan of study would use the "Noah" parameterization of evapotranspiration (Koren et al. 2010), which computes overall evapotranspiration from the root zone and splits it into soil layer evapotranspiration based on layer saturation and root distribution. The parameterization combines the Penman potential evaporation approach and the canopy resistance-based model of Ek and Mahrt (1991). Additionally, the dynamic vegetation processes described in Terink et al. (2015) will be incorporated to consider canopy storage effects. See *Supplementary Material: Parameterization of Evaporation in the "Noah" Land Surface Scheme* at the end of this annex for a detailed presentation of the parameterization.

Conclusion

More consistent water subtraction for evapotranspiration from upper and lower layers could be achieved by implementing vegetation effects based on canopy resistance parameterization. A new evapotranspiration computation module could be coupled with the SAC-SMA rainfall-runoff model to increase the accuracy and help evaluate effects on streamflows from land cover change. Moreover, the performance of this advanced SAC-SMA could be evaluated by intercomparison with the Variable Infiltration Capacity (VIC)-model, which also integrates the effects of vegetation.

References

Koren V et al. 2010. "Modification of Sacramento Soil Moisture Accounting Heat Transfer Component (SAC-HT) for Enhanced Evapotranspiration." NOAA Technical Report NWS 53

Terink W et al. 2015. "SPHY v2.0: Spatial Processes in Hydrology." Geosci. Model Dev., 8, 2009-2034

Supplementary Material: Parameterization of Evaporation in the "Noah" Land Surface Scheme

Actual evaporation is estimated from the Penman equation adjusted by soil moisture and canopy resistance effects. It contains three components: direct evaporation from the top soil layer, evaporation of precipitation intercepted by the canopy, and transpiration via canopy and roots.

3.1. Noah Direct Evaporation From the Top Soil Layer

$$E_{dir} = (1 - \sigma) \times E_p \times \left(\frac{\theta_1 - \theta_{min}}{\theta_s - \theta_{min}}\right)^{fx}$$

σ: green vegetation fraction = Par(32)
$E_p = pet$: potential evaporation
θ_1: soil moisture in the upper soil layer = Par(33)
θ_s: air dry (minimum) soil moisture = Par(34)
θ_{min}: saturation (porosity) soil moisture = Par(35)
fx: empirical coefficient; fx = 2 as recommended from Ek et al. (2003)

3.2. Wet Canopy Evaporation

$$E_c = \sigma \times E_p \times \left(\frac{W_c}{W_{max}}\right)$$

There are two ways to compute maximum allowed canopy interception (maximum canopy storage) and intercepted canopy water content (canopy storage).

Method 1: Noah model

W_{max}: maximum allowed canopy interception
W_c: intercepted canopy water content = Par(36)
Chen et al. (1996): $W_{max} = 0.5\ mm$; n = 0.5

$$\frac{\partial W_c}{\partial t} = \sigma \times P - P_d - E$$

$$\rightarrow W_c = (\sigma \times P - P_d - E)t\ with\ W_c = 0\ at\ t = 0$$

If W_c exceeds W_{max}, the excess precipitation P_d reaches the ground. Therefore, actual surface precipitation $P_s = (1 - \sigma) \times P + P_d$ with P is measured precipitation.

Method 2: Terink et al. (2015)

Maximum canopy storage

$$scan_{max} = 0.935 + 0.498 \times LAI - 0.00575 \times LAI^2 = W_{max}$$

Canopy storage

$$scan_t = scan_{t-1} + P_t$$

$scan$: canopy story at (t-1) [mm]
P_t: measured precipitation [mm]
Precipitation throughfall/effective precipitation is the precipitation that cannot be stored in canopy storage. It occurs if water stored in the canopy is bigger than maximum canopy storage.

$$Pe_t = max(0, scan_t - scan_{max,t})$$

Update canopy storage after computing effective precipitation

$$scan_t = scan_t - Pe_t$$

Intercepted water

$$Int_t = \min\left(1.5 \times ET_{r,t}, scan_t\right)[mm]$$

Update

$$scan_t = scan_t - Int$$

$$scan_t = W_c$$

3.3. Canopy Evapotranspiration

$$E_t = \sigma \times E_p \times B_c \left[1 - \left(\frac{W_c}{W_{max}}\right)^n\right]$$

$$B_c = \frac{1}{R_a + R_c} = \frac{C_h}{1 + C_h R_c}$$

R_a: atmosphere resistance = 230 Ω
R_c: total canopy resistance

$$R_c = \frac{R_{c,min}}{F_{sr} \times F_q \times F_T \times F_{sm} \times LAI}$$

$R_{c,min}$: minimal stomatal resistance [s/m]
Solar radiation effect

$$F_{sr} = \frac{\frac{R_{c,min}}{R_{c,max}} + f}{1 + f}$$

$R_{c,max}$: maximum stomatal resistance; $R_{c,max} = 5000 s/m$

$$f = 0.55 \times \frac{R_g}{R_{gl}} \times \frac{2}{LAI}$$

LAI: leaf area index; set to the universal value of 5 or extracted from land cover data (source: https://neo.sci.gsfc.nasa.gov/view.php?datasetId=MOD15A2_M_LAI)
R_{gl}: solar radiation limit value
R_g: solar radiation

$$K_t = \frac{R_g}{R_0} = A(1 - \exp(-B \times {T_d}^C))$$

A: maximum clear sky characteristics of the study area, vary with elevation and pollution; A = 0.7
B: how soon maximum K_t is achieved as T_d increases; winter: 0.01; summer: 0.004
C: how soon maximum K_t is achieved as T_d increases; 2.4
T_d: the difference between daily maximum and minimum temperature
R_0: extraterrestrial insulation is estimated from astronomical relationships

$$R_0 = 2 \times S_0 \times E_0[\cos(lat) \times \cos(\delta) \times \sin(0.5 \times rot \times t_{rs}) \times rot + \sin(lat) \times \sin(\delta) \times 0.5 \times t_{rs}$$

S_0: solar constant; S_0=117.54 cal/cm^{2}hr
E_0: eccentricity correction

$$E_0 = 1.00011 + 0.034221 \times cos\Gamma + 0.001280 \times sin\Gamma + 0.000719 \times cos2\Gamma + 0.000077\sin2\Gamma$$

Γ: day angle

$$\Gamma = \frac{2\pi(\mathrm{N_d} - 1)}{365}$$

$\mathrm{N_d}$ = day number, January 1 = day 1
Duffie and Backman (1991):

$$E_0 = 1 + 0.033 \times cos\left(\frac{2\pi \times \mathrm{N_d}}{365}\right)$$

lat: latitude
δ: sun declination

$$\delta = 23.45 * \sin [360 / 365 * (284 + \mathrm{N_d})]$$

$\mathrm{N_d}$ = day number, January 1 = day 1
rot: angular velocity of the earth's rotation; rot = 0.2618 rad/hr
t_{rs}: daylight time in hours

$$t_{rs} = \frac{arcCos[-tg(\delta)tg(lat)] - arcCos[-tg(\delta)tg(lat)]}{rot}$$

Vapor pressure effect

$$F_q = \frac{1}{1 + h_s[q_s(T_a) - q_a]}$$

h_s: empirical parameter
q_a: water vapor mixing ratio [kg/kg]

$$q_a = q(T_a) = \frac{0.622 \times e}{P_a - (1 - 0.622 \times e)}$$

$$e = 446.02 \times \exp(0.0579 \times t_a)$$

e: water vapor pressure [Pa]
t_a: air temperature [degrees Celsius]
q_s: saturation mixing ratio [kg/kg]

Tables of Saturation Mixing Ratios

Table for Fahrenheit Temperature	
Temperature (°F) Or Dew Point Temperature (°F)	Saturation Mixing Ratio (g / kg) Or Mixing Ratio (g / kg)
-40	0.12
-30	0.21
-20	0.35
-10	0.58
0	0.94
10	1.52
15	1.89
20	2.34
25	2.88
30	3.54
35	4.33
40	5.28
45	6.40
50	7.74
55	9.32
60	11.19
65	13.38
70	15.95
75	18.94
80	22.43
85	26.48
90	31.16
95	36.56
100	43.22

Table for Celsius Temperature	
Temperature (°C) Or Dew Point Temperature (°C)	Saturation Mixing Ratio (g / kg) Or Mixing Ratio (g / kg)
-40	0.1
-30	0.3
-20	0.8
-10	1.8
0	3.8
5	5.4
10	7.6
15	10.6
20	14.7
25	20.1
30	27.2
35	36.6
40	49.0

Air temperature effect

$$F_T = 1 - 0.0016 \times (T_{ref} - T_a)^2$$

T_{ref}: empirical parameter; $T_{ref} = 298\ K$
Soil moisture effect

$$F_{sm} = \sum_{i=1}^{nr} \frac{(\theta_i - \theta_w) \times d_i}{(\theta_f - \theta_w) \times d_{nr}}$$

θ_i: soil moisture content of soil layer I; maximum number of layers = 4;

$$\theta_1 = Par(33);\ \theta_2 = Par(37);\ \theta_3 = Par(38); \theta_4 = Par(39)$$

θ_f: field capacity = Par(40)
θ_w: wilting point = Par(41)
d_i: layer thickness; maximum number of layers = 4;

$$d_1 = Par(42);\ d_2 = Par(43);\ d_3 = Par(44); d_4 = Par(45)$$

d_{nr}: total root zone thickness = Par(42)+ Par(43)+ Par(44)+ Par(45)+
nr: number of root zone layers
T_a: air temperature

Parameters dependent on the vegetation class index

1: Evergreen Needleleaf Forest
2: Evergreen Broadleaf Forest
3: Deciduous Needleleaf Forest
4: Deciduous Broadleaf Forest
5: Mixed Forest
6: Woodland
7: Wooded Grassland
8: Closed Shrubland
9: Open Shrubland
10: Grassland
11: Cropland
12: Bare Ground
13: Urban and Built-up
14: Water

Vegetation class	Noah parameters					SAC-HTCR parameters (see Sections 3.5, & 4)		
	$R_{c,min}$	R_{gl}	h_z	Z_o	N_r	D_{50}	r_n	$R_{c,min}$
1	2	3	4	5	6	7	8	9
1	150	30	41.69	2.653	4	12	-1.88	70
2	100	30	54.53	0.826	4	21	-1.84	50
3	125	30	51.93	0.563	4	12	-1.88	60
4	150	30	47.35	1.098	4	23	-1.76	70
5	100	30	47.35	0.854	4	23	-1.76	50
6	70	65	54.53	0.856	4	23	-1.76	40
7	40	100	36.35	0.035	3	28	-1.91	40
8	300	100	42.00	0.238	3	28	-1.91	90
9	400	100	42.00	0.065	3	27	-2.05	250
10	150	100	42.00	0.076	2	7	-1.18	150
11	400	100	42.00	0.011	3	16	-1.45	200
12	40	100	36.35	0.035	3	16	-1.45	40
13	150	100	42.00	0.011	2	5	-1.45	100
14	100	30	51.75	0.001	0	0	-1.00	100

3.4. Total evapotranspiration

$$E_{total} = E_{dir} + E_c + E_t$$

Annex G: Adaptive Water Year Typing

DWR's water-year type calculation methodology is described on the California Data Exchange Center (CDEC) California Cooperative Snow Surveys website (http://cdec.water.ca.gov/cgi-progs/iodir_ss/wsihist). The Sacramento and San Joaquin water-year type indices classify the water available from Sacramento and San Joaquin river watersheds into one of five discrete states relative to long-term average streamflow values for each watershed: one "wet" classification, two "normal" classifications (above and below normal), and two "dry" classifications (dry and critical).

Water-year type classification systems "simplify complex hydrology into a single, numerical metric that can be used in rule-based decision making" (Null & Viers 2013), and have been applied to development of drought indices throughout the United States (Heim 2002; Quiring 2009), and to other uses, such as hydropower reservoir management in Chile (Olivares et al. 2015). Explicit linking of water system operations to a water-year type provides the opportunity for water system operations to better synchronize with the needs of aquatic ecosystems which depend on patterns of hydrologic variability for the integrity of their lifecycles (Richter et al. 1997).

The Sacramento and San Joaquin water-year type indices and their additive combination known as the "Eight River Index" determine water-year type for the State Water Project (SWP) and the Central Valley Project (CVP). Allocations for out-of-stream users, environmental flows, and limits to exports south of the Bay Delta are tied to water-year types (SWRCB 2000). Water-year types are therefore an integral part of water policy in the state and exert a significant effect on federal, state, and local agencies through the regulatory restrictions designed around them. The frequency distribution of Sacramento and San Joaquin water-year types is projected to change significantly with changes in hydroclimatic conditions (Null & Viers 2013), which will have effects on the Central Valley water system performance beyond the long-term persistent hydrologic shifts themselves.

The decision scaling platform uses water year typing to develop inputs for CalLite 3.0 which simulates the current regulatory framework built around water year types. This makes the platform capable of exploring how modifying water-year type thresholds or water-year index formula might alter the performance of the system. Adapting water-year type formulations and index thresholds to be based on a non-stationary climate is a potential strategy to ensure negative impacts caused by water scarcity are shared among water users in the way regulatory restrictions were originally designed to achieve.

Annex H: Groundwater Storage and Recovery

One potential solution to California's future water supply problem is enhanced groundwater storage and recovery. This activity proposes an exploration of the relative net benefits of various configurations of groundwater storage and recovery in the Central Valley System (CVS) using the suite of models presented in Figure 2. Due to the ease of simulating surface water flow and irrigation, most detailed modeling is carried out for surface-water processes, while the groundwater component is left based on approximations and gross simplifications. Groundwater models are computationally expensive and require a detailed examination of subsurface geology and flow in two dimensions.

The California Department of Water Resources (DWR) has developed detailed models for surface water allocation (CalSim) and groundwater movement (C2VSim). Unfortunately, the finely detailed groundwater modeling code causes long CalSim runs and is not amenable to testing non-natural major adjustments to the aquifer. There is promise in using CalLite 3.0, an aggregated version of CalSim-II with runtimes of around 10 minutes, as an environment for exploring how to better make use of groundwater resources. However, CalLite 3.0 may not be suitable for the representation of groundwater interactions. A first step to evaluating opportunities for North-of-Delta groundwater storage and South-of-Delta groundwater storage using the model workflow developed as part of this study is to fully explore opportunities for modifications to groundwater interactions using CalLite 3.0.

The prospect of using the simpler code and quicker runtimes of CalLite 3.0 to explore groundwater-focused model runs has previously been considered by DWR. The use of CalSim-II to experiment with non-natural groundwater scenarios would likely require a great deal of processing to rewrite the intensive coding to allow for modification, and even if reformatted, this model has slow runtimes. CalSim-III has a new feature that links to the C2VSim model via a collection of functions called the Dynamic Link Library (DLL) and thus allow CalSim-III to remotely simulate groundwater processes. Ideally, one could use the same concept to link C2VSim and CalLite 3.0, but there are two fundamental problems: different divisions of the Central Valley and different representations of surface-aquifer interactions.

The Central Valley is divided differently between these two models. The groundwater model, C2VSim, uses a fine-resolution finite element grid, seen in Figure 44, based on hydrologic considerations. CalSim-III is broken up into basins called *depletion study areas*, and the discrepancy between the two is represented in the DLL via a link-node representation of the groundwater system which makes the two conceptualizations coincident. The issue is that the basin units for CalLite 3.0 are different from CalSim-III, for which the DLL was made. This would require a reconceptualization of spatial units in CalLite 3.0.

Discussions with DWR professionals have revealed that the bigger problems in their previous effort were inconsistencies in the way that C2VSim and CalLite 3.0 dictate stream networks interaction with the aquifer system. In both models, points of interaction occur at discrete points called stream-aquifer (SA) nodes. In C2VSim, these nodes are usually located at the origin, midpoint, junctures, and ends of streams. The CalLite 3.0 system does not consider this level of detail. In addition, the number of streams indexed into CalLite 3.0 is fewer than those in the C2VSim. This inconsistency is shown in Figure 45. It is for this reason that the original effort to introduce the C2VSim processes into CalLite 3.0 was originally dropped. The issue is that one would have to map and distribute the sparser nodes in CalLite 3.0 into the more detailed C2VSim layout.

While these issues seem difficult to rectify, the hope is that with creative processing in GIS, the issue of different basic spatial units and different SA node representation can be carried out without long periods of pre-processing and validating CalSim-II code. GIS could be used to help redefine the CalLite 3.0 land divisions based on the CalSim-III method. The larger challenge of the SA node issue would require GIS software to use its ability to delineate streamflow to trace the connections between node systems and break up the less-detailed node system in the CalLite 3.0 code.

Formatting CalSim-II code could take a prohibitory amount of time. If GIS can be used to resolve these differences, the coding and changes would take place within CalLite 3.0, which is a much simpler process. The result would be the ability to explore groundwater storage as an option with the same level of confidence in the results as surface water models.

In the case that the simpler CalLite 3.0 approach described above proves infeasible, then the need to conduct experiments on augmented groundwater recharge would motivate a transition from CalLite 3.0 to CalSim-III in the fundamental model workflow developed for this study. In that case, groundwater augmentation analysis would feed into a substantially larger task involving embedding of CalSim-III into the model workflow in the place of CalLite 3.0.

Figure 44 Different Representations of the Central Valley

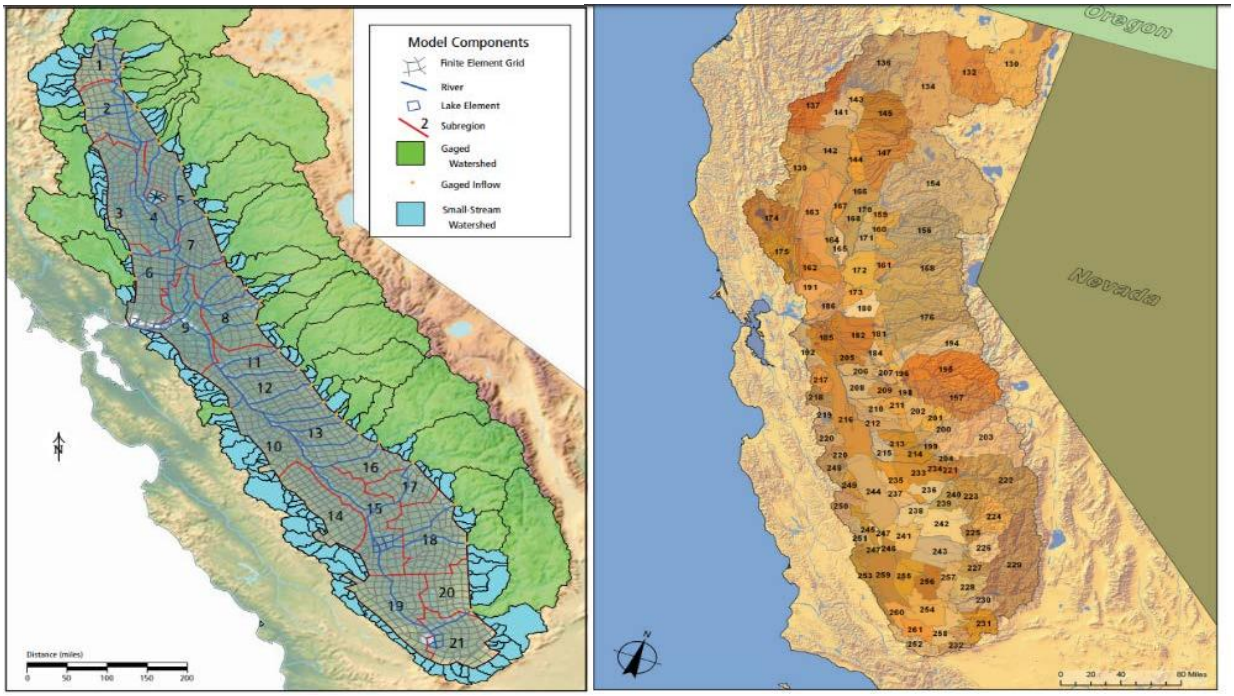

Note: The left-hand graphic shows the C2VSim representation and the right-hand graphic shows the CalSim/CalLite representation.

Figure 45 Representation of Stream-Aquifer Node Representation

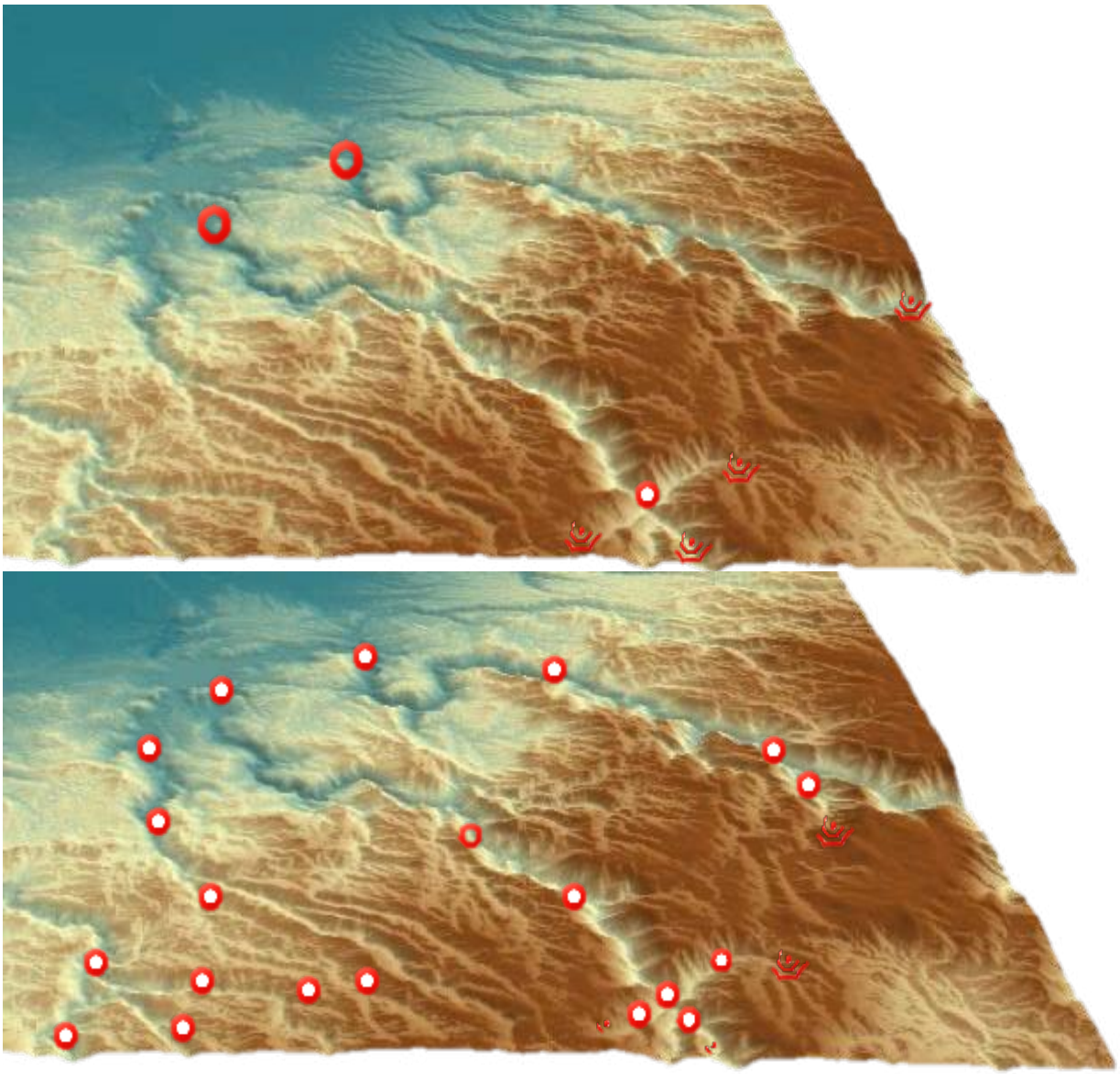

Note: The top graphic shows the CalLite representation and the bottom graphic shows the C2VSIM representation. Taken from a United States Geographic Survey (USGS) digital elevation model (DEM) of mid-San Joaquin Valley.

Annex I: Move From CalLite 3.0 to CalSim-III Operations Modeling

At the outset of DWR's Vulnerability Assessment with decision scaling study, CalLite 3.0 was chosen as the operations model to use in the analysis. CalLite 3.0 provided several benefits over California Department of Water Resources' (DWR's) flagship operations model at the time, CalSim-II, and is free and publicly available. CalLite 3.0 has a run time of 7–12 minutes for an 86-year simulation and is documented to provide results that are within about 1 percent of CalSim-II results, the production of which requires a comparative run time of 12 hours. Moreover, CalLite 3.0 requires 796 inputs as compared with the CalSim-II requirement of over 2,000 inputs. Because the decision scaling framework requires many hundreds of operational runs and a climatologically consistent method of perturbing model inputs, CalLite 3.0 held a distinct advantage over CalSim-II and was chosen as the operational model to be used in this study and provide a proof of concept.

With the completion of DWR's Vulnerability Assessment and progression to the evaluation of adaptation strategies, it is worth considering moving to DWR's newest operations model, CalSim-III. CalSim-III was released to the public for review in December 2017. While not fully accepted by DWR as its operational model, the model is close to a finished product and only minor changes are expected to be incorporated after public review.

Moving to CalSim-III would require a substantial effort to evaluate all of the input data CalSim-III requires (over 3,000 inputs) and develop a method of synthetically generating and perturbing those data based on available climatologic and hydrologic data. This effort would closely follow the process undertaken with CalLite 3.0.

A decision scaling framework built on CalSim-III would provide several benefits. CalSim-III links to the C2VSim model via a collection of functions called the Dynamic Link Library (DLL) which allows remote simulation of integrated groundwater-surface water processes. CalSim-III has refined spatial-scale and representation of Central Valley water demand through its novel implementation of "demand units" that can be aggregated into "Water Budget Areas." These two advancements, not available in CalLite 3.0, mean that CalSim-III simulations will more accurately account for climate change impacts on Central Valley groundwater and water demand and how those effects influence surface water conditions and deliveries. CalSim-III is fully supported and will continue to be improved and updated by DWR's Bay Delta Office. Studies completed using CalSim-III would be more consistent with studies being done by DWR and would be considered as slightly more robust. Finally, CalLite's simplifications add some level of error to results while CalSim-III's more sophisticated hydrologic inputs and water demand calculations, including groundwater, would likely improve the accuracy of the results.

This page is intentionally left blank.

2016 Six-Year Acoustic Telemetry Steelhead Study: Statistical Methods and Results

Prepared for:

Joshua Israel
U.S. Bureau of Reclamation
Sacramento, CA

Prepared by:

Rebecca Buchanan
Columbia Basin Research
School of Aquatic and Fishery Sciences
University of Washington
Seattle, WA

7 December 2018

Executive Summary

A total of 1,440 acoustic-tagged steelhead were released into the San Joaquin River at Durham Ferry in February, March, and April of 2016: 480 in February, 480 in March, and 480 in late April. Detection data were also available from 300 acoustic tags implanted into several species of predatory fish released in the Delta in April and May of 2014 and 2015. Acoustic tags were detectable on VEMCO hydrophones located at 44 stations throughout the lower San Joaquin River and Delta to Chipps Island (i.e., Mallard Slough) and Benicia Bridge. A rock barrier was installed at the head of Old River in early April 2016. Tagging and observation data were processed to construct detection histories, and data were passed through a predator filter to identify and remove detections thought to come from predators. Detection history data were analyzed using a multi-state release-recapture model to estimate survival, route selection, and transition probabilities throughout the Delta; receiver station detection probabilities were estimated concurrently from the release-recapture model. The survival and transition probabilities were adjusted for premature tag failure based on modeled tag survival from three tag-life studies. For all release groups, survival estimates included both the probability of migrating downriver and surviving, so that the complement included the probability of residualization as well as mortality.

Using only those detections classified as coming from juvenile steelhead by the predator filter, the estimates of total survival from Mossdale to Chipps Island, S_{Total}, ranged from 0.39 ($\widehat{SE} = 0.03$) for the February release group to 0.59 ($\widehat{SE} = 0.02$) for the April release group; the overall population estimate from all three releases (weighted average) was 0.47 ($\widehat{SE} = 0.02$). The estimated probability of entering Old River at its head was highest for the February release group (0.88, $\widehat{SE} = 0.02$), which passed mostly before the Head of Old River barrier was installed on April 1; estimates were still high (0.77, $\widehat{SE} = 0.02$) for the March release group, most of which passed before the barrier installation was complete, and were noticeably lower for the April release (0.04, $\widehat{SE} = 0.01$). The population estimate of Old River route selection over all three releases was 0.56 ($\widehat{SE} = 0.01$). There was a statistically significant preference for the Old River route for the February and March releases, and for the San Joaquin River route for the April release (P<0.0001 for each release group). Estimates of survival from Mossdale to Chipps Island via the San Joaquin River route $\left(S_A\right)$ ranged from 0.23 ($\widehat{SE} = 0.08$) for the February release group to 0.61 ($\widehat{SE} = 0.02$) for the April release; the population estimate, averaged over

all three release groups, was 0.45 ($\widehat{SE} = 0.03$) overall. In the Old River route, estimates of survival from Mossdale to Chipps Island $\left(S_B\right)$ ranged from 0.17 ($\widehat{SE} = 0.06$) for the April release to 0.41 ($\widehat{SE} = 0.04$) for the February release (population average = 0.33, $\widehat{SE} = 0.03$). The route-specific survival to Chipps Island was significantly different (at the 5% level) between routes for the April release group, when survival was higher in the San Joaquin River route than in the Old River route (P=0.0002). For the March release group, the point estimate of San Joaquin River route survival (0.50) was also higher than for the Old River route (0.40), but the difference was statistically significant only at the 10% level (P=0.0612). There was no significance difference in survival to Chipps Island between routes for the February release (P=0.1216). When combined over all three release groups, the population estimate of route-specific survival to Chipps Island was higher for the San Joaquin River route than for the Old River route (P=0.0034).

Travel time from release at Durham Ferry to Chipps Island ranged from 2.8 days to 41.2 days, and averaged 8.32 days ($\widehat{SE} = 0.19$ days) for all three release groups combined. Average travel time to Chipps Island was longest for the February release group (13.2 days), and shortest for the March release group (6.6 days); the April group had travel time similar to March (8.8 days). Average travel time to all detection sites was longest for the February release group. Travel time from release to the Mossdale receivers averaged approximately 6 days for the February release group, compared to 1.0 to 1.6 days for the March and April release groups. Travel time to the Turner Cut junction (i.e., receivers at either Turner Cut or MacDonald Island) ranged from 1.7 days to 32.8 days, and averaged 17.6 days for the February release, and approximately 5 days for the March and April releases.

A barrier was in place (i.e., after barrier closure during installation) at the head of Old River for passage of approximately 42% of the tagged steelhead in the 2016 tagging study. Of the 569 tagged steelhead that arrived at the head of Old River before the barrier closure during installation, 463 (81%) entered Old River. A route analysis was performed for the head of Old River using fish that arrived before barrier closure, using covariates measuring river discharge (flow), water velocity, export rates, fish length, river stage, and time of day of fish arrival at the river junction. Covariates that had significant associations with route selection at the head of Old River included a modeled estimate of flow at SJL (P<0.0001), river stage at MSD (P=0.0001), flow at MSD (P=0.0006), stage at OH1 (P=0.0009), OH1:MSD flow ratio (P=0.0015), and stage at SJL (P=0.0017) (Table 18). The regression model that accounted for the most variation in route selection at the head of Old River used river stage at MSD and

the 15-minute change in river stage at SJL. The model predicted that fish that arrived at the junction at higher river stages had a lower probability of entering Old River, and a higher probability of remaining in the San Joaquin River, whereas fish that arrived at the junction at higher levels of 15-minute change in river stage at SJL were more likely to enter Old River.

Route selection was analyzed at the Turner Cut junction using 389 tags, of which 24% entered Turner Cut, using measures of flow, water velocity, and river stage, export rates, fish length, and time of day of arrival at the junction. Covariates that had statistically significant associations with route selection at this river junction were the 15-minute change in river stage at the TRN gaging station in Turner Cut ($P<0.0001$) and both flow and velocity at TRN ($P=0.0003$). The regression model that accounted for the most variability in route selection at Turner Cut included the 15-minute change in river stage at TRN and flow at TRN. The modeled predicted that fish that arrived at the junction (i.e., passed the SJS receivers) at higher levels of the 15-minute change in river stage or higher levels of flow at TRN had a lower probability of entering Turner Cut.

Table of Contents

Acknowledgements

Funding for this project came from the U.S. Bureau of Reclamation (USBR). Many individuals from several agencies made this project possible. The tagging study was directed by the USBR (Josh Israel) and the U.S. Fish and Wildlife Service (USFWS: Pat Brandes). Individuals from the USFWS, USBR, California Department of Water Resources (CDWR), and the U.S. Geological Survey (USGS) implemented the tagging and release components of the project. The USFWS also implemented a fish health study (Ken Nichols). The USGS provided training for the surgeons (Theresa [Marty] Liedtke), helped design and installed, maintained, and retrieved the acoustic receiver array (Chris Vallee, Norbert VanderBranden, and Jon Burau), and pre-processed the data (Mike Simpson). Funding for data analysis and preparation of this report came from the USBR.

Introduction

A total of 1,440 acoustic-tagged juvenile steelhead were released into the San Joaquin River at Durham Ferry in February, March, and April of 2016; 480 were released in each of these months. Each steelhead was surgically implanted with a VEMCO V5 microacoustic tag. Each acoustic tag transmitted two unique identification codes: a traditional Pulse Position Modulation (PPM) code and a High Residence (HR) code, which provided detections on high residence receivers. The acoustic tags were detectable on hydrophones located at 44 stations throughout the lower San Joaquin River and Delta to Chipps Island (i.e., Mallard Slough) and Benicia Bridge. Detection data were also available from 300 acoustic tags implanted into several species of predatory fish released in the Delta in April and May of 2014 and 2015. A rock barrier was installed at the head of Old River in early April 2016; closure of the barrier was on 1 April 2016, and the barrier was breached on 1 June 2016.

VEMCO acoustic hydrophones and receivers were installed at 44 stations throughout the lower San Joaquin River and Delta in 2016 (Figure 1, Table 1). All of the receiver stations used in 2015 (Buchanan 2018b) were also used in 2016. One new receiver station was used in 2016, in the San Joaquin River near the Calaveras River (SJC = model code A10).

Statistical Methods

Data Processing for Survival Analysis

The University of Washington received the database of tagging and release data from the US Fish and Wildlife Service. The tagging database included the date and time of tag activation and tagging surgery for each tagged steelhead released in 2016, as well as the name of the surgeon (i.e., tagger), and the date and time of release of the tagged fish to the river. Fish size (length and weight), tag size, and any notes about fish condition were included, as well as the survival status of the fish at the time of release. Tag serial number and two unique tagging codes were provided for each tag, representing codes for various types of signal coding. Tagging data were summarized according to release group and tagger, and were cross-checked with Pat Brandes (USFWS) and Josh Israel (USBR) for quality control. All tags used in the survival study were activated only once.

Acoustic tag detection data collected at individual monitoring sites (Table 1) were transferred to the US Geological Survey (USGS) in Sacramento, California. A multiple-step process was used to identify and verify detections of fish in the data files and produce summaries of detection data suitable for

converting to tag detection histories. Detections were classified as valid if two or more pings were recorded within a 30 minute time frame on the hydrophones comprising a detection site from either of two tag codes associated with the tag; at the Central Valley Project trashrack receivers, a minimum of four pings were required within a 30 minute time frame for detections to be considered valid. The University of Washington received the primary database of autoprocessed detection data from the USGS. These data included the date, time, location, and tag codes and serial number of each valid detection of the acoustic steelhead tags on the fixed site receivers. The tag serial number indicated the acoustic tag ID, and were used to identify tag activation time, tag release time, and release group from the tagging database.

The autoprocessed database was cleaned to remove obviously invalid detections. The University of Washington identified potentially invalid detections based on unexpected travel times or unexpected transitions between detections, and queried the USGS processor about any discrepancies. All corrections were noted and made to the database. All subsequent analysis was based on this cleaned database.

The information for each tag in the database included the date and time of the beginning and end of each detection event when a tag was detected. Unique detection events were distinguished by detection on a separate hydrophone or by a time delay of 30 minutes between repeated hits on the same receiver. Separate events were also distinguished by unique signal coding schemes (i.e., PPM vs. HR). The cleaned detection event data were converted to detections denoting the beginning and end of receiver "visits;" consecutive visits to a receiver were separated either by a gap of at least 12 hours between detections on the receiver, or by detection on a different receiver array. Detections from receivers in dual or redundant arrays were pooled for this purpose, as were detections using different tag coding schemes.

The same data structure and data processing procedure were used to summarize detections of the acoustic-tagged predatory fish. Detections of the predatory fish were compared to detections of the steelhead tags to assist in distinguishing between detections of steelhead and detections of predators (see below).

Distinguishing between Detections of Steelhead and Predators

The possibility of predatory fish eating tagged study fish and then moving past one or more fixed site receivers complicated analysis of the detection data. The steelhead survival model depended on

the assumption that all detections of the acoustic tags represented live juvenile steelhead, rather than a mix of live steelhead and predators that temporarily had a steelhead tag in their gut. Without removing the detections that came from predators, the survival model would produce potentially biased estimates of survival of actively migrating juvenile steelhead through the Delta. The size of the bias depends on the amount of predation by predatory fish and the spatial distribution of the predatory fish after eating the tagged steelhead. To minimize bias, the detection data were filtered for predator detections, and detections assumed to come from predators were identified.

The predator filter used for analysis of the 2016 data was based on the predator filter designed and used in the analysis of the 2011–2015 data (USBR 2018a, 2018b, 2018c; Buchanan 2018a, 2018b). The 2011 predator filter was based on predator analyses presented by Vogel (2010, 2011), as well as conversations with fisheries biologists familiar with the San Joaquin River and Delta regions. The 2011 filter served as the basis for construction of the predator filters used in later years. The 2016 filter was applied to all detections of all tags implanted in steelhead. Two datasets were then constructed: the full steelhead-tag dataset of all detections, including those classified as coming from predators (i.e., "predator-type"), and the reduced dataset, restricted to those detections classified as coming from live steelhead smolts (i.e., "smolt-type"). The survival model was fit to both datasets separately. The results from the analysis of the reduced "smolt-type" dataset are presented as the final results of the 2016 tagging study. Results from analysis of the full dataset including "predator-type" detections were used to indicate the degree of uncertainty in survival estimates arising from the predator decision process.

The predator filter used for steelhead tagging data must account for both the possibility of extended rearing by steelhead in the Delta before eventual outmigration, and the possibility of residualization. These possibilities mean that some steelhead may have long residence or transition times, or they may move upstream either with or against the flow. Nevertheless, it was assumed that steelhead could not move against very high flow, and that their upstream excursions would be limited after entering the Delta at the head of Old River. Maximum residence times and transition times were imposed for most regions of the Delta, even allowing for extended rearing.

Even with these flexible criteria for steelhead, it was impossible to perfectly distinguish between a residualizing or extended rearing steelhead and a resident predator. A truly residualizing steelhead that is classified as a predator should not bias the overall estimate of successfully leaving the Delta at Chipps Island, because a residualizing steelhead would not be detected at Chipps Island. However, the

case of a steelhead exhibiting extended rearing or delayed migration before finally outmigrating past Chipps Island is more complicated. Such a steelhead may be classified as a predator based on long residence times, long transition times, and atypical movements within the Delta, or a combination of all three of these characteristics. Such a classification would negatively bias the overall estimate of true survival out of the Delta for steelhead. On the other hand, the survival model assumes common survival and detection probabilities for all steelhead, and thus is implicitly designed for actively migrating steelhead. With that understanding, the "survival" parameter estimated by the survival model is more properly interpreted as the joint probability of migration and survival, and its complement includes both mortality and extended rearing or residualization. The possibility of classifying steelhead with extended rearing times in the Delta as predators does not bias the survival model under this interpretation of the model parameters, and in fact is likely to improve model performance (i.e., fit) when these non-actively migrating steelhead detections are removed. In short, it was necessary either to limit survival analysis to actively migrating steelhead, or to assume that all detections came from steelhead. The first approach used the outcome of the predator filter described here for analysis. The second approach used all detection data.

The predator filter was based on assumed behavioral differences between actively migrating steelhead smolts and predators such as striped bass and channel catfish. For each steelhead tag, all detections were considered when implementing the filter, including detections from acoustic receivers that were not otherwise used in the survival model. As part of the decision process, environmental data including river flow, river stage, and water velocity were examined from several points throughout the Delta (Table 2), as available. Hydrologic data were downloaded from the California Data Exchange Center website (http://cdec.water.ca.gov/selectQuery.html) on 25 April 2017, and from the California Water Data Library (www.water.ca.gov/waterdatalibrary/) on 25–26 April 2017. Environmental data were reviewed for quality, and obvious errors were omitted. Daily pumping rates at the CVP and CCFB reservoir inflow rates were also used, downloaded from CDEC on 25 April 2016.

For each tag detection, several steps were performed to determine if it should be classified as predator or steelhead. Initially, all detections were assumed to be of live smolts. A tag was classified as a predator upon the first exhibition of predator-type behavior, with the acknowledged uncertainty that the steelhead smolt may actually have been eaten sometime before the first obvious predator-type detection. Once a detection was classified as coming from a predator, all subsequent detections of that

tag were likewise classified as predator detections. The assignment of predator status to a detection was made conservatively, with doubtful detections classified as coming from live steelhead.

A tag could be given a predator classification at a detection site on either arrival or departure from the site. A tag classified as being in a predator because of long travel time or movement against the flow was generally assigned a predator classification upon arrival at the detection site. On the other hand, a tag classified as being in a predator because of long residence time was assigned a predator classification upon departure from the detection site. Because the survival analysis estimated survival within reaches between sites, rather than survival during detection at a site, the predator classifications on departure from a site did not result in removal of the detection at that site from the reduced data set. However, all subsequent detections were removed from the reduced data set.

The predator filter used various criteria that addressed several spatial and temporal scales and fit under several categories (see USBR 2018a for more details): fish speed, residence time, upstream transitions, other unexpected transitions, travel time since release, and movements against flow. A predator score of at least 2 (i.e., failure to meet criteria of two or more predator filter components) was required to classify a tag as in a predator for a given transition if all previous detections had been classified as steelhead (USBR 2018a). If a previous detection had been classified as a predator, then all subsequent detections were classified as predators, also. The criteria used in the 2011–2015 studies were updated to reflect river conditions and observed tag detection patterns in 2016, and to represent transitions observed among the 2016 detection sites (Table 1). All receiver sites used in the 2015 study (Buchanan 2018b) were used in the 2016 study (Table 1). Additionally, there was a new receiver site installed in 2016 that was added to the predator filter: the San Joaquin River site near Calaveras River (SJC, site A10; Table 1).

Criteria for distinguishing between steelhead detections and predator detections were partially based on observed behavior of tags in fish that were presumed to have been transported from the holding tanks at either the State Water Project (SWP) or the Central Valley Project (CVP) to release sites in the lower San Joaquin River or Sacramento River, upstream of Chipps Island, under the assumption that such tags must have been in steelhead smolts rather than in steelhead predators. More weight was given to the data from tags that were presumed to have passed through the SWP than through the CVP, because steelhead predators can enter the CVP holding tank but are thought to be too large to pass through the louvers at the SWP (personal communication, Kevin Clark, California Department of Water

Resources). Tags presumed to have been transported from either SWP or CVP were used to identify the range of possible steelhead movement through the rest of the Delta. This was most helpful for detection sites in the western portion of the study area. This method mirrors that used for the 2011–2015 predator filters (USBR 2018a, 2018b, 2018c; Buchanan 2018a, 2018b).

Acoustic receivers were stationed inside the holding tanks at CVP, and tags that were observed in the holding tanks and then next observed at either Chipps Island (i.e., Mallard Island), Benicia Bridge, Jersey Point, False River, or Montezuma or Spoonbill sloughs (i.e., JPE/JPW–BBR) were assumed to have been transported. Acoustic receivers were not placed in the holding tanks at SWP, and so fish transported from SWP were identified with less certainty. It was presumed that tags were transported from SWP if they were detected either inside or outside the radial gates at the entrance to the Clifton Court Forebay (CCFB; the final receivers encountered before the SWP holding tank) and next detected at one of the JPE/JPW–BBR sites. This group may include tagged fish that migrated from the CCFB entrance to the JPE/JPW–BBR region in-river, evading detection at the multiple Old River and Middle River receivers north of the CCFB. While this in-river pathway was possible, it was deemed less likely than the SWP transport pathway for fish with no detections between CCFB and the downstream sites (i.e., JPE/JPW–BBR). More definitive information on transportation from the SWP was available in 2016 than in previous years, because the acoustic-tagged steelhead in the 2016 study were also PIT-tagged. The SWP release pipes that are used to return salvaged and transported fish to the San Joaquin River or Sacramento River at Sherman Island are outfitted with PIT-tag antennae. Thus, PIT-tag detections were available from 38 steelhead tags in 2016, detected 3–80 days after release at Durham Ferry; these detections were used to identify detections from steelhead, under the assumption that steelhead predators could not be transported from the SWP. Although not physically recaptured, the PIT-tag detection event is referred to as a "recapture event" and the acoustic tags associated with the detection PIT tags are referred to as "recapture tags" in what follows.

In addition to the PIT-tag detections, 17 acoustic-tagged steelhead were physically recaptured in the CVP holding tank, and 1 acoustic-tagged steelhead was recaptured in the Mossdale trawl[1]. The CVP holding tank recaptures occurred 3–19 days after initial release at Durham Ferry; the tag recaptured in

[1] One tagged steelhead was recaptured in the CVP holding tank at 2200 hours on 13 March 2016, with fork length 225 mm. The tag serial number was recorded as 1232894. This record was removed as inaccurate based on (1) the lack of detections of this tag downstream of the Durham Ferry receivers, (2) the fact that no other tags detected downstream of Mossdale passed Mossdale without detection, and (3) the large negative difference observed between fork length at tagging (237 mm) and fork length at recapture (225).

the Mossdale trawl was recaptured there 2 days after release at Durham Ferry. These recapture events provided evidence that the steelhead acoustic tag was still in a live steelhead at the time of recapture, rather than in a predator's gut. Combined over the tags recaptured in the CVP holding tank or in the Mossdale trawl and those associated with PIT-tag detections from the SWP transport truck release pipe, there were a total of 56 recaptured tags in 2016. The fixed site receiver detections of the recaptured steelhead tags that occurred prior to the recapture event provided information on the range of steelhead behavior, and were used to calibrate the predator filter for the regions represented by pre-recapture detections. In particular, the total score from the predator filter for each pre-recapture detection was required to be either 0 or 1, so that each pre-recapture detection was classified as coming from a likely steelhead rather than a likely predator. There was no limit placed on the predator score for detections of recaptured tags that occurred after the recapture event.

The criteria used in the predator filter were spatially explicit, with different limits defined for different receivers and transitions (Table 3). The overall approach used in the 2013–2015 studies was also used for the 2016 study; no new criteria were developed for the 2016 study. As in the 2014 and 2015 predator filters, the 2016 filter did not require upstream-directed transitions to have migration rate or body length per second (BLPS) less extreme than that observed on the downstream transition through the same reach. Components of the filter that are broadly applicable are described below, along with general criteria and/or exceptions for individual detection sites. This information largely complements that in Table 3, which provides detailed information on criteria for individual transitions. Only those transitions actually observed among either steelhead tags or predator tags (described below) are addressed. More information on the predator filter structure can be found in reports on the 2011–2015 studies in USBR (2018a, 2018b, 2018c), and Buchanan (2018a, 2018b).

The 2016 predator filter continued use of criteria relating to the maximum total visit length at a site (combined over multiple visits), time between visits to the same site, and large-scale movements from different regions of the study area. The maximum allowed time for detections anywhere since release at Durham Ferry was 1,000 hours. Although there was a PIT-tag detection in the SWP release pipes 80 days (approximately 1,929 hours) after Durham Ferry release, 37 of the 38 tags detected in the SWP release pipes were detected there <1,000 hours after Durham Ferry release. To the extent that steelhead may exhibit longer travel times or residencies in the study area, such steelhead are not actively migrating and are not well-represented by the survival model, as described above; thus, such detections were interpreted as more likely to indicate a predator than a migrating steelhead. The

default maximum total visit length at a site was 500 hours (approximately 21 days), although longer visits were allowed upstream of the head of Old River and at the radial gates (D1, D2). The maximum total visit length was further limited to the maximum of the mid-field residence time (i.e., duration from the first detection at a site without intervening detections elsewhere) or of the far-field (i.e., regional) residence time, if less than the default limit for the site. The maximum regional residence time that was allowed for transitions depended on the maximum values allowed for the mid-field residence time, travel time for the transition, and the regional residence time at previously detected sites in the region, if the tagged fish was coming from a site in the same region (see Table 4 for a description of the regions); if the tagged fish was coming from a different region, then the maximum allowed regional residence time was determined based only on the maximum mid-field residence time. More generally, regional residence times were limited to 1,000 hours upstream of the head of Old River and at the CVP (E1, E2), 800 hours in the vicinity of WCL (B3), OR4 (B4), and RGU/RGD (D1, D2), and 500 hours elsewhere in the study area; exceptions to this rule are indicated in Table 3. Unless otherwise specified, the maximum allowed length of an upstream foray (i.e., upstream directed movement that is uninterrupted by detections that indicated downstream movement between sites) was 20 km. The other criteria are specified below and in Table 3.

Detections in the San Joaquin River, Burns Cutoff (Rough and Ready Island, R1), and near the heads of Old and Middle Rivers (B1, B2, C1) after previous entry to the Interior Delta (sites B3, B4, C2, C3, D1, D2, E1, and E2) from near Stockton or sites farther downstream in the San Joaquin River ("lower San Joaquin River"; sites N6, N7, A8–A14, R1, F1, F2, and B5) were generally not allowed. The exceptions were at the San Joaquin River Shipping Channel (A11), MacDonald Island (A12), Turner Cut (F1), Medford Island (A13), and Disappointment Slough (A14). Once a tag had been detected arriving at either the CVP or the radial gates from the lower San Joaquin River, subsequent detection was allowed only at the CVP (E1, E2), the radial gates (D1/D2), Jersey Point (G1), False River (H1), Old River at its mouth (B5), Disappointment Slough (A14), Threemile Slough (T1), and the other sites downstream of Threemile Slough (T2, T3, G2, and G3). An exception was for West Canal (B3), for which post-facility transitions were allowed coming from the radial gates and Old River at Highway 4 (B4) for fish that came via the lower San Joaquin River. These restrictions were based on the assumption that juvenile steelhead that leave the lower San Joaquin River for the Interior Delta are not expected to return to the San Joaquin River, and those that leave the lower San Joaquin River for the water export facilities are not expected to subsequently leave the facilities other than through salvage and transport. Maximum

travel times were imposed on transitions in the Interior Delta and at the facilities for steelhead observed leaving the lower San Joaquin River for these regions. In general, travel time in the Interior Delta after entry to that region from the lower San Joaquin River was limited to 120 hours. For fish that entered the Interior Delta from the lower San Joaquin River and were then detected at the facilities, travel time in the Interior Delta after leaving the facilities was further limited to 100 hours; exceptions are noted below. Transitions from the northern Delta sites (G1, G2, G3, H1, T1, T2, T3) or western Delta sites (B2, B3, B4, C1, C2, D, E1, E2) back to the regions of the San Joaquin River upstream of Turner Cut were not allowed. Finally, transitions from ORS (B2) or the head of Middle River (C1) upstream to the head of Old River (B1) were not expected following detection in the lower San Joaquin River, whether the tagged fish used the Interior Delta or the head of Old River to move from the lower San Joaquin River to the B2/C1 region. More site-specific details and exceptions to these general rules are described below, and in Table 3.

DFU, DFD = Durham Ferry Upstream (A0) and Durham Ferry Downstream (A2): allow long residence and transition times and multiple visits; maximum total visit length (summed over visits that were separated by detections elsewhere) = 1,000 hours.

BDF1, BDF2 = Below Durham Ferry 1 (A3) and Below Durham Ferry 2 (A4): allow long transition times and multiple visits; maximum total visit length = 1,000 hours.

BCA, MOS, and HOR = Banta Carbona (A5), Mossdale (A6), and Head of Old River (B0): allow longer residence time if next transition is directed downstream (BCA, MOS); may have extra visits to A5, A6, and B0, or longer travel times to A6 and B0, if arrival flow is low. Transitions from Old River East (B1) are not allowed if the HOR barrier is installed. Maximum total visit length = 1,000 hours.

SJL = San Joaquin River near Lathrop (A7): transitions from Old River East (B1) are not allowed if the HOR barrier is in place. Maximum total visit length = 483 hours.

RS4–RS10 = Removal Study 4 (N1) through Removal Study 10 (N7): generally increasing regional residence times allowed for sites further downstream. Maximum total visit length = 75 hours.

ORE = Old River East (B1): require shorter residence times and/or fewer visits if the HOR barrier is in place; maximum total visit length = 324 hours. For transitions from ORS, no prior detections in the lower San Joaquin River.

SJG = San Joaquin River at Garwood Bridge (A8): repeat visits require arrival flow/velocity to be opposite direction from flow/velocity on previous departure. Maximum total visit length = 75 hours.

SJNB and RRI = San Joaquin River at Navy Bridge Drive (A10) and Rough and Ready Island (R1): fast transitions moving downstream require positive water velocity. Maximum total visit length = 40 hours.

SJC = San Joaquin River at the Calaveras River (A10): allow longer residence time if transition water velocity was low and positive for downstream transitions. Should not move against flow if coming from downstream; repeat visits require arrival flow/velocity to be opposite direction from flow/velocity on previous departure. Maximum total visit length = 85 hours.

SJS = San Joaquin River Shipping Channel (A11): should not move against flow if coming from downstream; repeat visits require arrival flow/velocity to be opposite direction from flow/velocity on previous departure. Maximum total visit length = 40 hours. No prior transition to the Interior Delta from the lower San Joaquin River if coming from upstream of SJS.

MAC = San Joaquin River at MacDonald Island (A12): allow more flexibility (longer regional residence time, transition time) if transition water velocity was low and positive for downstream transitions. Maximum total visit length = 60 hours. No prior transition to the Interior Delta from the lower San Joaquin River if coming from upstream of MAC.

MFE/MFW = Medford Island (A13): allow more flexibility (longer transition time) if transition water velocity was low and positive for downstream transitions; should not move against for transitions from downstream. Maximum total visit length = 500 hours. If coming from MID, no prior transition to Interior Delta from the lower San Joaquin River.

SJD = San Joaquin River at Disappointment Slough (A14): should not move against flow; repeat visits require arrival flow/velocity to be opposite direction from flow/velocity on previous departure. Maximum total visit length = 265 hours. No prior transition to facilities from the lower San Joaquin River if coming from MID, COL, or the San Joaquin River upstream of SJD.

TCE/TCW = Turner Cut (F1): should not move against flow. Maximum total visit length = 60 hours. If coming from SJS or MAC, no prior transition to the Interior Delta from the lower San Joaquin River.

COL = Columbia Cut (F2): no flow or velocity restrictions. Maximum total visit length = 500 hours.

OSJ = Old River at the San Joaquin (B5): should not move against flow; repeat visits require arrival flow/velocity to be opposite direction from flow/velocity on previous departure. Maximum total visit length = 325 hours. If coming from MFE/MFW or TCE/TCW, no prior transition to the facilities from the lower San Joaquin River. If coming from TCE/TCW, no prior detection in northwest Delta.

ORS = Old River South (B2): maximum total visit length = 500 hours. If coming from ORE, no prior detection in the northwest Delta. If coming from CVP, no prior detection in the lower San Joaquin River.

MRH = Middle River Head (C1): shorter residence times than at ORS; repeat visits are not allowed; maximum total visit length = 47 hours. If coming from ORE, no prior detection in the northwest Delta.

MR4 = Middle River at Highway 4 (C2): maximum total visit length = 80 hours. If coming from ORS, CVP, or WCL, no prior detections in the lower San Joaquin River. Maximum travel time in Interior Delta after detection at the facilities via the lower San Joaquin River = 10 hours.

MID = Middle River near Mildred Island (C3): should not move against flow; maximum total visit length = 134 hours. If coming from RS10, MFE/MFW, or TCE/TCW, no prior detection in northwest Delta. Maximum travel time in Interior Delta after detection at the facilities via the lower San Joaquin River = 10 hours.

CVP = Central Valley Project (E1): allow multiple visits; transitions from downstream Old River should not have departed Old River site against flow or arrived during low pumping. Maximum total visit length = 500 hours. Maximum cumulative upstream foray length = 23 km. If coming from ORS, no prior transition to Interior Delta or facilities from the lower San Joaquin River. Maximum travel time in the Interior Delta after entering that region from the lower San Joaquin River is unrestricted if coming from CVPtank, 180 hours for consecutive CVP transitions (i.e., CVP–CVP) and for transitions from WCL, MR4, and RGU/RGD, and 120 hours otherwise.

CVPtank = Central Valley Project holding tank (E2): assume that steelhead can leave tank and return (personal communication, Brent Bridges, USBR). Maximum total visit length = 500 hours. Maximum cumulative upstream foray length = 23 km.

WCL = West Canal (B3): allow many visits; should not arrive against flow or water velocity, or have departed RGU/RGD against strong inflow or CVP against strong pumping. Maximum total visit length = 40 hours. No prior transition to facilities from the lower San Joaquin River if coming from CVP, ORS, or MR4; no prior transition to Interior Delta from the lower San Joaquin River if coming from CVP or ORS.

OR4 = Old River at Highway 4 (B4): should not arrive move against flow or water velocity; maximum total visit length = 60 hours.

RGU/RGD = Radial Gates (D1, D2 = D): see OCAP 2015 [2013 report] for a general description of the residence time criteria at the radial gates. Maximum total visit length = 800 hours. Should not have moved against strong flow or CVP pumping. No prior transition to Interior Delta or facilities from the lower San Joaquin River if coming from ORS.

JPE/JPW and FRE/FRW = Jersey Point (G1) and False River (H1): no flow/velocity restrictions; maximum total visit length = 140 hours for JPE/JPW, and 83 hours for FRE/FRW. Maximum cumulative upstream foray length = 25 km if coming from JPE/JPW, FRE/FRW, or MAE/MAW. No prior transition to facilities from the lower San Joaquin River if coming from MFE/MFW, MID, MR4, OR4, or TCE/TCW; no prior detection in northwest Delta if coming from MFE/MFW or TCE/TCW.

TMS/TMN = Threemile Slough (T1): should not move against flow on departing from San Joaquin River sites. Maximum total visit length = 47 hours. Maximum cumulative upstream foray length = 25 km.

MTZ, SBS = Montezuma Slough (T2) and Spoonbill Slough (T3): No flow or velocity restrictions. Maximum total visit length = 10 hours for MTZ, and 4 hours for SBS; maximum cumulative upstream foray = 25 km.

MAE/MAW, BBR = Chipps Island (G2) and Benicia Bridge (G3): should not arrive from upstream against strong negative water velocity/flow (MAE/MAW). Maximum total visit length = 50 hours; maximum cumulative upstream foray = 25 km. No prior transition to facilities from the lower San Joaquin River if coming from MFE/MFW or TCE/TCW.

Fixed-site receiver detections were available from up to 150 predatory fish that had been implanted with acoustic tags as part of a predation study conducted by NMFS in 2014 and 2015: 78 Striped Bass *Morone saxatilis*, 128 Largemouth Bass *Micropterus salmoides*, 60 White Catfish *Ameiurus*

catus, and 34 Channel Catfish *Ictalurus punctatus*. Releases of tagged predatory fish took place in spring of 2014 and 2015, in reaches of the San Joaquin River between MOS (A6) and RS9 (N6) (Smith et al. 2016). The predator detections were used to assess the sensitivity (i.e., true positive rate) of the predator filter. A "positive" outcome was a predator score of two or more on at least one detection on the visit spatiotemporal scale during the detection history; earning a predator score ≥2 on every detection of the predator tag was not required. Filter sensitivity was measured as the proportion of the predator tags that were classified as in a predator at some point during their detection history within 2016. The sensitivity assessment excluded the "time since release" component of the predator filter because all predators were tagged before the current study year, and the observed time since release for the predator tags was outside the range observable for the steelhead tags for which the filter was designed. Only predator tags that were detected on at least one fixed site receiver were used in the sensitivity assessment. Some components of the predator filter use information from multiple detections, with the result that tags that have more observations are more likely to be classified as in a predator. Thus, the filter sensitivity was measured first using all detected predator tags, and then using only those that had at least five detections on the "visit" spatiotemporal scale. A sensitivity of 100% indicates a perfect ability to classify predators correctly, although it is still possible that live steelhead may be erroneously classified as predators.

The filter specificity (true negative rate) is the ability of the filter to correctly classify detections of steelhead as coming from steelhead rather than predatory fish. Assessing the filter specificity requires tags that are known to be in steelhead at some point after their initial release. There were 56 steelhead tags recaptured or detected via PIT tag after initial release in 2016. These 56 tags were used in calibrating the filter, however, and so it was not appropriate to use them also for assessing the filter specificity. No attempt was made to monitor filter specificity.

Constructing Detection Histories

For each tag, the detection data summarized on the "visit" scale were converted to a detection history (i.e., capture history) that indicated the chronological sequence of detections on the fixed site receivers throughout the study area. In cases in which a tag was observed passing a particular receiver array or river junction multiple times, the detection history represented the final route of the tagged fish past the array or junction. In particular, if a fish was observed even far downstream in one route but then returned to the river junction and finally selected the other route, then survival and detection in the later route were modeled. Detections from the receivers comprising certain dual arrays were

pooled to improve model fit, thereby converting the dual arrays to redundant arrays, which were treated as single arrays in the survival model: the San Joaquin River receivers at Durham Ferry Downstream (A2), Banta Carbona (A5), Mossdale (A6), Garwood Bridge (A8), and Calaveras River (A10); the Central Valley Project trash racks (E1); the radial gates receivers both outside (D1) and inside (D2) the Clifton Court Forebay; and Chipps Island (G2). For some release groups, it was necessary to pool detections across the lines in the dual array at Jersey Point (G1) to fit the model. The acoustic station on the San Joaquin River at the Navy Drive Bridge (A9) was designed as a dual array, but because no data were retrieved from one of the receivers within that array, the Navy Drive Bridge site was also treated as a single array in the model. One release group required pooling across the lines of the dual array at the Old River site at Highway 4 (B4) for fish that reached that site via the Old River route, although it was possible to use the full data from the dual array for fish that arrived there via from the San Joaquin River route. Treating the Chipps Island receivers as a redundant array rather than a dual array was possible because of the presence of the Benicia Bridge receivers (G3). The status of the radial gates (opened or closed) upon detection at the receivers just outside the radial gates (D1) was included in the detection history. Detections on receivers at the Head of Old River site (B0), the predator removal study sites (N1–N7), Montezuma Slough (T2), and Spoonbill Slough (T3) were used in determining the detection history, but were omitted from the survival model. Detections at Threemile Slough (T1) were included in the detection histories to represent the Sacramento River route to Chipps Island from the San Joaquin River receiver at Disappointment Slough (A14). Detections at West Canal (B3) were included in the model for the Old River from the head of Old River, but excluded from the San Joaquin River route.

Survival Model

A two-part multi-state statistical release-recapture model was developed and used to estimate perceived juvenile steelhead survival and migration route parameters throughout the study area. The release-recapture model was a modified version of the models used in the 2011–2015 steelhead analyses (USBR 2018a, 2018b, 2018c; Buchanan 2018a, 2018b), and similar to the model developed by Perry et al. (2010) and the model developed for the 2009–2011 VAMP studies (SJRGA 2010, 2011, 2013). Figure 1 shows the layout of the receivers using both descriptive labels for site names and the code names used in the survival model (Table 1). The survival model represented movement and perceived survival throughout the study area to the primary exit point at Chipps Island (i.e., Mallard Island) and on to Benicia Bridge (Figure 2, Figure 3). Individual receivers comprising dual arrays were identified separately, using “a” and “b” to represent the upstream and downstream receivers, respectively.

The statistical model depended on the assumption that all tagged steelhead in the study area were actively migrating, and that any residualization occurred upstream of the Durham Ferry release site. If, on the contrary, tagged steelhead residualized downstream of Durham Ferry, and especially within the study area (downstream of the Mossdale receiver, A6), then the multi-state statistical release-recapture model estimated perceived survival rather than true survival, where perceived survival is the joint probability of migrating and surviving. The complement of perceived survival includes both the probability of mortality and the probability of halting migration to rear or residualize. Unless otherwise specified, references to "survival" below should be interpreted to mean "perceived survival."

Fish moving through the Delta toward Chipps Island may have used any of several routes. The two primary routes modeled were the San Joaquin River route (Route A) and the Old River route (Route B). Route A followed the San Joaquin River past the distributary point with Old River near the town of Lathrop, CA, and past the city of Stockton, CA. Downstream of Stockton, fish in the San Joaquin River route (route A) may have remained in the San Joaquin River past its confluence with the Sacramento River and on to Chipps Island. Alternatively, fish in Route A may have exited the San Joaquin River for the interior Delta at any of several places downstream of Stockton, including Turner Cut, Columbia Cut (just upstream of Medford Island), and the confluence of the San Joaquin River with either Old River or Middle River, at Mandeville Island. Three of these four exit points from the San Joaquin River between Stockton and Jersey Point were monitored and used in the survival model: Turner Cut, Columbia Cut, and the Old River mouth (TCE/TCW, COL, and OSJ, respectively). Turner Cut and Columbia Cut were assigned route F, and treated as a subroute of route A. The Old River mouth route was treated as a subroute of route A, although as a site in Old River, it was given a model code name starting with "B" (B5). Fish that entered the interior Delta from the lower San Joaquin River may have either moved north through the interior Delta and reached Chipps Island by returning to the San Joaquin River and passing Jersey Point and the junction with False River, or they may have moved south through the interior Delta to the state or federal water export facilities, where they may have been salvaged and trucked to release points on the San Joaquin or Sacramento rivers just upstream of Chipps Island. All of these possibilities were included in both subroute F and route A. Another subroute of route A was Burns Cutoff around Rough and Ready Island, near Stockton, assigned subroute R; fish taking subroute R returned to the main stem San Joaquin River near the Calaveras River (SJC).

For fish that entered Old River at its distributary point on the San Joaquin River just upstream of Lathrop, CA (route B), there were several pathways available to Chipps Island. These fish may have migrated to Chipps Island either by moving northward in either the Old or Middle rivers through the interior Delta, or they may have moved to the state or federal water export facilities to be salvaged and trucked. The Middle River route (subroute C) was monitored and contained within Route B. Passage through the State Water Project via Clifton Court Forebay was monitored at the entrance to the Forebay and assigned a route (subroute D). Likewise, passage through the federal Central Valley Project was monitored at the entrance trashracks and in the facility holding tank and assigned a route (subroute E). Subroutes D and E were both contained in subroutes C (Middle River) and F (Turner Cut), as well as in primary routes A (San Joaquin River) and B (Old River). All routes and subroutes included multiple unmonitored pathways for passing through the Delta to Chipps Island.

Several exit points from the San Joaquin River were monitored and given route names for convenience, although they did not determine unique routes to Chipps Island. The first exit point encountered was False River, located off the San Joaquin River just upstream of Jersey Point. Fish entering False River from the San Joaquin River entered the interior Delta at that point, and would not be expected to reach Chipps Island without subsequent detection in another route. Thus, False River was considered an exit point of the study area, rather than a waypoint on the route to Chipps Island. It was given a route name (H) for convenience. Likewise, Jersey Point and Chipps Island were not included in unique routes. Jersey Point was included in many of the previously named routes (in particular, routes A and B, and subroutes C and F), whereas Chipps Island (the final exit point) was included in all previously named routes and subroutes except route H. Thus, Jersey Point and Chipps Island were given their own route name (G). Benicia Bridge was monitored in 2016; located downstream of Chipps Island, it was considered to be outside the study area, but facilitated estimating survival to Chipps Island; Benicia Bridge was also assigned route G. Several additional sets of receivers located in the San Joaquin River upstream of Stockton (Route A), Middle River (Subroute C) near Mildred Island, and in Montezuma and Spoonbill sloughs (Route T) were not used in the survival model. Threemile Slough (Route T) was used to represent a subroute of the San Joaquin River route (route A), namely a passage route from the lower San Joaquin to Chipps Island that uses the Sacramento River, rather than the San Joaquin River and Jersey Point, to pass Sherman Island. The routes, subroutes, and study area exit points are summarized as follows:

A = San Joaquin River: survival

B = Old River: survival

C = Middle River: survival

D = State Water Project: survival

E = Central Valley Project: survival

F = Turner Cut and Columbia Cut: survival

G = Jersey Point, Chipps Island, Benicia Bridge: survival, exit point

H = False River: exit point

N = Predator Removal Study: not used in survival model

R = Rough and Ready Island: survival

T = Threemile, Montezuma, and Spoonbill sloughs: survival (Threemile) or not used in survival model (Montezuma, Spoonbill)

The release-recapture model used parameters denoting the probability of detection (P_{hi}), route selection ("route entrainment", ψ_{hl}), perceived steelhead survival (the joint probability of migrating and surviving; S_{hi}), and transition probabilities equivalent to the joint probability of directed movement and survival ($\phi_{kj,hi}$) (Figure 2, Figure 3, Table A1). For each dual array, unique detection probabilities were estimated for the individual receivers in the dual array: P_{hia} represented the detection probability of the upstream receiver line at station i in route h, and P_{hib} represented the detection probability of the downstream receiver line.

The model parameters are:

P_{hi} = detection probability: probability of detection at telemetry station i within route h, conditional on surviving to station i, where $i = ia, ib$ for the upstream, downstream receiver lines in a dual array, respectively.

S_{hi} = perceived survival probability: joint probability of migration and survival from telemetry station i to i+1 within route h, conditional on surviving to station i.

ψ_{hl} = route selection probability: probability of a fish entering route h at junction l (l =1, 2, 3), conditional on fish surviving to junction l.

$\phi_{kj,hi}$ = transition probability: joint probability of migration, route selection, and survival; the probability of migrating, surviving, and moving from station j in route k to station i in route h, conditional on survival to station j in route k.

The transition parameters involving the receivers outside Clifton Court Forebay (site D1, RGU) depended on the status of the radial gates upon tag arrival at D1. Although fish that arrive at D1 when the gates are closed cannot immediately enter the gates to reach site D2 (RGD), they may linger in the area until the gates open. Thus, the parameters $\phi_{kj,D1O}$ and $\phi_{D1O,D2}$ represent transition to and from site D1 when the gates are open, and parameters $\phi_{kj,D1C}$ and $\phi_{D1C,D2}$ represent transition to and from D1 when the gates are closed. It was not possible to estimate unique detection probabilities at site D1 for open and closed gates, so a common probability of detection, P_{D1}, was assumed at that site regardless of gate status upon arrival.

A variation on the parameter naming convention was used for parameters representing the transition probability to the junction of False River with the San Joaquin River, just upstream of Jersey Point (Figure 1). This river junction marks the distinction between routes G and H, so transition probabilities to this junction are named $\phi_{kj,GH}$ for the joint probability of surviving and moving from station j in route k to the False River junction. Fish may arrive at the junction either from the San Joaquin River or from the interior Delta. The complex tidal forces present in this region prevent distinguishing between individuals using False River as an exit from the San Joaquin and individuals using False River as an entrance to the San Joaquin from Frank's Tract. Regardless of which approach the fish used to reach this junction, the $\phi_{kj,GH}$ parameter (e.g. $\phi_{A14,GH}$) is the transition probability to the junction of False River with the San Joaquin River via any route; ψ_{G1} is the probability of moving downstream toward Jersey Point from the junction; and $\psi_{H1} = 1 \quad \psi_{G1}$ is the probability of exiting (or re-exiting) the San Joaquin River to False River from the junction (Figure 2, Figure 3). In the event that sparse detections at False River prevented separate estimation of $\phi_{kj,GH}$ and ψ_{G1}, the parameter $\phi_{kj,G1} = \phi_{kj,GH}\psi_{G1}$ was estimated directly and used to compute estimates of Mid-Delta survival (defined below).

For fish that reached the interior receivers at the State Water Project (D2) or the Central Valley Project (E2), the parameters $\phi_{D2,G2}$ and $\phi_{E2,G2}$, respectively, represent the joint probability of migrating and surviving to Chipps Island, including survival during and after collection and transport (Figure 2). Some salvaged and transported fish were released in the San Joaquin River between Jersey Point and Chipps Island, and others were released in the Sacramento River upstream of the confluence with the San Joaquin River; records of the release location were not available for individual fish. Because salvaged fish were not required to pass Jersey Point and the False River junction, and in particular those released in the Sacramento River, it was not possible to estimate the transition probability to Chipps Island via Jersey Point for salvaged fish. Thus, only the overall probability of making the transition to Chipps Island was estimated for fish passing through the water export facilities.

Because of the complexity of routing in the vicinity of MacDonald Island on the San Joaquin River, Turner Cut, Columbia Cut, Medford Island, and Disappointment Slough, and the possibility of reaching the interior Delta via either route A or route B, the full survival model that represented all routes was decomposed into two submodels for analysis, as in the 2011–2015 analyses (USBR 2018a, 2018b, 2018c; Buchanan 2018a, 2018b). Submodel I modeled the overall migration from release at Durham Ferry to arrival at Chipps Island without modeling the specific routing from the lower San Joaquin River (i.e., from the Turner Cut Junction) through the interior Delta to Chipps Island, although it included detailed subroutes in route B for fish that entered Old River at its upstream junction with the San Joaquin River (Figure 2). In Submodel I, transitions from MacDonald Island (A12) and Turner Cut (F1) to Chipps Island were interpreted as survival probabilities ($S_{A12,G2}$ and $S_{F1,G2}$) because they represented all possible pathways from these sites to Chipps Island. Submodel II, on the other hand, focused entirely on Route A, and used a virtual release of tagged fish detected at the San Joaquin River receiver array near Lathrop (A7, SJL) to model the detailed routing from the lower San Joaquin River near MacDonald Island and Turner Cut through or around the interior Delta to Jersey Point and Chipps Island (Figure 3). Submodel II included the Medford Island and Disappointment Slough detection sites (A13 and A14), as well as Columbia Cut (F2) and the northern Old River site (B5), all of which were omitted from Submodel I because of complex routing in that region. Submodel II also included the Old and Middle River receivers near Highway 4 (B4 and C2), as well as the water export facilities (D1, D2, E1, E2), Jersey Point/False River (G1/H1), and Threemile Slough (T1) (Figure 3).

The two submodels I and II were fit concurrently using common detection probabilities at certain shared receivers: D1 (RGU), D2 (RGD), E1 (CVP), E2 (CVP holding tank), G1 (JPE/JPW), and H1 (FRE/FRW). While submodels I and II both modeled detections at these receivers, actual detections modeled at these receivers came from different tagged fish in the two submodels: detections from Route B fish were used in Submodel I, and detections from Route A fish were used in Submodel II. Detections at all other sites included in Submodel II either included the same fish as in Submodel I (i.e., sites SJG, SJNB, RRI, SJC, SJS, MAC, TCE/TCW, MAE/MAW, and BBR, model codes A8–A12, R1, F1, G2, and G3), or else were unique to Submodel II (i.e., sites MFE/MFW, COL, SJD, OSJ, TMN/TMS = A13, F2, A14, B5, T1). Detection probabilities at sites that shared detections between the submodels were estimated separately for submodels I and II to avoid double-counting. As in the 2011 study (USBR 2018a), unique transition parameters through the water export facility sites (i.e., $\phi_{D1O,D2}$, $\phi_{D1C,D2}$, $\phi_{D2,G2}$, $\phi_{E1,E2}$, and $\phi_{E2,G2}$) were estimated for Submodels I and II, under the assumption that fish that arrive outside the CVP or the Clifton Court Forebay coming from the head of Old River might have a different likelihood of reaching the interior receivers than fish that came from the lower San Joaquin River.

In addition to the model parameters, performance metrics measuring migration route probabilities and survival were estimated as functions of the model parameters. Both route selection probabilities and route-specific survival were estimated for the two primary routes determined by routing at the head of Old River (routes A and B). Route selection and route-specific survival were also estimated for the major subroutes of routes A and B, when possible from the available data. These subroutes were identified by a two-letter code, where the first letter indicates routing used at the head of Old River (A or B), and the second letter indicates routing used at the next river junction encountered: A or F at the Turner Cut Junction, and B or C at the head of Middle River. Thus, the route selection probabilities for the subroutes were:

$\psi_{AA} = \psi_{A1}\psi_{A3}$: probability of remaining in the San Joaquin River past both the head of Old River and the Turner Cut Junction,

$\psi_{AF} = \psi_{A1}\psi_{F3}$: probability of remaining in the San Joaquin River past the head of Old River, and exiting to the interior Delta at Turner Cut,

$\psi_{BB} = \psi_{B1}\psi_{B2}$: probability of entering Old River at the head of Old River, and remaining in Old River past the head of Middle River,

$\psi_{BC} = \psi_{B1}\psi_{C2}$: probability of entering Old River at the head of Old River, and entering Middle River at the head of Middle River,

where $\psi_{B1} = 1 \quad \psi_{A1}$, $\psi_{F3} = 1 \quad \psi_{A3}$, and $\psi_{C2} = 1 \quad \psi_{B2}$.

The probability of surviving from the entrance of the Delta near Mossdale Bridge (site A6, MOS) through an entire migration pathway to Chipps Island was estimated as the product of survival probabilities that trace that pathway:

$S_{AA} = S_{A6}S_{A7}S_{A8,A10}S_{A10}S_{A11}S_{A12,G2}$: Delta survival for fish that remained in the San Joaquin River past the head of Old River,

$S_{AF} = S_{A6}S_{A7}S_{A8,A10}S_{A10}S_{A11}S_{F1,G2}$: Delta survival for fish that entered Turner Cut from the San Joaquin River,

$S_{BB} = S_{A6}S_{B1}S_{B2,G2}$: Delta survival for fish that entered Old River at its head, and remained in Old River past the head of Middle River,

$S_{BC} = S_{A6}S_{B1}S_{C1,G2}$: Delta survival for fish that entered Old River at its head, and entered Middle River at its head.

The measure $S_{A8,A10}$ is the probability of surviving from Garwood Bridge (A8) to the receivers in the San Joaquin River near the Calaveras River (A10 = SJC), and includes both passing Rough and Ready Island via the San Joaquin River (ψ_{A2}) and passing it via Burns Cutoff ($\psi_{R2} = 1 \quad \psi_{A2}$):

$$S_{A8,A10} = S_{A8}\left(\psi_{A2}S_{A9} \quad \psi_{R2}S_{R1}\right).$$

In cases where detections were sparse at site C1 in route B, Delta survival could not be estimated for the Middle River subroute of route B.

The parameters $S_{A12,G2}$ and $S_{F1,G2}$ represent the probabilities of getting to Chipps Island (i.e., Mallard Island, site MAE/MAW) from sites A12 and F1, respectively. Both parameters represent multiple pathways around or through the Delta to Chipps Island (Figure 1). Fish that were detected at the A12 receivers (MacDonald Island) may have remained in the San Joaquin River all the way to Chipps Island, or they may have entered the interior Delta downstream of Turner Cut. Fish that entered the interior Delta either at Turner Cut or farther downstream may have migrated through the interior Delta to Chipps Island via Frank's Tract or Fisherman's Cut, False River, and Jersey Point; returned to the San Joaquin River via its downstream confluence with either Old or Middle River at Mandeville Island; or gone through salvage and trucking from the water export facilities. All such routes are represented in the $S_{A12,G2}$ and $S_{F1,G2}$ parameters, which were estimated directly using Submodel I (Figure 2).

Survival probabilities $S_{B2,G2}$ and $S_{C1,G2}$ represent survival to Chipps Island for fish that remained in Old River at B2 (ORS), or entered the Middle River at C1 (MRH), respectively. Fish in both these routes may have subsequently been salvaged and trucked from the water export facilities, or have migrated through the interior Delta to Jersey Point and on to Chipps Island (Figure 1). Because there were many unmonitored river junctions within the "reach" between sites B2 or C1 and Chipps Island, it was impossible to separate the probability of taking a specific pathway from the probability of survival along that pathway. Thus, only the joint probability of movement and survival to the next receivers along a route (i.e., the $\phi_{kj,hi}$ parameters defined above and in Figure 2) could be estimated. However, the overall survival probability from B2 ($S_{B2,G2}$) or C1 ($S_{C1,G2}$) to Chipps Island was estimable by summing products of the $\phi_{kj,hi}$ parameters:

$$\begin{aligned} S_{B2,G2} &= \left(\phi_{B2,D1O}\phi_{D1O,D2} + \phi_{B2,D1C}\phi_{D1C,D2}\right)\phi_{D2,G2} + \phi_{B2,E1}\phi_{E1,E2}\phi_{E2,G2} + \\ &\quad \left(\phi_{B2,B3}\phi_{B3,B4}\phi_{B4,GH} + \phi_{B2,C2}\phi_{C2,GH}\right)\psi_{G1}\phi_{G1,G2} \end{aligned}$$

and

$$\begin{aligned} S_{C1,G2} &= \left(\phi_{C1,D1O}\phi_{D1O,D2} + \phi_{C1,D1C}\phi_{D1C,D2}\right)\phi_{D2,G2} + \phi_{C1,E1}\phi_{E1,E2}\phi_{E2,G2} + \\ &\quad \left(\phi_{C1,B3}\phi_{B3,B4}\phi_{B4,GH} + \phi_{C1,C2}\phi_{C2,GH}\right)\psi_{G1}\phi_{G1,G2}. \end{aligned}$$

In cases where detections were sparse at site C1, the survival parameter $S_{C1,G2}$ was estimated directly from the model, and no attempt was made to decompose it into individual transition parameters.

Fish in the Old River route that successfully bypassed the water export facilities and reached the receivers in Old River or Middle River near Highway 4 (sites B4 or C2, respectively) may have used any of several subsequent routes to reach Chipps Island. In particular, they may have remained in Old or Middle rivers until they rejoined the San Joaquin downstream of Medford Island, and then migrated in the San Joaquin, or they may have passed through Frank's Tract and False River or Fisherman's Cut to rejoin the San Joaquin River. As described above, these routes were all included in the transition probabilities $\phi_{B4,GH}$ and $\phi_{C2,GH}$, which represent the probability of moving from site B4 or C2, respectively, to the False River junction with the San Joaquin.

Both route selection and route-specific survival were also estimated on the large routing scale, focusing on routing only at the head of Old River. The route selection parameters were defined as:

$\psi_A = \psi_{A1}$: probability of remaining in the San Joaquin River at the head of Old River

$\psi_B = \psi_{B1}$: probability of entering Old River at the head of Old River.

The probability of surviving from the entrance of the Delta (site A6, MOS) through an entire large-scale migration pathway to Chipps Island was defined as a function of the finer-scale route-specific survival probabilities and route selection probabilities:

$S_A = \psi_{A3} S_{AA} \quad \psi_{F3} S_{AF}$: Delta survival (from Mossdale to Chipps Island) for fish that remained in the San Joaquin River at the head of Old River, and

$S_B = \psi_{B2} S_{BB} \quad \psi_{C2} S_{BC}$: Delta survival for fish that entered Old River at the head of Old River.

Using the estimated migration route probabilities and route-specific survival for these two primary routes (A and B), survival of the population from A6 (Mossdale) to Chipps Island was defined as:

$$S_{Total} = \psi_A S_A \quad \psi_B S_B.$$

Survival was also estimated from Mossdale to the Jersey Point/False River junction, both by route and overall. Survival through this region ("Mid-Delta" or MD) was estimated only for fish that migrated entirely in-river, without being trucked from either of the water export facilities, because trucked fish were not required to pass the Jersey Point/False River junction in order to reach Chipps

Island. The route-specific Mid-Delta survival for the large-scale San Joaquin River and Old River routes was defined as follows:

$S_{A(MD)} = \psi_{A3} S_{AA(MD)} + \psi_{F3} S_{AF(MD)}$: Mid-Delta survival for fish that remained in the San Joaquin River past the head of Old River, and

$S_{B(MD)} = \psi_{B2} S_{BB(MD)} + \psi_{C2} S_{BC(MD)}$: Mid-Delta survival for fish that entered Old River at its head, where

$$S_{AA(MD)} = S_{A6} S_{A7} S_{A8,A10} S_{A10} S_{A11} S_{A12(MD)},$$

$$S_{AF(MD)} = S_{A6} S_{A7} S_{A8,A10} S_{A10} S_{A11} \phi_{F1,GH},$$

$$S_{BB(MD)} = S_{A6} S_{B1} \left(\phi_{B2,B3} \phi_{B3,B4} \phi_{B4,GH} + \phi_{B2,C2} \phi_{C2,GH} \right), \text{ and}$$

$$S_{BC(MD)} = S_{A6} S_{B1} \left(\phi_{C1,B3} \phi_{B3,B4} \phi_{B4,GH} + \phi_{C1,C2} \phi_{C2,GH} \right).$$

The parameter $S_{A12(MD)}$ is derived from the parameters of Submodel II:

$$S_{A12(MD)} = \phi_{A12,A13} S_{A13(MD)} + \phi_{A12,F2} S_{F2(MD)},$$

where

$$S_{A13(MD)} = \phi_{A13,GH} + \phi_{A13,A14} \phi_{A14,GH} + \phi_{A13,B4} \phi_{B4,GH} + \phi_{A13,C2} \phi_{C2,GH} + \phi_{A13,B5} S_{B5(MD)},$$

$$S_{F2(MD)} = \phi_{F2,GH} + \phi_{F2,A14} \phi_{F2,GH} + \phi_{F2,B4} \phi_{B4,GH} + \phi_{F2,C2} \phi_{C2,GH} + \phi_{F2,B5} S_{B5(MD)},$$

and

$$S_{B5(MD)} = \phi_{B5,GH} + \phi_{B5,B4} \phi_{B4,GH} + \phi_{B5,C2} \phi_{C2,GH}.$$

In cases where detections were sparse at sites downstream of A13 and at F2, the parameter $S_{A12(MD)}$ was derived as follows:

$$S_{A12(MD)} = \phi_{A12,GH} + \phi_{A12,A13} \phi_{A13,GH},$$

where $\phi_{A12,GH}$ represents the probability of moving directly from A12 to the Jersey Point/False River junction without passing A13, and $\phi_{A13,GH}$ represents the total probability of moving from A13 to the Jersey Point/False River junction. In cases where detections were sparse at the Highway 4 sites (B4, C2) in the Old River route, the subroute-specific estimates of Mid-Delta survival within the Old River route were derived as:

$$S_{BB(MD)} = S_{A6} S_{B1} \phi_{B2,GH}, \text{ and}$$

$$S_{BC(MD)} = S_{A6} S_{B1} \phi_{C1,GH},$$

where $\phi_{B2,GH}$ and $\phi_{C1,GH}$ were estimated in the model directly.

Total Mid-Delta survival (i.e., from Mossdale to the Jersey Point/False River junction) was defined as $S_{Total(MD)} = \psi_A S_{A(MD)} \quad \psi_B S_{B(MD)}$. Mid-Delta survival was estimated only for those release groups with sufficient tag detections to model transitions through the entire south Delta and lower San Joaquin River and to the Jersey Point/False River junction. In cases where detections at False River were too sparse to be modeled, the estimate of survival through the Mid-Delta region should be interpreted as survival to Jersey Point, rather than to the Jersey Point/False River junction. In cases where detections were too sparse at the Middle River Head (C1) receivers in the Old River route to estimate transition probabilities from that site, no estimate was available of Mid-Delta survival for the Middle River component of the Old River route.

Survival was also estimated through the southern portions of the Delta ("South Delta" or SD), both within each primary route and overall:

$$S_{A(SD)} = S_{A6} S_{A7} S_{A8,A10} S_{A10} S_{A11}, \text{ and}$$

$$S_{B(SD)} = S_{A6} S_{B1} \left(\psi_{B2} S_{B2(SD)} + \psi_{C2} S_{C1(SD)} \right),$$

where $S_{B2(SD)}$ and $S_{C1(SD)}$ are defined as:

$$S_{B2(SD)} = \phi_{B2,B3} \phi_{B3,B4} \quad \phi_{B2,C2} \quad \phi_{B2,D1O} \quad \phi_{B2,D1C} \quad \phi_{B2,E1}, \text{ and}$$

$$S_{C1(SD)} = \phi_{C1,B3}\phi_{B3,B4} \quad \phi_{C1,C2} \quad \phi_{C1,D1O} \quad \phi_{C1,D1C} \quad \phi_{C1,E1}.$$

Total survival through the South Delta was defined as:

$$S_{Total(SD)} = \psi_A S_{A(SD)} \quad \psi_B S_{B(SD)}.$$

In cases where detection data were too sparse in the Old River route to estimate transitions to the water export facilities or Highway 4 from both Old River South (B2) and Middle River Head (C1) (e.g., first release group), estimates of South Delta survival were not available for either the Old River route or overall.

The probability of reaching Mossdale from the release point at Durham Ferry, $\phi_{A1,A6}$, was defined as the product of the intervening reach survival probabilities:

$$\phi_{A1,A6} = \phi_{A1,A2} S_{A2} S_{A3} S_{A4} S_{A5}.$$

This measure reflects a combination of mortality and residualization upstream of Old River.

Individual detection histories (i.e., capture histories) were constructed for each tag as described above. More details and examples of detection history construction and model parameterization are available in USBR (2018a). Under the assumptions of common survival, route selection, and detection probabilities and independent detections among the tagged fish in each release group, the likelihood function for the survival model for each release group is a multinomial likelihood with individual cells denoting the possible capture histories.

Parameter Estimation

The multinomial likelihood model described above was fit numerically to the observed set of detection histories according to the principle of maximum likelihood using Program USER software, developed at the University of Washington (Lady et al. 2009). Point estimates and standard errors were computed for each parameter. Standard errors of derived performance measures were estimated using the delta method (Seber 2002: 7-9). Sparse data prevented some parameters from being freely estimated for some release groups. Transition, survival, detection, and route selection probabilities were fixed to 1 or 0 in the USER model as appropriate, based on the observed detections. The model was fit separately for each release group. For each release group, the complete data set that included

possible detections from predatory fish was analyzed separately from the reduced data set that was restricted to detections classified as steelhead detections. Population-level estimates of parameters and performance measures were estimated as weighted averages of the release-specific estimates, using weights proportional to release size.

In cases in which a survival or transition parameter was estimated at 0, the 95% upper bound on survival was estimated using a binomial error structure (Louis 1981); correction for tag failure was calculated using an assumed travel time that was based on travel time either from other release groups, from previous years, or to nearby sites, together with the fitted tag survival model. Likewise, in cases in which a survival parameter was estimated at 1, the 95% lower bound on survival was estimated.

The significance of the radial gates status on arrival at the outside receiver (RGU, site D1) was assessed for the each release group separately using a likelihood ratio test to indicate a significant difference in model fit (Sokal and Rohlf 1995). If the effect of the gates was found to be insignificant using this criterion, then a simplified model was used for parameter estimation in which $\phi_{kj,D1O} = \phi_{kj,D1C}$ for station k in route j, and $\phi_{D1O,D2} = \phi_{D1C,D2}$. The overall probability of transitioning from station k in route j to site D1 was modeled as $\phi_{kj,D2} = \phi_{kj,D1O}$ $\phi_{kj,D1C}$ under this simplified model. A likelihood ratio test was also used to test for the significance of route effects on the transition probabilities through the water export facilities: $\phi_{D1O,D2}$, $\phi_{D1C,D2}$ (or $\phi_{D1,D2}$ if the gate effect test was not significant), $\phi_{E1,E2}$, and $\phi_{E2,G2}$. Likewise, a likelihood ratio test was used to test for the significance of route effects on the transition probability from Jersey Point to Chipps Island ($\phi_{G1,G2}$). Only parameters that could be estimated separately in both routes were included in testing. All testing was performed at the 95% level (α=0.05). For each model, goodness-of-fit was assessed visually using Anscombe residuals (McCullagh and Nelder 1989). The sensitivity of parameter and performance metric estimates to inclusion of detection histories with large absolute values of Anscombe residuals was examined for each release group individually.

For each release group, the effect of primary route (San Joaquin River or Old River) on estimates of survival to Chipps Island was tested with a two-sided *Z*-test on the log scale:

$$Z = \frac{\ln\left(\hat{S}_A\right) - \ln\left(\hat{S}_B\right)}{\sqrt{\hat{V}}},$$

where

$$V = \frac{Var\left(\hat{S}_A\right)}{\hat{S}_A^2} + \frac{Var\left(\hat{S}_B\right)}{\hat{S}_B^2} - \frac{2Cov\left(\hat{S}_A, \hat{S}_B\right)}{\hat{S}_A \hat{S}_B}.$$

The parameter *V* was estimated using Program USER. Estimates of survival to Jersey Point and False River (i.e., $S_{A(MD)}$ and $S_{B(MD)}$) were also compared in this way. Also tested was whether tagged steelhead showed a route preference at the head of Old River, using a two-sided *Z*-test with the test statistic:

$$Z = \frac{\hat{\psi}_A - 0.5}{SE\left(\hat{\psi}_A\right)}.$$

Statistical significance was tested at the 5% level (α=0.05). Tests that were significant only at the 10% level (α=0.10) were noted.

Analysis of Tag Failure

Three in-tank tag-life studies of VEMCO V5 tags were implemented for the 2016 steelhead survival study. Each study used 33 acoustic tags. Tags in the February study were activated on 24 February 2016, and were last detected on 10 May 2016. The April tag-life study used tags that were activated on 5 April 2016, and last detected on 11 June 2016. The tags in the May tag-life study were activated on 8 May 2016, and last detected on 18 July 2016. Total time of battery activation was used in the tag-life study. Tags were monitored in tanks using fixed-site hydrophones and receivers, and were pooled across tanks for analysis.

Six acoustic hydrophones and receivers were used in the 2016 tag-life study. Receiver 300959 failed in the May tag-life study, resulting in missing failure times for the 17 tags monitored on this receiver. The last detection times for these 17 tags was at day 55.82 after tag activation, compared to a median tag failure time among the remaining 82 tags of approximately 64 days (pooled over all three studies). Because receiver 300959 failed relatively early compared to observed failure of tags monitored on other receivers, and because the equipment failure was in the monitoring equipment rather than the tag battery, the last detection times recorded for these 17 tags were expected to have been unrelated to the actual failure time. These 17 tags were omitted from analysis of tag failure.

For each tag-life study, the observed tag survival was modeled using the 4-parameter vitality curve (Li and Anderson, 2009). Tag failure times were truncated at day 69 to improve model fit (USBR 2018b). The improvement in model fit attained by stratifying by tag-life study was assessed using the Akaike Information Criterion (AIC; Burnham and Anderson, 2002).

The fitted tag survival model from the tag failure data was used to adjust estimated fish survival and transition probabilities for premature tag failure using methods adapted from Townsend et al. (2006). In Townsend et al. (2006), the probability of tag survival through a reach is estimated based on the average observed travel time of tagged fish through that reach. For this study, travel time and the probability of tag survival to Chipps Island were estimated separately for the different routes (e.g., San Joaquin route vs. Old River route). Subroutes using truck transport were handled separately from subroutes using only in-river travel. Standard errors of the tag-adjusted fish survival and transition probabilities were estimated using the inverse Hessian matrix of the fitted joint fish-tag survival model. The additional uncertainty introduced by variability in tag survival parameters was not estimated, with the result that standard errors may have been slightly low. In previous studies, however, variability in tag-survival parameters has been observed to contribute little to the uncertainty in the fish survival estimates when compared with other, modeled sources of variability (Townsend et al. 2006); thus, the resulting bias in the standard errors was expected to be small.

Analysis of Surgeon Effects

The potential effects of different surgeons (i.e., taggers) on steelhead survival were analyzed in several ways. The simplest method used contingency tests of independence on the number of tag detections at key detection sites throughout the study area. Specifically, a lack of independence (i.e., heterogeneity) between the detections distribution and surgeon was tested using a chi-squared test (α=0.05; Sokal and Rohlf, 1995). Lack of independence may be caused by differences in survival, route selection, or detection probabilities among surgeons. Detections from those downstream sites with sparse data were omitted for this test in order to achieve adequate cell counts.

A second method of assessing possible surgeon effects visually compared estimates of cumulative steelhead survival throughout the study area among surgeons; an F-test was used to test for a surgeon effect on cumulative survival through each major route (routes A and B). Although differences in cumulative survival can provide compelling indication of possible surgeon effects on survival, they are inconclusive alone, because survival differences in the first few reaches can persist in estimates of cumulative survival even if individual reach survival estimates are equal among surgeons in

those downstream reaches. Thus, it is necessary to augment the cumulative survival assessment with additional evidence. Accordingly, a third method of assessment used Analysis of Variance to test for a surgeon effect on individual reach survival estimates. Finally, the nonparametric Kruskal-Wallis rank sum test (Sokal and Rohlf 1995, ch. 13) was used to test for whether one or more surgeons performed consistently more poorly than others, based on individual reach survival or transition probabilities through key reaches. In the event that survival was different for the steelhead tagged by a particular surgeon, the model was refit to the pooled release groups without tags from the surgeon in question, and the difference in survival estimates due to the surgeon was tested using a two-sided Z-test on the lognormal scale. The reduced data set (without predator detections), pooled over release groups, was used for these analyses.

Analysis of Travel Time

Travel time was measured from release at Durham Ferry to each detection site. Travel time was also measured through each reach for tags detected at the beginning and end of the reach, and summarized across all tags with observations. Travel time between two sites was defined as the time delay between the beginning of the detections at the first site and the first detection at the second site. In cases where the tagged fish was observed to make multiple visits to a site, the final visit was used for travel time calculations. When possible, travel times were measured separately for different routes through the study area. Detection sites, routes, or transitions that were omitted from the survival model because of sparse data were also omitted from the travel time analysis. The harmonic mean was used to summarize travel times.

Route Selection Analysis

A temporary rock barrier was installed at the head of Old River through part of the 2016 tagging study, effectively blocking most access to the upper reaches of Old River when the barrier was in place. Culverts in the barrier allowed water and fish to pass through the barrier, but few (10) tagged steelhead were observed at the upper Old River detection sites when the barrier was in place in 2016. Analysis of route selection at the head of Old River used those fish that passed before the barrier was installed. Route selection was also analyzed for the Turner Cut junction. In both cases, acoustic tag detections used in these analysis were restricted to those detected at the acoustic receiver arrays located just downstream of the junction in question: SJL (model code A7) or ORE (B1) for the head of Old River junction, and MAC (A12) or TCE/TCW (F1) for the Turner Cut junction. Tags were further restricted to those whose final pass of the junction came from either upstream sites or from the opposite leg of the

junction; tags whose final pass of the junction came either from downstream sites or from a previous visit to the same receivers (e.g., repeated visits to the SJL receivers for the head of Old River junction) were excluded from this analysis. Tags were restricted in this way to limit the delay between initial arrival at the junction, when hydrologic covariates were measured, and the tagged fish's final route selection at the junction. Predator-type detections were excluded.

As in previous years (USBR 2018a, 2018b, 2018c; Buchanan 2018a, 2018b), the effects of variability in hydrologic conditions on route selection at the head of Old River and Turner Cut were explored using statistical generalized linear models (GLMs) with a binomial error structure and logit link (McCullagh and Nelder, 1989). Hydrologic metrics used in the analyses are defined below for each junction. In addition to the hydrologic metrics, fork length at tagging (L), release group (RG), and time of day of arrival at the junction were also considered as factors potentially affecting route selection. Time of day of arrival was measured as dawn, day, dusk, or night. Dawn was assumed to end at sunrise, and dusk began at sunset. A separate measure indicated whether fish arrived at the junction during the day.

Head of Old River

The head of Old River barrier closure date during installation was 1 April 2016; only those tag detections from either the San Joaquin River receivers at Lathrop (SJL, site A7) or the Old River receivers at Old River East (ORE, site B1) from before 1500 hours on that date were used in the covariate analysis of route selection at the head of Old River. The estimated detection probabilities at both these sites were 1.0 for all release groups, so no detections from downstream sites in either route were needed to augment the route selection data. All tags detected at SJL or ORE before barrier closure date came from the February and March release groups. Tags used in the analysis were restricted to those estimated to have spent no more than 3 hours between passing the head of Old River junction and being detected at the receivers at either SJL or ORE on their final pass through the river junction, using linear interpolation and the average travel rate through that reach for the tag in question. Tags were restricted in this way to limit the time delay between arrival at the junction and final route selection. When restricted to this set of the tags observed passing the head of Old River before barrier closure, there were 88 tags detected at the San Joaquin River receiver (SJL), and 442 tags detected at the Old River receiver (ORE), providing at most 88 degrees of freedom for the route selection analysis.

The same set of possible covariates were formatted for the simple route selection analysis at the head of Old River in 2016 as in previous years: measures of flow, water velocity, and river stage at the estimated time of arrival at the head of Old River junction, the 15-minute change in these measures, daily export rates from the Central Valley Project and State Water Project on the day of arrival at the junction, fish fork length at the time of tagging, and time of day at fish arrival at the junction. Methods used to compile and format the data were those used in previous years; see USBR (2018c) for more details. As in 2014 and 2015, no flow or water velocity data were available from the Lathrop gaging station (SJL) in the San Joaquin River in 2016; this lack of data meant that the flow proportion into the San Joaquin River was also missing for 2016. Flow, velocity, and river stage data were available from the Mossdale gaging station (MSD), and these data were used as covariates in 2016 (Table 2). The OH1 gaging station was located 0.86–0.92 km upstream of the ORE receivers; the SJL gaging station was located 0.30–0.40 km from the SJL receivers. The covariates considered were:

- C_{SJL}, ΔC_{SJL} = SJL river stage (C) and the 15-minute change in SJL river stage at the estimated time of tag passage of the head of Old River junction;
- Q_{OH1}, ΔQ_{OH1}, V_{OH1}, ΔV_{OH1}, C_{OH1}, ΔC_{OH1} = OH1 river flow (i.e., discharge: Q), water velocity (V), and river stage (C), and the 15-minute changes in OH1 flow, water velocity, and river stage at the estimated time of tag passage of the head of Old River junction;
- Q_{MSD}, ΔQ_{MSD}, V_{MSD}, ΔV_{MSD}, C_{MSD}, ΔC_{MSD} = MSD river flow (i.e., discharge: Q), water velocity (V), and river stage (C), and the 15-minute changes in MSD flow, water velocity, and river stage at the estimated time of tag passage of the head of Old River junction;
- E_{CVP}, E_{SWP} = Daily export rate at the CVP and SWP at the estimated time of tag passage of the head of Old River junction, as reported by Dayflow (https://water.ca.gov/Programs/Environmental-Services/Compliance-Monitoring-And-Assessment/Dayflow-Data);
- P_{CVP} = Percent of combined daily CVP/SWP export rate that was attributable to the CVP; = E_{CVP} /(E_{CVP} + E_{SWP});
- *day* = Indicator variable defined to be 1 if tag was estimated to have passed the head of Old River junction during the day, and 0 otherwise;
- *Time of day* = Categorical variable for the time of day of tag passage of the head of Old River, defined as *dawn, day, dusk*, or *night*;
- L = Fork length at tagging;
- RG = Release group (categorical variable).

In addition to the covariates that represented environmental conditions measured at individual monitoring stations, two additional covariates were developed that combined flow measures at the MSD and OH1 monitoring stations. The difference between the flow at MSD and flow at OH1 at the time of estimated passage of head of Old River junction was used as a first-order approximation of flow at the SJL station at the same time, in the absence of measured flow data from SJL:

$$qQ_{SJL} = Q_{MSD} \quad Q_{OH1},$$

where "qQ" indicates a modeled approximation of flow (Q). This modeled flow at SJL makes the simplifying assumption that there was no loss or gain in flow between the MSD station and the SJL and OH1 stations.

Another new covariate is the signed ratio of flow at OH1 to the flow at MSD, r_Q. To avoid complications of interpretation when flow at these two stations was measured as moving in different directions (i.e., positive flow measure at one station and negative flow measure at the other station), this ratio measure was defined to be 0 when the two flow measurements had different signs:

$$r_Q = \begin{cases} \dfrac{Q_{OH1}}{Q_{MSD}}, & Q_{MSD}, Q_{OH1} \text{ both } > 0; \\ -1 \times \dfrac{Q_{OH1}}{Q_{MSD}}, & Q_{MSD}, Q_{OH1} \text{ both } < 0; \\ 0, & Q_{MSD} < 0 \text{ or } Q_{OH1} < 0 \text{ but not both.} \end{cases}$$

If all flow passing the OH1 gaging station in Old River either came from or went to the San Joaquin River upstream of the MSD gaging station, then the magnitude of the measure r_Q is always ≤ 1 and can be interpreted as the OH1 proportion of MSD flow, approximately. However, under some stages of the tidal cycle, water directed downstream in Old River past the OH1 station may have come partially from the San Joaquin River past MSD and partially from the lower San Joaquin River past the SJL gaging station; in this case, r_Q is sometimes > 1, and it is misleading to interpret it as a proportion of MSD flow. For this reason, the measure r_Q is more properly referred to as the OH1:MSD flow ratio, or more simply the "flow ratio."

The route selection analysis in previous years included a factor variable (U) that indicated whether flow at OH1 was negative at the time of tag arrival at the river junction. In 2016, OH1 flow was positive for all but 4 records used in the route selection analysis, and so this variable was omitted from analysis.

As in previous years, all continuous covariates were standardized, i.e.,

$$\tilde{x}_{ij} = \frac{x_{ij} - \overline{x}_j}{s(x_j)}$$

for the observation x of covariate j from tag i. Categorical variables (e.g., release group, time of day) were not standardized.

The form of the generalized linear model was

$$\ln\left(\frac{\psi_{iA}}{\psi_{iB}}\right) = \beta_0 + \beta_1\left(\tilde{x}_{i1}\right) + \beta_2\left(\tilde{x}_{i2}\right) + \cdots + \beta_p\left(\tilde{x}_{ip}\right)$$

where $\tilde{x}_{i1}, \tilde{x}_{i2}, \ldots, \tilde{x}_{ip}$ are the observed values of standardized covariates for tag i (covariates 1, 2, …, p, see below), ψ_{iA} is the predicted probability that the fish with tag i selected route A (San Joaquin River route), and $\psi_{iB} = 1 - \psi_{iA}$ (B = Old River route). Route choice for tag i was determined based on detection of tag i at either site A7 (route A) or site B1 (route B).

Single-variate regression was performed first, and covariates were ranked by P-values from the appropriate F-test (if the model was over-dispersed) or χ^2 test otherwise (McCullagh and Nelder 1989). Significance was determined at the experimentwise level of 5%; the Bonferroni correction for multiple comparisons was used within each step of the stepwise regression (Sokal and Rohlf 1995). In the event that significant associations were found from the single-variate models, covariates were then analyzed together in a series of multiple regression models. Because of high correlation between flow and velocity measured from the same site, the covariates flow and velocity were analyzed in separate models. River stage was analyzed both separately from flow, velocity, and the OH1:MSD flow ratio, and together with flow. A flow ratio model was developed using the OH1:MSD flow ratio, r_Q. The general forms of the various multivariate models were:

Flow model: $Q_{OH1} + \Delta Q_{OH1} + Q_{MSD} + \Delta Q_{MSD} + day + E_{CVP} + E_{SWP} + P_{CVP} + L + RG$

Flow ratio model: $r_Q + day + E_{CVP} + E_{SWP} + P_{CVP} + L + RG$

Velocity model: $V_{OH1} + V_{MSD} + \Delta V_{OH1} + \Delta V_{MSD} + day + E_{CVP} + E_{SWP} + P_{CVP} + L + RG$

Stage model:

$$C_{MSD} + \Delta C_{MSD} + C_{SJL} + \Delta C_{SJL} + C_{OH1} + \Delta C_{OH1} + day + E_{CVP} + E_{SWP} + P_{CVP} + L + RG$$

Flow + Stage model:

$$Q_{OH1} + Q_{MSD} + \Delta Q_{OH1} + \Delta Q_{MSD} + C_{MSD} + \Delta C_{MSD} + C_{SJL} + \Delta C_{SJL} + C_{OH1} + \Delta C_{OH1} + day + E_{CVP} + E_{SWP} + P_{CVP} + L + RG.$$

An alternative flow model was developed that used the modeled SJL flow (qQ_{SJL}) in place of Q_{OH1} and Q_{MSD}.

Backwards selection with F-tests was used to find the most parsimonious model in each category (flow, flow ratio, velocity, stage, and stage + flow) that explained the most variation in the data (McCullagh and Nelder 1989). Main effects were considered using the full model; two-way interaction effects were considered using the reduced model found from backwards selection on the main effects model. The model that resulted from the selection process in each model category was compared using an F-test to the full model (or a χ^2-test if the data were not overdispersed from the model) from that category to ensure that all significant main effects were included. AIC and assessment of model fit were used to select among the flow, flow ratio, velocity, stage, and flow + stage models (Burnham and Anderson 2002). Model fit was assessed by grouping data into discrete classes according to the independent covariate, and comparing predicted and observed frequencies of route selection into the San Joaquin using the Pearson chi-squared test (Sokal and Rohlf 1995). The variance inflation factor (VIF) for each covariate was also calculated as a measure of multicollinearity among the covariates, and models with maximum VIF greater than 10 or mean VIF considerably greater than 1 were excluded (Kutner et al. 2004).

Turner Cut Junction

The acoustic receiver arrays MAC (A12) and TCE/TCW (F1) were located 1.2–3.4 km downstream of the Turner Cut junction; detections at the SJS receiver array (A11), 0.39 km upstream of the Turner Cut junction, were also used. In addition to the data restrictions described above, tags were limited to those whose observed travel time from the SJS receiver to either MAC or TCE/TCW was ≤ 8 hours. Also excluded were tags whose last detection before their final visit to the MAC or TCE/TCW receivers came from the opposite leg of the river junction. These requirements were used to ensure that environmental conditions measured at the time of departure from SJS represented conditions when fish reached the Turner Cut junction.

The covariates used in previous years were again used for the 2016 analysis: measures of river discharge (flow), river velocity, and river stage measured at the TRN gaging station at the time of tag departure from SJS (model code A11), the 15-minute change in flow, velocity, and stage at TRN, measures of the average magnitude (i.e., the Root Mean Square, or RMS) of flow and velocity at the SJG gaging station (Table 2) during the tagged individual's transition from the SJG telemetry station (model code A8) to SJS, daily export rates at the CVP and SWP upon tag departure from SJS, the CVP proportion of combined exports from the CVP and SWP, fork length at tagging, release group, and time of day of arrival at the junction. The covariates considered were:

- Q_{TRN}, ΔQ_{TRN}, V_{TRN}, ΔV_{TRN}, C_{TRN}, ΔC_{TRN} = TRN river flow (i.e., discharge: Q), water velocity (V), and river stage (C), and the 15-minute changes in TRN flow, water velocity, and river stage at the observed time of tag departure from the SJS receivers;
- Q_{SJG}, V_{SJG} = Root Mean Square (RMS) of San Joaquin River flow (Q) and water velocity (V) measured at the SJG gaging station at Garwood Bridge, from the time of the final tag detection at the SJG telemetry station (site A8) until the observed time of tag departure from SJS;
- U = Indicator variable defined to be 1 if flow at TRN was negative, and 0 otherwise
- E_{CVP}, E_{SWP} = Daily export rate at the CVP and SWP on the day of tag departure from the SJS receivers, as reported by Dayflow;
- P_{CVP} = Percent of combined daily CVP/SWP export rate that was attributable to the CVP; = E_{CVP} /(E_{CVP} + E_{SWP});
- day = Indicator variable defined to be 1 if tag departed the SJS receivers during the day, and 0 otherwise;

- *Time of day* = Categorical variable for the time of day of tag departure from the SJS receivers, defined as *dawn, day, dusk*, or *night*;
- L = Fork length at tagging;
- RG = Release group (categorical variable).

The TRN gaging station was located 0.13–0.19 km northeast of the TCE and TCW receivers (i.e., between the Turner Cut junction with the San Joaquin River and the TCE/TCW receivers (Table 2). Negative flow at the TRN station was interpreted as being directed into the interior Delta, away from the San Joaquin River (Cavallo et al. 2013). No gaging station was available in the San Joaquin River close to the MAC receivers. Thus, although measures of hydrologic conditions were available in Turner Cut, measures of flow proportion into Turner Cut were not available. The SJG gaging station was approximately 14 km upstream from the Turner Cut junction. More details on the definition and construction of the covariates are available in the report for the 2012 study (USBR 2018b). One change was made in the data formatting procedure from the 2012 analysis. In the 2012 analysis, environmental conditions were measured at the estimated time of arrival at the Turner Cut junction, based on observed travel time and travel distance to the TCE/TCW or MAC receivers. For the 2016 analysis, environmental conditions were measured instead at the observed time of tag departure from the SJS (A11) receivers, which exhibited less uncertainty than estimates of junction arrival time; this approach mirrors that used in 2015 (Buchanan 2018b).

As in previous years, all continuous covariates were standardized, i.e.,

$$\tilde{x}_{ij} = \frac{x_{ij} - \overline{x}_j}{s(x_j)}$$

for the observation x of covariate j from tag i. Categorical variables (e.g., release group, time of day) were not standardized.

The form of the generalized linear model was

$$\ln\left(\frac{\psi_{iA}}{\psi_{iF}}\right) = \beta_0 + \beta_1\left(\tilde{x}_{i1}\right) + \beta_2\left(\tilde{x}_{i2}\right) + \cdots + \beta_p\left(\tilde{x}_{ip}\right)$$

where $\tilde{x}_{i1}, \tilde{x}_{i2}, \ldots, \tilde{x}_{ip}$ are the observed values of standardized covariates for tag i (covariates 1, 2, …, p, see below), ψ_{iA} is the predicted probability that the fish with tag i selected route A (San Joaquin River route), and $\psi_{iF} = 1 \quad \psi_{iA}$ (F = Turner Cut route). Route choice for tag i was determined based on detection of tag i at either site A12 (route A) or site F1 (route F).

Single-variate regression was performed first, and covariates were ranked by P-values from the appropriate F-test (if the model was over-dispersed) or χ-square test otherwise (McCullagh and Nelder 1989). Significance was determined at the experimentwise level of 5%; the Bonferroni correction for multiple comparisons was used within each step of the stepwise regression (Sokal and Rohlf 1995). If individual covariates were found to have significant associations with route selection, covariates were then analyzed together in a series of multiple regression models. Because of high correlation between flow and velocity measured from the same site, the covariates flow and velocity were analyzed in separate models. River stage was analyzed both separately from flow and velocity, and together with flow. The exception was that the flow index in the reach from SJG to the TCE/TCW or MAC receivers (Q_{SJG}) was included in the river stage models. The general forms of the three multivariate models were:

Flow model: $Q_{TRN} + Q_{SJG} + \Delta Q_{TRN} + U + day + E_{CVP} + E_{SWP} + P_{CVP} + L + RG$

Velocity model: $V_{TRN} + V_{SJG} + \Delta V_{TRN} + U + day + E_{CVP} + E_{SWP} + P_{CVP} + L + RG$

Stage model: $C_{TRN} + \Delta C_{TRN} + Q_{SJG} + day + E_{CVP} + E_{SWP} + P_{CVP} + L + RG$

Flow + Stage model:

$$Q_{TRN} + Q_{SJG} + \Delta Q_{TRN} + U + C_{TRN} + \Delta C_{TRN} + day + E_{CVP} + E_{SWP} + P_{CVP} + L + RG.$$

Backwards selection with F-tests was used to find the most parsimonious model in each category (flow, velocity, stage, and flow + stage) that explained the most variation in the data (McCullagh and Nelder 1989). Main effects were considered using the full model; two-way interaction effects were considered using the reduced model found from backwards selection on the main effects model. The model that resulted from the selection process in each category (flow, velocity, stage, or flow + stage) was compared using an F-test to the full model (or a χ^2-test if the data were not

overdispersed from the model) from that category to ensure that all significant main effects were included. AIC was used to select among the flow, velocity, and stage models (Burnham and Anderson 2002). Model fit was assessed by grouping data into discrete classes according to the independent covariate, and comparing predicted and observed frequencies of route selection into the San Joaquin using the Pearson chi-squared test (Sokal and Rohlf 1995).

Survival through Facilities

A supplemental analysis was performed to estimate the probability of survival of tagged fish from the interior receivers at the water export facilities through salvage to release on the San Joaquin or Sacramento rivers. Overall salvage survival from the interior receivers at site $k2$, $S_{k2(salvage)}$ (k=D, E), was defined as

$$S_{k2(salvage)} = \phi_{k2,GH} + \phi_{k2,G2} + \phi_{k2,T1} + \phi_{k2,T2} + \phi_{k2,T3},$$

where $\phi_{k2,G2}$ is as defined above, and $\phi_{k2,GH}$, $\phi_{k2,T1}$, $\phi_{k2,T2}$, and $\phi_{k2,T3}$ are the joint probabilities of surviving and moving from site $k2$ to the Jersey Point/False River junction (GH), Threemile Slough (T1), Montezuma Slough (T2), and Spoonbill Slough (T3), respectively, without going on to Chipps Island. The subset of detection histories that included detection at site $k2$ (k=D, E) was used for this analysis; predator-type detections were excluded. Detections from the full data set were used to estimate the detection probability at sites G1, G2, H1, T1, T2, and T3, although only data from tags detected at either D2 or E2 were used to estimate salvage survival. Because there were many tags detected at H1 that were later detected elsewhere such that their H1 detections were not used in the full survival model, all presumed steelhead tags ever detected at H1 were used to estimate the detection probability at H1; only detections from the final visit to H1 were used for detection probability estimation. The same procedure was used for estimating the detection probability at sites T1, T2, and T3. Detections at G1 and G2 were treated in the same way as in the full survival model, namely, detections from the lines forming the dual array at each site were pooled and these sites were treated as single arrays in the salvage survival model. The detection probability at Chipps Island was estimated based on all tags detected at Benicia Bridge (G3), as in the full survival model. Profile likelihood was used to estimate the 95% confidence intervals for both $S_{D2(salvage)}$ and $S_{E2(salvage)}$ when those parameters were estimated freely; in the event that the parameter estimates were on the boundary of the permissible interval (i.e.,

either 0 or 1), the sample size and the 95% upper bound (for a point estimate of 0) or the 95% lower bound (for a point estimate of 1) were reported.

Comparison among Release Groups

In order to address the issue of whether a single release group consistently had higher or lower survival and transition probability estimates compared to the other two release groups, parameter estimates were compared using a two-way analysis of variance and F-test (Sokal and Rohlf 1995). Only survival parameters representing non-overlapping regions, and transition probabilities for non-competing reaches, were used in this analysis; reaches considered were further limited to those with at least 5 tags detected per release group at the upstream end of the reach. The parameters considered were: transition probability from the release site at Durham Ferry to the first downstream detection site ($\phi_{A1,A2}$), reach-specific survival from Durham Ferry Downstream (A2) to the Turner Cut junction (A12, F1) ($S_{A2},\ldots,S_{A11}$), overall survival from MacDonald Island (A12) to Chipps Island ($S_{A12,G2}$) and from Turner Cut (F1) to Chipps Island ($S_{F1,G2}$), survival in Old River from the receivers near its head (B1) to the receivers near the head of Middle River (B2, C1) (S_{B1}), and overall survival from the Old River South receivers (B2) to Chipps Island ($S_{B2,G2}$). Both parameter and release group were treated as factors. In the event of a significant F-test indicating a consistent effect of release group on parameter estimates, three two-sided pairwise *t*-tests were used to test for comparisons between pairs of release groups. Significance was assessed at the testwise 10% level.

Linear contrasts were used to test whether estimates of survival in key regions and routes were different for one release group compared to the others. In particular, for release group i ($i=1,2,3$) and survival parameter θ, the linear contrast $L_{i\theta}$ was estimated as:

$$\hat{L}_{i\theta} = \hat{\theta}_i \quad 0.5\sum_{j\neq i}\hat{\theta}_j \ .$$

For each release group i, $\hat{L}_{i\theta}$ was compared to 0 using a Z-test. The survival parameters considered were the composite parameters $\phi_{A1,A6}$, S_A, S_B, and overall survival S_{Total}. The Bonferroni multiple comparison correction was used for 12 tests with a 10% experimentwise significance level (Sokal and Rohlf, 1995). A contrast that is positive (negative) and significantly different from 0 indicates that the release in question had higher (lower) survival than the other two release groups.

Results

Detections of Acoustic-Tagged Fish

A total of 1,440 tags were released in juvenile steelhead at Durham Ferry in 2016 and used in the survival study. Of these, 1,331 (92%) were detected on one or more receivers either upstream or downstream of the release site (Table 5), including any predator-type detections. A total of 1,300 (90%) were detected at least once downstream of the release site, and 1,020 (71%) were detected in the study area from Mossdale to Chipps Island (Table 5). One hundred thirty (130) tags were detected upstream of the release site; 99 of these were also detected downstream of the release site. A total of 21 tags were detected at Mossdale or downstream without having been detected between the Durham Ferry release site and Mossdale.

Overall, there were 630 tags detected on one or more receivers in the San Joaquin River route downstream of the head of Old River, including possible predator detections (Table 5). In general, tag detections decreased within each migration route as distance from the release point increased, after fish reached Mossdale. Of the 630 tags detected in the San Joaquin River route, all but one were detected on the receivers near Lathrop, CA (SJL); the single tag that was not detected at SJL was observed at Turner Cut (F1) and Calaveras River (A10) after taking the Old River route at the head of Old River and passing the Highway 4 receiver on Middle River (MR4). A total of 572 tags were detected on one or more of the receivers used in the predator removal study (RS4–RS10); 496 were detected on one or more receivers near Stockton, CA (SJG, SJNB, or RRI); 481 were detected on the receivers at Calaveras River or near the Turner Cut (SJC, SJS, MAC, or TCE/TCW); and 328 were detected at Medford Island or Columbia Cut (MFE/MFW or COL) (Table 6). A total of 289 tags were detected at either Disappointment Slough or the northern Old River site (SJD or OSJ) (Table 6); 2 of those tags had been observed taking the Old River route at the head of Old River. The majority of the tags from the February release group (release 1) that were detected in the San Joaquin River downstream of the head of Old River were not assigned to the San Joaquin River route for the survival model, because they were subsequently detected in the Old River route or upstream of Old River (Table 5). Most of the tags detected in the San Joaquin River route from the March and April release groups (releases 2 and 3) were also assigned to that route for survival analysis (Table 5). Overall, 521 tags were assigned to the San Joaquin River route for the survival model, mostly from the April release group (Table 5). One additional tag was detected in the San Joaquin River route but was captured in the Mossdale trawl before its San Joaquin River route detections, and its detection history was right-censored (i.e., truncated) at site A6 (MOS); this tag was

not included in the total 521 tags assigned to the San Joaquin River route. Of the 521 tags, 143 were detected at the receivers in Turner Cut, although 16 of those tags were subsequently detected in the San Joaquin River, and so were not assigned to the Turner Cut route for analysis. Of the 521 tags assigned to the San Joaquin River route, 71 were detected in Columbia Cut (COL, site F2), 57 at the northern Middle River receivers (MID, site C3), 48 at the northern Old River receivers (OSJ, site B5), 60 at the Old or Middle River receivers near Highway 4 (OR4 and MR4, sites B4 and C2), 49 at West Canal (WCL, site B3), and 50 at the water export facilities (including the radial gates at the entrance to the Clifton Court Forebay) (Table 6). A total of 293 San Joaquin River route tags were detected at the Jersey Point/False River receivers, including 65 on the False River receivers (Table 6). However, most of the tags detected at False River were later detected either at Jersey Point or Chipps Island, and so only one tag detected at False River from the San Joaquin River route was available for use in the survival model (Table 7). Forty-four (44) tags from the San Joaquin River route were detected at Threemile Slough; all but two had come from the Disappointment Slough receivers, although some had intervening detections at Jersey Point. One Threemile Slough tag came from the northern Old River site (OSJ), and one came from the CVP holding tank. A total of 291 San Joaquin River route tags were eventually detected at Chipps Island, including predator-type detections, mostly from the April release group (Table 6).

The majority of the tags from the February and March release groups that were detected downstream of the head of Old River were detected in the Old River route (472 tags); the April release group had many fewer tags detected in the Old River route compared to the San Joaquin River route (19 vs 415) (Table 5). All 491 tags detected in the Old River route were detected at the Old River East receivers near the head of Old River; 479 were detected near the head of Middle River, 417 at the receivers at the water export facilities, 118 at West Canal, and 21 at the Old or Middle River receivers near Highway 4 in the interior Delta (Table 6). The majority of the tags detected at West Canal entered the interior Delta from the head of Old River, while the majority of the tags detected at Highway 4 (OR4, MR4) entered the interior Delta from the San Joaquin River downstream of Stockton (Table 6).

The large majority of tags detected in the Old River route were also assigned to that route for the survival model, although up to three tags in each release group were detected in the Old River route but assigned to the San Joaquin River route because of subsequent detections in that route. One tag detected in the Old River route was subsequently detected upstream of the head of Old River, and was not assigned to the Old River route. In all, 483 tags were assigned to the Old River route at the head of Old River based on the full sequence of tag detection (Table 5). Of these 483 tags, 341 were detected at

the CVP trash racks, although only 285 such tags were used in the survival model for the CVP because the others were subsequently detected at the radial gates, Old River, or Middle River (Table 6, Table 7). Likewise, 231 of the tags assigned to the Old River route were detected at the radial gates, and only 113 of those detections were available for use in the survival model (Table 6, Table 7). A total of 31 of the Old River route tags were detected at either Jersey Point or False River (Table 6), 21 of which came via the CVP, 6 via the CCFB, and 4 via Old River at Highway 4, before being detected at Jersey Point or False River. Ten tags from the Old River route were detected at False River, but all were later detected at Jersey Point, Chipps Island, Benicia Bridge, or Threemile Slough, so there were no False River detections available for the survival model from the Old River route (Table 6, Table 7). Of the 483 tags assigned to the Old River route at the head of Old River, 184 were detected at Chipps Island, including predator-type detections (Table 6, Table 7).

In addition to the northern Middle River receivers (MID), tag detections were recorded at the Montezuma Slough and Spoonbill Slough receivers but were purposely omitted from the survival model. Two tags were detected at the Montezuma Slough receivers (both from the Old River route), and nine tags were detected at the Spoonbill Slough receivers (six from the Old River route); all were subsequently detected at Chipps Island. Threemile Slough was used only in the San Joaquin River route; four tags from the Old River route were detected at Threemile Slough after detection at either the water export facilities (three tags) or the Old River receivers near Highway 4 (one tag) (Table 6).

The predator filter used to distinguish between detections of juvenile steelhead and detections of predatory fish that had eaten the tagged steelhead classified 161 of the 1,440 tags (11%) released as being detected in a predator at some point during the study (Table 8). Of the 1,020 tags detected in the study area (i.e., at Mossdale or points downstream), 139 tags (14%) were classified as being in a predator, although some had also been identified as a predator before entering the study area. A total of 131 tags (13% of 1,020) were first classified as a predator within the study area. Relatively few (31, 2%) of the 1,310 tags detected upstream of Mossdale were assigned a predator classification in that region; 1 of those 31 tags was first classified as a predator downstream of Mossdale, and then returned to the upstream region.

The detection site with the most first-time predator classifications was the CVP trashrack (E1; 33 of 351, 9.4%) (Table 8). The detection site upstream of Durham Ferry (A0) also had a high number of first-time predator classifications (14 of 130, 10.8%). Within the study area, the detection sites with the largest number of first-time predator-type detections, aside from the CVP trashrack (E1), were the

Radial Gates Upstream receivers (D1; 11 of 268, 4.1%) and Predator Removal Study 6 (N3; 7 of 524, 1.3%) (Table 8). The majority of the first-time predator classifications assigned within the study area were assigned to tags on departure from the site in question (77) rather than on arrival at the site (54). Predator classifications on arrival were typically due to unexpected travel time, unexpected transitions between detection sites, or lengthy detection histories at individual sites, and were most common at Durham Ferry Upstream (A0), the CVP trashrack (E1), Banta Carbona (A5), and the third and fourth predator removal study sites (N3, N4) (Table 8). Predator classifications on departure were typically due to long residence times, and were most prevalent at the CVP trashrack (E1) and outside the radial gates (D1) (Table 8). Only detections classified as from predators on arrival were removed from the survival model, along with any detections subsequent to the first predator-type detection for a given tag.

The predator filter performance was assessed using acoustic telemetry detections of predatory fish including Striped Bass, Largemouth Bass, White Catfish, and Channel Catfish. A total of 89 tagged predatory fish were detected in the 2016 steelhead survival study: 22 that had been released in 2014, and 67 that had been released in 2015. Of the 89 predator tags detected, a total of 71 tags were classified as being in a predator at some point during their detection history, based on a score of at least 2 from the predator filter, resulting in a filter sensitivity of 79.8%. When predator tags that had fewer than 5 detections events on the visit scale were omitted, the filter sensitivity increased to 98.5%: 66 of 67 predator tags tested positive as a predator.

When the detections classified as coming from predators were removed from the detection data, there was little change in the overall number of tags detected, although the patterns of detections changed somewhat (Table 9, Table 10, and Table 11). With the predator-type detections removed, 1,297 of the 1,440 (90%) tags released were detected downstream of the release site, and 1,012 (70% of those released) were detected in the study area from Mossdale to Chipps Island (Table 9). A total of 122 tags were detected upstream of the release site with steelhead-type detections; 90 of these were also detected downstream of the release site. With or without the predator-type detections, the April release group had the most detections in the study area, and the February release group had the fewest (Table 5, Table 9).

The Old River route was used more than the San Joaquin River route for the February and March release groups, while the April release group used the San Joaquin River route more (Table 9). Most detection sites had fewer detections in the reduced, steelhead-only data set (Table 10 vs Table 6). However, because some tags were observed moving upriver or to an alternate route after the predator

classification from the predator filter, the number of detections available for use in the survival model was actually higher in the steelhead-only data set for some detection sites (DFD, WCL, and MRH; Table 11 vs Table 7). The largest change in the number of detections available for the survival analysis occurred at the Navy Drive Bridge (SJNB), where the reduced data set had 19 fewer detections than the full data set that included the predator-type detection (Table 11 vs Table 7). Comparable reductions in the number of detections were observed at the Calaveras River (SJC; reduction = 18), Chipps Island (reduction = 17), and Benicia Bridge (reduction = 16) (Table 11 vs Table 7). The number of tags detected at Chipps Island changed from 461 when the predator-type detections were included, to 444 when such detections were excluded (Table 6 vs Table 10). Of the 518 tags that were assigned to the San Joaquin River route at the head of Old River when predator-type detections were excluded, 93 were subsequently detected in the interior Delta, 131 were detected in Turner Cut, 68 were detected in Columbia Cut, and 46 were detected at the northern Old River site (OSJ), compared to 275 tags that were detected only in the main stem San Joaquin River downstream of the head of Old River; 277 (53%) of the tags assigned to the San Joaquin River route were detected at Jersey Point, and 276 (53%) were detected at Chipps Island (Table 10). Of the 479 tags assigned to the Old River route at the head of Old River, 304 (63%) were detected at the CVP trash racks, 224 (47%) at the radial gates, 30 (6%) at Jersey Point, and 182 (38%) at Chipps Island (Table 10). Detection counts used in the survival model largely follow a similar pattern (Table 11).

Survival Model Modifications for Individual Release Groups

Modifications to the survival model were required for the individual release groups because of sparse data.

Modifications for February Release Group

Most of the fish from the February release group that reached the head of Old River arrived at that junction before the temporary rock barrier was installed, and the majority of tags from this release were observed using the Old River route through the Delta. Detections were too sparse in the San Joaquin River route to fit the full reach-specific survival model to those data. Survival could be estimated along the San Joaquin River to Turner Cut, MacDonald Island, and Medford Island, and from those sites to Chipps Island, but the finer-grained spatial detail between those sites and Chipps Island could not be estimated. No attempt was made to estimate transition probabilities from the lower San Joaquin River to the Highway 4 sites (OR4, MR4) or the water export facility sites (RGU, RGD, CVP, CVPtank), or to Chipps Island specifically via Columbia Cut, the northern Old River site (OSJ), or

Disappointment Slough (SJD). Detection sites A14, B4, B5, C2, D1, D2, E1, E2, F2, G1, and T1 were all omitted from Submodel II because of sparse detections (Figure 4). False River was omitted entirely from both submodels.

In the Old River route, only one tag was detected at the Middle River Head (MRH, C1) site; the detection history for that tag was right-censored (i.e., truncated) at that site, so that it contributed to estimation of survival to that site but no attempt was made to estimate transition probabilities starting at site C1. The majority of the Old River route tags observed downstream of the Old River South station (ORS, B2) were detected at the water export facilities (CVP, CVP tank, RGU, and RGD). Too few tags were detected at the Highway 4 sites (OR4, MR4) to estimate transition probabilities from those sites, although transition probabilities were estimated to those sites, under the assumption of 100% detection. There were also too few tags detected at West Canal (WCL, B3) to estimate the transition probability from that site; WCL was omitted from Submodel I. No Old River route tags were detected at Jersey Point (JPE/JPW, G1), so that site was omitted from the model. The estimates of total Delta survival in both routes and overall estimated from the full model were confirmed by fitting a simplified model that estimated survival from the Old River East (ORE = B1) site to Chipps Island directly.

Modifications for March Release Group

The majority of tags detected downstream of the head of Old River from the March release group were observed taking the Old River route. Within the Old River route, the majority of tags were observed taking the routes through the water export facilities rather than past Highway 4. The sparse detections at the Old River receivers at Highway 4 (OR4 = B4) required pooling the detections from the dual array at that site and treating it as a single array for Submodel I. Sparse detection data in the San Joaquin River route at the water export facilities and Highway 4 receivers (OR4, MR4) required removing those sites from Submodel II. This resulted in parameters $\phi_{A13,GH}$, $\phi_{B5,GH}$, $\phi_{F1,GH}$, and $\phi_{F2,GH}$ encompassing not only the probability of directly moving from sites MFE/MFW (A13), OSJ (B5), TCE/TCW (F1), and COL (F2) directly to the Jersey Point/False River junction as implied in the full Submodel II (Figure 3), but also the probability of moving first to the Highway 4 region (OR4, MR4) before moving on to Jersey Point or False River (Figure 5). It was also necessary to pool detections across the dual array at Jersey point (G1) for both major routes, and at Old River South (ORS = B2) in the Old River route. Only one tag was detected using the Threemile Slough route, but that tag was subsequently detected downstream at Benicia Bridge (BBR = G3), so it was necessary to retain Threemile Slough in the model to avoid biasing estimates of transitions past Jersey Point. It was also necessary to assume 100% detection

probability at Threemile Slough and complete transitions from that site to Chipps Island (i.e., $\phi_{T1,G2} = 1$); the limitations of these assumptions were explored. False River was omitted entirely from both submodels. Through-Delta survival estimates from the full model were confirmed using a simpler model that estimated survival directly from ORS to Chipps Island in the Old River route.

Modifications for April Release Group

The head of Old River barrier was installed for passage of the majority of fish from the April release group. The presence of the barrier resulted in few April tags detected in the Old River route, and sparse detections downstream of the Old River South/Middle River Head receivers (ORS = B2, MRH = C1). The majority of tag detections at the water export facilities, and all detections at the Highway 4 sites (OR4 = B4, MR4 = C2) and Jersey Point (JPE/JPW = G1), came from tags observed taking the San Joaquin River route at the head of Old River. Under the assumption of common detection probabilities regardless of route, it was possible to retain most detection sites in both submodels, although it was not possible to estimate all transition probabilities in the Old River route. In particular, because there were no detections at the stations at West Canal (WCL = B3) or Highway 4, it was not possible to estimate transition probabilities from those sites ($\phi_{B3,B4}$, $\phi_{B4,GH}$, and $\phi_{C2,GH}$) and WCL was omitted from the model. Estimates of mid-Delta survival in the Old River route ($S_{B(MD)}$) and overall ($S_{Total(MD)}$) could nevertheless be estimated based on the pattern of detections at upstream sites (ORE, ORS, and MR4) and Jersey Point (JPE/JPW), using the Jersey Point detection probability from the San Joaquin River route fish. Sparse detections at the Middle River Head station (MRH = C1) required right-censoring (i.e., truncating) detection histories at that site; no attempt was made to estimate transition probabilities or survival from that site. The estimates of through-Delta survival and mid-Delta from the Old River route (S_B and $S_{B(MD)}$) and overall (S_{Total} and $S_{Total(MD)}$) were all based on the assumption that no tags successfully reached either Jersey Point or Chipps Island via the MR4 detection site. Although it was not possible to estimate transition probabilities from the MRH site, the low observed usage of that site across all release groups, and the lack of any subsequent detections of MRH tags, provides support for that assumption. Because the sparse detection data in the Old River route presented challenges in fitting the full model in that route, the estimates of through-Delta survival in the Old River route and overall were confirmed by fitting a simplified model that omitted all detailed transitions between the Old River East (ORE = B1) site near the head of Old River and Chipps Island.

False River was omitted entirely from both submodels. It was necessary to pool detections within the dual array at Columbia Cut (COL = F2) when the predator-type detections were removed, and at Jersey Point with and without the predator-type detections. Model fit was improved by pooling detections within the lines comprising the dual arrays at MacDonald Island (MAC = A12); each of these sites was treated as a single array in the model.

Tag-Survival Model and Tag-Life Adjustments

Observed tag failure times ranged from 22.92 days to 76.01 days; all but 1 of the 82 tags with failure times survived at least 57 days. Model fit was improved by right-censoring (i.e., truncating) failure time data at 69 days; there were 15 tags with tag failure times > 69 days. Model fit comparisons using AIC to compare analyses that pooled over tag-life study resulted in selection of the pooled model (ΔAIC = 30.15). Thus, a single tag survival model was fitted and used to adjust fish survival estimates for premature tag failure. The estimated mean time to failure from the pooled data was 63.9 days ($\widehat{SE} =$ 6.4 days) (Figure 6).

The complete set of acoustic-tag detection data from those tags released in steelhead to the river at Durham Ferry, including any detections that may have come from predators, contained several detections that occurred after the tags began dying (Figure 7, Figure 8). The sites with the latest detections were the CVP trashracks, Durham Ferry Downstream, Medford Island, and Chipps Island (Figure 7, Figure 8). Some of these late-arriving detections may have come from predators, or from residualizing steelhead. Without the predator-type detections, the late-arriving detections were largely removed (e.g., Figure 9). Tag-life corrections were made to survival estimates to account for the premature tag failure observed in the tag-life studies. All of the estimates of reach tag survival were greater than or equal to 0.9812, and most were greater than 0.998, out of a possible range of 0 to 1; cumulative tag survival to Chipps Island was estimated at 0.9955 without predator-type detections (0.9950 with predator-type detections). Thus, there was little effect of either premature tag failure or corrections for tag failure on the estimates of steelhead reach survival in 2016.

Surgeon Effects

Steelhead in the release groups were evenly distributed across surgeon (Table 12). Additionally, for each surgeon, the number of steelhead tagged was well-distributed across release group. A chi-squared test found no evidence of lack of independence of surgeon across release group (χ^2 = 0.533, df = 4, P = 0.9702). The distribution of tags detected at various key detection sites was also well-distributed

across surgeons and showed no evidence of a surgeon effect on survival, route selection, or detection probabilities at these sites (χ^2 = 17.253, df = 52, P > 0.9999; Table 13).

Estimates of cumulative fish survival throughout the San Joaquin River route to Chipps Island showed similar patterns of survival across all surgeons. Surgeon A had consistently lower point estimates of cumulative survival through the San Joaquin River route, and in the Old River route through Old River South and the head of Middle River (Figure 10, Figure 11). The estimate of cumulative survival to the Turner Cut junction (i.e., to the MacDonald Island or Turner Cut receivers) in the San Joaquin River route was 0.56 ($\widehat{SE} = 0.03$) for fish tagged by surgeon A, compared to 0.62 ($\widehat{SE} = 0.03$) for surgeon B, and 0.60 ($\widehat{SE} = 0.03$) for surgeon C (Figure 10). Survival to Chipps Island via the San Joaquin River route was estimated at 0.37 surgeon A, compared to 0.41 and 0.42 for surgeons B and C, respectively ($\widehat{SE} = 0.03$ for each surgeon). Despite the lower point estimates of survival in the San Joaquin River route for fish tagged by surgeon A, there was no significant difference in cumulative survival to any sites in that route among surgeons (P≥0.2019, Figure 10). In the Old River route, the differences between the surgeons were smaller, and had disappeared by the export facilities, West Canal, and Highway 4; no differences were statistically significant (P≥0.6312; Figure 11). In particular, there was no difference in survival to Chipps Island in the Old River route (P=0.7049; Figure 11). Analysis of variance found no effect of surgeon on reach survival in the two routes collectively (P=0.2070). Rank tests found no evidence of consistent differences in reach survival for fish from different surgeons either upstream of the Head of Old River (P=0.9810), in the San Joaquin River route (P=0.6977), or in the Old River route (P=0.9810).

Survival and Route Selection Probabilities

Likelihood ratio tests found that transitions to the exterior receivers at the Clifton Court Forebay, and on to the interior receivers of the Forebay, depended on whether the radial gates were open or closed at the time of arrival at the exterior receivers (P≤0.0036) for the February and March release groups. No strong gate effect was observed for the April release group (P=0.0575), so the April model was fit without differentiating between open and closed gates. Model fit was not significantly improved by including an effect of route selection at the head of Old River on the transition probabilities from the water export facility detection sites ($\phi_{D1,D2}$, $\phi_{D2,G2}$, $\phi_{E1,E2}$, and $\phi_{E2,G2}$ for the April release group (P=0.6139); detection data at the water export facility sites from the San Joaquin River tags were too sparse to include those sites in the February and March models. Model fit was also not improved by

including an effect of route selection on the transition probability from Jersey Point to Chipps Island ($\phi_{G1,G2}$) for the March release group (P=0.5949); detections at Jersey Point were too sparse in one or both routes for testing in the February and April release groups.

Some parameters were unable to be estimated because of sparse detection data; see above for details on modifications to the release-recapture model required for each release group. For all release groups, detections at the Middle River Head site (C1) were too sparse to estimate transition probabilities from that site to telemetry stations downstream. Estimates of survival through the South Delta were available only when there was no evidence of tags selecting the Middle River route (i.e., $\psi_{BC} = 0$; March release without predator-type detections, and March and April releases with predator-type detections) (Table 14, Table 15), and estimates of survival through the South Delta, Mid-Delta region (i.e., to Jersey Point), or total (i.e., to Chipps Island) depended on the assumption (consistent with the data) that either use of the Middle River route or survival in that route was 0. Selection of the Middle River route was based on the assumption of 100% detection probability at site C1. While this assumption could not be tested within each release group, it is consistent with the pattern of detections observed over all release groups (i.e., all tags detected at the C1 array were detected on both lines of the array).

Sparse detection data at the Highway 4 sites (OR4, MR4) in the February and April release groups prevented estimation of transition probabilities from those sites to Jersey Point and Chipps Island; estimates of Old River route survival to either Jersey Point or Chipps Island depended on the assumption that the Highway 4 routes were not viable, which was consistent with the data. Sparse detection data at Jersey Point from the February release group prevented estimation of survival through the Mid-Delta region for both primary routes (Table 14, Table 15). No transition probabilities could be estimated to or from the Highway 4 sites and the water export facility sites for fish that took the San Joaquin River route at the head of Old River from the February and March release groups, because of sparse detections at those sites. Likewise, detection counts in the San Joaquin River route were too low for the February release to estimate transition probabilities among the detection sites between the region around MacDonald Island, Medford Island, and Turner Cut, and Chipps Island.

Although the full survival model separately estimates the transition probabilities to the Jersey Point/False River junction ($\phi_{kj,GH}$) and the route selection probability at that junction $\left(\psi_{G1}\right)$, it was not

possible to estimate these two parameter separately for any release group in 2016. Of the 75 steelhead tags observed on the False River receivers, all but one of them were later detected at either Jersey Point or Chipps Island. There were too few detections available in the modeled detection histories at False River to reliably estimate the detection probability at that site. This meant that it was not possible to separately estimate the survival transition parameters $\phi_{kj,GH}$ from the route selection probability ψ_{G1}, for transitions from station j in route k. Instead, only their product was estimable: $\phi_{kj,G1} = \phi_{kj,GH}\psi_{G1}$, for kj = A12, A13, A14, B4, B5, C2, F1, and F2. However, in some cases, even those parameters could not be estimated because of sparse data. Because there were some detections at the H1 receivers, it is must be that $\psi_{G1} < 1$ and $\phi_{kj,G1} \neq \phi_{kj,G1}$. Although not possible to estimate the difference between these parameters, the fact that 74 of 75 (99%) of the tags detected at H1 were later detected at G1 or G2 suggests that the difference between $\phi_{kj,G1}$ and $\phi_{kj,GH}$ was small. Omitting H1 meant also that the estimates of survival through the Mid-Delta region should be interpreted as survival to Jersey Point, rather than to the Jersey Point/False River junction.

Few tags were detected using the Burns Cutoff route around Rough and Ready Island (i.e., passing the RRI = R1 telemetry station), and no tags were detected at that site from the February and March release groups (Table 11). The estimates of route selection at Burns Cutoff (ψ_{A2}) were based on the assumption of 100% detection probability at site R1 for the February and March release groups. No estimate of survival from the R1 site to the Calaveras River detection site (SJC = A10) was available for the February and March release groups. Likewise, the estimate of the transition probability to Threemile Slough ($\phi_{A14,T1}$) was based on the assumption of 100% detection probability at Threemile Slough for the March release group. Alternative assumptions of 50% detection probability at Threemile Slough raised the estimate of $\phi_{A14,T1}$ by 0.01, a difference which was less than the standard error.

Using only those detections classified as coming from juvenile steelhead by the predator filter, the estimates of total survival from Mossdale to Chipps Island, S_{Total}, ranged from 0.39 ($\widehat{SE} = 0.03$) for the February release group to 0.59 ($\widehat{SE} = 0.02$) for the April release group; the overall population estimate from all three releases (weighted average) was 0.47 ($\widehat{SE} = 0.02$) (Table 14). The estimated probability of entering Old River at its head was highest for the February release group (0.88, $\widehat{SE} =$ 0.02), which passed mostly before the Head of Old River barrier was installed on April 1; estimates were

still high (0.77, $\widehat{SE} = 0.02$) for the March release group, most of which passed before the barrier installation was complete, and were noticeably lower for the April release (0.04, $\widehat{SE} = 0.01$). The population estimate of Old River route selection over all three releases was 0.56 ($\widehat{SE} = 0.01$) (Table 14). There was a statistically significant preference for the Old River route for the February and March releases, and for the San Joaquin River route for the April release (P<0.0001 for each release group). Estimates of survival from Mossdale to Chipps Island via the San Joaquin River route $\left(S_A\right)$ ranged from 0.23 ($\widehat{SE} = 0.08$) for the February release group to 0.61 ($\widehat{SE} = 0.02$) for the April release; the population estimate, averaged over all three release groups, was 0.45 ($\widehat{SE} = 0.03$) overall (Table 14). In the Old River route, estimates of survival from Mossdale to Chipps Island $\left(S_B\right)$ ranged from 0.17 ($\widehat{SE} = 0.06$) for the April release to 0.41 ($\widehat{SE} = 0.04$) for the February release (population average = 0.33, $\widehat{SE} = 0.03$) (Table 14). The route-specific survival to Chipps Island was significantly different (at the 5% level) between routes for the April release group, when survival was higher in the San Joaquin River route than in the Old River route (P=0.0002; Table 14). For the March release group, the point estimate of San Joaquin River route survival (0.50) was also higher than for the Old River route (0.40), but the difference was statistically significant only at the 10% level (P=0.0612). There was no significance difference in survival to Chipps Island between routes for the February release (P=0.1216; Table 14). When combined over all three release groups, the population estimate of route-specific survival to Chipps Island was higher for the San Joaquin River route than for the Old River route (P=0.0034; Table 14).

Survival was estimated to the Jersey Point/False River junction for routes that did not pass through the holding tanks at the CVP or the CCFB. This survival measure ($S_{Total(MD)}$) was estimable only for the March and April release groups: $\hat{S}_{Total(MD)} = 0.14$ ($\widehat{SE} = 0.02$) for March, and 0.53 ($\widehat{SE} = 0.02$) for April (Table 14). This was a minimum estimate, because it excluded the possibility of going to False River rather than to Jersey Point; however, no tags from these two release groups were detected at False River without also being detected at either Jersey Point or Chipps Island (Table 11), suggesting that the bias in the estimate of $S_{Total(MD)}$ was small. Survival to Jersey Point was different for the two routes for both the March and April releases (P<0.0001), and was higher for fish in the San Joaquin River route (Table 14). However, over 75% of the Old River route fish from the March release group were detected at the radial gates at the entrance to the Clifton Court Forebay or at the CVP trashracks (Table 11); the

survivors of these fish would not have contributed to survival to Jersey Point or False River, because those sites were not on the migration route downstream from the CVP or SWP holding tanks. Because $S_{Total(MD)}$ does not reflect survival to downstream regions via salvage, it does not necessarily indicate overall survival to Chipps Island (S_{Total}), in particular in the absence of a barrier at the head of Old River. The barrier was absent for the majority of fish passing the head of Old River from the March release, and approximately 77% of fish used the Old River route from that release group. Only 4% of fish from the April release group used the Old River route, and the estimates of mid-Delta survival and total Delta survival were similar for that group (0.53 ($\widehat{SE} = 0.02$) for mid-Delta survival and 0.59 ($\widehat{SE} = 0.02$) for total Delta survival; Table 14).

Survival was estimated through the South Delta for San Joaquin River route fish ($S_{A(SD)}$) for all three release groups, and for Old River route fish only for the March release group ($S_{B(SD)}$). The "South Delta" region corresponded to the region studied for Chinook salmon survival in the 2009 VAMP study (SJRGA 2010). Survival through the San Joaquin River portion of the South Delta, i.e. from Mossdale to the Turner Cut or MacDonald Island receivers, had estimates ranging from 0.58 ($\widehat{SE} = 0.09$; February) to 0.89 ($\widehat{SE} = 0.02$; April); the population level estimate was 0.73 ($\widehat{SE} = 0.04$; Table 14). Survival through the Old River portion of the South Delta, i.e., from Mossdale to the CVP trashracks (CVP), radial gates exterior receivers (RGU), and Highway 4 receivers (OR4, MR4), was estimated only for the March release: 0.0.83 ($\widehat{SE} = 0.02$; Table 14). Total estimated survival through the entire South Delta region ($S_{Total(SD)}$) was estimable only for the March group (0.81, $\widehat{SE} = 0.02$; Table 14).

Including the predator-type detections in the analysis had a negligible effect on the survival estimates in most regions for the February and March release groups, and moderate effects for the April release group (Table 15). The measures of through-Delta survival and Mid-Delta survival had higher estimates for the April release group when predators were included (Table 15) than when they were excluded (Table 14); the increases ranged from 0.03 for Mid-Delta survival through the San Joaquin River Route ($S_{A(MD)}$) to 0.08 for the Old River route survival from Mossdale to Chipps Island $\left(S_B\right)$. Also notable was the ability to estimate South Delta survival in the Old River route ($S_{B(SD)}$) for the April release when predator-type detections were included, although with only moderate precision (0.67,

$\widehat{SE} = 0.12$; Table 15). The differences in April through-Delta survival estimates when the predator-type detections were included arose from additional tags detected at Chipps Island, along with small increases in detection counts at sites throughout the study area (Table 7, Table 11, Table 14, Table 15).

Estimates of survival through the South Delta tended to be higher when predator-type detections were included, if survival was estimable at all, for all release groups. The estimates of South Delta survival in the San Joaquin River route for the three release groups increased from 0.58 ($\widehat{SE} =$ 0.09), 0.74 ($\widehat{SE} = 0.05$), and 0.89 ($\widehat{SE} = 0.02$) without the predator-type detections to 0.65 ($\widehat{SE} = 0.09$), 0.77 ($\widehat{SE} = 0.05$) and 0.93 ($\widehat{SE} = 0.01$) when predator-type detections were included (Table 14, Table 15). For the March release group, estimates of South Delta survival in the Old River route and overall both increased by 0.03 when predator-type detections were included. For the April release group, South Delta survival in the Old River route ($S_{B(SD)}$) could be estimated only when the predator-type detections were included (0.67, $\widehat{SE} = 0.12$; Table 15). No estimates of Old River route South Delta survival could be estimated for the February release group, whether or not predator-type detections were included.

Detection probability estimates were high (>0.95) at most receiver arrays throughout the Delta (Table A2). However, some detection sites upstream of Mossdale had estimated detection probabilities as low as 0.30 (BDF1 = A3 for the April release; Table A2). The estimated probability of detection at Chipps Island ranged from 0.93 ($\widehat{SE} = 0.02$) for the April release to 0.95 ($\widehat{SE} = 0.03$) for the February release (Table A2), based on the pattern of detections at Chipps Island and Benicia Bridge. The estimates of survival to Chipps Island are adjusted for imperfect detection, so detection probabilities < 1.0 are not expected to bias the survival estimates.

Survival estimates in reaches varied throughout the study. For most reaches upstream of the San Joaquin River Navy Drive Bridge (SJNB = A9), the estimated survival was highest for the April release, and lowest for the February release (Table A2). The estimated total probability of survival from release at Durham Ferry to Mossdale was considerably lower for the February release (0.44, $\widehat{SE} = 0.02$) compared to March (0.78, $\widehat{SE} = 0.02$) or April (0.89, $\widehat{SE} = 0.01$) (Table 14). This pattern of lower perceived survival to Mossdale in February was observed both with and without the predator-type detections (Table 14, Table 15). The probability of turning upstream from the release site ($\phi_{A1,A0}$) had

similar estimates for all three releases (0.02 to 0.08; Table A2), suggesting that the lower estimate of cumulative survival to Mossdale for February was due either to mortality or to permanent rearing between Durham Ferry and Mossdale rather than farther upstream.

Reach-specific estimates in the San Joaquin River route tended to be less precise (larger standard errors) for the February release group, when relatively few tags were observed in that route compared to the March and April release groups (Table A2). Survival from Mossdale through the head of Old River, to the SJL or ORE receivers, had high estimates all three release groups, ranging from 0.96 ($\widehat{SE} = 0.01$) for February to 1.00 ($\widehat{SE} < 0.01$) for April (Table A2). Survival in the San Joaquin River from Lathrop (SJL) to Garwood Bridge (SJG, site A8) varied from 0.72 ($\widehat{SE} = 0.09$) for the February release group to 0.96 ($\widehat{SE} = 0.01$) for the April release group (Table A2). Reach-specific survival estimates in the reaches between Garwood Bridge and the MacDonald Island/Turner Cut receivers were consistently high (0.92 to 1.00) across the release groups (Table A2). From MacDonald Island, most fish continued in the San Joaquin River to Medford Island, represented by the transition parameter $\phi_{A12,A13}$; estimates were higher for the later release groups (0.97, $\widehat{SE} = 0.05$ for March, and 0.75, $\widehat{SE} = 0.03$ for April) than for February (0.44, $\widehat{SE} = 0.17$) (Table A2). Most fish from the March and April release groups that were observed at Medford Island continued down the San Joaquin to Disappointment Slough ($\hat{\phi}_{A13,A14} = 0.72$ to 0.81, $\widehat{SE} \leq 0.07$), although some moved past the northern Old River receivers (OSJ, site B5) instead ($\hat{\phi}_{A13,B5} = 0.10$ to 0.21, $\widehat{SE} \leq 0.06$ (Table A2). Total survival from Disappointment Slough to either Jersey Point (G1) or Threemile Slough (T1) was > 0.95 for both the March and April release groups. The probability of moving from OSJ to Jersey Point was also high (≥0.93) for March and April, whereas the estimated transition probability from Jersey Point to Chipps Island ranged from 0.84 to 0.98 ($\widehat{SE} \leq 0.05$) (Table A2). Too few tags from the February release were detected in the San Joaquin River route to monitor detailed migration pathways downstream of MacDonald Island and Turner Cut for that release. Most tags detected coming from Disappointment Slough past Threemile Slough were later detected at Chipps Island ($\hat{\phi}_{T1,G2} = 0.95$, $\widehat{SE} = 0.03$ population estimate, Table A2). Consistent with the relatively low survival in the upstream reaches for the February release group compared to the March and April releases, the February release had the lowest estimate of total survival to Chipps Island from MacDonald Island: 0.34 ($\widehat{SE} = 0.16$), compared to 0.81 to 0.83 for the March and April releases (Table A2). On the

other hand, the February group had the highest estimated survival from Turner Cut to Chipps Island but with low precision because of small sample size: 0.50, $\widehat{SE} = 0.21$ for February, compared to 0.31 to 0.33 ($\widehat{SE} = 0.05$ to 0.11) for March and April (Table A2). The February group also had the highest probability of leaving the San Joaquin River for Turner Cut (0.40; $\widehat{SE} = 0.13$; Table A2).

In the Old River route, the estimated probability of surviving from the first detection site (ORE, site B1) to the head of Middle River (S_{B1}) was very high (≥0.97) for all three release groups; the February and March estimates had high precision ($\widehat{SE} = 0.01$), while the smaller sample size in April resulted in lower precision (95% lower bound = 0.82; Table A2). For all release groups, the estimate of S_{B1} was dependent on the assumption of 100% detection at the Middle River site MRH (site C1); pooling detections across all three release groups, the dual array estimate of the detection probability at that site was 1.0. No tags observed taking the Middle River route had subsequent detections. All release groups had a low estimated probability of moving and surviving from ORS to the Highway 4 sites (≤0.04 for each release group for OR4 and MR4; Table A2); because no February tags were detected at MR4, the MR4 transition probability for that group was based on the untested assumption of 100% detection probability. The estimated probability of moving from the Old River site at Highway 4 (OR4) to Jersey Point was highest for March (0.38, $\widehat{SE} = 0.17$), and either very low (0.04, $\widehat{SE} = 0.04$) or unestimable for the other release groups (Table A2). No tags detected at the Middle River Highway 4 site (MR4) were later detected at Jersey Point (95% upper bound = 0.56 for March and 0.14 for April for $\phi_{C2,G1}$; Table A2). The transition probability from ORS to the CCFB radial gates (exterior site, D1) had similar estimates for the three release groups (0.21 to 0.39), while the estimated transition probability from ORS to the CVP was considerably lower for April (0.23, $\widehat{SE} = 0.12$) than for February (0.67, $\widehat{SE} = 0.04$) or March (0.57, $\widehat{SE} = 0.03$) (Table A2). The majority of tags that were detected at the exterior radial gate receivers (D1) and did not return to either the CVP or Highway 4 were eventually observed entering Clifton Court Forebay and were detected on the interior receivers (D2): 0.82 to 1.04. The transition probability from the interior radial gate receivers to Chipps Island, presumably through the Forebay and salvage, ranged from 0.33 ($\widehat{SE} = 0.12$) for April, to 0.56 ($\widehat{SE} = 0.06$) for March (Table A2). Of the February and March tagging steelhead that reached the CVP trashracks (E1) without later being detected at the CCFB radial gates (D1, D2) or Highway 4 receivers, just over half were estimated to have

survived to the holding tank (0.54 to 0.59, $\widehat{SE} \leq 0.05$), whereas under half were observed entering the CVP holding tank from the April release (0.44, $\widehat{SE} = 0.10$) (Table A2). From the holding tank to Chipps Island, the transition probability estimate ranged from 0.85 ($\widehat{SE} = 0.05$) for February to 0.92 ($\widehat{SE} = 0.08$) for April (Table A2). Although including predator-type detections resulted in modified transition and survival probabilities for some reaches, similar overall patterns of movement and survival were estimated whether or not predator-type detections were included (Table A3).

Travel Time

For tags classified as being in steelhead, travel time through the system from release at Durham Ferry to Chipps Island ranged from 2.8 days to 41.2 days, and averaged 8.32 days ($\widehat{SE} = 0.19$ days) for all three release groups combined (Table 16a). Average travel time to Chipps Island was longest for the February release group (13.2 days), and shortest for the March release group (6.6 days); the April group had travel time similar to March (8.8 days) (Figure 12). Average travel time to Chipps Island was slightly longer for fish in the San Joaquin River route than for the Old River route: combined over all releases, fish in the San Joaquin River route took an average of 8.92 days ($\widehat{SE} =$ 0.21 days) from release at Durham Ferry, compared to an average of 7.52 days ($\widehat{SE} = 0.33$ days) for fish in the Old River route (Table 16a). However, variability between release groups complicates comparisons of route effects on travel time. For example, although the average travel time was shorter for the Old River route within each release group, the average travel time in the Old River route for the February release (12.8 days, $\widehat{SE} = 0.9$ days) was considerably longer than the average San Joaquin River travel time for either the March (9.1 days, $\widehat{SE} = 0.4$ days) or April (8.8 days, $\widehat{SE} = 0.2$ days) release group (Table 16a). Over 80% of the tags that were observed at Chipps Island arrived within 15 days of release at Durham Ferry. There were 56 tags that took 16–41 days, evenly split between the San Joaquin River route and the Old River route. Travel time from release at Durham Ferry to Chipps Island via salvage at the CVP ranged from 2.8 days to 38.3 days, and was observed in all release groups. Of the 123 tags that took this migration route, 19 had travel time > 15 days from Durham Ferry to Chipps Island: 17 were released at Durham Ferry in February and 2 were released in April, and all but 4 used the Old River route to the CVP. Travel time from Durham Ferry to Chipps Island via presumed salvage at the SWP ranged from 4.0 days to 41.2 days. Of the 57 tags observed taking this route, 11 had travel time > 15 days, all from the Old River migration route and all but 3 from the February release group.

Average travel time to all detection sites was longest for the February release group (Table A16a). For most detection sites, the March release group had lower average travel time than the April release, but the difference was typically small (average difference = 1.2 days). However, the average travel time to the CCFB radial gates was approximately 6 days longer for April (10.0 days, $\widehat{SE} = 1.2$ days) than for March (3.5 days, $\widehat{SE} = 0.2$ days) (Table 16a), while the April release tended to arrive at Columbia Cut or Disappointment Slough approximately 1 day faster than the March release (approximately 5 to 7 days for both releases) (Table 16a). Travel time from release to the Mossdale receivers averaged approximately 6 days for the February release group, compared to 1.0 to 1.6 days for the March and April release groups (Table 16a). Travel time to the Turner Cut junction (i.e., either Turner Cut receivers or MacDonald Island receivers) ranged from 1.7 days to 32.8 days, and averaged 17.6 days for the February release, approximately 5 days for the March and April releases. The majority (362 of 439, 82%) of the tags detected at the Turner Cut or MacDonald Island receivers came from the April release group (Table 16a). Travel time from release to the CVP trash racks ranged from 1.4 days to 37.1 days, and averaged 10.1 days, 4.0 days, and 8.9 days ($\widehat{SE} \leq 0.9$ days) for the February, March, and April release groups, respectively (Table 16a). Travel time to the radial gates receivers outside Clifton Court Forebay (RGU) followed a similar distribution as to the CVP trash racks (Table 16a). For both the CVP trash racks and the CCFB exterior receivers, travel time from Durham Ferry was longer for the San Joaquin River route than for the Old River route for the April release, and too few San Joaquin River route tags were detected from February and March to estimate travel time.

Few tags were detected at the Highway 4 detection sites (OR4, MR4) from the February release group from either route, and from the March release group from the San Joaquin River route. For tags taking the Old River route from the March release, average travel times were approximately 6.5 days to MR4 and 9.6 days to OR4 ($\widehat{SE} \leq 1.7$ days) (Table 16a). Considerably more tags were detected at the Highway 4 sites from the April release, all from the San Joaquin River route, and travel times averaged 8 – 10 days at both sites (Table 16a). Too few tags were detected at Jersey Point coming from either route to estimate travel time to that site for the February release group. The majority of tags observed at Jersey Point from March and April came from the San Joaquin River site, and had an average travel time of approximately 7-8 days (Table 16a). The three tags observed at Jersey Point from the Old River route (all from March) had travel times ranging from 9.8 days to 19.7 days.

Including detections from tags classified as predators tended to lengthen average travel times slightly, but the general pattern across routes and release groups was the same as without predator-type detections (Table 16b). The average travel time from release to Chipps Island via all routes, including the predator-type detections, was 8.49 days ($SE = 0.20$) (Table 16b). Increases in travel time with the predator-type detections reflect the travel time criteria in the predator filter, which assumes that predatory fish may move more slowly through the study area than migrating steelhead. Travel time increases may also reflect multiple visits to a site by a predator, because the measured travel time reflects time from release to the start of the final visit to the site. The Old River site at Highway 4 (OR4) had lower average travel times when the predator-type detections were included; this can happen when the predator filter removes repeat movement to sites that were previously visited.

Average travel time through reaches for tags classified as being in steelhead ranged from 0.008 days (approximately 12 minutes) from the entrance channel receivers at the Clifton Court Forebay (RGU) to the interior forebay receivers (RGD), to 4.48 days from Turner Cut (TCE/TCW) to Chipps Island (Table 17a; all releases). The "reach" from the exterior to the interior radial gate receivers (RGU to RGD) was the shortest, so it is not surprising that it would have the shortest travel time, as well. Travel times from the San Joaquin River receiver near Lathrop (SJL) to Garwood Bridge (SJG) averaged 1 day over all tags (~18 rkm); for tags released in February and March, average travel time through this reach was approximately 1.6 to 1.7 days (Table 17a). Average travel time from Old River South (ORS) to the CVP trashracks was approximately 1.4 day over all tags (~18 rkm). Average travel time to Chipps Island was approximately 2.9 days from MacDonald Island (~54 rkm via the San Joaquin River), and approximately 4.5 days from Turner Cut (also ~54 rkm via Frank's Tract) (Table 17a; all releases). From Jersey Point to Chipps Island was approximately 1 day (~26 rkm). Including the predator-type detections had little effect on average travel time through reaches (Table 17b).

Route Selection Analysis

Head of Old River

A total of 997 tags were detected at either the ORE or SJL telemetry receiver sites in 2018. Estimated detection probabilities were 1.0 for both sites A7 and B1 for all releases, without predator-type detections (Appendix Table A2). Of these 997 tags, 569 were estimated to have arrived at the head

of Old River junction before closure of the barrier during installation ("before barrier installation"). The majority of the tags that arrived before barrier installation selected the Old River route (463 tags = 82%).

When slow-moving tags and tags coming from either downstream or making repeated visits to the ORE or SJL receiver sites were removed, route selection data were available for 919 tags. Of these 919 tags, 530 were estimated to have arrived at the head of Old River junction before barrier installation. A total of 88 of the tags that arrived before barrier installation selected the San Joaquin River route (16.6%), whereas 374 tags arriving after barrier installation (and before barrier opening) selected the San Joaquin River route (97.4%) (Figure 13). The remaining analysis used only those tags that arrived before barrier installation.

San Joaquin River flow (discharge) at the MSD gaging station (near Mossdale Bridge), at the estimated time of arrival of the tagged juvenile steelhead at the head of Old River, ranged from -1,073 cfs to 5,114 cfs (average = 2,866 cfs), for study fish that arrived at the river junction before barrier closure on 1 April 2016. The flow at MSD was negative for 9 of 530 (1.7%) tags upon arrival at the river junction. Water velocity ranged from -0.48 ft/s to 1.8 ft/s (average = 1.22 ft/s) at tag arrival at the junction. Flow and velocity at MSD were highly correlated (r=0.92). At the Old River gaging station OH1, flow at estimated time of fish arrival at the river junction ranged from -114 cfs to 3,441 cfs (average = 1,829 cfs), and was negative for arrival of 4 of 530 (0.7%) tags at the junction. Water velocity at OH1 ranged from -0.06 ft/s to 1.93 ft/s (average = 1.13 ft/s) at tag arrival at the junction. Flow and velocity at OH1 were highly correlated (r=0.94), whereas flow at the MSD and OH1 stations were only moderately correlated (r=0.64). There was high correlation between river stage measurements from the different gaging stations (MSD, SJL, and OH1; r≥0.98), and low correlation between stage and the 15-minute change in stage for each station ($|r| \leq 0.21$). Export rates averaged 3,334 cfs at CVP, and 3,159 cfs at SWP, and the average CVP proportion of combined (CVP + SWP) export rates was 52%, on the days of fish arrival at the head of Old River. There was moderate correlation between total Delta exports and flow at OH1 (r=0.72) and flow at MSD (r=0.76) upon fish arrival at the river junction.

Of the 530 tags detected at SJL or ORE and used in the route selection analysis at the head of Old River, 19 were estimated to have arrived at head of Old River junction at dawn, 233 during the day, 6 during dusk, and 272 at night. Thirty-four of the 88 tagged steelhead that selected the San Joaquin River route arrived during the day, 48 arrived at night, one at dusk, and 5 at dawn. Steelhead that entered Old River tended to have more variable measures of flow and OH1 flow proportion, river stage,

15-minute change in river stage, and SWP export rates (Figure 14). Those that entered Old River also tended to have lower flow at MSD and lower modeled SJL flow, lower SJL river stage, higher 15-minute change in river stage, and lower SWP export rates (Figure 14). Similar patterns of river stage and route selection were observed for the OH1 and MSD gaging stations as for the SJL gaging station (not shown). Flow and velocity measures at the same stations were highly correlation ($r \geq 0.92$) at the estimated time of tag arrival at the head of Old River junction; thus, no velocity plot is shown.

Although the majority of tagged steelhead that arrived at the head of Old River junction before barrier closure in 2016 selected the Old River route, the proportion of fish selecting the San Joaquin River route tended to be highest in the middle of March, which was also when flow, velocity, river stage, and SWP exports were highest (Figure 15–Figure 18). Of the 530 tags used in the route selection analysis at the head of Old River, 442 (83%) selected Old River. This left a maximum of 87 degrees of freedom for the regression models.

The single-variate analyses found significant associations (experimentwise α=0.05) between route selection at the head of Old River and modeled flow at SJL ($P<0.0001$), river stage at MSD ($P=0.0001$), flow at MSD ($P=0.0006$), stage at OH1 ($P=0.0009$), OH1:MSD flow ratio ($P=0.0015$), and stage at SJL ($P=0.0017$) (Table 18). The 15-minute change in river stage SJL, OH1, and MSD, velocity and 15-minute change in velocity at MSD, SWP export rate and total export rate throughout the Delta, and CVP proportion of CVP and SWP exports all had associations with route selection that were significant at the testwise 5% level ($P<0.05$), but not at the more stringent experimentwise 5% level ($P<0.0021$ required). The other measures all had associations with route selection that were non-significant even at the testwise 5% level ($P \geq 0.0928$) (Table 18).

Multiple regression found significant associations between route selection and measures of flow at OH1 and MSD, the OH1:MSD flow ratio, water velocity at OH1, stage at MSD and OH1 and the 15-minute change in stage at SJL, and the SWP export rate (Table 19). The flow + stage model had the lowest AIC, and used river stage from two different stations (OH1 and MSD). River stage from these two stations was highly correlated ($r=0.98$), and the maximum variance inflation factor (VIF) for this model was 34.7, indicating that the level of multicollinearity among the covariates may be influencing the regression coefficient estimates to a large extent (Kutner et al. 2004). When river stage from either OH1 or MSD was omitted from the flow + stage model, the flow measure at OH1 no longer accounted for a

significant amount of variation in route selection (P≥0.0901), suggesting that the flow + stage model was over-fitting the data.

The best-fitting stage model used the measure of river stage at the MSD station (C_{MSD}) and the 15-minute change in river stage at the SJL station (ΔC_{SJL}), and fit almost as well as the flow + stage model based on AIC (ΔAIC=0.80; Table 19). The stage model also had acceptable fit based on the Pearson chi-squared test (P=0.6550), and both the mean and maximum VIF was 1.0 (acceptable). Model fit was better for lower levels of the predicted probability of taking the San Joaquin River route, compared to higher levels (Figure 19: Stage Model 1). All other models had ΔAIC≥8.46. An alternate stage model was considered that used river stage and the 15-minute change in river stage measured from the same station, SJL. This model made similar predictions as the river stage model that used river stage at MSD and the change in river stage from SJL, but had markedly lower fit based on AIC (ΔAIC=7.75; Figure 19: Stage Model 2). Thus, the stage model that used river stage at MSD and change in river stage at SJL was selected as the final model for route selection at the head of Old River.

The stage model predicted the probability of remaining in the San Joaquin River at the head of Old River according to:

$$\psi_A = \frac{\exp\left(-11.37 + 1.60 C_{MSD} - 16.99 \Delta C_{SJL}\right)}{1 + \exp\left(-11.37 + 1.60 C_{MSD} - 16.99 \Delta C_{SJL}\right)},$$

where C_{MSD} and ΔC_{SJL} represent the river stage at MSD and 15-minute change in river stage at SJL, respectively, measured upon estimated time of tagged fish arrival at the head of Old River junction (Table 19). Equivalently, the probability of entering Old River was modeled as

$$\psi_B = \left[1 + \exp\left(-11.37 + 1.60 C_{MSD} - 16.99 C_{SJL}\right)\right]^{-1}.$$

This model shows an effect of both river stage and the 15-minute change in river stage on the probability of entering Old River: fish that arrived at the junction at higher river stages had a lower probability of entering Old River, and a higher probability of remaining in the San Joaquin River, whereas fish that arrived at the junction at higher levels of 15-minute change in river stage at SJL were more likely to enter Old River (Figure 20, Figure 21). If the 15-minute change in river stage can be interpreted as a surrogate for the phase of the tidal cycle, the stage model indicates that fish are more likely to take the Old River route if they reach the head of Old River on an incoming tide (Figure 21).

Turner Cut Junction

A total of 440 tags were detected at the MAC (A12) and TCE/TCW (F1) telemetry receiver arrays in 2016. Estimated detection probabilities were 0.995 to 1.0 for site A12, and 1.0 for site F1 for all release groups (Appendix Table A2). Overall, 39 tags were excluded from the route selection analysis because of transition type (i.e., repeated visits at MAC or TCE/TCW, transitions between MAC and TCE/TCW, or transitions from downstream or the interior Delta), and 12 tags were excluded because of slow travel. Detections from a total of 389 tags were used in this analysis: 13 from the February release group, 54 from the March release group, and 322 from the April release group. Of these 389 tags, 93 (24%) selected the Turner Cut route, and 296 (76%) selected the San Joaquin River route.

River flow (discharge) at the Turner Cut gaging station (TRN) at the time of tag passage of the SJS receivers ranged from -4,447 cfs to 2,851 cfs (average = -796 cfs) in 2016. The flow in Turner Cut was negative (directed into Turner Cut from the San Joaquin River) for 236 of 389 (61%) of the tags detected. Water velocity at TRN ranged from -0.79 ft/s to 0.58 ft/s (average = -0.13 ft/s) at the time of SJS passage in 2016; there was high correlation between river flow and water velocity at the TRN station (r=0.999). River stage at TRN ranged from 6.3 ft to 11.1 ft (average = 9.0 ft) at tag passage of SJS; correlation between river stage and either flow or water velocity was moderate (r=-0.85). The average magnitude (root mean square, RMS) of river flow at Garwood Bridge (gaging station SJG) in the San Joaquin River during fish travel from the SJG telemetry station to SJS ranged from 2,163 cfs to 4,113 cfs (average = 2,854 cfs). Daily export rates at CVP ranged from 414 cfs to 3,439 cfs (average = 1,714 cfs); SWP export ranged from 393 cfs to 4,595 cfs, and averaged 1,404 cfs. The CVP proportion of combined export rates ranged from 37% to 68% (average = 56%). There was moderate correlation between either CVP exports or SWP exports and flow at Turner Cut ($|r| \leq 0.12$ for both).

Of the 389 tags detected at MAC or TCE/TCW and used in the route selection analysis at the Turner Cut junction, 7 were estimated to have passed the SJS receivers at dawn, 326 during the day, 7 at dusk, and 49 at night. Only 1 (14%) of the 7 tags passing at dawn, and 2 (29%) of the 7 tags passing at dusk, selected the Turner Cut route; 74 (23%) and 16 (33%) of those passing SJS during the day and night, respectively, selected the Turner Cut route. Steelhead that selected the San Joaquin River route tended to have passed SJS with more positive river flow at TRN than those that selected the Turner Cut route (Figure 22); positive flow at TRN indicated flow directed out of Turner Cut into the San Joaquin River. Fish that selected the Turner Cut route tended to have passed SJS when the river stage at TRN was higher than for fish that selected the alternate route, but there was considerable overlap in river

stage values between the two routes (Figure 22). The 15-minute change in river stage at TRN was considerably less variable and lower (i.e., more negative, indicating falling river stage levels) for fish that selected the San Joaquin River route than for those that selected the Turner Cut route (Figure 22). There was little difference in the RMS of river flow at SJG during transition from the SJG telemetry station to SJS for fish that eventually took the two routes, or in exports or fork length at tagging (Figure 22).

The majority of the tagged steelhead detected at either Turner Cut or MacDonald Island in 2016 were observed at MacDonald Island, and most were detected there in the second week of May; smaller groups were detected there in the third week of May and the fourth week of March (Figure 23). There was little obvious pattern in variations in route selection and either flow (Figure 23), velocity (Figure 24), river stage (Figure 25), or exports (Figure 26), summarized on the weekly time scale. Although the average values of flow at TRN for steelhead detected at the junction varied considerably between weeks, the extreme values of TRN flow were observed in weeks when only one or two fish were detected (Figure 23). There was lower variation in the RMS of flow at SJG during the steelhead transition from the SJG telemetry station to SJS (Figure 23). Similar patterns were seen with velocity (Figure 24). River stage at TRN tended to be slightly higher for fish that selected the San Joaquin River route than those that selected the Turner Cut route, but the pattern was not wholly consistent (Figure 25). For fish arriving at the Turner Cut junction in March and April, fish that stayed in the San Joaquin River tended to pass SJS when the combined CVP and SWP exports were higher; for fish that arrived at the junction in May, the pattern was reversed but weak, when viewed on the weekly scale (Figure 26). Overall, the tendency of the tagged steelhead to arrive at the Turner Cut junction in only a few weeks meant that the weekly time scale had little ability to highlight patterns in the data.

Of the 389 tags used in the Turner Cut route selection analysis, 296 (76%) selected the San Joaquin River route, and 93 (24%) selected the Turner Cut route. This left a maximum of 92 degrees of freedom for the regression models. Observations of the 15-minute change in river flow, river stage, and water velocity at the TRN gaging station were missing for 8 records, of which 3 tags were observed in the Turner Cut route; for those covariates and for the multiple regression models, there were only 89 degrees of freedom available.

The single-variate analyses found significant associations (experimentwise α=0.05) between route selection at the Turner Cut junction and the 15-minute change in river stage at TRN ($P<0.0001$),

and both flow and velocity at TRN (P=0.0003) (Table 20). The 15-minute change in flow and velocity at TRN and the presence of negative flow at TRN (i.e., directed into the interior Delta) each had associations with route selection that were significant at the testwise 5% level (P<0.05), but not at the more stringent experimentwise 5% level (P<0.0029 required). The other measures all had associations with route selection that were non-significant even at the testwise 5% level (P≥0.0928) (Table 20).

Multiple regression found significant associations between route selection and measures of flow, velocity, and the 15-minute change in river stage at TRN (Table 21). The flow + stage model had the lowest AIC (ΔAIC≥13.53), although the F-test of the significance of the effect of flow at TRN was significant only at the testwise 5% level rather than the experimentwise 5% level (P=0.0364 vs P<0.0250 required). The strongly improved model fit indicated by the AIC compared to the stage-only model (ΔAIC=13.53), combined with the nearly significant flow effect, suggests that flow at TRN was a moderately important component in route selection in 2016, although not as important as the 15-minute change in river stage (P=0.0004). The model that used measures of flow instead of measures of river stage ("flow model") used the 15-minute change in flow and the indicator variable for negative flow as well as the measure of flow itself at TRN, but was not selected by AIC (ΔAIC=15.95 compared to the flow + stage model) (Table 21). Both models had adequate fit based on the Pearson chi-squared test (P≥0.9998), but the strong relationship between the observations of flow at TRN and the presence of negative flow at that station made the flow model unreliable. For the flow + stage model, the VIF was 1.2, which indicates an acceptably low level of multicollinearity between the covariates. Model fit was markedly better for the flow + stage model compared to the other models (Figure 27). Thus, the flow + stage model was selected as the final model for route selection at the Turner Cut Junction.

The flow + stage model predicted the probability of remaining in the San Joaquin River at the Turner Cut junction according to:

$$\psi_A = \frac{\exp\left(-1.21 - 9.92\Delta C_{TRN} + 0.0003 Q_{TRN}\right)}{1 + \exp\left(-1.21 - 9.92\Delta C_{TRN} + 0.0003 Q_{TRN}\right)},$$

where ΔC_{TRN} and Q_{TRN} represent the 15-minute change in river stage at TRN and the flow at TRN, respectively, measured upon the final tag detection at the SJS telemetry station (Table 21). Equivalently, the probability of entering Turner Cut was modeled as

$$\psi_F = \left[1 + \exp\left(1.21 + 9.92\Delta C_{TRN} - 0.0003 Q_{TRN}\right)\right]^{-1}.$$

This model shows an effect both of the 15-minute change in river stage at TRN and flow at TRN on the probability of entering Turner Cut: fish that passed SJS at higher levels of the 15-minute change in river stage at TRN or lower levels of flow at TRN had a higher probability of entering Turner Cut (Figure 28, Figure 29). If the 15-minute change in river stage can be interpreted as a surrogate for the phase of the tidal cycle, the stage model indicates that fish are more likely to enter Turner Cut if they pass SJS (e.g., arrive at the function) on an incoming tide (Figure 28) and when flow is directed into Turner Cut (Figure 29).

Survival through Facilities

Survival through the water export facilities was estimated as the overall probability of reaching Chipps Island, Jersey Point, False River, Threemile Slough, Montezuma Slough, or Spoonbill Slough after being last detected in the CVP holding tank (site E2, for the federal facility) or the interior receivers at the radial gates at the entrance to the Clifton Court Forebay (site D2, for the receivers closest to the SWP state facility). Thus, survival for the federal facility (CVP) is conditional on being entrained in the holding tank, while survival for the state facility (SWP) is conditional on entering and not leaving the Clifton Court Forebay, and includes survival through the Forebay to the holding tanks. Results are reported for the individual release groups, and also for the pooled data set from all release groups (population estimate); predator-type detections were excluded. Conditional detection probabilities were estimated for all sites used.

Estimated survival from the CVP holding tank to the receivers located near the salvage release sites (Chipps Island, Jersey Point, False River, Threemile Slough, Montezuma Slough, and Spoonbill Slough) ranged from 0.86 ($\widehat{SE} = 0.05$) for the February release group, with a 95% profile likelihood interval of (0.75, 0.93), to 1.00 (95% lower bound = 0.78) for the April release group (Table 22). For the state facility, estimated survival from the radial gates to the receivers near the release sites ranged from 0.33 ($\widehat{SE} = 0.12$) for April release group (95% profile likelihood interval = (0.13, 0.58)), to 0.56 ($\widehat{SE} =$ 0.06) for the March release group (95% profile likelihood interval = (0.44, 0.68); Table 22). Release-specific sample sizes ranged from 12 to 79 for the CVP analysis, and from 15 to 66 for the SWP analysis. Estimated survival to receivers after release was consistently higher for the CVP holding tank compared to the Clifton Court Forebay radial gate (SWP); this is consistent with the estimates of the probability of successfully moving from those sites to Chipps Island that were calculated from the full survival model: $\hat{\phi}_{D2,G2} =$ 0.33 to 0.56 ($\widehat{SE} \leq 0.12$), and $\hat{\phi}_{E2,G2} =$ 0.85 to 0.92 ($\widehat{SE} \leq 0.08$) (Table A2).

Comparison among Release Groups

Analysis of variance found that the effect of release group on parameter estimates of reach-specific survival and transition probability parameters was just non-significant at the 10% level ($F_{2,28} =$ 2.452, P=0.1044). Pairwise *t*-tests found a significant difference between estimates from the February release and those from the March and April releases ($t_{28} =$ 1.845, P=0.0756 for February vs March, and $t_{28} =$ 1.983, P=0.0573 for February vs April). The effect of the February release group was negative in both cases, indicating that survival estimates for February tended to be lower than those from the latter two release groups. There was no significant difference found in estimates between the March and April release groups ($t_{28} =$ 0.138, P=0.8915).

Linear contrasts found differences in survival from Durham Ferry to Mossdale among all three release groups, with estimates from February being lower than the other releases (P<0.0001) (Table 23). Survival from Mossdale to Chipps Island via the San Joaquin River route was lower in February and higher in April (P≤0.0003), whereas survival from Mossdale to Chipps Island via the Old River route was lower in April (P=0.0003). Overall survival from Mossdale to Chipps Island followed the pattern for the San Joaquin River route, and was lower in February and higher in April (P≤0.0025) (Table 23).

Discussion

Predator Filter and Predator-type Detections

The 2016 predator filter had similar sensitivity to the 2015 filter, and lower sensitivity than the 2014 filter. As in the case of the 2015 filter, this is partly a result of the modifications to the calibration of the 2016 filter to reflect the detection histories of the recapture tags prior to the recapture event. When predator tags that had fewer than 5 detection events were omitted, the 2016 filter had higher sensitivity (98.%) than either the 2014 (92.9%) or 2015 (87.1%) filters. Because some components of the predator filter use the pattern of detections over multiple detection sites and time periods, it is reasonable that the filter sensitivity was improved for tags with longer detection histories.

The increase in total Delta survival seen when predator-type detections were included for the April release (i.e., increase of 0.04), but not for the February or March releases, suggests either that steelhead predators were leaving the Delta in April, or that steelhead were more likely to engage in temporary Delta rearing or delayed migration behavior in April than earlier in the spring. A comparable

increase (i.e., increase of 0.03) was observed for survival through the South Delta survival for the March release group when predators were observed, but not through the Mid-Delta or the entire Delta; this pattern is consistent with high predation activity around the water export facilities or Highway 4 in March, but not further downstream. In general, the spatial patterns in the survival differences with and without predator-type detections may reflect a reduced ability to distinguish between behavior of steelhead and predators from the available tagging data as fish approach Jersey Point and Chipps Island, especially from the Old River route.

Comparison among Release Groups

The estimate of total Delta survival from Mossdale to Chipps Island was lower for the February release group than for the later groups (P=0.0025; Table 23). Examination of the reach-specific survival estimates suggests that it was primarily survival between MacDonald Island and Chipps Island that accounted for the lower Delta survival estimate for the February release (Table A2). That release group also had lower survival from Durham Ferry to Mossdale than the other groups (P<0.0001; Table 23), driven by lower transition probabilities from Durham Ferry to Banta Carbona (Table A2). The April release group, on the other hand, had the highest total Delta survival estimate (P<0.0001) and the highest survival from Durham Ferry to Mossdale (P<0.0001), but the lowest estimated survival to Chipps Island via the Old River route (P=0.0003; Table 14, Table 23).

There was considerable variation in river conditions among the time periods when fish from the different release groups were migrating through the Delta. Measures of Delta inflow, export rates, the I:E ratio, and water temperature were averaged for each release group through the time period that extended from the first day of release through the last day of release, and further extended by the median observed travel time from release to Chipps Island for the release group: 15 days for the February release, 8 days for the March release, and 10 days for the April release (Figure 30–Figure 33). Delta inflow measured at Vernalis (VNS gaging station) was lowest for the February release (average = 1,209 cfs) compared to average VNS flows of 2,508 cfs and 2,649 cfs for the March and April releases, respectively (Figure 30). Delta inflow was highest (up to 6,100 cfs) immediately before and during the first day of the March release period, before a steep decline through the 8 days over which conditions were summarized (Figure 30). Exports were highest for the February and March releases (average combined CVP-SWP export rate = 5,900 cfs for February, and 6,030 cfs for March), and lowest for the April release (2,553 cfs; Figure 31). The I:E ratio (ratio of Delta inflow at VNS to total Delta exports, measured on daily time scale) was lowest for the February release and highest for the April release

(Figure 32). The highest daily I:E ratio values occurred in mid-April, shortly before the start of the April release period (Figure 32). Average I:E values for the three release groups were 0.20, 0.39, and 0.93, respectively. Water temperatures measured at the MSD gaging station near Mossdale tended to be highest for the March release group (average = 16.6°C). The February and April groups experienced similar temperatures (average = 17.8°C and 16.4°C, respectively), but there was more variability during the April summarization period (Figure 33). The highest water temperatures occurred between the March and April releases, when water temperature at MSD reached 22.2°C (Figure 33).

The prevailing conceptual model of how water project operations and river conditions influence survival through the Delta is that survival is higher during periods of higher Delta inflow, lower export rates, higher I:E, and lower water temperatures (SST 2017). The survival estimates from the 2016 six-year study support the conceptual model regarding Delta inflow, exports, and the I:E ratio. In particular, the release group that experienced the lowest Delta inflow (February) had the lowest total survival to Chipps Island, and the release group that experienced the lowest export rates (April) had the highest total survival through the Delta. However, the March release group experienced similarly high Delta inflow compared to the April release on average (Figure 30), but had lower survival. Also, the March release group experienced export rates as high as the February release (Figure 31), but had higher survival. It may be that the high export rates experienced by the March release prevented the full benefit of high Delta inflow for that group, or that the high inflow may have partially offset potential negative effects of high export rates. Alternatively, despite the very high Delta inflow experienced by the first fish released in March, the steep decline in Delta inflow shortly after the beginning of the March release period may have resulted in lower survival compared with the more moderate but also more stable Delta inflow conditions experienced by the April release group. It is notable that when compared to the I:E ratio, which combines both Delta inflow and export conditions, the expected pattern of higher survival associated with higher I:E was observed when comparing all three release groups (Figure 32).

Within the Old River route, the February and March release groups had higher survival than the April release ($P=0.0003$; Table 14). These first two release groups also experienced higher levels of combined export rates from the SWP and CVP facilities, and migrated before installation of the barrier at the head of Old River was complete (Figure 31). This pattern suggests that for fish that enter Old River at its head, higher export rates may provide some benefit by drawing migrants into the salvage tanks faster. However, the estimates of the transition probability from the CVP trashrack into the holding tank (≤0.59), and from the entrance of the Clifton Court Forebay through the Forebay and

salvage facility to Chipps Island (≤0.56) (Table A2) indicate that the salvage routes have considerable mortality risks, even at relatively high export rates. It is also notable that even with the high export rates in February and March, survival to Chipps Island was not higher in the Old River route than in the San Joaquin River route (Table 14).

Within the San Joaquin River route, the April release group had the highest survival to Chipps Island ($P<0.0001$), and survival was higher in this route than in the Old River route ($P=0.0002$) (Table 14). In addition to experiencing low combined export rates, the April release group was the only release that passed the head of Old River with the barrier in place. The rock barrier diverted both fish and river flow away from Old River and into the San Joaquin River route, and in this way may have extended the protective effect of increased Delta inflow further downstream in the San Joaquin River.

Water temperature may also have contributed to differences in survival among the three release groups. Despite the initially high Delta inflows experienced by the March release group, fish from that release also migrated with consistently higher water temperatures than the February or April groups (Figure 33). The warmer water temperatures may have limited the benefit of the higher inflow for the March group. The February and April releases had similar average water temperatures, but the longer travel time of the February release meant that the February fish had longer exposure to warmer water than for the April release (Figure 33), which may have then contributed to the lower survival of that release group. Despite the higher survival estimated for the April release group during this study, the high water temperatures (up to 22°C) and low flow in early and mid-April suggest that run-of-river (untagged) steelhead migrating in the interval between the March release and the April release were likely to have had lower survival than those study fish that migrated in late April.

Survival Through Central Valley Project

Survival through the water export facilities was estimable for all three release groups (Table 22). Pooled over all release groups, the large majority of tags detected at either facility came from the Old River route (Table 11), and the head of Old River barrier prevented most access to the Old River route for the April release group. More tags were detected at the facilities from the San Joaquin River route from the April release group compared to earlier releases, possibly reflecting the larger number of tags observed taking the San Joaquin River route when the barrier was in place. Based on tag detections in regions near the transport release sites (Jersey Point, False River, Chipps Island, Benicia Bridge, Threemile Slough, Montezuma Slough, and Spoonbill Slough), survival was higher through the CVP facility than through the SWP (Table 22). However, the SWP survival included survival through the

Clifton Court Forebay, whereas the CVP survival started from the trashracks located just outside the facility.

The probability of successfully reaching the CVP holding tank from the trashracks ($\phi_{E1,E2}$) was estimated at 0.44 to 0.59 ($\widehat{SE} \leq 0.10$) for each release group (Table A2). The transition parameter $\phi_{E1,E2}$ is the product of the probability of moving from the trashracks toward the louvers and holding tank, and the probability of surviving during that process. Its complement includes both mortality before passing the louvers and within the facility, and the possibility of returning from the trashracks to Old River and moving either upstream toward Middle River or downstream toward the Clifton Court Forebay and Highway 4. Tagged fish whose modeled detection histories included the CVP trashracks (i.e., as tabulated in Table 11) were those fish that were not detected at Old River, Middle River, or radial gate sites (i.e., Clifton Court Forebay) after their CVP detection (excluding the predator-type detections), which means that the extent to which the probability $1-\phi_{E1,E2}$ includes leaving the trashracks for non-CVP sites is limited by the probability of non-detection at those sites (conditional on tag presence), and the possibility of mortality before reaching those sites. The estimated conditional probability of detection was 1.0 for most Old River route sites outside the CVP (Table A2), but was 0.75 at Highway 4 (site B4) for the March release group, and ≥ 0.93 at the exterior receiver at Clifton Court Forebay (RGU, site D1). Additionally, there were too few detections at the Middle River sites in some releases to freely estimate the detection probability at those sites (Table A2). The imperfect detection probabilities at some sites means that some component of the estimated value of $1-\phi_{E1,E2}$ includes the probability of exiting the CVP into the interior Delta and reaching Old and Middle River sites without detection. Nevertheless, the moderate to high estimates of the conditional detection probabilities in Old and Middle Rivers suggest that the majority of the probability $1-\phi_{E1,E2}$ reflects mortality either between the CVP trashracks and those interior Delta sites, or between the CVP trashracks and the CVP holding tank. The complex Delta routing and tidal influence in the southwest region of the Delta prevent estimating the probability of mortality outside the CVP for fish that may have left the trashracks, or to separate that mortality from mortality outside the louvers or within the facility. Comparison of Table 10 and Table 11 shows that of the 336 tags were detected at the CVP trashracks (site E1), 91% (305) were assigned the trashracks detection for the survival model. The other 9% (31 tags) were subsequently observed at non-CVP sites (i.e., B2, B3, B4, C1, C2, D1, D2). While not a reliable estimate of the final probability of leaving the CVP for the interior Delta, the relatively low rate of total CVP tags that were

later detected elsewhere in the interior Delta suggests that most tagged steelhead detected at the CVP trashracks in 2016 attempted to pass into the facility. This result is similar to the pattern observed in 2014, when 96% of the CVP tags were assigned to the CVP route, but considerably different from 2015, when only 59% of the CVP tags were assigned to that route (Buchanan 2018a, 2018b). The estimates of $\phi_{E1,E2}$ in 2016 were similar to those from 2014 (0.50–0.51) and higher than in 2015 (0.36–0.37), implying continued high mortality between the CVP trashracks and either the holding tank or in the Delta following CVP exit.

Once in the CVP holding tank, the probability of successfully reaching Chipps Island ($\phi_{E2,G2}$) was estimated at 0.85–0.92 ($\widehat{SE} \leq 0.08$) for the three release groups (Table A2). Thus, the majority of the perceived loss between the CVP trashrack receivers and Chipps Island occurred between detection at the trashracks and arrival in the holding tanks; survival during and after salvage was relatively high (0.86–1.00; Table 22).

The daily export rate at the CVP, on the day of tag detection at the trashracks (site E1), was between 3,000 cfs and 3,500 cfs for 202 of the 305 (66%) tags used to estimate $\phi_{E1,E2}$; all tags that arrived when the CVP export rate was > 3,000 cfs came from the February and March release groups (Figure 31). The other 103 tags detected at the CVP trashracks were detected there on days when the daily export rate was between 956 cfs and 2,746 cfs. A likelihood ratio test found a difference in estimates of $\phi_{E1,E2}$ for conditions of export rates >3,000 cfs versus <1,000 cfs at tag detection at the CVP trashracks (P=0.0179), pooled over all releases. Combined over releases, the estimated transition probability from the CVP trashracks to the holding tank ($\hat{\phi}_{E1,E2}$) was 0.60 ($\widehat{SE} = 0.03$) for tags that arrived the CVP export rate >3,000, and 0.46 ($\widehat{SE} = 0.05$) when the export rate ≤3,000 cfs.

The route via the Old River route through the CVP to Chipps Island accounted for 0.5% to 66% of the total survival to Chipps Island in 2016, depending on the release group. The estimate of the probability of getting from Mossdale to Chipps Island via Old River and the CVP was unavailable for the February release group because of sparse data at certain sites; however, of the 79 tags detected at either Chipps Island or Benicia Bridge from the February release group, 52 (66%) had been detected in the CVP holding tank. For the March release group in 2016, the route via the CVP to Chipps Island accounted for approximately 45% of the total survival to Chipps Island: total Delta survival was

estimated at 0.42 ($\widehat{SE} = 0.02$), and the total probability of getting from Mossdale to Chipps Island via Old River and the CVP was 0.20 ($\widehat{SE} = 0.02$). The head of Old River barrier was installed for the April release group, and the Old River route via the CVP contributed considerably less to total Delta survival for that group: the probability of getting from Mossdale to Chipps Island via the Old River route and the CVP was <0.01, whereas the total Delta survival was higher than for the other groups (0.59, $\widehat{SE} = 0.02$) (Table 11, Table 14). The proportion of the total Delta survival that represents the CVP salvage route depends on a variety of factors: the probability of taking the Old River route at the head of Old River, the probability of entering the CVP rather than migrating past it to the radial gates or Highway 4, and relative survival in both Old River between its head and the CVP, within the CVP, and during and after salvage, compared to survival throughout the San Joaquin River to Chipps Island. If a barrier blocks most access to Old River, then the CVP is unlikely to represent a significant migration route to Chipps Island, unless survival is also very low in the San Joaquin River. In 2016, the February release group had both a relatively high probability of entering Old River at its head (0.88, $\widehat{SE} = 0.02$) and relatively low survival in the San Joaquin River route (0.23, $\widehat{SE} = 0.08$), compared to the later release groups (Table 14); these two factors contributed to the CVP representing a higher proportion of total Delta survival for February release groups compared to the March and April releases.

References

Buchanan, R. A. (2018a). 2014 Six-Year Acoustic Telemetry and Steelhead Study: Statistical Methods and Results. Technical report to the U.S. Bureau of Reclamation. Available online at http://www.cbr.washington.edu/papers.

Buchanan, R. A. (2018b). 2015 Six-Year Acoustic Telemetry and Steelhead Study: Statistical Methods and Results. Technical report to the U.S. Bureau of Reclamation. Available online at http://www.cbr.washington.edu/papers.

Burnham, K. P., and D. R. Anderson (2002). Model selection and multimodel inference: A practical information-theoretic approach. 2nd edition. Springer. New York, NY. 488 pp.

Cavallo, B., P. Gaskill, and J. Melgo (2013). Investigating the influence of tides, inflows, and exports on sub-daily flow in the Sacramento-San Joaquin Delta. Cramer Fish Sciences Report. 64 pp. Available online at: http://www.fishsciences.net/reports/2013/Cavallo_et_al_Delta_Flow_Report.pdf.

Kutner, M. H., C. J. Nachtsheim, and J. Neter (2004). Applied linear regression models. 4th edition. McGraw-Hill Irwin, San Francisco, CA.

Lady, J. M., and J. R. Skalski (2009). USER 4: User-Specified Estimation Routine. School of Aquatic and Fishery Sciences. University of Washington. Available from http://www.cbr.washington.edu/paramest/user/.

Li, T., and J. J. Anderson (2009). The Vitality model: A Way to understand population survival and demographic heterogeneity. Theoretical Population Biology 76: 118-131.

Louis, T. A. (1981). Confidence intervals for a binomial parameter after observing no successes. The American Statistician 35:154.

McCullagh, P., and J. Nelder (1989). Generalized linear models. 2nd edition. Chapman and Hall, London.

Perry, R. W., J. R. Skalski, P. L. Brandes, P. T. Sandstrom, A. P. Klimley, A. Ammann, and B. MacFarlane (2010). Estimating survival and migration route probabilities of juvenile Chinook salmon in the Sacramento-San Joaquin River Delta. North American Journal of Fisheries Management 30: 142-156.

Salmon Scoping Team (SST) (2017). Effects of water project operations on juvenile salmonid migration and survival in the South Delta. Volume 1: Findings and Recommendations, and Appendices. Technical report prepared for Collaborative Adaptive Management Team, January 2017. Available: https://www.westcoast.fisheries.noaa.gov/central_valley/water_operations/OCAPreports.html. Accessed 19 Nov 2018.

San Joaquin River Group Authority (SJRGA) (2010). 2009 Annual Technical Report: On Implementation and Monitoring of the San Joaquin River Agreement and the Vernalis Adaptive Management Plan (VAMP). Prepared for the California Water Resources Control Board.

San Joaquin River Group Authority (SJRGA) (2011). 2010 Annual Technical Report: On Implementation and Monitoring of the San Joaquin River Agreement and the Vernalis Adaptive Management Plan (VAMP). Prepared for the California Water Resources Control Board.

San Joaquin River Group Authority (SJRGA) (2013). 2011 Annual Technical Report: On Implementation and Monitoring of the San Joaquin River Agreement and the Vernalis Adaptive Management Plan (VAMP). Prepared for the California Water Resources Control Board.

Seber, G. A. F. (2002). The estimation of animal abundance. Second edition. Blackburn Press, Caldwell, New Jersey.

Sokal, R. R., and Rohlf, F. J. (1995). Biometry, 3rd ed. W.H. Freeman and Co., New York, NY, USA.

Smith, J., D. Huff, C. Michel, D. Demer, G. Cutter, S. Manugian, T. Quinn, and S. Hayes (2016). Quantifying the abundance, distribution, and predation of salmon by non-native fish predators in the San Joaquin River. Oral presentation to Bay-Delta Science Conference, November 15–17, 2016, Sacramento, CA.

Townsend, R. L., J. R. Skalski, P. Dillingham, and T. W. Steig (2006). Correcting Bias in Survival Estimation Resulting from Tag Failure in Acoustic and Radiotelemetry Studies. Journal of Agricultural, Biological, and Environmental Statistics 11: 183-196.

U.S. Bureau of Reclamation (USBR) (2018a). NMFS Biological Opinion RPA IV.2.2: 2011 Six-Year Acoustic Telemetry Steelhead Study. Contributions by Buchanan, R., J. Israel, P. Brandes. E. Buttermore. Reclamation Bay-Delta Office, Mid-Pacific Region, Sacramento, CA. FINAL REPORT May 14, 2018, 144p.

U.S. Bureau of Reclamation (USBR) (2018b). NMFS Biological Opinion RPA IV.2.2: 2012 Six-Year Acoustic Telemetry Steelhead Study. Contributions by Buchanan, P. Brandes, R., J. Israel, E. Buttermore. Reclamation Bay-Delta Office, Mid-Pacific Region, Sacramento, CA. FINAL REPORT May 16, 2018, 172p.

U.S. Bureau of Reclamation (USBR) (2018c). NMFS Biological Opinion RPA IV.2.2: 2013 Six-Year Acoustic Telemetry Steelhead Study. Contributions by: R. Buchanan, P. Brandes, J. Israel, and E. Buttermore. U.S. Bureau of Reclamation. Bay-Delta Office, Mid-Pacific Region, Sacramento, CA. FINAL REPORT. June 2018, 213 pp.

Vogel, D. A. (2010). Evaluation of acoustic-tagged juvenile Chinook salmon movements in the Sacramento-San Joaquin delta during the 2009 Vernalis Adaptive Management Program. Technical Report for San Joaquin River Group Authority. 72 p. Available http://www.sjrg.org/technicalreport/ (accessed 13 December 2011).

Vogel, D. A. (2011). Evaluation of acoustic-tagged juvenile Chinook salmon and predatory fish movements in the Sacramento-San Joaquin Delta during the 2010 Vernalis Adaptive Management

Program. Technical report for San Joaquin River Group Authority. Available http://www.sjrg.org/technicalreport/ (accessed 13 December 2011).

Figures

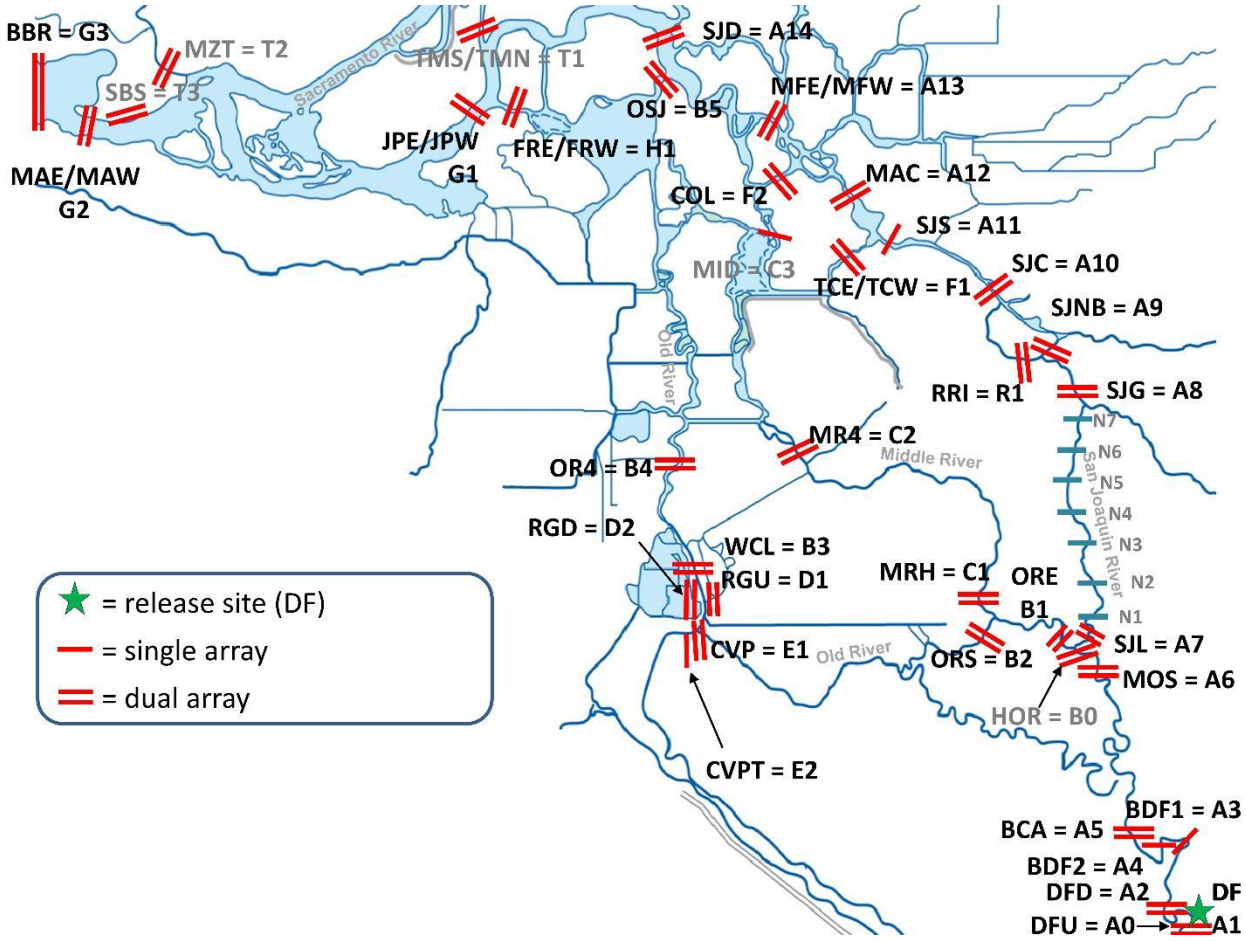

Figure 1. Locations of acoustic receivers and release site used in the 2016 steelhead tagging study, with site code names (3- or 4-letter code) and model code (letter and number string). Site A1 is the release site at Durham Ferry. Sites in gray were omitted from the survival model.

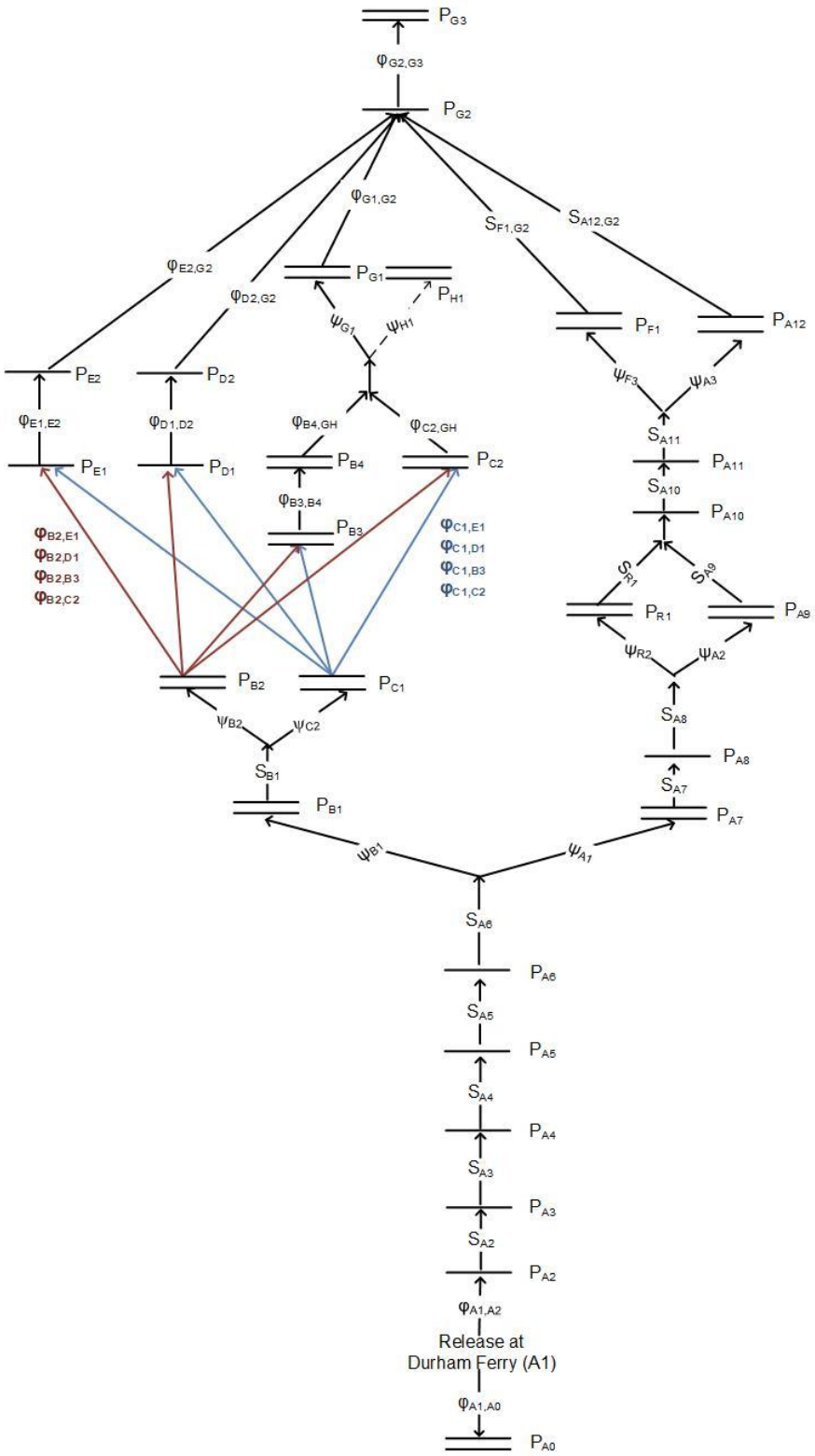

Figure 2. Schematic of 2016 mark-recapture Submodel I with estimable parameters. Single lines denote single-array or redundant multi-line telemetry stations, and double lines denote dual-array telemetry stations, respectively. Names of telemetry stations correspond to site labels in Figure 1. Migration pathways to sites B3 (WCL), C2 (MR4), D1 (RGU), and E1 (CVP) are color-coded by departure site.

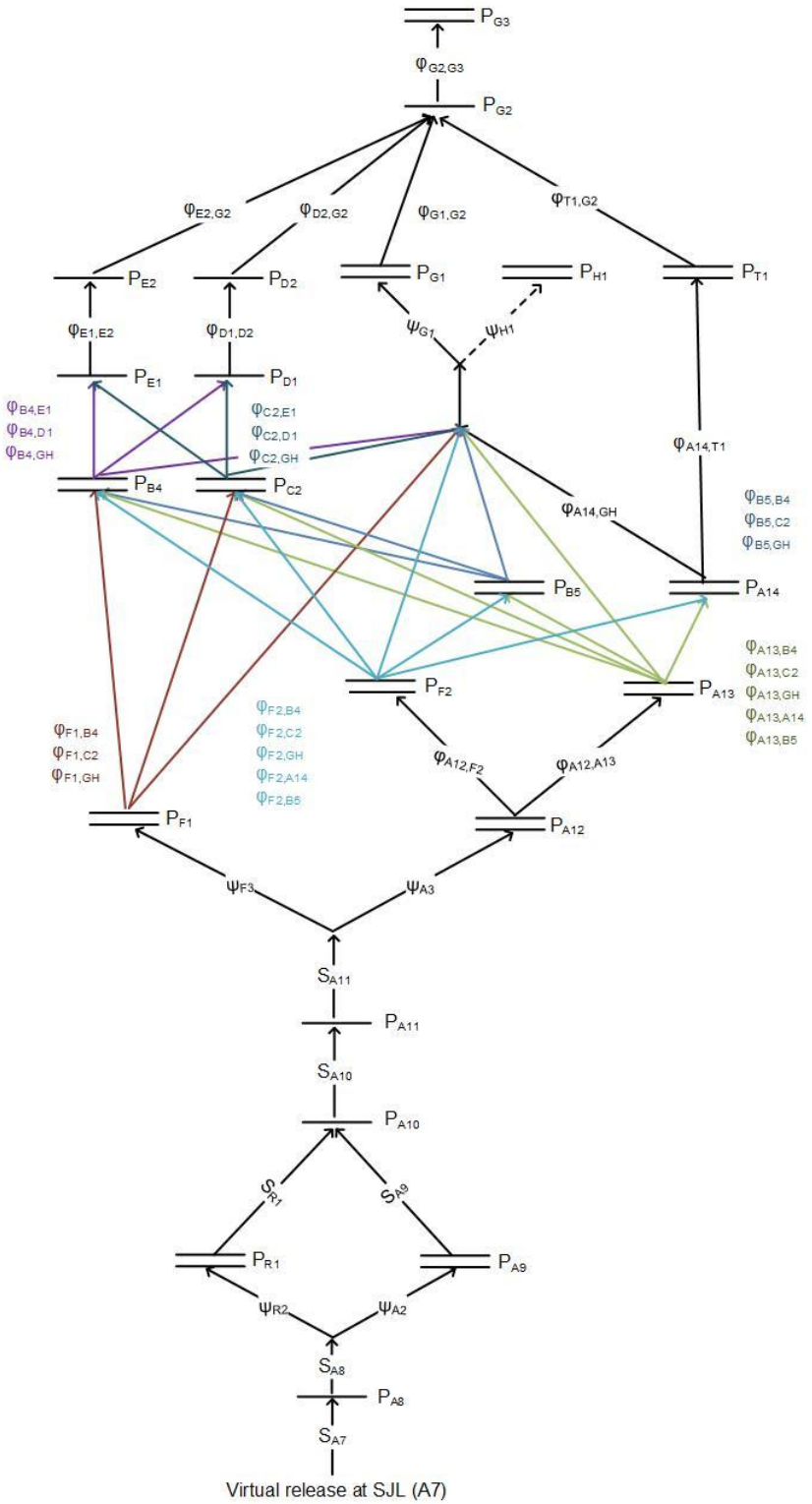

Figure 3. Schematic of 2016 mark-recapture Submodel II with estimable parameters. Single lines denote single-array or redundant multi-line telemetry stations, and double lines denote dual-array telemetry stations. Names of telemetry stations correspond to site labels in Figure 1. Migration pathways to sites A14 (SJD), B4 (OR4), B5 (OSJ), C2 (MR4), D1 (RGU), E1 (CVP), and the G1-H1 junction (JPE/JPW – FRE/FRW) are color-coded by departure site.

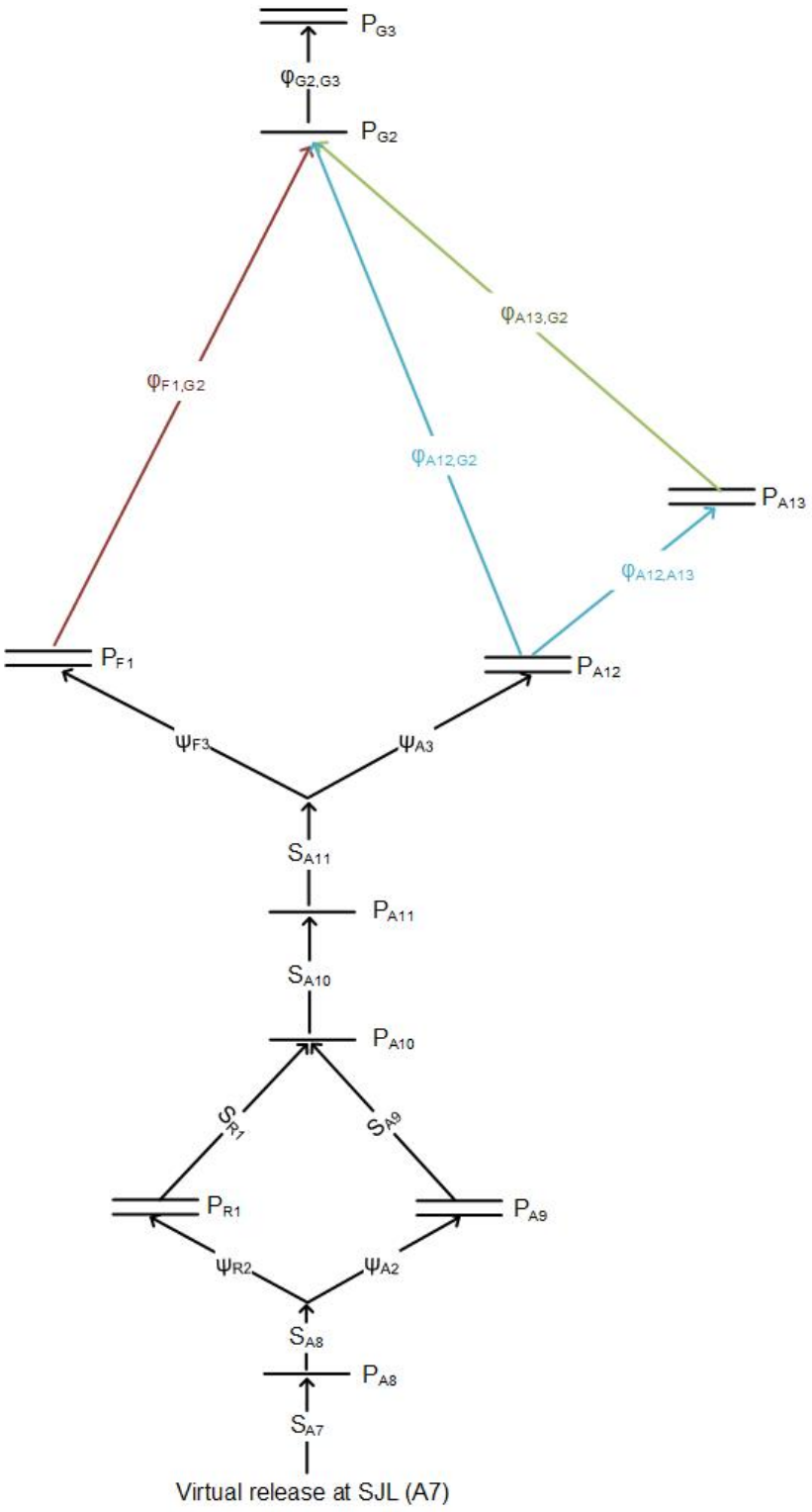

Figure 4. Schematic of simplified 2016 mark-recapture Submodel II with estimable parameters, used for the February release group (release 1). Single lines denote single-array or redundant multi-line telemetry stations, and double lines denote dual-array telemetry stations. Names of telemetry stations correspond to site labels in Figure 1. Migration pathways from sites A12 (MAC), A13 (MFE/MFW), and F1 (TCE/TCW) are color-coded by departure site.

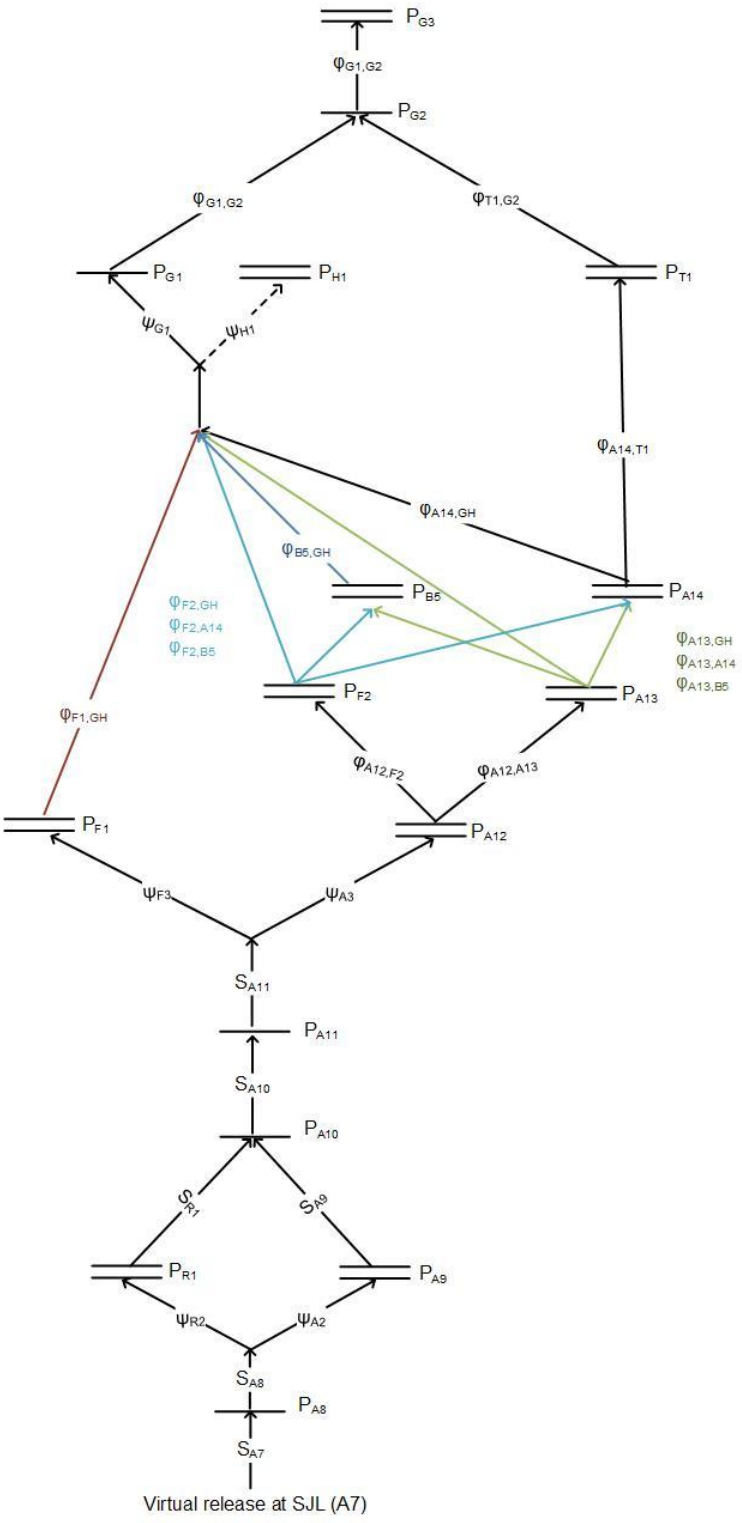

Figure 5. Schematic of simplified 2016 mark-recapture Submodel II with estimable parameters, used for the March release group (release 2). Single lines denote single-array or redundant multi-line telemetry stations, and double lines denote dual-array telemetry stations. Names of telemetry stations correspond to site labels in Figure 1. Migration pathways to sites A14 (SJD), B5 (OSJ), and the G1-H1 junction (JPE/JPW – FRE/FRW) are color-coded by departure site.

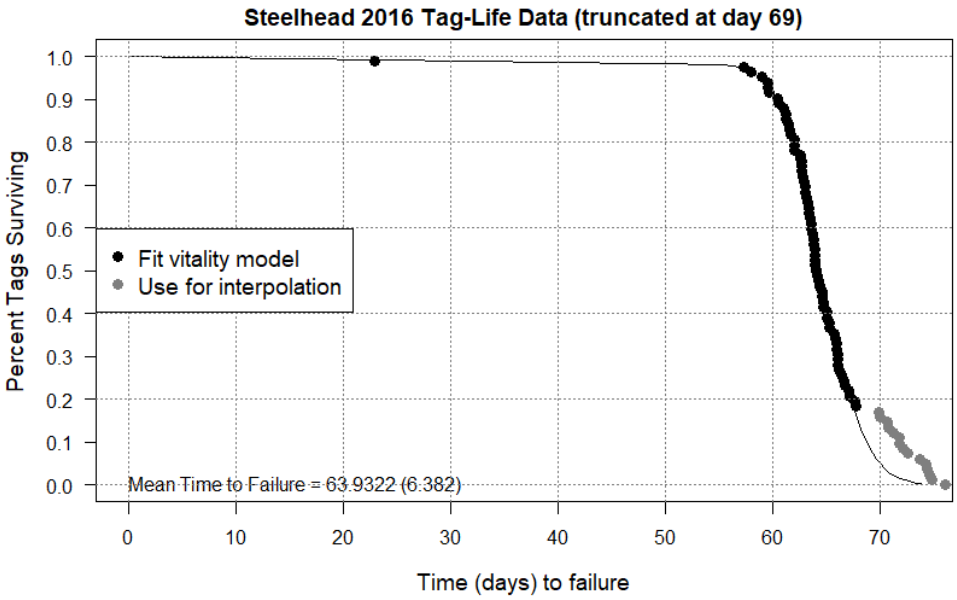

Figure 6. Observed tag failure times from the 2016 tag-life studies (pooled over the February, April, and May studies), and fitted four-parameter vitality curve. Tags without final failure times were omitted (17 tags). Failure times were truncated at day 69 to improve fit of the model. Tag failure times used to fit the model are represented by black dots; failure times past the truncation point are in gray.

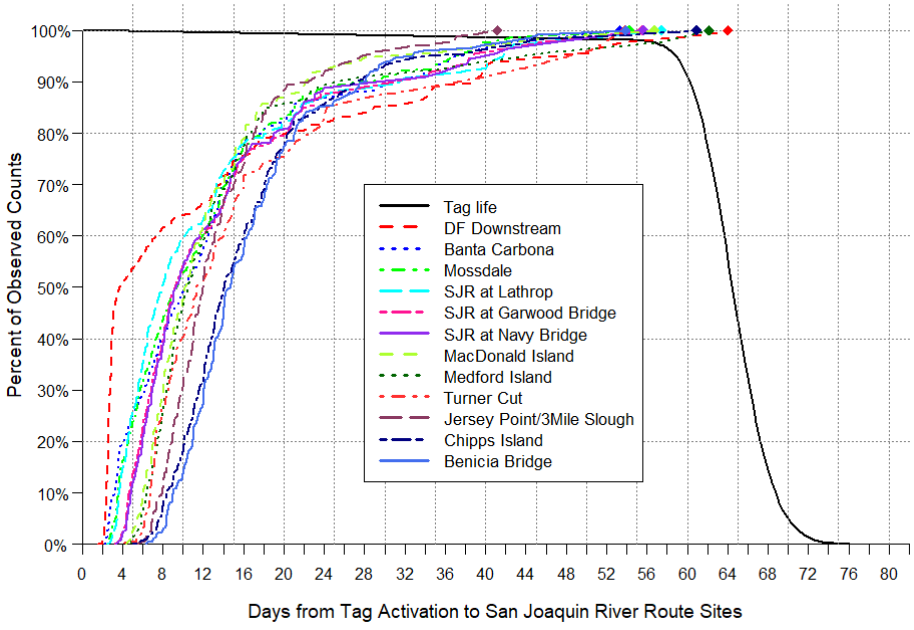

Figure 7. Four-parameter vitality survival curve for tag survival, and the cumulative arrival timing of acoustic-tagged juvenile steelhead at receivers in the San Joaquin River route to Chipps Island in 2016, including detections that may have come from predators; tag-life data were pooled across tag-life studies, and arrival time data were pooled across releases. The tag survival curve was estimated only to day 69, to improve model fit.

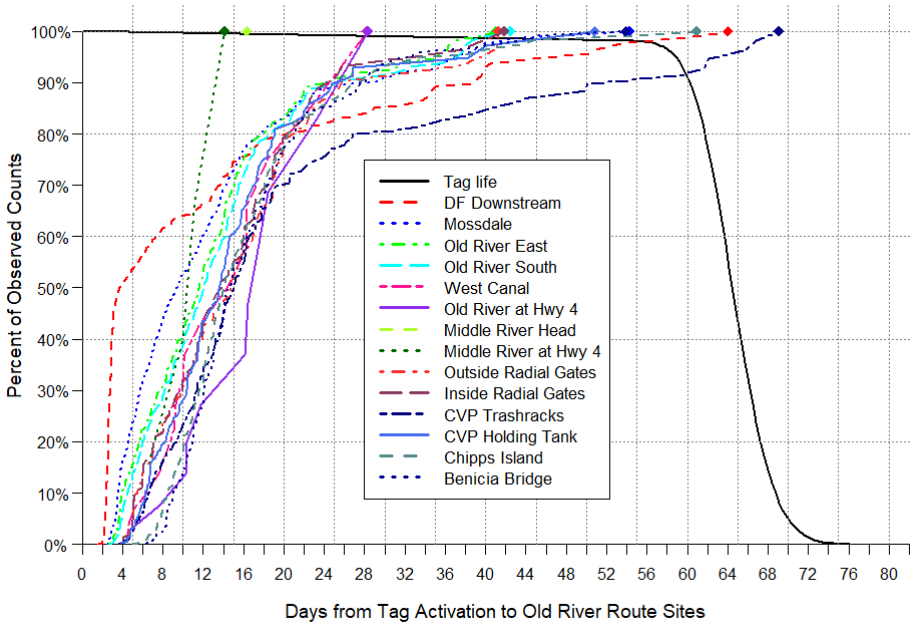

Figure 8. Four-parameter vitality survival curve for tag survival, and the cumulative arrival timing of acoustic-tagged juvenile steelhead at receivers in the Old River route to Chipps Island in 2016, including detections that may have come from predators; tag-life data were pooled across tag-life studies, and arrival time data were pooled across releases. The tag survival curve was estimated only to day 69, to improve model fit.

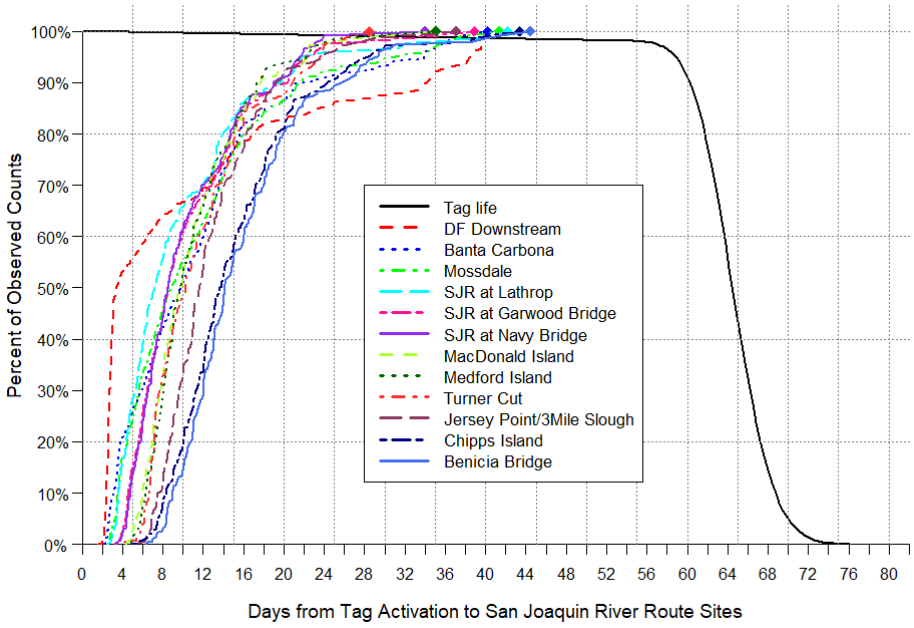

Figure 9. Four-parameter vitality survival curve for tag survival, and the cumulative arrival timing of acoustic-tagged juvenile steelhead at receivers in the San Joaquin River route to Chipps Island in 2016, excluding detections that were deemed to have come from predators; tag-life data were pooled across tag-life studies, and arrival time data were pooled across releases. The tag survival curve was estimated only to day 69, to improve model fit.

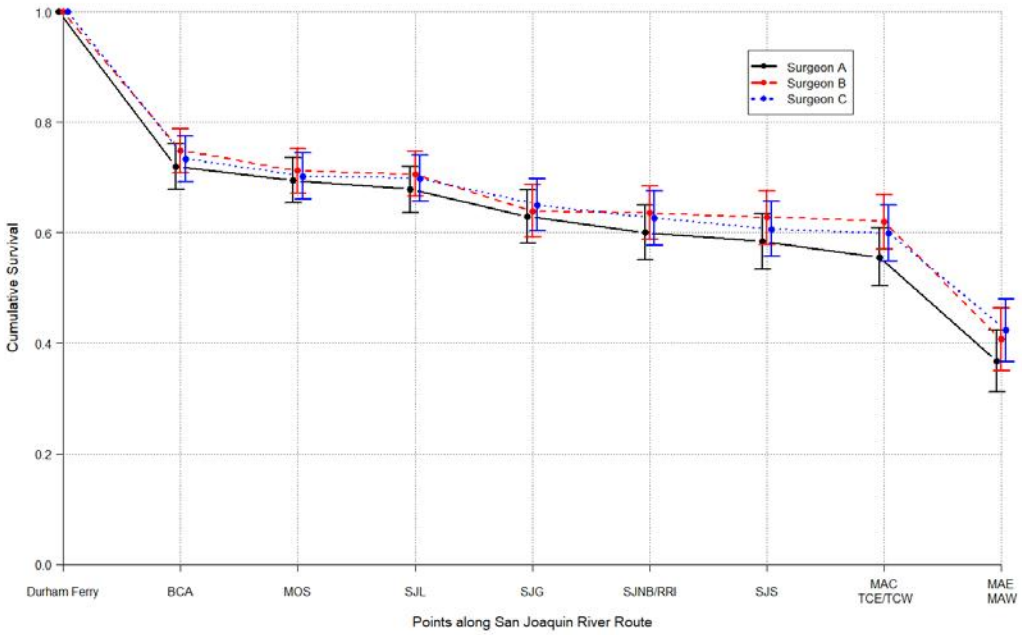

Figure 10. Cumulative survival from release at Durham Ferry to various points along the San Joaquin River route to Chipps Island, by surgeon. Error bars are 95% confidence intervals.

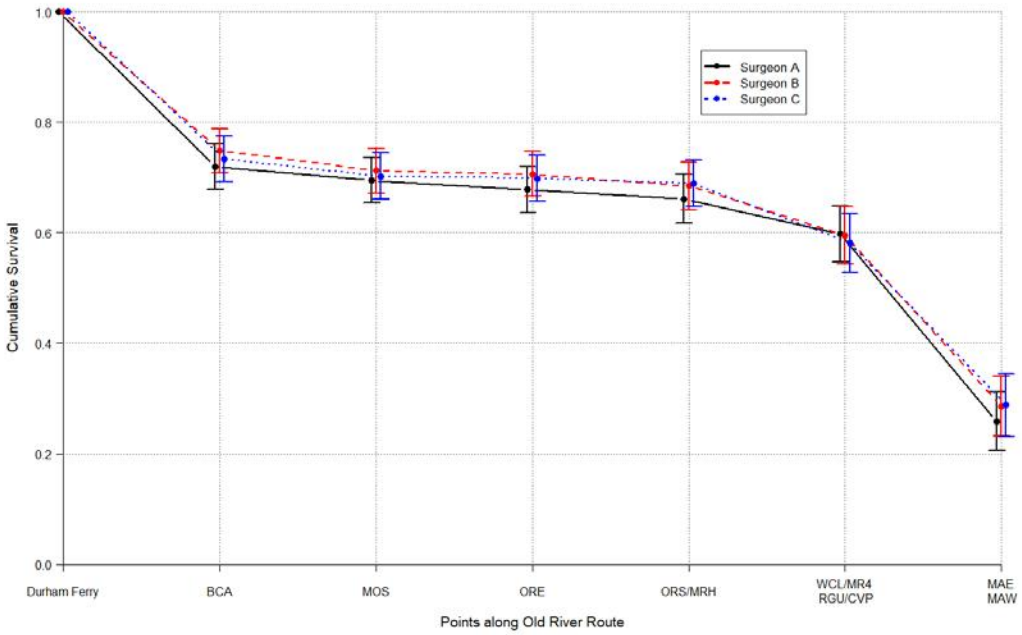

Figure 11. Cumulative survival from release at Durham Ferry to various points along the Old River route to Chipps Island, by surgeon. Error bars are 95% confidence intervals.

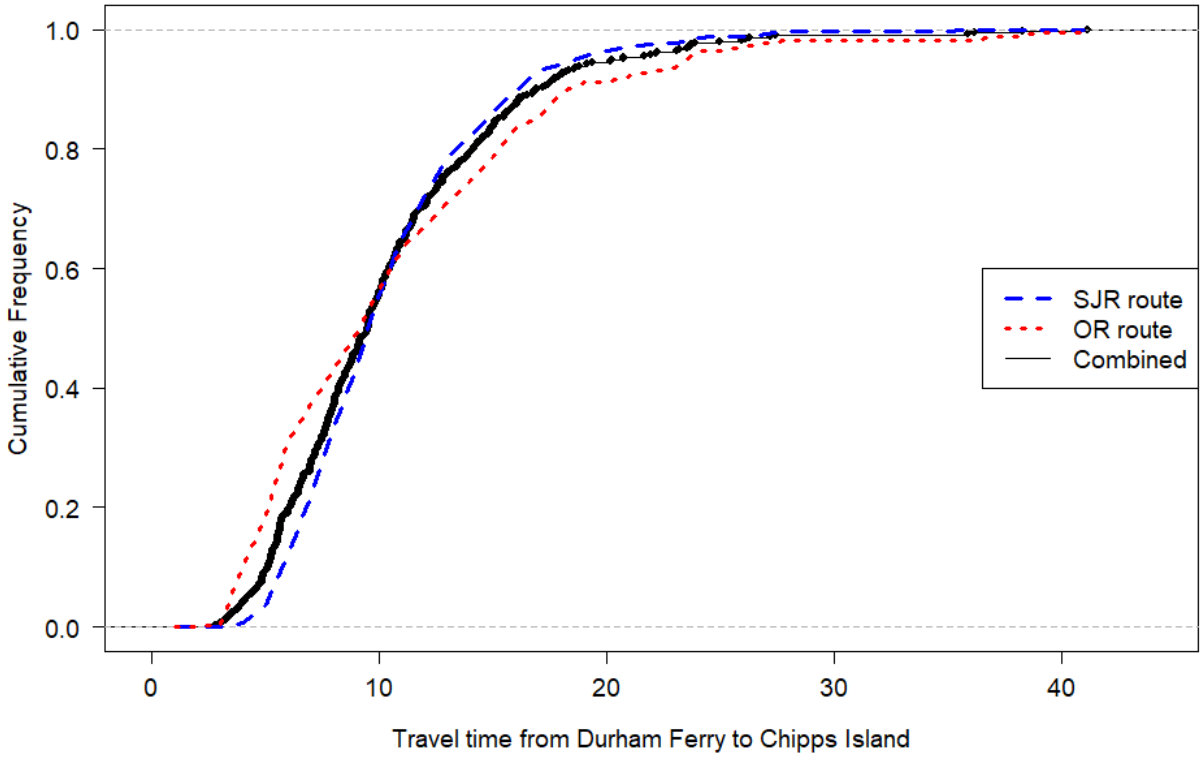

Figure 12. Empirical cumulative travel time distribution from Durham Ferry to Chipps Island for juvenile steelhead tagged and released at Durham Ferry in the 2016 Six-Year Study. Migration route (SJR = San Joaquin River, OR = Old River) was defined based on route selection at the head of Old River. Black points represent observed travel time for both routes combined. All release groups are represented.

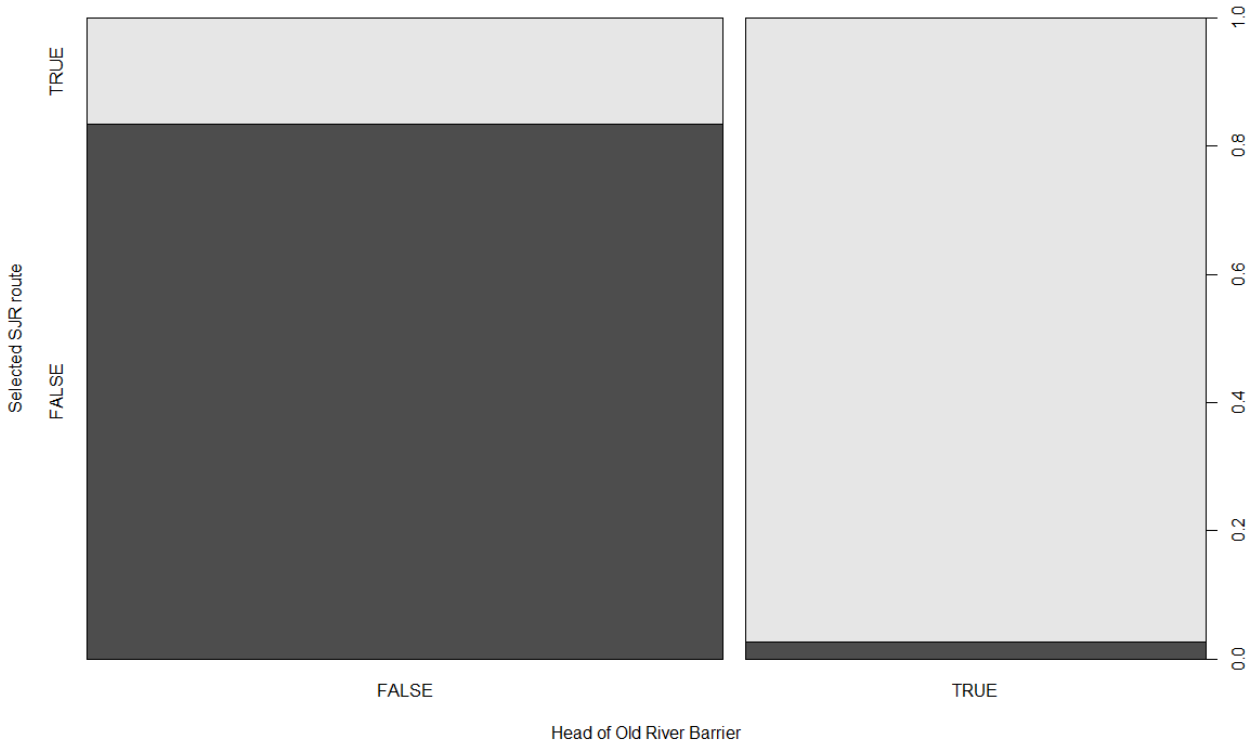

Figure 13. Relative proportions of 914 tags in the head of Old River route selection analysis observed selecting the San Joaquin River route (light shading) based on barrier status at time of arrival at the head of Old River in 2016. The short, dark region, denoting the "barrier" and "Old River route" combination, represented 10 tags. Tags observed at the junction after barrier opening and removal were omitted.

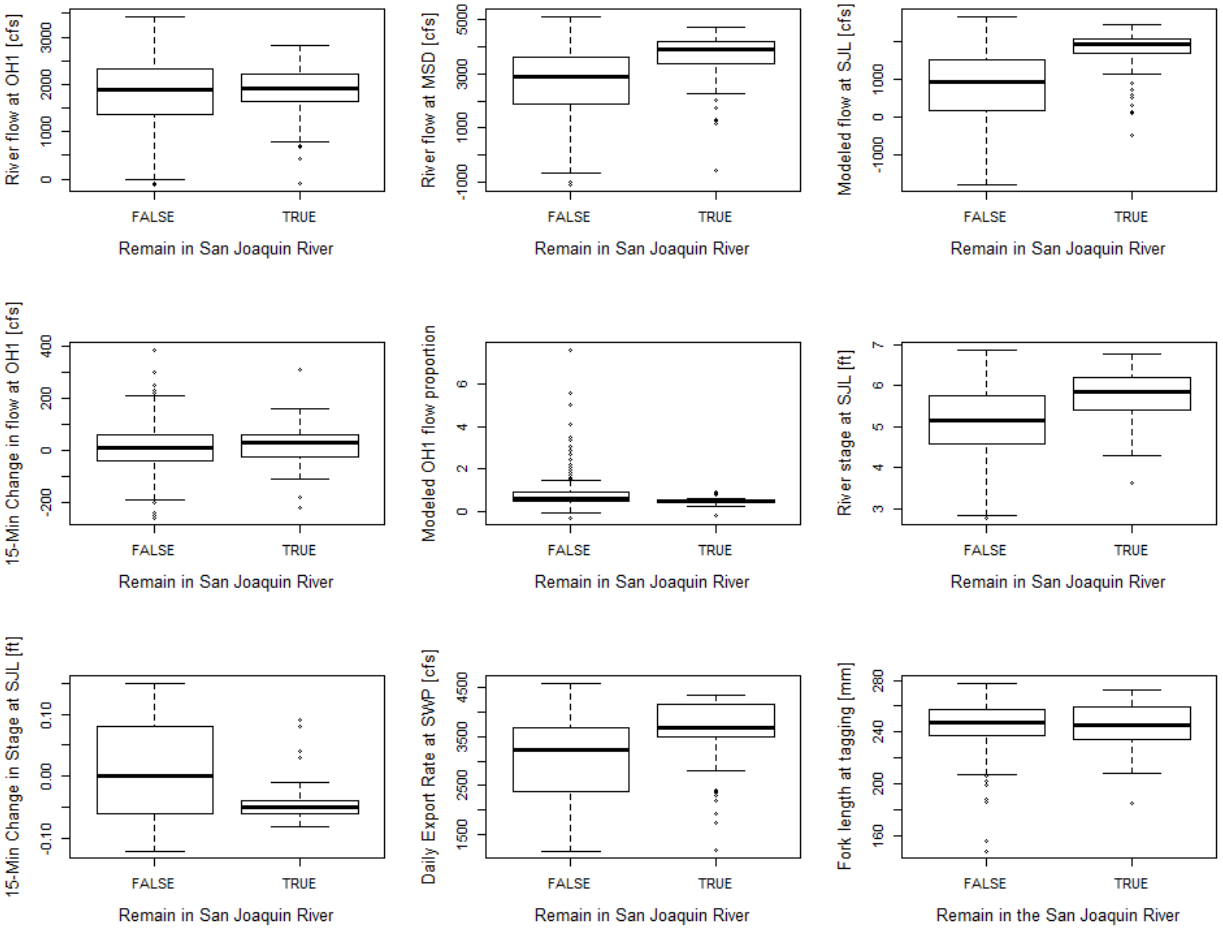

Figure 14. Conditions upon the estimated time of arrival at the head of Old River junction, daily export rates, and fork length at tagging, for steelhead detected at the SJL or ORE receivers and estimated to have arrived at the head of Old River junction before 1500 hours on 1 April 2016 (closure date for the head of Old River barrier). Data represent tags whose most recent detections were either upstream or in the other river branch, and did not linger in the vicinity of the river junction longer than 3 hours; predator-type detections were omitted. Bolded horizontal bar is median measure, upper and lower boundaries of box are the 25th and 75th quantiles (defining the interquartile range), and whiskers are the extremes or 1.5 × the interquartile range.

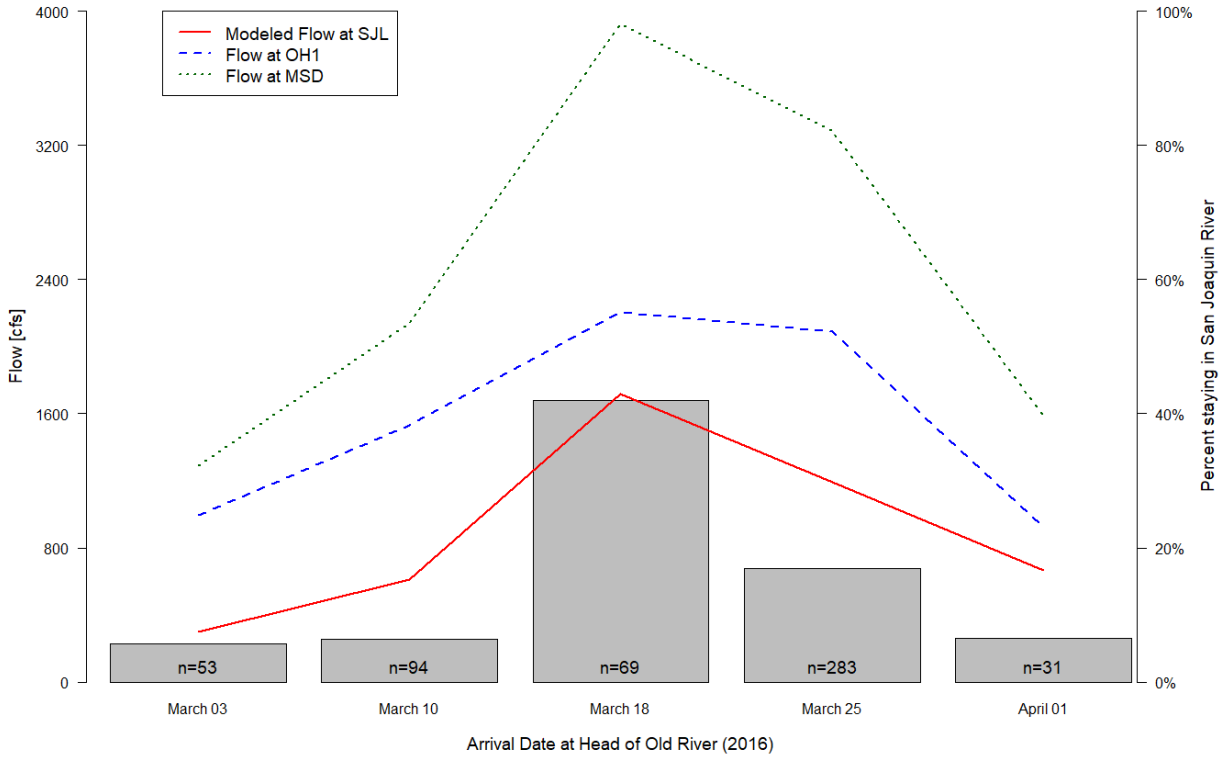

Figure 15. The observed proportion of tagged juvenile steelhead that remained in the San Joaquin River at the head of Old River during the 2016 tagging study (gray bars, representing weekly periods; n = weekly sample size), and the measured flow at the OH1 and MSD gaging stations and modeled flow at the SJL gaging station at the estimated time of fish arrival at the junction, averaged over fish, for steelhead estimated to have arrived at the junction before 1500 hours on 1 April 2016. Proportion of fish remaining in the San Joaquin River is shown only for time periods with at least 10 fish detected.

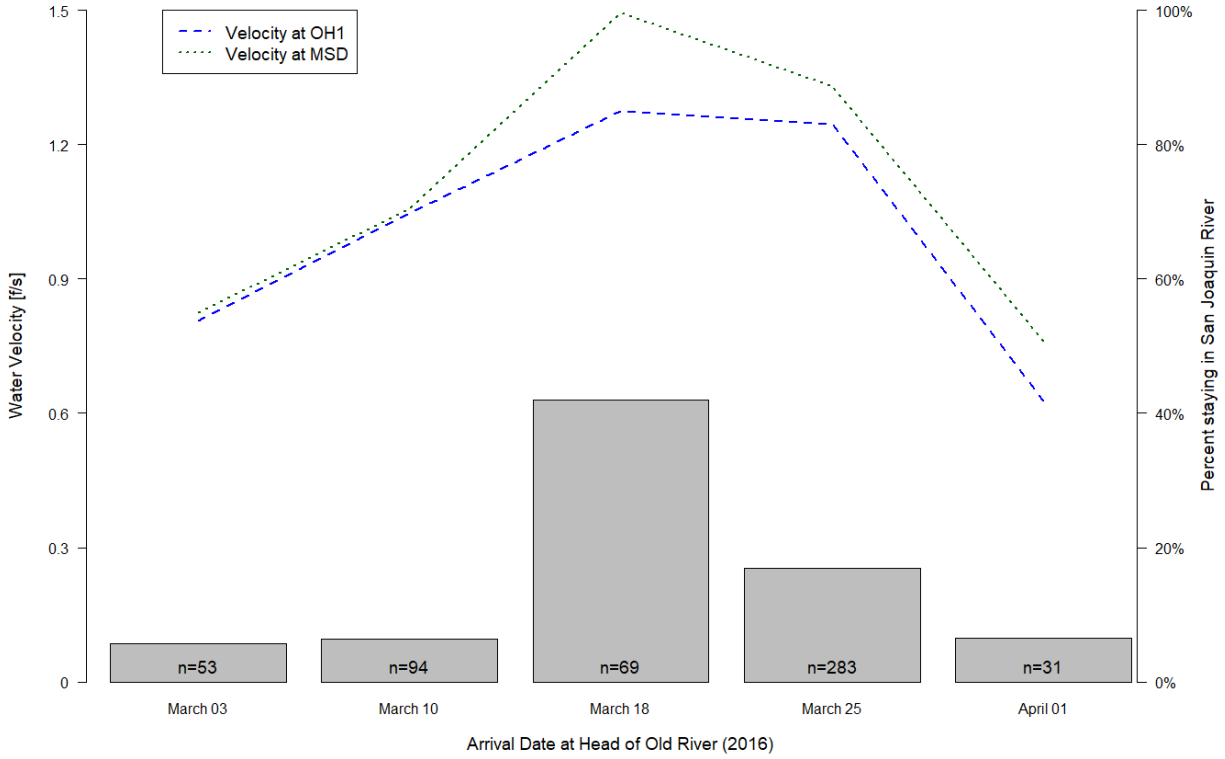

Figure 16. The observed proportion of tagged juvenile steelhead that remained in the San Joaquin River at the head of Old River during the 2016 tagging study (gray bars, representing weekly periods; n = weekly sample size), and the measured water velocity at the OH1 and MSD gaging stations at the estimated time of fish arrival at the junction, averaged over fish, for steelhead estimated to have arrived at the junction before 1500 hours on 1 April 2016. Proportion of fish remaining in the San Joaquin River is shown only for time periods with at least 10 fish detected.

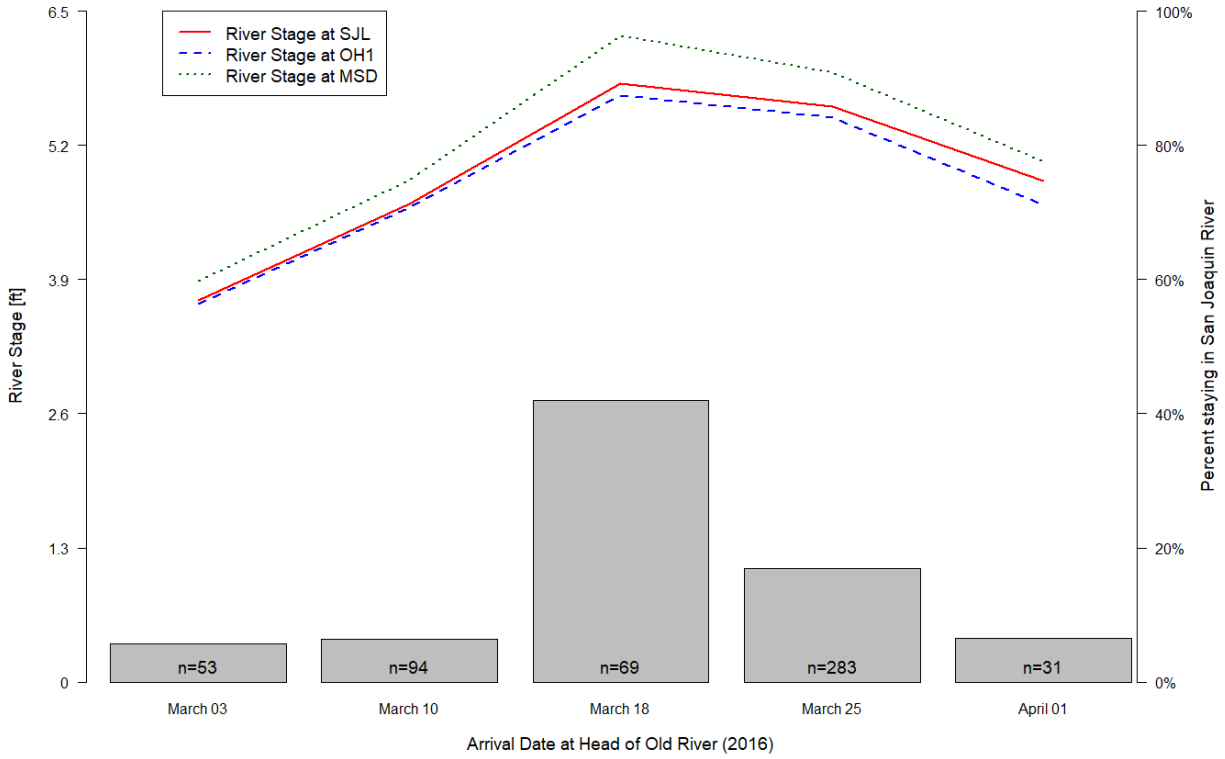

Figure 17. The observed proportion of tagged juvenile steelhead that remained in the San Joaquin River at the head of Old River during the 2016 tagging study (gray bars, representing weekly periods; n = weekly sample size), and the measured river stage at the SJL, OH1, and MSD gaging stations at the estimated time of fish arrival at the junction, averaged over fish, for steelhead estimated to have arrived at the junction before 1500 hours on 1 April 2016. Proportion of fish remaining in the San Joaquin River is shown only for time periods with at least 10 fish detected.

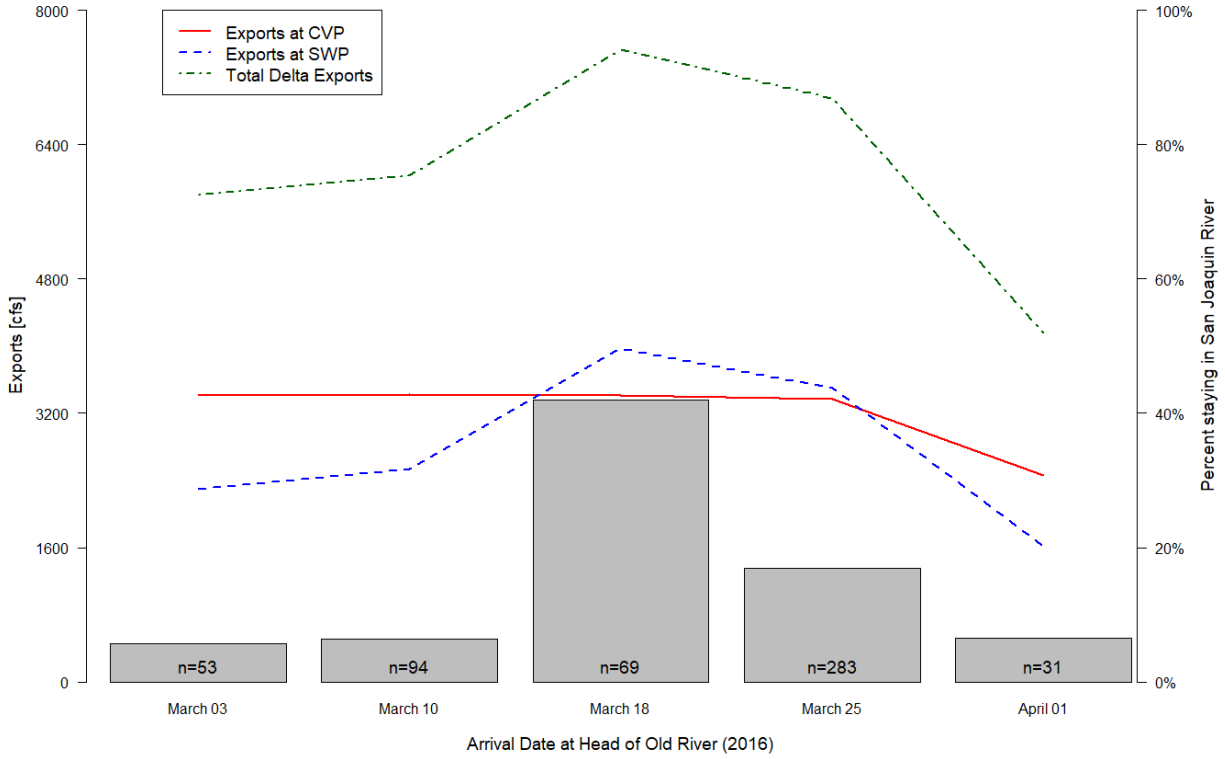

Figure 18. The observed proportion of tagged juvenile steelhead that remained in the San Joaquin River at the head of Old River during the 2016 tagging study (gray bars, representing weekly periods; n = weekly sample size), and the measured daily export rate at CVP, SWP, and total in the Delta on the estimated day of fish arrival at the junction, averaged over fish, for steelhead estimated to have arrived at the junction before 1500 hours on 1 April 2016. Proportion of fish remaining in the San Joaquin River is shown only for time periods with at least 10 fish detected.

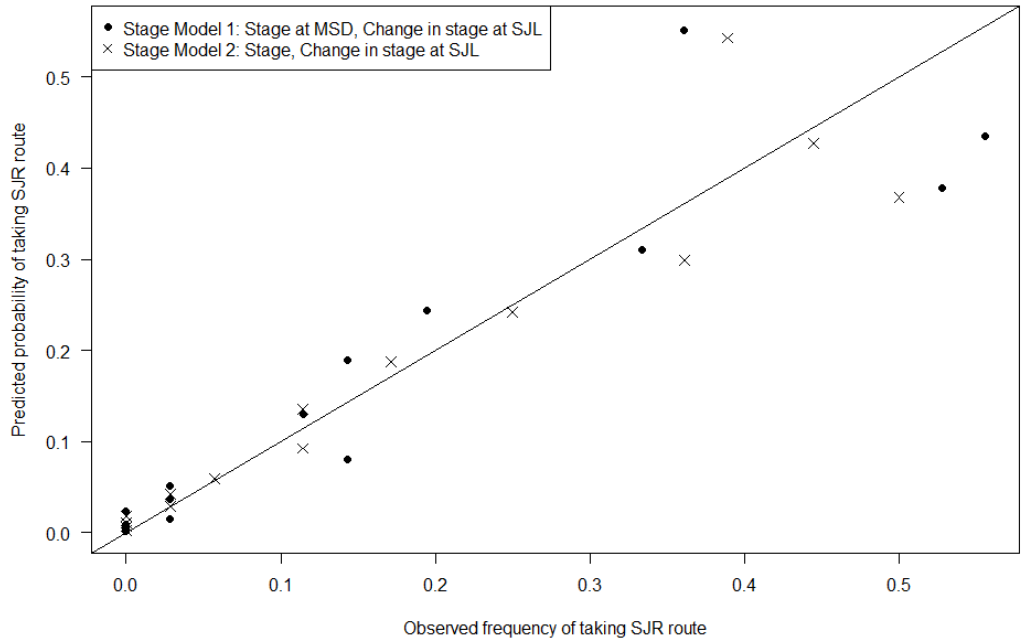

Figure 19. Predicted probability versus observed frequency of taking the San Joaquin River (SJR) route at the head of Old River, for two river stage models for route selection at the head of Old River. Dashed line is 1-1 line.

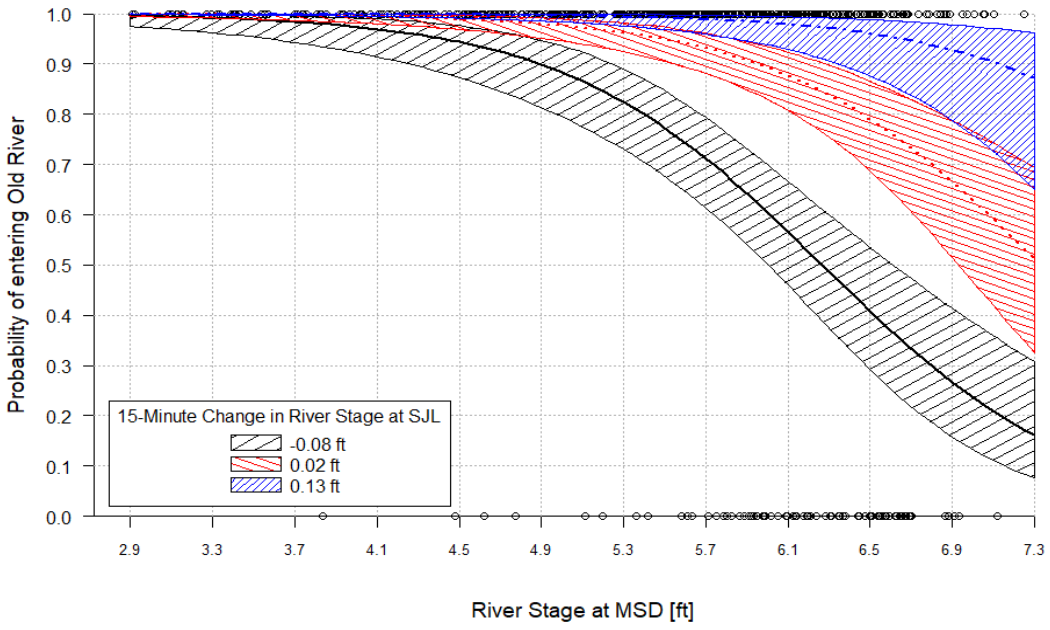

Figure 20. Fitted probability of entering Old River at its head versus river stage measured at the MSD gaging station in the San Joaquin River, for 15-minute change in river stage at SJL = -0.08, 0.02, and 0.13 ft, with 95% confidence bands, in 2016. Covariates were measured at the time of estimated tagged fish arrival at the head of Old River junction. Points indicate the observed route selection (0 = San Joaquin River, 1 = Old River) for each observed value of river stage.

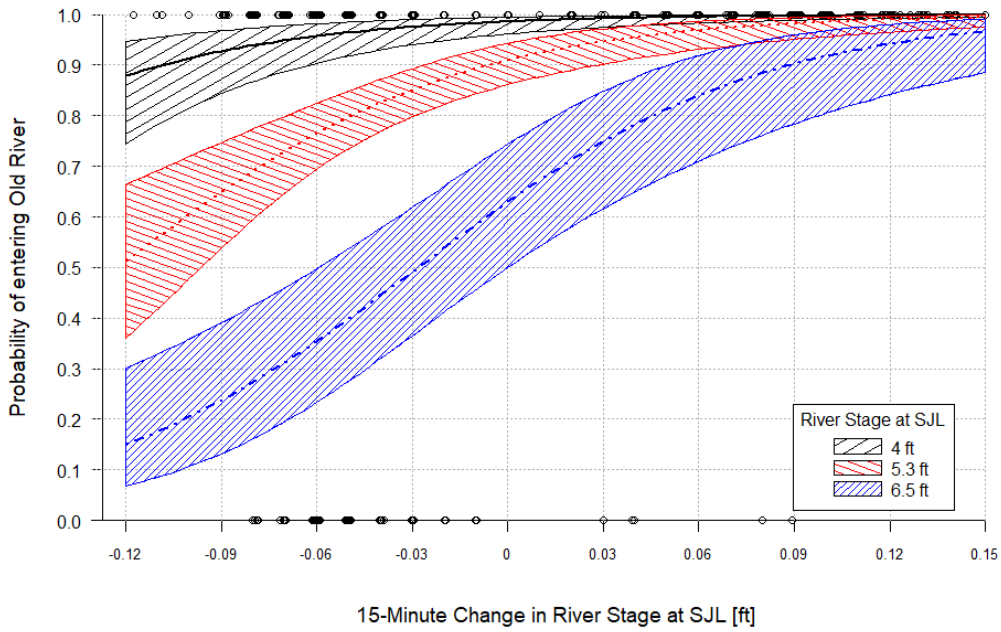

Figure 21. Fitted probability of entering Old River at its head versus the 15-minute change in river stage measured at the SJL gaging station in the San Joaquin River, for river stage at MSD = 4, 5.3, and 6.5 ft, with 95% confidence bands, in 2016. Covariates were measured at the time of estimated tagged fish arrival at the head of Old River junction. Points indicate the observed route selection (0 = San Joaquin River, 1 = Old River) for each observed value of 15-minute change in river stage; observed 15-minute change in river stage values have been offset slightly to avoid overlap in plotting.

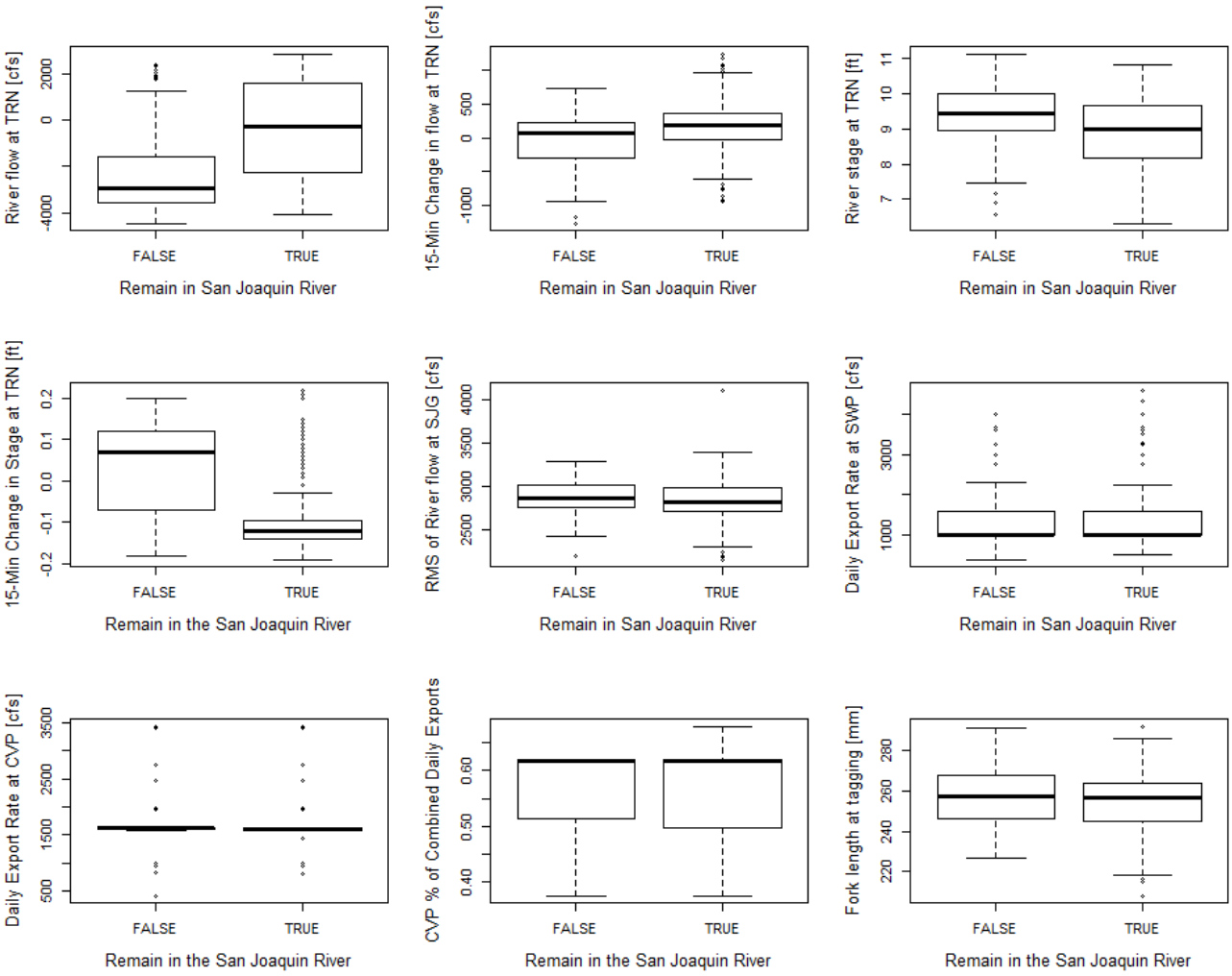

Figure 22. Hydrological conditions upon the estimated time of tag passage at the SJS receiver (0.39 km upstream of the Turner Cut junction), daily export rates, and fork length at tagging, for steelhead detected at the MAC or TCE/TCW receivers. Data represent tags that whose most recent detections were upstream and with travel time ≤8 hours from SJS to either MAC or TCE/TCW; predator-type detections were omitted. Bolded horizontal bar is median measure, upper and lower boundaries of box are the 25th and 75th quantiles (defining the interquartile range), and whiskers are the extremes or 1.5 × the interquartile range.

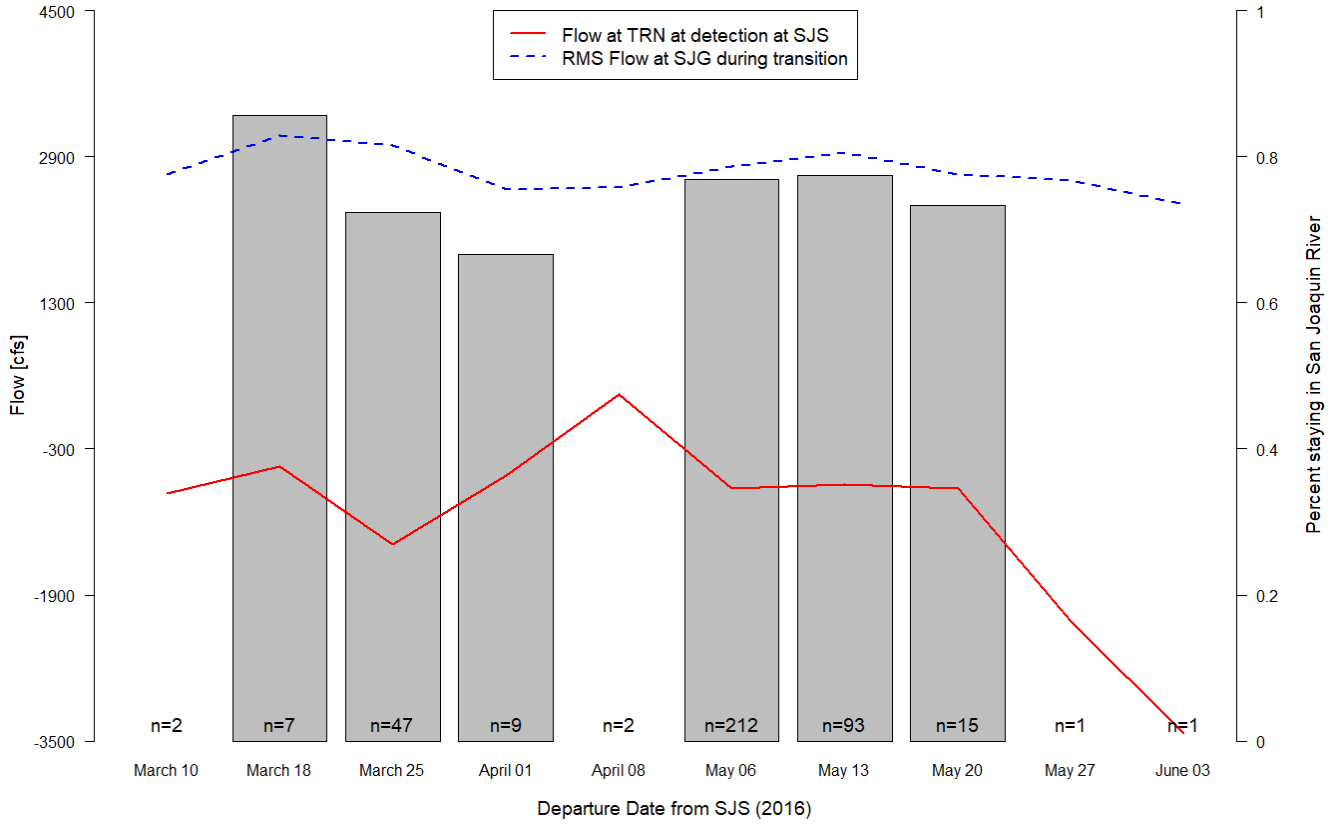

Figure 23. The observed proportion of tagged juvenile steelhead that remained in the San Joaquin River at the Turner Cut junction during the 2016 tagging study (gray bars, representing weekly periods; n = weekly sample size), the measured river discharge (flow) at the TRN gaging station in Turner Cut at the time of tag passage of the SJS receivers, averaged over fish (solid line), and the Root Mean Square (RMS) of river flow measured at the SJG gaging station during fish transition from the SJG telemetry receiver to the SJS receivers, averaged over fish (dashed line). Proportion of fish remaining in the San Joaquin River is shown only for time periods with at least 5 fish detected.

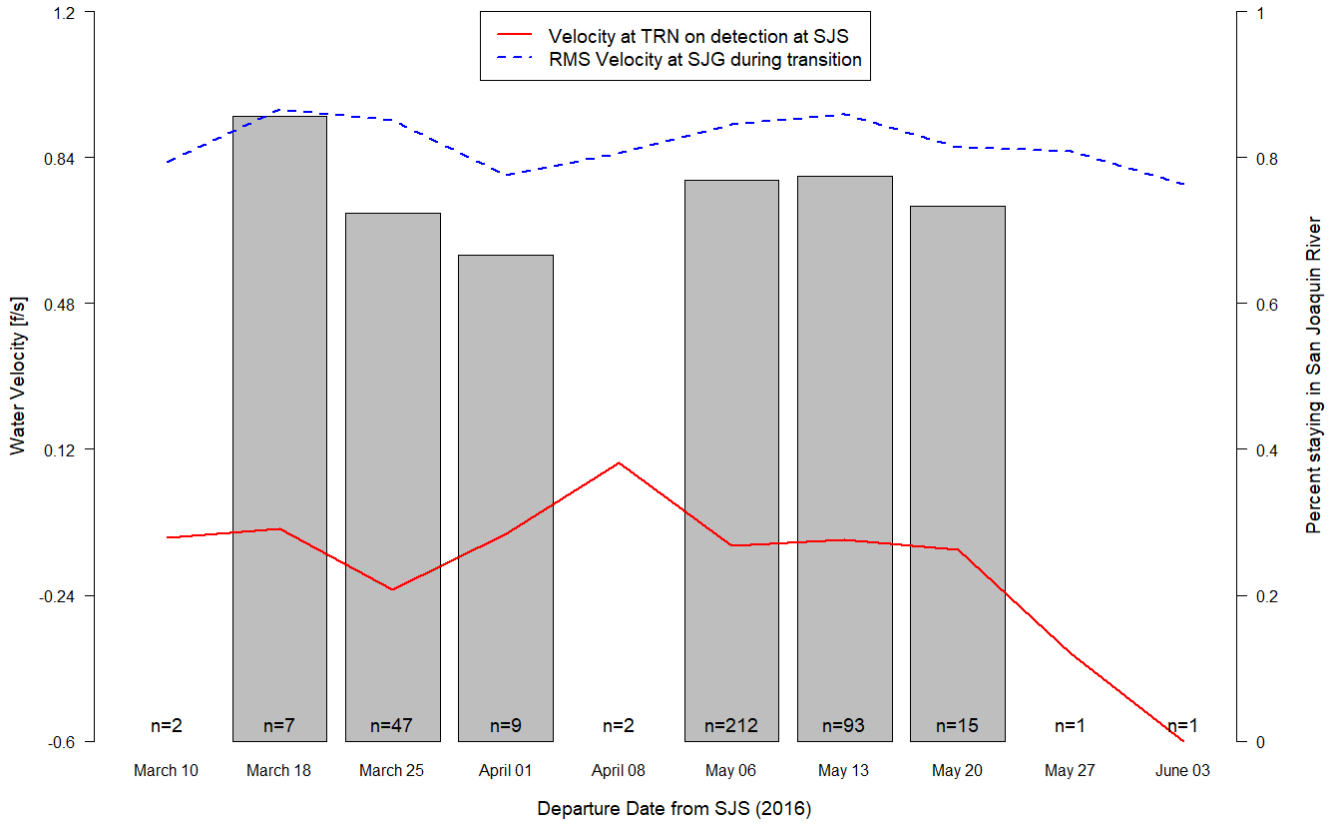

Figure 24. The observed proportion of tagged juvenile steelhead that remained in the San Joaquin River at the Turner Cut junction during the 2016 tagging study (gray bars, representing weekly periods; n = weekly sample size), the measured water velocity at the TRN gaging station in Turner Cut at the time of tag passage of the SJS receivers, averaged over fish (solid line), and the Root Mean Square (RMS) of water velocity measured at the SJG gaging station during fish transition from the SJG acoustic receiver to the SJS receivers, averaged over fish (dashed line). Proportion of fish remaining in the San Joaquin River is shown only for time periods with at least 5 fish detected.

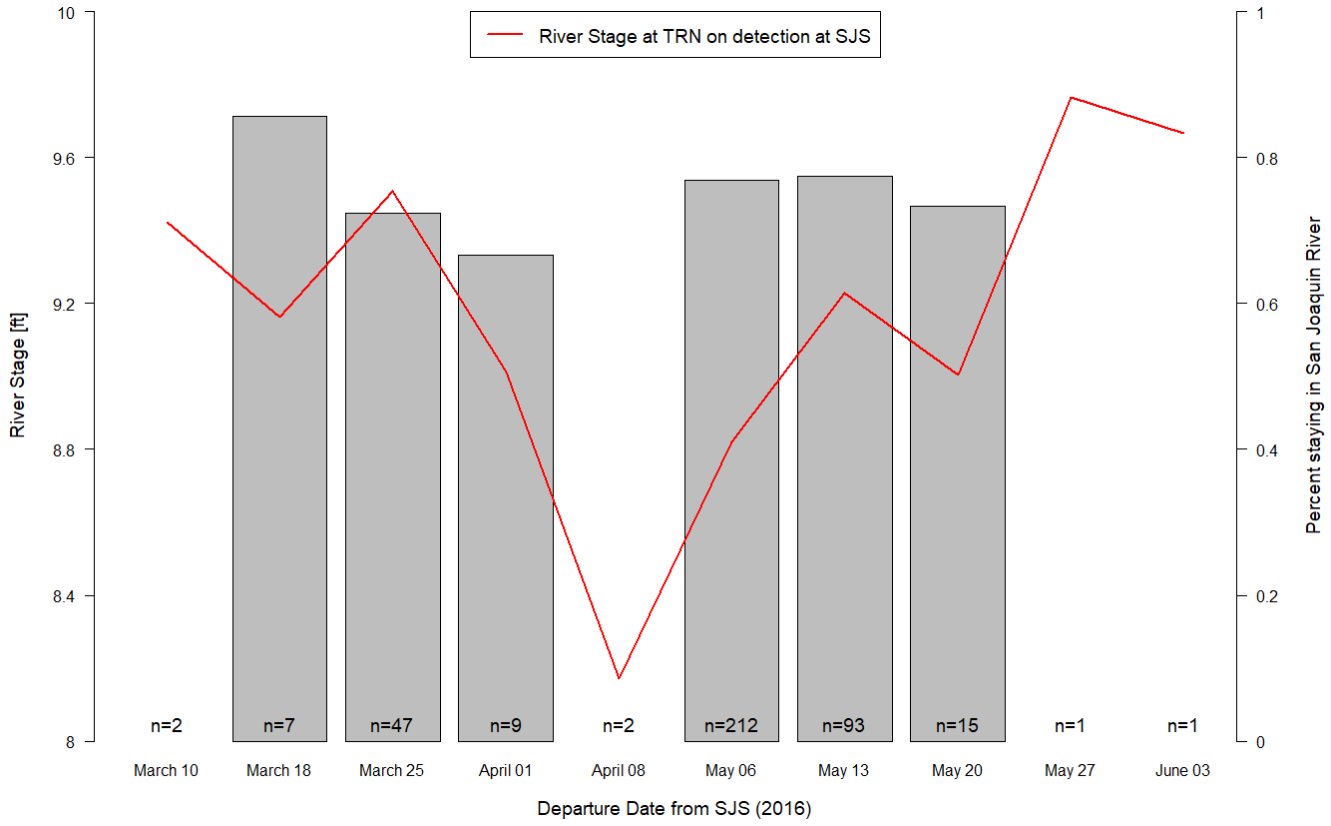

Figure 25. The observed proportion of tagged juvenile steelhead that remained in the San Joaquin River at the Turner Cut junction during the 2016 tagging study (gray bars, representing weekly periods; n = weekly sample size), and the measured river stage at the TRN gaging station in Turner Cut at the time of tag passage of the SJS receivers, averaged over fish. Proportion of fish remaining in the San Joaquin River is shown only for time periods with at least 5 fish detected.

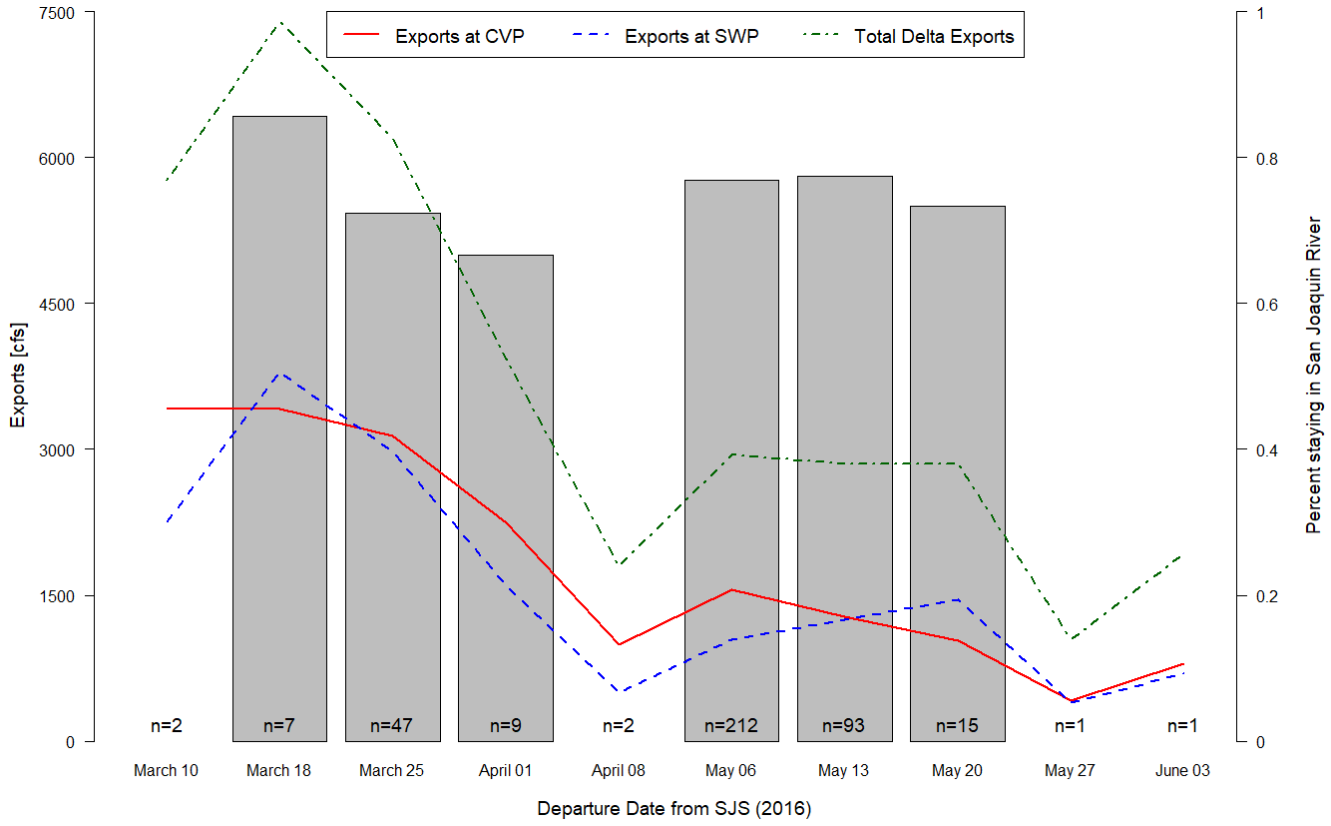

Figure 26. The observed proportion of tagged juvenile steelhead that remained in the San Joaquin River at the Turner Cut junction during the 2016 tagging study (gray bars, representing weekly periods; n = weekly sample size), and the measured daily export rate at CVP, SWP, and total in the Delta at the time of tag passage of the SJS receivers. Proportion of fish remaining in the San Joaquin River is shown only for time periods with at least 5 fish detected.

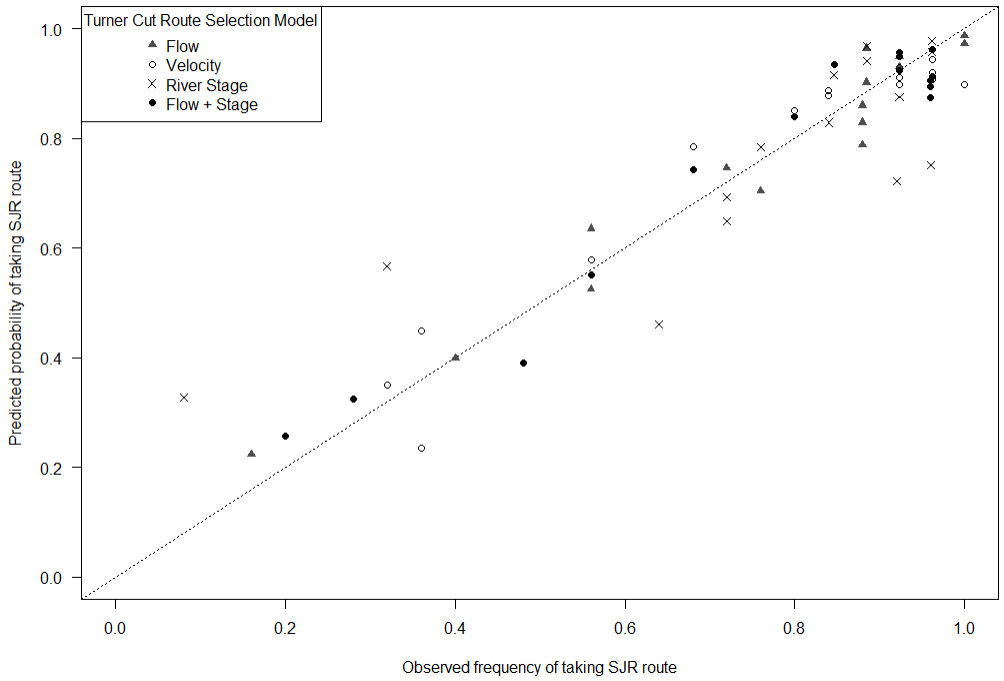

Figure 27. Predicted probability versus observed frequency of taking the San Joaquin River (SJR) route at the Turner Cut Junction, for the candidate models. Dashed line is 1-1 line.

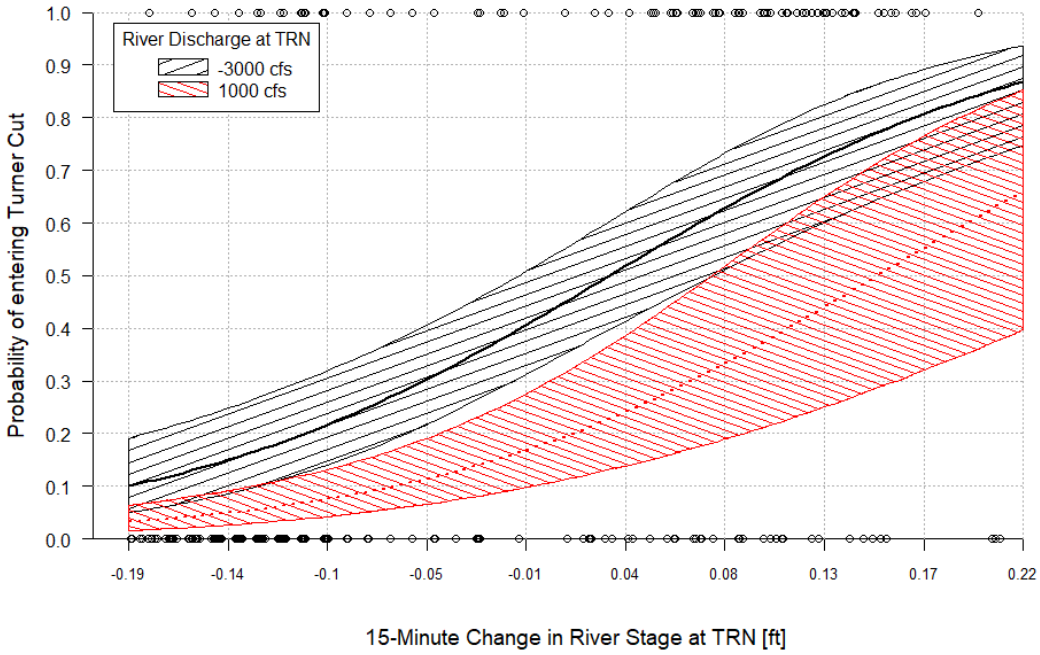

Figure 28. Fitted probability of entering Turner Cut versus 15-minute change in river stage measured at the TRN gaging station in Turner Cut, for river discharge (flow) at TRN = -3,000 cfs and 1,000 cfs, with 95% confidence bands, in 2016. Covariates were measured at the time of tag passage at the SJS receivers. Points indicate the observed route selection (0 = San Joaquin River, 1 = Turner Cut) for each observed value of 15-minute change in river stage; observed 15-minute change in river stage values have been offset slightly to avoid overlap in plotting.

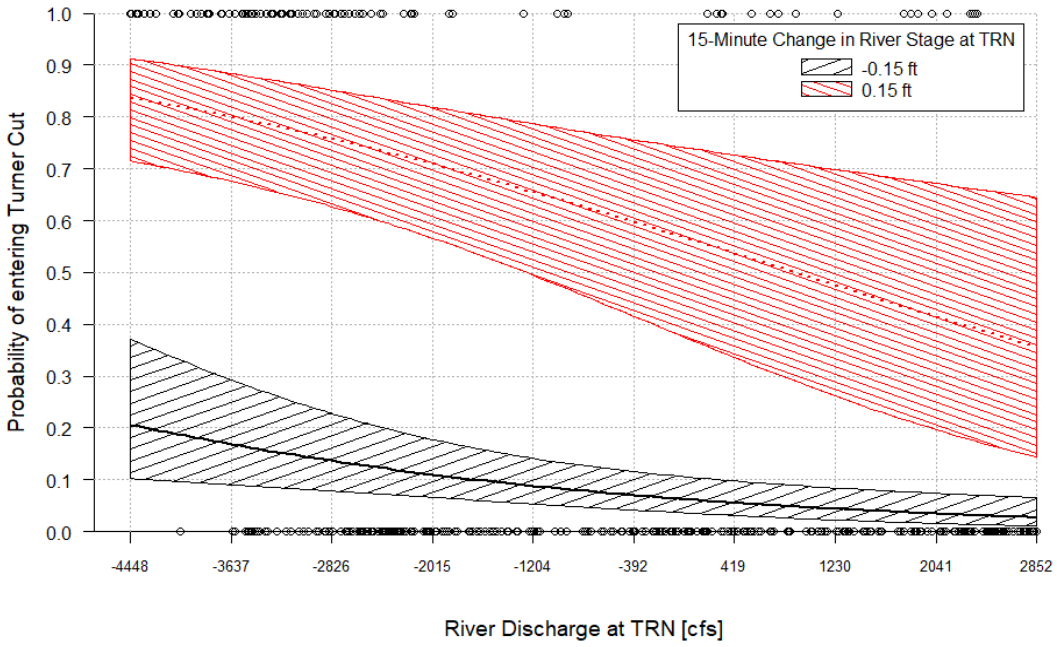

Figure 29. Fitted probability of entering Turner Cut versus river discharge (flow) measured at the TRN gaging station in Turner Cut, for 15-minute change in river stage at TRN = -0.15 ft and 0.15 ft, with 95% confidence bands, in 2016. Covariates were measured at the time of tag passage at the SJS receivers. Points indicate the observed route selection (0 = San Joaquin River, 1 = Turner Cut) for each observed value of river discharge.

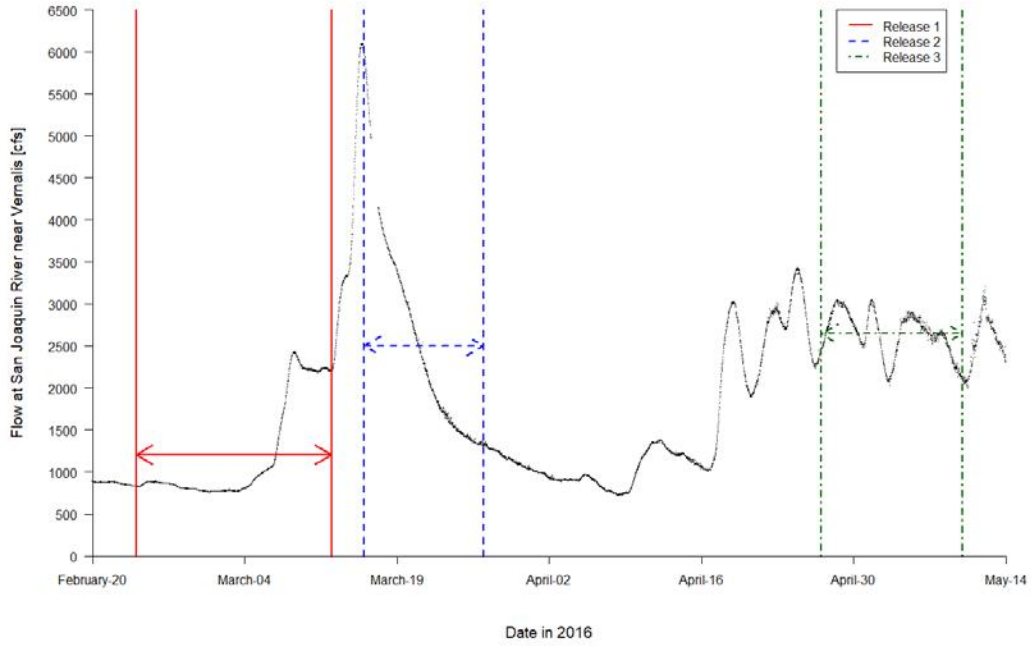

Figure 30. Delta inflow represented as river discharge (flow) measured at the San Joaquin River gaging station near Vernalis (VNS) during the 2016 study. Vertical lines represent the time period from the first day through the final day of release, plus the median observed travel time to Chipps Island for the release. Arrow height indicates mean discharge: 1,209 cfs, 2,508 cfs, and 2,649 cfs, respectively.

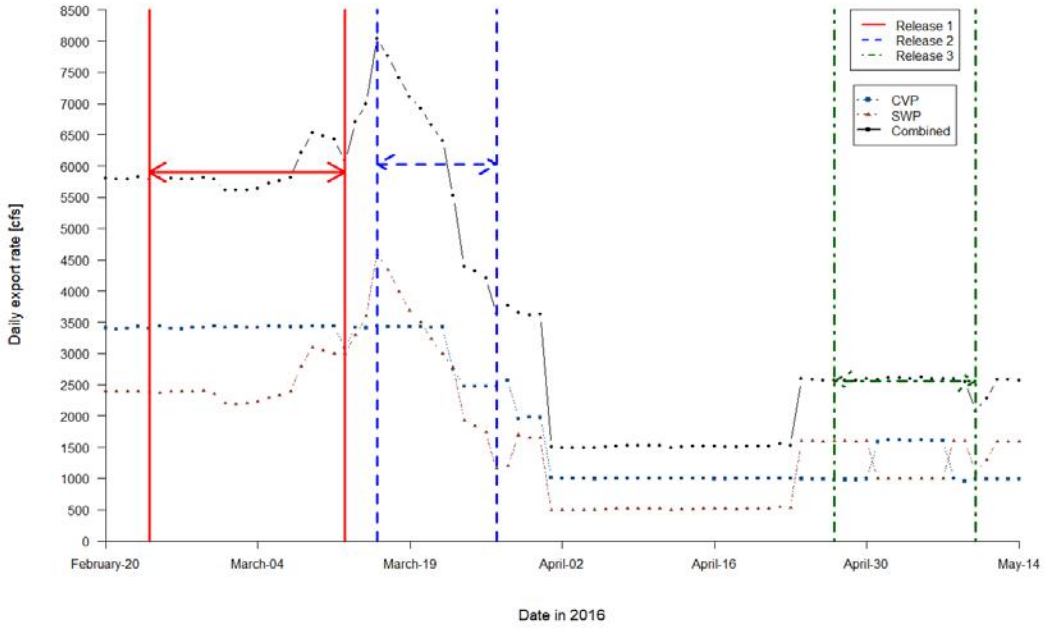

Figure 31. Daily export rate at CVP and SWP during the 2016 study. Vertical lines represent the time period from the first day through the final day of release, plus the median observed travel time to Chipps Island for the release. Arrow height indicates mean combined export rate: 5,899 cfs, 6,030 cfs, and 2,553 cfs, respectively.

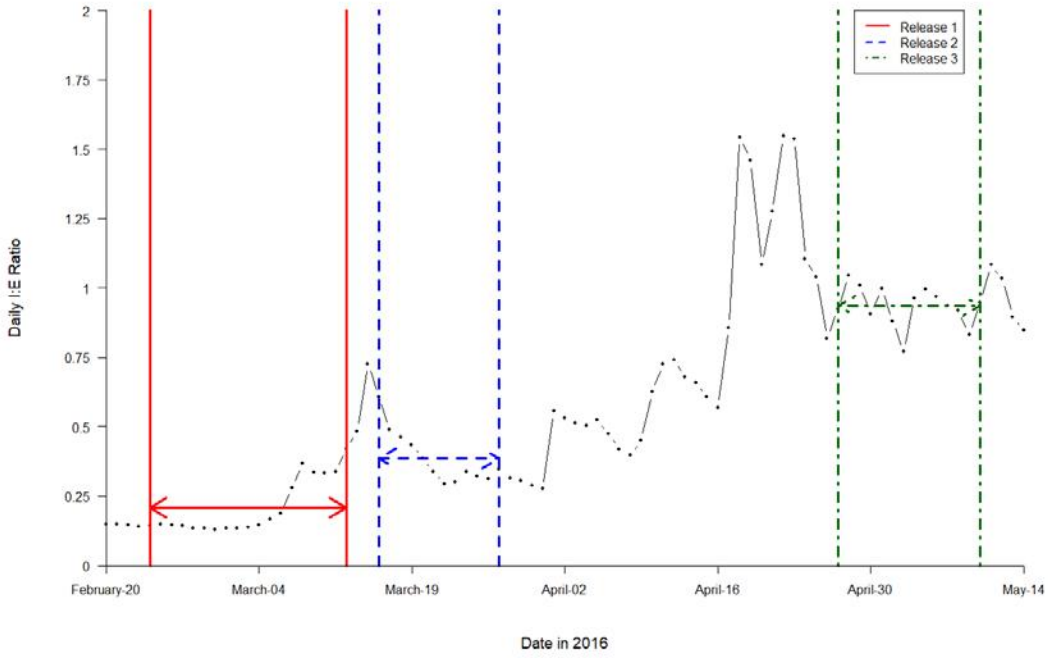

Figure 32. Daily Inflow : Export (I:E) ratio during the 2016 study, where I:E = VNS inflow : total Delta Export Rate; data from Dayflow. Vertical lines represent the time period from the first day through the final day of release, plus the median observed travel time to Chipps Island for the release. Arrow height indicates mean I:E ratio: 0.20, 0.39, and 0.93, respectively.

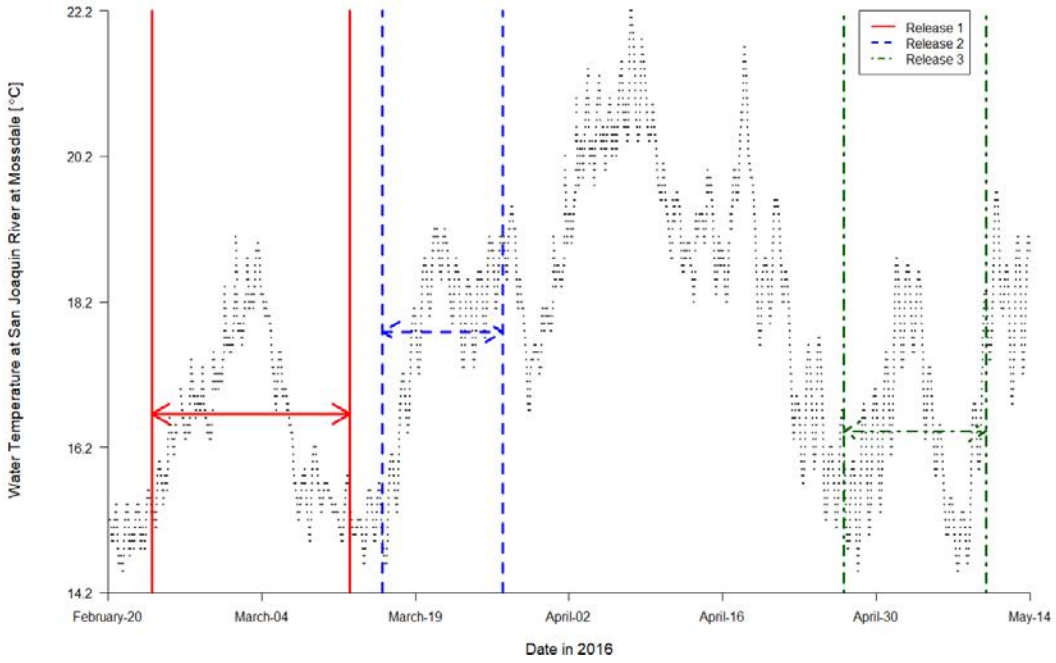

Figure 33. Water temperature at the San Joaquin River gaging station near Mossdale Bridge (MSD) during the 2016 study. Vertical lines represent the time period from the first day through the final day of release, plus the median observed travel time to Chipps Island for the release. Arrow height indicates mean temperature: 16.6°C, 17.8°C, and 16.4°C, respectively.

Tables

Table 1. Names and descriptions of receivers and hydrophones used in the 2016 Steelhead tagging study, with receiver codes used in Figure 1, the survival model (Figures 2 – 5), and in data processing by the United States Geological Survey (USGS). The release site was located at Durham Ferry. Average latitude and longitude are given for sites with multiple hydrophones. Receiver codes starting with "46" are high residency receivers (VEMCO HRR); all others are VEMCO VR2W or VR2C receivers.

Individual Receiver Name and Description	Hydrophone Location		Receiver Code	Survival Model Code	Data Processing Code
	Latitude (°N)	Longitude (°W)			
San Joaquin River near Durham Ferry upstream of the release site, upstream	37.68565	-121.2564	DFU1	A0a	300944
San Joaquin River near Durham Ferry upstream of the release site, downstream	37.68643	-121.2567	DFU2	A0b	300911
San Joaquin River near Durham Ferry; release site	37.68678	-121.2641	DF		
San Joaquin River near Durham Ferry downstream of the release site, upstream	37.68862	-121.2761	DFD1	A2a	300985 460084
San Joaquin River near Durham Ferry downstream of the release site, downstream	37.68875	-121.276	DFD2	A2b	460085
San Joaquin River below Durham Ferry, upstream	37.72132	-121.2622	BDF1	A3	460035
San Joaquin River below Durham Ferry, downstream	37.71787	-121.2783	BDF2	A4	460036
San Joaquin River near Banta Carbona, upstream	37.72778	-121.2987	BCAU	A5a	301503
San Joaquin River near Banta Carbona, downstream	37.72833	-121.2986	BCAD	A5b	460021
San Joaquin River near Mossdale Bridge, upstream	37.79173	-121.3070	MOSU	A6a	300928
San Joaquin River near Mossdale Bridge, downstream	37.79255	-121.3068	MOSD	A6b	300717
San Joaquin River near Lathrop, upstream	37.81103	-121.3196	SJLU	A7a	300721 300991
San Joaquin River near Lathrop, downstream	37.81162	-121.3187	SJLD	A7b	300957 301501
San Joaquin River near Garwood Bridge, upstream	37.93508	-121.3300	SJGU	A8a	300934 300892
San Joaquin River near Garwood Bridge, downstream	37.93529	-121.3305	SJGD	A8b	300903 300918
San Joaquin river near Navy Bridge, upstream[a]	37.94670	-121.3398	SJNBU	A9a	300723
San Joaquin river near Navy Bridge, downstream	37.94677	-121.3395	SJNBD	A9b	300888
San Joaquin River near Calaveras River, upstream	37.96895	-121.3718	SJCU	A10a	300952 300954
San Joaquin River near Calaveras River, downstream	37.96955	-121.3724	SJCD	A10b	300982 301153
San Joaquin River Shipping Channel	37.99562	-121.4404	SJS	A11	300729 300887 300724

a = no data reported

Table 1. (Continued)

Individual Receiver Name and Description	Hydrophone Location		Receiver Code	Survival Model Code	Data Processing Code
	Latitude (°N)	Longitude (°W)			
San Joaquin River near MacDonald Island, upstream	38.01763	-121.4620	MACU	A12a	300922 300883
San Joaquin River near MacDonald Island, downstream	38.02247	-121.4653	MACD	A12b	301163 300912
San Joaquin River near Medford Island, upstream (east)	38.05322	-121.5115	MFE	A13a	300920 300915
San Joaquin River near Medford Island, downstream (west)	38.05377	-121.5132	MFW	A13b	300712 300935
San Joaquin River near Disappointment Slough, upstream	38.09159	-121.5747	SJDU	A14a	300932 300956 300986
San Joaquin River near Disappointment Slough, downstream	38.09240	-121.5752	SJDD	A14b	300897 300899 300950
San Joaquin River upstream of Head of Old River, upstream[b]	37.80597	-121.3188	HORU	B0a	300866 300940
San Joaquin River upstream of Head of Old River, downstream[b]	37.80584	-121.3197	HORD	B0b	300905 300958
Old River East, near junction with San Joaquin, upstream	37.81186	-121.3356	OREU	B1a	300718 300930
Old River East, near junction with San Joaquin, downstream	37.81239	-121.3356	ORED	B1b	301452 300890
Old River South, upstream	37.82052	-121.3776	ORSU	B2a	300943
Old River South, downstream	37.82000	-121.3778	ORSD	B2b	300726
West Canal, upstream	37.84663	-121.5596	WCLU	B3a	300863
West Canal, downstream	37.84738	-121.5599	WCLD	B3b	300931
Old River near Highway 4, upstream	37.89294	-121.5673	OR4U	B4a	300902 300722
Old River near Highway 4, downstream	37.89380	-121.5671	OR4D	B4b	300713 301161
Old River at the San Joaquin River, upstream (closer to Old River mouth)	38.06233	-121.5811	OSJU	B5a	301512 301157 300885
Old River at the San Joaquin River, downstream (farther from Old River mouth)	38.06179	-121.5820	OSJD	B5b	300715 301510 301508
Middle River Head, upstream	37.82448	-121.3794	MRHU	C1a	300896
Middle River Head, downstream	37.82473	-121.3802	MRHD	C1b	300858
Middle River near Highway 4, upstream	37.89610	-121.4930	MR4U	C2a	300719 301165
Middle River near Highway 4, downstream	37.89680	-121.4933	MR4D	C2b	300948 300881
Middle River near Mildred Island, upstream[b]	38.00180	-121.5117	MIDU	C3a	300942 300913

b = not used in survival model

Table 1. (Continued)

Individual Receiver Name and Description	Hydrophone Location		Receiver Code	Survival Model Code	Data Processing Code
	Latitude (°N)	Longitude (°W)			
Middle River near Mildred Island, downstream[b]	38.00232	-121.5117	MIDD	C3b	300981 300714
Radial Gate at Clifton Court Forebay, upstream (in entrance channel to forebay), array 1 in dual array	37.83003	-121.5566	RGU1	D1a	300908
Radial Gate at Clifton Court Forebay, upstream (in entrance channel to forebay), array 2 in dual array	37.82960	-121.5570	RGU2	D1b	300910
Radial Gate at Clifton Court Forebay, downstream (inside forebay), array 1 in dual array	37.83019	-121.5575	RGD1	D2a	460009 300904
Radial Gate at Clifton Court Forebay, downstream (inside forebay), array 2 in dual array	37.83019	-121.5575	RGD2	D2b	460010 300980
Central Valley Project trashracks, upstream	37.81687	-121.5584	CVPU	E1a	460012 460023
Central Valley Project trashracks, downstream	37.81665	-121.5589	CVPD	E1b	300939
Central Valley Project holding tanks	37.81585	-121.5591	CVPT	E2	300891 300938 300876
Turner Cut, east	37.99167	-121.4549	TCE	F1a	450043 300868
Turner Cut, west	37.99133	-121.4555	TCW	F1b	300900 450024
Columbia Cut, upstream	38.02729	-121.5009	COLU	F2a	300898 300869
Columbia Cut, downstream	38.02697	-121.5017	COLD	F2b	300862 301502
San Joaquin River at Jersey Point, upstream (east)	38.05630	-121.6870	JPE	G1a	300889 300873 300867 300941 301511 300720 300895 301164
San Joaquin River at Jersey Point, downstream (west)	38.05556	-121.6884	JPW	G1b	301504 300877 301002 300994 301000 301001 301024 301156

b = not used in survival model

Table 1. (Continued)

Individual Receiver Name and Description	Hydrophone Location		Receiver Code	Survival Model Code	Data Processing Code
	Latitude (°N)	Longitude (°W)			
Chipps Island (aka Mallard Island), upstream (east)	38.04810	-121.9313	MAE	G2a	300936 300727 300906 301154 300865 300929 300886 301505 300880 301158 301509
Chipps Island (aka Mallard Island), downstream (west)	38.04926	-121.9328	MAW	G2b	300923 300731 300921 300728 300864 300990 300955 300909 300882 300989 301159
Benicia Bridge pier, upstream (east)	38.04275	-122.1215	BBE	G3a	301617 301615 300949 300946 300960 300961 300945 301616 301614
Benicia Bridge pier, downstream (west)	38.04066	-122.1235	BBW	G3b	301493 301492 301489 301490 301488 301487 301486 301491
False River, west (closer to San Joaquin)	38.05635	-121.6643	FRW	H1a	301507 300730
False River, east (farther from San Joaquin)	38.05635	-121.6637	FRE	H1b	301506 300984
Predator Removal Study Site 4[b]	37.81862	-121.3174	RS4	N1	300870 301166
Predator Removal Study Site 5[b]	37.83189	-121.3122	RS5	N2	300901 300872
Predator Removal Study Site 6[b]	37.85138	-121.3221	RS6	N3	300884 300924
Predator Removal Study Site 7[b]	37.86450	-121.3236	RS7	N4	300917 300879
Predator Removal Study Site 8[b]	37.88777	-121.3302	RS8	N5	300878 300861
Predator Removal Study Site 9[b]	37.90577	-121.3234	RS9	N6	300871 300937
Predator Removal Study Site 10[b]	37.91825	-121.3206	RS10	N7	300916 300914

b = not used in survival model

Table 1. (Continued)

Individual Receiver Name and Description	Hydrophone Location		Receiver Code	Survival Model Code	Data Processing Code
	Latitude (°N)	Longitude (°W)			
Burns Cutoff at Rough and Ready Island, upstream	37.94023	-121.3510	RRIU	R1a	300859
Burns Cutoff at Rough and Ready Island, downstream	37.94015	-121.3512	RRID	R1b	301155
Threemile Slough, south	38.10748	-121.6840	TMS	T1a	300875 301162
Threemile Slough, north	38.11111	-121.6832	TMN	T1b	300933 300732
Montezuma Slough, upstream[b]	38.07138	-121.8686	MTZU	T2a	301018
Montezuma Slough, downstream[b]	38.07148	-121.8697	MTZD	T2b	300860
Spoonbill Slough, upstream[b]	38.05525	-121.8953	SBSU	T3a	301014
Spoonbill Slough, downstream[b]	38.05542	-121.8955	SBSD	T3b	300999

b = not used in survival model

Table 2. Environmental monitoring sites used in predator decision rule and route entrainment analysis for 2016 Steelhead study. Database = CDEC (http://cdec.water.ca.gov/) or Water Library (http://www.water.ca.gov/waterdatalibrary/).

Environmental Monitoring Site			Detection Site	Data Available					Database
Site Name	Latitude (°N)	Longitude (°W)		River Flow	Water Velocity	River Stage	Pumping	Reservoir Inflow	
BDT	37.8650	121.3231	RS6, RS7, RS8	Yes	Yes	Yes	No	No	Water Library
CLC	37.8298	121.5574	RGU, RGD	No	No	No	No	Yes	CDEC
CSE	38.0740	121.8501	MTZ	No	No	Yes	No	No	CDEC
FAL	38.0554	121.6672	FRE/FRW	Yes	Yes	Yes	No	No	CDEC
GCT	37.8200	121.4498	ORS	No	No	Yes	No	No	Water Library
HLT	38.0030	121.5108	COL, MID	Yes	Yes	Yes	No	No	CDEC
MAL	38.0428	121.9201	MTZ, SBS, MAE/MAW	No	Yes	Yes[b]	No	No	CDEC
MDB	37.8908	121.4883	MR4	No	No	Yes	No	No	Water Library
MDM	37.9425	121.5340	MR4	Yes	Yes	No	No	No	CDEC
MRU	37.8339	121.3860	MRH	Yes	Yes	No	No	No	Water Library
MRZ	38.0276	122.1405	BBR	No	No	Yes	No	No	CDEC
MSD	37.7860	121.3060	HOR, MOS	Yes	Yes	Yes	No	No	Water Library
ODM	37.8101	121.5419	CVP/CVPtank	Yes	Yes	Yes	No	No	CDEC[a]
OH1	37.8080	121.3290	ORE	Yes	Yes	Yes	No	No	Water Library
OH4	37.8900	121.5697	OR4	Yes	Yes	Yes	No	No	CDEC
ORX	37.8110	121.3866	ORS	Yes	Yes	No	No	No	Water Library
OSJ	38.0711	121.5789	OSJ	Yes	Yes	Yes	No	No	CDEC
PRI	38.0593	121.5575	MAC, MFE/MFW, SJD	Yes	Yes	Yes	No	No	CDEC
RMID040	37.8350	121.3838	MRH	No	No	Yes	No	No	Water Library
ROLD040	37.8286	121.5531	RGU, RGD, WCL	No	No	Yes	No	No	Water Library
RRI	37.9360	121.3650	SJC, SJS	Yes	Yes	Yes	No	No	Water Library
SJD	37.8223	131.3177	RS4, RS5	Yes	Yes	No	No	No	Water Library
SJG	37.9351	121.3295	RS9, RS10, SJG, SJNB, RRI	Yes	Yes	Yes	No	No	CDEC
SJJ	38.0520	121.6891	JPE/JPW	Yes	Yes	Yes	No	No	CDEC

[a] = California Water Library was used for river stage.

[b] = Used for river stage for SBS and MAE/MAW.

Table 2. (Continued)

Environmental Monitoring Site			Detection Site	Data Available					Database
Site Name	Latitude (°N)	Longitude (°W)		River Flow	Water Velocity	River Stage	Pumping	Reservoir Inflow	
SJL	37.8100	121.3230	SJL	No	No	Yes	No	No	Water Library
TRN	37.9927	121.4541	TCE/TCW	Yes	Yes	Yes	No	No	CDEC
TRP	37.8165	121.5596	CVP/CVPtank	No	No	No	Yes	No	CDEC
TSJ	38.0900	121.6869	TMS/TMN	No	No	Yes	No	No	Water Library
TSL	38.1004	121.6866	TMS/TMN	Yes	Yes	No	No	No	CDEC
VNS	37.6670	121.2670	DFU, DFD, BDF1, BDF2, BCA	Yes	No	Yes	No	No	CDEC
WCI	37.8316	121.5541	RGU, RGD, WCL	Yes	Yes	No	No	No	Water Library

[a] = California Water Library was used for river stage.

[b] = Used for river stage for SBS and MAE/MAW.

Table 3a. Cutoff values used in predator filter in 2016. Observed values past cutoff or unmet conditions indicate a predator. Time durations are in hours unless otherwise specified. See Table 3b for Flow, Water Velocity, Extra Conditions, and Comment. Footnotes refer to both this table and Table 3b.

Detection Site	Previous Site	Residence Time[a] (hr)			Migration Rate[b, c] (km/hr)		Time since last visit (hr)	BLPS (Magnitude)	No. of Visits	No. of Cumulative Upstream Forays
		Near Field	Mid-field	Far-field						
		Maximum	Maximum	Maximum	Minimum	Maximum	Maximum	Maximum	Maximum	Maximum
DFU	DF	200	400	800	0	4			1	0
	DFU	200	800	1,000					2	2
	DFD, BDF1	200	400	800	0	4			2	2
	TCE/TCW	1	2	4	0.2	4			0	2
DFD	DF	300	600	1,000	0	4.5			1	0
	DFU, DFD	300	600 (1,000[f])	1,000	0	4.5 (NA[f])			10	2
	BDF1, BDF2, BCA	300	600	1,000		4			3	2
BDF1	DF	30	60	1,000	0	4.5			1	0
	DFD	30	60	1,000	0	4.5			10	0
	BDF1	60	440	1,000					10	1
	BDF2	30	60	1,000	0	4.5			3	2
	BCA	30	60	1,000	0.1	4.5			3	2
BDF2	DF, DFD, BDF1	30	60	1,000	0	4.5			10 (1[f])	0
	BDF2	60	440	1,000					10	1
	BCA	30	60	1,000	0.1	4.5			3	2
BCA	DF, DFU	30 (1000[f])	60 (1000[f])	1,000	0	4.5			1	0
	DFD, BDF1, BDF2	30 (1000[f])	60 (1000[f])	1,000	0	4.5			4	0
	BCA	60 (1000[f])	340 (1000[f])	1,000					5	1
	MOS	1	2	1,000	0.1	4			2	2
	MOS	30	300	1,100					5	5
	HOR, RS7	24	48	1,100		6	400	4.5	8	7

a = Near-field residence time includes up to 12 hours missing between detections, while mid-field residence time includes entire time lag between first and last detections without intervening detections elsewhere; far-field ("regional") residence time includes all time from entry in region to arrival at and departure from current site

b = Approximate migration rate calculated on most direct pathway

c = Missing values for transitions to and from same site: travel times must be 12 to 24 hours, unless otherwise specified under "Extra conditions"

f = See comments for alternate criteria

Table 3a. (Continued)

Detection Site	Previous Site	Residence Time[a] (hr) Near Field Maximum	Residence Time[a] (hr) Mid-field Maximum	Residence Time[a] (hr) Far-field Maximum	Migration Rate[b, c] (km/hr) Minimum	Migration Rate[b, c] (km/hr) Maximum	Time since last visit (hr) Maximum	BLPS (Magnitude) Maximum	No. of Visits Maximum	No. of Cumulative Upstream Forays Maximum
MOS	DF, DFU, DFD, BDF1, BDF2, BCA	50 (100[f])	100 (200[f])	1,000		6		4.6	1	0
	MOS	30	250	1,000					4	4
	HOR	30	60	1,000		6		4.6	3	5
SJL	HOR	24	48	96	0.1	6	25	4.6	5	0
	SJL	5	164	385					4	2
	ORE	5 (1[f])	10 (2[f])	20 (4[f])	0.5	6	20 (15[f])	4.6	3 (0[f])	0
	RS4	10	20	483	0.1	4		4.6	5	5
RS4	SJL	24	48	448	0.1	6	25	4.6	5	0
	RS4	5	139	500					4	2
	RS5	12	24	500 (160[e])	0.1	4	168	4.6	5	7
	TCE/TCW	12	24	367 (160[e])	2.1	4	168	4.6	4	7
RS5	RS4	24	48	500	0.1	6	50	4.6	5	0
	RS5	5	139	500					4	3
	RS6	12	24	500 (140[e])	0.2	4	144	4.6	5	7
RS6	RS5	24	48	500	0.1	6	100	4.6	8	0
	RS6	5	139	500					8	4
	RS7	12	24	500 (130[e])	0.2	4	100	4.6	8	7
RS7	RS6	27	59	500	0.1	6	100	4.6	8	0
	RS7	5	82	500					9	5
	RS8	12	24	500 (130[e])	0.2	4	100	4.6	8	7
RS8	RS7	27	59	500	0.1	6	123	4.6	8	0

a = Near-field residence time includes up to 12 hours missing between detections, while mid-field residence time includes entire time lag between first and last detections without intervening detections elsewhere; far-field ("regional") residence time includes all time from entry in region to arrival at and departure from current site

b = Approximate migration rate calculated on most direct pathway

c = Missing values for transitions to and from same site: travel times must be 12 to 24 hours, unless otherwise specified under "Extra conditions"

e = Condition at departure from previous site

f = See comments for alternate criteria

Table 3a. (Continued)

Detection Site	Previous Site	Residence Time[a] (hr) Near Field Maximum	Residence Time[a] (hr) Mid-field Maximum	Residence Time[a] (hr) Far-field Maximum	Migration Rate[b, c] (km/hr) Minimum	Migration Rate[b, c] (km/hr) Maximum	Time since last visit (hr) Maximum	BLPS (Magnitude) Maximum	No. of Visits Maximum	No. of Cumulative Upstream Forays Maximum
RS8	RS8	5	82	500					6	3
	RS9	12	24	500 (200[e])	0.1	4	100	4.6	9	9
RS9	RS5, RS8	24	48	500	0.1	6	125	4.6	8	0
	RS9	5	79	500					3	3
	RS10	12	24	500 (200[e])	0.1	4	100	4.6	8	9
RS10	RS9	24	48	500	0.1	6	130	4.6	6	0
	RS10	5	79	500					3	3
	SJG, SJNB	12	24	500 (200[e])		4	130	4.6	6	6
SJG	RS6, RS10	30	60	500	0.1	6	140	4.6	5 (3[f])	0
	SJG	15	79	500					3	3
	SJNB, RRI	10	20	500		4	140	4.6	4	10
SJNB	SJG	30	60	500	0.1	6 (2[f])	140	4.6	5	0
	SJNB	15	90	500					3	4
	RRI	15	30	500	0.1	6	140		3	2
	SJC	15	30	500	0.1	4	140	4.6	5	10
RRI	SJG	20	40	500	0.1	6 (2[f])	25	4.6	2	0
	RRI	5	70	500					2	4
	SJNB	5	10	500	0.1	6	25		2	2
	SJC	2	4	500	0.2	4	25	4.6	2	6
SJC	SJG	55 (30[f])	110 (60[f])	500	0.1	6	75	4.6	1	0
	SJNB, RRI	55 (30[f])	110 (60[f])	500	0.1	6	75	4.6	3	0
	SJC	24	129	500					3	4

a = Near-field residence time includes up to 12 hours missing between detections, while mid-field residence time includes entire time lag between first and last detections without intervening detections elsewhere; far-field ("regional") residence time includes all time from entry in region to arrival at and departure from current site

b = Approximate migration rate calculated on most direct pathway

c = Missing values for transitions to and from same site: travel times must be 12 to 24 hours, unless otherwise specified under "Extra conditions"

e = Condition at departure from previous site

f = See comments for alternate criteria

Table 3a. (Continued)

Detection Site	Previous Site	Residence Time[a] (hr) Near Field Maximum	Residence Time[a] (hr) Mid-field Maximum	Residence Time[a] (hr) Far-field Maximum	Migration Rate[b, c] (km/hr) Minimum	Migration Rate[b, c] (km/hr) Maximum	Time since last visit (hr) Maximum	BLPS (Magnitude) Maximum	No. of Visits Maximum	No. of Cumulative Upstream Forays Maximum
SJC	SJS	24	48	180	0.6	4	75	4.6	4	10
	MFE/MFW	2	4	500	1.3	4	75	4.6	1	4
SJS	SJG, SJC	30	60	120	0.1	6	50	4.6	1 (4[f])	0
	SJS	24	104	264					3	6
	MAC, TCE/TCW	24	48	402 (500[f])	0.3 (0.1[f])	4	50	4.6 (5[f])	6	10
MAC	SJS	20	40	342 (317[f])	0.1 (0.3[f])	6	24	4.6	3	0
	MAC	15	69	435					2	4
	TCE/TCW	15	30	500	0.2	6	24		2	1
	MFE/MFW	15	30	500	0.4	4	36	4.6	3	10
	COL	15	30	500	0.3	4	24	4.6	2	4
MFE/MFW	SJC	20	40	500	0.1 (0.3[f])	6	36	4.6	1	0
	MAC	20	40	500 (496[f])	0.1 (0.3[f])	6	36	4.6	2	0
	MFE/MFW	10	100	500					2	4
	COL	12	24	500	0.1	6	24	4.6	2	1
	SJD	12	24	48	0.7	4	36	4.6	2	4
	MAE/MAW	1	2	4	0.1	4	36	4.6	0	4
	MID	20	40	80	0.1	4	36	4.6	2	4
SJD	MAC, MID	24	48	96	0.1 (0.3[f])	6	36	4.6	1	0
	MFE/MFW, COL	24	48	96	0.1 (0.3[f])	6	36	4.6	2	0
	SJD	15	109 (69[f])	265 (185[f])					2	4
	OSJ	15	30	192	0.2	4	36	4.6	2	2
	JPE/JPW, FRE/FRW, TMN/TMS	15	30	60		4	36	4.6	2	4

a = Near-field residence time includes up to 12 hours missing between detections, while mid-field residence time includes entire time lag between first and last detections without intervening detections elsewhere; far-field ("regional") residence time includes all time from entry in region to arrival at and departure from current site

b = Approximate migration rate calculated on most direct pathway

c = Missing values for transitions to and from same site: travel times must be 12 to 24 hours, unless otherwise specified under "Extra conditions"

f = See comments for alternate criteria

Table 3a. (Continued)

Detection Site	Previous Site	Residence Time[a] (hr) Near Field Maximum	Mid-field Maximum	Far-field Maximum	Migration Rate[b, c] (km/hr) Minimum	Maximum	Time since last visit (hr) Maximum	BLPS (Magnitude) Maximum	No. of Visits Maximum	No. of Cumulative Upstream Forays Maximum
HOR	MOS	25 (100[f])	50 (200[f])	1,000		6		4.6	3	0
	HOR	25	250	1,000					6	4
	SJL	15 (10[f])	30 (20[f])	1,000	0.2	6	192 (100[f])	4.6	10	10
	ORE	35 (1[f])	30 (2[f])	1,000	0.2 (0.6[f])	6	192 (5[f])	4.6	4 (0[f])	4
ORE	HOR	15	30	60	0.1	6	25	5	2 (1[f])	0
	ORE	5 (2[f])	90 (87[f])	210 (207[f])					2	1
	SJL	5 (2[f])	10 (4[f])	20 (8[f])	0.3	6	20 (15[f])	5	2 (1[f])	0
	ORS	3 (1[f])	6 (2[f])	324 (315[f])		4	25	5	2 (1[f])	2 (1[f])
ORS	ORE	24	48	308	0.1	6	40	4.6	1	0
	ORS	12	146	500					4	2
	MRH	12	24	380	0.2	6	40	4.6	2	2
	CVP	12	24	48	0.3	4	40	4.6	2	3
WCL	RGU/RGD	15	30	800	0.2	5	100	5	5	0
	CVP	15	30	800	0.1	4	100	4.6	5	0
	ORS	15	30	800	0.1	4	100	4.6	1	0
	WCL	2	82	800					5	4
	MR4	15	30	60	0.1	4	100	4.6	1	0
	OR4	15	30	800	0.1	4	100	4.6	5	7
OR4	WCL	20	40	800	0.1	4.5	100	4.6	3	0
	OR4	20	200	800					3	4
	JPE/JPW	20	40	80	0.1	4	100	4.6	1	4
	MR4	20	40	80	0.1	4	100	4.6	2	0
	MID, TCE/TCW	20	40	80	0.1	4	100	4.6	2 (1[f])	0

a = Near-field residence time includes up to 12 hours missing between detections, while mid-field residence time includes entire time lag between first and last detections without intervening detections elsewhere; far-field ("regional") residence time includes all time from entry in region to arrival at and departure from current site

b = Approximate migration rate calculated on most direct pathway

c = Missing values for transitions to and from same site: travel times must be 12 to 24 hours, unless otherwise specified under "Extra conditions"

f = See comments for alternate criteria

Table 3a. (Continued)

Detection Site	Previous Site	Residence Time[a] (hr) Near Field Maximum	Residence Time[a] (hr) Mid-field Maximum	Residence Time[a] (hr) Far-field Maximum	Migration Rate[b, c] (km/hr) Minimum	Migration Rate[b, c] (km/hr) Maximum	Time since last visit (hr) Maximum	BLPS (Magnitude) Maximum	No. of Visits Maximum	No. of Cumulative Upstream Forays Maximum
OSJ	MFE/MFW	15	30	60	0.1	6	36	4.6	2	0
	TCE/TCW, MID	15	30	60	0.1	6	36	4.6	1	0
	COL	15	30	60	0.1	6	36	4.6	2	0
	OSJ	5	54	138					2	4
	SJD	10	20	325	0.1	4	36	4.6	2	2
	FRE/FRW	2	4	8	0.7	4	36	4.6	2	4
MRH	ORE	10	20	280	0.1	6	40	4.6	1	0
	MRH	3	47	351					0	2
	ORS	3	6	500	0.2	6	40	4.6	1	2
MR4	ORS	10	20	40	0.1	4.5		4.6	1	0
	MR4	10	80	170					2	2
	MID	10	20	217	0.1	4	100	4.6	2	2
	CVP, WCL	10	20	40	0.1	4	100	4.6	1	0
	TCE/TCW	10	20	40	0.1	4	100	4.6	1	0
MID	RS10	12	24	48	0.2	4	100	4.6	1	0
	MFE/MFW, SJD	12	24	48	0.1	4	100	4.6	1	0 ([3]f)
	MID	12	134	282					3	2
	TCE/TCW	12	24	48	0.1	4	100	4.6	1	0
	COL	12	24	48		4	100	4.6	2	0
	OSJ	12	24	48	0.1	4	100	4.6	1	4
RGU/RGD	ORS	80 (336[h]; 800[i])	80 (336[h]; 800[i])	800	0.1	4.5	150	4.6	1	0

a = Near-field residence time includes up to 12 hours missing between detections, while mid-field residence time includes entire time lag between first and last detections without intervening detections elsewhere; far-field ("regional") residence time includes all time from entry in region to arrival at and departure from current site

b = Approximate migration rate calculated on most direct pathway

c = Missing values for transitions to and from same site: travel times must be 12 to 24 hours, unless otherwise specified under "Extra conditions"

f = See comments for alternate criteria

h = If returned to Forebay entrance channel from Clifton Court Forebay and most detections were at RGU (not RGD)

i = If known presence at gates < 80 hours, or if present at RGU < 80% of total residence time and returned to Forebay entrance channel from RGD

Table 3a. (Continued)

Detection Site	Previous Site	Residence Time[a] (hr) Near Field Maximum	Residence Time[a] (hr) Mid-field Maximum	Residence Time[a] (hr) Far-field Maximum	Migration Rate[b, c] (km/hr) Minimum	Migration Rate[b, c] (km/hr) Maximum	Time since last visit (hr) Maximum	BLPS (Magnitude) Maximum	No. of Visits Maximum	No. of Cumulative Upstream Forays Maximum
RGU/RGD	CVP	80 (336[h]; 800[i])	80 (336[h]; 800[i])	800	0.1	4.5	150	4.6	4	0
	WCL	80 (336[h]; 800[i])	80 (336[h]; 800[i])	800	0.1	5	150	4.6	5	4
	MR4	10 (336[h]; 100[j])	10 (336[h]; 100[j])	800	0.4	4.5	150	4.6	1	0
CVP	ORS	100	200	1,000	0.1	4.5	200	4	1	0
	CVP	25	236	1,000					4	3
	CVPtank	25	263	1,000		1			5	3
	RGU/RGD	80	160	1,000	0.1	4	200	4	4 (1[f])	4
	WCL	80	160	1,000	0.1	4	200	4	4 (1[f])	4
	MR4	80	160	1,000	0.1	4.5	200	4	4 (1[f])	0
CVPtank	CVP	30	90	1,000					2	4
TCE/TCW	SJS	24	48	328	0.1	6	24	4.6	3	0
	TCE/TCW	12	106	494					2	4
	MAC	12	24	483	0.2	6	24	4.6	2	1
	MR4	12	24	48	0.1	4	24	4.6	2	4
	MID	12	24	48	0.1	4	24	4.6	2	4
COL	MAC	24	48	500	0.1	6	36	4.6	2	0
	MFE/MFW	12	24	500	0.1	6	36	4.6	2	1

a = Near-field residence time includes up to 12 hours missing between detections, while mid-field residence time includes entire time lag between first and last detections without intervening detections elsewhere; far-field ("regional") residence time includes all time from entry in region to arrival at and departure from current site

b = Approximate migration rate calculated on most direct pathway

c = Missing values for transitions to and from same site: travel times must be 12 to 24 hours, unless otherwise specified under "Extra conditions"

f = See comments for alternate criteria

h = If returned to Forebay entrance channel from Clifton Court Forebay and most detections were at RGU (not RGD)

i = If known presence at gates < 80 hours, or if present at RGU < 80% of total residence time and returned to Forebay entrance channel from RGD

j = Maximum residence time is 100 hours if known presence at gates < 10 hours, or 800 hours if present at RGU < 80% of total residence time and returned to Forebay entrance channel from RGD

Table 3a. (Continued)

Detection Site	Previous Site	Residence Time[a] (hr) Near Field Maximum	Residence Time[a] (hr) Mid-field Maximum	Residence Time[a] (hr) Far-field Maximum	Migration Rate[b, c] (km/hr) Minimum	Migration Rate[b, c] (km/hr) Maximum	Time since last visit (hr) Maximum	BLPS (Magnitude) Maximum	No. of Visits Maximum	No. of Cumulative Upstream Forays Maximum
JPE/JPW	MFE/MFW, TCE/TCW, OR4, MID, SJD, OSJ	40	80	160	0.2	4.5	30	4.6	1	0
	TMN/TMS	40	80	224	0.2	4.5	30	4.6	2	0
	RGU/RGD, CVPtank	40	80	160	0.1		30	4.6	1	3
	JPE/JPW	20	140	414					3	3
	FRE/FRW	20	140	414	0.2	7	30		3	3
	MAE/MAW	2	4	500	1	4	30	4.6	2	3
MAE/MAW	SJD, MFE/MFW, TCE/TCW, WCL, OSJ, TMN/TMS, JPE/JPW, FRE/FRW	40	200	500	0.2	4.5	50	4.6	1	0
	CVPtank	40	200	500		4	50	4.6	1	0
	RGU/RGD	40	200	500		5	50	4.6	1	0
	MTZ, SBS	40	200	500	0.2	4.5	50	4.6	2	0
	MAE/MAW	20	100	500					3	3
	BBR	10	50	500	0.2	4.5	50	4.6	3	4
BBR	TCE/TCW	40	200	500	0.2	6		4.6	1	0
	TMN/TMS, JPE/JPW, MTZ	40	200	500	0.2	6		4.6	1	0
	CVPtank	40	200	500	0.2	7		4.6	1	0
	RGU/RGD	40	200	500		8		4.6	1	0
	MAE/MAW	40	200	500	0.2	6		4.6	2	0
	BBR	10	50	500					3	0

a = Near-field residence time includes up to 12 hours missing between detections, while mid-field residence time includes entire time lag between first and last detections without intervening detections elsewhere; far-field ("regional") residence time includes all time from entry in region to arrival at and departure from current site

b = Approximate migration rate calculated on most direct pathway

c = Missing values for transitions to and from same site: travel times must be 12 to 24 hours, unless otherwise specified under "Extra conditions"

Table 3a. (Continued)

Detection Site	Previous Site	Residence Time[a] (hr)			Migration Rate[b, c] (km/hr)		Time since last visit (hr)	BLPS (Magnitude)	No. of Visits	No. of Cumulative Upstream Forays
		Near Field	Mid-field	Far-field						
		Maximum	Maximum	Maximum	Minimum	Maximum	Maximum	Maximum	Maximum	Maximum
FRE/FRW	OR4, MR4, MID, TCE/TCW, SJD	20	40	80	0.2	4.5	15	4.6	1	0
	OSJ	20	40	80	0.2	4.5	15	4.6	2	0
	JPE/JPW	20	83	193	0.2	7	15		3	3
	FRE/FRW	3	83	193					3	3
TMN/TMS	SJD	10	20	40	0.2	4.5	15	4.6	1	0
	RGU/RGD, CVPtank	10	20	40	0.2 (0.1[f])	4.5	15	4.6	1	4
	TMN/TMS	3	47	111					2	3
	JPE/JPW	10	20	278	0.2	4.5	15	4.6	2	4
	FRE/FRW	10	20	137	0.2	4.5	15	4.6	2	4
	SBS, MAE/MAW	10	20	500	0.2	4.5	15	4.6	1	4
MTZ	RGU/RGD	5	10	20	0.1	4.5	15	4.6	1	0
	CVPtank	5	10	20	0.2	4.5	15	4.6	1	0
SBS	TMN/TMS, JPE/JPW	2	4	500	0.2	4.5	15	4.6	1	0
	SBS	1	37	500					2	3
	MAE/MAW	2	4	500	0.2	4.5	15	4.6	1	4

a = Near-field residence time includes up to 12 hours missing between detections, while mid-field residence time includes entire time lag between first and last detections without intervening detections elsewhere; far-field ("regional") residence time includes all time from entry in region to arrival at and departure from current site

b = Approximate migration rate calculated on most direct pathway

c = Missing values for transitions to and from same site: travel times must be 12 to 24 hours, unless otherwise specified under "Extra conditions"

f = See comments for alternate criteria

Table 3b. Cutoff values used in predator filter in 2016. Observed values past cutoff or unmet conditions indicate a predator. Time durations are in hours unless otherwise specified. Footnotes, Extra Conditions and Comment refer to both this table and Table 3a.

		Flow[d] (cfs)		Water Velocity[d] (ft/sec)			Extra Conditions	Comment
Detection Site	Previous Site	At arrival	At departure[e]	At arrival	At departure[e]	Average during transition		
DFU	DF						Travel time < 300	
	DFU						Travel time < 700	
	DFD, BDF1						Travel time < 300	
	TCE/TCW						Travel time < 300	Observed only among predator tags; not allowed
DFD	DF						Travel time < 300	
	DFU, DFD						Travel time < 300	Alternate value if coming from DFD
	BDF1, BDF2, BCA						Travel time < 50	
BDF1	DF						Travel time < 500	
	DFD						Travel time < 500	
	BDF1						Travel time < 300; known presence in detection range < 30	
	BDF2						Travel time < 100	
	BCA							
BDF2	DF, DFD, BDF1						Travel time < 500	Alternate value if coming from DF
	BDF2						Travel time < 300; known presence in detection range < 30	
	BCA							
BCA	DF, DFU						Travel time < 500	Alternate value if next transition is downstream
	DFD, BDF1, BDF2						Travel time < 500	Alternate value if next transition is downstream

d = Flow or velocity condition referred to in "Comment" is used to select criteria that prompts Comment. Otherwise, classified as predator if flow or velocity condition is violated

e = Condition at departure from previous site

Table 3b. (Continued)

Detection Site	Previous Site	Flow[d] (cfs)		Water Velocity[d] (ft/sec)			Extra Conditions	Comment
		At arrival	At departure[e]	At arrival	At departure[e]	Average during transition		
BCA	BCA						Maximum of 3 visits if arrival flow > 12000 cfs; Travel time < 200 (500[f])	Alternate value if next transition is downstream; otherwise, known presence in detection range < 30 hours.
	MOS		< 5000					
MOS	DF, DFU, DFD, BDF1, BDF2, BCA						Travel time < 200; allow 3 visits, travel time < 500 if arrival flow < 11,000 cfs	Alternate value if next transition is downstream
	MOS	<14000				<2.7	Travel time < 48	
	HOR	<14000				<3	Travel time < 60	
SJL	HOR							
	SJL						Travel time < 125	
	ORE						Regional residence time < 25 (15[f]) on departure from ORE	Alternate value if HOR barrier
	RS4							
RS4	SJL							
	RS4						Travel time < 100	
	RS5							
	TCE/TCW						Next transition must be downstream	Observed only among predator tags; not allowed
RS5	RS4							
	RS5						Travel time < 100	
	RS6							
RS6	RS5	>-500						
	RS6						Travel time < 100	

d = Flow or velocity condition referred to in "Comment" is used to select criteria that prompts Comment. Otherwise, classified as predator if flow or velocity condition is violated

e = Condition at departure from previous site

f = See comments for alternate criteria

Table 3b. (Continued)

Detection Site	Previous Site	Flow[d] (cfs)		Water Velocity[d] (ft/sec)			Extra Conditions	Comment
		At arrival	At departure[e]	At arrival	At departure[e]	Average during transition		
RS6	RS7	<1200						
RS7	RS6	>-500						
	RS7						Travel time < 40	
	RS8	<1200						
RS8	RS7	>-500						
	RS8						Travel time < 40	
	RS9	<1200						
RS9	RS5, RS8							
	RS9						Travel time < 40	
	RS10							
RS10	RS9							
	RS10						Travel time < 40	
	SJG, SJNB						Travel time < 15	
SJG	RS6, RS10							Alternate value if coming from RS6
	SJG	<2000 (>-2000)[g]	>-2000 (<2000)[g]	<0.5 (>-0.5)[g]	>-0.5 (<0.5)[g]	<0.8	Travel time < 24	
	SJNB, RRI	<3900	<3900	<1.4	<1.4	<1.4	Travel time < 15	
SJNB	SJG					>-0.15		Alternate value if water velocity condition is not met
	SJNB						Travel time < 35	
	RRI							
	SJC							

d = Flow or velocity condition referred to in "Comment" is used to select criteria that prompts Comment. Otherwise, classified as predator if flow or velocity condition is violated

e = Condition at departure from previous site

g = High flow/velocity on departure requires low values on arrival (and vice versa)

Table 3b. (Continued)

Detection Site	Previous Site	Flow[d] (cfs)		Water Velocity[d] (ft/sec)			Extra Conditions	Comment
		At arrival	At departure[e]	At arrival	At departure[e]	Average during transition		
RRI	SJG					>-0.15		Alternate value if water velocity condition is not met
	RRI						Travel time < 35	
	SJNB							
	SJC							
SJC	SJG					0.05 to 0.25		Alternate value if water velocity condition is not met
	SJNB, RRI					0.05 to 0.25		Alternate value if water velocity condition is not met
	SJC	<2000 (>-2000)[g]	>-2000 (<2000)[g]	<0.13 (>-0.13)[g]	>-0.13 (<0.13)[g]		Travel time < 40	
	SJS	<3500	<3900	<0.22	<0.22		Travel time < 12	
	MFE/MFW	<3500	<3900	<0.22	<0.22		Travel time < 12	
SJS	SJG, SJC							Alternate value if coming from SJC
	SJS	<3000 (>-3000)[g]	>-3000 (<3000)[g]	<0.18 (>-0.18)[g]	>-0.18 (<0.18)[g]		Travel time < 40	
	MAC, TCE/TCW	<4000	<40000 (NA[f])	<0.25	<0.75 (NA[f])		Travel time < 12	Alternate value if coming from TCE/TCW
MAC	SJS					-0.1 to 0.4		Alternate value if water velocity condition is not met
	MAC	<40000 (>-40000)[g]	>-40000 (<40000)[g]	<0.75 (>-0.75)[g]	>-0.75 (<0.75)[g]		Travel time < 24	
	TCE/TCW							

d = Flow or velocity condition referred to in "Comment" is used to select criteria that prompts Comment. Otherwise, classified as predator if flow or velocity condition is violated

e = Condition at departure from previous site

f = See comments for alternate criteria

g = High flow/velocity on departure requires low values on arrival (and vice versa)

Table 3b. (Continued)

Detection Site	Previous Site	Flow[d] (cfs)		Water Velocity[d] (ft/sec)			Extra Conditions	Comment
		At arrival	At departure[e]	At arrival	At departure[e]	Average during transition		
MAC	MFE/MFW			<0.5				
	COL			<0.5				
MFE/MFW	SJC					-0.1 to 0.4		Alternate value if water velocity condition is not met
	MAC					-0.1 to 0.4		Alternate value if water velocity condition is not met
	MFE/MFW	<40000 (>-40000)[g]	>-40000 (<40000)[g]	<0.75 (>-0.75)[g]	>-0.75 (<0.75)[g]		Travel time < 60	
	COL						Travel time < 24	
	SJD			<0.5		<0.1	Travel time < 12	
	MAE/MAW			<0.5		<0.1		Observed only among predator tags; not allowed
	MID		>-2000		>-0.1			
SJD	MAC, MID	>-27000		>-0.5		-0.1 to 0.4		Alternate value if condition for water velocity during transition is not met
	MFE/MFW, COL	>-27000		>-0.5		-0.1 to 0.4		Alternate value if condition for water velocity during transition is not met
	SJD	<40000 (>-40000)[g]	>-40000 (<40000)[g]	<0.75 (>-0.75)[g]	>-0.75 (<0.75)[g]	-0.1 to 0.4	Travel time < 60 (20[f])	Alternate value if condition for water velocity during transition is not met

d = Flow or velocity condition referred to in "Comment" is used to select criteria that prompts Comment. Otherwise, classified as predator if flow or velocity condition is violated

e = Condition at departure from previous site

f = See comments for alternate criteria

g = High flow/velocity on departure requires low values on arrival (and vice versa)

Table 3b. (Continued)

Detection Site	Previous Site	Flow[d] (cfs) At arrival	Flow[d] (cfs) At departure[e]	Water Velocity[d] (ft/sec) At arrival	Water Velocity[d] (ft/sec) At departure[e]	Water Velocity[d] (ft/sec) Average during transition	Extra Conditions	Comment
SJD	OSJ				>-0.1		Travel time < 24	
	JPE/JPW, FRE/FRW, TMN/TMS	<27000		<0.5		<0.1 (NA[f])	Travel time < 12	Alternate value if coming from JPE/JPW or FRE/FRW
HOR	MOS						Travel time < 50; allow 4 visits, travel time < 100 if arrival flow < 11,000 cfs	Alternate value if next transition is downstream
	HOR	<14000				<2.7	Travel time < 48	
	SJL	<14000 (5000[f])				<3	Regional residence time < 180 (120[f]) at departure from SJL	Alternate value if HOR barrier
	ORE	<14000 (5000[f])				<3	Regional residence time < 50 (15[f]) at departure from ORE	Alternate value if HOR barrier
ORE	HOR							Alternate value if HOR barrier
	ORE						Travel time < 60	Alternate value if HOR barrier
	SJL	>-200 (>200[f])		>-0.1 (>0.2[f])			Regional residence time < 60 (30[f]) on departure from SJL; travel time < 6	Alternate value if HOR barrier
	ORS	<3000					Travel time < 10 (5[f])	Alternate value if HOR barrier
ORS	ORE						Travel time < 50	
	ORS	<1200 (>-1100)[g]	>-1100 (<1200)[g]	<0.5 (>-0.5)[g]	>-0.5 (<0.5)[g]		Travel time < 100	
	MRH						Travel time < 5	
	CVP					<1.5	Travel time < 70	
WCL	RGU/RGD	>-9000		>-1.5			Travel time < 12; CCFB inflow < 4000 cfs on departure[e]	

d = Flow or velocity condition referred to in "Comment" is used to select criteria that prompts Comment. Otherwise, classified as predator if flow or velocity condition is violated

e = Condition at departure from previous site

f = See comments for alternate criteria

g = High flow/velocity on departure requires low values on arrival (and vice versa)

Table 3b. (Continued)

Detection Site	Previous Site	Flow[d] (cfs)		Water Velocity[d] (ft/sec)			Extra Conditions	Comment
		At arrival	At departure[e]	At arrival	At departure[e]	Average during transition		
WCL	CVP	>-9000	>-2000	>-1.5	>-0.8		CVP pumping < 4000 cfs on departure[e]	
	ORS	>-9000		>-1.5				
	WCL						Travel time < 50	
	MR4							
	OR4	<150	<4500	<0	<0.6			
OR4	WCL	>-6000		>-0.8				
	OR4						Travel time < 150	
	JPE/JPW	<6000		<0.8				
	MR4						Travel time < 150	
	MID, TCE/TCW	<6000		<0.8	<0.1 (0.2[f])		Travel time < 150; known presence in detection range < 5	Alternate value if coming from TCE/TCW
OSJ	MFE/MFW			<0.1				
	TCE/TCW, MID							
	COL							
	OSJ	<4000 (>-4000)[g]	>-4000 (<4000)[g]	<0.2 (>-0.2)[g]	>-0.2 (<0.2)[g]		Travel time < 24	
	SJD			<0.1				
	FRE/FRW						Travel time < 12	
MRH	ORE						Travel time < 50	
	MRH						Travel time < 24	Not allowed
	ORS						Travel time < 5	
MR4	ORS						Travel time < 180	
	MR4	<6500 (>-6500)[g]	>-6500 (<6500)[g]	<0.5 (>-0.5)[g]	>-0.5 (<0.5)[g]		Travel time < 50	

d = Flow or velocity condition referred to in "Comment" is used to select criteria that prompts Comment. Otherwise, classified as predator if flow or velocity condition is violated

e = Condition at departure from previous site

f = See comments for alternate criteria

g = High flow/velocity on departure requires low values on arrival (and vice versa)

Table 3b. (Continued)

Detection Site	Previous Site	Flow[d] (cfs)		Water Velocity[d] (ft/sec)			Extra Conditions	Comment
		At arrival	At departure[e]	At arrival	At departure[e]	Average during transition		
MR4	MID			<0.5	<0.1	<0.1		
	CVP, WCL						CVP pumping < 4000 cfs on departure[e] from CVP	
	TCE/TCW			<0.5	<0.2			
MID	RS10						Travel time < 120	
	MFE/MFW, SJD	<2500		<0.1			Travel time < 120	Alternate value if coming from SJD
	MID	<2500 (>-2500)[g]	>-2500 (<2500)[g]	<0.1 (>-0.1)[g]	>-0.1 (<0.1)[g]		Travel time < 100	
	TCE/TCW	>-2500		>-0.1	<0.2		Travel time < 120	
	COL	<2500		<0.1			Travel time < 120	
	OSJ	<2500		<0.1			Travel time < 120	
RGU/RGD	ORS							
	CVP		>-2000		>-0.8		CVP pumping < 4000 cfs at departure[e]	
	WCL		<3500		<0.6		Travel time < 30	
	MR4						Travel time < 30	
CVP	ORS							
	CVP						Travel time < 100; CVP pumping > 800 cfs on arrival, and < 2500 cfs on departure from previous visit	
	CVPtank						Travel time < 3; CVP pumping < 1000 cfs on arrival	
	RGU/RGD	<2000		<0.8			CVP pumping > 800 cfs on arrival	Alternate value if came from lower SJR via Interior Delta

d = Flow or velocity condition referred to in "Comment" is used to select criteria that prompts Comment. Otherwise, classified as predator if flow or velocity condition is violated

e = Condition at departure from previous site

g = High flow/velocity on departure requires low values on arrival (and vice versa)

Table 3b. (Continued)

Detection Site	Previous Site	Flow[d] (cfs)		Water Velocity[d] (ft/sec)			Extra Conditions	Comment
		At arrival	At departure[e]	At arrival	At departure[e]	Average during transition		
CVP	WCL	<2000	<3500	<0.8	<0.6		CVP pumping > 800 cfs on arrival	Alternate value if came from lower SJR via Interior Delta
	MR4	<2000		<0.8				Alternate value if came from lower SJR via Interior Delta
CVPtank	CVP						Travel time < 20	
TCE/TCW	SJS			<0.1				
	TCE/TCW	<1500 (>-1500)[g]	>-1500 (<1500)[g]	<0.3 (>-0.3)[g]	>-0.3 (<0.3)[g]		Travel time < 60	
	MAC			<0.1		<0.1	Travel time < 24	
	MR4	>-500	>-6500	>-0.1	>-0.5	>-0.2		
	MID	>-500	<2000	>-0.1	<0.1	>-0.2		
COL	MAC							
	MFE/MFW							
JPE/JPW	MFE/MFW, TCE/TCW, OR4, MID, SJD, OSJ							
	TMN/TMS							
	RGU/RGD, CVPtank						Travel time 2 to 80 hours	
	JPE/JPW						Travel time < 50	
	FRE/FRW						No minimum travel time	
	MAE/MAW							

d = Flow or velocity condition referred to in "Comment" is used to select criteria that prompts Comment. Otherwise, classified as predator if flow or velocity condition is violated

e = Condition at departure from previous site

g = High flow/velocity on departure requires low values on arrival (and vice versa)

Table 3b. (Continued)

Detection Site	Previous Site	Flow[d] (cfs)		Water Velocity[d] (ft/sec)			Extra Conditions	Comment
		At arrival	At departure[e]	At arrival	At departure[e]	Average during transition		
MAE/MAW	SJD, MFE/MFW, TCE/TCW, WCL, OSJ, TMN/TMS, JPE/JPW, FRE/FRW			>-1				
	CVPtank			>-1			Travel time 5 to 100	
	RGU/RGD			>-1			Travel time 5 to 500	
	MTZ, SBS			>-1				
	MAE/MAW						Travel time < 36	
	BBR			<1				
BBR	TCE/TCW							
	TMN/TMS, JPE/JPW, MTZ							
	CVPtank						Travel time 5 to 180	
	RGU/RGD						Travel time 5 to 600	
	MAE/MAW							
	BBR						Travel time < 36	
FRE/FRW	OR4, MR4, MID, TCE/TCW, SJD OSJ							
	JPE/JPW						No minimum travel time	
	FRE/FRW						Travel time < 30	
TMN/TMS	SJD		>-27000		>-0.5			
	RGU/RGD, CVPtank							Alternate value if coming from RGU/RGD
	TMN/TMS	<0 (>0)[g]	>0 (<0)[g]	<0 (>0)[g]	>0 (<0)[g]		Travel time < 24	

d = Flow or velocity condition referred to in "Comment" is used to select criteria that prompts Comment. Otherwise, classified as predator if flow or velocity condition is violated

e = Condition at departure from previous site

g = High flow/velocity on departure requires low values on arrival (and vice versa)

Table 3b. (Continued)

Detection Site	Previous Site	Flow[d] (cfs)		Water Velocity[d] (ft/sec)			Extra Conditions	Comment
		At arrival	At departure[e]	At arrival	At departure[e]	Average during transition		
TMN/TMS	JPE/JPW							
	FRE/FRW							
	SBS, MAE/MAW							
MTZ	RGU/RGD							
	CVPtank							
SBS	TMN/TMS, JPE/JPW							
	SBS						Travel time < 24	
	MAE/MAW							

d = Flow or velocity condition referred to in "Comment" is used to select criteria that prompts Comment. Otherwise, classified as predator if flow or velocity condition is violated

e = Condition at departure from previous site

Table 4. Regions used in the far-field residence time components of the predator filter in 2016.

Region	Detection Sites
I	DFU, DFD, BDF1, BDF2, BCA, MOS, HOR
IIA	SJL, RS4–RS10, SJG, SJNB, RRI, SJC
IIB	ORE, ORS, MRH
IIIA	SJS, MAC, MFE/MFW, TCE/TCW, COL
IIIB	WCL, OR4, RGU, RGD, CVP, CVPtank
IIIC	MR4, MID
IV	JPE/JPW, MAE/MAW, FRE/FRW, TMN/TMS, MTZ, SBS, BBE/BBW
IVB	SJD, OSJ

Table 5. Number of tags from each release group that were detected after release in 2016, including predator-type detections and detections omitted from the survival analysis. Releases are: 1 = February, 2 = March, 3 = April.

Release Group	1	2	3	Total
Number Released	480	480	480	1,440
Number Detected	399	461	471	1,331
Number Detected Downstream	379	458	463	1,300
Number Detected Upstream of Study Area	399	444	467	1,310
Number Detected in Study Area	217	376	427	1,020
Number Detected in San Joaquin River Route	72	143	415	630
Number Detected in Old River Route	182	290	19	491
Number Assigned to San Joaquin River Route	27	85	409	521
Number Assigned to Old River Route	180	288	15	483

Table 6. Number of tags observed from each release group at each detection site in 2016, including predator-type detections. Routes (SJR = San Joaquin River, OR = Old River) represent route assignment at the head of Old River. Pooled counts are summed over all receivers in array and all routes. Route could not be identified for some tags. Releases are: 1 = February, 2 = March, 3 = April.

Detection Site	Site Code	Survival Model Code	Release Group 1	2	3	Total
Release site at Durham Ferry			480	480	480	1,440
Durham Ferry Upstream, Upstream	DFU1	A0a	79	16	33	128
Durham Ferry Upstream, Downstream	DFU2	A0b	69	11	19	99
Durham Ferry Upstream (Pooled)	DFU	A0	80	16	34	130
Durham Ferry Downstream, Upstream	DFD1	A2a	378	370	419	1,167
Durham Ferry Downstream, Downstream	DFD2	A2b	378	288	358	1,024
Durham Ferry Downstream (Pooled)	DFD	A2	378	396	434	1,208
Below Durham Ferry 1	BDF1	A3	234	136	203	573
Below Durham Ferry 2	BDF2	A4	236	170	213	619
Banta Carbona, Upstream	BCAU	A5a	220	150	337	707
Banta Carbona, Downstream	BCAD	A5b	223	164	310	697
Banta Carbona (Pooled)	BCA	A5	231	208	384	823
Mossdale, Upstream	MOSU	A6a	217	374	427	1,018
Mossdale, Downstream	MOSD	A6b	217	376	427	1,020
Mossdale (Pooled)	MOS	A6	217	376	427[a]	1,020
Head of Old River (Pooled)	HOR	B0	214	374	427	1,015
Lathrop, Upstream	SJLU	A7a	72	142	410	624
Lathrop, Downstream	SJLD	A7b	71	141	415	627
Lathrop (Pooled)	SJL	A7	72	142	415	629
Predator Removal Study 4	RS4	N1	49	112	411	572
Predator Removal Study 5	RS5	N2	41	97	408	546
Predator Removal Study 6	RS6	N3	31	87	406	524
Predator Removal Study 7	RS7	N4	27	83	406	516
Predator Removal Study 8	RS8	N5	25	81	405	511
Predator Removal Study 9	RS9	N6	24	79	404	507
Predator Removal Study 10	RS10	N7	24	77	404	505
Garwood Bridge, Upstream	SJGU	A8a	22	72	402	496
Garwood Bridge, Downstream	SJGD	A8b	22	72	402	496
Garwood Bridge (Pooled)	SJG	A8	22	72	402	496
Navy Drive Bridge	SJNB	A9	21	69	396	486
Rough and Ready Island, Upstream	RRIU	R1a	1	4	41	46
Rough and Ready Island, Downstream	RRID	R1b	1	4	41	46
Rough and Ready Island (Pooled)	RRI	R1	1	4	41	46
Calaveras River, Upstream	SJCU	A10a	20	67	392	479
Calaveras River, Downstream	SJCD	A10b	20	67	394	481
Calaveras River (Pooled)	SJC	A10	20	67	394	481
San Joaquin River Shipping Channel	SJS	A11	19	67	386	472
MacDonald Island Upstream	MACU	A12a	13	58	318	389

a = One tagged steelhead was recaptured after detection at MOS and then returned to the river

Table 6. (Continued)

Detection Site	Site Code	Survival Model Code	Release Group 1	2	3	Total
MacDonald Island Downstream	MACD	A12b	12	55	307	374
MacDonald Island (Pooled)	MAC	A12	13	58	319	390
Turner Cut, Upstream	TCE	F1a	8	22	114	144
Turner Cut, Downstream	TCW	F1b	8	22	114	144
Turner Cut (Pooled)	TCE/TCW	F1	8	22	114	144
Medford Island East	MFE	A13a	5	42	229	276
Medford Island West	MFW	A13b	5	42	230	277
Medford Island (Pooled)	MFE/MFW	A13	5	42	230	277
Columbia Cut, Upstream	COLU	F2a	2	5	62	69
Columbia Cut, Downstream	COLD	F2b	2	5	64	71
Columbia Cut (Pooled)	COL	F2	2	5	64	71
Disappointment Slough, Upstream	SJDU	A14a	6	41	223	270
Disappointment Slough, Downstream	SJDD	A14b	6	40	218	264
Disappointment Slough (Pooled)	SJD	A14	6	41	223	270
Old River at the San Joaquin, Upstream	OSJU	B5a	3	10	34	47
Old River at the San Joaquin, Downstream	OSJD	B5b	3	10	35	48
Old River at the San Joaquin (Pooled)	OSJ	B5	3	10	35	48
Old River East, Upstream	OREU	B1a	182	290	19	491
Old River East, Downstream	ORED	B1b	182	290	19	491
Old River East (Pooled)	ORE	B1	182	290	19	491
Old River South, Upstream	ORSU	B2a	179	283	17	479
Old River South, Downstream	ORSD	B2b	179	282	17	478
Old River South (Pooled)	ORS	B2	179	283	17	479
West Canal, Upstream	WCLU	B3a	42	83	42	167
West Canal, Downstream	WCLD	B3b	39	81	42	162
West Canal: SJR Route	WCL	B3	4	5	40	49
West Canal: OR Route	WCL	B3	38	78	2	118
West Canal (Pooled)	WCL	B3	42	83	42	167
Old River at Highway 4, Upstream	OR4U	B4a	7	19	31	57
Old River at Highway 4, Downstream	OR4D	B4b	7	19	30	56
Old River at Highway 4, SJR Route	OR4	B4	4	5	30	39
Old River at Highway 4, OR Route	OR4	B4	3	14	1	18
Old River at Highway 4 (Pooled)	OR4	B4	7	19	31	57
Middle River Head, Upstream	MRHU	C1a	4	1	2	7
Middle River Head, Downstream	MRHD	C1b	4	1	2	7
Middle River Head (Pooled)	MRH	C1	4	1	2	7
Middle River at Highway 4, Upstream	MR4U	C2a	1	5	29	35
Middle River at Highway 4, Downstream	MR4D	C2b	1	5	29	35
Middle River at Highway 4, SJR Route	MR4	C2	1	1	29	31
Middle River at Highway 4, OR Route	MR4	C2	0	4	0	4
Middle River at Highway 4 (Pooled)	MR4	C2	1	5	29	35

Table 6. (Continued)

Detection Site	Site Code	Survival Model Code	Release Group 1	2	3	Total
Middle River near Mildred Island	MID	C3	1	5	51	57
Radial Gates Upstream #1	RGU1	D1a	84	137	38	259
Radial Gates Upstream #2	RGU2	D1b	85	138	37	260
Radial Gates Upstream: SJR Route	RGU	D1	2	4	34	40
Radial Gates Upstream: OR Route	RGU	D1	84	138	6	228
Radial Gates Upstream (Pooled)	RGU	D1	86	142	40	268
Radial Gates Downstream #1	RGD1	D2a	30	65	16	111
Radial Gates Downstream #2	RGD2	D2b	34	68	17	119
Radial Gates Downstream: SJR Route	RGD	D2	0	2	12	14
Radial Gates Downstream: OR Route	RGD	D2	34	66	5	105
Radial Gates Downstream (Pooled)	RGD	D2	34	68	17	119
Central Valley Project Trashrack, Upstream	CVPU	E1a	127	187	37	351
Central Valley Project Trashrack, Downstream	CVPD	E1b	122	177	36	335
CVP Trashrack: SJR Route	CVP	E1	4	2	31	37
CVP Trashrack: OR Route	CVP	E1	123	185	6	314
CVP Trashrack (Pooled)	CVP	E1	127	187	37	351
CVP Holding Tank: SJR Route	CVPtank	E2	2	0	13	15
CVP Holding Tank: OR Route	CVPtank	E2	70	85	2	157
CVP Holding Tank	CVPtank	E2	72[b]	85[c]	15	172
Threemile Slough, Upstream	TMS	T1a	1	9	38	48
Threemile Slough, Downstream	TMN	T1b	1	8	36	45
Threemile Slough: SJR Route	TMS/TMN	T1	0	6	38	44
Threemile Slough: OR Route	TMS/TMN	T1	1	3	0	4
Threemile Slough (Pooled)	TMS/TMN	T1	1	9	38	48
Jersey Point East	JPE	G1a	20	61	241	322
Jersey Point West	JPW	G1b	20	60	242	322
Jersey Point: SJR Route	JPE/JPW	G1	5	47	242	294
Jersey Point: OR Route	JPE/JPW	G1	15	15	0	30
Jersey Point (Pooled)	JPE/JPW	G1	20	62	242	324
False River West	FRW	H1a	4	18	31	53
False River East	FRE	H1b	8	19	45	72
False River: SJR Route	FRE/FRW	H1	4	15	46	65
False River: OR Route	FRE/FRW	H1	4	6	0	10
False River (Pooled)	FRE/FRW	H1	8	21	46	75
Montezuma Slough, Upstream	MTZU	T2a	0	2	0	2
Montezuma Slough, Downstream	MTZD	T2b	0	1	0	1
Montezuma Slough (Pooled)	MTZ	T2	0	2	0	2
Spoonbill Slough, Upstream	SBSU	T3a	2	0	2	4

[b] = Ten tagged steelhead were recaptured in the CVP holding tank after detection, and then returned to the river

[c] = Six tagged steelhead were recaptured in the CVP holding tank after detection, and then returned to the river

Table 6. (Continued)

Detection Site	Site Code	Survival Model Code	Release Group 1	2	3	Total
Spoonbill Slough, Downstream	SBSD	T3b	3	4	2	9
Spoonbill Slough (Pooled)	SBS	T3	3	4	2	9
Chipps Island East	MAE	G2a	78	135	246	459
Chipps Island West	MAW	G2b	77	135	243	455
Chipps Island: SJR Route	MAE/MAW	G2	6	38	247	291
Chipps Island: OR Route	MAE/MAW	G2	73	107	4	184
Chipps Island (Pooled)	MAE/MAW	G2	79	145	251	475
Benicia Bridge, East	BBE	G3a	73	151	253	477
Benicia Bridge, West	BBW	G3b	72	150	265	487
Benicia Bridge: SJR Route	BBE/BBW	G3	6	43	263	312
Benicia Bridge: OR Route	BBE/BBW	G3	68	109	4	181
Benicia Bridge (Pooled)	BBE/BBW	G3	74	152	267	493

Table 7. Number of tags observed from each release group at each detection site in 2016 and used in the survival analysis, including predator-type detections. Numbers in parentheses are counts of tags whose detection histories were right-censored at that site. Pooled counts are summed over all receivers in array. Route could not be identified for some tags. Releases are: 1 = February, 2 = March, 3 = April.

Detection Site	Site Code	Survival Model Code	Release Group			Total
			1	2	3	
Release site at Durham Ferry			480	480	480	1,440
Durham Ferry Upstream, Upstream	DFU1	A0a	38	10	22	70
Durham Ferry Upstream, Downstream	DFU2	A0b	26	6	13	45
Durham Ferry Upstream (Pooled)	DFU	A0	38	10	23	71
Durham Ferry Downstream	DFD	A2	360	389	419	1,168
Below Durham Ferry 1	BDF1	A3	226	126	192	544
Below Durham Ferry 2	BDF2	A4	221	165	199	585
Banta Carbona	BCA	A5	224	203	377	804
Mossdale	MOS	A6	214	376	426 (1)	1,016
Lathrop, Upstream	SJLU	A7a	27	83	402	512
Lathrop, Downstream	SJLD	A7b	27	85	409	521
Lathrop (Pooled)	SJL	A7	27	85	409	521
Garwood Bridge	SJG	A8	21	69	399	489
Navy Drive Bridge	SJNB	A9	20	67	387	474
Rough and Ready Island, Upstream	RRIU	R1a	0	0	7	7
Rough and Ready Island, Downstream	RRID	R1b	0	0	7	7
Rough and Ready Island (Pooled)	RRI	R1	0	0	7	7
San Joaquin River near Calaveras	SJC	A10	20	66	389	475
San Joaquin River Shipping Channel	SJS	A11	19	66	384	469
MacDonald Island Upstream	MACU	A12a	10	46	274	330
MacDonald Island Downstream	MACD	A12b	9	46	277	332
MacDonald Island (Pooled)	MAC	A12	10	46	280	336
Turner Cut, Upstream	TCE	F1a	8	20	99	127
Turner Cut, Downstream	TCW	F1b	8	20	99	127
Turner Cut (Pooled)	TCE/TCW	F1	8	20	99	127
Medford Island East	MFE	A13a	5	40	209	254
Medford Island West	MFW	A13b	5	40	211	256
Medford Island (Pooled)	MFE/MFW	A13	5	40	212	257
Columbia Cut, Upstream	COLU	F2a	2[a]	5	56	63
Columbia Cut, Downstream	COLD	F2b	2[a]	5	56	63
Columbia Cut (Pooled)	COL	F2	2[a]	5	56	63
Disappointment Slough, Upstream	SJDU	A14a	3[a]	32	203	238
Disappointment Slough, Downstream	SJDD	A14b	3[a]	32	197	232
Disappointment Slough (Pooled)	SJD	A14	3[a]	32	203	238
Old River at the San Joaquin, Upstream	OSJU	B5a	2[a]	8	29	39
Old River at the San Joaquin, Downstream	OSJD	B5b	2[a]	8	29	39

a = detections were not used in the survival model

Table 7. (Continued)

Detection Site	Site Code	Survival Model Code	Release Group 1	2	3	Total
Old River at the San Joaquin (Pooled)	OSJ	B5	2[a]	8	29	39
Old River East, Upstream	OREU	B1a	180	288	15	483
Old River East, Downstream	ORED	B1b	180	288	15	483
Old River East (Pooled)	ORE	B1	180	288	15	483
Old River South, Upstream	ORSU	B2a	175	281	14	470
Old River South, Downstream	ORSD	B2b	177	281	15	473
Old River South (Pooled)	ORS	B2	177	282	15	474
West Canal, Upstream	WCLU	B3a	1[a]	16	0[a]	17
West Canal, Downstream	WCLD	B3b	1[a]	16	0[a]	17
West Canal: OR Route (Pooled)	WCL	B3	1[a]	16	0[a]	17
Old River at Highway 4, Upstream	OR4U	B4a	5	15	29	49
Old River at Highway 4, Downstream	OR4D	B4b	5	15	29	49
Old River at Highway 4, SJR Route	OR4	B4	4[a]	5[a]	29	38
Old River at Highway 4, OR Route	OR4	B4	1 (1)	10	0	11
Old River at Highway 4 (Pooled)	OR4	B4	5 (1)	15	29	49
Middle River Head, Upstream	MRHU	C1a	1	0	0	1
Middle River Head, Downstream	MRHD	C1b	1	0	0	1
Middle River Head (Pooled)	MRH	C1	1 (1)	0	0	1
Middle River at Highway 4, Upstream	MR4U	C2a	1	4	20	25
Middle River at Highway 4, Downstream	MR4D	C2b	1	4	20	25
Middle River at Highway 4, SJR Route	MR4	C2	1[a]	0[a]	20	21
Middle River at Highway 4, OR Route	MR4	C2	0	4	0	4
Middle River at Highway 4 (Pooled)	MR4	C2	1	4	20	25
Radial Gates Upstream: SJR Route	RGU	D1	0[a]	2[a]	14	16
Radial Gates Upstream: OR Route	RGU	D1	38	65	4	107
Radial Gates Upstream (Pooled)	RGU	D1	38	67	18	123
Radial Gates Downstream: SJR Route	RGD	D2	0[a]	2[a]	11	13
Radial Gates Downstream: OR Route	RGD	D2	34	66	5	105
Radial Gates Downstream (Pooled)	RGD	D2	34	68	16	118
CVP Trashrack: SJR Route	CVP	E1	4[a]	2[a]	24	30
CVP Trashrack: OR Route	CVP	E1	120	160	5	285
CVP Trashrack (Pooled)	CVP	E1	124	162	29	315
CVP Holding Tank: SJR Route	CVPtank	E2	2[a]	0[a]	13	15
CVP Holding Tank: OR Route	CVPtank	E2	70 (10)	84 (6)	2	156
CVP Holding Tank (Pooled)	CVPtank	E2	72 (10)	84 (6)	15	171
Threemile Slough, Upstream	TMS	T1a	0[a]	1	23	24
Threemile Slough, Downstream	TMN	T1b	0[a]	1	23	24
Threemile Slough: SJR Route (Pooled)	TMS/TMN	T1	0[a]	1	23	24

a = detections were not used in the survival model

Table 7. (Continued)

Detection Site	Site Code	Survival Model Code	Release Group 1	2	3	Total
Jersey Point East	JPE	G1a	4[a]	50	226	280
Jersey Point West	JPW	G1b	4[a]	48	227	279
Jersey Point: SJR Route	JPE/JPW	G1	4[a]	47	227	278
Jersey Point: OR Route	JPE/JPW	G1	0[a]	3	0	3
Jersey Point (Pooled)	JPE/JPW	G1	4[a]	50	227	281
False River West	FRW	H1a	0[a]	0[a]	0[a]	0
False River East	FRE	H1b	1[a]	0[a]	0[a]	1
False River: SJR Route	FRE/FRW	H1	1[a]	0[a]	0[a]	1
False River: OR Route	FRE/FRW	H1	0[a]	0[a]	0[a]	0
False River (Pooled)	FRE/FRW	H1	1[a]	0[a]	0[a]	0
Chipps Island: SJR Route	MAE/MAW	G2	6	38	245	289
Chipps Island: OR Route	MAE/MAW	G2	65	103	4	172
Chipps Island (Pooled)	MAE/MAW	G2	71	141	249	461
Benicia Bridge, East	BBE	G3a	63	143	247	453
Benicia Bridge, West	BBW	G3b	62	144	261	467
Benicia Bridge: SJR Route	BBE/BBW	G3	6	43	260	309
Benicia Bridge: OR Route	BBE/BBW	G3	58	103	3	164
Benicia Bridge (Pooled)	BBE/BBW	G3	64	146	263	473

a = detections were not used in the survival model

Table 8. Number of tags from each release group in 2016 first classified as in a predator at each detection site, based on the predator filter.

Detection Site and Code			Durham Ferry Release Groups							
			Classified as Predator on Arrival at Site				Classified as Predator on Departure from Site			
Detection Site	Site Code	Survival Model Code	1	2	3	Total	1	2	3	Total
Durham Ferry Upstream	DFU	A0	6	0	7	13	1	0	0	1
Durham Ferry Downstream	DFD	A2	2	1	0	3	0	0	0	0
Below Durham Ferry 1	BDF1	A3	0	0	1	1	0	1	0	1
Below Durham Ferry 2	BDF2	A4	2	1	0	3	3	0	0	3
Banta Carbona	BCA	A5	3	0	2	5	0	0	0	0
Mossdale	MOS	A6	0	0	1	1	0	0	0	0
Head of Old River	HOR	B0	0	2	0	2	1	0	1	2
Lathrop	SJL	A7	0	0	0	0	1	0	1	2
Predator Removal Study 4	RS4	N1	0	0	0	0	0	2	1	3
Predator Removal Study 5	RS5	N2	0	0	1	1	1	0	1	2
Predator Removal Study 6	RS6	N3	0	1	3	4	0	0	3	3
Predator Removal Study 7	RS7	N4	1	1	2	4	0	0	1	1
Predator Removal Study 8	RS8	N5	1	0	1	2	0	1	0	1
Predator Removal Study 9	RS9	N6	0	0	0	0	0	1	2	3
Predator Removal Study 10	RS10	N7	0	0	2	2	0	0	0	0
Garwood Bridge	SJG	A8	0	0	0	0	0	1	2	3
Navy Drive Bridge	SJNB	A9	0	0	0	0	0	0	0	0
Rough and Ready Island	RRI	R1	0	0	0	0	0	0	1	1
San Joaquin River at Calaveras River	SJC	A10	0	0	2	2	0	0	2	2
San Joaquin River Shipping Channel	SJS	A11	0	1	1	2	0	0	1	1
MacDonald Island	MAC	A12	0	0	2	2	1	1	1	3
Medford Island	MFE/MFW	A13	0	0	1	1	0	0	2	2
San Joaquin River at Disappointment Slough	SJD	A14	0	0	1	1	0	1	1	2
Old River East	ORE	B1	1	0	1	2	0	2	0	2
Old River South	ORS	B2	0	0	1	1	1	0	0	1
West Canal	WCL	B3	0	0	2	2	0	0	0	0
Old River at Highway 4	OR4	B4	0	1	2	3	1	0	1	2
Old River at the San Joaquin Mouth	OSJ	B5	0	0	0	0	0	0	2	2
Middle River Head	MRH	C1	0	0	1	1	1	0	1	2
Middle River at Highway 4	MR4	C2	0	0	0	0	0	0	1	1
Middle River near Mildred Island	MID	C3	0	0	0	0	0	0	0	0
Radial Gates Upstream	RGU	D1	1	1	0	2	6	2	1	9
Radial Gates Downstream	RGD	D2	0	0	0	0	0	1	0	1
Central Valley Project Trashrack	CVP	E1	1	8	1	10	4	14	5	23
Central Valley Project Holding Tank	CVPtank	E2	0	0	0	0	0	0	0	0
Turner Cut	TCE/TCW	F1	0	0	3	3	0	0	0	0

Table 8. (Continued)

Detection Site and Code			Durham Ferry Release Groups							
			Classified as Predator on Arrival at Site				Classified as Predator on Departure from Site			
Detection Site	Site Code	Survival Model Code	1	2	3	Total	1	2	3	Total
Columbia Cut	COL	F2	0	0	0	0	0	0	0	0
Jersey Point	JPE/JPW	G1	0	1	1	2	0	0	0	0
Chipps Island	MAE/MAW	G2	0	0	1	1	2	0	0	2
Benicia Bridge	BBR	G3	1	1	0	2	0	1	0	1
False River	FRE/FRW	H1	0	0	0	0	0	0	0	0
Threemile Slough	TMS/TMN	T1	0	1	0	1	0	0	0	0
Montezuma Slough	MTZ	T2	0	0	0	0	0	0	0	0
Spoonbill Slough	SBS	T3	0	0	0	0	0	0	0	0
Total Tags			19	20	40	79	23	28	31	82

Table 9. Number of tags from each release group that were detected after release in 2016, excluding predator-type detections and detections omitted from the survival analysis. Releases are: 1 = February, 2 = March, 3 = April.

Release Group	1	2	3	Total
Number Released	480	480	480	1,440
Number Detected	399	461	469	1,329
Number Detected Downstream	378	458	461	1,297
Number Detected Upstream of Study Area	399	444	465	1,308
Number Detected in Study Area	212	374	426	1,012
Number Detected in San Joaquin River Route	67	141	413	621
Number Detected in Old River Route	181	286	16	483
Number Assigned to San Joaquin River Route	25	85	408	518
Number Assigned to Old River Route	178	286	15	479

Table 10. Number of tags observed from each release group at each detection site in 2016, excluding predator-type detections. Routes (SJR = San Joaquin River, OR = Old River) represent route assignment at the head of Old River. Pooled counts are summed over all receivers in array and all routes. Route could not be identified for some tags. Releases are: 1 = February, 2 = March, 3 = April.

Detection Site	Site Code	Survival Model Code	Release Group			Total
			1	2	3	
Release site at Durham Ferry			480	480	480	1,440
Durham Ferry Upstream, Upstream	DFU1	A0a	77	16	27	120
Durham Ferry Upstream, Downstream	DFU2	A0b	67	11	12	90
Durham Ferry Upstream (Pooled)	DFU	A0	78	16	28	122
Durham Ferry Downstream, Upstream	DFD1	A2a	377	370	417	1,164
Durham Ferry Downstream, Downstream	DFD2	A2b	377	288	355	1,020
Durham Ferry Downstream (Pooled)	DFD	A2	377	396	432	1,205
Below Durham Ferry 1	BDF1	A3	231	136	198	565
Below Durham Ferry 2	BDF2	A4	233	170	209	612
Banta Carbona, Upstream	BCAU	A5a	214	149	336	699
Banta Carbona, Downstream	BCAD	A5b	217	163	309	689
Banta Carbona (Pooled)	BCA	A5	225	207	383	815
Mossdale, Upstream	MOSU	A6a	212	372	426	1,010
Mossdale, Downstream	MOSD	A6b	212	374	426	1,012
Mossdale (Pooled)	MOS	A6	212	374	426[a]	1,012
Head of Old River (Pooled)	HOR	B0	209	372	425	1,006
Lathrop, Upstream	SJLU	A7a	67	140	408	615
Lathrop, Downstream	SJLD	A7b	66	139	413	618
Lathrop (Pooled)	SJL	A7	67	140	413	620
Predator Removal Study 4	RS4	N1	44	109	409	562
Predator Removal Study 5	RS5	N2	37	94	405	536
Predator Removal Study 6	RS6	N3	27	85	402	514
Predator Removal Study 7	RS7	N4	23	81	400	504
Predator Removal Study 8	RS8	N5	21	79	396	496
Predator Removal Study 9	RS9	N6	20	77	395	492
Predator Removal Study 10	RS10	N7	20	75	393	488
Garwood Bridge, Upstream	SJGU	A8a	18	70	391	479
Garwood Bridge, Downstream	SJGD	A8b	18	70	391	479
Garwood Bridge (Pooled)	SJG	A8	18	70	391	479
Navy Drive Bridge	SJNB	A9	18	67	383	468
Rough and Ready Island, Upstream	RRIU	R1a	0	3	36	39
Rough and Ready Island, Downstream	RRID	R1b	0	3	36	39
Rough and Ready Island (Pooled)	RRI	R1	0	3	36	39
San Joaquin River near Calaveras, Upstream	SJCU	A10a	17	63	382	462
San Joaquin River near Calaveras, Downstream	SJCD	A10b	17	63	384	464
San Joaquin River near Calaveras (Pooled)	SJC	A10	17	63	384	464
San Joaquin River Shipping Channel	SJS	A11	16	63	375	454

[a] = One tagged steelhead was recaptured after detection at MOS and then returned to the river

Table 10. (Continued)

Detection Site	Site Code	Survival Model Code	Release Group 1	2	3	Total
MacDonald Island Upstream	MACU	A12a	12	56	310	378
MacDonald Island Downstream	MACD	A12b	11	54	298	363
MacDonald Island (Pooled)	MAC	A12	12	56	311	379
Turner Cut, Upstream	TCE	F1a	6	20	106	132
Turner Cut, Downstream	TCW	F1b	6	20	106	132
Turner Cut (Pooled)	TCE/TCW	F1	6	20	106	132
Medford Island East	MFE	A13a	4	41	219	264
Medford Island West	MFW	A13b	4	41	220	265
Medford Island (Pooled)	MFE/MFW	A13	4	41	220	265
Columbia Cut, Upstream	COLU	F2a	2	5	59	66
Columbia Cut, Downstream	COLD	F2b	2	5	61	68
Columbia Cut (Pooled)	COL	F2	2	5	61	68
Disappointment Slough, Upstream	SJDU	A14a	5	40	212	257
Disappointment Slough, Downstream	SJDD	A14b	5	39	207	251
Disappointment Slough (Pooled)	SJD	A14	5	40	212	257
Old River at the San Joaquin, Upstream	OSJU	B5a	3	10	32	45
Old River at the San Joaquin, Downstream	OSJD	B5b	3	10	33	46
Old River at the San Joaquin (Pooled)	OSJ	B5	3	10	33	46
Old River East, Upstream	OREU	B1a	181	286	16	483
Old River East, Downstream	ORED	B1b	181	286	16	483
Old River East (Pooled)	ORE	B1	181	286	16	483
Old River South, Upstream	ORSU	B2a	177	279	15	471
Old River South, Downstream	ORSD	B2b	177	278	15	470
Old River South (Pooled)	ORS	B2	177	279	15	471
West Canal, Upstream	WCLU	B3a	38	80	39	157
West Canal, Downstream	WCLD	B3b	35	78	39	152
West Canal: SJR Route	WCL	B3	2	4	37	43
West Canal: OR Route	WCL	B3	36	76	2	114
West Canal (Pooled)	WCL	B3	38	80	39	157
Old River at Highway 4, Upstream	OR4U	B4a	5	16	27	48
Old River at Highway 4, Downstream	OR4D	B4b	5	16	26	47
Old River at Highway 4, SJR Route	OR4	B4	2	4	26	32
Old River at Highway 4, OR Route	OR4	B4	3	12	1	16
Old River at Highway 4 (Pooled)	OR4	B4	5	16	27	48
Middle River Head, Upstream	MRHU	C1a	3	1	2	6
Middle River Head, Downstream	MRHD	C1b	3	1	2	6
Middle River Head (Pooled)	MRH	C1	3	1	2	6
Middle River at Highway 4, Upstream	MR4U	C2a	1	5	26	32
Middle River at Highway 4, Downstream	MR4D	C2b	1	5	26	32
Middle River at Highway 4, SJR Route	MR4	C2	1	1	26	28
Middle River at Highway 4, OR Route	MR4	C2	0	4	0	4

Table 10. (Continued)

Detection Site	Site Code	Survival Model Code	Release Group 1	2	3	Total
Middle River at Highway 4 (Pooled)	MR4	C2	1	5	26	32
Middle River near Mildred Island, Upstream	MIDU	C3a	1	5	49	55
Middle River near Mildred Island, Downstream	MIDD	C3b	1	5	49	55
Middle River near Mildred Island (Pooled)	MID	C3	1	5	49	55
Radial Gates Upstream #1	RGU1	D1a	78	133	36	247
Radial Gates Upstream #2	RGU2	D1b	79	134	35	248
Radial Gates Upstream: SJR Route	RGU	D1	0	3	32	35
Radial Gates Upstream: OR Route	RGU	D1	80	135	6	221
Radial Gates Upstream (Pooled)	RGU	D1	80	138	38	256
Radial Gates Downstream #1	RGD1	D2a	29	63	15	107
Radial Gates Downstream #2	RGD2	D2b	33	66	16	115
Radial Gates Downstream: SJR Route	RGD	D2	0	1	11	12
Radial Gates Downstream: OR Route	RGD	D2	33	65	5	103
Radial Gates Downstream (Pooled)	RGD	D2	33	66	16	115
Central Valley Project Trashrack, Upstream	CVPU	E1a	122	182	32	336
Central Valley Project Trashrack, Downstream	CVPD	E1b	118	171	31	320
CVP Trashrack: SJR Route	CVP	E1	2	2	28	32
CVP Trashrack: OR Route	CVP	E1	120	180	4	304
CVP Trashrack (Pooled)	CVP	E1	122	182	32	336
CVP Holding Tank: SJR Route	CVPtank	E2	2	0	11	13
CVP Holding Tank: OR Route	CVPtank	E2	69	85	1	155
CVP Holding Tank (Pooled)	CVPtank	E2	71[b]	85[c]	12	168
Threemile Slough, Upstream	TMS	T1a	1	8	33	42
Threemile Slough, Downstream	TMN	T1b	1	7	32	40
Threemile Slough: SJR Route	TMS/TMN	T1	0	6	33	39
Threemile Slough: OR Route	TMS/TMN	T1	1	2	0	3
Threemile Slough (Pooled)	TMS/TMN	T1	1	8	33	42
Jersey Point East	JPE	G1a	19	61	225	305
Jersey Point West	JPW	G1b	19	60	226	305
Jersey Point: SJR Route	JPE/JPW	G1	4	47	226	277
Jersey Point: OR Route	JPE/JPW	G1	15	15	0	30
Jersey Point (Pooled)	JPE/JPW	G1	19	62	226	307
False River West	FRW	H1a	4	18	28	50
False River East	FRE	H1b	7	19	40	66
False River: SJR Route	FRE/FRW	H1	3	15	42	60
False River: OR Route	FRE/FRW	H1	4	6	0	10
False River (Pooled)	FRE/FRW	H1	7	21	42	70

[b] = Ten tagged steelhead were recaptured in the CVP holding tank after detection, and then returned to the river

[c] = Six tagged steelhead were recaptured in the CVP holding tank after detection, and then returned to the river

Table 10. (Continued)

Detection Site	Site Code	Survival Model Code	Release Group 1	2	3	Total
Montezuma Slough, Upstream	MTZU	T2a	0	2	0	2
Montezuma Slough, Downstream	MTZD	T2b	0	1	0	1
Montezuma Slough (Pooled)	MTZ	T2	0	2	0	2
Spoonbill Slough, Upstream	SBSU	T3a	1	0	2	3
Spoonbill Slough, Downstream	SBSD	T3b	2	4	2	8
Spoonbill Slough (Pooled)	SBS	T3	2	4	2	8
Chipps Island East	MAE	G2a	77	135	231	443
Chipps Island West	MAW	G2b	76	135	227	438
Chipps Island: SJR Route	MAE/MAW	G2	6	38	232	276
Chipps Island: OR Route	MAE/MAW	G2	72	107	3	182
Chipps Island (Pooled)	MAE/MAW	G2	78	145	235	458
Benicia Bridge, East	BBE	G3a	72	151	239	462
Benicia Bridge, West	BBW	G3b	71	150	249	470
Benicia Bridge: SJR Route	BBE/BBW	G3	6	43	248	297
Benicia Bridge: OR Route	BBE/BBW	G3	67	109	3	179
Benicia Bridge (Pooled)	BBE/BBW	G3	73	152	251	476

Table 11. Number of tags observed from each release group at each detection site in 2016 and used in the survival analysis, excluding predator-type detections. Numbers in parentheses are counts of tags whose detection histories were right-censored at that site. Pooled counts are summed over all receivers in array. Route could not be identified for some tags. Releases are: 1 = February, 2 = March, 3 = April.

Detection Site	Site Code	Survival Model Code	Release Group			Total
			1	2	3	
Release site at Durham Ferry			480	480	480	1,440
Durham Ferry Upstream, Upstream	DFU1	A0a	37	10	18	65
Durham Ferry Upstream, Downstream	DFU2	A0b	25	6	8	39
Durham Ferry Upstream (Pooled)	DFU	A0	37	10	19	66
Durham Ferry Downstream	DFD	A2	361	389	421	1171
Below Durham Ferry 1	BDF1	A3	227	126	190	543
Below Durham Ferry 2	BDF2	A4	222	164	198	584
Banta Carbona	BCA	A5	221	201	379	801
Mossdale	MOS	A6	211	374	426 (1)	1011
Lathrop, Upstream	SJLU	A7a	25	83	402	510
Lathrop, Downstream	SJLD	A7b	25	85	408	518
Lathrop (Pooled)	SJL	A7	25	85	408	518
Garwood Bridge	SJG	A8	18	69	390	477
Navy Drive Bridge	SJNB	A9	17	64	374	455
Rough and Ready Island, Upstream	RRIU	R1a	0	0	6	6
Rough and Ready Island, Downstream	RRID	R1b	0	0	6	6
Rough and Ready Island (Pooled)	RRI	R1	0	0	6	6
San Joaquin River near Calaveras	SJC	A10	17	63	380	460
San Joaquin River Shipping Channel	SJS	A11	16	63	372	451
Lathrop, Upstream	SJLU	A7a	25	83	402	510
MacDonald Island Upstream	MACU	A12a	9	45	265	319
MacDonald Island Downstream	MACD	A12b	8	45	268	321
MacDonald Island (Pooled)	MAC	A12	9	45	271	325
Turner Cut, Upstream	TCE	F1a	6	18	91	115
Turner Cut, Downstream	TCW	F1b	6	18	91	115
Turner Cut (Pooled)	TCE/TCW	F1	6	18	91	115
Medford Island East	MFE	A13a	4	39	202	245
Medford Island West	MFW	A13b	4	39	205	248
Medford Island (Pooled)	MFE/MFW	A13	4	39	205	248
Columbia Cut, Upstream	COLU	F2a	2[a]	5	54	61
Columbia Cut, Downstream	COLD	F2b	2[a]	5	54	61
Columbia Cut (Pooled)	COL	F2	2[a]	5	54	61
Disappointment Slough, Upstream	SJDU	A14a	2[a]	31	192	225
Disappointment Slough, Downstream	SJDD	A14b	2[a]	31	186	219
Disappointment Slough (Pooled)	SJD	A14	2[a]	31	192	225
Old River at the San Joaquin, Upstream	OSJU	B5a	2[a]	8	28	38

a = detections were not used in the survival model

Table 11. (Continued)

Detection Site	Site Code	Survival Model Code	Release Group			Total
			1	2	3	
Old River at the San Joaquin, Downstream	OSJD	B5b	2[a]	8	28	38
Old River at the San Joaquin (Pooled)	OSJ	B5	2[a]	8	28	38
Old River East, Upstream	OREU	B1a	178	286	15	479
Old River East, Downstream	ORED	B1b	178	286	15	479
Old River East (Pooled)	ORE	B1	178	286	15	479
Old River South, Upstream	ORSU	B2a	173	276	12	461
Old River South, Downstream	ORSD	B2b	175	276	13	464
Old River South (Pooled)	ORS	B2	175	277	13	465
West Canal, Upstream	WCLU	B3a	2[a]	16	0[a]	18
West Canal, Downstream	WCLD	B3b	2[a]	16	0[a]	18
West Canal: OR Route (Pooled)	WCL	B3	2[a]	16	0[a]	18
Old River at Highway 4, Upstream	OR4U	B4a	4	12	25	41
Old River at Highway 4, Downstream	OR4D	B4b	4	12	25	41
Old River at Highway 4, SJR Route	OR4	B4	2[a]	4[a]	25	31
Old River at Highway 4, OR Route	OR4	B4	2 (2)	8	0	10
Old River at Highway 4 (Pooled)	OR4	B4	4 (2)	12	25	41
Middle River Head, Upstream	MRHU	C1a	1	0	2	3
Middle River Head, Downstream	MRHD	C1b	1	0	2	3
Middle River Head (Pooled)	MRH	C1	1 (1)	0	2 (2)	3
Middle River at Highway 4, Upstream	MR4U	C2a	1	4	20	25
Middle River at Highway 4, Downstream	MR4D	C2b	1	4	20	25
Middle River at Highway 4, SJR Route	MR4	C2	1[a]	0[a]	20	21
Middle River at Highway 4, OR Route	MR4	C2	0	4	0	4
Middle River at Highway 4 (Pooled)	MR4	C2	1	4	20	25
Radial Gates Upstream: SJR Route	RGU	D1	0[a]	1[a]	13	14
Radial Gates Upstream: OR Route	RGU	D1	36	63	4	103
Radial Gates Upstream (Pooled)	RGU	D1	36	64	17	117
Radial Gates Downstream: SJR Route	RGD	D2	0[a]	1[a]	10	11
Radial Gates Downstream: OR Route	RGD	D2	33	65	5	103
Radial Gates Downstream (Pooled)	RGD	D2	33	66	15	114
CVP Trashrack: SJR Route	CVP	E1	2[a]	2[a]	24	28
CVP Trashrack: OR Route	CVP	E1	117	157	3	277
CVP Trashrack (Pooled)	CVP	E1	119	159	27	305
CVP Holding Tank: SJR Route	CVPtank	E2	2[a]	0[a]	11	13
CVP Holding Tank: OR Route	CVPtank	E2	69 (10)	85 (6)	1	155
CVP Holding Tank (Pooled)	CVPtank	E2	71 (10)	85 (6)	12	168
Threemile Slough, Upstream	TMS	T1a	0[a]	1	21	22
Threemile Slough, Downstream	TMN	T1b	0[a]	1	21	22

a = detections were not used in the survival model

Table 11. (Continued)

Detection Site	Site Code	Survival Model Code	Release Group			Total
			1	2	3	
Threemile Slough: SJR Route (Pooled)	TMS/TMN	T1	0[a]	1	21	22
Jersey Point East	JPE	G1a	4[a]	50	212	266
Jersey Point West	JPW	G1b	4[a]	48	213	265
Jersey Point: SJR Route	JPE/JPW	G1	4[a]	47	213	264
Jersey Point: OR Route	JPE/JPW	G1	0[a]	3	0	3
Jersey Point (Pooled)	JPE/JPW	G1	4[a]	50	213	267
False River West	FRW	H1a	0[a]	0[a]	0[a]	0
False River East	FRE	H1b	0[a]	0[a]	0[a]	0
False River: SJR Route	FRE/FRW	H1	0[a]	0[a]	0[a]	0
False River: OR Route	FRE/FRW	H1	0[a]	0[a]	0[a]	0
False River (Pooled)	FRE/FRW	H1	0[a]	0[a]	0[a]	0
Chipps Island: SJR Route	MAE/MAW	G2	6	38	230	274
Chipps Island: OR Route	MAE/MAW	G2	64	103	3	170
Chipps Island (Pooled)	MAE/MAW	G2	70	141	233	444
Benicia Bridge, East	BBE	G3a	62	145	234	441
Benicia Bridge, West	BBW	G3b	61	144	246	451
Benicia Bridge: SJR Route	BBE/BBW	G3	6	43	246	295
Benicia Bridge: OR Route	BBE/BBW	G3	57	103	2	162
Benicia Bridge (Pooled)	BBE/BBW	G3	63	146	248	457

a = detections were not used in the survival model

Table 12. Number of juvenile Steelhead tagged by each surgeon in each release group during the 2016 tagging study. Releases are: 1 = February, 2 = March, 3 = April.

	Release Group			
Surgeon	1	2	3	Total Tags
A	160	160	160	480
B	160	160	168	488
C	160	160	152	472
Total Tags	480	480	480	1,440

Table 13. Release size and counts of juvenile Steelhead tag detections at key detection sites by surgeon in 2016, excluding predator-type detections. * = omitted from chi-square test of independence because of low counts.

Detection Site	Surgeon A	Surgeon B	Surgeon C
Release at Durham Ferry	480	488	472
Below Durham Ferry 1 (BDF1)	181	200	162
Below Durham Ferry 2 (BDF2)	184	215	185
Banta Carbona (BCA)	259	286	256
Mossdale (MOS)	333	347	331
Lathrop (SJL)	165	179	174
Garwood Bridge (SJG)	153	162	162
Navy Bridge (SJNB)	144	159	152
Rough and Ready Island (RRI)*	2	1	3
Calaveras River (SJC)	145	160	155
Shipping Channel (SJS)	142	159	150
MacDonald Island (MAC)	99	121	105
Turner Cut (TCE/TCW)	36	36	43
Medford Island (MFE/MFW)	75	91	82
Columbia Cut (COL)	17	23	21
Disappointment Slough	71	77	77
Old River Mouth (OSJ)	8	17	13
Old River East (ORE)	159	165	155
Old River South (ORS)	155	159	151
West Canal (WCL)*	8	7	3
Old River at Highway 4 (OR4)	15	12	14
Middle River Head (MRH)*	0	1	2
Middle River at Highway 4 (MR4)	8	6	11
Clifton Court Forebay Exterior (RGU)	38	39	40
Clifton Court Forebay Interior (RGD)	37	36	41
Central Valley Project Trash Rack (CVP)	104	104	97
Central Valley Project Holding Tank (CVPtank)	57	59	52
Threemile Slough (TMN/TMS)	8	6	8
Jersey Point (JPT/JPE/JPW)	82	95	90
Chipps Island (MAT/MAE/MAW)	131	157	156
Benicia Bridge (BBR)	138	159	160

Table 14. Performance metric estimates (standard errors or 95% bound [UB = upper bound, LB = lower bound] in parentheses) for tagged juvenile Steelhead released in the 2016 tagging study, excluding predator-type detections. South Delta ("SD") survival extended to MacDonald Island and Turner Cut in Route A, and the Central Valley Project trash rack, exterior radial gate receiver at Clifton Court Forebay, and Old River and Middle River receivers at Highway 4 in Route B. Population-level estimates were weighted averages over the available release-specific estimates, using weights proportional to release size. Releases are: 1 = February, 2 = March, 3 = April.

Parameter	Release 1[ab]	Release 2	Release 3[b]	Population Estimate
ψ_{AA}	0.07 (0.02)	0.16 (0.02)	0.72 (0.02)	0.32 (0.01)
ψ_{AF}	0.05 (0.02)	0.07 (0.01)	0.24 (0.02)	0.12 (0.01)
ψ_{BB}	0.87 (0.02)	0.77 (0.02)	0.03 (0.01)	0.56 (0.01)
ψ_{BC}	0.00 (<0.01)	0	0.00 (<0.01)	0.00 (<0.01)
S_{AA}	0.19 (0.10)	0.61 (0.06)	0.72 (0.02)	0.51 (0.04)
S_{AF}	0.29 (0.13)	0.25 (0.08)	0.27 (0.04)	0.27 (0.05)
S_{BB}	0.41 (0.04)	0.40 (0.03)	0.20 (0.06)	0.34 (0.03)
S_{BC}[c]	NA	NA	NA	NA
ψ_{A}	0.12[d] (0.02)	0.23[d] (0.02)	0.96[e] (0.01)	0.44[d] (0.01)
ψ_{B}	0.88[d] (0.02)	0.77[d] (0.02)	0.04[e] (0.01)	0.56[d] (0.01)
S_{A}	0.23 (0.08)	0.50[f] (0.05)	0.61[g] (0.02)	0.45[g] (0.03)
S_{B}	0.41 (0.04)	0.40[f] (0.03)	0.17[g] (0.06)	0.33[g] (0.03)
S_{Total}	0.39 (0.03)	0.42 (0.03)	0.59 (0.02)	0.47 (0.02)
$S_{A(MD)}$[h]	NA	0.58[g] (0.05)	0.55[g] (0.02)	0.56[gi] (0.03)
$S_{B(MD)}$[h]	NA	0.01[g] (0.01)	0[g] (95% UB: 0.19)	0.01[gi] (<0.01)
$S_{Total(MD)}$[h]	NA	0.14 (0.02)	0.53 (0.02)	0.34[i] (0.02)
$S_{A(SD)}$	0.58 (0.09)	0.74 (0.05)	0.89 (0.02)	0.73 (0.04)
$S_{B(SD)}$	NA	0.83 (0.02)	NA	NA
$S_{Total(SD)}$	NA	0.81 (0.02)	NA	NA
ϕ_{A1A6}	0.44 (0.02)	0.78 (0.02)	0.89 (0.01)	0.70 (0.01)

a = there were too few tags detected at Jersey Point to estimate survival through the Mid-Delta region

b = there were too few tags detected at Highway 4 to estimate survival in the South Delta region

c = there were too few tags detected in the Middle River route to estimate route-specific survival

d = significant preference for route B (Old River Route) (α=0.05)

e = significant preference for route A (San Joaquin River Route) (α=0.05)

f = estimated survival is significantly higher in route A (San Joaquin River Route) than in route B (Old River Route) (α=0.10) (tested only for Delta and Mid-Delta survival)

g = estimated survival is significantly higher in route A (San Joaquin River Route) than in route B (Old River Route) (α=0.05) (tested only for Delta and Mid-Delta survival)

h = estimates are the joint probability of surviving to the Jersey Point/False River junction, and moving downstream from that junction toward Jersey Point

i = population estimate is based on only two release groups

Table 15. Performance metric estimates (standard error or 95% bound [UB = upper bound, LB = lower bound] in parentheses) for tagged juvenile Steelhead released in the 2016 tagging study, including predator-type detections. South Delta ("SD") survival extended to MacDonald Island and Turner Cut in Route A, and the Central Valley Project trash rack, exterior radial gate receiver at Clifton Court Forebay, and Old River and Middle River receivers at Highway 4 in Route B. Population-level estimates were weighted averages over the available release-specific estimates, using weights proportional to release size. Releases are: 1 = February, 2 = March, 3 = April.

Parameter	Release 1[ab]	Release 2	Release 3	Population Estimate
ψ_{AA}	0.07 (0.02)	0.16 (0.02)	0.71 (0.02)	0.31 (0.01)
ψ_{AF}	0.06 (0.02)	0.07 (0.01)	0.25 (0.02)	0.13 (0.01)
ψ_{BB}	0.86 (0.02)	0.77 (0.02)	0.04 (0.01)	0.56 (0.01)
ψ_{BC}	0.00 (<0.01)	0	0	0.00 (<0.01)
S_{AA}	0.20 (0.10)	0.62 (0.06)	0.77 (0.02)	0.53 (0.04)
S_{AF}	0.24 (0.12)	0.23 (0.08)	0.29 (0.04)	0.26 (0.05)
S_{BB}	0.42 (0.04)	0.39 (0.03)	0.25 (0.07)	0.35 (0.03)
S_{BC}[c]	NA	NA	NA	NA
ψ_{A}	0.13[d] (0.02)	0.23[d] (0.02)	0.96[e] (0.01)	0.44[d] (0.01)
ψ_{B}	0.87[d] (0.02)	0.77[d] (0.02)	0.04[e] (0.01)	0.56[d] (0.01)
S_{A}	0.22[f] (0.08)	0.50[g] (0.05)	0.65[h] (0.02)	0.46[h] (0.03)
S_{B}	0.41[f] (0.04)	0.39[g] (0.03)	0.25[h] (0.07)	0.35[h] (0.03)
S_{Total}	0.39 (0.03)	0.42 (0.03)	0.63 (0.02)	0.48 (0.02)
$S_{A(MD)}$[i]	NA	0.58[h] (0.05)	0.58[h] (0.02)	0.58[hj] (0.03)
$S_{B(MD)}$[i]	NA	0.01[h] (0.01)	0[h] (95% UB: 0.19)	0.01[hj] (<0.01)
$S_{Total(MD)}$[i]	NA	0.14 (0.02)	0.56 (0.02)	0.35[j] (0.02)
$S_{A(SD)}$	0.65 (0.09)	0.77 (0.05)	0.93 (0.01)	0.78 (0.03)
$S_{B(SD)}$	NA	0.86 (0.02)	0.67 (0.12)	0.76[j] (0.06)
$S_{Total(SD)}$	NA	0.84 (0.02)	0.92 (0.01)	0.88[j] (0.01)
ϕ_{A1A6}	0.45 (0.02)	0.78 (0.02)	0.89 (0.01)	0.71 (0.01)

a = there were too few tags detected at Jersey Point to estimate survival through the Mid-Delta region

b = there were too few tags detected at Highway 4 to estimate survival in the South Delta region

c = there were too few tags detected in the Middle River route to estimate route-specific survival

d = significant preference for route B (Old River Route) (α=0.05)

e = significant preference for route A (San Joaquin River Route) (α=0.05)

f = estimated survival is significantly higher in route B (Old River Route) than in route A (San Joaquin River Route) (α=0.10) (tested only for Delta and Mid-Delta survival)

g = estimated survival is significantly higher in route A (San Joaquin River Route) than in route B (Old River Route) (α=0.10) (tested only for Delta and Mid-Delta survival)

h = estimated survival is significantly higher in route A (San Joaquin River Route) than in route B (Old River Route) (α=0.05) (tested only for Delta and Mid-Delta survival)

i = estimates are the joint probability of surviving to the Jersey Point/False River junction, and moving downstream from that junction toward Jersey Point

j = population estimate is based on only two release groups

Table 16a. Average travel time in days (harmonic mean) of acoustic-tagged juvenile Steelhead from release at Durham Ferry during the 2016 tagging study, without predator-type detections. Standard errors are in parentheses. NA entries for N (sample size) correspond to detection sites or routes that were removed from the survival model because of sparse data. See Table 16b for travel time from release with predator-type detections. Releases are: 1 = February, 2 = March, 3 = April.

	Without Predator-Type Detections							
	All releases		Release 1		Release 2		Release 3	
Detection Site and Route	N	Travel Time	N	Travel Time	N	Travel Time	N	Travel Time
Durham Ferry Upstream (DFU)	66	0.56 (0.16)	37	0.48 (0.16)	10	0.45 (0.37)	19	1.11 (0.45)
Durham Ferry Downstream (DFD)	1170	0.04 (<0.01)	360	0.10 (0.01)	389	0.03 (<0.01)	421	0.04 (<0.01)
Below Durham Ferry 1 (BDF1)	543	0.32 (0.02)	227	0.78 (0.09)	126	0.19 (0.01)	190	0.26 (0.02)
Below Durham Ferry 2 (BDF2)	584	0.42 (0.02)	222	1.32 (0.16)	164	0.26 (0.02)	198	0.33 (0.02)
Banta Carbona (BCA)	800	0.67 (0.03)	220	2.53 (0.30)	201	0.50 (0.03)	379	0.54 (0.03)
Mossdale (MOS)	1010	1.44 (0.05)	210	6.18 (0.46)	374	0.95 (0.04)	426	1.56 (0.07)
Lathrop (SJL)	517	1.82 (0.07)	24	8.48 (2.55)	85	1.02 (0.07)	408	2.07 (0.08)
Garwood Bridge (SJG)	476	3.35 (0.10)	17	16.07 (1.28)	69	2.59 (0.17)	390	3.41 (0.11)
Navy Drive Bridge (SJNB)	454	3.54 (0.11)	16	15.95 (1.13)	64	2.75 (0.18)	374	3.60 (0.12)
Rough and Ready Island (RRI)	6	4.74 (1.18)	0	NA	0	NA	6	4.74 (1.18)
San Joaquin River near Calaveras (SJC)	459	4.29 (0.12)	16	16.46 (1.21)	63	3.66 (0.21)	380	4.27 (0.12)
San Joaquin Shipping Channel (SJS)	450	4.99 (0.12)	15	17.53 (1.40)	63	4.76 (0.23)	372	4.88 (0.13)
MacDonald Island (MAC)	324	5.13 (0.14)	8	17.59 (2.06)	45	5.20 (0.28)	271	5.01 (0.15)
Turner Cut (TCE/TCW)	115	5.71 (0.24)	6	17.74 (2.41)	18	5.05 (0.45)	91	5.60 (0.25)
Turner Cut Junction (MAC or TCE/TCW)	439	5.27 (0.12)	14	17.65 (1.50)	63	5.16 (0.24)	362	5.15 (0.13)
Medford Island (MFE/MFW)	247	5.54 (0.16)	3	15.94 (4.28)	39	5.64 (0.29)	205	5.47 (0.18)
Columbia Cut (COL)	61	5.54 (0.37)	NA	NA	5	6.56 (1.64)	54	5.33 (0.36)
Disappointment Slough (SJD)	225	6.18 (0.18)	NA	NA	31	6.82 (0.40)	192	6.05 (0.20)
Old River at the San Joaquin (OSJ)	37	5.99 (0.41)	NA	NA	8	5.49 (0.39)	28	5.98 (0.50)
Old River East (ORE)	479	2.10 (0.10)	178	7.10 (0.47)	286	1.44 (0.06)	15	3.71 (0.88)
Old River South (ORS)	465	2.68 (0.12)	175	7.90 (0.45)	277	1.86 (0.08)	13	5.36 (1.19)
West Canal (WCL)	18	5.61 (1.20)	NA	NA	16	5.16 (1.10)	0	NA
Old River at Highway 4 (OR4), SJR Route	31	10.13 (0.69)	NA	NA	NA	NA	25	9.82 (0.74)
Old River at Highway 4 (OR4), OR Route	10	10.74 (1.90)	2	19.89 (8.88)	8	9.63 (1.70)	0	NA
Old River at Highway 4 (OR4)	41	10.27 (0.68)	2	19.89 (8.88)	8	9.63 (1.70)	25	9.82 (0.74)
Middle River Head (MRH)	3	6.69 (2.59)	1	9.36 (NA)	0	NA	2	5.86 (3.20)

Table 16a. (Continued)

Detection Site and Route	Without Predator-Type Detections							
	All releases		Release 1		Release 2		Release 3	
	N	Travel Time	N	Travel Time	N	Travel Time	N	Travel Time
Middle River at Highway 4 (MR4), SJR Route	21	8.73 (0.82)	NA	NA	NA	NA	20	8.46 (0.77)
Middle River at Highway 4 (MR4), OR Route	4	6.48 (1.65)	0	NA	4	6.48 (1.65)	0	NA
Middle River at Highway 4 (MR4)	25	8.27 (0.75)	0	NA	4	6.48 (1.65)	20	8.46 (0.77)
Radial Gates Upstream (DFU), SJR Route	14	10.91 (0.69)	NA	NA	NA	NA	13	10.85 (0.73)
Radial Gates Upstream (DFU), OR Route	103	4.50 (0.32)	36	10.81 (1.28)	63	3.31 (0.21)	4	7.30 (2.13)
Radial Gates Upstream (DFU)	117	4.84 (0.34)	36	10.81 (1.28)	63	3.31 (0.21)	17	9.73 (1.02)
Radial Gates Downstream (DFD), SJR Route	11	11.33 (0.83)	NA	NA	NA	NA	10	11.28 (0.91)
Radial Gates Downstream (DFD), OR Route	103	4.61 (0.33)	33	10.90 (1.35)	65	3.47 (0.23)	5	8.08 (2.16)
Radial Gates Downstream (DFD)	114	4.89 (0.35)	33	10.90 (1.35)	65	3.47 (0.23)	15	9.96 (1.20)
Central Valley Project Trashrack (CVP), SJR Route	28	10.36 (0.77)	NA	NA	NA	NA	24	10.15 (0.81)
Central Valley Project Trashrack (CVP), OR Route	277	5.36 (0.24)	117	10.02 (0.53)	157	3.99 (0.19)	3	4.47 (0.54)
Central Valley Project Trashrack (CVP)	305	5.61 (0.24)	117	10.02 (0.53)	157	3.99 (0.19)	27	8.89 (0.85)
Central Valley Project Holding Tank (CVPtank), SJR Route	13	10.26 (1.27)	NA	NA	NA	NA	11	9.47 (1.14)
Central Valley Project Holding Tank (CVPtank), OR Route	155	5.44 (0.31)	69	9.98 (0.71)	85	3.99 (0.23)	1	3.71 (NA)
Central Valley Project Holding Tank (CVPtank)	168	5.65 (0.31)	69	9.98 (0.71)	85	3.99 (0.23)	12	8.39 (1.26)
Threemile Slough (TMN/TMS)	22	7.71 (0.69)	NA	NA	1	8.18 (NA)	21	7.69 (0.72)
Jersey Point (JPE/JPW), SJR Route	264	7.31 (0.19)	NA	NA	47	7.59 (0.33)	213	7.15 (0.20)
Jersey Point (JPE/JPW), OR Route	3	14.35 (3.31)	NA	NA	3	14.35 (3.31)	0	NA
Jersey Point (JPE/JPW)	267	7.35 (0.19)	NA	NA	50	7.81 (0.36)	213	7.15 (0.20)
Chipps Island (MAE/MAW), SJR Route	273	8.92 (0.21)	5	22.47 (1.75)	38	9.11 (0.41)	230	8.78 (0.22)
Chipps Island (MAE/MAW), OR Route	170	7.52 (0.33)	64	12.76 (0.88)	103	5.99 (0.26)	3	7.52 (2.80)
Chipps Island (MAE/MAW)	443	8.32 (0.19)	69	13.17 (0.89)	141	6.60 (0.25)	233	8.76 (0.22)
Benicia Bridge (BBR)	456	9.31 (0.19)	62	14.85 (0.95)	146	7.53 (0.23)	248	9.75 (0.22)

Table 16b. Average travel time in days (harmonic mean) of acoustic-tagged juvenile Steelhead from release at Durham Ferry during the 2016 tagging study, with predator-type detections. Standard errors are in parentheses. NA entries for N (sample size) correspond to detection sites or routes that were removed from the survival model because of sparse data. See Table 16a for travel time from release without predator-type detections. Releases are: 1 = February, 2 = March, 3 = April.

	With Predator-Type Detections							
	All releases		Release 1		Release 2		Release 3	
Detection Site and Route	N	Travel Time	N	Travel Time	N	Travel Time	N	Travel Time
Durham Ferry Upstream (DFU)	71	0.66 (0.20)	38	0.54 (0.20)	10	0.45 (0.37)	23	1.46 (0.66)
Durham Ferry Downstream (DFD)	1167	0.04 (<0.01)	359	0.10 (0.01)	389	0.03 (<0.01)	419	0.04 (<0.01)
Below Durham Ferry 1 (BDF1)	544	0.32 (0.02)	226	0.78 (0.09)	126	0.19 (0.01)	192	0.26 (0.02)
Below Durham Ferry 2 (BDF2)	585	0.43 (0.02)	221	1.38 (0.18)	165	0.27 (0.02)	199	0.34 (0.03)
Banta Carbona (BCA)	803	0.67 (0.03)	223	2.57 (0.31)	203	0.50 (0.03)	377	0.53 (0.03)
Mossdale (MOS)	1015	1.45 (0.05)	213	6.25 (0.46)	376	0.96 (0.04)	426	1.56 (0.07)
Lathrop (SJL)	520	1.85 (0.07)	26	9.03 (2.69)	85	1.04 (0.08)	409	2.08 (0.08)
Garwood Bridge (SJG)	488	3.43 (0.11)	20	17.78 (1.68)	69	2.61 (0.17)	399	3.47 (0.11)
Navy Drive Bridge (SJNB)	473	3.66 (0.11)	19	17.75 (1.61)	67	2.87 (0.20)	387	3.69 (0.12)
Rough and Ready Island (RRI)	7	5.33 (1.43)	0	NA	0	NA	7	5.33 (1.43)
San Joaquin River near Calaveras (SJC)	474	4.40 (0.12)	19	18.34 (1.70)	66	3.82 (0.24)	389	4.35 (0.13)
San Joaquin Shipping Channel (SJS)	468	5.13 (0.13)	18	19.59 (1.91)	66	4.96 (0.26)	384	4.99 (0.14)
MacDonald Island (MAC)	335	5.25 (0.15)	9	19.02 (2.62)	46	5.30 (0.31)	280	5.12 (0.16)
Turner Cut (TCE/TCW)	127	6.01 (0.26)	8	20.89 (3.45)	20	5.54 (0.60)	99	5.78 (0.26)
Turner Cut Junction (MAC or TCE/TCW)	462	5.44 (0.13)	17	19.86 (2.05)	66	5.37 (0.28)	379	5.28 (0.14)
Medford Island (MFE/MFW)	256	5.71 (0.17)	4	19.36 (6.10)	40	5.77 (0.32)	212	5.62 (0.19)
Columbia Cut (COL)	63	5.65 (0.38)	NA	NA	5	6.56 (1.64)	56	5.45 (0.37)
Disappointment Slough (SJD)	238	6.36 (0.19)	NA	NA	32	7.00 (0.45)	203	6.21 (0.20)
Old River at the San Joaquin (OSJ)	38	6.13 (0.44)	NA	NA	8	5.49 (0.39)	29	6.16 (0.54)
Old River East (ORE)	483	2.12 (0.10)	180	7.14 (0.47)	288	1.45 (0.07)	15	3.71 (0.88)
Old River South (ORS)	474	2.72 (0.12)	177	7.93 (0.45)	282	1.89 (0.08)	15	5.73 (1.23)
West Canal (WCL)	17	5.36 (1.13)	NA	NA	16	5.16 (1.10)	0	NA
Old River at Highway 4 (OR4), SJR Route	38	11.26 (0.85)	NA	NA	NA	NA	29	10.36 (0.76)
Old River at Highway 4 (OR4), OR Route	11	7.09 (2.46)	1	13.75 (NA)	10	6.76 (2.45)	0	NA
Old River at Highway 4 (OR4)	49	9.95 (1.21)	1	13.75 (NA)	10	6.76 (2.45)	29	10.36 (0.76)
Middle River Head (MRH)	1	13.43 (NA)	1	13.43 (NA)	0	NA	0	NA

Table 16b. (Continued)

Detection Site and Route	With Predator-Type Detections							
	All releases		Release 1		Release 2		Release 3	
	N	Travel Time	N	Travel Time	N	Travel Time	N	Travel Time
Middle River at Highway 4 (MR4), SJR Route	21	8.99 (0.94)	NA	NA	NA	NA	20	8.71 (0.88)
Middle River at Highway 4 (MR4), OR Route	4	6.48 (1.65)	0	NA	4	6.48 (1.65)	0	NA
Middle River at Highway 4 (MR4)	25	8.46 (0.84)	0	NA	4	6.48 (1.65)	20	8.71 (0.88)
Radial Gates Upstream (DFU), SJR Route	16	12.10 (1.10)	NA	NA	NA	NA	14	11.48 (0.94)
Radial Gates Upstream (DFU), OR Route	107	4.62 (0.34)	38	11.03 (1.28)	65	3.40 (0.23)	4	7.30 (2.13)
Radial Gates Upstream (DFU)	123	5.03 (0.36)	38	11.03 (1.28)	65	3.40 (0.23)	18	10.19 (1.13)
Radial Gates Downstream (DFD), SJR Route	13	12.48 (1.24)	NA	NA	NA	NA	11	11.72 (0.99)
Radial Gates Downstream (DFD), OR Route	105	4.67 (0.34)	34	10.92 (1.32)	66	3.52 (0.24)	5	8.08 (2.16)
Radial Gates Downstream (DFD)	118	5.01 (0.36)	34	10.92 (1.32)	66	3.52 (0.24)	16	10.27 (1.23)
Central Valley Project Trashrack (CVP), SJR Route	30	11.57 (1.08)	NA	NA	NA	NA	24	10.44 (0.90)
Central Valley Project Trashrack (CVP), OR Route	285	5.65 (0.26)	120	10.21 (0.55)	160	4.22 (0.22)	5	6.10 (1.47)
Central Valley Project Trashrack (CVP)	315	5.94 (0.27)	120	10.21 (0.55)	160	4.22 (0.22)	29	9.30 (0.90)
Central Valley Project Holding Tank (CVPtank), SJR Route	15	11.17 (1.46)	NA	NA	NA	NA	13	10.51 (1.42)
Central Valley Project Holding Tank (CVPtank), OR Route	156	5.48 (0.31)	70	10.10 (0.73)	84	3.97 (0.23)	2	5.94 (3.58)
Central Valley Project Holding Tank (CVPtank)	171	5.74 (0.32)	70	10.10 (0.73)	84	3.97 (0.23)	15	9.53 (1.48)
Threemile Slough (TMN/TMS)	24	7.83 (0.66)	NA	NA	1	8.18 (NA)	23	7.82 (0.69)
Jersey Point (JPE/JPW), SJR Route	278	7.46 (0.19)	NA	NA	47	7.62 (0.35)	227	7.33 (0.21)
Jersey Point (JPE/JPW), OR Route	3	14.35 (3.31)	NA	NA	3	14.35 (3.31)	0	NA
Jersey Point (JPE/JPW)	281	7.50 (0.19)	NA	NA	50	7.84 (0.37)	227	7.33 (0.21)
Chipps Island (MAE/MAW), SJR Route	288	9.14 (0.22)	5	22.47 (1.75)	38	9.11 (0.41)	245	9.03 (0.24)
Chipps Island (MAE/MAW), OR Route	172	7.59 (0.34)	65	12.98 (0.91)	103	5.99 (0.26)	4	8.70 (2.99)
Chipps Island (MAE/MAW)	460	8.49 (0.20)	70	13.39 (0.92)	141	6.60 (0.25)	249	9.03 (0.24)
Benicia Bridge (BBR)	472	9.46 (0.19)	63	15.02 (0.97)	146	7.56 (0.24)	263	9.98 (0.23)

Table 17a. Average travel time in days (harmonic mean) of acoustic-tagged juvenile Steelhead through the San Joaquin River Delta river reaches during the 2016 tagging study, without predator-type detections. Standard errors are in parentheses. NA entries for N (sample size) correspond to detection sites or routes that were removed from the survival model because of sparse data. * = all routes combined between upstream and downstream boundaries. Reaches that were not modeled for individual release groups were excluded. Releases are: 1 = February, 2 = March, 3 = April. See Table 17b for travel time through reaches with predator-type detections.

Upstream Reach Boundary	Downstream Reach Boundary	All Releases: N	All Releases: Travel Time	Release 1: N	Release 1: Travel Time	Release 2: N	Release 2: Travel Time	Release 3: N	Release 3: Travel Time
Durham Ferry (Release)	DFU	66	0.56 (0.16)	37	0.48 (0.16)	10	0.45 (0.37)	19	1.11 (0.45)
	DFD	1170	0.04 (<0.01)	360	0.10 (0.01)	389	0.03 (<0.01)	421	0.04 (<0.01)
DFD	BDF1	512	0.22 (0.01)	227	0.44 (0.04)	104	0.14 (0.01)	181	0.16 (0.01)
BDF1	BDF2	359	0.06 (<0.01)	198	0.07 (<0.01)	58	0.06 (0.01)	103	0.04 (<0.01)
BDF2	BCA	465	0.15 (0.01)	197	0.17 (0.01)	97	0.16 (0.01)	171	0.13 (0.01)
BCA	MOS	766	0.51 (0.01)	201	0.65 (0.03)	189	0.47 (0.03)	376	0.47 (0.02)
MOS	SJL	517	0.24 (0.01)	24	0.43 (0.08)	85	0.22 (0.01)	408	0.24 (0.01)
	ORE	479	0.23 (0.01)	178	0.27 (0.01)	286	0.21 (0.01)	15	0.42 (0.11)
SJL	SJG	476	1.01 (0.03)	17	1.68 (0.30)	69	1.53 (0.09)	390	0.93 (0.03)
SJG	SJNB	454	0.09 (<0.01)	16	0.11 (0.02)	64	0.09 (0.01)	374	0.09 (<0.01)
	RRI	6	0.28 (0.03)	0	NA	0	NA	6	0.28 (0.03)
SJNB	SJC	452	0.33 (0.01)	16	0.32 (0.07)	63	0.48 (0.06)	373	0.31 (0.01)
RRI		5	0.62 (0.14)	0	NA	0	NA	5	0.62 (0.14)
SJC	SJS	450	0.34 (0.01)	15	0.54 (0.12)	63	0.52 (0.06)	372	0.31 (0.01)
SJS	MAC	324	0.11 (<0.01)	8	0.12 (0.03)	45	0.15 (0.02)	271	0.11 (<0.01)
	TCE/TCW	115	0.12 (0.01)	6	0.26 (0.09)	18	0.18 (0.05)	91	0.11 (0.01)
MAC	MFE/MFW	246	0.20 (0.01)	3	0.30 (0.15)	39	0.35 (0.04)	204	0.18 (0.01)
	COL*	61	0.22 (0.11)	NA	NA	5	0.18 (0.06)	54	0.23 (0.13)
	SJD*	224	0.71 (0.03)	NA	NA	31	0.93 (0.10)	191	0.68 (0.03)
	OSJ*	37	0.72 (0.08)	NA	NA	8	0.85 (0.11)	28	0.67 (0.09)
	JPE/JPW*	197	1.62 (0.05)	NA	NA	29	2.09 (0.10)	167	1.57 (0.05)
	OR4/MR4*	15	2.75 (0.23)	NA	NA	NA	NA	15	2.75 (0.23)
MFE/MFW	SJD	194	0.28 (0.02)	NA	NA	28	0.35 (0.07)	165	0.27 (0.02)
	OSJ	29	0.43 (0.06)	NA	NA	8	0.42 (0.07)	20	0.42 (0.07)
	JPE/JPW*	172	1.19 (0.05)	NA	NA	27	1.65 (0.10)	145	1.13 (0.05)
	OR4/MR4*	7	2.18 (0.11)	NA	NA	NA	NA	7	2.18 (0.11)

Table 17a. (Without predators: continued)

Upstream Reach Boundary	Downstream Reach Boundary	All Releases: N	All Releases: Travel Time	Release 1: N	Release 1: Travel Time	Release 2: N	Release 2: Travel Time	Release 3: N	Release 3: Travel Time
SJD	JPE/JPW	192	0.65 (0.04)	NA	NA	28	0.92 (0.07)	163	0.63 (0.04)
	TMN/TMS	22	0.72 (0.12)	NA	NA	1	1.95 (NA)	21	0.69 (0.12)
TCE/TCW	JPE/JPW	23	3.01 (0.31)	NA	NA	9	3.05 (0.59)	14	2.99 (0.35)
	OR4/MR4	37	2.04 (0.22)	NA	NA	NA	NA	30	1.94 (0.23)
COL	SJD	31	0.58 (0.09)	NA	NA	3	0.79 (0.29)	27	0.56 (0.09)
	OSJ	7	0.71 (0.14)	NA	NA	0	NA	7	0.71 (0.14)
	JPE/JPW*	26	1.52 (0.15)	NA	NA	2	1.30 (0.13)	23	1.57 (0.18)
	OR4/MR4*	8	2.46 (0.33)	NA	NA	NA	NA	8	2.46 (0.33)
OSJ	JPE/JPW	32	0.43 (0.05)	NA	NA	8	0.44 (0.09)	23	0.43 (0.06)
	OR4/MR4	0	NA	NA	NA	NA	NA	0	NA
ORE	ORS	465	0.28 (0.01)	175	0.30 (0.01)	277	0.26 (0.01)	13	0.48 (0.15)
	MRH	3	0.94 (0.42)	1	0.62 (NA)	0	NA	2	1.27 (1.07)
ORS	WCL	18	1.21 (0.38)	NA	NA	16	1.22 (0.43)	NA	NA
	OR4*	10	1.71 (0.91)	2	1.69 (1.25)	8	1.72 (1.14)	0	NA
	MR4	4	2.11 (0.93)	0	NA	4	2.11 (0.93)	0	NA
	RGU	103	1.37 (0.07)	36	1.52 (0.12)	63	1.30 (0.08)	4	1.32 (0.42)
	CVP	277	1.39 (0.05)	117	1.42 (0.07)	157	1.40 (0.06)	3	0.74 (0.35)
WCL	OR4	10	0.21 (0.08)	NA	NA	8	0.22 (0.09)	NA	NA
OR4 via OR	JPE/JPW	3	1.13 (0.62)	NA	NA	3	1.13 (0.62)	0	NA
OR4 via SJR	JPE/JPW	1	1.90 (NA)	NA	NA	NA	NA	1	1.90 (NA)
	RGU	6	0.36 (0.14)	NA	NA	NA	NA	5	0.32 (0.12)
	CVP	19	0.45 (0.09)	NA	NA	NA	NA	15	0.60 (0.09)
MRH	WCL	0	NA	NA	NA	0	NA	NA	NA
	OR4	0	NA	NA	NA	0	NA	NA	NA
	MR4	0	NA	NA	NA	0	NA	NA	NA
	RGU	0	NA	NA	NA	0	NA	NA	NA
	CVP	0	NA	NA	NA	0	NA	NA	NA
MR4 via OR	JPE/JPW	0	NA	NA	NA	0	NA	0	NA
MR4 via SJR	JPE/JPW	1	1.82 (NA)	NA	NA	NA	NA	0	NA

Table 17a. (Without predators: continued)

Upstream Reach Boundary	Downstream Reach Boundary	All Releases: N	All Releases: Travel Time	Release 1: N	Release 1: Travel Time	Release 2: N	Release 2: Travel Time	Release 3: N	Release 3: Travel Time
MR4 via SJR	RGU	8	0.73 (0.29)	NA	NA	NA	NA	8	0.73 (0.29)
	CVP	9	1.18 (0.22)	NA	NA	NA	NA	9	1.18 (0.22)
RGU via OR	RGD	97	0.01 (<0.01)	32	0.01 (<0.01)	61	0.01 (<0.01)	4	0.01 (0.01)
RGU via SJR	RGD	11	0.01 (<0.01)	NA	NA	NA	NA	10	0.01 (<0.01)
CVP via OR	CVPtank	155	0.06 (0.01)	69	0.06 (0.01)	85	0.06 (0.01)	1	0.02 (NA)
CVP via SJR	CVPtank	13	0.07 (0.04)	NA	NA	NA	NA	11	0.16 (0.06)
JPE/JPW	MAE/MAW* (Chipps Island)	233	1.04 (0.03)	NA	NA	38	1.00 (0.06)	192	1.04 (0.03)
TMN/TMS		19	1.03 (0.08)	NA	NA	0	NA	19	1.03 (0.08)
MAC		237	2.85 (0.06)	2	2.95 (0.60)	32	3.09 (0.13)	203	2.81 (0.07)
MFE/MFW		200	2.43 (0.06)	1	3.54 (NA)	31	2.66 (0.12)	168	2.39 (0.06)
SJD		193	1.89 (0.05)	NA	NA	25	1.96 (0.12)	167	1.88 (0.05)
TCE/TCW		35	4.48 (0.30)	3	4.91 (1.40)	6	5.30 (0.84)	26	4.29 (0.33)
COL		37	2.78 (0.18)	NA	NA	1	1.80 (NA)	35	2.84 (0.19)
OSJ		26	1.83 (0.12)	NA	NA	5	1.99 (0.14)	20	1.84 (0.16)
OR4		3	3.41 (0.79)	0	NA	2	3.63 (1.49)	1	3.03 (NA)
MR4		1	2.83 (NA)	1	2.83 (NA)	0	NA	0	NA
RGD		54	2.93 (0.16)	14	3.10 (0.46)	35	2.87 (0.16)	5	2.90 (0.55)
CVPtank		123	1.11 (0.05)	50	1.28 (0.09)	64	1.01 (0.07)	9	1.16 (0.18)
MAE/MAW	BBR	425	0.70 (0.02)	59	0.88 (0.07)	136	0.72 (0.04)	230	0.66 (0.03)

Table 17b. Average travel time in days (harmonic mean) of acoustic-tagged juvenile Steelhead through the San Joaquin River Delta river reaches during the 2016 tagging study, with predator-type detections. Standard errors are in parentheses. NA entries for N (sample size) correspond to detection sites or routes that were removed from the survival model because of sparse data. * = all routes combined between upstream and downstream boundaries. Reaches that were not modeled for individual release groups were excluded. Releases are: 1 = February, 2 = March, 3 = April. See Table 17a for travel time through reaches without predator-type detections.

Upstream Reach Boundary	Downstream Reach Boundary	All Releases: N	All Releases: Travel Time	Release 1: N	Release 1: Travel Time	Release 2: N	Release 2: Travel Time	Release 3: N	Release 3: Travel Time
Durham Ferry (Release)	DFU	71	0.66 (0.20)	38	0.54 (0.20)	10	0.45 (0.37)	23	1.46 (0.66)
	DFD	1167	0.04 (<0.01)	359	0.10 (0.01)	389	0.03 (<0.01)	419	0.04 (<0.01)
DFD	BDF1	513	0.22 (0.01)	226	0.43 (0.04)	104	0.14 (0.01)	183	0.16 (0.01)
BDF1	BDF2	360	0.06 (<0.01)	197	0.07 (<0.01)	58	0.06 (0.01)	105	0.04 (<0.01)
BDF2	BCA	468	0.15 (0.01)	199	0.17 (0.01)	98	0.16 (0.01)	171	0.13 (0.01)
BCA	MOS	771	0.51 (0.01)	204	0.65 (0.03)	191	0.47 (0.02)	376	0.48 (0.02)
MOS	SJL	520	0.24 (0.01)	26	0.43 (0.08)	85	0.22 (0.01)	409	0.24 (0.01)
	ORE	483	0.23 (0.01)	180	0.27 (0.01)	288	0.21 (0.01)	15	0.42 (0.11)
SJL	SJG	488	1.02 (0.03)	20	1.80 (0.30)	69	1.50 (0.09)	399	0.95 (0.03)
SJG	SJNB	473	0.09 (<0.01)	19	0.11 (0.02)	67	0.09 (0.01)	387	0.09 (<0.01)
	RRI	7	0.33 (0.06)	0	NA	0	NA	7	0.33 (0.06)
SJNB	SJC	465	0.33 (0.01)	19	0.35 (0.08)	66	0.49 (0.05)	380	0.31 (0.01)
RRI		7	0.67 (0.15)	0	NA	0	NA	7	0.67 (0.15)
SJC	SJS	468	0.34 (0.01)	18	0.47 (0.09)	66	0.52 (0.06)	384	0.32 (0.01)
SJS	MAC	335	0.11 (<0.01)	9	0.12 (0.02)	46	0.15 (0.02)	280	0.11 (<0.01)
	TCE/TCW	127	0.12 (0.01)	8	0.23 (0.06)	20	0.18 (0.05)	99	0.11 (0.01)
MAC	MFE/MFW	255	0.20 (0.01)	4	0.31 (0.12)	40	0.33 (0.04)	211	0.19 (0.01)
	COL*	63	0.22 (0.11)	NA	NA	5	0.18 (0.06)	56	0.23 (0.13)
	SJD*	237	0.72 (0.03)	NA	NA	32	0.84 (0.11)	202	0.70 (0.03)
	OSJ*	38	0.72 (0.08)	NA	NA	8	0.85 (0.11)	29	0.67 (0.09)
	JPE/JPW*	207	1.64 (0.05)	NA	NA	29	2.09 (0.10)	177	1.59 (0.05)
	OR4/MR4*	16	2.94 (0.31)	NA	NA	NA	NA	16	2.94 (0.31)
MFE/MFW	SJD	205	0.28 (0.02)	NA	NA	29	0.33 (0.06)	174	0.27 (0.02)
	OSJ	30	0.43 (0.05)	NA	NA	8	0.42 (0.07)	21	0.42 (0.07)
	JPE/JPW*	181	1.19 (0.05)	NA	NA	27	1.65 (0.10)	154	1.14 (0.05)
	OR4/MR4*	7	2.18 (0.11)	NA	NA	NA	NA	7	2.18 (0.11)

Table 17b. (With predators: continued)

Upstream Reach Boundary	Downstream Reach Boundary	All Releases: N	All Releases: Travel Time	Release 1: N	Release 1: Travel Time	Release 2: N	Release 2: Travel Time	Release 3: N	Release 3: Travel Time
SJD	JPE/JPW	202	0.64 (0.04)	NA	NA	28	0.92 (0.07)	173	0.61 (0.04)
	TMN/TMS	24	0.74 (0.12)	NA	NA	1	1.95 (NA)	23	0.72 (0.12)
TCE/TCW	JPE/JPW	24	3.05 (0.31)	NA	NA	9	3.09 (0.63)	15	3.03 (0.34)
	OR4/MR4	43	2.16 (0.22)	NA	NA	NA	NA	33	2.06 (0.24)
COL	SJD	33	0.61 (0.09)	NA	NA	3	0.79 (0.29)	29	0.59 (0.10)
	OSJ	7	0.65 (0.09)	NA	NA	0	NA	7	0.65 (0.09)
	JPE/JPW*	27	1.53 (0.15)	NA	NA	2	1.30 (0.13)	24	1.59 (0.18)
	OR4/MR4*	9	2.76 (0.50)	NA	NA	NA	NA	9	2.76 (0.50)
OSJ	JPE/JPW	34	0.42 (0.04)	NA	NA	8	0.44 (0.09)	25	0.42 (0.05)
	OR4/MR4	1	2.99 (NA)	NA	NA	NA	NA	1	2.99 (NA)
ORE	ORS	474	0.28 (0.01)	177	0.30 (0.01)	282	0.26 (0.01)	15	0.54 (0.17)
	MRH	1	4.29 (NA)	1	4.29 (NA)	0	NA	0	NA
ORS	WCL	17	1.20 (0.39)	NA	NA	16	1.22 (0.43)	NA	NA
	OR4*	11	1.30 (0.58)	1	0.97 (NA)	10	1.35 (0.68)	0	NA
	MR4	4	2.11 (0.93)	0	NA	4	2.11 (0.93)	0	NA
	RGU	107	1.40 (0.07)	38	1.54 (0.12)	65	1.33 (0.09)	4	1.32 (0.42)
	CVP	285	1.43 (0.05)	120	1.45 (0.07)	160	1.45 (0.07)	5	0.98 (0.40)
WCL	OR4	11	0.16 (0.04)	NA	NA	10	0.17 (0.05)	NA	NA
OR4 via OR	JPE/JPW	3	1.13 (0.62)	NA	NA	3	1.13 (0.62)	0	NA
OR4 via SJR	JPE/JPW	2	2.02 (0.13)	NA	NA	NA	NA	2	2.02 (0.13)
	RGU	9	0.50 (0.19)	NA	NA	NA	NA	7	0.43 (0.18)
	CVP	21	0.52 (0.12)	NA	NA	NA	NA	15	0.63 (0.10)
MRH	WCL	0	NA	NA	NA	0	NA	0	NA
	OR4	0	NA	NA	NA	0	NA	0	NA
	MR4	0	NA	NA	NA	0	NA	0	NA
	RGU	0	NA	NA	NA	0	NA	0	NA
	CVP	0	NA	NA	NA	0	NA	0	NA
MR4 via OR	JPE/JPW	0	NA	NA	NA	0	NA	0	NA
MR4 via SJR	JPE/JPW	1	1.82 (NA)	NA	NA	NA	NA	0	NA

Table 17b. (With predators: continued)

Upstream Reach Boundary	Downstream Reach Boundary	All Releases: N	All Releases: Travel Time	Release 1: N	Release 1: Travel Time	Release 2: N	Release 2: Travel Time	Release 3: N	Release 3: Travel Time
MR4 via SJR	RGU	7	0.76 (0.36)	NA	NA	NA	NA	7	0.76 (0.36)
	CVP	9	1.32 (0.31)	NA	NA	NA	NA	9	1.32 (0.31)
RGU via OR	RGD	99	0.01 (<0.01)	33	0.01 (<0.01)	62	0.01 (<0.01)	4	0.01 (0.01)
RGU via SJR	RGD	13	0.01 (<0.01)	NA	NA	NA	NA	11	0.01 (<0.01)
CVP via OR	CVPtank	156	0.06 (0.01)	70	0.06 (0.01)	84	0.06 (0.01)	2	0.04 (0.03)
CVP via SJR	CVPtank	15	0.08 (0.05)	NA	NA	NA	NA	13	0.18 (0.08)
JPE/JPW	MAE/MAW* (Chipps Island)	243	1.04 (0.03)	NA	NA	38	1.00 (0.06)	202	1.05 (0.03)
TMN/TMS		21	1.07 (0.09)	NA	NA	0	NA	21	1.07 (0.09)
MAC		249	2.91 (0.06)	2	2.95 (0.60)	32	3.09 (0.13)	215	2.88 (0.07)
MFE/MFW		209	2.46 (0.06)	1	3.54 (NA)	31	2.66 (0.12)	177	2.43 (0.07)
SJD		202	1.91 (0.05)	NA	NA	25	1.96 (0.12)	176	1.90 (0.05)
TCE/TCW		38	4.64 (0.31)	3	4.91 (1.40)	6	5.30 (0.84)	29	4.50 (0.35)
COL		40	2.90 (0.20)	NA	NA	1	1.80 (NA)	38	2.97 (0.21)
OSJ		29	1.96 (0.16)	NA	NA	5	1.99 (0.14)	23	1.99 (0.20)
OR4		4	3.34 (0.54)	0	NA	2	3.63 (1.49)	2	3.09 (0.07)
MR4		1	2.83 (NA)	1	2.83 (NA)	0	NA	0	NA
RGD		54	2.93 (0.16)	14	3.10 (0.46)	35	2.87 (0.16)	5	2.90 (0.55)
CVPtank		127	1.13 (0.06)	51	1.31 (0.09)	64	1.01 (0.07)	12	1.27 (0.18)
MAE/MAW	BBR	440	0.70 (0.02)	60	0.88 (0.07)	136	0.72 (0.04)	244	0.66 (0.03)

Table 18. Results of single-variate analyses of 2016 route selection at the Head of Old River, for tags estimated to have arrived at the river junction before 1500 on April 1, 2016 (date of barrier closure). The values df1 and df2 are the degrees of freedom for the F-test. Covariates are ordered by P-value and F statistic.

Covariate	*F*	df1	df2	*P*	Sign
Modeled flow at SJL[a]	26.2586	1	86	<0.0001	+
Stage at MSD[a]	15.9108	1	86	0.0001	+
Flow at MSD[a]	12.8721	1	86	0.0006	+
Stage at OH1[a]	11.8732	1	86	0.0009	+
OH1:MSD flow ratio flow[a]	10.7756	1	86	0.0015	-
Stage at SJL[a]	10.4644	1	86	0.0017	+
Change in stage at SJL	9.9023	1	86	0.0023	-
Exports at SWP	9.5779	1	86	0.0027	+
Total Exports in Delta	9.0747	1	86	0.0034	+
Change in stage at OH1	8.9801	1	86	0.0036	-
CVP Proportion of Exports	8.7290	1	86	0.0040	-
Change in stage at MSD	5.8212	1	86	0.0180	-
Change in velocity at MSD	4.8349	1	86	0.0306	+
Velocity at MSD	4.7283	1	86	0.0324	+
Change in flow at MSD	2.8893	1	86	0.0928	+
Release Group	2.5835	1	86	0.1117	+
Velocity at OH1	1.0762	1	86	0.3025	-
Exports at CVP	1.0714	1	96	0.3035	+
Change in velocity at OH1	0.3194	1	86	0.5734	+
Arrive at junction during day	0.2218	1	86	0.6389	-
Change in flow at OH1	0.0410	1	86	0.8401	+
Time of day of arrival	0.1212	3	84	0.9474	-[b]
Flow at OH1	0.0017	1	86	0.9673	-
Fork Length	0.0001	1	86	0.9932	+

a = Significant at experimentwise 5% level

b = Regression coefficients for day, dusk, and night relative to dawn

Table 19. Results of multivariate analyses of route selection at the head of Old River in 2016. Modeled response is the probability of selecting the San Joaquin River route. The columns labeled *t*, df, and P refer to the *t*-tests.

Model Type	Covariate[a]	Estimate	S.E.	*t*	df	*P*
Flow: Q_{MSD} and Q_{OH1}	Intercept	-2.5287	0.2324	-10.8823	85	<0.0001
	Q_{MSD}	2.4960	0.3217	7.7585	85	<0.0001
	Q_{OH1}	-1.6322	0.2685	-6.0799	85	<0.0001
	Goodness-of-fit: χ^2= 16.7583, df=13, P=0.2106; AIC = 368.55					
Flow: qQ_{SJL}	Intercept	-2.4853	0.2254	-11.0272	86	<0.0001
	qQ_{SJL}	1.8587	0.2382	7.8040	86	<0.0001
	Goodness-of-fit: χ^2= 26.6220, df=13, P=0.0140; AIC = 369.06					
Flow Ratio	Intercept	-2.8211	0.2581	-10.9303	85	<0.0001
	r_Q	-3.1826	0.4855	-6.5548	85	<0.0001
	SWP	1.0639	0.1651	6.4432	85	<0.0001
	Goodness-of-fit: χ^2= 8.2192, df=13, P=0.8290; AIC = 375.22					
Velocity	Intercept	-2.1791	0.1750	-12.4521	85	<0.0001
	V_{OH1}	-1.2177	0.1681	-7.2440	85	<0.0001
	SWP	1.6839	0.1987	8.4752	85	<0.0001
	Goodness-of-fit: χ^2= 19.7497, df=13, P=0.1016; AIC = 375.40					
Stage	Intercept	-2.6012	0.2433	-10.6920	85	<0.0001
	C_{MSD}	1.4480	0.2116	6.8441	85	<0.0001
	ΔC_{SJL}	-1.2317	0.2244	-5.4880	85	<0.0001
	Goodness-of-fit: χ^2= 10.4716, df=13, P=0.6550; AIC = 360.89					
Flow + Stage	Intercept	-2.578	0.2308	-11.1696	84	<0.0001
	Q_{OH1}	-1.1397	0.2036	-5.5980	84	<0.0001
	C_{OH1}	-5.0271	0.9141	-5.4996	84	<0.0001
	C_{MSD}	7.1223	1.0642	6.6930	84	<0.0001
	Goodness-of-fit: χ^2= 9.1204, df=13, P=0.7638; AIC = 360.10					

a = continuous covariates (Q_{MSD}, Q_{OH1}, qQ_{SJL}, r_Q, SWP, V_{OH1}, C_{MSD}, ΔC_{SJL}, C_{OH1}) are standardized. Intercept and slope estimates for the unstandardized covariates are -11.3675 (SE=1.4558), 1.5972 (SE=0.2334; C_{MSD}), and -16.9854 (SE=3.0950; ΔC_{SJL}) for the stage model.

Table 20. Results of single-variate analyses of 2016 route selection at the Turner Cut junction. The values df1 and df2 are the degrees of freedom for the F-test. Covariates are ordered by P-value and F statistic.

Covariate	*F*	df1	df2	*P*	Sign
Change in stage at TRN[a]	28.5919	1	88	0.0000	-
Flow at TRN[a]	14.1468	1	91	0.0003	+
Velocity at TRN[a]	13.7104	1	91	0.0003	+
Change in flow at TRN	6.9271	1	88	0.0100	+
Change in velocity at TRN	6.5850	1	88	0.0120	+
Negative flow at TRN	4.3586	1	91	0.0396	-
Stage at TRN	3.5000	1	91	0.0646	-
Velocity during transition from SJG	1.1272	1	91	0.2912	-
Flow during transition from SJG	0.6115	1	91	0.4362	-
Leave SJS during day	0.3303	1	91	0.5669	+
Fork Length	0.3086	1	91	0.5799	-
Time of Day of Departure from SJS	0.1857	3	89	0.9059	-[b]
Exports at CVP	0.0539	1	91	0.8170	-
Release Group	0.0530	2	90	0.9484	+[c]
Total Exports in Delta	0.0394	1	91	0.8430	-
Exports at SWP	0.0368	1	91	0.8483	-
CVP Proportion of Exports	0.0002	1	91	0.9891	+

a = Significant at experimentwise 5% level

b = Regression coefficients for day, dusk, and night relative to dawn

c = Regression coefficients for Release Groups 2 and 3 relative to Group 1

Table 21. Results of multivariate analyses of route selection at the Turner Cut junction in 2016. Modeled response is the probability of selecting the San Joaquin River route. The columns labeled *t*, df, and P refer to the *t*-tests.

Model Type	Covariate[a]	Estimate	S.E.	*t*	df	*P*
Flow	Intercept	-0.3727	0.4182	-0.8912	86	0.3753
	Q_{TRN}	2.4583	0.3774	6.5133	86	<0.0001
	ΔQ_{TRN}	0.6901	0.1510	4.5685	86	0.0002
	U_{QTRN}: $Q_{TRN} < 0$	3.3722	0.7423	4.5430	86	0.0002
	Goodness-of-fit: χ^2=1.4554, df=13, P=1.0000; AIC =320.84					
Velocity	Intercept	-0.2701	0.3869	-0.6982	87	0.4869
	V_{TRN}	2.4159	0.3621	6.6716	87	<0.0001
	U_{VTRN}: $V_{TRN} < 0$	3.0464	0.3776	4.4978	87	<0.0001
	Goodness-of-fit: χ^2=1.4554, df=13, P=0.4758; AIC = 344.01					
Stage	Intercept	1.4933	0.1552	9.6196	88	<0.0001
	ΔC_{TRN}	-1.2375	0.1365	-9.0646	88	<0.0001
	Goodness-of-fit: χ^2=3.2045, df=13, P=0.9971; AIC = 318.42					
Flow + Stage	Intercept	1.6133	0.1705	9.4621	87	<0.0001
	Q_{TRN}	0.6600	0.1755	3.7597	87	0.0003
	ΔC_{TRN}	-1.0096	0.1394	-7.2432	87	<0.0001
	Goodness-of-fit: χ^2=1.9068, df=13, P=0.9998; AIC = 304.89					

a = continuous covariates (Q_{TRN}, ΔQ_{TRN}, $V_{TRN,}$ ΔC_{TRN}) are standardized. Intercept and slope estimates for the unstandardized covariates are -1.2132 (SE=0.2098), -9.9211 (SE=1.3697; ΔC_{TRN}), and 0.0003 (SE=0.0001; Q_{TRN}) for the flow + stage model.

Table 22. Estimates of survival from downstream receivers at water export facilities (CVP holding tank or interior of Clifton Court Forebay at radial gates) through salvage to receivers* after release from truck in 2016, excluding predator-type detections (95% profile likelihood interval or 95% lower bound [LB] in parentheses). Population estimate is based on data pooled from all releases. * = receiver sites indicating survival were G1, G2, G3, H1, T1, T2, and T3. Estimates are based on assumption of 100% detection probability at T2 and T3.

Facility	Upstream Site Code	Release 1	Release 2	Release 3	Population Estimate
CVP	E2	0.86 (0.75, 0.93)	0.88 (0.79, 0.94)	1 (95% LB: 0.78)	0.88 (0.82, 0.92)
SWP	D2	0.43 (0.27, 0.60)	0.56 (0.44, 0.68)	0.33 (0.13, 0.58)	0.49 (0.40, 0.58)

Table 23. Estimates (standard errors in parentheses) of linear contrasts comparing estimates of survival from release group in question to average estimates from the other two release groups. Estimates were based on data that excluded predator-type detections. * = significant difference from 0 for experimentwise α=0.10 (testwise α=0.0083). Releases are: 1 =February, 2 = March, 3 = April.

Parameter	Release 1	Release 2	Release 3
ϕ_{A1A6}	-0.39* (0.02)	0.11* (0.02)	0.28* (0.02)
S_A	-0.32* (0.09)	0.08 (0.07)	0.24* (0.06)
S_B	0.13 (0.05)	0.10 (0.04)	-0.23* (0.06)
S_{Total}	-0.12* (0.04)	-0.07 (0.03)	0.19* (0.03)

* = significant difference from 0 for experimentwise α=0.10

Appendix A. Survival Model Parameters

Table A1. Definitions of parameters used in the release-recapture survival model in the 2016 tagging study. Parameters used only in particular submodels are noted. * = estimated directly or derived from model.

Parameter	Definition
S_{A2}	Probability of survival from Durham Ferry Downstream (DFD) to Below Durham Ferry 1 (BDF1)
S_{A3}	Probability of survival from Below Durham Ferry 1 (BDF1) to Below Durham Ferry 2 (BDF2)
S_{A4}	Probability of survival from Below Durham Ferry 2 (BDF2) to Banta Carbona (BCA)
S_{A5}	Probability of survival from Banta Carbona (BCA) to Mossdale (MOS)
S_{A6}	Probability of survival from Mossdale (MOS) to Lathrop (SJL) or Old River East (ORE)
S_{A7}	Probability of survival from Lathrop (SJL) to Garwood Bridge (SJG)
S_{A8}	Probability of survival from Garwood Bridge (SJG) to Navy Drive Bridge (SJNB) or Rough and Ready Island (RRI)
$S_{A8,G2}$	Overall survival from Garwood Bridge (SJG) to Chipps Island (MAE/MAW) (derived from Submodel I)
S_{A9}	Probability of survival from Navy Drive Bridge (SJNB) to San Joaquin River near Calaveras River (SJC)
$S_{A9,G2}$	Overall survival from Navy Drive Bridge (SJNB) to Chipps Island (MAE/MAW) (derived from Submodel I)
S_{A10}	Probability of survival from San Joaquin River near Calaveras River (SJC) to San Joaquin River Shipping Channel (SJS)
$S_{A10,G2}$	Overall survival from San Joaquin River near Calaveras River (SJC) to Chipps Island (MAE/MAW) (derived from Submodel I)
S_{A11}	Probability of survival from San Joaquin River Shipping Channel (SJS) to MacDonald Island (MAC) or Turner Cut (TCE/TCW)
$S_{A11,G2}$	Overall survival from San Joaquin River Shipping Channel (SJS) to Chipps Island (MAE/MAW) (derived from Submodel I)
$S_{A12,G2}$	Overall survival from MacDonald Island (MAC) to Chipps Island (MAE/MAW) (Submodel I)
$S_{A13,G2}$	Overall survival from Medford Island (MFE/MFW) to Chipps Island (MAE/MAW) (derived from Submodel II)
S_{B1}	Probability of survival from Old River East (ORE) to Old River South (ORS) or Middle River Head (MRH) (Submodel I)
$S_{B2,G2}$	Overall survival from Old River South (ORS) to Chipps Island (MAE/MAW) (derived from Submodel I)
$S_{B2(SD)}$	Overall survival from Old River South (ORS) to the exit points of the Route B South Delta Region: OR4, MR4, RGU, CVP (derived from Submodel I)
$S_{C1,G2}$	Overall survival from head of Middle River (MRH) to Chipps Island (MAE/MAW) (derived from Submodel I)
$S_{C1(SD)}$	Overall survival from head of Middle River (MRH) to the exit points of the Route B South Delta Region: OR4, MR4, RGU, CVP (derived from Submodel I)
$S_{F1,G2}$	Overall survival from Turner Cut (TCE/TCW) to Chipps Island (MAE/MAW) (Submodel I)
S_{R1}	Probability of survival from Rough and Ready Island (RRI) to San Joaquin River near Calaveras River (SJC)
$\phi_{A1,A0}$	Joint probability of moving from Durham Ferry release site upstream toward DFU, and surviving to DFU
$\phi_{A1,A2}$	Joint probability of moving from Durham Ferry release site downstream toward DFD, and surviving to DFD
$\phi_{A1,A5}$	Joint probability of moving from Durham Ferry release site downstream toward BCA, and surviving to BCA; = $\phi_{A1,A2}$ S_{A2} S_{A3} S_{A4}
$\phi_{A1,A6}$	Joint probability of moving from Durham Ferry release site downstream toward MOS, and surviving to MOS; = $\phi_{A1,A2}$ S_{A2} S_{A3} S_{A4} S_{A5}
$\phi_{A12,A13}$	Joint probability of moving from MAC toward MFE/MFW, and surviving from MAC to MFE/MFW (Submodel II)
$\phi_{A12,F2}$	Joint probability of moving from MAC toward COL, and surviving from MAC to COL (Submodel II)
$\phi_{A12,G2}$	Joint probability of moving from MAC toward MAE/MAW without passing MFE/MFW, and surviving from MAC to MAE/MAW (Submodel II*)
$\phi_{A13,A14}$	Joint probability of moving from MFE/MFW toward SJD, and surviving from MFE/MFW to SJD (Submodel II)
$\phi_{A13,B4}$	Joint probability of moving from MFE/MFW directly toward OR4, and surviving from MFE/MFW to OR4 (Submodel II)
$\phi_{A13,B5}$	Joint probability of moving from MFE/MFW directly toward OSJ, and surviving from MFE/MFW to OSJ (Submodel II)
$\phi_{A13,C2}$	Joint probability of moving from MFE/MFW directly toward MR4, and surviving from MFE/MFW to MR4 (Submodel II)

Table A1. (Continued)

Parameter	Definition
$\phi_{A13,GH}$	Joint probability of moving from MFE/MFW directly toward Jersey Point (JPE/JPW) or False River (FRE/FRW), and surviving to JPE/JPW or FRE/FRW (Submodel II*)
$\phi_{A13,G1}$	Joint probability of moving from MFE/MFW directly toward Jersey Point (JPE/JPW) and surviving to JPE/JPW (Submodel II*); = $\phi_{A13,GH(A)}\psi_{G1}$
$\phi_{A13,G2}$	Joint probability of moving from MFE/MFW toward MAE/MAW, and surviving from MFE/MFW to MAE/MAW (Submodel II*)
$\phi_{A14,GH}$	Joint probability of moving from SJD toward Jersey Point (JPE/JPW) or False River (FRE/FRW), and surviving to JPE/JPW or FRE/FRW (Submodel II)
$\phi_{A14,G1}$	Joint probability of moving from SJD toward Jersey Point (JPE/JPW) and surviving to JPE/JPW (Submodel II); = $\phi_{A14,GH(A)}\psi_{G1}$
$\phi_{A14,T1}$	Joint probability of moving from SJD toward TMS/TMN and surviving to TMS/TMN (Submodel II)
$\phi_{B2,B3}$	Joint probability of moving from ORS toward WCL, and surviving from ORS to WCL (Submodel I)
$\phi_{B2,B4}$	Joint probability of moving from ORS toward OR4, and surviving from ORS to OR4 (Submodel I*); = $\phi_{B2,B3}\phi_{B3,B4}$
$\phi_{B2,C2}$	Joint probability of moving from ORS toward MR4, and surviving from ORS to MR4 (Submodel I)
$\phi_{B2,D1O}$	Joint probability of moving from ORS toward RGU, surviving to RGU, and arriving when the radial gates are open (Submodel I)
$\phi_{B2,D1C}$	Joint probability of moving from ORS toward RGU, surviving to RGU, and arriving when the radial gates are closed (Submodel I)
$\phi_{B2,D1}$	Joint probability of moving from ORS toward RGU, and surviving from ORS to RGU (Submodel I)
$\phi_{B2,E1}$	Joint probability of moving from ORS toward CVP, and surviving from ORS to CVP (Submodel I)
$\phi_{B3,B4}$	Joint probability of moving from WCL toward OR4, and surviving from WCL to OR4 (Submodel I)
$\phi_{B4,D1O}$	Joint probability of moving from OR4 toward RGU, surviving to RGU, and arriving when the radial gates are open (Submodel II)
$\phi_{B4,D1C}$	Joint probability of moving from OR4 toward RGU, surviving to RGU, and arriving when the radial gates are closed (Submodel II)
$\phi_{B4,D1}$	Joint probability of moving from OR4 toward RGU and surviving to RGU (Submodel II)
$\phi_{B4,E1}$	Joint probability of moving from OR4 toward CVP and surviving to CVP (Submodel II)
$\phi_{B4,GH(A)}$	Joint probability of moving from OR4 toward Jersey Point (JPE/JPW) or False River (FRE/FRW), and surviving from OR4 to JPE/JPW or FRE/FRW (Submodel II)
$\phi_{B4,GH(B)}$	Joint probability of moving from OR4 toward Jersey Point (JPE/JPW) or False River (FRE/FRW), and surviving from OR4 to JPE/JPW or FRE/FRW (Submodel I)
$\phi_{B4,G1(A)}$	Joint probability of moving from OR4 toward Jersey Point (JPE/JPW) and surviving from OR4 to JPE/JPW (Submodel II); = $\phi_{B4,GH(A)}\psi_{G1}$
$\phi_{B4,G1(B)}$	Joint probability of moving from OR4 toward Jersey Point (JPE/JPW) and surviving from OR4 to JPE/JPW (Submodel I); = $\phi_{B4,GH(B)}\psi_{G1}$
$\phi_{B5,B4}$	Joint probability of moving from OSJ directly toward OR4, and surviving from OSJ to OR4 (Submodel II)
$\phi_{B5,C2}$	Joint probability of moving from OSJ directly toward MR4, and surviving from OSJ to MR4 (Submodel II)
$\phi_{B5,GH}$	Joint probability of moving from OSJ directly toward Jersey Point (JPE/JPW) or False River (FRE/FRW), and surviving to JPE/JPW or FRE/FRW (Submodel II*)
$\phi_{B5,G1}$	Joint probability of moving from OSJ directly toward Jersey Point (JPE/JPW) and surviving to JPE/JPW (Submodel II*); = $\phi_{B5,GH(A)}\psi_{G1}$
$\phi_{C1,B3}$	Joint probability of moving from MRH toward WCL, and surviving from MRH to WCL (Submodel I)
$\phi_{C1,B4}$	Joint probability of moving from MRH toward OR4, and surviving from MRH to OR4 (Submodel I*); = $\phi_{C1,B3}\phi_{B3,B4}$
$\phi_{C1,C2}$	Joint probability of moving from MRH toward MR4, and surviving from MRH to MR4 (Submodel I)
$\phi_{C1,D1O}$	Joint probability of moving from MRH toward RGU, surviving to RGU, and arriving when the radial gates are open (Submodel I)
$\phi_{C1,D1C}$	Joint probability of moving from MRH toward RGU, surviving to RGU, and arriving when the radial gates are closed (Submodel I)
$\phi_{C1,D1}$	Joint probability of moving from MRH toward RGU, and surviving from MRH to RGU (Submodel I)
$\phi_{C1,E1}$	Joint probability of moving from MRH toward CVP, and surviving from MRH to CVP (Submodel I)

Table A1. (Continued)

Parameter	Definition
$\phi_{C2,D1O}$	Joint probability of moving from MR4 toward RGU, surviving to RGU, and arriving when the radial gates are open (Submodel II)
$\phi_{C2,D1C}$	Joint probability of moving from MR4 toward RGU, surviving to RGU, and arriving when the radial gates are closed (Submodel II)
$\phi_{C2,D1}$	Joint probability of moving from MR4 toward RGU and surviving to RGU (Submodel II)
$\phi_{C2,E1}$	Joint probability of moving from MR4 toward CVP and surviving to CVP (Submodel II)
$\phi_{C2,GH(A)}$	Joint probability of moving from MR4 toward Jersey Point (JPE/JPW) or False River (FRE/FRW), and surviving from MR4 to JPE/JPW or FRE/FRW (Submodel II)
$\phi_{C2,GH(B)}$	Joint probability of moving from MR4 toward Jersey Point (JPE/JPW) or False River (FRE/FRW), and surviving from MR4 to JPE/JPW or FRE/FRW (Submodel I)
$\phi_{C2,G1(A)}$	Joint probability of moving from MR4 toward Jersey Point (JPE/JPW) and surviving from MR4 to JPE/JPW (Submodel II); = $\phi_{C2,GH(A)}\psi_{G1}$
$\phi_{C2,G1(B)}$	Joint probability of moving from MR4 toward Jersey Point (JPE/JPW) and surviving from MR4 to JPE/JPW (Submodel I); = $\phi_{C2,GH(B)}\psi_{G1}$
$\phi_{D1O,D2(A)}$	Joint probability of moving from RGU toward RGD, and surviving from RGU to RGD, conditional on arrival at RGU when the radial gates are open (Submodel II)
$\phi_{D1O,D2(B)}$	Joint probability of moving from RGU toward RGD, and surviving from RGU to RGD, conditional on arrival at RGU when the radial gates are open (Submodel I)
$\phi_{D1C,D2(A)}$	Joint probability of moving from RGU toward RGD, and surviving from RGU to RGD, conditional on arrival at RGU when the radial gates are closed (Submodel II)
$\phi_{D1C,D2(B)}$	Joint probability of moving from RGU toward RGD, and surviving from RGU to RGD, conditional on arrival at RGU when the radial gates are closed (Submodel I)
$\phi_{D1,D2(A)}$	Joint probability of moving from RGU toward RGD, and surviving from RGU to RGD (Submodel II)
$\phi_{D1,D2(B)}$	Joint probability of moving from RGU toward RGD, and surviving from RGU to RGD (Submodel I)
$\phi_{D2,G2(A)}$	Joint probability of moving from RGD toward Chipps Island (MAE/MAW) and surviving from RGD to MAE/MAW (Submodel II)
$\phi_{E1,E2(A)}$	Joint probability of moving from CVP toward CVPtank and surviving from CVP to CVPtank (Submodel II)
$\phi_{E1,E2(B)}$	Joint probability of moving from CVP toward CVPtank and surviving from CVP to CVPtank (Submodel I)
$\phi_{E2,G2(A)}$	Joint probability of moving from CVPtank toward Chipps Island (MAE/MAW) and surviving from CVPtank to MAE/MAW (Submodel II)
$\phi_{E2,G2(B)}$	Joint probability of moving from CVPtank toward Chipps Island (MAE/MAW) and surviving from CVPtank to MAE/MAW (Submodel I)
$\phi_{F1,B4}$	Joint probability of moving from TCE/TCW directly toward OR4, and surviving from TCE/TCW to OR4 (Submodel II)
$\phi_{F1,C2}$	Joint probability of moving from TCE/TCW directly toward MR4, and surviving from TCE/TCW to MR4 (Submodel II)
$\phi_{F1,GH}$	Joint probability of moving from TCE/TCW directly toward Jersey Point (JPE/JPW) or False River (FRE/FRW), and surviving to JPE/JPW or FRE/FRW (Submodel II*)
$\phi_{F1,G1}$	Joint probability of moving from TCE/TCW directly toward Jersey Point (JPE/JPW) and surviving to JPE/JPW (Submodel II*); = $\phi_{F1,GH(A)}\psi_{G1}$
$\phi_{F1,G2}$	Joint probability of moving from TCE/TCW toward MAE/MAW, and surviving from TCE/TCW to MAE/MAW (Submodel II*)
$\phi_{F2,A14}$	Joint probability of moving from COL toward SJD, and surviving from COL to SJD (Submodel II)
$\phi_{F2,B4}$	Joint probability of moving from COL directly toward OR4, and surviving from COL to OR4 (Submodel II)
$\phi_{F2,B5}$	Joint probability of moving from COL directly toward OSJ, and surviving from COL to OSJ (Submodel II)
$\phi_{F2,C2}$	Joint probability of moving from COL directly toward MR4, and surviving from COL to MR4 (Submodel II)
$\phi_{F2,GH}$	Joint probability of moving from COL directly toward Jersey Point (JPE/JPW) or False River (FRE/FRW), and surviving to JPE/JPW or FRE/FRW (Submodel II*)
$\phi_{F2,G1}$	Joint probability of moving from COL directly toward Jersey Point (JPE/JPW) and surviving to JPE/JPW (Submodel II*); = $\phi_{F2,GH(A)}\psi_{G1}$
$\phi_{G1,G2(A)}$	Joint probability of moving from JPE/JPW toward Chipps Island (MAE/MAW), and surviving to MAE/MAW (Submodel II)

Table A1. (Continued)

Parameter	Definition
$\phi_{G1,G2(B)}$	Joint probability of moving from JPE/JPW toward Chipps Island (MAE/MAW), and surviving to MAE/MAW (Submodel I)
$\phi_{G2,G3}$	Joint probability of moving from Chipps Island (MAE/MAW) toward Benicia Bridge (BBR), and surviving from MAE/MAW to BRR
$\phi_{T1,G2}$	Joint probability of moving from TMS/TMN toward Chipps Island (MAE/MAW), and surviving to MAE/MAW (Submodel II)
ψ_{A1}	Probability of remaining in the San Joaquin River at the head of Old River; = 1 - ψ_{B1}
ψ_{A2}	Probability of remaining in the San Joaquin River at its upstream junction with Burns Cutoff; = 1 - ψ_{R2}
ψ_{A3}	Probability of remaining in the San Joaquin River at the junction with Turner Cut; = 1 - ψ_{F3}
ψ_{B1}	Probability of entering Old River at the head of Old River; = 1 - ψ_{A1}
ψ_{B2}	Probability of remaining in Old River at the head of Middle River; = 1 - ψ_{C2}
ψ_{C2}	Probability of entering Middle River at the head of Middle River; = 1 - ψ_{B2}
ψ_{F3}	Probability of entering Turner Cut at the junction with the San Joaquin River; = 1 - ψ_{A3}
ψ_{G1}	Probability of moving downriver in the San Joaquin River at the Jersey Point/False River junction (equated between submodels); = 1 - ψ_{H1}
ψ_{H1}	Probability of entering False River at the Jersey Point/False River junction (equated between submodels); = 1 - ψ_{G1}
ψ_{R2}	Probability of entering Burns Cutoff at its upstream junction with the San Joaquin River; = 1 - ψ_{R2}
P_{A0a}	Conditional probability of detection at DFU1
P_{A0b}	Conditional probability of detection at DFU2
P_{A0}	Conditional probability of detection at DFU (either DFU1 or DFU2)
P_{A2}	Conditional probability of detection at DFD
P_{A3}	Conditional probability of detection at BDF1
P_{A4}	Conditional probability of detection at BDF2
P_{A5}	Conditional probability of detection at BCA
P_{A6}	Conditional probability of detection at MOS
P_{A7a}	Conditional probability of detection at SJLU
P_{A7b}	Conditional probability of detection at SJLD
P_{A7}	Conditional probability of detection at SJL (either SJLU or SJLD)
P_{A8}	Conditional probability of detection at SJG
P_{A9}	Conditional probability of detection at SJNB
P_{A10}	Conditional probability of detection at SJC
P_{A11}	Conditional probability of detection at SJS
P_{A12a}	Conditional probability of detection at MACU
P_{A12b}	Conditional probability of detection at MACD
P_{A12}	Conditional probability of detection at MAC (either MACU or MACD)
P_{A13a}	Conditional probability of detection at MFE
P_{A13b}	Conditional probability of detection at MFW
P_{A13}	Conditional probability of detection at MFE/MFW (either MFE or MFW)
P_{A14a}	Conditional probability of detection at SJDU
P_{A14b}	Conditional probability of detection at SJDD
P_{A14}	Conditional probability of detection at SJD (either SJDU or SJDD)
P_{B1a}	Conditional probability of detection at OREU
P_{B1b}	Conditional probability of detection at ORED

Table A1. (Continued)

Parameter	Definition
P_{B1}	Conditional probability of detection at ORE (either OREU or ORED)
P_{B2a}	Conditional probability of detection at ORSU
P_{B2b}	Conditional probability of detection at ORSD
P_{B2}	Conditional probability of detection at ORS (either ORSU or ORSD)
P_{B3a}	Conditional probability of detection at WCLU
P_{B3b}	Conditional probability of detection at WCLD
P_{B3}	Conditional probability of detection at WCL (either WCLU or WCLD)
P_{B4a}	Conditional probability of detection at OR4U
P_{B4b}	Conditional probability of detection at OR4D
P_{B4}	Conditional probability of detection at OR4 (either OR4U or OR4D)
P_{B5a}	Conditional probability of detection at OSJU
P_{B5b}	Conditional probability of detection at OSJD
P_{B5}	Conditional probability of detection at OSJ (either OSJU or OSJD)
P_{C1a}	Conditional probability of detection at MRHU
P_{C1b}	Conditional probability of detection at MRHD
P_{C1}	Conditional probability of detection at MRH (either MRHU or MRHD)
P_{C2a}	Conditional probability of detection at MR4U
P_{C2b}	Conditional probability of detection at MR4D
P_{C2}	Conditional probability of detection at MR4 (either MR4U or MR4D)
P_{D1}	Conditional probability of detection at RGU
P_{D2}	Conditional probability of detection at RGD
P_{E1}	Conditional probability of detection at CVP
P_{E2}	Conditional probability of detection at CVPtank
P_{F1a}	Conditional probability of detection at TCE
P_{F1b}	Conditional probability of detection at TCW
P_{F1}	Conditional probability of detection at TCE/TCW (either TCE or TCW)
P_{F2a}	Conditional probability of detection at COLU
P_{F2b}	Conditional probability of detection at COLD
P_{F2}	Conditional probability of detection at COL (either COLU or COLD)
P_{G1a}	Conditional probability of detection at JPE
P_{G1b}	Conditional probability of detection at JPW
P_{G1}	Conditional probability of detection at JPE/JPW (either JPE or JPW)
P_{G2}	Conditional probability of detection at MAE/MAW
P_{G3a}	Conditional probability of detection at BBE
P_{G3b}	Conditional probability of detection at BBW
P_{G3}	Conditional probability of detection at BBR (either BBE or BBW)
P_{H1a}	Conditional probability of detection at FRW
P_{H1b}	Conditional probability of detection at FRE
P_{H1}	Conditional probability of detection at FRE/FRW (either FRE or FRW)
P_{R1a}	Conditional probability of detection at RRIU
P_{R1b}	Conditional probability of detection at RRID

Table A1. (Continued)

Parameter	Definition
P_{R1}	Conditional probability of detection at RRI (either RRIU or RRID)
P_{T1a}	Conditional probability of detection at TMS
P_{T1b}	Conditional probability of detection at TMN
P_{T1}	Conditional probability of detection at TMS/TMN (either TMS or TMN)

Table A2. Parameter estimates (standard errors or 95% bound [UB = upper bound, LB = lower bound] in parentheses) for tagged juvenile Steelhead released in 2016, excluding predator-type detections. Parameters without standard errors were estimated at fixed values in the model. Population-level estimates are weighted averages of the available release-specific estimates. Some parameters were not estimable because of sparse data.

Parameter	Release 1	Release 2	Release 3	Population Estimate
S_{A2}	0.74 (0.02)	0.93 (0.02)	0.98 (0.01)	0.88 (0.01)
S_{A3}	0.95 (0.02)	0.98 (0.03)	1.00 (0.01)	0.97 (0.01)
S_{A4}	0.91 (0.02)	0.95 (0.02)	0.98 (0.01)	0.95 (0.01)
S_{A5}	0.91 (0.02)	0.94 (0.02)	0.99 (<0.01)	0.95 (0.01)
S_{A6}	0.96 (0.01)	0.99 (<0.01)	1.00 (<0.01)	0.98 (<0.01)
S_{A7}	0.72 (0.09)	0.81 (0.04)	0.96 (0.01)	0.83 (0.03)
S_{A8}	0.94 (0.05)	0.93 (0.03)	0.98 (0.01)	0.95 (0.02)
$S_{A8,G2}$	0.34 (0.11)	0.63 (0.06)	0.64 (0.02)	0.53 (0.04)
S_{A9}	1 (95% LB: 0.84)	0.98 (0.02)	1.00 (<0.01)	0.99 (0.01)
$S_{A9,G2}$	0.36 (0.12)	0.67 (0.06)	0.65 (0.02)	0.56 (0.04)
S_{A10}	0.94 (0.06)	1 (95% LB: 0.95)	0.98 (0.01)	0.97 (0.02)
$S_{A10,G2}$	0.36 (0.12)	0.69 (0.06)	0.65 (0.02)	0.57 (0.04)
S_{A11}	0.94 (0.06)	1 (95% LB: 0.95)	0.97 (0.01)	0.97 (0.02)
$S_{A11,G2}$	0.38 (0.12)	0.69 (0.06)	0.67 (0.02)	0.58 (0.05)
$S_{A12,G2}$	0.34 (0.16)	0.83 (0.06)	0.81 (0.02)	0.66 (0.06)
$S_{A13,G2}$	0.50 (0.25)	0.79 (0.06)	0.87 (0.02)	0.72 (0.09)
S_{B1}	0.99 (0.01)	0.97 (0.01)	1 (95% LB: 0.82)	0.99 (<0.01)
$S_{B2,G2}$	0.43 (0.04)	0.41 (0.03)	0.20 (0.07)	0.35 (0.03)
$S_{B2(SD)}$	0.89 (0.02)	0.86 (0.02)	0.62 (0.14)	0.79 (0.05)
$S_{C1,G2}$				
$S_{C1(SD)}$				
$S_{F1,G2}$	0.50 (0.21)	0.33 (0.11)	0.31 (0.05)	0.38 (0.08)
S_{R1}			0.83 (0.15)	
$\phi_{A1,A0}$	0.08 (0.01)	0.02 (0.01)	0.04 (0.01)	0.05 (0.01)
$\phi_{A1,A2}$	0.76 (0.02)	0.96 (0.01)	0.94 (0.01)	0.88 (0.01)
$\phi_{A1,A5}$	0.48 (0.02)	0.83 (0.02)	0.90 (0.01)	0.74 (0.01)
$\phi_{A1,A6}$	0.44 (0.02)	0.78 (0.02)	0.89 (0.01)	0.70 (0.01)
$\phi_{A12,A13}$	0.44 (0.17)	0.87 (0.05)	0.75 (0.03)	0.69 (0.06)
$\phi_{A12,F2}$		0.11 (0.05)	0.20 (0.02)	0.16 (0.03)
$\phi_{A12,G2}$	0.11 (0.10)	0.07 (0.04)	0.15 (0.02)	0.11 (0.04)
$\phi_{A13,A14}$		0.72 (0.07)	0.81 (0.03)	0.76 (0.04)
$\phi_{A13,B4}$			0.01 (0.01)	
$\phi_{A13,B5}$		0.21 (0.06)	0.10 (0.02)	0.15 (0.03)
$\phi_{A13,C2}$			0.02 (0.01)	
$\phi_{A13,GH}$				
$\phi_{A13,G1}$		0.03[a] (0.03)	0.02[b] (0.01)	0.03 (0.01)
$\phi_{A13,G2}$	0.50 (0.25)	0.79 (0.06)	0.87 (0.02)	0.72 (0.09)

a = includes possibility of passing via OR4 or MR4 on way to JPE/JPW

b = probability of going to JPE/JPW directly without passing OR4 or MR4

Table A2. (Continued)

Parameter	Release 1	Release 2	Release 3	Population Estimate
$\phi_{A14,GH}$				
$\phi_{A14,G1}$		0.95 (0.05)	0.85 (0.03)	0.90 (0.03)
$\phi_{A14,T1}$		0.03 (0.03)	0.11 (0.02)	0.07 (0.02)
$\phi_{B2,B3}$		0.06 (0.01)		
$\phi_{B2,B4}$	0.01 (0.01)	0.04 (0.01)	0 (95% UB: 0.20)	0.02 (0.01)
$\phi_{B2,C2}$	0 (95% UB: 0.02)	0.01 (0.01)	0 (95% UB: 0.20)	0.00 (<0.01)
$\phi_{B2,D1O}$	0.17 (0.03)	0.21 (0.02)	0.19 (0.07)	0.19 (0.03)
$\phi_{B2,D1C}$	0.04 (0.02)	0.03 (0.01)	0.19 (0.07)	0.09 (0.02)
$\phi_{B2,D1}$	0.21 (0.03)	0.24 (0.03)	0.39 (0.14)	0.28 (0.05)
$\phi_{B2,E1}$	0.67 (0.04)	0.57 (0.03)	0.23 (0.12)	0.49 (0.04)
$\phi_{B3,B4}$		0.67 (0.19)		
$\phi_{B4,D1O}$			0.10 (0.04)	
$\phi_{B4,D1C}$			0.10 (0.04)	
$\phi_{B4,D1}$			0.20 (0.08)	
$\phi_{B4,E1}$			0.60 (0.10)	
$\phi_{B4,GH(A)}$				
$\phi_{B4,GH(B)}$				
$\phi_{B4,G1(A)}$			0.04 (0.04)	
$\phi_{B4,G1(B)}$		0.38 (0.17)		
$\phi_{B5,B4}$			0 (95% UB: 0.10)	
$\phi_{B5,C2}$			0 (95% UB: 0.10)	
$\phi_{B5,GH}$				
$\phi_{B5,G1}$		1[a] (95% LB: 0.74)	0.93[b] (0.05)	0.96 (0.02)
$\phi_{C1,B3}$				
$\phi_{C1,B4}$				
$\phi_{C1,C2}$				
$\phi_{C1,D1O}$				
$\phi_{C1,D1C}$				
$\phi_{C1,D1}$				
$\phi_{C1,E1}$				
$\phi_{C2,D1O}$			0.20 (0.06)	
$\phi_{C2,D1C}$			0.20 (0.06)	
$\phi_{C2,D1}$			0.40 (0.11)	
$\phi_{C2,E1}$			0.45 (0.11)	
$\phi_{C2,GH(A)}$				
$\phi_{C2,GH(B)}$				
$\phi_{C2,G1(A)}$			0 (95% UB: 0.14)	
$\phi_{C2,G1(B)}$		0 (95% UB: 0.56)		

a = includes possibility of passing via OR4 or MR4 on way to JPE/JPW

b = probability of going to JPE/JPW directly without passing OR4 or MR4

Table A2. (Continued)

Parameter	Release 1	Release 2	Release 3	Population Estimate
$\phi_{D1O,D2(A)}$			0.82[cd] (0.09)	
$\phi_{D1O,D2(B)}$	1.05 (0.06)	0.99 (0.02)	0.82[cd] (0.09)	0.96 (0.04)
$\phi_{D1C,D2(A)}$			0.82[cd] (0.09)	
$\phi_{D1C,D2(B)}$	1 (95% LB: 0.57)	1 (95% LB: 0.75)	0.82[cd] (0.09)	0.94 (0.03)
$\phi_{D1,D2(A)}$			0.82[c] (0.09)	
$\phi_{D1,D2(B)}$	1.04 (0.05)	0.99 (0.02)	0.82[c] (0.09)	0.95 (0.04)
$\phi_{D2,G2(A)}$			0.33[c] (0.12)	
$\phi_{D2,G2(B)}$	0.45 (0.08)	0.56 (0.06)	0.33[c] (0.12)	0.45 (0.05)
$\phi_{E1,E2(A)}$			0.44[c] (0.10)	
$\phi_{E1,E2(B)}$	0.59 (0.05)	0.54 (0.04)	0.44[c] (0.10)	0.53 (0.04)
$\phi_{E2,G2(A)}$			0.92[c] (0.08)	
$\phi_{E2,G2(B)}$	0.85 (0.05)	0.86 (0.04)	0.92[c] (0.08)	0.88 (0.03)
$\phi_{F1,B4}$			0.21 (0.04)	
$\phi_{F1,C2}$			0.12 (0.03)	
$\phi_{F1,GH}$				
$\phi_{F1,G1}$		0.56[a] (0.12)	0.21[b] (0.04)	0.39 (0.06)
$\phi_{F1,G2}$	0.50 (0.20)	0.47 (0.10)	0.31 (0.04)	0.43 (0.08)
$\phi_{F2,A14}$		0.60 (0.22)	0.49 (0.07)	0.55 (0.11)
$\phi_{F2,B4}$			0.07 (0.04)	
$\phi_{F2,B5}$		0 (95% UB: 0.45)	0.15 (0.05)	0.07 (0.02)
$\phi_{F2,C2}$			0.07 (0.04)	
$\phi_{F2,GH}$				
$\phi_{F2,G1}$		0.20[a] (0.18)	0.13[b] (0.04)	0.16 (0.09)
$\phi_{G1,G2(A)}$		0.84[c] (0.05)	0.98 (0.01)	0.91 (0.03)
$\phi_{G1,G2(B)}$		0.84[c] (0.05)		
$\phi_{G2,G3}$	0.86 (0.04)	0.96 (0.02)	0.99 (0.01)	0.94 (0.02)
$\phi_{T1,G2}$		1 (95% LB: 0.05)	0.91 (0.06)	0.95 (0.03)
ψ_{A1}	0.12 (0.02)	0.23 (0.02)	0.96 (0.01)	0.44 (0.01)
ψ_{A2}	1	1	0.98 (0.01)	0.99 (<0.01)
ψ_{A3}	0.60 (0.13)	0.71 (0.06)	0.75 (0.02)	0.69 (0.05)
ψ_{B1}	0.88 (0.02)	0.77 (0.02)	0.04 (0.01)	0.56 (0.01)
ψ_{B2}	0.99 (0.01)	1	0.87 (0.09)	0.95 (0.03)
ψ_{C2}	0.01 (0.01)	0	0.13 (0.09)	0.05 (0.03)
ψ_{F3}	0.40 (0.13)	0.29 (0.06)	0.25 (0.02)	0.31 (0.05)
ψ_{G1}				
ψ_{H1}				
ψ_{R2}	0	0	0.02 (0.01)	0.01 (<0.01)
P_{A0a}	1	1	0.88 (0.12)	0.96 (0.04)

a = includes possibility of passing via OR4 or MR4 on way to JPE/JPW

b = probability of going to JPE/JPW directly without passing OR4 or MR4

c = parameter equated between submodels Ic and IIa based on likelihood ratio test ($\alpha \geq 0.05$)

d = parameter equated between open and closed gate status based on likelihood ratio test ($\alpha \geq 0.05$)

Table A2. (Continued)

Parameter	Release 1	Release 2	Release 3	Population Estimate
P_{A0b}	0.68 (0.08)	0.60 (0.15)	0.39 (0.11)	0.55 (0.07)
P_{A0}	1	1	0.92 (0.08)	0.97 (0.03)
P_{A2}	1.00 (<0.01)	0.85 (0.02)	0.93 (0.01)	0.93 (0.01)
P_{A3}	0.84 (0.02)	0.30 (0.02)	0.43 (0.02)	0.52 (0.01)
P_{A4}	0.87 (0.02)	0.39 (0.02)	0.45 (0.02)	0.57 (0.01)
P_{A5}	0.96 (0.01)	0.51 (0.03)	0.88 (0.02)	0.78 (0.01)
P_{A6}	1	1	1	1
P_{A7a}	1	0.98 (0.02)	0.99 (0.01)	0.99 (0.01)
P_{A7b}	1	1	1	1
P_{A7}	1	1	1	1
P_{A8}	1	1	1	1
P_{A9}	1	1	0.99 (<0.01)	0.99 (<0.01)
P_{A10}	1	1	1	1
P_{A11}	1	1	1.00 (<0.01)	1.00 (<0.01)
P_{A12a}	1	1		1
P_{A12b}	0.89 (0.10)	1		0.94 (0.05)
P_{A12}	1	1	1.00 (<0.01)	1.00 (<0.01)
P_{A13a}	1	1	0.99 (0.01)	1.00 (<0.01)
P_{A13b}	1	1	1	1
P_{A13}	1	1	1	1
P_{A14a}		1	1	1
P_{A14b}		1	0.97 (0.01)	0.98 (0.01)
P_{A14}		1	1	1
P_{B1a}	1	1	1	1
P_{B1b}	1	1	1	1
P_{B1}	1	1	1	1
P_{B2a}	0.99 (0.01)		0.92 (0.07)	0.96 (0.04)
P_{B2b}	1		1	1
P_{B2}	1	1	1	1
P_{B3a}		1		
P_{B3b}		1		
P_{B3}		1		
P_{B4a}	1		1	1
P_{B4b}	1		1	1
P_{B4}	1	0.75 (0.22)	1	0.92 (0.07)
P_{B5a}		1	1	1
P_{B5b}		1	1	1
P_{B5}		1	1	1
P_{C1a}	1^{e}	1^{e}	1	1
P_{C1b}	1^{e}	1^{e}	1	1
P_{C1}	1^{e}	1^{e}	1	1

e = assumed value; data too sparse to estimate freely

Table A2. (Continued)

Parameter	Release 1	Release 2	Release 3	Population Estimate
P_{C2a}	1[e]	1	1	1
P_{C2b}	1[e]	1	1	1
P_{C2}	1[e]	1	1	1
P_{D1}	0.97 (0.03)	0.94 (0.03)	0.93 (0.06)	0.95 (0.03)
P_{D2}	0.86 (0.08)	0.98 (0.02)	1	0.94 (0.03)
P_{E1}	1	1	1	1
P_{E2}	1	1	1	1
P_{F1a}	1	1	1	1
P_{F1b}	1	1	1	1
P_{F1}	1	1	1	1
P_{F2a}		1		
P_{F2b}		1		
P_{F2}		1	0.98 (0.02)	0.99 (0.01)
P_{G1a}				
P_{G1b}				
P_{G1}		0.94 (0.04)	0.96 (0.01)	0.95 (0.02)
P_{G2}	0.95 (0.03)	0.93 (0.02)	0.93 (0.02)	0.94 (0.01)
P_{G3a}	0.98 (0.02)	0.99 (0.01)	0.94 (0.01)	0.97 (0.01)
P_{G3b}	0.97 (0.02)	0.99 (0.01)	0.99 (0.01)	0.98 (0.01)
P_{G3}	1.00 (<0.01)	1.00 (<0.01)	1.00 (<0.01)	1.00 (<0.01)
P_{H1a}				
P_{H1b}				
P_{H1}				
P_{R1a}	1[e]	1[e]	1	1
P_{R1b}	1[e]	1[e]	1	1
P_{R1}	1[e]	1[e]	1	1
P_{T1a}		1[e]	1	1
P_{T1b}		1[e]	1	1
P_{T1}		1[e]	1	1

e = assumed value; data too sparse to estimate freely

Table A3. Parameter estimates (standard errors or 95% bound [UB = upper bound, LB = lower bound] in parentheses) for tagged juvenile Steelhead released in 2016, including predator-type detections. Parameters without standard errors were estimated at fixed values in the model. Population-level estimates are weighted averages of the available release-specific estimates. Some parameters were not estimable because of sparse data.

Parameter	Release 1	Release 2	Release 3	Population Estimate
S_{A2}	0.74 (0.02)	0.92 (0.02)	0.98 (0.01)	0.88 (0.01)
S_{A3}	0.95 (0.02)	0.99 (0.03)	0.99 (0.01)	0.98 (0.01)
S_{A4}	0.92 (0.02)	0.95 (0.02)	0.97 (0.01)	0.95 (0.01)
S_{A5}	0.92 (0.02)	0.94 (0.02)	1.00 (<0.01)	0.95 (0.01)
S_{A6}	0.97 (0.01)	0.99 (<0.01)	1.00 (<0.01)	0.99 (<0.01)
S_{A7}	0.78 (0.08)	0.81 (0.04)	0.98 (0.01)	0.86 (0.03)
S_{A8}	0.95 (0.05)	0.97 (0.02)	0.99 (<0.01)	0.97 (0.02)
$S_{A8,G2}$	0.29 (0.10)	0.63 (0.06)	0.66 (0.02)	0.53 (0.04)
S_{A9}	1 (95% LB: 0.86)	0.99 (0.01)	0.98 (0.01)	0.99 (0.01)
$S_{A9,G2}$	0.30 (0.10)	0.64 (0.06)	0.67 (0.02)	0.54 (0.04)
S_{A10}	0.95 (0.05)	1 (95% LB: 0.96)	0.99 (0.01)	0.98 (0.02)
$S_{A10,G2}$	0.30 (0.10)	0.65 (0.06)	0.68 (0.02)	0.55 (0.04)
S_{A11}	0.95 (0.05)	1 (95% LB: 0.96)	0.99 (0.01)	0.98 (0.02)
$S_{A11,G2}$	0.32 (0.11)	0.65 (0.06)	0.69 (0.02)	0.55 (0.04)
$S_{A12,G2}$	0.30 (0.15)	0.81 (0.06)	0.83 (0.02)	0.65 (0.05)
$S_{A13,G2}$	0.40 (0.22)	0.77 (0.06)	0.89 (0.02)	0.69 (0.08)
S_{B1}	0.99 (0.01)	0.98 (0.01)	1 (95% LB: 0.82)	0.99 (<0.01)
$S_{B2,G2}$	0.44 (0.04)	0.40 (0.03)	0.25 (0.07)	0.36 (0.03)
$S_{B2(SD)}$	0.91 (0.02)	0.88 (0.02)	0.67 (0.12)	0.82 (0.04)
$S_{C1,G2}$				
$S_{C1(SD)}$				
$S_{F1,G2}$	0.38 (0.17)	0.30 (0.10)	0.31 (0.05)	0.33 (0.07)
S_{R1}			1 (95% LB: 0.65)	
$\phi_{A1,A0}$	0.08 (0.01)	0.02 (0.01)	0.05 (0.01)	0.05 (0.01)
$\phi_{A1,A2}$	0.75 (0.02)	0.96 (0.01)	0.94 (0.01)	0.88 (0.01)
$\phi_{A1,A5}$	0.49 (0.02)	0.83 (0.02)	0.89 (0.01)	0.74 (0.01)
$\phi_{A1,A6}$	0.45 (0.02)	0.78 (0.02)	0.89 (0.01)	0.71 (0.01)
$\phi_{A12,A13}$	0.50 (0.16)	0.87 (0.05)	0.76 (0.03)	0.71 (0.06)
$\phi_{A12,F2}$		0.11 (0.05)	0.20 (0.02)	0.15 (0.03)
$\phi_{A12,G2}$	0.10 (0.09)	0.07 (0.03)	0.15 (0.02)	0.11 (0.03)
$\phi_{A13,A14}$		0.73 (0.07)	0.82 (0.03)	0.77 (0.04)
$\phi_{A13,B4}$			0.01 (0.01)	
$\phi_{A13,B5}$		0.20 (0.06)	0.10 (0.02)	0.15 (0.03)
$\phi_{A13,C2}$			0.02 (0.01)	
$\phi_{A13,GH}$				
$\phi_{A13,G1}$		0.03[a] (0.02)	0.02[b] (0.01)	0.02 (0.01)
$\phi_{A13,G2}$	0.40 (0.22)	0.77 (0.06)	0.89 (0.02)	0.69 (0.08)

a = includes possibility of passing via OR4 or MR4 on way to JPE/JPW

b = probability of going to JPE/JPW directly without passing OR4 or MR4

Table A3. (Continued)

Parameter	Release 1	Release 2	Release 3	Population Estimate
$\phi_{A14,GH}$				
$\phi_{A14,G1}$		0.92 (0.05)	0.86 (0.02)	0.89 (0.03)
$\phi_{A14,T1}$		0.03 (0.03)	0.11 (0.02)	0.07 (0.02)
$\phi_{B2,B3}$		0.06 (0.01)		
$\phi_{B2,B4}$	0.01 (0.01)	0.05 (0.02)	0 (95% UB: 0.18)	0.02 (0.01)
$\phi_{B2,C2}$	0 (95% UB: 0.02)	0.01 (0.01)	0 (95% UB: 0.18)	0.00 (<0.01)
$\phi_{B2,D1O}$	0.17 (0.03)	0.21 (0.02)	0.17 (0.06)	0.18 (0.02)
$\phi_{B2,D1C}$	0.05 (0.02)	0.04 (0.01)	0.17 (0.06)	0.09 (0.02)
$\phi_{B2,D1}$	0.22 (0.03)	0.25 (0.03)	0.34 (0.12)	0.27 (0.04)
$\phi_{B2,E1}$	0.68 (0.04)	0.58 (0.03)	0.33 (0.12)	0.53 (0.04)
$\phi_{B3,B4}$		0.83 (0.22)		
$\phi_{B4,D1O}$			0.12 (0.04)	
$\phi_{B4,D1C}$			0.12 (0.04)	
$\phi_{B4,D1}$			0.24 (0.08)	
$\phi_{B4,E1}$			0.52 (0.09)	
$\phi_{B4,GH(A)}$				
$\phi_{B4,GH(B)}$				
$\phi_{B4,G1(A)}$			0.07 (0.05)	
$\phi_{B4,G1(B)}$		0.30 (0.15)		
$\phi_{B5,B4}$			0.03 (0.03)	
$\phi_{B5,C2}$			0 (95% UB: 0.10)	
$\phi_{B5,GH}$				
$\phi_{B5,G1}$		1[a] (95% LB: 0.74)	0.97[b] (0.03)	0.98 (0.02)
$\phi_{C1,B3}$				
$\phi_{C1,B4}$				
$\phi_{C1,C2}$				
$\phi_{C1,D1O}$				
$\phi_{C1,D1C}$				
$\phi_{C1,D1}$				
$\phi_{C1,E1}$				
$\phi_{C2,D1O}$			0.18 (0.05)	
$\phi_{C2,D1C}$			0.18 (0.05)	
$\phi_{C2,D1}$			0.35 (0.11)	
$\phi_{C2,E1}$			0.45 (0.11)	
$\phi_{C2,GH(A)}$				
$\phi_{C2,GH(B)}$				
$\phi_{C2,G1(A)}$			0 (95% UB: 0.14)	
$\phi_{C2,G1(B)}$		0 (95% UB: 0.56)		

a = includes possibility of passing via OR4 or MR4 on way to JPE/JPW

b = probability of going to JPE/JPW directly without passing OR4 or MR4

Table A3. (Continued)

Parameter	Release 1	Release 2	Release 3	Population Estimate
$\phi_{D1O,D2(A)}$			0.83[cd] (0.09)	
$\phi_{D1O,D2(B)}$	1.08 (0.08)	0.99 (0.02)	0.83[cd] (0.09)	0.97 (0.04)
$\phi_{D1C,D2(A)}$			0.83[cd] (0.09)	
$\phi_{D1C,D2(B)}$	0.99 (0.13)	0.91 (0.10)	0.83[cd] (0.09)	0.91 (0.06)
$\phi_{D1,D2(A)}$			0.83[cd] (0.09)	
$\phi_{D1,D2(B)}$	1.06 (0.08)	0.98 (0.02)	0.83[cd] (0.09)	0.96 (0.04)
$\phi_{D2,G2(A)}$			0.31[c] (0.12)	
$\phi_{D2,G2(B)}$	0.42 (0.09)	0.55 (0.06)	0.31[c] (0.12)	0.43 (0.05)
$\phi_{E1,E2(A)}$			0.52[c] (0.09)	
$\phi_{E1,E2(B)}$	0.58 (0.04)	0.52 (0.04)	0.52[c] (0.09)	0.54 (0.04)
$\phi_{E2,G2(A)}$			0.94[c] (0.06)	
$\phi_{E2,G2(B)}$	0.86 (0.05)	0.87 (0.04)	0.94[c] (0.06)	0.89 (0.03)
$\phi_{F1,B4}$			0.21 (0.04)	
$\phi_{F1,C2}$			0.12 (0.03)	
$\phi_{F1,GH}$				
$\phi_{F1,G1}$		0.51[a] (0.11)	0.20[b] (0.04)	0.35 (0.06)
$\phi_{F1,G2}$	0.37 (0.17)	0.43 (0.10)	0.31 (0.04)	0.37 (0.07)
$\phi_{F2,A14}$		0.60 (0.22)	0.52 (0.07)	0.56 (0.11)
$\phi_{F2,B4}$			0.09 (0.04)	
$\phi_{F2,B5}$		0 (95% UB: 0.45)	0.13 (0.04)	0.06 (0.02)
$\phi_{F2,C2}$			0.05 (0.03)	
$\phi_{F2,GH}$				
$\phi_{F2,G1}$		0.20[a] (0.18)	0.13[b] (0.04)	0.16 (0.09)
$\phi_{G1,G2(A)}$		0.84[c] (0.05)	0.97 (0.01)	0.90 (0.03)
$\phi_{G1,G2(B)}$		0.84[c] (0.05)		
$\phi_{G2,G3}$	0.86 (0.04)	0.97 (0.02)	0.98 (0.01)	0.94 (0.02)
$\phi_{T1,G2}$		1 (95% LB: 0.05)	0.92 (0.06)	0.96 (0.03)
ψ_{A1}	0.13 (0.02)	0.23 (0.02)	0.96 (0.01)	0.44 (0.01)
ψ_{A2}	1	1	0.98 (0.01)	0.99 (<0.01)
ψ_{A3}	0.56 (0.12)	0.70 (0.06)	0.74 (0.02)	0.66 (0.04)
ψ_{B1}	0.87 (0.02)	0.77 (0.02)	0.04 (0.01)	0.56 (0.01)
ψ_{B2}	0.99 (0.01)	1	1	1.00 (<0.01)
ψ_{C2}	0.01 (0.01)	0	0	0.00 (<0.01)
ψ_{F3}	0.44 (0.12)	0.30 (0.06)	0.26 (0.02)	0.34 (0.04)
ψ_{G1}				
ψ_{H1}				
ψ_{R2}	0	0	0.02 (0.01)	0.01 (<0.01)
P_{A0a}	1	1	0.92 (0.07)	0.97 (0.02)

a = includes possibility of passing via OR4 or MR4 on way to JPE/JPW

b = probability of going to JPE/JPW directly without passing OR4 or MR4

c = parameter equated between submodels Ic and IIa based on likelihood ratio test ($\alpha \geq 0.05$)

d = parameter equated between open and closed gate status based on likelihood ratio test ($\alpha \geq 0.05$)

Table A3. (Continued)

Parameter	Release 1	Release 2	Release 3	Population Estimate
P_{A0b}	0.68 (0.08)	0.60 (0.15)	0.55 (0.11)	0.61 (0.07)
P_{A0}	1	1	0.97 (0.04)	0.99 (0.01)
P_{A2}	1.00 (<0.01)	0.85 (0.02)	0.93 (0.01)	0.93 (0.01)
P_{A3}	0.84 (0.02)	0.30 (0.02)	0.44 (0.02)	0.53 (0.01)
P_{A4}	0.87 (0.02)	0.39 (0.02)	0.45 (0.02)	0.57 (0.01)
P_{A5}	0.96 (0.01)	0.51 (0.03)	0.88 (0.02)	0.78 (0.01)
P_{A6}	1	1	1	1
P_{A7a}	1	0.98 (0.02)	0.98 (0.01)	0.99 (0.01)
P_{A7b}	1	1	1	1
P_{A7}	1	1	1	1
P_{A8}	1	1	1	1
P_{A9}	1	1	0.99 (0.00)	1.00 (<0.01)
P_{A10}	1	1	1	1
P_{A11}	1	1	1.00 (0.00)	1.00 (<0.01)
P_{A12a}	1	1		1
P_{A12b}	0.90 (0.09)	1		0.95 (0.05)
P_{A12}	1	1	1.00 (<0.01)	1.00 (<0.01)
P_{A13a}	1	1	0.98 (0.01)	0.99 (<0.01)
P_{A13b}	1	1	0.99 (0.01)	1.00 (<0.01)
P_{A13}	1	1	1.00 (<0.01)	1.00 (<0.01)
P_{A14a}		1	1	1
P_{A14b}		1	0.97 (0.01)	0.99 (0.01)
P_{A14}		1	1	1
P_{B1a}	1	1	1	1
P_{B1b}	1	1	1	1
P_{B1}	1	1	1	1
P_{B2a}	0.99 (0.01)		0.93 (0.06)	0.96 (0.03)
P_{B2b}	1		1	1
P_{B2}	1	1	1	1
P_{B3a}		1		
P_{B3b}		1		
P_{B3}		1		
P_{B4a}	1^{e}		1	1
P_{B4b}	1^{e}		1	1
P_{B4}	1^{e}	0.75 (0.22)	1	0.92 (0.07)
P_{B5a}		1	1	1
P_{B5b}		1	1	1
P_{B5}		1	1	1
P_{C1a}	1^{e}	1^{e}	1^{e}	1^{e}
P_{C1b}	1^{e}	1^{e}	1^{e}	1^{e}
P_{C1}	1^{e}	1^{e}	1^{e}	1^{e}

e = assumed value; data too sparse to estimate freely

Table A3. (Continued)

Parameter	Release 1	Release 2	Release 3	Population Estimate
P_{C2a}	1[e]	1	1	1
P_{C2b}	1[e]	1	1	1
P_{C2}	1[e]	1	1	1
P_{D1}	0.97 (0.03)	0.94 (0.03)	0.94 (0.06)	0.95 (0.02)
P_{D2}	0.82 (0.09)	0.97 (0.03)	1	0.93 (0.03)
P_{E1}	1	1	1	1
P_{E2}	1	1	1	1
P_{F1a}	1	1	1	1
P_{F1b}	1	1	1	1
P_{F1}	1	1	1	1
P_{F2a}		1	1	1
P_{F2b}		1	1	1
P_{F2}		1	1	1
P_{G1a}				
P_{G1b}				
P_{G1}		0.94 (0.04)	0.96 (0.01)	0.95 (0.02)
P_{G2}	0.95 (0.03)	0.93 (0.02)	0.93 (0.02)	0.94 (0.01)
P_{G3a}	0.98 (0.02)	0.98 (0.01)	0.94 (0.01)	0.97 (0.01)
P_{G3b}	0.97 (0.02)	0.99 (0.01)	0.99 (0.01)	0.98 (0.01)
P_{G3}	1.00 (<0.01)	1.00 (<0.01)	1.00 (<0.01)	1.00 (<0.01)
P_{H1a}				
P_{H1b}				
P_{H1}				
P_{R1a}	1[e]	1[e]	1	1
P_{R1b}	1[e]	1[e]	1	1
P_{R1}	1[e]	1[e]	1	1
P_{T1a}		1[e]	1	1
P_{T1b}		1[e]	1	1
P_{T1}		1[e]	1	1

e = assumed value; data too sparse to estimate freely

OBAN: ONCORHYNCHUS BAYESIAN ANALYSIS

A STATISTICAL LIFE-CYCLE MODEL FOR SALMON

PREDATION WORKSHOP
JULY 20, 2013
UC DAVIS

NOBLE HENDRIX, QEDA CONSULTING

Collaborators:
Ray Hilborn, Curry Cunningham, Bob Lessard, University of Washington
Correigh Greene, Tim Beechie, NOAA Fisheries

Acknowledgements

- Delta Stewardship Council
- NMFS
- CDFW
- USFWS
- DWR
- USBR

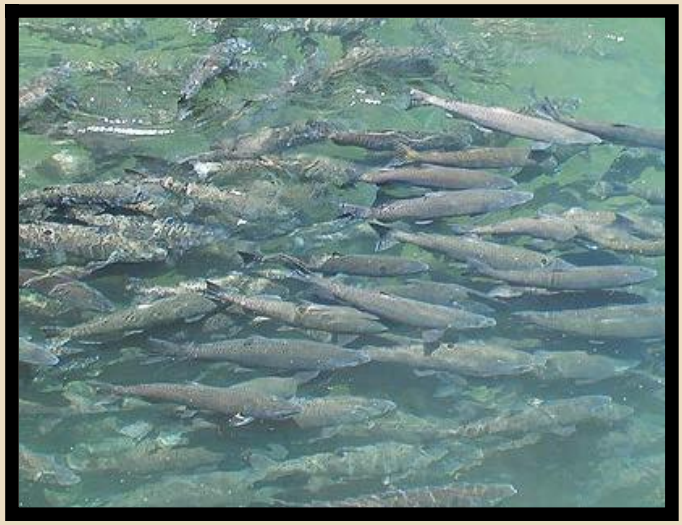

Central Valley spring-run Chinook

MOTIVATION:

Factors hypothesized to affect WR population dynamics

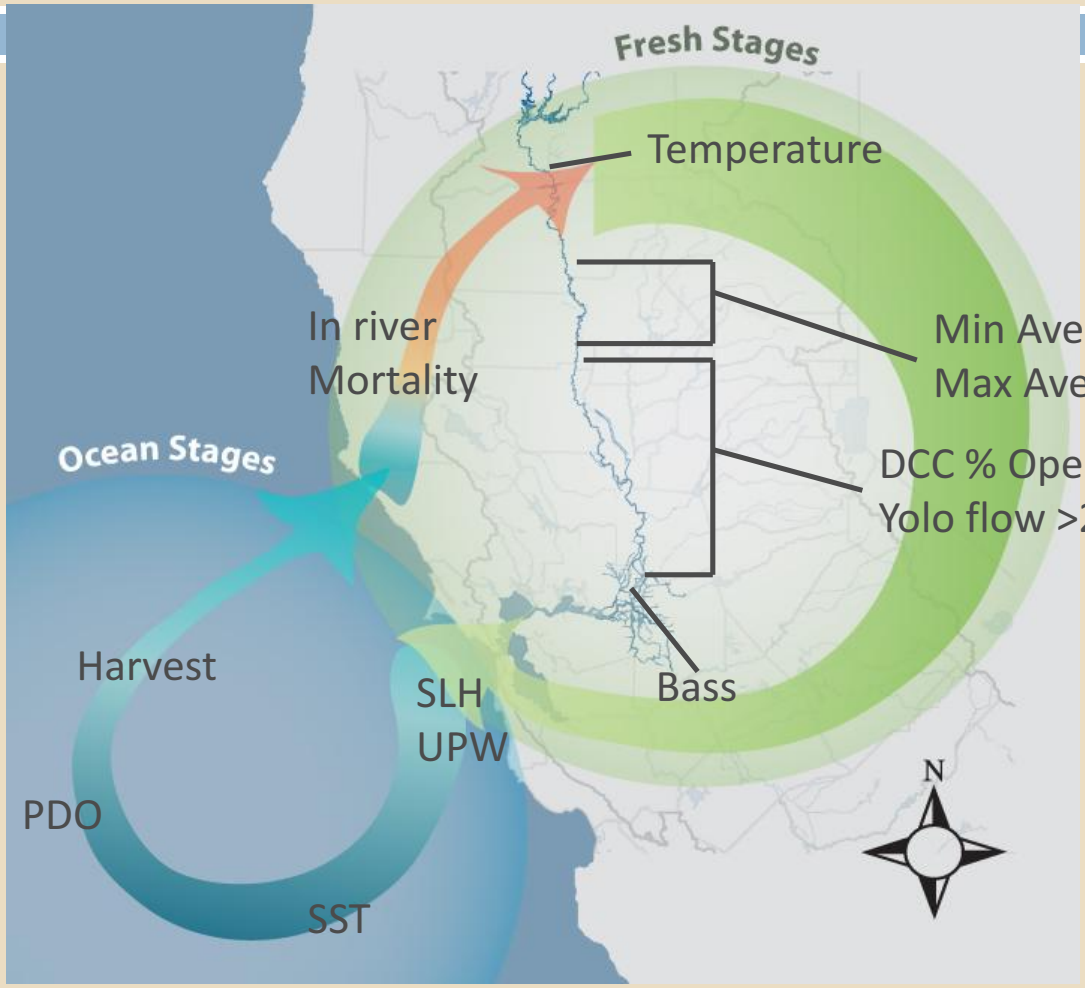

OBAN objectives:

- Evaluate whether hypothesized factors explain dynamic vital rates (e.g., survival) through the entire life-cycle
- Estimate effects of factors by statistically fitting predictions of the population dynamics model to observed indices of abundance
- Explicitly incorporate uncertainty in the estimation procedure by using a Bayesian framework

1st Level: Stage Transitions

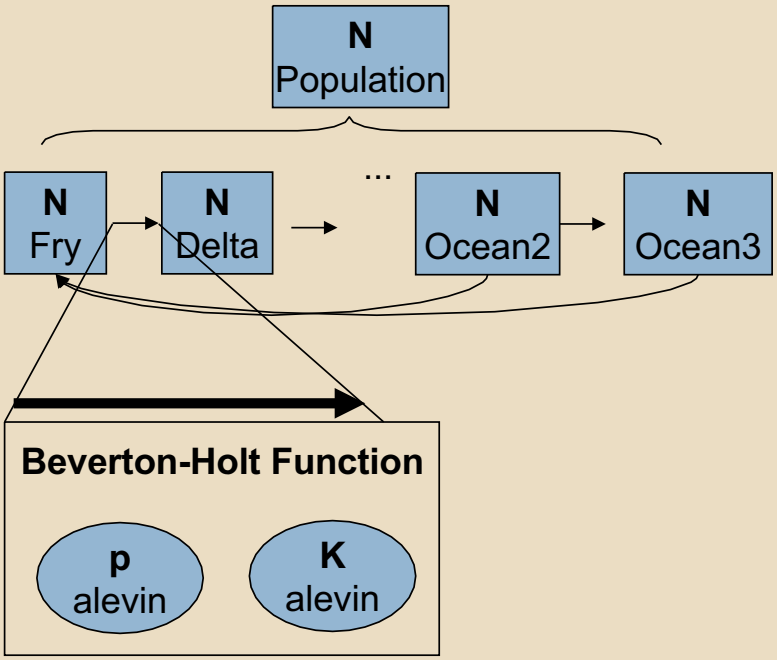

Beverton-Holt Function for Transitions

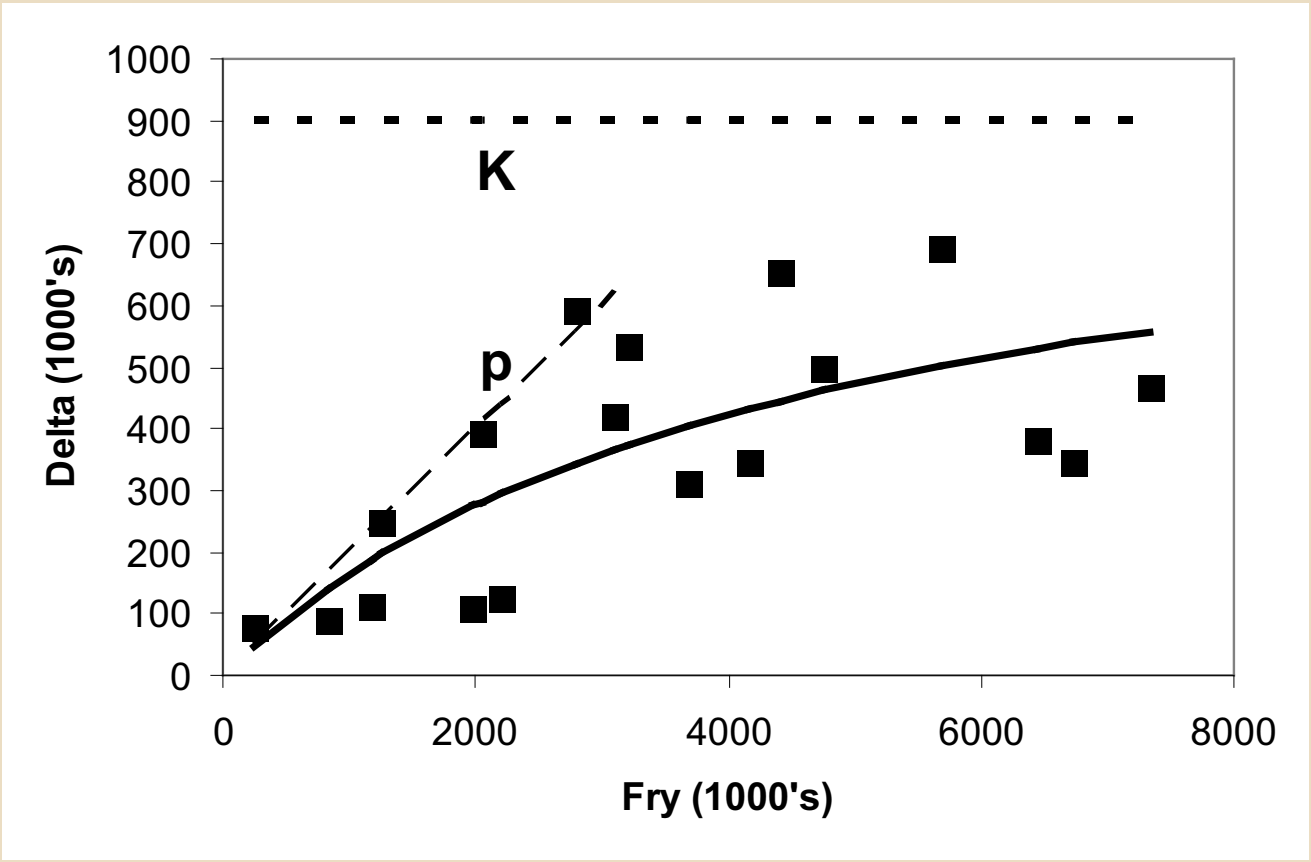

Full Hierarchy

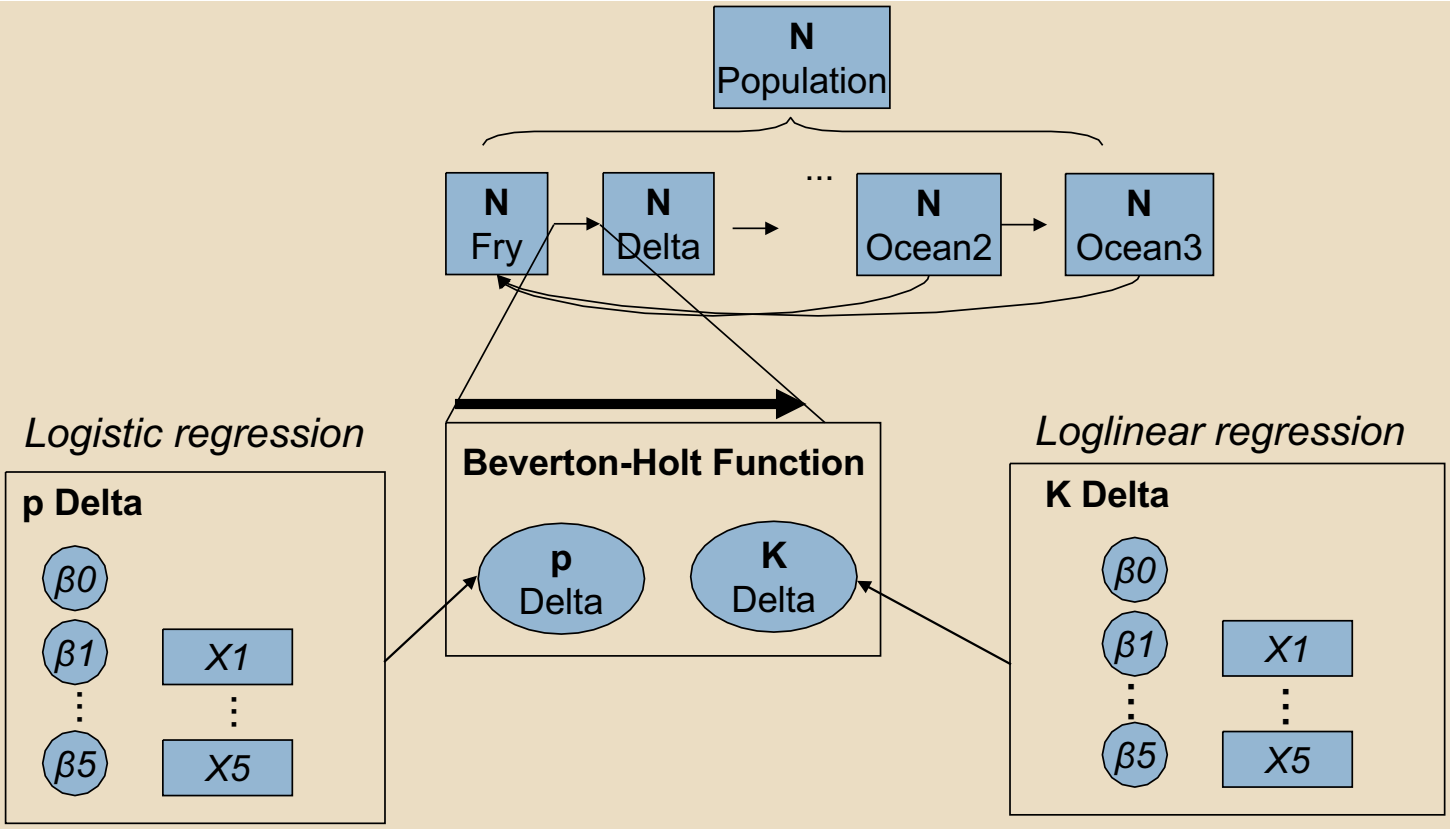

Maximum Likelihood Modeling Tool

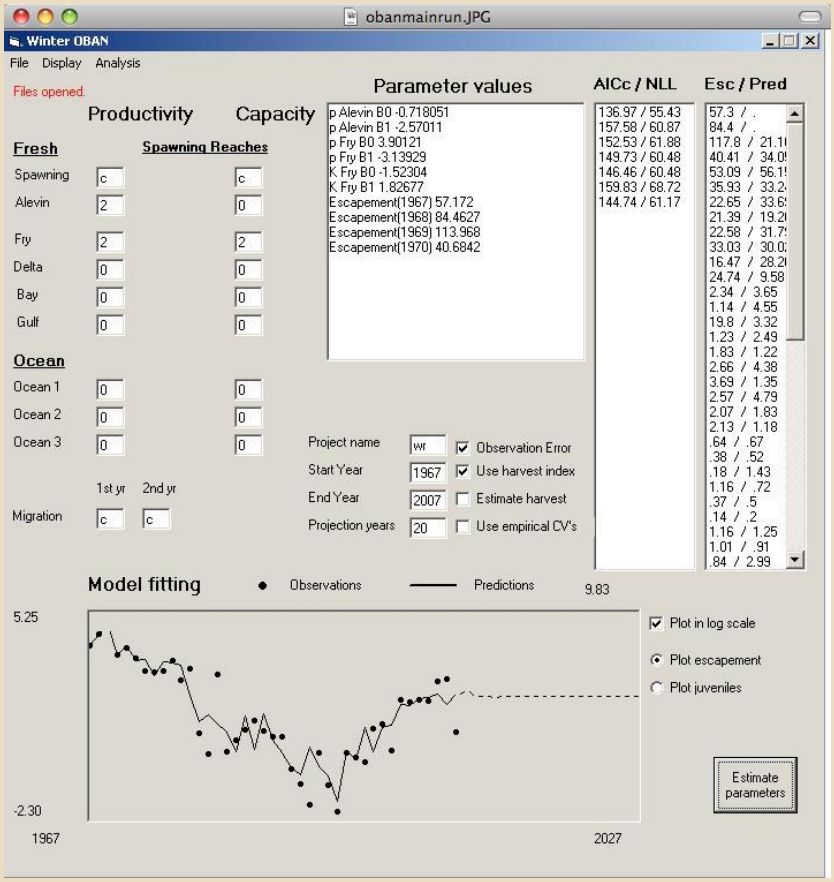

- Delivers point estimates (MLE)
- Estimation via ADMB
- Stable and available to public
- Easy to convert competing hypotheses into model structural forms (GUI based)
- Easy to compare competing hypotheses with AIC

Model Assumptions and Limitations

- Assumptions similar to generalized linear models:
  - Identify relationships, but does not specify the underlying causal mechanism
  - Multicollinearity of factors
  - Distributional assumptions
- Forecasting Limitations
  - Large changes to the ecosystem that are not captured in the historical conditions are difficult to forecast

Butte Creek spring-run

Photo Credit: UC Davis (aacook@gmail.com)

Butte Creek Potential Factors

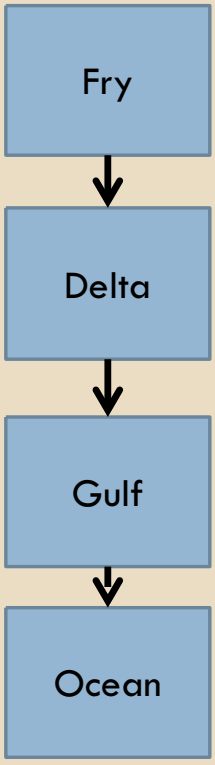

- Fry stage: Flow and Temperature (y-1) metrics
- Delta stage: **BASS** (Catch), YOLO, DCC, EXPT
- Gulf stage: UPW, SLH, SST, and CURL
- Ocean 2 and Ocean 3 stages: Harvest

Model Fit (lowest AIC)

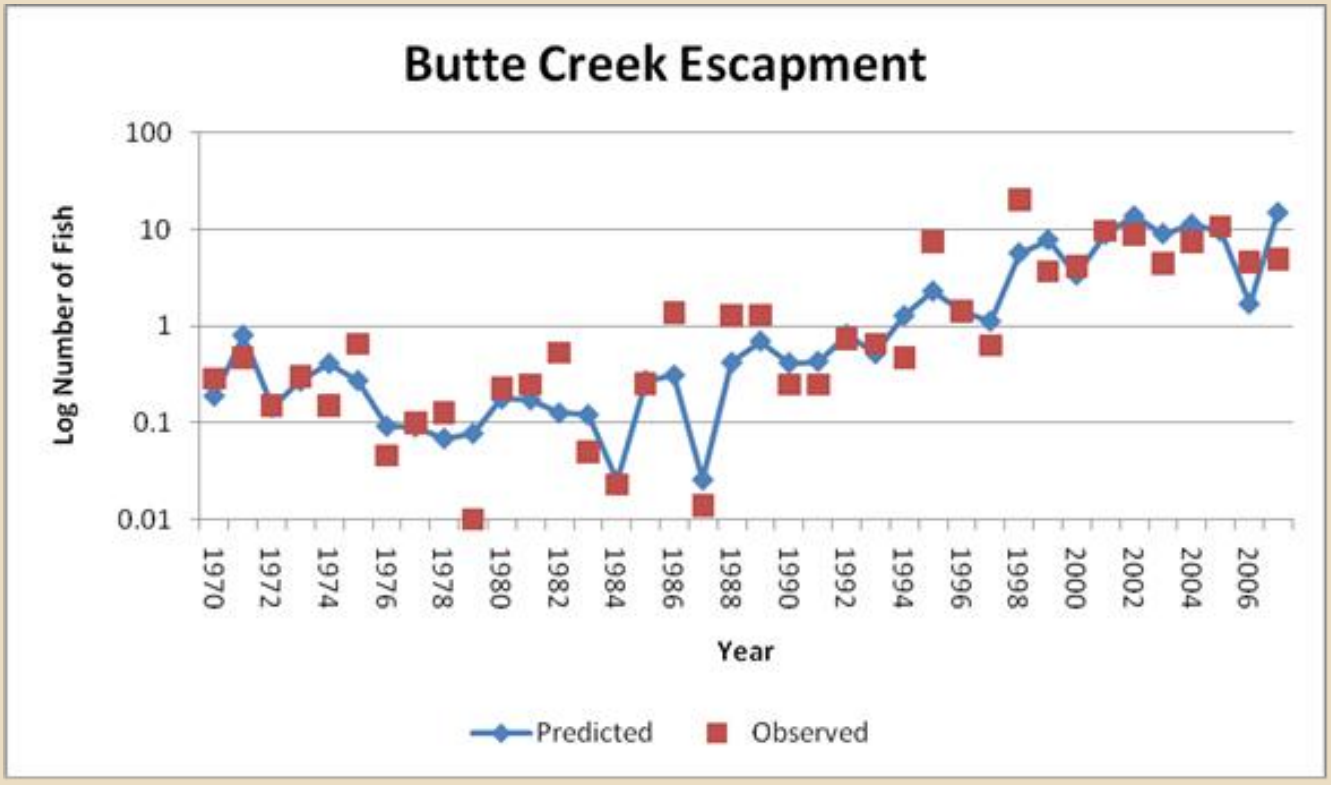

Model structural uncertainty

Delta Stage	Gulf Stage	AIC_C Score	Δ AIC_C
BASS;	CURL; SLH;	110.33	0.00
	CURL; SLH;	112.76	2.43
EXPT; BASS;	CURL; SLH;	113.62	3.29
BASS;	PDO; UPW;	115.97	5.64
YOLO;	PDO; UPW;	116.55	6.22

Model selection weights (Burnham and Anderson 2002), of approximately 0.57, 0.17, and 0.11 for the top three models.

Influence of Factors on Butte Creek SR

Factor	Model 1	Model 3
BASS	-1.24 (0.51)	-1.39 (0.60)
CURL	6.75 (1.5)	6.65 (1.49)
SLH	-3.65 (0.94)	-3.63 (0.92)
EXPT		-3.09 (0.71)

- SR survival increases when:
  - Striped bass abundance is low
  - Curl is positive (i.e., periods of more offshore upwelling)
  - SLH is low (i.e., El Niño years are bad)
  - Exports are lower than average

Winter OBAN

- Bayesian state-space model
- Estimation via MCMC – Metropolis and distribution free adaptive rejection steps (log concave densities) in WinBUGS
- 50,000 (50% burn-in) samples from 3 chains with diagnostics via the Brooks-Gelman- Rubin statistic (Brooks and Gelman 1998)

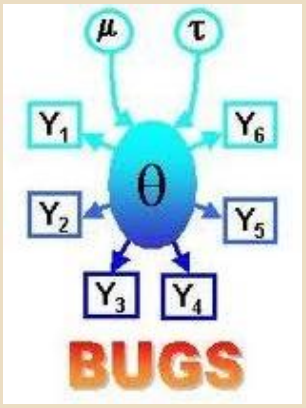

CDFG

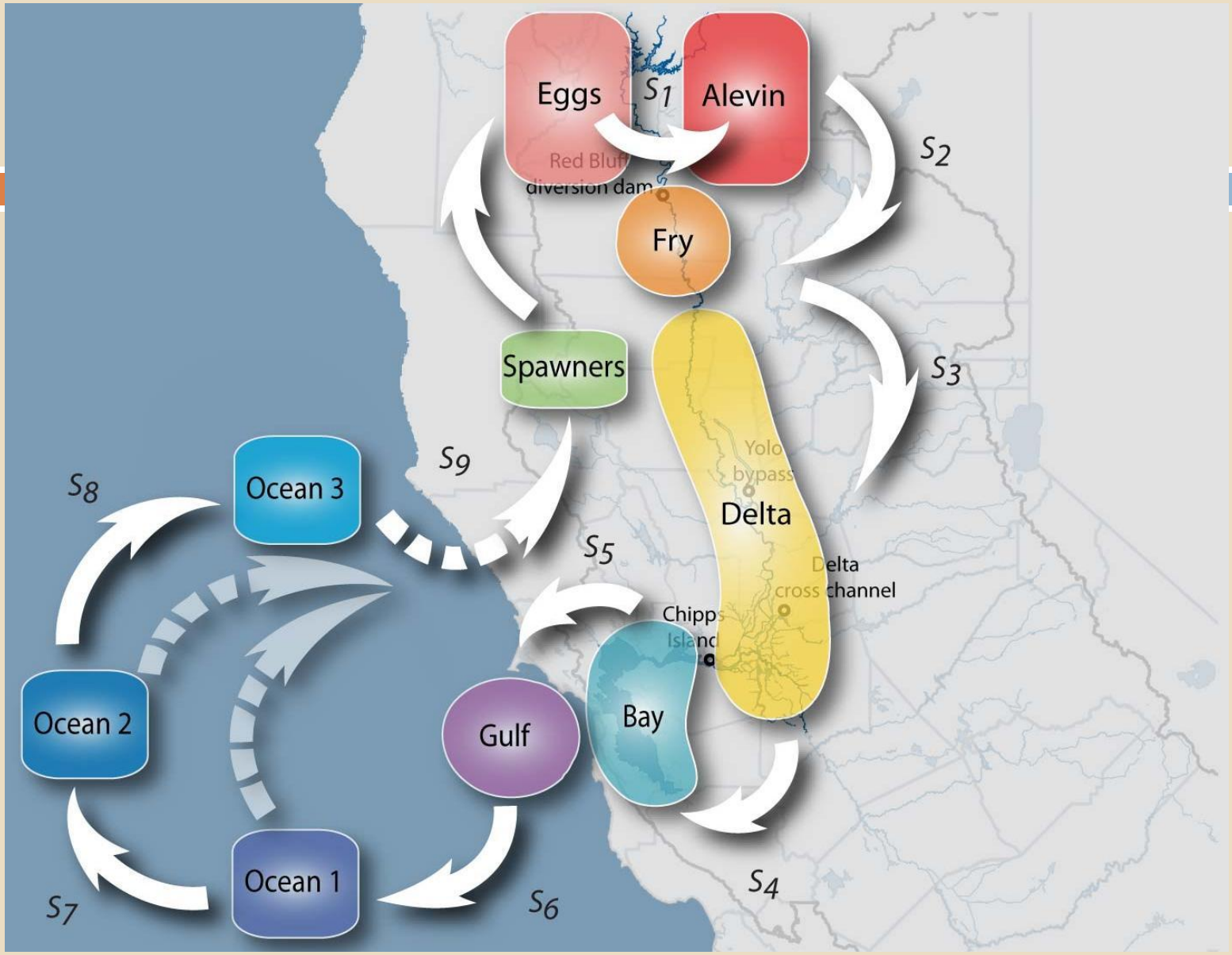
Eggs
S_1
Alevin
S_2
Red Bluff
diversion dam
Fry
S_3
Spawners
S_9
Yolo
bypass
Delta
Delta
cross channel
S_5
Chipps
Island
Bay
Gulf
S_4
S_6
S_7
S_8
Ocean 3
Ocean 2
Ocean 1

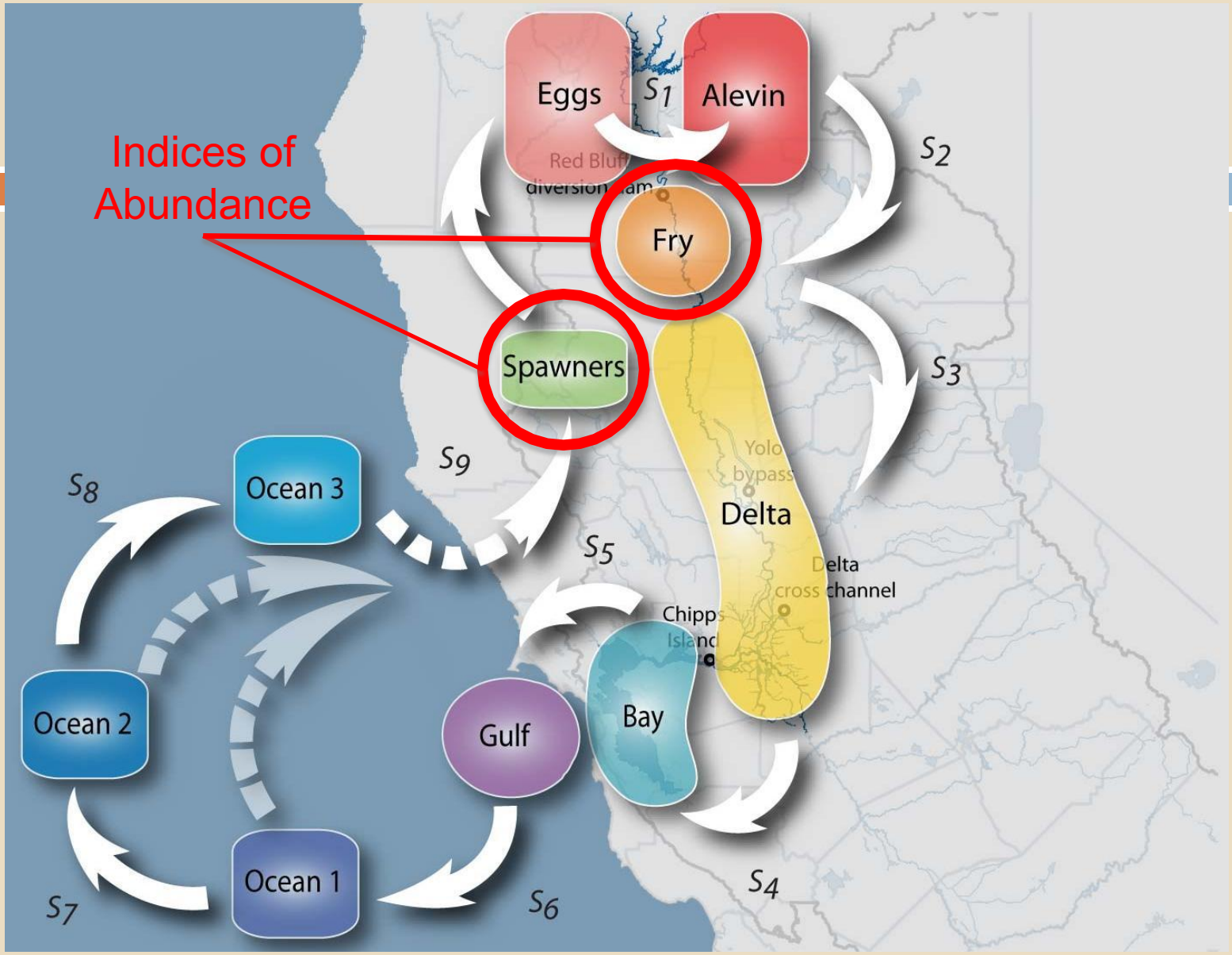
Indices of Abundance
Eggs
S_1
Alevin
S_2
Red Bluff diversion dam
Fry
Spawners
S_3
S_9
S_8
Ocean 3
Yolo bypass
Delta
S_5
Delta cross channel
Chipps Island
Ocean 2
Gulf
Bay
Ocean 1
S_7
S_6
S_4

Winter Run Model details

- Period of retrospective analysis: 1967 – 2008
- Data
  - Annual escapement: 1967 – 2008
    - 1967 – 1987 counts conducted via a weir type setting
    - 1988 – 2001 expansion assuming 15% of the run after May 15th
    - 2002 – 2008 carcass surveys
  - Juvenile production indices: 1995 – 1999, 2002-2007
- Assumptions:
  - Harvest rates reflect relative levels of exploitation
  - Maturation rates from analysis of ’98, ’99, ’00 CWT data

Winter OBAN

Factors affecting survival transitions:

- Covariates incorporated into Winter OBAN
  - Alevin: TEMP- Temperature in spawning reaches
  - Fry: MINFLOW - Minimum Flow at Bend Bridge
  - Delta: EXPT, YOLO, **BASS**
    - Two BASS covariates were evaluated
  - Gulf: CURL - upwelling index
  - Ocean: Harvest

BASS:

Standardized Predation Covariates

- Log Striped Bass Catch
- Log Striped Bass Peterson Abundance Estimate

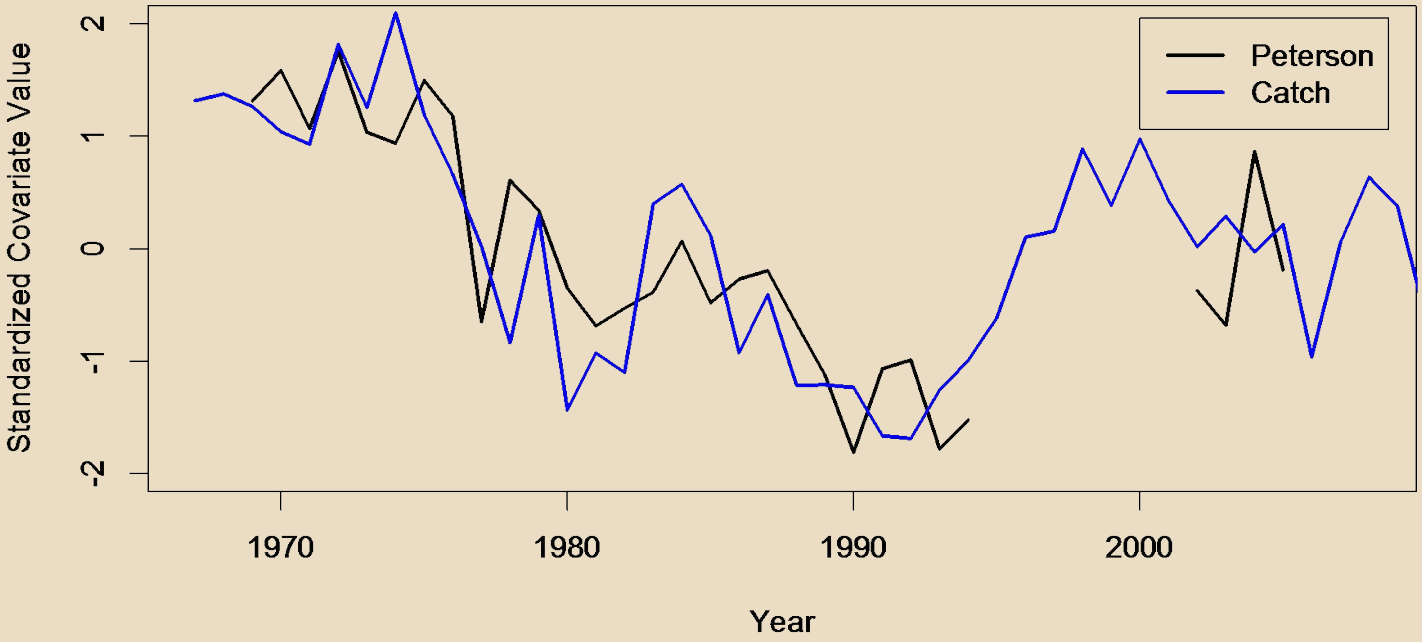

WR escapement

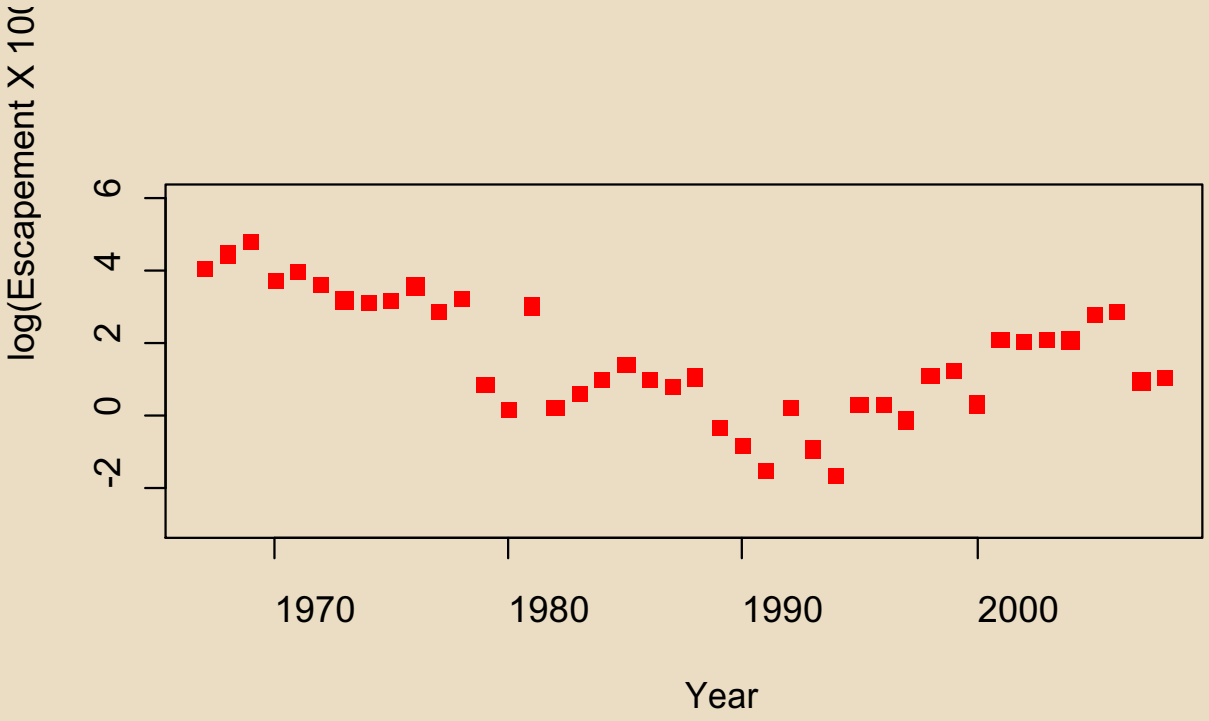

Escapement with measurement error

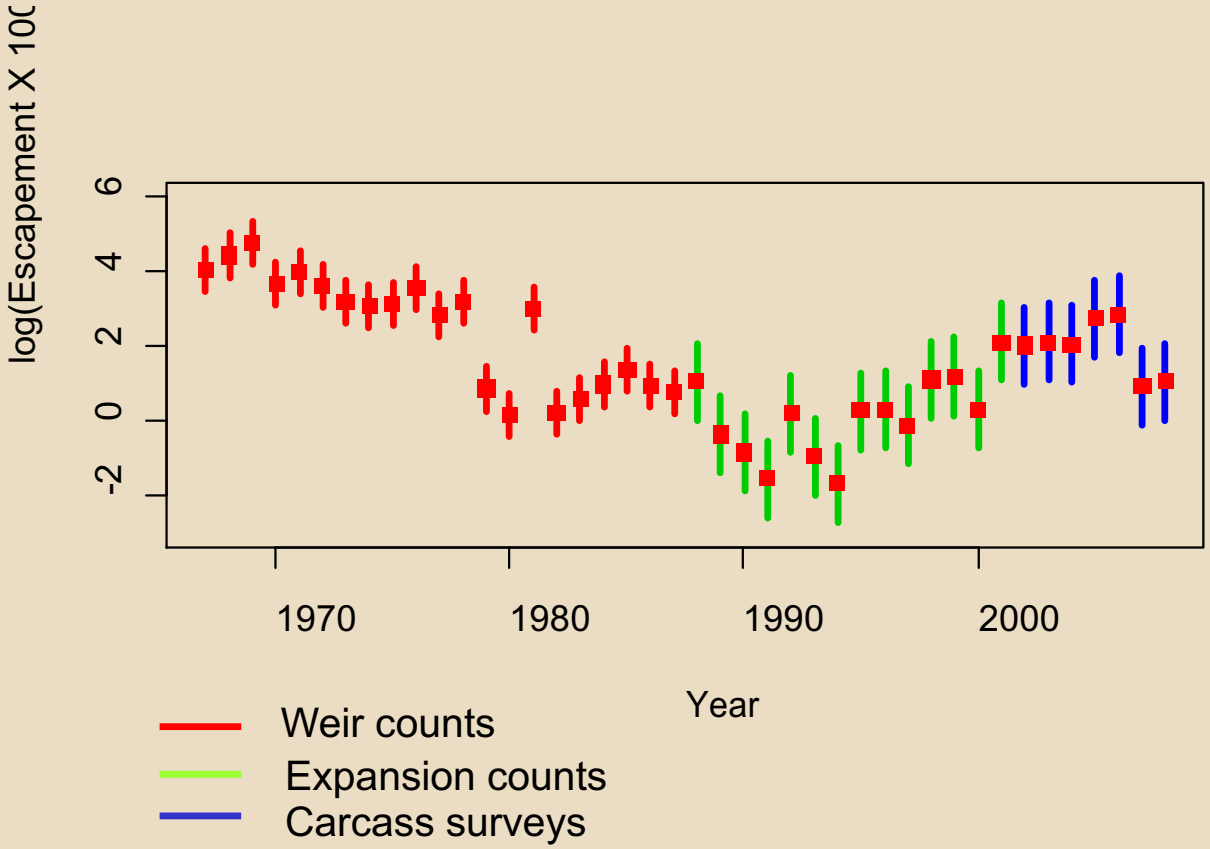

OBAN fit to WR escapement

mean predictions

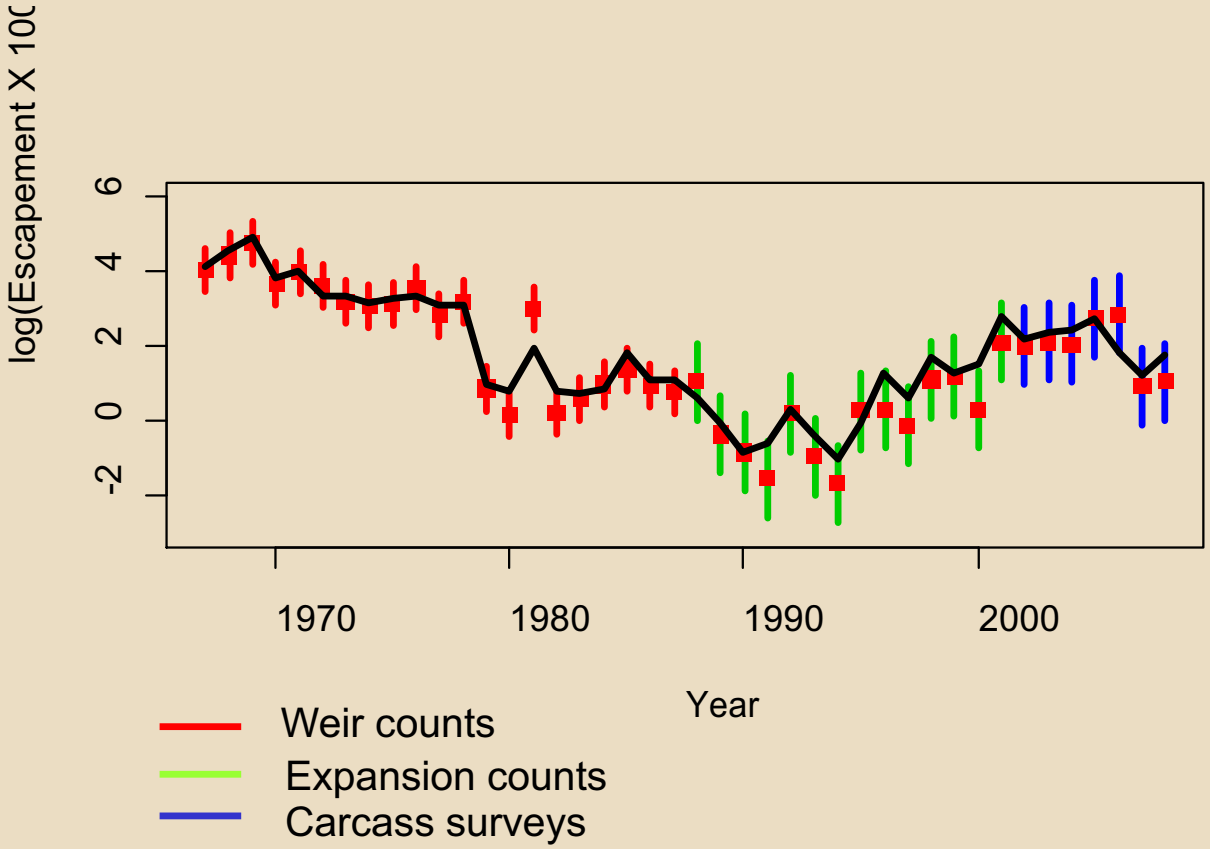

OBAN fit to WR escapement

mean predictions with 95% credible intervals

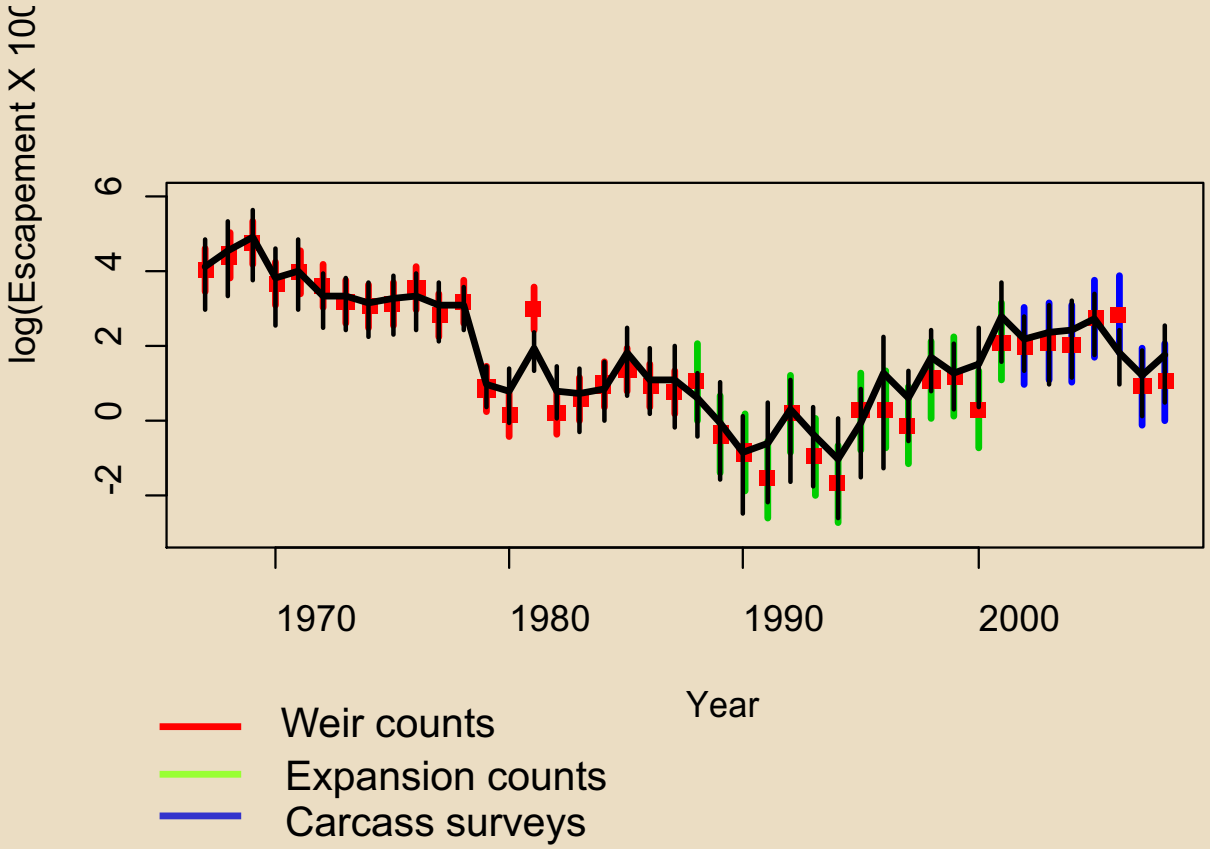

Posterior distributions of coefficients BASS log Catch

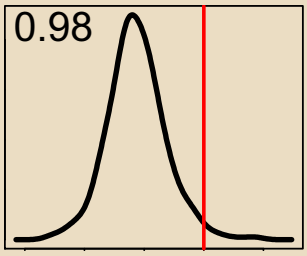

0.96

0.32

0.18

0.62

nsity

0.18

BASS:

Imputing the Peterson Abundance Index for missing years

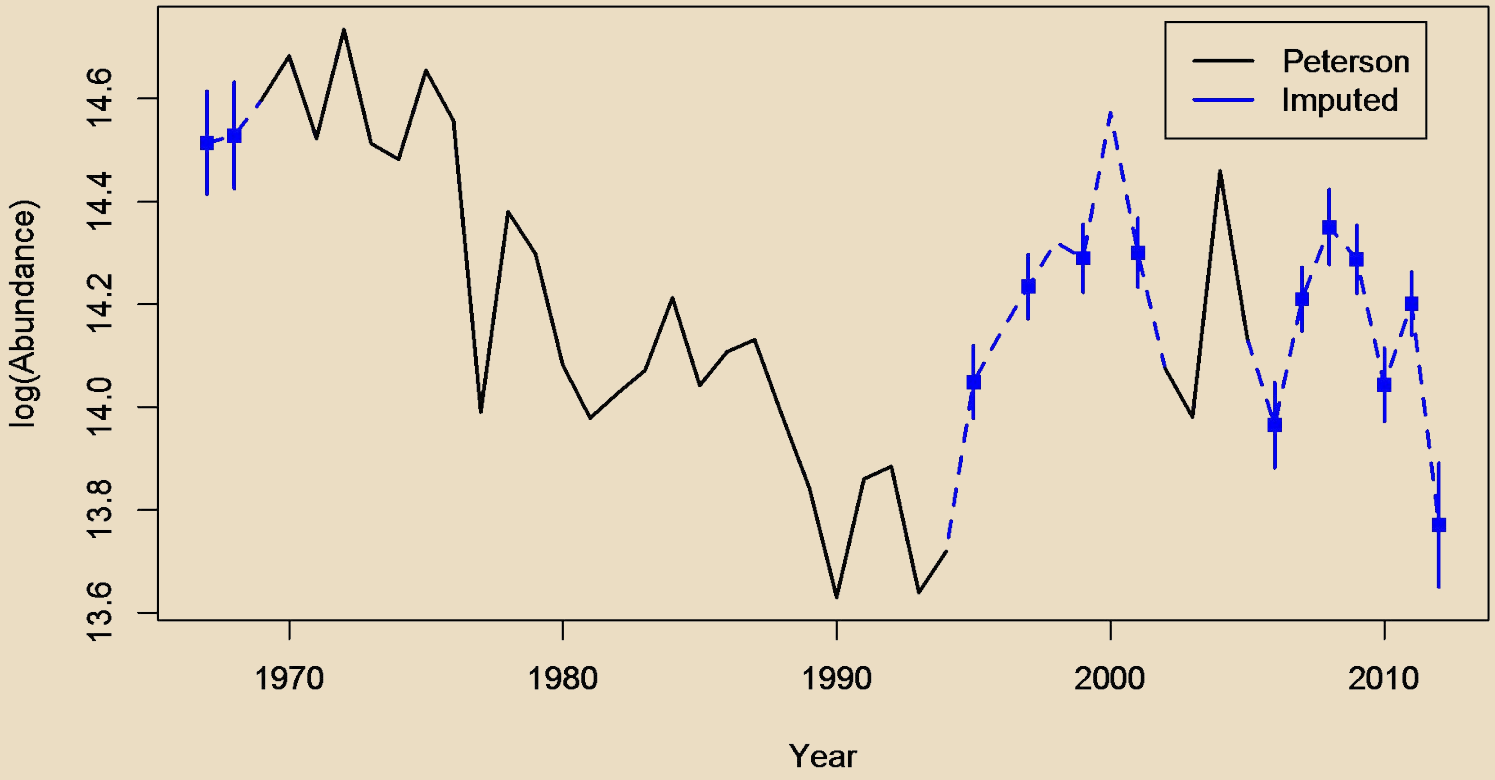

Posterior distributions of coefficients BASS log Abundance

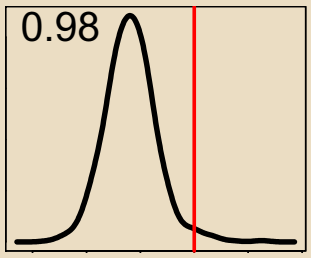

0.94

0.26

0.17

0.51

0.18

Probability Density

Winter-run Summary

- Winter OBAN factors hypothesized to increase abundance (posterior probabilities):
  - Lower temperatures in spawning reaches (0.98)
  - Increased flows during outmigration (0.82)
  - Reduced exports (0.94)
  - Increased access to Yolo bypass (0.6)
  - Decreased wind stress curl/upwelling (0.6 – 0.7)
  - Decreased striped bass (0.18)

Discussion

- Differential response to striped bass:
  - Winter-run are weakly related to striped bass Catch or Abundance*
  - Spring-run in Butte Creek negatively related to striped bass Catch
- Chinook abundance and timing of outmigration
  - Winter-run is a small component of salmon production and timing is asynchronous with other runs
  - Spring-run outmigration timing more similar to fall-run, which may be targeted by striped bass

*Abundance includes imputed values for missing years

Discussion II

Catch and Abundance* reflecting predation pressure?

- Metrics available that are better correlated to Peterson Abundance estimates – CPUE, trip success, etc.
- Striped bass predation pressure related to population dynamics
  - Catch affects abundance of striped bass adults
  - Recruitment dynamics – temporal mismatch between Peterson estimates (ages 3 to 8+) and juvenile predation
  - Juvenile bass abundance estimates and predation pressure

*Abundance includes imputed values for missing years

QUESTIONS?

Contact:
noblehendrix@gmail.com

Quartz Pool, Butte Creek
Photo Credit: Allen Harthorn, Friends of Butte Creek

Additional Slides OBAN Structure

Modeling the BH **p** parameter

logit() transformation

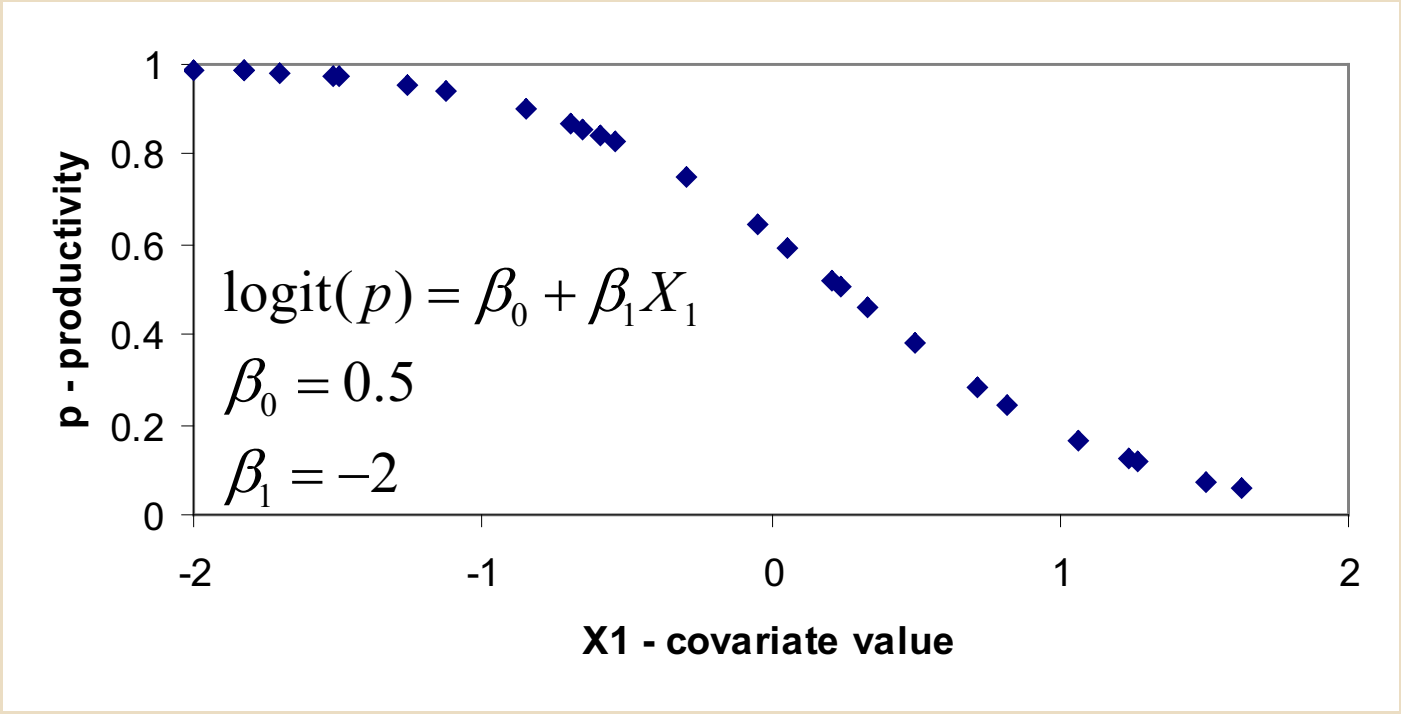

Modeling the BH **K** parameter

log() transformation

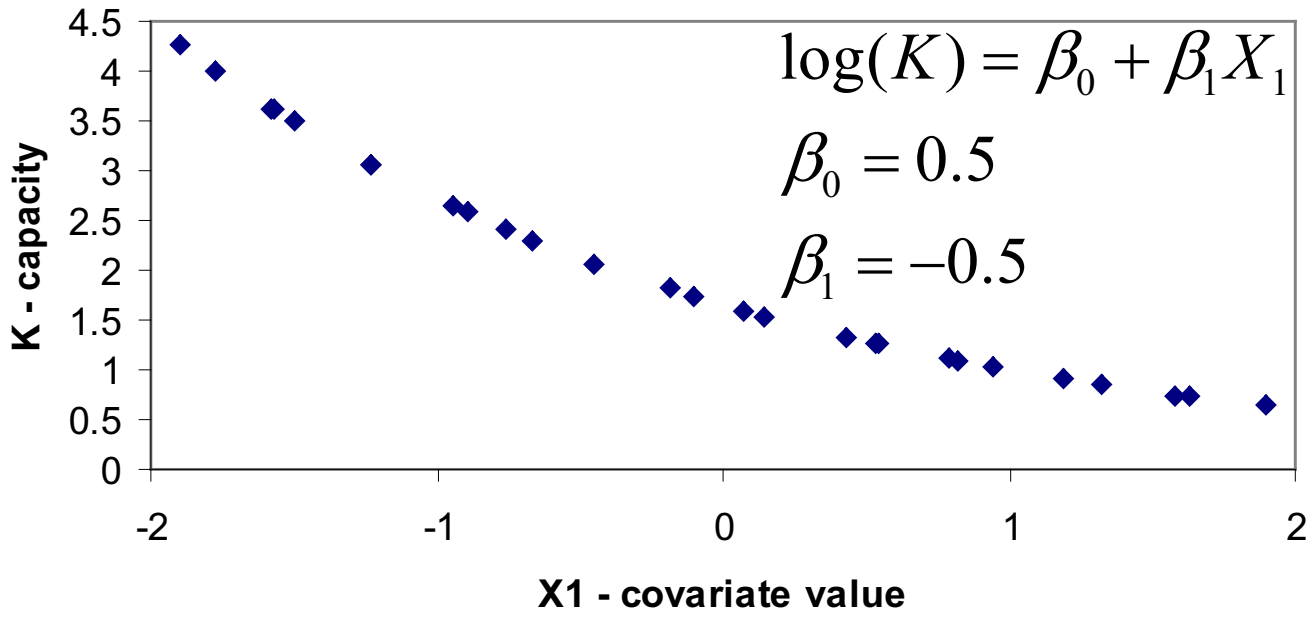

Additional Slides Spring-Run

Butte Creek spring-run life-cycle

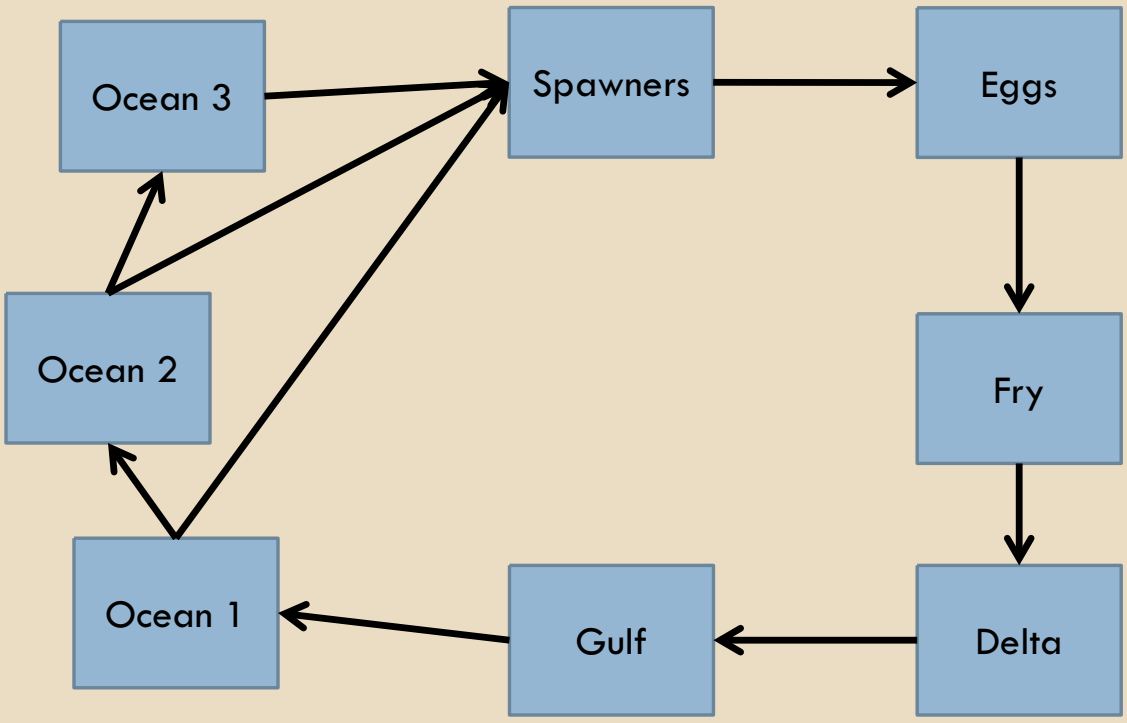

Data

- Adult escapement from 1970 to 2007 (missing 1991)
- Juvenile screw trap data (not used)
- Conditional Maturation schedule (Grover et al. 2004)
  - Age 2 - 1%
  - Age 3 - 35%
  - Age 4 - 100%

Butte Creek Juvenile data

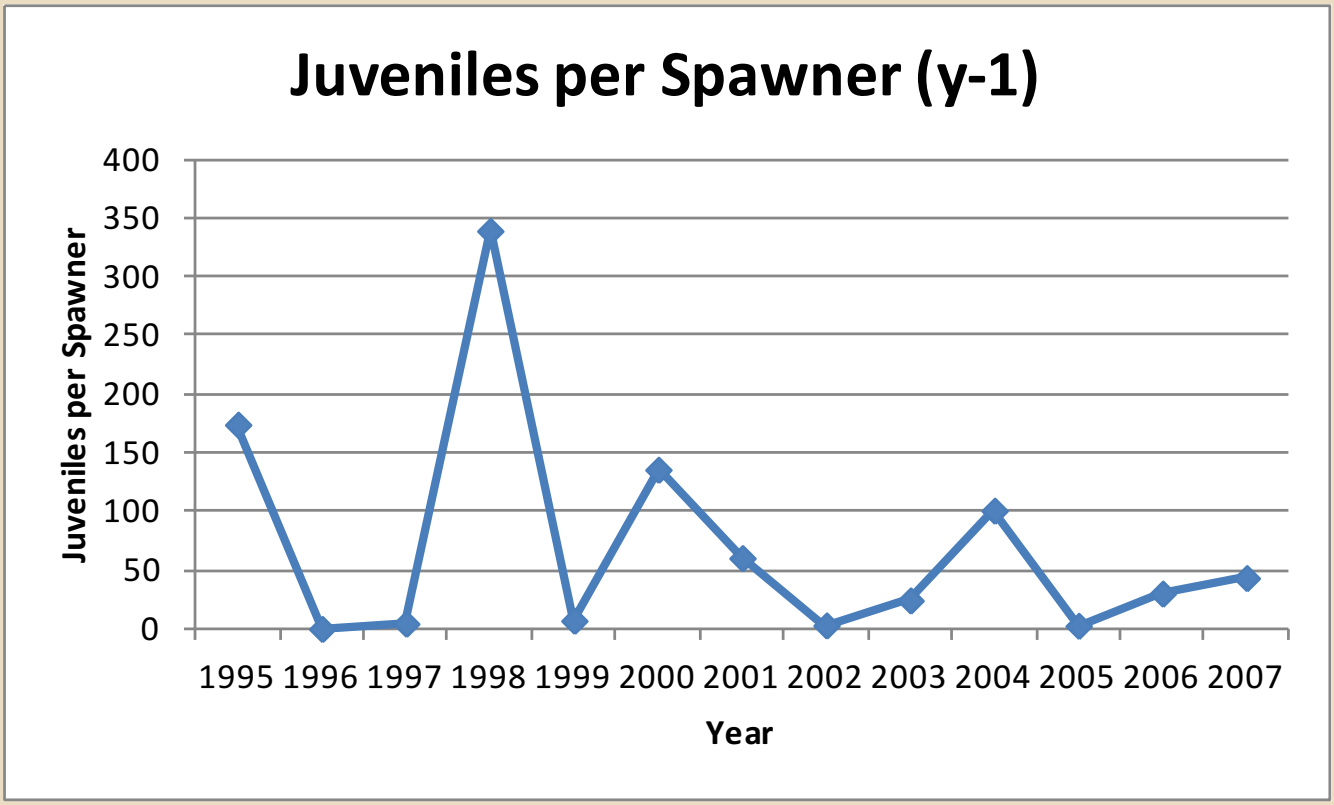

Additional Slides Winter-Run

Additional Information

- *Conditional Maturation rates*
  - *Age 2 ~ Beta(1,10), [95%CI: 0.002, 0.31]*
  - *Age 3 ~ Beta(10,1), [95%CI: 0.69, 0.99]*
  - *Age 4 = 100%*
  - Consistent with Analysis of CWT 1998 – 2000 brood years (Grover, A. 2004)
    - 0.01 – 0.17 Age 2 Maturation
    - 0.96-0.97 Age 3 Conditional Maturation Rate
    - 1.0 Age 4 Conditional Maturation Rate
- *Structuring of escapement measurement error*

$$\sigma_{weir} \leq \sigma_{carcass} \leq \sigma_{expansion}$$

Measurement error estimates from different escapement data sources

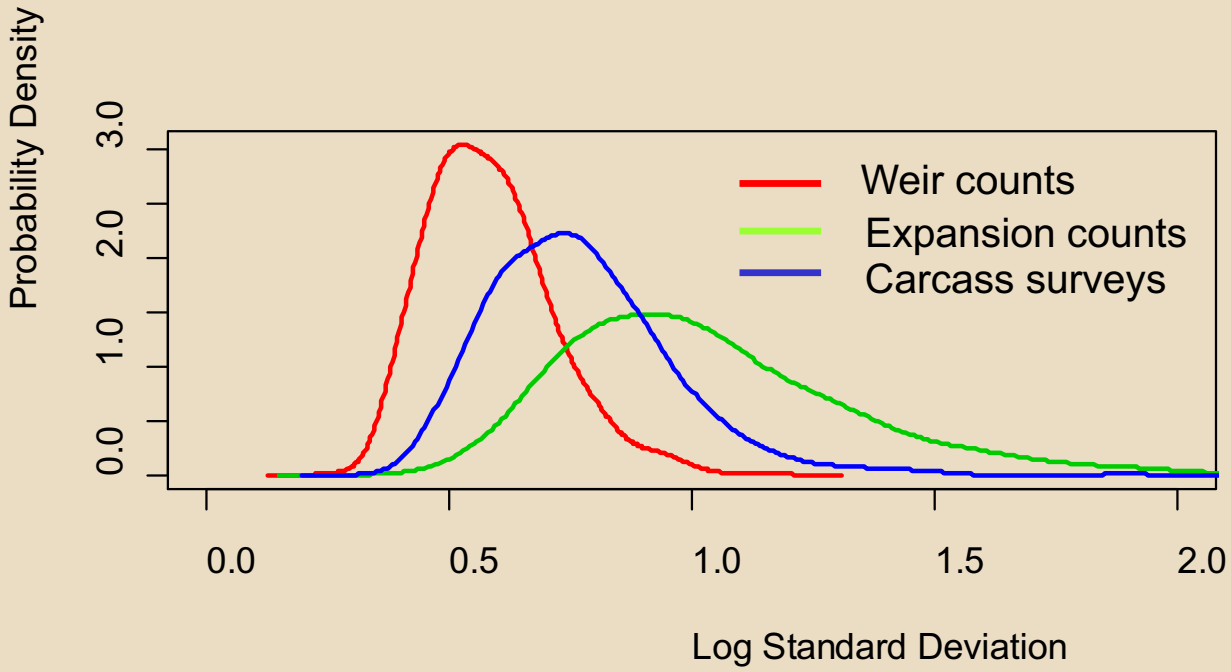

Absolute abundance estimates of juvenile spring-run and winter-run Chinook salmon at Chipps Island

Funded by

Delta Science of the Delta Stewardship Council

(previously CALFED Bay-Delta Program)

Grant Agreement Number 1049

Awarded September 1, 2007

Prepared by:

Brian Pyper[1], **Tommy Garrison**, and **Steve Cramer**
Cramer Fish Sciences
Gresham, OR

Patricia L. Brandes
U.S. Fish and Wildlife Service
Lodi, CA

David P. Jacobson and Michael A. Banks
Coastal Oregon Marine Experiment Station
Department of Fisheries & Wildlife
Oregon State University
Newport, Oregon

July 1, 2013

[1]Current address: Fish Metrics, 2027 SE Spokane St., Portland, OR

U.S.
Fish & Wildlife
Service

Oregon State University

Acknowledgments

We would like to acknowledge Jonathan Speegle for database help, Denise Barnard and Jonathan Thompson for leading the organization and checking of DNA samples, and all the biological technicians and biologists who took tissue samples at Chipps Island as part of sampling by the U.S. Fish and Wildlife on behalf of the Interagency Ecological Program (IEP). We thank Eric Volkman, Pete Hrodey, Denise Barnard and John Netto who oversaw the tissue collections at Chipps Island. We would also like to thank the California Department of Fish and Wildlife's Central Valley tissue archive laboratory for splitting tissue samples prior to sending them to Oregon State University. California's Departments of Water Resources and Fish and Wildlife graciously funded the splitting of the tissue samples. We thank Ken Newman, mathematical statistician for the Stockton FWS office, for his invaluable support and suggestions throughout the project, and Casey Justice for his contributions in developing a statistical sampling plan. We thank Delta Science for funding the project and IEP for supporting the sampling at Chipps Island.

Table of Contents

List of Figures

List of Tables

Executive Summary

In this study, we estimated juvenile Chinook salmon abundance by run using catch in midwater trawling at the confluence of the Sacramento and San Joaquin Rivers and entrance to San Francisco Bay near Chipps Island. Juveniles captured since 1993 by this trawling effort have been assigned to run based on their length and date captured. Instead, we report the results of run assignments based on genetic (DNA) markers for trawl samples collected from October, 2007 to June, 2011. Independent blind-test data were used to estimate, and account for, error rates in DNA assignments. In a companion report, Pyper et al. (2013) examined alternative methods and data from the historical sampling period to estimate trawl capture efficiency. The results of that study were used in conjunction with the DNA run assignments to estimate total abundance of juveniles from each run reaching San Francisco Bay.

Across years, DNA assignments indicated that fall run composed between 84.0% and 92.8% of the annual juvenile abundance, late-fall run composed 1.9% to 4.4%, and Butte Creek spring run ranged between 3.9% and 9.0%. Mill-Deer creek spring run and winter run each composed less than 3% of the total abundance in 2008, and less than 2% in subsequent years. However, estimates of DNA assignments were highly uncertain for late-fall run and Mill-Deer spring run due to uncertainty in potential misclassifications of true fall run to these runs.

DNA-based estimates of race composition often differed substantially from those based on length-at-date criteria. Across all four years, more fish were assigned to fall run (+2.4%), and far fewer fish were assigned to spring and winter runs based on DNA compared to length criteria. Winter-run DNA assignments had the closest fit to their expected length-at-date range, with only a few fish overlapping the adjacent late-fall and spring ranges. However, relatively large numbers of fall, late-fall, and spring run fish overlapped with the winter-run length criteria. Similarly, large numbers of fall run (based on DNA) overlapped with the spring-run length criteria. Consequently, use of DNA assignments provided much more accurate, and reduced, annual estimates of run composition for the spring and winter runs, which were one half to one sixth of the run compositions based on length criteria across years.

Juvenile abundance was estimated assuming that trawl efficiency was constant across biweekly periods and years. Abundances were compared for four different efficiency estimates (Pyper et al. 2013), including three empirical estimates that were independently derived using coded-wire-tag release data (Pyper et al. 2013). The fourth approach examined was the “fish flux” method of Kimmerer (2008), which had an implied efficiency that was substantially higher than the empirical estimates, and was considered to be likely biased.

The ranges in annual abundances from 2008 (August 1, 2007 to July 31, 2008) to 2011 based on the trawl efficiency estimate for Jersey Point releases (the midrange of empirical estimates) were as follows: 1.4 million to 7.5 million for fall run; 71thouand to 186 thousand for late-fall run; 67 thousand to 331 thousand for Butte Creek spring run; 36 thousand to 92 thousand for Mill-Deer

creek spring run; and 45 thousand to 63 thousand for winter run. Annual abundances were lowest for all runs in 2008, while the highest abundances were observed in 2011 for fall and late-fall runs, and in 2010 for spring and winter runs. The most precise estimates of annual abundance were for fall run, with coefficients of variation (CVs) of 21% or less. Abundances of were also relatively precise for Butte Creek spring run (CVs of 30% or less) and winter run (37% or less). Abundance estimates for late-fall run and Mill-Deer creek spring run were very imprecise (CVs > 75%) due to uncertainty in potential misclassifications of true fall run.

While the precision estimates for Butte Creek spring run and winter run are encouraging, they should be interpreted cautiously because abundances were sensitive to the choice of efficiency estimate (a roughly two-fold difference among the three empirical estimates), and because efficiency was assumed to be constant over time. It is currently unclear which of the efficiency estimates we examined is most accurate, and to what extent trawl efficiency may vary seasonally or among years. These and other uncertainties we identify warrant further investigation.

Introduction

Two of the most important metrics for monitoring anadromous salmonid populations are the abundances of spawners and the number of juveniles they produce. In the Central Valley of California where adult Chinook salmon production supports major fisheries in the ocean and freshwater, the numbers of juveniles leaving freshwater during the spring has been sampled annually since 1978 by means of midwater trawling in the San Francisco Estuary near Chipps Island (Figure 1) (Brandes and McLain 2001). Chipps Island is located downstream from the junction of the Sacramento and San Joaquin rivers, and thus is located where all juvenile Chinook salmon produced in the two basins must pass enroute to the ocean. The area sampled near Chipps Island is relatively constricted (3/4 of a mile across the channel), which provides the most concentrated opportunity for sampling juveniles as they leave the Central Valley.

Since 1993, trawling has also occurred at Chipps Island in other months of the year to estimate juvenile abundance by run. The four runs in the Central Valley and more specifically the Sacramento River basin are fall, late-fall, spring, and winter run (Fisher 1994). The San Joaquin tributaries support only a fall-run population. These runs are named after the season in which adults return to freshwater. Winter run is listed as endangered and spring run is listed as threatened under the federal Endangered Species Act (ESA)(NMFS 1994), and thus distinction of these runs and estimation of their abundance is critical to gauging the success of management actions aimed at recovering these stocks. Abundance at Chipps Island has historically been estimated using two methods to expand catches: (1) using the proportion of time and channel width sampled to expand catches; and (2) using an estimate of trawl efficiency to expand catches (USFWS 1997). Trawl efficiency is based on the proportion of marked fish surviving to the trawl and recovered in the trawl from releases made upstream, corrected for sampling effort. Differences in abundance estimates between methods of catch expansion have raised uncertainty as to which method is most reliable.

In addition to uncertainty regarding catch expansion, genetic analyses indicate that length-at-date methods used to apportion total juvenile abundance into the various runs of Chinook salmon have been inaccurate. Those methods used length and date of capture to assign fish to a given race (Fisher, 1992 and S. Greene, California Department of Water Resources, pers. comm.). Because the fall run composes over 90% of adult Chinook returning to the Central Valley (CHINOOKPROD, www.fws.gov/stockton/afrp/, accessed 6/20/13), small errors in classification of individuals from this run can cause large errors in the numbers assigned to other runs.

In recent years, genetic markers have been developed that make it possible to distinguish race of Chinook with greater than 95% accuracy (Banks and Jacobson 2004). Fin tissue for DNA analysis was collected for 6 years from a subset of juveniles sampled at the Delta fish facilities, and results showed that true winter run (determined by DNA) composed between 4 to 84% (with an average of 49%) of the juvenile salmon that were designated as winter run based on length-at-date criteria (Hedgecock 2002). Although most genetic winter run were within their designated

length-at-date range (95.5%), roughly half the Chinook in that length range were actually of a different run (Hedgecock 2002). These results indicate that use of length-at-date criteria can result in large overestimates of juvenile winter-run abundance. The length-at-date method may be even less accurate for spring run because their length and time of juvenile migration overlap considerably with the fall run.

To reduce these sources of uncertainty, the study reported here was designed with two objectives: (1) to determine the most reliable methods for expanding trawl catches to total abundance; and (2) to sample genetic composition of the juvenile catches at Chipps Island and estimate the abundance that each genetically distinct group composed. Expansion of trawl catches to total abundance is based on estimates of capture efficiency (proportion of available fish captured). Chipps Island trawl efficiency was estimated using several alternative methods and is the focus of a separate report (Pyper et al. 2013). Here, we focus on the results of genetic sampling of juvenile salmon catches from October, 2007 to June, 2011 to estimate the abundance and proportionate contribution to total juvenile production from each run. Note that catches of fall, spring and late-fall run within each annual period likely incorporate progeny from two brood years. Although we report abundance estimates of all four runs, our focus is on spring and winter run because (1) the statistical power of individual-based genetic assignments of these runs is more established than for the other runs (Banks 2005), and (2) there is an urgent need for accurate estimates of their juvenile abundance to facilitate understanding of their population dynamics and status (Cramer et al. 2004).

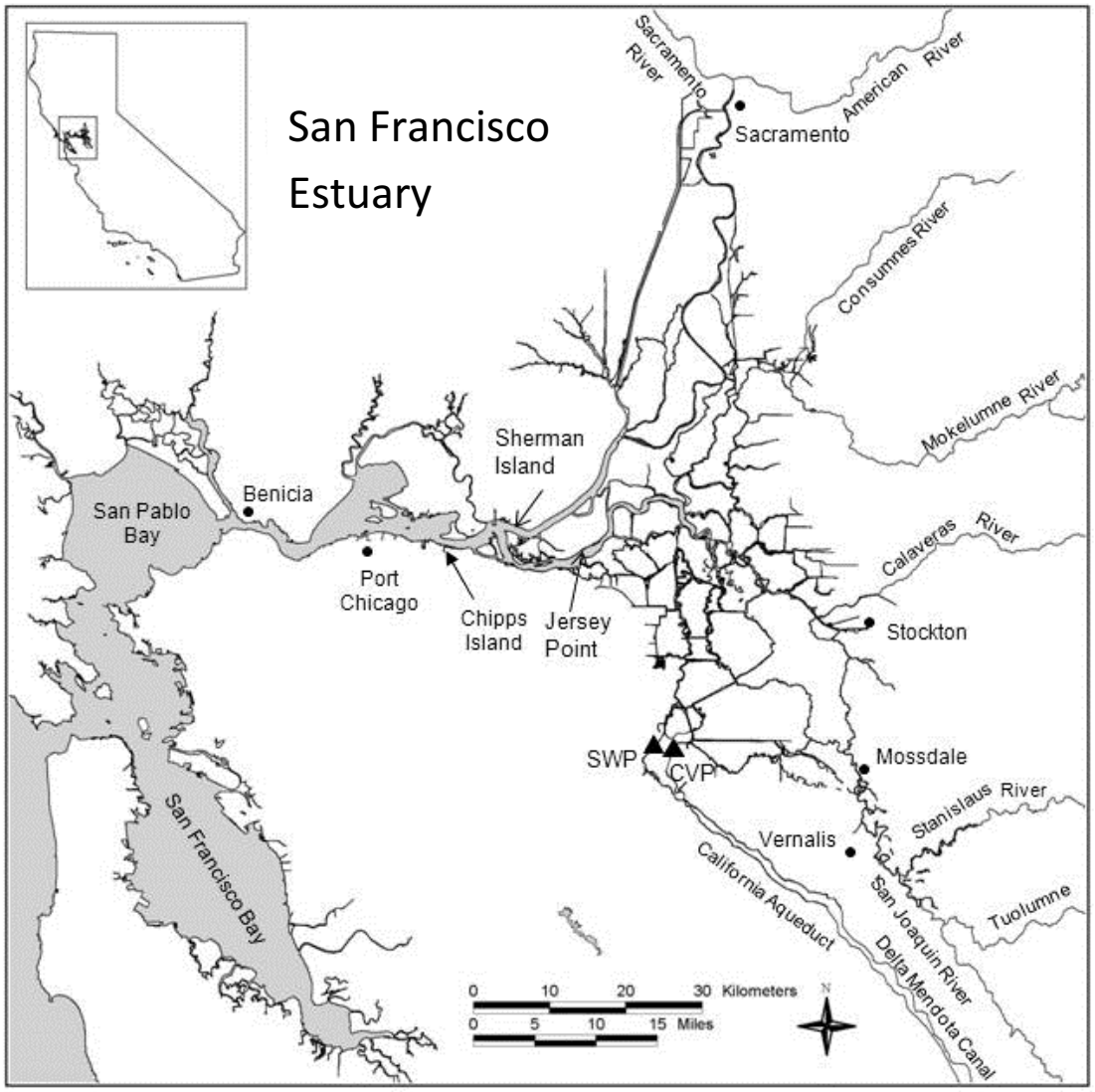

Figure 1. Map of San Francisco Estuary showing location of Chipps Island where trawling for smolts has been conducted annually.

Methods

The following sections describe the steps we used to estimate absolute abundances (N) by run of juvenile Chinook salmon migrating past Chipps Island. A simple overview of the key sampling processes and estimators is shown in Figure 2; actual estimates were more complicated. In short, there were three main steps to estimating absolute abundances: (1) estimation of "corrected" run assignments (x) in samples of trawl catch based on observed DNA assignments (y) and blind-test data; (2) estimation of total catch (X) by run given the fraction (f) of catch sampled; and (3) estimation of total abundance (N) given estimates of trawl efficiency (E) and trawl effort (p).

Data collection

Chipps Island trawl

Midwater trawling has been conducted at Chipps Island between April and June since 1978. This sampling was initiated to gain relative abundance and survival information on juvenile salmon emigrating from the Delta towards the Pacific Ocean (Brandes and McLain, 2001). In October, 1993, sampling was expanded to continue through June, 1994 and since October of 1994 year-round sampling has been conducted to better understand the temporal patterns of juvenile salmon emigration downstream. Generally, ten 20-minute tows were conducted three to seven days each week from April to June (Brandes and McLain, 2001). Sampling was conducted seven days per week during recovery of experimental releases of coded-wire-tagged (CWT) salmon (usually December-January and April-May) to increase the numbers recovered from these experimental fish released upstream and in the Delta.

Trawls were conducted within a 3 km section of river upstream of the western tip of Chipps Island (Brandes and McLain, 2001). Trawls were conducted in both directions (upstream and downstream) regardless of tide in three channel locations: north, south, and middle. Occasionally, inclement weather, mechanical problems, or excessive delta smelt or salmon catch reduced tow duration or number of tows per day.

Between October, 2007 and June, 2011, ten 20-minute tows were usually conducted two to three days per week but at times, tow duration was reduced or days were cancelled to stay within daily or annual delta smelt incidental take limits as managed through the Interagency Ecological Program. For instance, between February 5 and March 10 of 2008, trawling at Chipps Island was cancelled due to concerns about high delta smelt incidental take. A similar curtailment period occurred between June and October of 2007. During some periods, tows were limited to as little as 5 minutes to assess delta smelt take prior to conducting tows of 15 or 20 minutes.

Recent measurements conducted in 2009 determined that the trawl net fished at Chipps Island has a mean effective-fishing mouth size of 12.7 m^2 (Whitesel) or 13.0 m^2 (Confluence) depending on the vessel used (preliminary unpublished data). These values differ from the value of 18.5m^2 reported in Brandes and McLain (2001), which was based on fishing-net dimensions

reported in 1993 (USFWS 1994). Importantly, measurements of volume sampled in the current trawl database (and used in this report) do not reflect these changes in mouth size (i.e., database volumes and those reported here are based on an assumed mouth size of 18.5 m^2). However, there was only one instance – in the estimation of abundance using the "fish flux" method discussed below – where modifications were required to incorporate the recent (improved) estimate of effective-fishing mouth size.

Fin tissue for DNA analysis was collected from juvenile Chinook salmon captured in the trawl sampling conducted at Chipps Island per a modified sampling plan.

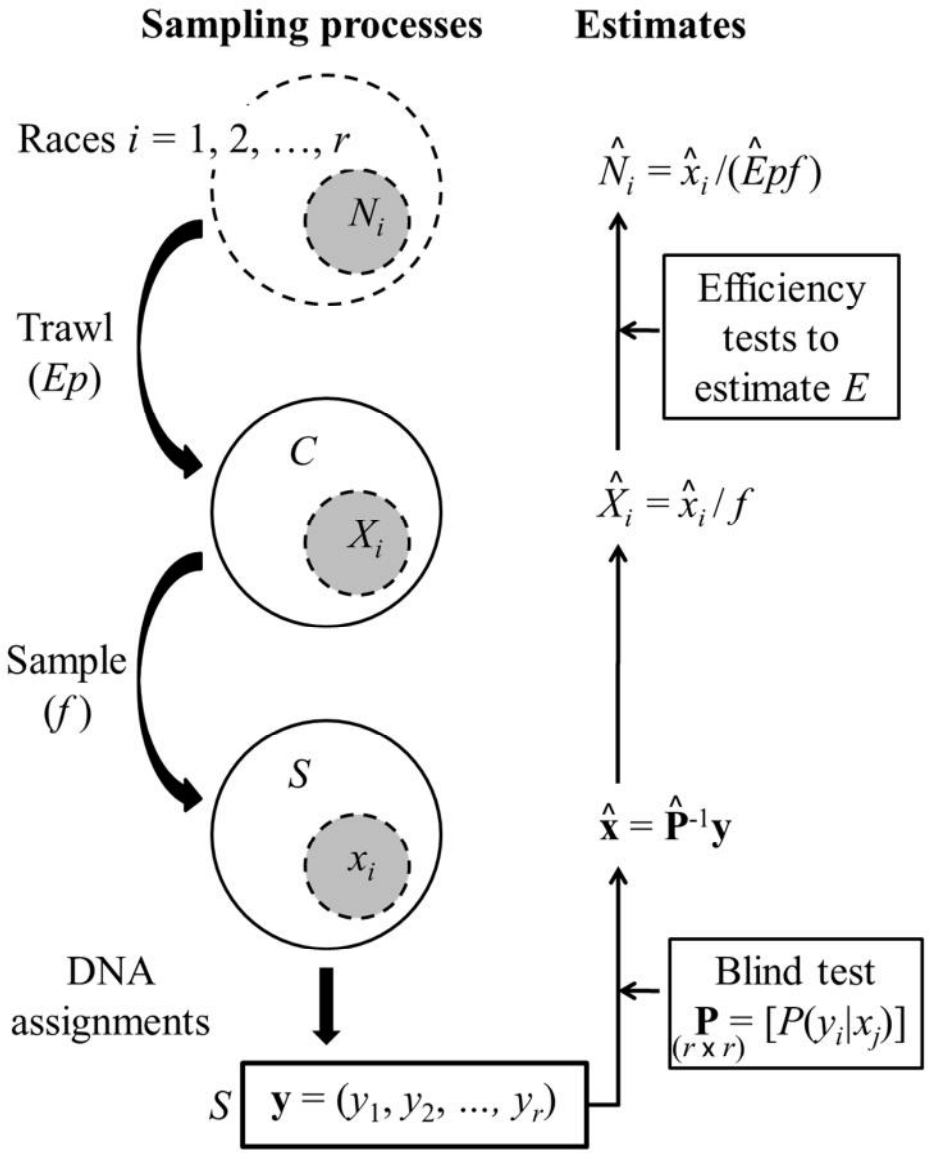

Figure 2. Overview of sampling process and estimators that lead to total abundance estimates. Race is the same as run (e.g. winter run).

Sampling plan

The original sampling plan (Attachment A) recommended tissue collection from all unmarked juvenile salmon caught between December and June that had lengths either within or greater than the river model's length-at-date criteria for winter run (Fisher, 1992). Juvenile salmon within the spring run and fall run length-at-date criteria were also to be tissue sampled, but maximum sample sizes were specified depending on the length class and time of year. This original plan was designed to optimally allocate the annual target of 3000 samples for evaluating winter and spring run, recognizing that many fall run would likely be included in the spring length-at-date criteria, and a few true spring run would be included in the fall-run length-at-date criteria.

It should be noted that almost 100% of hatchery late-fall run, winter run, and spring run were marked with CWTs during these sample years and, thus, were not tissue sampled (Kormos et al. 2012; USFWS 2011, p.186). In addition, since 2007, a minimum of 25% of the fall-run hatchery production from the Central Valley hatcheries has been marked and tagged (USFWS, 2011). Thus some of the unmarked juvenile Chinook salmon sampled for tissue for this study were unmarked fall-run hatchery fish.

The original sampling plan was modified during the first year of the study because of the unexpected curtailment (temporarily) in February, 2008, and reduction of sampling at Chipps Island thereafter, due to delta smelt take concerns. Given reduced sampling and a coincidental reduction in salmon abundance, attempts were made to tissue sample all juvenile salmon caught in the trawl, with some minor exceptions. Some sub-sampling was incorporated during late April and early May when many unmarked fall-run hatchery fish were assumed to be in the catch, based on the number of tagged hatchery fish being caught. During those times, 5 fish in the fall-run length-at-date category were to be tissue sampled per tow (50 per day). In addition, juvenile salmon under 50 millimeters were not sampled because it was determined that tissue sampling would cause mortality.

After sampling at Chipps Island was interrupted in February 2008, we obtained permission from California Bay-Delta Authority (our funders at the time) and modified our ESA take permit to allow tissue sampling of juvenile salmon collected near Sacramento in regular IEP trawling between March 2008 and June 2011. These tissue samples were processed for genetic run designation and will be the basis for future analyses.

Sampling protocols for collecting tissue from juvenile Chinook salmon captured in the trawl at Chipps Island were similar to those at the State Water Project (SWP) and Central Valley Project (CVP) fish facilities, although samples were placed on filter paper and air dried instead of using a buffer solution as has been the protocol at the SWP and CVP (Harvey et al. in press). A 1 X 2 mm or 2 X 4 mm triangular piece of tissue was taken in the field from the top or bottom lobe of the caudal fin shortly after a juvenile was caught. The tissue was placed on filter paper, folded over twice, and inserted into a labeled coin envelope for drying back in the laboratory, prior to

placing it in a plastic bag for longer-term storage. Samples were given a unique ID number and were linked to individual catches in the trawl catch database.

Once organized and checked, tissue samples were sent to the California Department of Fish and Game's (now California Department of Fish and Wildlife) Central Valley Archive lab for splitting. Samples were then sent to Michael Banks's genetics laboratory at Oregon State University for analyses and run determination. Note that some juveniles were tissue sampled but were not included in the final run-assignment data because their tissue samples were lost, damaged, or yielded inconclusive run assignments (i.e., no run assignment was given).

Genetic analyses and run assignments

Samples where characterized using a 21 microsatellite panel named HMSC21 using protocols detailed in Banks et al. (in review). HMCS21 includes the following loci: *Ots-104, -107* (Nelson and Beacham 1999); *Ots-201b, -208b, -209 -211, -212, -215* (Greig et al. 2003); *Ots-G78b, -G83b, -G249, -G253, -G311, -G422, -G409* (Williamson et al. 2002); *Ost515* (Naish and Park 2002); and five microsatellites derived from research characterizing alternate copies of the circadian rhythm transcription factor C*ryptochome*, including *Cry2b.1, Cry2b.2, Cry3* (O'Malley et al. 2010), *Ots-701* (GeneBank accession # KF163438), and *Ots-702* (GeneBank accession # KF163440) . Alternate microsatellite alleles were resolved through electrophoresis utilizing an Applied Biosystems (AB) 3730xl DNA analyzer and scored using AB GeneMapper software (Version 4).

Data for the 21 microsatellites for each sample were assessed against the Hatfield Marine Science Center HMSC21 baseline utilizing the "assign individual to baseline population" option available in the computer application ONCOR (Kalinowski 2008 *www.montana.edu/kalinowski/Software/ONCOR.htm)* to determine the most likely sub-population origin for each sample. Data in this baseline are comprised of five primary sub-populations as described in Banks et al. (2000). These sub-populations or runs are named fall, late-fall, winter, and two reproductively isolated spring runs: (1) spring run from Butte creek; and (2) spring run from neighboring Mill and Deer creeks. The fall run sub-population includes mainstem spawning populations from throughout the Sacramento and San Joaquin as well as both early (putative spring) and late (putative fall) returns to the Feather River (spring run) because of difficulty in resolving sub-structure among these stocks (Banks et al. 2000; Hedgecock et al. 2001).

ONCOR assigns individuals in a mixture sample to the baseline population that has the highest probability of producing the given genotype in the mixture. Emphasis is placed on the phrase "in the mixture" because ONCOR uses both genotype frequencies and mixture proportions when estimating the origin of individuals. ONCOR performs these calculations as follows. Let p_{ij} denote the probability that individual i (of unknown origin) belongs to baseline population j. This probability p_{ij} can be estimated from the genotype frequencies in each baseline population and an estimate of the stock composition of the fishery. Let f_{ij} be the frequency of the ith fish's

genotype in the *j*th population and let m_j be the estimated stock composition of the sample. Following Rannala and Mountain (1997), an estimate of p_{ij}, which we refer to as the run assignment probability, is given by

$$\hat{p}_{ij} = \frac{m_j f_{ij}}{\sum_j m_j f_{ij}} . \quad (1)$$

Typically when using genetic assignment data, an overall assignment error rate is controlled for by determining a run assignment probability threshold at which individual observations are discarded. This allows for determination of a false-positive detection rate (i.e., Type I error in statistical hypothesis testing). For instance, Harvey et al. (in press) used blind-test data (described below) and a bootstrap procedure in an attempt to control for assignment error rates by determining a threshold that would yield a desired test-wide error rate. However, their results were inconclusive because the desired error rate was either never achieved for a run (i.e., too few fish were miss-assigned), or error rates were only achieved at the highest assignment probability of 1.00, which would require exclusion of all fish with assignment probability ≤ 1.00. Furthermore, the blind-test evaluations revealed that ONCOR assignment probabilities did not correlate well with actual assignment accuracy for some runs (Harvey et al. in press). Thus, we did not attempt to restrict assignment data based solely on a threshold value for ONCOR assignment probability. Instead, we used blind-test data to quantify and account for likely assignment errors, as outlined in the next section.

Sample estimates of corrected assignments by run

We utilized blind-test data of 623 known origin Chinook adult salmon to account for false positive (wrongly assigning any other run to be run of interest) and false negative (wrongly assigning run of interest to be any other run) error rates when estimating abundances by run in samples of trawl catch. A complete description of the adult sampling and genetic analyses of the blind-test data is found in Banks et al. (in review). Determining assignment error rates from blind-test data allows us to compute "corrected" estimates that should more accurately reflect the "true" numbers of fish by run in a given field sample.

Run assignment corrections: Example with two runs

The following example uses blind-test data to correct a new sample of assignments when there are only two runs, *a* and *b*. Let *n* be the total number of fish in the sample, let *y* be the number assigned by run, and let *x* be the true number of fish by run. The expected number of fish assigned to run *a* in the sample is given by (Ken Newman, personal communication):

$$E(y_a) = x_a P(a \mid a) + x_b P(a \mid b) , \quad (2)$$

where $P(a|a)$ is the conditional probability that a fish of run *a* is correctly assigned as run *a* and $P(a|b)$ is the probability that a fish of run *b* is incorrectly assigned as run *a* (i.e. the false positive

error rate). To express Equation (2) as function of the false negative error rate, the following two substitutions are made

$$x_b = n - x_a$$
$$P(a \mid a) = 1 - P(b \mid a), \tag{3}$$

where $P(b|a)$ is the false negative error rate. The method-of-moments approach (e.g., Mood et al. 1974, p. 274) can then be used to solve for x_a:

$$\hat{x}_a = \frac{y_a - nP(a \mid b)}{1 - P(a \mid b) - P(b \mid a)}. \tag{4}$$

The blind-test data is used to estimate $P(a|b)$ and $P(b|a)$ by constructing a 2×2 table T where the rows are the numbers of fish assigned to runs a and b based on genetics and the columns are the true known numbers of run a and b

		True Run	
		a	b
Genetic Assignment	a	T_{aa}	T_{ab}
	b	T_{ba}	T_{bb}

Conditioning on the true values (i.e., the column totals), the estimates of false positive and false negative error rates are then given by

$$P(a \mid b) = T_{ab} / (T_{ab} + T_{bb})$$
$$P(b \mid a) = T_{ba} / (T_{aa} + T_{ba}). \tag{5}$$

Run assignment corrections: Example with several runs

The approach above can be generalized for a set of runs $i = 1, 2, \ldots, r$. In brief, for each run, we can specify an equation for the expected assignment ($E[y_i]$) analogous to Equation (2). This provides a classic "system of linear equations" that has a vector-matrix form $\mathbf{y} = \mathbf{Px}$, where the vector $\mathbf{y}$ is the set of expected run assignments $\{E[y_i]\}$, the column vector $\mathbf{x}$ is the set of true numbers by run $\{x_i\}$, and $\mathbf{P}$ is an $r \times r$ matrix (with rows i and columns j) of conditional probabilities, $P(i|j)$ (i.e., the probability that a fish of true run j is assigned to run i, where $j \in i$). Given an estimate of $\mathbf{P}$ from blind-test data and a new sample of assignments $\{y_i\}$, we can estimate the true numbers by run

$$\hat{\mathbf{x}} = \hat{\mathbf{P}}^{-1}\mathbf{y}, \tag{6}$$

where the column vector $\mathbf{y} = (y_1, y_2, \ldots, y_r)$ holds the observed run assignments and $\hat{\mathbf{P}}^{-1}$ denotes the matrix inverse of $\hat{\mathbf{P}}$. We refer to these estimates of x_i as "corrected run assignments." As discussed below, negative estimates of x_i can occur and require special consideration.

The blind-test data are used to estimate each entry in the matrix **P**. Let T be an $r \times r$ table where the rows are the assigned numbers by run i and the columns are the true known numbers by run j ($j \in i$). An estimate of $P(i|j)$ is obtained by

$$\hat{P}(i \mid j) = T_{ij} \big/ T_{\cdot j} \ , \tag{7}$$

where $T_{\cdot j}$ is the sum across all entries i in column j. The false positive and negative error rates are the off diagonal elements of $\hat{\mathbf{P}}$.

To estimate the variance of each estimate $\hat{x}_i$, we used a parametric bootstrap procedure. Specifically, we assumed that each column of T (the blind-test data) was an independent multinomial sample with probabilities $\hat{P}(i \mid j)$, and accordingly, generated 1,000 bootstrap replicates for **P** and hence $\mathbf{P}^{-1}$. We then estimated the variance-covariance matrix of $\mathbf{P}^{-1}$, denoted **Q**, and used the relevant component of this matrix (i.e., the ith row) to estimate the variance of $\hat{x}_i$ given a new sample of assignments **y**:

$$\hat{\sigma}^2_{\hat{x}_i} = \mathbf{y}' \hat{\mathbf{Q}}_i \mathbf{y} \ . \tag{8}$$

Note that in this report, we unintentionally omitted an important source of variance in the corrected estimates $\hat{x}_i$ (Ken Newman, U.S. Fish and Wildlife Service, pers. comm.). In the formulation above, the observed assignments $\{y_i\}$ in a given sample are assumed to be multinomial variables conditional on the true numbers by run $\{x_i\}$ and true probabilities $\{P(i|j)\}$. However, Equation (8) only accounts for uncertainty in estimates of $P(i|j)$ derived from blind-test data, and hence, we ignored the multinomial variation or "sampling error" associated with each new sample $\{y_i\}$ that should also be accounted for in the variance estimate for $\hat{x}_i$. As noted in the Discussion, we do not expect (in general) that this omission would have large effects on our estimates and conclusions regarding precisions of abundance estimates, in particular for annual estimates.

Application of blind-test data

The blind-test data provided by Banks et al. (in review) are shown in Table 1. Sample sizes were large for true fall and winter run, whereas very few spring run were collected, particularly from Mill and Deer Creek. After examining the data in relation to ONCOR assignment probabilities,

we determined that there was merit in splitting the blind-test data into two groups: (A) run assignments with ONCOR probabilities = 1; and (B) run assignments with ONCOR probabilities < 1. Modified versions of these two datasets, which form the basis for our run-assignment corrections, are shown in Table 2. The rationale for splitting the data is evident in the assignments for true fall run and true winter run (Table 2). For example, of the 295 true fall run with ONCOR assignment probabilities = 1, only one fish (0.3%) was misclassified (assigned as late-fall run). However, of the 46 true fall run with ONCOR probabilities < 1, five fish (10.9%) were misclassified. Similarly, assignments for true winter run were very accurate for ONCOR probabilities = 1, but were incorrect in all cases for ONCOR probabilities < 1. Thus, we split the data to account for these different error rates associated with ONCOR assignment probabilities (the data were insufficient to justify further stratification by ONCOR assignment probabilities).

Due to limited data, we modified the blind-test data as follows (see Table 2). First, there were insufficient numbers of true spring Mill-Deer creek fish (n = 2; Table 1) and true spring-Butte Creek fish with assignment probabilities < 1 (only 1 fish) to provide meaningful estimates of error rates for these groups. We therefore pooled all true spring run assignments (n = 15) and assumed they were equally applicable to both Butte Creek and Mill-Deer creek spring runs for both assignment-probability categories (Table 2). Second, for assignments with ONCOR probabilities < 1, no true winter-run fish was correctly identified as winter run and no fish of a different run was incorrectly assigned as winter run. This resulted in a row of zeros in the matrix **P**, which violates a condition of matrix inversion. We therefore added one true winter run fish as being correctly assigned to winter run in this probability category (Table 2).

Table 3 shows the conditional probabilities $P(i|j)$ (i.e., the probability that a fish of true run j is assigned to run i) based on the two assignment tables (Table 2). The non-diagonal entries in Table 3 are the false positive error rates (when interpreted across a given row) and false negative error rates (when interpreted down a given column). The largest error rates were observed for assignments of true late-fall run, which were often misclassified as fall run regardless of ONCOR assignment probability.

In our application, we were interested in sample estimates of true numbers by run ($\hat{x}_i$) summed across both categories of ONCOR assignment probability:

$$\hat{\mathbf{x}} = \hat{\mathbf{P}}_{\mathrm{A}}^{-1}\mathbf{y}_{\mathrm{A}} + \hat{\mathbf{P}}_{\mathrm{B}}^{-1}\mathbf{y}_{\mathrm{B}} \ , \tag{9}$$

where subscripts "A" and "B" distinguish between ONCOR assignment probabilities = 1 and < 1, respectively. Thus, a sample of assignments **y** provided two possible subsets of assignments ($\mathbf{y}_{\mathrm{A}}$ and $\mathbf{y}_{\mathrm{B}}$) depending on the data. The estimates of the conditional probability matrices ($\mathbf{P}_{\mathrm{A}}$ and $\mathbf{P}_{\mathrm{B}}$) are given in Table 3.

Table 1. Classification table of blind-test data for the number of fish by true known run and DNA run assignment.

		True run				
		Fall	Late-fall	Spring Butte	Spring Mill-Deer	Winter
DNA Assignment	Fall	333	34	1	1	2
	Late-fall	6	40	0	0	4
	Spring Butte	0	0	12	0	1
	Spring Mill–Deer	2	2	0	1	1
	Winter	0	1	0	0	168
	Total	341	77	13	2	176

Table 2. Modified classification table of the number of fish by true known run and DNA run assignment for two categories of ONCOR assignment probability.

		True run				
(A) ONCOR Assignment Probability = 1		Fall	Late-fall	Spring Butte*	Spring M-D*	Winter
DNA Assignment	Fall	294	13	2	2	1
	Late-fall	1	16	0	0	1
	Spring Butte	0	0	13	0	0
	Spring Mill–Deer	0	0	0	13	1
	Winter	0	1	0	0	168
	Total	295	30	15	15	171

(B) ONCOR Assignment Probability < 1		Fall	Late-fall	Spring Butte*	Spring M-D*	Winter
DNA Assignment	Fall	39	21	2	2	1
	Late-fall	5	24	0	0	3
	Spring Butte	0	0	13	0	1
	Spring Mill–Deer	2	2	0	13	0
	Winter	0	0	0	0	1**
	Total	46	47	15	15	6

* Column data are combined true spring-run assignments (Butte and Mill-Deer, both ONCOR probability categories)

** Not observed; one fish added to allow matrix inversions (see text)

Table 3. Conditional probabilities of run assignments (for a fish of a given true run) for two categories of ONCOR assignment probability. Off-diagonal elements correspond to false positive error rates (rows: probability of wrongly assigning a different run to be the run of interest) and false negative error rates (columns: probability of wrongly assigning the run of interest to a different run).

		True run				
(A) ONCOR Assignment Probability = 1		Fall	Late-fall	Spring Butte	Spring M-D	Winter
DNA Assignment	Fall	0.997	0.433	0.133	0.133	0.006
	Late-fall	0.003	0.533	0.000	0.000	0.006
	Spring Butte	0.000	0.000	0.867	0.000	0.000
	Spring Mill-Deer	0.000	0.000	0.000	0.867	0.006
	Winter	0.000	0.033	0.000	0.000	0.982

(B) ONCOR Assignment Probability < 1		Fall	Late-fall	Spring Butte	Spring M-D	Winter
DNA Assignment	Fall	0.848	0.447	0.133	0.133	0.167
	Late-fall	0.109	0.511	0.000	0.000	0.500
	Spring Butte	0.000	0.000	0.867	0.000	0.167
	Spring Mill–Deer	0.043	0.043	0.000	0.867	0.000
	Winter	0.000	0.000	0.000	0.000	0.167

The variance estimate for a given run-specific estimate $\hat{x}_i$ is given by

$$\hat{\sigma}^2_{\hat{x}_i} = \mathbf{y}'_{\mathrm{A}}\hat{\mathbf{Q}}_{\mathrm{A}i}\mathbf{y}_{\mathrm{A}} + \mathbf{y}'_{\mathrm{B}}\hat{\mathbf{Q}}_{\mathrm{B}i}\mathbf{y}_{\mathrm{B}} \ , \tag{10}$$

where estimates of the variance-covariance matrices ($\mathbf{Q}_{\mathrm{A}}$ and $\mathbf{Q}_{\mathrm{B}}$) were derived using the bootstrap procedure described above.

As an example of the magnitude and direction of run-assignment corrections, assume we had a sample of observed assignments with ONCOR probabilities = 1 and assignment numbers {100, 10, 5, 5, 5} for fall, late-fall, Butte Creek, Mill-Deer creek, and winter run, respectively. The corrected estimates, which are given by the first term in Equation (9) and then rounded to whole numbers, are {91, 18, 6, 6, 4} fish respectively. In this example, using the blind-test data (Table 3) to correct observed assignments had the largest numerical effect on assignments for fall and late-fall-runs, though proportional effects were also large for the numerically small assignments (e.g., the winter-run assignment changed from 5 to 4 fish, a 20% decline).

Treatment of negative estimates

Estimates of corrected assignments were often negative for the late-fall and spring Mill-Deer creek runs, in particular when these runs had very low observed assignments (y_i) relative to fall run. In such cases, we (1) set negative values of $\hat{x}_i$ to zero, (2) computed the sum $\sum \hat{x}_i$, and (3) multiplied the corrected assignments by the ratio $\sum y_i / \sum \hat{x}_i$. This procedure ensured that the total number of final corrected assignments was equal to the number of observed assignments ($\sum y_i$). For example, suppose a set of 24 observed assignments yielded corrected estimates {20, -8, 4, 4, 4}. After setting -8 to zero, $\sum \hat{x}_i$ = 32 (i.e., the non-negative corrections contain eight more fish than were actually observed). Multiplying $\{ \hat{x}_i \}$ by $\sum y_i / \sum \hat{x}_i$ (= 24/32 = 0.75) yields the final corrected estimates {15, 0, 3, 3, 3}. In sum, we set negative corrections to zero and scaled the remaining corrections in a manner that retained their relative proportions and ensured consistency between total numbers of observed and corrected assignments.

Stratification and sums across strata

To estimate abundances by run, we first stratified catch and sample data into biweekly time periods and several fork-length strata. This was done for the following reasons. First, because not all juveniles caught in the Chipps Island trawl were tissue sampled and DNA-assigned to run, some level of temporal stratification was required to expand sample estimates to the total catch. After inspecting the data, we chose biweekly periods for stratification because they provided a reasonable balance between ensuring sufficient sample sizes (i.e., to reliably apply assignment corrections and estimate run components in the unanalyzed catch) and depicting seasonal migration patterns by run. Second, with respect to fork length, we expect differences in juvenile length by run at Chipps Island (e.g., Fisher 1992). Consequently, the original sampling plan (Attachment A) recommended targeting larger juveniles during specific periods to improve

estimates for the winter and spring runs. Although such length-selective tissue sampling was largely abandoned due to limited catches, it is still useful from a statistical perspective to stratify by length because we expect differences across length strata in both run composition and sampling fractions (due to chance or non-random length sampling), in particular for larger length classes where we expect few fish but potentially high proportions of spring, winter, or late-fall run.

Two "biweekly" periods were defined for each month, with days 1-15 forming the first period and the remaining days forming the second period (e.g., days 16-30 for April or days 16-31 for May). For fish length, we defined six strata: < 80 mm; 80-89 mm; 90-99 mm; 100-109 mm; 110-119 mm; and ≥ 120 mm. In addition, data and estimates were summarized for each of four "sampling years" (2008-2011), which were defined from August 1 of the previous sampling year through July 31 of the sampling year (e.g., the 2008 sampling year comprised the period from August 1, 2007 through July 31, 2008).

Estimates of corrected run assignments ($\hat{x}_i$; Equation 9) were computed for a given biweekly period and length stratum using the sample DNA assignments for that period-length combination. We then estimated biweekly totals across length strata for each run; these are the primary estimates we report. Let t denote the tth biweekly period and k denote the kth length stratum ($k = 1, 2, \ldots, 6$). For a given run i, we are interested in the biweekly sum of corrected assignments across length strata:

$$\hat{x}_{it.} = \sum_k \hat{x}_{itk} \quad , \tag{11}$$

which has a variance estimate given by (e.g., Mood et al. 1974, p. 178)

$$\begin{aligned} \hat{\sigma}^2_{\hat{x}_{it.}} &= \sum_k \hat{\sigma}^2_{\hat{x}_{itk}} + 2\sum_k \sum_{l \neq k} \operatorname{cov}\left[\hat{x}_{itk}, \hat{x}_{itl}\right] \\ &= \sum_k \hat{\sigma}^2_{\hat{x}_{itk}} + 2\sum_k \sum_{l \neq k} \left(\mathbf{y}'_{\mathrm{A}tk} \hat{\mathbf{Q}}_{\mathrm{A}i} \mathbf{y}_{\mathrm{A}tl} + \mathbf{y}'_{\mathrm{B}tk} \hat{\mathbf{Q}}_{\mathrm{B}i} \mathbf{y}_{\mathrm{B}tl}\right). \end{aligned} \tag{12}$$

The second term of Equation (12) is the sum of estimated covariances (across all combinations of length strata k and l, where $l \neq k$) that arise because all assignment corrections ($\hat{x}_{itk}$) are based on the same estimates of $\mathbf{P}_\mathrm{A}$ and $\mathbf{P}_\mathrm{B}$ (i.e., they are not independent because they are based on the same blind-test data).

We also computed sums of corrected assignments across biweekly periods for each sample year. These estimates were analogous to those above, but with summations across all period and length stratum combinations.

Total catch estimates by run

Estimates of total catch by run were obtained by expanding the corrected assignments by the fraction of catch that was sampled and DNA analyzed (e.g., Figure 2). Let C_{tk} be the trawl catch for biweekly period t and length stratum k, let S_{tk} be the sample of catch that was DNA assigned to run, and let f_{tk} (= S_{tk} / C_{tk}) be the fraction of catch that was sampled and assigned to run. For cases where $f_{tk} < 1$ (i.e., not all of the catch was assigned to run), we want to estimate the true abundance of each run in the catch. We denote this "total catch" for the ith run as X_{itk}. When deriving estimators for X_{itk} and its variance, there are two processes to consider: (1) the sampling of catch, which determines the distribution of true abundances, x_{itk}, in the sample; and (2) the estimation of x_{itk} given the observed run assignments $\{y_{itk}\}$ and blind-test data. As detailed in Appendix A, the combination of these processes provides the following estimate of X_{itk} :

$$\hat{X}_{itk} = \frac{\hat{x}_{itk}}{f_{tk}} \tag{13}$$

with an approximate variance given by (Appendix A)

$$\hat{\sigma}^2_{\hat{X}_{itk}} = \frac{1}{f_{tk}^2}\left(\hat{\sigma}^2_{\hat{x}_{itk}} + \hat{X}_{itk} f_{tk} (1 - f_{tk}) \frac{C_{tk} - \hat{X}_{itk}}{C_{tk} - 1} \right). \tag{14}$$

Again, we were primarily interested in biweekly totals (by run) across all length strata:

$$\hat{X}_{it.} = \sum_k \hat{X}_{itk} \quad . \tag{15}$$

As was the case for sums of assignment corrections (see Equation (12)), the variance estimate for $\hat{X}_{it.}$ needs to account for covariances among estimates due to the use of blind-test data:

$$\begin{aligned} \hat{\sigma}^2_{\hat{X}_{it.}} &= \sum_k \hat{\sigma}^2_{\hat{X}_{itk}} + 2 \sum_k \sum_{l \neq k} \operatorname{cov}\left[\hat{X}_{itk}, \hat{X}_{itl} \right] \\ &= \sum_k \hat{\sigma}^2_{\hat{X}_{itk}} + 2 \sum_k \sum_{l \neq k} \frac{1}{f_{tk}} \frac{1}{f_{tl}} \operatorname{cov}\left[\hat{x}_{itk}, \hat{x}_{itl} \right] \\ &= \sum_k \hat{\sigma}^2_{\hat{X}_{itk}} + 2 \sum_k \sum_{l \neq k} \frac{1}{f_{tk}} \frac{1}{f_{tl}} \left(\mathbf{y}'_{\mathrm{A}tk} \hat{\mathbf{Q}}_{\mathrm{A}i} \mathbf{y}_{\mathrm{A}tl} + \mathbf{y}'_{\mathrm{B}tk} \hat{\mathbf{Q}}_{\mathrm{B}i} \mathbf{y}_{\mathrm{B}tl} \right). \end{aligned} \tag{16}$$

Similar estimators were used for annual sums of total catch estimates by run, but with summations across all biweekly periods as well as length strata.

As a baseline for comparison, we also computed total catch estimates based on observed run assignments. To obtain these estimates, we replaced $\hat{x}_{itk}$ with y_{itk} in Equation (13), and removed the variance and covariance terms for $\hat{x}$ in Equations (14) and (16).

Total abundance estimates by run

Estimates of the total (or "absolute") abundance of juveniles passing Chipps Island were computed for biweekly periods and then summed for each sampling year. Derivations and assumptions for abundance estimates, in particular for variances, are detailed in Appendix A. Here, we outline the essential steps and equations.

To estimate abundance, trawl catches are expanded to account for trawl efficiency (the proportion of migrating fish that is captured when the trawl is operating) and trawl effort (e.g., the proportion of time trawled within a given period). For example, in USFWS (2006), abundances were estimated on a monthly basis by dividing total catches of juveniles by an estimate of trawl efficiency and the proportion of time trawled. In our application, this is analogous to the following equation for a given run *i* (as depicted in Figure 2):

$$\hat{N}_i = \frac{\hat{X}_i}{\hat{E}p} = \frac{\hat{x}_i}{\hat{E}pf} \quad , \tag{17}$$

were *N* denotes total abundance, *E* denotes trawl efficiency, and *p* is the proportion of time sampled. The use of Equation (17) is only illustrative (e.g., it implies a generic period with no length stratification).

In this report, we take additional steps to better account for trawl effort, and hence, we use a different notation for abundance estimates. In descriptive terms, we computed the total number of fish (all runs) that would have been caught had the trawl operated continuously throughout a biweekly period, and multiplied this amount by the estimated proportion of fish composed of run *i* during that period. This provided an estimate of catch for run *i*, expanded to account for trawl effort. Abundance was estimated by dividing this expanded catch by the trawl efficiency.

Specifically, biweekly abundances by run (across length strata) were estimated as

$$\hat{N}_{it.} = \frac{\hat{\rho}_{it}\hat{\gamma}_t}{\hat{E}}, \tag{18}$$

where $\hat{\rho}_{it}$ is an estimate of the proportion of migrating juveniles composed of run *i* in period *t*, and $\hat{\gamma}_t$ is an estimate of the total catch of juveniles (all runs) that would have been observed had the trawl operated continuously throughout the period. The estimate $\hat{\rho}_{it}$ was given by

$$\hat{\rho}_{it} = \frac{\hat{X}_{it.}}{C_{t.}}, \tag{19}$$

where $\hat{X}_{it.}$ is the estimated total catch for run *i* (across length strata; see Equation (15)) and $C_{t.}$ is the total observed catch of all juveniles (summed across length strata).

The estimate $\hat{\gamma}_t$ accounted for missing days (i.e., days with no trawling) as well as variation in catch per unit effort among days. Let subscript *d* denote day, let D_t be the total days in biweekly period *t*, and let M_t be the number of missing days (where $M_t < D_t$). For each day of trawling, there is an observed total catch, C_{td} (across all runs and length strata), and a computed proportion of the day trawled, p_{td}. The estimate $\hat{\gamma}_t$ was given by

$$\hat{\gamma}_t = \sum_{d}^{D_t - M_t} \frac{C_{td}}{p_{td}} + M_t \bar{c}_t = D_t \bar{c}_t \ , \tag{20}$$

where $\bar{c}_t$ is mean of the set of $(D_t - M_t)$ daily observations $\{C_{td} / p_{td}\}$, which are analogous to catch-per-unit-effort data. Note that in our application, we estimated p_{td} as a standardized proportion of water volume trawled (see Appendix A), which matched the definition for efficiency estimates.

An approximate variance estimator for the biweekly abundance estimate (Equation (18)) is given by

$$\hat{\sigma}^2_{\hat{N}_{it.}} \cong \frac{\hat{\gamma}_t^2}{\hat{E}^2} \hat{\sigma}^2_{\hat{\rho}_{it}} + \frac{\hat{\rho}_{it}^2}{\hat{E}^2} \hat{\sigma}^2_{\hat{\gamma}_t} + \frac{\hat{\rho}_{it}^2 \hat{\gamma}_t^2}{\hat{E}^4} \hat{\sigma}^2_{\hat{E}} \ . \tag{21}$$

Expressions for the variances of $\hat{\rho}_{it}$ and $\hat{\gamma}_t$ are provided in Appendix A. Estimates of trawl efficiency, $\hat{E}$, and its variance were obtained from Pyper et al. (2013), as discussed below.

It is useful to decompose Equation (21) further with respect to the variance for $\hat{\rho}_{it}$ (the estimate of the proportion of migrating juveniles composed of run *i* in period *t*):

$$\hat{\sigma}^2_{\hat{N}_{it.}} \cong \frac{\hat{\gamma}_t^2}{\hat{E}^2 C_{t.}^2} \left(\sum_k \sum_l \frac{1}{f_{tk}} \frac{1}{f_{tl}} \left(\mathbf{y}'_{\mathrm{A}tk} \hat{\mathbf{Q}}_{\mathrm{A}i} \mathbf{y}_{\mathrm{A}tl} + \mathbf{y}'_{\mathrm{B}tk} \hat{\mathbf{Q}}_{\mathrm{B}i} \mathbf{y}_{\mathrm{B}tl} \right) + \sum_k \frac{\hat{x}_{itk}}{f_{tk}^2} \right) + \frac{\hat{\rho}_{it}^2}{\hat{E}^2} \hat{\sigma}^2_{\hat{\gamma}_t} + \frac{\hat{\rho}_{it}^2 \hat{\gamma}_t^2}{\hat{E}^4} \hat{\sigma}^2_{\hat{E}} \tag{22}$$

The four additive terms in Equation (22) correspond respectively to (1) measurement error in DNA assignment corrections; (2) sampling variation in trawl captures of the run of interest; (3) variance in biweekly catch due to missing days; and (4) variation in the estimate of trawl efficiency. Potentially large components of variation have been omitted, specifically, temporal variation in efficiency and/or catch (e.g., overdispersion due to clumpy spatial and/or temporal patterns of fish migration).

Last, we computed annual sums of abundance by run across biweekly periods. The estimators for annual abundance are provided in Appendix A.

As a baseline for comparison, we also computed abundance estimates based on observed run assignments. To obtain these estimates, we replaced corrected assignments ($\hat{x}$) with observed assignments (y) and removed all variance and covariance terms for $\hat{x}$.

Estimates of efficiency

Total abundances were estimated using four different estimates of Chipps Island trawl efficiency as reported in Pyper et al. (2013). In Pyper et al. (2013), data for paired-release tests (across numerous years) were used to examine relationships between estimated efficiency and potential covariates (e.g., run, fork length, temperature, turbidity and flow). They found little evidence of such relationships, and concluded that variation in efficiencies (across tests and years) was largely driven by confounding effects of differing ocean recovery rates (e.g., survival rates) between control releases and fish of upstream releases passing Chipps Island. Following their recommendation, we assumed that trawl efficiency was constant across periods and years. Thus, one estimate of efficiency we used was the mean efficiency across paired-release tests (Table 4).

Pyper et al. (2013) also evaluated efficiency estimates based on proximal releases (i.e., releases made close to Chipps Island) for the Jersey Point and Pittsburg release locations. These estimates differed, but both were considerably higher than the mean efficiency for paired-release tests (Table 4). As discussed in Pyper et al. (2013), it was unclear which efficiency estimate was preferable; there were advantages and disadvantages to each of three datasets (paired-release tests, Jersey Point, and Pittsburg) and the different methods used to estimate efficiency. We therefore compared abundance estimates based on each of the three efficiency estimates. However, we chose the Jersey Point estimate (the midrange) as the baseline for comparisons.

Table 4. Estimates of Chipps Island trawl efficiency and standard errors (SE) as reported in Pyper et al. (2013). All estimates assume (i.e., are standardized to) a volume-sampled rate of 1000 m^3/minute (based on volume measurements in the current trawl database). No standard error is provided for the fish-flux method, which is based on a set of assumed constants.

	Estimate	SE
Paired-release tests	0.0064	0.0007
Jersey Point releases	0.0088	0.0018
Pittsburg releases	0.0124	0.0016
Fish flux	0.04	-

The fourth approach we used to estimate abundance was the "fish flux" method of Kimmerer (2008). This is an expansion method in which trawl catch is expanded by the ratio of the volume of water trawled versus the (assumed) volume of water that a migrating fish occupies. As detailed in Pyper et al. (2013), the fish-flux method has an implied (constant) efficiency, which was estimated to be 0.041 or 0.042 depending on the vessel used (Confluence or Whitesel). For simplicity, we assumed an efficiency of 0.04 for the fish-flux method (Table 4). Because the fish-flux method is based on a set of assumed constants (e.g., average migration speed and the

channel width and water depth occupied by a migrating fish), there is no variance for this efficiency.

An important detail for all efficiency estimates (Table 4) is that they are standardized by volume sampled, that is, they are estimates of efficiency when the trawl is fishing at a rate of 1000 m^3/minute. This convention was adopted by Pyper et al. (2013) to standardize trawl effort as a function of volume sampled rather than time sampled (see Pyper et al. 2013 for the rationale and evidence in support of using volume rather than time), and was accounted for when estimating abundances because daily values of trawl effort (p_{td}) were standardized accordingly (see Appendix A).

As noted earlier, the effective-fishing mouth size of the trawl net fished at Chipps Island was recently estimated to be 12.7 m^2 (Whitesel) or 13.0 m^2 (Confluence), as opposed to the value of 18.5m^2 that is currently used to compute volume sampled in the trawl database (the data used here). However, such a change would not affect our abundance estimates, except in the case of the fish-flux method. The paired- and proximal-release efficiencies were derived using the same volumes and standardized effort as used here, so a simple scalar change to all trawl volumes would not affect abundance estimates (only the definition of "standardized effort" would change). In contrast, the fish-flux method depends on actual volumes sampled. To correctly apply the fish-flux method to current database volumes, Pyper et al. (2013) adjusted implied efficiency by the ratio of recent ("correct") verses database ("incorrect") estimates of net-mouth areas. (Note that similar three-decimal values for implied efficiency are obtained for both the recent estimate of 12.7 m^2 for the Whitesel (0.041) and 13.0m^2 (0.042) for the Confluence.)

Results

Summaries of trawl effort, catch, and DNA samples

Trawl effort at Chipps Island, as measured by hours sampled, was reasonably similar across biweekly periods for sample years 2009-2011 (Table 5, Figure 3). By comparison, effort in the 2008 sample year was relatively high during December/January, but low during February/March (there was no trawling from February 5 through March 10 due to concerns for delta smelt). In most biweekly periods and sample years, trawling occurred in less than half of the total days available.

Total catches and DNA sample numbers are reported for biweekly periods in Table 6. Catches were low in all biweekly periods from August through March, with a high of 27 fish caught in the March 16-31, 2010 period. Beginning in April, catches steadily increased in most years and peaked in either the April 16-30 or May 1-15 period. Total annual catches increased in each sample year. From June through mid-April, the fraction of catch that was tissue sampled and DNA-assigned to run was typically greater than 80%. However, during the periods of relatively high catch from mid-April through mid-May, the fraction of catch that was DNA analyzed was

often less than 50%. Overall, a much larger fraction of catch was DNA analyzed in sample years 2008 and 2011 compared to 2009 and 2010.

Fork length distributions for DNA-analyzed and non-analyzed fish were similar for most biweekly periods in which there was partial sampling of catch (Figure 4). However, notable differences were evident in some March and April periods, and in general, the largest fish caught (i.e., high outliers in fork length) were predominantly found among DNA-analyzed fish. This result is not surprising given that the smaller, fall run were sometimes subsampled whereas the larger fish were not.

Observed DNA run assignments

There were stark differences among runs in the ONCOR probability categories ($P < 1$ or $P = 1$) for DNA assignments. Observed DNA run assignments, tabulated by biweekly period and ONCOR probability category, are shown in Table 7 for all sample years combined. Assignments for winter-run had the highest proportion (98%) of ONCOR probabilities = 1, followed by Butte Creek spring run (70%) and fall run (63%). In contrast, proportions of ONCOR probabilities = 1 were very low for assignments of late-fall run (5%) and Mill-Deer creek spring run (18%). In the case of fall run, there was a much lower proportion of ONCOR probabilities = 1 from July to March (i.e., 23 of 88 assignments, or 26%) than from April to June (64%), suggesting that fall-run assignments were less certain in months outside the peak migration period (April to June). Across years, total DNA assignments (n = 5104) were dominated by fall run (4,326; 84.8%), followed by Butte Creek spring run (301; 5.9%), late-fall run (272; 5.3%), winter run (105; 2.1%), and Mill-Deer creek spring run (100; 2.0%).

Relationships between fork length and capture date of fish that were DNA assigned to run are shown in Figure 5 (the top panel highlights fall and late-fall runs; the bottom panel highlights spring and winter runs). Fish assigned to the fall and late-fall runs prior to the spring emigration period had relatively high fork lengths. Winter-run assignments were more confined in length and time, and were generally larger in size, than spring-run assignments. A greater number of spring Mill-Deer creek assignments overlapped in length and time with winter run than did Butte Creek assignments. The peak for winter- run assignments occurred in mid-March, whereas the peak for the both spring runs occurred in April.

Table 5. Chipps Island trawl effort summaries by biweekly period and sampling year. A " – " indicates that no trawling was conducted during this strata. Sample year 2008 is defined as August 1st, 2007 – July 31st, 2008 and similarly for 2009, 2010 and 2011. Sampling effort summaries are not presented from August 1st – September 30th, 2007, which preceded the onset of DNA sampling and from July 1- 30th , 2011 when DNA sampling concluded.

		Days of trawling				Minutes trawled				Volume trawled (thousands of m^3)			
Period	Days	2008	2009	2010	2011	2008	2009	2010	2011	2008	2009	2010	2011
Aug 1-15	15		4	6	6		780	1,200	1,120		846	1,376	1,249
Aug 16-31	16		4	7	7		793	1,400	1,277		829	1,595	1,437
Sep 1-15	15		5	6	7		1,000	1,100	1,320		1,104	1,202	1,365
Sep 16-30	15		4	7	6		799	1,400	1,140		847	1,521	1,175
Oct 1-15	15	6	4	6	7	1,196	780	1,100	1,286	1,296	806	1,204	1,366
Oct 16-31	16	7	5	7	6	1,400	1,000	1,360	1,200	1,413	980	1,458	1,289
Nov 1-15	15	7	4	6	7	1,340	800	1,182	1,355	1,330	824	1,245	1,296
Nov 16-30	15	6	4	7	6	1,100	700	1,300	1,100	1,139	664	1,426	1,067
Dec 1-15	15	12	6	6	7	2,210	1,080	1,140	1,280	2,232	1,048	1,262	1,483
Dec 16-31	16	15	5	8	6	3,015	920	1,506	1,100	3,087	889	1,619	1,097
Jan 1-15	15	5	6	6	6	960	1,160	1,200	1,155	919	1,194	1,347	1,283
Jan 16-31	16	15	7	4	6	2,772	1,360	795	1,080	2,885	1,417	854	1,190
Feb 1-15	15	4	6	6	7	520	1,200	1,200	1,400	571	1,329	1,313	1,565
Feb 16-28	13	-	6	6	6	0	1,200	1,200	1,200	-	1,290	1,271	1,392
Mar 1-15	15	2	6	7	6	315	1,215	1,400	1,200	341	1,264	1,561	1,327
Mar 16-31	16	5	7	7	7	980	1,400	1,396	1,400	1,045	1,382	1,571	1,440
Apr 1-15	15	4	8	6	7	800	2,280	1,181	1,400	900	2,262	1,302	1,426
Apr 16-30	15	4	7	7	6	780	1,830	1,380	1,200	853	1,813	1,482	1,323
May 1-15	15	5	8	6	6	1,000	1,865	1,180	1,200	1,053	1,893	1,300	1,160
May 16-31	16	4	6	6	7	745	1,140	1,120	1,260	810	1,259	1,159	1,405
Jun 1-15	15	6	7	7	7	1,200	1,360	1,398	1,400	1,308	1,430	1,532	1,521
Jun 16-30	15	7	6	7	6	1,380	1,200	1,298	1,220	1,543	1,326	1,515	1,374
Jul 1-15	15	4	7	6		660	1,300	1,120		749	1,476	1,297	
Jul 16-31	16	5	7	6		810	1,380	912		914	1,571	1,030	
Total	365	123	139	153	142	23,183	28,542	29,468	27,293	24,388	29,743	32,442	29,230

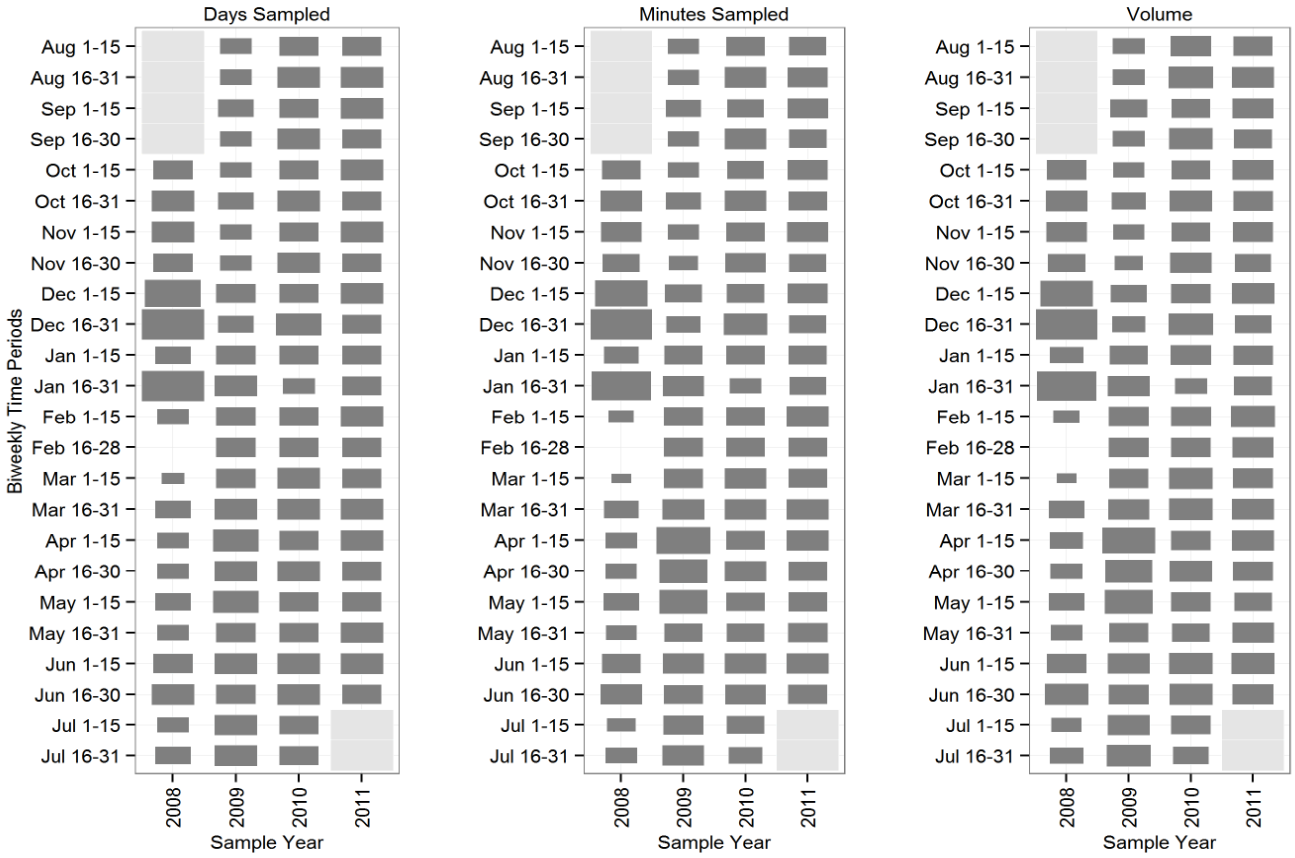

Figure 3. Graphical display of Chipps Island trawl effort summaries by biweekly period and sampling year. The size of each rectangle is proportional to the value in Table 5. Sample year 2008 is defined as August 1st, 2007 – July 31st, 2008 and similarly for 2009, 2010 and 2011.

Table 6. Raw catch and number of DNA samples (assigned to run) taken at Chipps Island by biweekly period and sampling year. A " – " indicates that no sampling (trawl or DNA) was conducted during this period. Blank entries indicate either zero catch or no DNA samples. Catch is not reported from August-September in sample year 2008 and July in sample year 2011 because no DNA samples were taken during these periods.

	Catch (*C*)				DNA samples analyzed (*S*)				Fraction analyzed (*f* = *S*/*C*)			
	2008	2009	2010	2011	2008	2009	2010	2011	2008	2009	2010	2011
Aug 1-15		1	0	2	-	1		2	-	1.00		1.00
Aug 16-31		0	0	1	-			1	-			1.00
Sep 1-15		0	1	2	-		1	2	-		1.00	1.00
Sep 16-30		0	1	0	-		1		-		1.00	
Oct 1-15	1	0	0	1	0			1	0.00			1.00
Oct 16-31	0	2	0	0		0				0.00		
Nov 1-15	1	2	3	3	1	1	3	3	1.00	0.50	1.00	1.00
Nov 16-30	1	0	0	1	1			1	1.00			1.00
Dec 1-15	9	1	0	1	6	1		1	0.67	1.00		1.00
Dec 16-31	10	0	2	4	10		2	4	1.00		1.00	1.00
Jan 1-15	6	6	1	3	5	6	1	3	0.83	1.00	1.00	1.00
Jan 16-31	14	0	4	1	8		4	0	0.57		1.00	0.00
Feb 1-15	0	1	6	1		1	6	1		1.00	1.00	1.00
Feb 16-28	-	12	7	6	-	10	7	6	-	0.83	1.00	1.00
Mar 1-15	5	24	24	7	5	16	23	7	1.00	0.67	0.96	1.00
Mar 16-31	17	24	27	18	17	23	24	17	1.00	0.96	0.89	0.94
Apr 1-15	27	122	62	67	25	111	57	66	0.93	0.91	0.92	0.99
Apr 16-30	134	690	1,740	845	124	268	462	699	0.93	0.39	0.27	0.83
May 1-15	316	1,059	764	1,763	141	198	307	790	0.45	0.19	0.40	0.45
May 16-31	45	71	371	687	33	50	235	447	0.73	0.70	0.63	0.65
Jun 1-15	40	37	194	641	39	32	170	424	0.98	0.86	0.88	0.66
Jun 16-30	28	16	37	144	26	16	33	86	0.93	1.00	0.89	0.60
Jul 1-15	1	11	12		1	10	12	-	1.00	0.91	1.00	-
Jul 16-31	1	6	2		1	6	2	-	1.00	1.00	1.00	-
Total	656	2,085	3,258	4,198	443	750	1,350	2,561	0.68	0.36	0.41	0.61

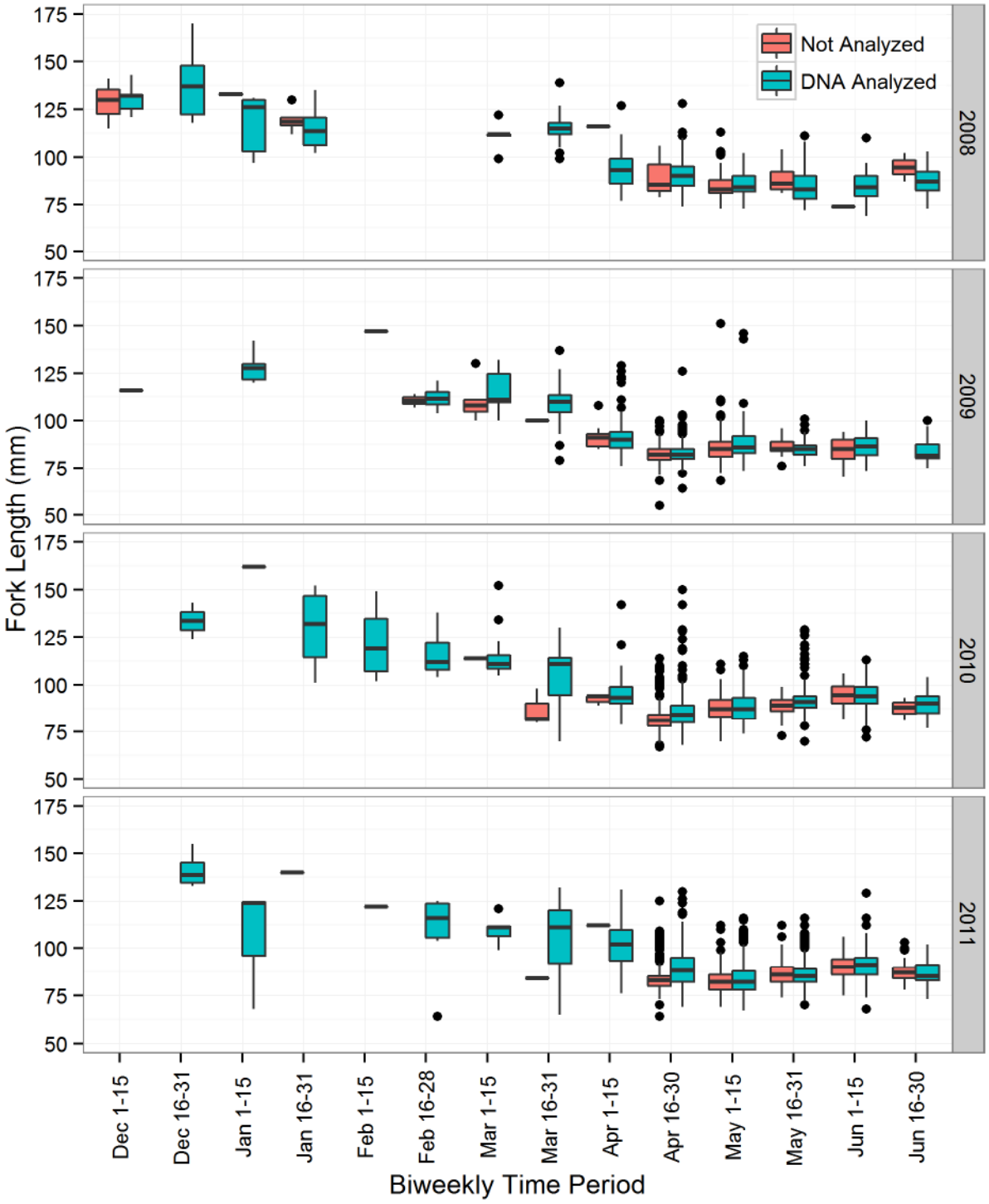

Figure 4. Boxplots of fork length (mm) by period and sample year for DNA-analyzed and not-analyzed juvenile Chinook salmon caught in Chipps Island trawl. Boxplots show medians (horizontal lines), 25th-75th percentiles (boxes), 1.5× (75th- 25th percentiles) (whiskers). Data points beyond the end of the whiskers are outliers. Sample years include December from the previous year (2008, includes December of 2007, etc.).

Comparisons with assignments based on length-at-date criteria

Total run assignments based on DNA often differed substantially with those based on the river model's length-at-date criteria (Fisher 1992). Across all four years, more fish were DNA assigned to the fall and late-fall runs, and far fewer fish were DNA assigned to spring and winter runs, than compared to length-at-date assignments (Figure 6). These trends were consistent for both observed and corrected DNA assignments (Figure 6) (corrected assignments are reported below). Scatter plots of length and capture date for observed DNA assignments illustrate the differences between DNA assignments and their expected length-at-date ranges (Figure 7). For example, many fish that were DNA assigned to fall run were contained within the length-at-date range for spring run, and to a lesser extent, within the late-fall and winter run ranges. The length-at-date distributions for late-fall DNA-assignments were similar to those for fall-run assignments, and were spread across the length-at-date ranges for all runs. Spring-run DNA assignments were centered in the spring-run length-at date range, but also overlapped considerably with the adjacent winter and fall-run length-at-date ranges. Winter-run DNA assignments had the closest fit to their expected length-at-date range, with only a few fish overlapping the adjacent late-fall and spring-run ranges (Figure 7).

Table 7. Number of fish assigned to run by biweekly period and ONCOR assignment-probability category. All sample years are combined.

	ONCOR assignment probability (P < 1 or P = 1)									
	Fall		Late-Fall		Spring Butte		Spring Mill-Deer		Winter	
	<1	=1	<1	=1	<1	=1	<1	=1	<1	=1
Aug 1-15	1		2							
Aug 16-31	1									
Sep 1-15	1	1	1							
Sep 16-30		1								
Oct 1-15			1							
Oct 16-31										
Nov 1-15	3	2	3							
Nov 16-30	1		1							
Dec 1-15	2	1	4							1
Dec 16-31	6	2	6	2						
Jan 1-15	5	1	5	1						3
Jan 16-31	7		3							2
Feb 1-15	2	1	2							3
Feb 16-28	1		3				1		1	17
Mar 1-15	9		5				5	3		29
Mar 16-31	12	10	6	1	1	3	10	5	1	32
Apr 1-15	61	92	8		24	54	9	2		9
Apr 16-30	486	825	55		42	108	28	2		7
May 1-15	480	839	52		11	33	20	1		
May 16-31	221	507	21	1	6	6	2	1		
Jun 1-15	216	379	49	2	6	5	5	3		
Jun 16-30	53	79	21	3	1	1	2	1		
Jul 1-15	9	4	7	3						
Jul 16-31	5		3	1						
Total	1,582	2,744	258	14	91	210	82	18	2	103
% of total	37%	63%	95%	5%	30%	70%	82%	18%	2%	98%

Figure 5. Scatterplot of juvenile Chinook salmon caught in Chipps Island trawl and DNA-assigned to run as a function of fork length and sample day (all four years of study data combined). Run abbreviations are fall (F), late-fall (LF), spring Butte (SB), spring Mill and Deer (SMD), and winter (W).

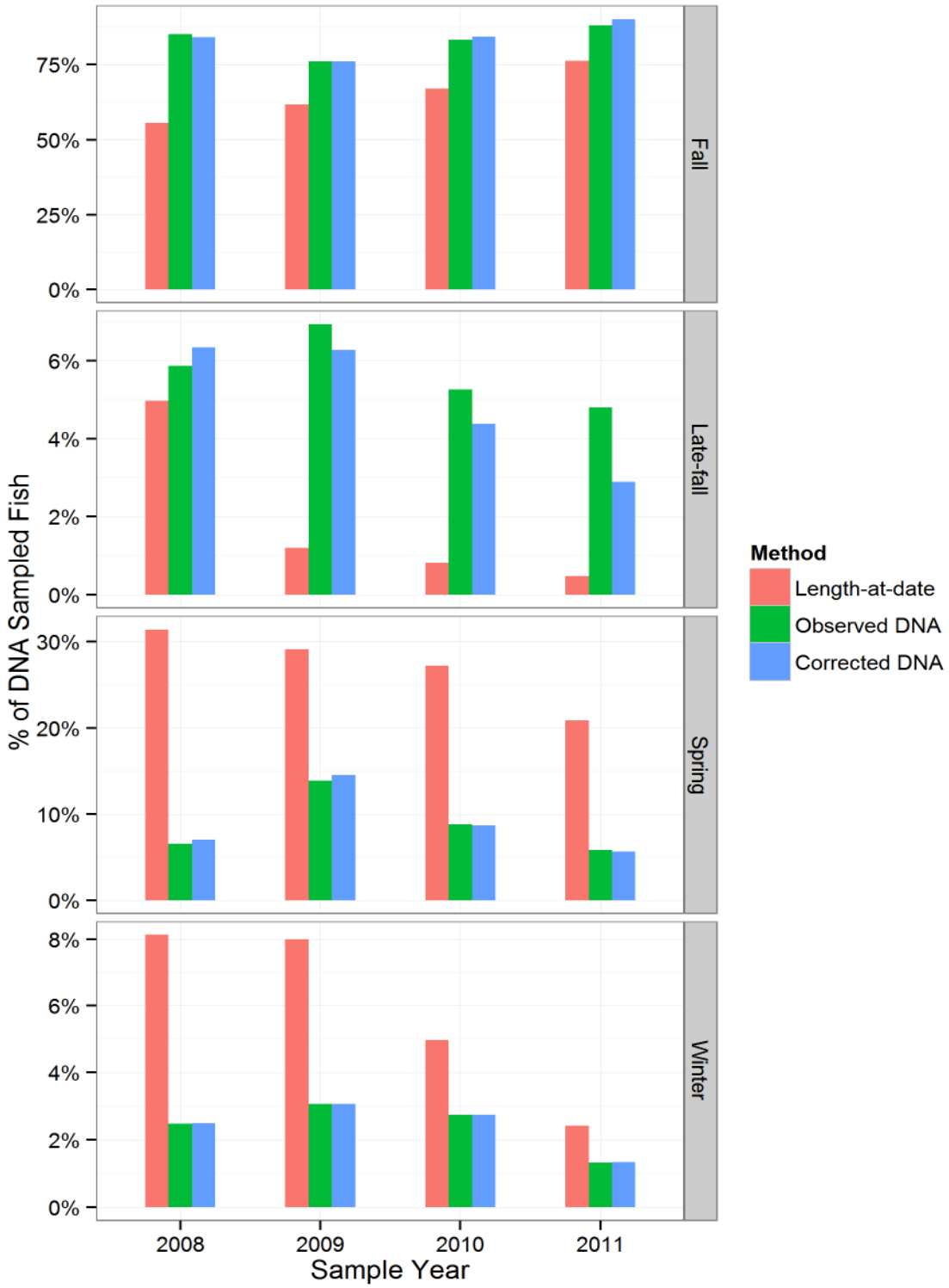

Figure 6. Comparison of run assignments based on length-at-date criteria versus DNA (observed and corrected) for juvenile Chinook salmon caught in Chipps Island trawl and DNA assigned to run. For each sample year and assignment method, the percentage of total juveniles assigned to each run is shown. Sample year 2008 is defined as August 1st, 2007 – July 31st, 2008 and similarly for 2009, 2010 and 2011.

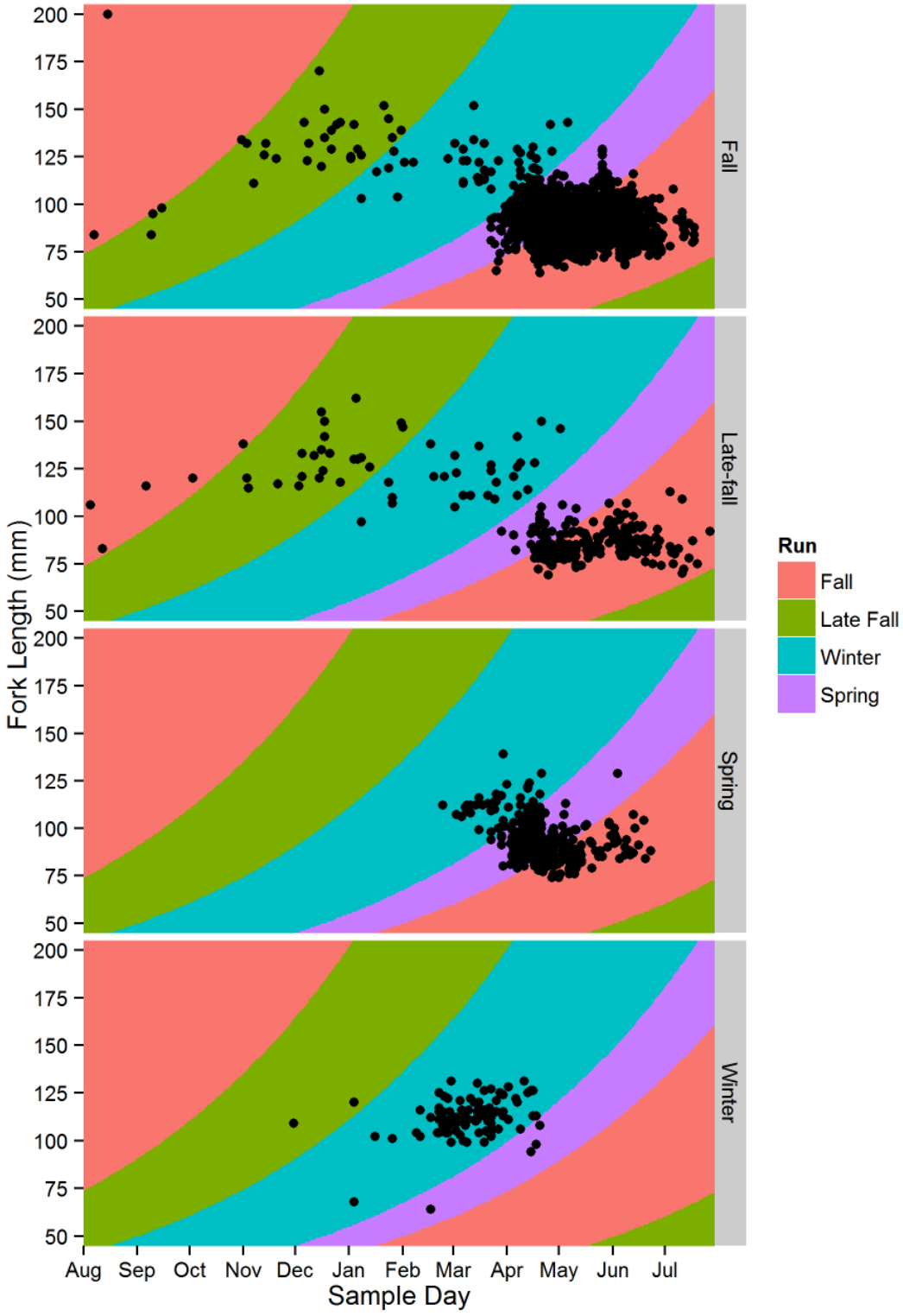

Figure 7. Scatterplot of juvenile Chinook salmon caught in Chipps Island trawl and DNA assigned to run (panels) as a function of fork length and sample day (all four years of study data combined). The color regions correspond to length-at-date criteria for run assignment.

Assignment corrections and total catch estimates by run

Observed and corrected DNA assignments, and their corresponding total catch estimates, are presented for each run in Table 8-Table 12. Comparisons of observed DNA assignments (y) and corrected assignments ($\hat{x}$) show the effects of using blind-test data to "correct" assignments (i.e., accounting for empirical error rates in DNA assignments). The total catch estimates ($\hat{X}$) are simple expansions that account for the proportion of trawl catch that was not DNA assigned to run. Standard errors, shown in parentheses, reflect two sources of uncertainty. First, there is estimation error in assignment corrections, and second, there is additional (hypergeometric) sampling error in estimates of total catch (i.e., for those periods in which some catch was not DNA assigned to run).

Note that because the reported estimates for biweekly periods are *sums* across length strata, the apparent expansion factors to total catch may differ for observed and corrected assignments. For example, during the May 1-15 period in 2009, there were eight observed assignments for late-fall run with a corresponding total catch estimate of 37 fish, a more than four-fold expansion (Table 9). In contrast, the corrected assignments for this period summed to only two fish, with a corresponding total catch estimate of only three fish (after rounding). This difference in the observed and corrected expansions to total catch was due to the differing proportions of catch sampled within length strata (i.e., observed assignments were more numerous in length strata with low proportions of sampled catch).

Fall run

Fish that were DNA assigned to fall run were observed throughout the sampling year, with the largest numbers observed in the April 16-30 and May 1-15 periods (Table 8). Two year classes are evident, with the older young of the year from the previous brood year migrating between August and April, and the current brood year migrating between April and July (Figure 7). Across years, observed and corrected assignments for fall run were reasonably similar (Table 8; see also Figure 6). The largest annual difference was in 2011, with 2,255 observed assignments and 2,309 corrected assignments (i.e., a 2.4% increase in corrected assignments relative to observed).

Estimates of total annual catch increased each year from roughly 600 fall run in 2008 to almost 4,000 in 2011. Total catch estimates based on observed and corrected assignments were similar, though standard errors were typically much larger for estimates based on corrected assignments.

Late-fall run

Late-fall fish were also identified throughout the sampling year, with relatively high numbers from mid-April to late June in most years (Table 9). Like fall run, late-fall run display two year classes, with the older young of the year from the previous brood year migrating between August and May, while the current brood year migrates between April and July (Figure 7). However, there were often large differences between observed and corrected DNA assignments of late-fall run. In particular, corrected assignments tended to be much lower than observed assignments in

the three biweekly periods extending from mid-April to the end of May, when fall-run abundances were high. Outside these periods, corrected assignments were typically equal to, or somewhat larger than, the observed assignments. The largest annual difference was in 2011, with 123 observed and 74 corrected assignments (a 39.8% decrease in corrected assignments relative to observed).

For sample years 2009-2011, estimates of total annual catch based on corrected assignments were considerably lower (roughly half) compared to estimates based on observed assignments. Standard errors for the corrected catch estimates were very large, reflecting the high uncertainty in estimates of corrected assignments for late-fall run.

Butte Creek spring run

Butte Creek spring run were identified from March through June, with relatively high numbers in the three biweekly periods extending from April to mid-May (Table 10). It is likely that spring run outmigrants during this period contain both yearlings and young-of-the-year. Corrected DNA assignments tended to be slightly higher than observed DNA assignments (e.g., annual totals of corrected assignments were roughly 10% higher than for observed assignments). Similar differences were observed for total catch estimates. For example, annual totals of corrected catch estimates were roughly 10% larger than estimates based on observed assignments for years 2009-2011. Estimates of corrected assignments and total catch for Butte Creek spring run were relatively precise (i.e., had low standard errors).

Mill-Deer spring run

Assignments of Mill-Deer creek spring run (Table 11) were far less numerous than for Butte Creek. The timing of peak counts for Mill-Deer creek assignments varied across years, ranging from late March (2008) to early May (2011). Spring run outmigrants during this period likely consist of both yearlings and young of the year. Corrected assignments declined each year in comparison to observed assignments. There was no difference in 2008, while the largest annual difference was in 2011, with 30 observed and 10 corrected assignments (a 63% decrease in corrected assignments relative to observed). Larger differences were observed for total catch estimates across years, with reductions in corrected catch estimates ranging from 9% (2008) to 72% (2011) relative to estimates based on observed assignments. As was the case for late-fall run, estimates of corrected assignments and total catch for Mill-Deer creek spring run were highly uncertain (large standard errors).

Winter run

Most assignments of winter run occurred in three biweekly periods from late February through March, though 12 of the 34 observed assignments in 2011 were identified in April (Table 12). In all periods and years, corrected assignments and total catch estimates (after rounding) were very precise and were identical to the observed values. Because assignments of winter run occurred in time periods and length strata with high proportions of sampled catch (typically 100%), total catch estimates were equal to, or only slightly larger than, the corresponding assignment

numbers. Annual total catch estimates for winter run were low, ranging from just 12 fish in 2008 to a high of 38 fish in 2010.

Negative estimates of corrected assignments

As detailed in the Methods section, when corrected run assignments were negative for a given biweekly period and length stratum, we set negative estimates to zero and scaled the remaining run corrections to equal the total number of observed assignments. Negative estimates can be indication of biased or insufficient blind-test data, so we note their prevalence here for each run.

The frequency of negative estimates was much greater for assignments with ONCOR probabilities < 1 than for probabilities = 1. For probabilities < 1, there was a total of 180 combinations of period-length strata (across years) with at least one observed DNA assignment. Among these 180 cases, negative corrections occurred in 34 (19% of cases) for fall run, 54 (30%) for late-fall run, 2 (1%) for Butte Creek spring run, and 26 (14%) for Mill-Deer creek spring run. The negative estimates for fall run tended to occur when observed fall-run assignments were low relative to late-fall assignments (e.g., December through March), while negative estimates for the late-fall and Mill-Deer creek runs occurred when observed assignments of these runs were low relative to fall-run assignments (e.g., April through June). In contrast, among the 178 period-length combinations with ONCOR assignment probabilities = 1, negative corrections occurred in only 8 cases (4.5%) for fall run and 10 cases (5.6%) for late-fall run. There were no negative estimates for winter run in either ONCOR probability category.

Table 8. Number of fall-run juvenile Chinook salmon by biweekly period and sample year that were DNA assigned to run (observed and corrected assignments) and corresponding estimates of total catch based on observed and corrected assignments. Standard errors for estimates are reported in parentheses. A " – " indicates that no trawl sampling was conducted during this strata. Periods with zero catch or no fish sampled for DNA are left blank. Sample year 2008 is defined as August 1st, 2007 – July 31st, 2008 and similarly for 2009, 2010 and 2011.

	Observed assignments				Corrected assignments				Total catch based on observed assignments				Total catch based on corrected assignments			
	2008	2009	2010	2011	2008	2009	2010	2011	2008	2009	2010	2011	2008	2009	2010	2011
Aug 1-15		1		0		1 (0.2)		0 (1.2)		1 (0)		0 (0)		1 (0.2)		0 (1.2)
Aug 16-31				1				1 (0.2)				1 (0)				1 (0.2)
Sep 1-15			1	1			1 (0)	1 (0.4)			1 (0)	1 (0)			1 (0)	1 (0.4)
Sep 16-30			1				1 (0)				1 (0)				1 (0)	
Oct 1-15				0				0 (0.6)				0 (0)				0 (0.6)
Oct 16-31																
Nov 1-15	1	1	1	2	1 (0)	1 (0.2)	0 (1)	2 (0.4)	1 (0)	2 (0)	1 (0)	2 (0)	1 (0)	2 (0.5)	0 (1)	2 (0.4)
Nov 16-30	1			0	1 (0.2)			0 (0.6)	1 (0)			0 (0)	1 (0.2)			0 (0.6)
Dec 1-15	3	0		0	1 (1.4)	0 (0.6)		0 (0)	4 (0.9)	0 (0)		0 (0)	1 (2)	0 (0.6)		0 (0)
Dec 16-31	7		1	0	6 (0.9)		0 (0.4)	0 (1.8)	7 (0)		1 (0)	0 (0)	6 (0.9)		0 (0.4)	0 (1.8)
Jan 1-15	2	2	0	2	1 (1.6)	0 (0.9)	0 (0.4)	2 (0.5)	2 (0.6)	2 (0)	0 (0)	2 (0)	1 (1.9)	0 (0.9)	0 (0.4)	2 (0.5)
Jan 16-31	4		3		2 (1.2)		3 (0.7)		7 (1.5)		3 (0)		4 (2.3)		3 (0.7)	
Feb 1-15		0	2	1		0 (0.6)	1 (0.4)	1 (0.2)		0 (0)	2 (0)	1 (0)		0 (0.6)	1 (0.4)	1 (0.2)
Feb 16-28	-	0	0	1	-	0 (0.6)	0 (2.5)	1 (0.2)	-	0 (0)	0 (0)	1 (0)	-	0 (0.6)	0 (2.5)	1 (0.2)
Mar 1-15	0	6	2	1	0 (0.2)	5 (1.1)	1 (0.7)	0 (0.4)	0 (0)	8 (1.2)	2 (0)	1 (0)	0 (0.2)	7 (2.1)	1 (0.7)	0 (0.4)
Mar 16-31	4	5	6	7	3 (0.7)	4 (2.3)	6 (0.8)	7 (3.6)	4 (0)	5 (0.4)	8 (0.5)	8 (0)	3 (0.7)	4 (2.5)	8 (1)	8 (3.7)
Apr 1-15	17	56	43	37	16 (1.1)	50 (6.2)	43 (3.4)	35 (2.7)	18 (0)	61 (1.7)	47 (1)	37 (0.5)	17 (1.1)	54 (7.1)	48 (3.8)	36 (2.8)
Apr 16-30	112	231	389	579	113 (9.1)	240 (16.1)	400 (25.1)	590 (37.9)	121 (1)	596 (11.3)	1,531 (21.6)	706 (4.2)	123 (9.8)	620 (42.3)	1,589 (101)	721 (46.6)
May 1-15	132	175	275	737	134 (8.2)	182 (12.4)	284 (19.6)	771 (47.2)	295 (4.8)	930 (23.9)	686 (10.3)	1,648 (11.4)	301 (18.6)	967 (67.1)	708 (50)	1,728 (105.3)
May 16-31	32	44	225	427	33 (2.5)	43 (3.2)	229 (12.1)	438 (23.6)	44 (0.7)	62 (1.9)	355 (3.1)	656 (4.1)	44 (3.5)	61 (5)	362 (19.9)	673 (36)
Jun 1-15	38	29	143	385	38 (3.2)	28 (2.2)	138 (8.2)	390 (20.4)	39 (0)	34 (0.6)	163 (2)	583 (5.2)	39 (3.2)	32 (2.7)	157 (9.6)	589 (31.2)
Jun 16-30	24	10	24	74	23 (0.9)	7 (2.2)	21 (1.9)	69 (4.4)	26 (0.4)	10 (0)	27 (0.9)	123 (3.6)	25 (1.2)	7 (2.2)	24 (2.3)	115 (8.5)
Jul 1-15	0	7	6		0 (0.6)	6 (1.2)	6 (1.6)		0 (0)	8 (0)	6 (0)		0 (0.6)	7 (1.2)	6 (1.6)	
Jul 16-31	0	4	1		0 (0.6)	4 (0.8)	1 (0.4)		0 (0)	4 (0)	1 (0)		0 (0.6)	4 (0.8)	1 (0.4)	
Total	377	571	1,123	2255	372 (23.2)	571 (37.6)	1,136 (69)	2,309 (133.8)	569 (5.3)	1,723 (26.6)	2,835 (24.2)	3,770 (14.3)	566 (34.9)	1,766 (117.4)	2,910 (182.4)	3,878 (224.7)

Table 9. Number of late-fall-run juvenile Chinook salmon by biweekly period and sample year that were DNA assigned to run (observed and corrected assignments) and corresponding estimates of total catch based on observed and corrected assignments. Standard errors for estimates are reported in parentheses. A " – " indicates that no trawl sampling was conducted during this strata. Periods with zero catch or no fish sampled for DNA are left blank. Sample year 2008 is defined as August 1st, 2007 – July 31st, 2008 and similarly for 2009, 2010 and 2011.

	Observed assignments				Corrected assignments				Total catch based on observed assignments				Total catch based on corrected assignments			
	2008	2009	2010	2011	2008	2009	2010	2011	2008	2009	2010	2011	2008	2009	2010	2011
Aug 1-15		0		2		0 (0.2)		2 (1.2)		0 (0)		2 (0)		0 (0.2)		2 (1.2)
Aug 16-31				0				0 (0.2)				0 (0)				0 (0.2)
Sep 1-15			0	1			0 (0)	1 (0.4)			0 (0)	1 (0)			0 (0)	1 (0.4)
Sep 16-30			0				0 (0)				0 (0)				0 (0)	
Oct 1-15				1				1 (0.6)				1 (0)				1 (0.6)
Oct 16-31																
Nov 1-15	0	0	2	1	0 (0)	0 (0.2)	3 (1)	1 (0.4)	0 (0)	0 (0)	2 (0)	1 (0)	0 (0)	0 (0.4)	3 (1)	1 (0.4)
Nov 16-30	0			1	0 (0.2)			1 (0.6)	0 (0)			1 (0)	0 (0.2)			1 (0.6)
Dec 1-15	3	1		0	5 (1.4)	1 (0.6)		0 (0)	4 (0.9)	1 (0)		0 (0)	7 (2)	1 (0.6)		0 (0)
Dec 16-31	3		1	4	4 (0.9)		2 (0.4)	4 (1.8)	3 (0)		1 (0)	4 (0)	4 (0.9)		2 (0.4)	4 (1.8)
Jan 1-15	3	2	1	0	4 (1.6)	4 (0.9)	1 (0.4)	0 (0.4)	4 (0.6)	2 (0)	1 (0)	0 (0)	5 (1.9)	4 (0.9)	1 (0.4)	0 (0.4)
Jan 16-31	3		0		5 (1.2)		0 (0.7)		6 (1.5)		0 (0)		9 (2.3)		0 (0.7)	
Feb 1-15		1	1	0		1 (0.6)	2 (0.4)	0 (0.2)		1 (0)	1 (0)	0 (0)		1 (0.6)	2 (0.4)	0 (0.2)
Feb 16-28	-	1	2	0	-	1 (0.6)	2 (3.4)	0 (0.2)	-	1 (0)	2 (0)	0 (0)	-	1 (0.6)	2 (3.4)	0 (0.2)
Mar 1-15	0	3	1	1	0 (0.1)	4 (1.1)	2 (0.5)	2 (0.4)	0 (0)	5 (1.7)	1 (0)	1 (0)	0 (0.1)	6 (2.6)	2 (0.5)	2 (0.4)
Mar 16-31	1	5	1	0	2 (0.4)	6 (2.3)	2 (0.5)	0 (4.2)	1 (0)	5 (0.4)	1 (0.4)	0 (0)	2 (0.4)	6 (2.4)	2 (0.7)	0 (4.3)
Apr 1-15	1	2	3	2	1 (0.9)	3 (3.5)	2 (3.1)	3 (1.9)	1 (0)	2 (0)	3 (0.4)	2 (0.3)	1 (0.9)	3 (3.9)	2 (3.4)	3 (1.9)
Apr 16-30	2	11	15	27	0 (8.6)	1 (15.1)	5 (23.4)	11 (35)	2 (0.4)	29 (6.7)	53 (12.6)	33 (2.7)	0 (9.3)	4 (38.7)	5 (94)	14 (43.1)
May 1-15	5	8	10	29	2 (7.8)	2 (11.7)	1 (18.6)	1 (44.8)	12 (4)	37 (12.6)	25 (6)	66 (9.1)	5 (17.4)	3 (60.1)	2 (46.7)	3 (99.9)
May 16-31	1	4	5	12	0 (2.4)	5 (3)	0 (11.6)	2 (22.5)	1 (0.7)	6 (1.6)	9 (2.5)	19 (3.2)	1 (3.4)	7 (4.6)	0 (18.8)	3 (34.2)
Jun 1-15	0	3	17	31	0 (3)	4 (2.1)	22 (7.8)	30 (19.4)	0 (0)	3 (0.6)	19 (1.6)	46 (4.7)	0 (3.1)	5 (2.6)	25 (9.1)	46 (29.6)
Jun 16-30	2	6	5	11	3 (0.9)	9 (2.2)	8 (1.8)	15 (4.2)	2 (0.4)	6 (0)	6 (0.8)	19 (3.5)	3 (1.1)	9 (2.2)	9 (2.2)	27 (8.3)
Jul 1-15	1	3	6		1 (0.6)	4 (1.2)	6 (1.7)		1 (0)	3 (0)	6 (0)		1 (0.6)	4 (1.2)	6 (1.7)	
Jul 16-31	1	2	1		1 (0.6)	2 (0.8)	1 (0.4)		1 (0)	2 (0)	1 (0)		1 (0.6)	2 (0.8)	1 (0.4)	
Total	26	52	71	123	29 (21.9)	46 (34.5)	58 (64.8)	74 (126.1)	38 (4.5)	103 (14.5)	131 (14.3)	196 (11.6)	39 (32.8)	56 (107.4)	64 (171.1)	108 (212.4)

Table 10. Number of spring-run (Butte Creek) juvenile Chinook salmon by biweekly period and sample year that were DNA assigned to run (observed and corrected assignments) and corresponding estimates of total catch based on observed and corrected assignments. Standard errors for estimates are reported in parentheses. A " – " indicates that no trawl sampling was conducted during this strata. Periods with zero catch or no fish sampled for DNA are left blank. Sample year 2008 is defined as August 1st, 2007 – July 31st, 2008 and similarly for 2009, 2010 and 2011.

	Observed assignments				Corrected assignments				Total catch based on observed assignments				Total catch based on corrected assignments			
	2008	2009	2010	2011	2008	2009	2010	2011	2008	2009	2010	2011	2008	2009	2010	2011
Aug 1-15		0		0		0 (0)		0 (0)		0 (0)		0 (0)		0 (0)		0 (0)
Aug 16-31				0				0 (0)				0 (0)				0 (0)
Sep 1-15			0	0			0 (0)	0 (0)			0 (0)	0 (0)			0 (0)	0 (0)
Sep 16-30			0				0 (0)				0 (0)				0 (0)	
Oct 1-15				0				0 (0)				0 (0)				0 (0)
Oct 16-31																
Nov 1-15	0	0	0	0	0 (0)	0 (0)	0 (0)	0 (0)	0 (0)	0 (0)	0 (0)	0 (0)	0 (0)	0 (0)	0 (0)	0 (0)
Nov 16-30	0			0	0 (0)			0 (0)	0 (0)			0 (0)	0 (0)			0 (0)
Dec 1-15	0	0		0	0 (0)	0 (0)		0 (0)	0 (0)	0 (0)		0 (0)	0 (0)	0 (0)		0 (0)
Dec 16-31	0		0	0	0 (0)		0 (0)	0 (0)	0 (0)		0 (0)	0 (0)	0 (0)		0 (0)	0 (0)
Jan 1-15	0	0	0	0	0 (0)	0 (0)	0 (0)	0 (0)	0 (0)	0 (0)	0 (0)	0 (0)	0 (0)	0 (0)	0 (0)	0 (0)
Jan 16-31	0		0		0 (0)		0 (0)		0 (0)		0 (0)		0 (0)		0 (0)	
Feb 1-15		0	0	0		0 (0)	0 (0)	0 (0)		0 (0)	0 (0)	0 (0)		0 (0)	0 (0)	0 (0)
Feb 16-28	-	0	0	0	-	0 (0)	0 (1)	0 (0)	-	0 (0)	0 (0)	0 (0)	-	0 (0)	0 (1)	0 (0)
Mar 1-15	0	0	0	0	0 (0)	0 (0)	0 (0)	0 (0)	0 (0)	0 (0)	0 (0)	0 (0)	0 (0)	0 (0)	0 (0)	0 (0)
Mar 16-31	1	2	1	0	1 (0.1)	2 (0.3)	1 (0.1)	0 (1)	1 (0)	2 (0)	1 (0.4)	0 (0)	1 (0.1)	2 (0.3)	1 (0.4)	0 (1)
Apr 1-15	5	46	9	18	5 (0.5)	52 (4.7)	10 (0.9)	20 (1.6)	5 (0)	50 (1.7)	9 (0.8)	18 (0.5)	5 (0.5)	57 (5.5)	11 (1.3)	20 (1.7)
Apr 16-30	9	21	41	79	10 (0.9)	24 (2.3)	46 (4)	89 (7.9)	10 (0.9)	53 (8.8)	101 (13.3)	90 (3)	10 (1.3)	61 (11)	112 (16.7)	101 (9.4)
May 1-15	4	10	16	14	5 (0.4)	11 (1.2)	18 (1.7)	16 (1.3)	9 (3.1)	64 (18.3)	41 (7.8)	26 (4.8)	9 (3.2)	74 (20.9)	46 (9.2)	29 (5.6)
May 16-31	0	2	5	5	0 (0)	2 (0.3)	5 (0.5)	6 (0.5)	0 (0)	3 (1.1)	8 (2.2)	8 (2.1)	0 (0)	3 (1.1)	8 (2.3)	9 (2.3)
Jun 1-15	0	0	9	2	0 (0)	0 (0)	10 (0.8)	2 (0.2)	0 (0)	0 (0)	11 (1.2)	3 (1)	0 (0)	0 (0)	11 (1.6)	3 (1.1)
Jun 16-30	0	0	1	1	0 (0)	0 (0)	1 (0.1)	1 (0.1)	0 (0)	0 (0)	1 (0)	2 (1.3)	0 (0)	0 (0)	1 (0.1)	2 (1.3)
Jul 1-15	0	0	0		0 (0)	0 (0)	0 (0)		0 (0)	0 (0)	0 (0)		0 (0)	0 (0)	0 (0)	
Jul 16-31	0	0	0		0 (0)	0 (0)	0 (0)		0 (0)	0 (0)	0 (0)		0 (0)	0 (0)	0 (0)	
Total	19	81	82	119	21 (1.8)	92 (8.7)	92 (7.9)	133 (11.3)	25 (3.2)	172 (20.4)	172 (15.6)	147 (6.3)	25 (4)	197 (29)	190 (22.9)	164 (15.2)

Table 11. Number of spring-run (Mill-Deer creek) juvenile Chinook salmon by biweekly period and sample year that were DNA assigned to run (observed and corrected assignments) and corresponding estimates of total catch based on observed and corrected assignments. Standard errors for estimates are reported in parentheses. A " – " indicates that no trawl sampling was conducted during this strata. Periods with zero catch or no fish sampled for DNA are left blank. Sample year 2008 is defined as August 1st, 2007 – July 31st, 2008 and similarly for 2009, 2010 and 2011.

	Observed assignments				Corrected assignments				Total catch based on observed assignments				Total catch based on corrected assignments			
	2008	2009	2010	2011	2008	2009	2010	2011	2008	2009	2010	2011	2008	2009	2010	2011
Aug 1-15		0		0		0 (0.1)		0 (0.2)		0 (0)		0 (0)		0 (0.1)		0 (0.2)
Aug 16-31				0				0 (0.1)				0 (0)				0 (0.1)
Sep 1-15			0	0			0 (0)	0 (0.1)			0 (0)	0 (0)			0 (0)	0 (0.1)
Sep 16-30			0				0 (0)				0 (0)				0 (0)	
Oct 1-15				0				0 (0.1)				0 (0)				0 (0.1)
Oct 16-31																
Nov 1-15	0	0	0	0	0 (0)	0 (0.1)	0 (0.2)	0 (0.1)	0 (0)	0 (0)	0 (0)	0 (0)	0 (0)	0 (0.1)	0 (0.2)	0 (0.1)
Nov 16-30	0			0	0 (0.1)			0 (0.1)	0 (0)			0 (0)	0 (0.1)			0 (0.1)
Dec 1-15	0	0		0	0 (0.2)	0 (0.1)		0 (0)	0 (0)	0 (0)		0 (0)	0 (0.3)	0 (0.1)		0 (0)
Dec 16-31	0		0	0	0 (0.2)		0 (0.1)	0 (0.3)	0 (0)		0 (0)	0 (0)	0 (0.2)		0 (0.1)	0 (0.3)
Jan 1-15	0	0	0	0	0 (0.3)	0 (0.2)	0 (0)	0 (0.1)	0 (0)	0 (0)	0 (0)	0 (0)	0 (0.3)	0 (0.2)	0 (0)	0 (0.1)
Jan 16-31	0		0		0 (0.2)		0 (0.2)		0 (0)		0 (0)		0 (0.4)		0 (0.2)	
Feb 1-15		0	0	0		0 (0.1)	0 (0.1)	0 (0.1)		0 (0)	0 (0)	0 (0)		0 (0.1)	0 (0.1)	0 (0.1)
Feb 16-28	-	1	0	0	-	1 (0.2)	0 (0.2)	0 (0.1)	-	1 (0.4)	0 (0)	0 (0)	-	1 (0.5)	0 (0.2)	0 (0.1)
Mar 1-15	2	2	4	0	2 (0.2)	2 (0.3)	4 (0.4)	0 (0.1)	2 (0)	4 (1.5)	4 (0.3)	0 (0)	2 (0.2)	3 (1.5)	4 (0.5)	0 (0.1)
Mar 16-31	5	6	4	0	5 (0.5)	6 (0.7)	3 (0.6)	0 (0.6)	5 (0)	6 (0)	4 (0.5)	0 (0)	5 (0.5)	6 (0.7)	4 (0.8)	0 (0.6)
Apr 1-15	1	6	2	2	1 (0.3)	6 (1.1)	2 (0.9)	2 (0.6)	2 (0.7)	6 (0.7)	2 (0.5)	2 (0)	1 (0.8)	6 (1.4)	2 (1.1)	2 (0.6)
Apr 16-30	1	3	17	9	1 (2.2)	1 (4.1)	11 (6.5)	3 (9.6)	1 (0.3)	8 (3.6)	57 (12.7)	11 (1.5)	1 (2.4)	2 (10.7)	34 (27.3)	4 (11.8)
May 1-15	0	5	6	10	0 (2.1)	2 (3.2)	3 (5)	2 (12.2)	0 (0)	27 (11.2)	15 (4.5)	23 (5.3)	0 (4.7)	14 (18.3)	7 (12.8)	3 (27.2)
May 16-31	0	0	0	3	0 (0.6)	0 (0.9)	0 (3.1)	1 (6)	0 (0)	0 (0)	0 (0)	5 (1.7)	0 (0.9)	0 (1.2)	0 (5)	2 (9.2)
Jun 1-15	1	0	1	6	1 (0.8)	0 (0.6)	0 (2.2)	3 (5.6)	1 (0)	0 (0)	1 (0.4)	9 (2.2)	1 (0.8)	0 (0.7)	0 (2.5)	3 (8.5)
Jun 16-30	0	0	3	0	0 (0.2)	0 (0.4)	3 (0.5)	0 (1.2)	0 (0)	0 (0)	3 (0.5)	0 (0)	0 (0.3)	0 (0.4)	3 (0.8)	0 (1.9)
Jul 1-15	0	0	0		0 (0.1)	0 (0.2)	0 (0.2)		0 (0)	0 (0)	0 (0)		0 (0.1)	0 (0.2)	0 (0.2)	
Jul 16-31	0	0	0		0 (0.1)	0 (0.2)	0 (0.1)		0 (0)	0 (0)	0 (0)		0 (0.1)	0 (0.2)	0 (0.1)	
Total	10	23	37	30	10 (6.2)	18 (9.9)	27 (18.1)	10 (35)	11 (0.8)	52 (11.9)	86 (13.5)	50 (6.1)	10 (9.3)	32 (31.1)	54 (47.9)	14 (58.9)

Table 12. Number of winter-run juvenile Chinook salmon by biweekly period and sample year that were DNA assigned to run (observed and corrected assignments) and corresponding estimates of total catch based on observed and corrected assignments. Standard errors for estimates are reported in parentheses. A " – " indicates that no trawl sampling was conducted during this strata. Periods with zero catch or no fish sampled for DNA are left blank. Sample year 2008 is defined as August 1st, 2007 – July 31st, 2008 and similarly for 2009, 2010 and 2011.

	Observed assignments				Corrected assignments				Total catch based on observed assignments				Total catch based on corrected assignments			
	2008	2009	2010	2011	2008	2009	2010	2011	2008	2009	2010	2011	2008	2009	2010	2011
Aug 1-15		0		0		0 (0)		0 (0)		0 (0)		0 (0)		0 (0)		0 (0)
Aug 16-31				0				0 (0)				0 (0)				0 (0)
Sep 1-15			0	0			0 (0)	0 (0)			0 (0)	0 (0)			0 (0)	0 (0)
Sep 16-30			0				0 (0)				0 (0)				0 (0)	
Oct 1-15				0				0 (0)				0 (0)				0 (0)
Oct 16-31																
Nov 1-15	0	0	0	0	0 (0)	0 (0)	0 (0)	0 (0)	0 (0)	0 (0)	0 (0)	0 (0)	0 (0)	0 (0)	0 (0)	0 (0)
Nov 16-30	0			0	0 (0)			0 (0)	0 (0)			0 (0)	0 (0)			0 (0)
Dec 1-15	0	0		1	0 (0)	0 (0)		1 (0)	0 (0)	0 (0)		1 (0)	0 (0)	0 (0)		1 (0)
Dec 16-31	0		0	0	0 (0.1)		0 (0)	0 (0.1)	0 (0)		0 (0)	0 (0)	0 (0.1)		0 (0)	0 (0.1)
Jan 1-15	0	2	0	1	0 (0)	2 (0)	0 (0.1)	1 (0)	0 (0)	2 (0)	0 (0)	1 (0)	0 (0)	2 (0)	0 (0.1)	1 (0)
Jan 16-31	1		1		1 (0)		1 (0)		1 (0)		1 (0)		1 (0)		1 (0)	
Feb 1-15		0	3	0		0 (0)	3 (0)	0 (0)		0 (0)	3 (0)	0 (0)		0 (0)	3 (0)	0 (0)
Feb 16-28	-	8	5	5	-	8 (0.1)	5 (1.7)	5 (0.1)	-	10 (0.4)	5 (0)	5 (0)	-	10 (0.4)	5 (1.7)	5 (0.1)
Mar 1-15	3	5	16	5	3 (0)	5 (0.1)	16 (0.2)	5 (0.1)	3 (0)	7 (1.8)	17 (0.3)	5 (0)	3 (0)	7 (1.8)	17 (0.3)	5 (0.1)
Mar 16-31	6	5	12	10	6 (0.1)	5 (0.1)	12 (0.1)	10 (1.7)	6 (0)	6 (0.6)	12 (0)	10 (0)	6 (0.1)	6 (0.6)	12 (0.1)	10 (1.7)
Apr 1-15	1	1	0	7	1 (0)	1 (0)	0 (0)	7 (0.1)	2 (0.7)	1 (0)	0 (0)	7 (0.4)	2 (0.7)	1 (0)	0 (0)	7 (0.4)
Apr 16-30	0	2	0	5	0 (0)	2 (0.1)	0 (0.1)	5 (0.2)	0 (0)	3 (1.6)	0 (0)	5 (0.8)	0 (0)	3 (1.6)	0 (0.4)	5 (0.8)
May 1-15	0	0	0	0	0 (0)	0 (0)	0 (0.1)	0 (0.2)	0 (0)	0 (0)	0 (0)	0 (0)	0 (0.1)	0 (0.2)	0 (0.2)	0 (0.4)
May 16-31	0	0	0	0	0 (0)	0 (0.1)	0 (0.1)	0 (0.1)	0 (0)	0 (0)	0 (0)	0 (0)	0 (0)	0 (0.1)	0 (0.1)	0 (0.2)
Jun 1-15	0	0	0	0	0 (0)	0 (0)	0 (0)	0 (0.1)	0 (0)	0 (0)	0 (0)	0 (0)	0 (0)	0 (0)	0 (0)	0 (0.2)
Jun 16-30	0	0	0	0	0 (0)	0 (0.1)	0 (0.1)	0 (0.1)	0 (0)	0 (0)	0 (0)	0 (0)	0 (0)	0 (0.1)	0 (0.1)	0 (0.1)
Jul 1-15	0	0	0		0 (0)	0 (0)	0 (0.2)		0 (0)	0 (0)	0 (0)		0 (0)	0 (0)	0 (0.2)	
Jul 16-31	0	0	0		0 (0)	0 (0)	0 (0.1)		0 (0)	0 (0)	0 (0)		0 (0)	0 (0)	0 (0.1)	
Total	11	23	37	34	11 (0.1)	23 (0.3)	37 (1.8)	34 (1.8)	12 (0.7)	29 (2.5)	38 (0.3)	34 (0.9)	12 (0.7)	29 (2.5)	38 (1.9)	34 (2.1)

Total abundance estimates by run

Biweekly estimates of total (absolute) abundance, both for observed and corrected DNA assignments, are presented for each run in Table 13 - Table 17. These biweekly abundances, which were derived using the Jersey Point estimate of Chipps Island trawl efficiency, followed similar seasonal patterns to those discussed above for DNA assignments and total catch. In the remainder of this section, we focus on comparisons of annual abundance estimates.

Annual abundance estimates varied considerably across years for most runs. For example, based on estimates derived using corrected assignments and the Jersey Point efficiency, the ranges in annual abundances by run were as follows (summarized in Table 18): 1.4 million (in 2008) to 7.5 million (2011) for fall run; 71 thousand (2008) to 186 thousand (2011) for late-fall run; 67 thousand (2008) to 331 thousand (2010) for Butte Creek spring run; 36 thousand (2008) to 92 thousand (2010) for Mill-Deer creek spring run; and 45 thousand (2008) to 63 thousand (2010) for winter run. Regardless of how estimates were derived, annual abundances were lowest for all runs in sample year 2008, while the highest abundances were observed in sample year 2011 for fall and late-fall runs, and in sample year 2010 for spring and winter runs (Table 18).

Abundance estimates were strongly influenced by the choice of efficiency estimate (Table 18). Note that because abundance is inversely proportional to trawl efficiency (e.g., a low efficiency yields a high abundance estimate), and because efficiency was assumed to be constant, abundances based on different efficiencies had the same relative differences regardless of year, run, or assignment type. Thus, the largest abundance estimates were based on the lowest, paired-release estimate of efficiency (0.0064; see Table 4), while the lowest abundances were based on the high efficiency (0.04) implied by the fish-flux method. Relative to Jersey Point estimates, abundances were always 38% higher based on the paired-release efficiency, 29% lower for the Pittsburg efficiency, and 78% lower for the fish-flux method (Table 18). These large and consistent differences in abundance estimates based on the differing efficiencies apply to biweekly estimates as well, as illustrated for winter run in Figure 8.

Annual abundances based on corrected DNA assignments were often much lower than those based on observed assignments for late-fall run and Mill-Deer creek spring run (e.g., Table 18). Percentage differences in corrected versus observed estimates are presented in Table 19 (these were the same regardless of the efficiency estimate used). In sample years 2009-2011, abundances based on corrected assignments for the late-fall and Mill-Deer creek runs were 35% to 73% lower than those based on observed assignments (these fish were mostly transferred to fall run, accounting for the small percentage increases in corrected abundances of fall run). Note that the slight annual differences shown for winter run (Table 19) were not due to differences in observed and corrected assignments, which were always equal (see Table 12); rather, these differences were due to rounding errors in sums of total (corrected) catch estimates across runs, which affected estimates of winter-run proportions in a few biweekly periods.

Across years, fall run composed between 84.0% and 92.8% of the total annual abundance across runs, based on corrected assignments (Figure 9). Late-fall run composed 1.9% to 4.4%, while Butte Creek spring run ranged between 3.9% and 9.0%. Mill-Deer creek spring run and winter run each composed less than 3% of the total abundance in sample year 2008, and less than 2% in subsequent years. Abundance proportions based on observed assignments (not shown) were notably higher for the late-fall and Mill-Deer creek runs in sample years 2009-2011.

Components of variance

The precision of annual abundance estimates, as reflected by their standard errors, varied considerably depending on run, assignment type (observed or corrected), and efficiency estimate (Table 18). Variances for abundances based on corrected assignments were larger than those for observed assignments because of measurement errors in assignment corrections. Note that variances for abundances based on the fish-flux method were biased low because there was no estimate of precision associated with this efficiency (see Table 4).

An assessment of the variance components for annual abundances is presented in Table 20. These results are for abundances based on corrected assignments and the Jersey Point efficiency (similar results were found for the paired-release and Pittsburg efficiencies). Note that corrected assignments provide a much better reflection of true uncertainty than observed assignments, which assume no error in DNA assignments. The four variance components in Table 20 were defined in Equation 22. In addition, as a relative measure of precision, Table 20 reports the coefficient of variation (CV = standard error/estimate) for abundance estimates.

The most precise estimates were for fall run, with CVs of 21% or less (Table 20). Variances for fall-run abundances were largely driven by two components: variances in catch (due to missing sampling days) and efficiency. Abundances for Butte Creek spring run and winter run were also reasonably precise, though their variance components differed. For Butte Creek estimates, all four components contributed 20% or more of the variance, depending on the year. For winter run, sampling error (i.e., low numbers of assignments) was the dominant source of variance (50% or more), while measurement error in corrected assignments contributed little (6% or less). In contrast, abundance estimates for late-fall run and Mill-Deer creek spring run were very imprecise (CVs > 75%) because of measurement error in corrected assignments.

Table 13. Absolute abundance estimates for juvenile fall-run Chinook salmon by biweekly period and sample year based on observed and corrected DNA assignments and using the Jersey Point (proximal release) estimate of Chipps Island trawl efficiency. Standard errors for estimates are reported in parentheses. A " – " indicates that no trawl sampling was conducted during this strata. Periods with zero catch or no fish sampled for DNA are left blank. Sample year 2008 is defined as August 1st, 2007 – July 31st, 2008 and similarly for 2009, 2010 and 2011.

	Abundance based on observed assignments				Abundance based on corrected assignments			
	2008	2009	2010	2011	2008	2009	2010	2011
Aug 1-15		3,370 (4,490)		0 (0)		3,370 (4,554)		0 (3,752)
Aug 16-31				3,287 (3,714)				3,287 (3,788)
Sep 1-15			4,509 (5,118)	1,567 (1,763)			4,509 (5,118)	1,567 (1,890)
Sep 16-30			3,252 (3,656)				3,252 (3,656)	
Oct 1-15				0 (0)				0 (930)
Oct 16-31								
Nov 1-15	1,562 (1,961)	5,684 (7,573)	1,913 (2,197)	3,670 (2,985)	1,562 (1,961)	5,684 (7,682)	0 (1,914)	3,670 (3,090)
Nov 16-30	3,007 (3,854)			0 (0)	3,007 (3,913)			0 (1,169)
Dec 1-15	5,918 (3,422)	0 (0)		0 (0)	1,479 (2,958)	0 (1,259)		0 (17)
Dec 16-31	6,156 (2,709)		1,613 (1,808)	0 (0)	5,277 (2,579)		0 (702)	0 (3,438)
Jan 1-15	5,873 (5,560)	4,389 (3,657)	0 (0)	3,814 (3,409)	2,936 (6,541)	0 (1,911)	0 (654)	3,814 (3,516)
Jan 16-31	6,378 (3,643)		9,303 (6,629)		3,644 (3,419)		9,303 (6,954)	
Feb 1-15		0 (0)	3,790 (2,991)	1,655 (2,077)		0 (1,149)	1,895 (2,172)	1,655 (2,110)
Feb 16-28	-	0 (0)	0 (0)	1,536 (1,723)	-	0 (1,060)	0 (4,152)	1,536 (1,759)
Mar 1-15	0 (0)	15,358 (7,424)	3,142 (2,355)	1,772 (1,870)	0 (1,703)	14,022 (7,689)	1,571 (1,945)	0 (775)
Mar 16-31	10,533 (5,800)	9,273 (5,359)	13,613 (7,532)	14,169 (6,666)	7,899 (5,271)	7,419 (6,473)	13,109 (7,589)	14,169 (9,348)
Apr 1-15	47,159 (17,584)	75,467 (23,450)	92,678 (26,429)	66,292 (24,263)	47,965 (17,771)	66,254 (22,481)	91,645 (27,269)	62,603 (23,637)
Apr 16-30	346,378 (106,015)	781,219 (189,985)	2,502,152 (674,205)	1,371,401 (422,320)	352,104 (111,272)	811,500 (204,293)	2,599,928 (718,837)	1,400,539 (440,542)
May 1-15	698,262 (245,006)	1,214,466 (296,072)	1,306,498 (431,479)	3,455,630 (972,025)	714,726 (254,279)	1,262,784 (318,272)	1,355,467 (457,132)	3,623,379 (1,042,399)
May 16-31	146,679 (59,541)	128,054 (41,796)	752,419 (225,346)	1,261,971 (323,185)	146,679 (60,650)	125,989 (42,265)	771,403 (234,651)	1,296,559 (339,010)
Jun 1-15	72,503 (21,591)	56,061 (21,686)	261,213 (77,549)	936,173 (220,114)	72,503 (22,404)	52,764 (20,988)	252,901 (76,632)	945,808 (227,770)
Jun 16-30	42,160 (13,318)	18,742 (8,827)	54,928 (21,362)	196,979 (60,615)	40,539 (13,030)	13,119 (7,916)	48,825 (19,805)	184,168 (58,196)
Jul 1-15	0 (0)	14,872 (6,934)	11,090 (5,424)		0 (2,004)	13,013 (6,758)	11,090 (6,167)	
Jul 16-31	0 (0)	6,603 (4,442)	1,891 (2,441)		0 (1,397)	6,603 (4,616)	1,891 (2,572)	
Total	1,392,577 (275,465)	2,333,565 (356,147)	5,024,010 (835,987)	7,319,925 (1,131,567)	1,400,328 (286,062)	2,382,526 (382,209)	5,166,794 (887,687)	7,542,762 (1,204,820)

Table 14. Absolute abundance estimates for juvenile late-fall-run Chinook salmon by biweekly period and sample year based on observed and corrected DNA assignments and using the Jersey Point (proximal release) estimate of Chipps Island trawl efficiency. A " – " indicates that no trawl sampling was conducted during this strata. Time periods with zero catch or no fish sampled for DNA are left blank. Sample year 2008 is defined as August 1st, 2007 – July 31st, 2008 and similarly for 2009, 2010 and 2011.

	Abundance based on observed assignments				Abundance based on corrected assignments			
	2008	2009	2010	2011	2008	2009	2010	2011
Aug 1-15		0 (0)		6,468 (5,312)		0 (732)		6,468 (6,516)
Aug 16-31				0 (0)				0 (714)
Sep 1-15			0 (0)	1,567 (1,763)			0 (30)	1,567 (1,894)
Sep 16-30			0 (0)				0 (21)	
Oct 1-15				1,603 (2,012)				1,603 (2,219)
Oct 16-31								
Nov 1-15	0 (0)	0 (0)	3,826 (3,462)	1,835 (1,977)	0 (10)	0 (1,234)	5,739 (5,022)	1,835 (2,137)
Nov 16-30	0 (0)			2,016 (2,583)	0 (653)			2,016 (2,838)
Dec 1-15	5,918 (3,422)	2,171 (2,781)		0 (0)	10,357 (5,496)	2,171 (3,056)		0 (23)
Dec 16-31	2,638 (1,635)		1,613 (1,808)	7,735 (5,187)	3,518 (2,078)		3,226 (2,895)	7,735 (6,240)
Jan 1-15	11,746 (9,289)	4,389 (3,657)	1,800 (2,307)	0 (0)	14,683 (12,416)	8,778 (6,165)	1,800 (2,412)	0 (829)
Jan 16-31	5,467 (3,454)		0 (0)		8,200 (4,790)		0 (2,021)	
Feb 1-15		1,980 (2,537)	1,895 (2,008)	0 (0)		1,980 (2,788)	3,790 (3,107)	0 (359)
Feb 16-28	-	1,653 (1,766)	3,313 (2,778)	0 (0)	-	1,653 (2,046)	3,313 (6,280)	0 (346)
Mar 1-15	0 (0)	9,599 (6,062)	1,571 (1,618)	1,772 (1,870)	0 (531)	12,019 (7,764)	3,142 (2,465)	3,544 (2,887)
Mar 16-31	2,633 (2,702)	9,273 (5,359)	1,701 (1,848)	0 (0)	5,266 (4,083)	11,128 (7,525)	3,277 (2,830)	0 (7,607)
Apr 1-15	2,619 (2,807)	2,474 (1,856)	5,915 (3,723)	3,583 (2,814)	2,821 (3,654)	3,680 (5,268)	3,818 (7,172)	5,216 (4,907)
Apr 16-30	5,725 (4,522)	38,012 (14,468)	86,619 (33,262)	64,102 (23,158)	0 (26,650)	5,235 (50,690)	8,181 (153,807)	27,194 (84,480)
May 1-15	28,403 (15,944)	48,317 (21,657)	47,612 (21,556)	138,392 (46,448)	11,872 (41,767)	3,917 (78,510)	3,829 (89,294)	6,290 (209,515)
May 16-31	3,333 (4,186)	12,392 (7,074)	19,075 (9,985)	36,551 (13,916)	3,333 (11,779)	14,457 (11,863)	0 (39,955)	5,779 (66,007)
Jun 1-15	0 (0)	4,946 (3,488)	30,448 (11,461)	73,866 (21,629)	0 (5,742)	8,244 (6,291)	40,270 (20,208)	73,866 (51,674)
Jun 16-30	3,243 (2,526)	11,245 (6,040)	12,206 (6,685)	30,427 (12,625)	4,864 (3,571)	16,867 (9,162)	18,309 (9,856)	43,239 (20,149)
Jul 1-15	3,454 (4,603)	5,577 (3,537)	11,090 (5,424)		3,454 (5,025)	7,436 (4,725)	11,090 (6,228)	
Jul 16-31	2,408 (3,166)	3,301 (2,767)	1,891 (2,441)		2,408 (3,464)	3,301 (3,038)	1,891 (2,585)	
Total	77,594	155,335	230,582	369,923	70,782	100,874	111,681	186,359
	(21,392)	(29,947)	(43,982)	(59,991)	(54,026)	(96,100)	(184,217)	(242,200)

Table 15. Absolute abundance estimates for juvenile spring-run (Butte Creek) Chinook salmon by biweekly period and sample year based based on observed and corrected DNA assignments and using the Jersey Point (proximal release) estimate of Chipps Island trawl efficiency. Standard errors for estimates are reported in parentheses. A " – " indicates that no trawl sampling was conducted during this strata. Periods with zero catch or no fish sampled for DNA are left blank. Sample year 2008 is defined as August 1st, 2007 – July 31st, 2008 and similarly for 2009, 2010 and 2011.

	Abundance based on observed assignments				Abundance based on corrected assignments			
	2008	2009	2010	2011	2008	2009	2010	2011
Aug 1-15		0 (0)		0 (0)		0 (0)		0 (0)
Aug 16-31				0 (0)				0 (0)
Sep 1-15			0 (0)	0 (0)			0 (0)	0 (0)
Sep 16-30			0 (0)				0 (0)	
Oct 1-15				0 (0)				0 (0)
Oct 16-31								
Nov 1-15	0 (0)	0 (0)	0 (0)	0 (0)	0 (0)	0 (0)	0 (0)	0 (0)
Nov 16-30	0 (0)			0 (0)	0 (0)			0 (0)
Dec 1-15	0 (0)	0 (0)		0 (0)	0 (0)	0 (0)		0 (0)
Dec 16-31	0 (0)		0 (0)	0 (0)	0 (0)		0 (0)	0 (0)
Jan 1-15	0 (0)	0 (0)	0 (0)	0 (0)	0 (0)	0 (0)	0 (0)	0 (0)
Jan 16-31	0 (0)		0 (0)		0 (0)		0 (0)	
Feb 1-15		0 (0)	0 (0)	0 (0)		0 (0)	0 (0)	0 (0)
Feb 16-28	-	0 (0)	0 (0)	0 (0)	-	0 (0)	0 (1,739)	0 (0)
Mar 1-15	0 (0)	0 (0)	0 (0)	0 (0)	0 (0)	0 (0)	0 (0)	0 (0)
Mar 16-31	2,633 (2,702)	3,709 (2,935)	1,701 (1,848)	0 (0)	2,633 (2,721)	3,709 (2,974)	1,638 (1,859)	0 (1,859)
Apr 1-15	13,099 (7,026)	61,858 (19,616)	17,746 (7,403)	32,250 (13,005)	14,107 (7,275)	69,935 (22,832)	21,002 (8,584)	34,779 (14,230)
Apr 16-30	28,626 (12,580)	69,470 (22,320)	165,066 (51,925)	174,824 (56,855)	28,626 (12,861)	79,841 (25,995)	183,254 (58,760)	196,192 (65,689)
May 1-15	21,302 (12,607)	83,576 (33,080)	78,085 (32,020)	54,518 (21,280)	21,370 (12,777)	96,634 (37,755)	88,067 (36,215)	60,809 (23,703)
May 16-31	0 (0)	6,196 (4,620)	16,955 (9,065)	15,389 (7,821)	0 (0)	6,196 (4,676)	17,047 (9,285)	17,338 (8,489)
Jun 1-15	0 (0)	0 (0)	17,627 (7,593)	4,817 (3,431)	0 (0)	0 (0)	17,719 (7,756)	4,817 (3,468)
Jun 16-30	0 (0)	0 (0)	2,034 (2,142)	3,202 (3,166)	0 (0)	0 (0)	2,034 (2,159)	3,202 (3,185)
Jul 1-15	0 (0)	0 (0)	0 (0)		0 (0)	0 (0)	0 (0)	
Jul 16-31	0 (0)	0 (0)	0 (0)		0 (0)	0 (0)	0 (0)	
Total	65,663	224,811	299,219	285,004	66,738	256,317	330,764	317,140
	(19,337)	(44,803)	(62,643)	(62,750)	(19,723)	(51,510)	(70,679)	(71,952)

Table 16. Absolute abundance estimates for juvenile spring-run (Mill-Deer) Chinook salmon by biweekly period and sample year based on observed and corrected DNA assignments and using the Jersey Point (proximal release) estimate of Chipps Island trawl efficiency. Standard errors for estimates are reported in parentheses. A " – " indicates that no trawl sampling was conducted during this strata. Periods with zero catch or no fish sampled for DNA are left blank. Sample year 2008 is defined as August 1st, 2007 – July 31st, 2008 and similarly for 2009, 2010 and 2011.

	Abundance based on observed assignments				Abundance based on corrected assignments			
	2008	2009	2010	2011	2008	2009	2010	2011
Aug 1-15		0 (0)		0 (0)		0 (183)		0 (660)
Aug 16-31				0 (0)				0 (179)
Sep 1-15			0 (0)	0 (0)			0 (0)	0 (119)
Sep 16-30			0 (0)				0 (0)	
Oct 1-15				0 (0)				0 (163)
Oct 16-31								
Nov 1-15	0 (0)	0 (0)	0 (0)	0 (0)	0 (0)	0 (309)	0 (329)	0 (140)
Nov 16-30	0 (0)			0 (0)	0 (163)			0 (206)
Dec 1-15	0 (0)	0 (0)		0 (0)	0 (430)	0 (221)		0 (14)
Dec 16-31	0 (0)		0 (0)	0 (0)	0 (176)		0 (123)	0 (592)
Jan 1-15	0 (0)	0 (0)	0 (0)	0 (0)	0 (967)	0 (336)	0 (1)	0 (208)
Jan 16-31	0 (0)		0 (0)		0 (386)		0 (507)	
Feb 1-15		0 (0)	0 (0)	0 (0)		0 (202)	0 (150)	0 (90)
Feb 16-28	-	1,653 (1,890)	0 (0)	0 (0)	-	1,653 (1,920)	0 (325)	0 (101)
Mar 1-15	15,059 (11,238)	7,679 (5,809)	6,284 (3,538)	0 (0)	15,059 (11,326)	6,009 (5,054)	6,284 (3,610)	0 (150)
Mar 16-31	13,166 (6,625)	11,128 (6,020)	6,806 (4,024)	0 (0)	13,166 (6,745)	11,128 (6,146)	6,554 (4,104)	0 (1,042)
Apr 1-15	5,239 (4,913)	7,422 (3,750)	3,943 (3,041)	3,583 (2,758)	2,821 (3,506)	7,361 (4,022)	3,818 (3,547)	3,477 (2,915)
Apr 16-30	2,862 (3,078)	10,486 (6,462)	93,156 (34,692)	21,367 (9,597)	2,862 (7,573)	2,617 (14,125)	55,630 (48,084)	7,769 (23,421)
May 1-15	0 (0)	35,258 (18,231)	28,567 (14,732)	48,227 (20,133)	0 (11,219)	18,282 (24,772)	13,401 (25,449)	6,290 (57,159)
May 16-31	0 (0)	0 (0)	0 (0)	9,618 (5,951)	0 (2,939)	0 (2,513)	0 (10,646)	3,853 (18,049)
Jun 1-15	1,859 (1,916)	0 (0)	1,602 (1,760)	14,452 (6,809)	1,859 (2,406)	0 (1,162)	0 (3,941)	4,817 (13,902)
Jun 16-30	0 (0)	0 (0)	6,103 (4,209)	0 (0)	0 (463)	0 (715)	6,103 (4,386)	0 (3,117)
Jul 1-15	0 (0)	0 (0)	0 (0)		0 (353)	0 (433)	0 (431)	
Jul 16-31	0 (0)	0 (0)	0 (0)		0 (246)	0 (279)	0 (103)	
Total	38,188	73,629	146,465	97,249	35,769	47,053	91,793	26,209
	(14,405)	(21,490)	(38,463)	(24,225)	(19,634)	(30,086)	(56,134)	(65,994)

Table 17. Absolute abundance estimates for juvenile winter-run Chinook salmon by biweekly period and sample year based on observed and corrected DNA assignments and using the Jersey Point (proximal release) estimate of Chipps Island trawl efficiency. Standard errors for estimates are reported in parentheses. A " – " indicates that no trawl sampling was conducted during this strata. Periods with zero catch or no fish sampled for DNA are left blank. Sample year 2008 is defined as August 1st, 2007 – July 31st, 2008 and similarly for 2009, 2010 and 2011.

	Abundance based on observed assignments				Abundance based on corrected assignments			
	2008	2009	2010	2011	2008	2009	2010	2011
Aug 1-15		0 (0)		0 (0)		0 (0)		0 (0)
Aug 16-31				0 (0)				0 (0)
Sep 1-15			0 (0)	0 (0)			0 (1)	0 (0)
Sep 16-30			0 (0)				0 (1)	
Oct 1-15				0 (0)				0 (0)
Oct 16-31								
Nov 1-15	0 (0)	0 (0)	0 (0)	0 (0)	0 (0)	0 (0)	0 (0)	0 (0)
Nov 16-30	0 (0)			0 (0)	0 (0)			0 (0)
Dec 1-15	0 (0)	0 (0)		2,000 (2,511)	0 (0)	0 (0)		2,000 (2,511)
Dec 16-31	0 (0)		0 (0)	0 (0)	0 (67)		0 (0)	0 (148)
Jan 1-15	0 (0)	4,389 (3,657)	0 (0)	1,907 (2,173)	0 (1)	4,389 (3,658)	0 (138)	1,907 (2,173)
Jan 16-31	911 (932)		3,101 (3,360)		911 (932)		3,101 (3,360)	
Feb 1-15		0 (0)	5,685 (3,841)	0 (0)		0 (0)	5,685 (3,841)	0 (0)
Feb 16-28	-	16,533 (8,506)	8,284 (5,257)	7,684 (5,201)	-	16,533 (8,508)	8,284 (5,970)	7,684 (5,202)
Mar 1-15	22,589 (14,112)	13,438 (7,362)	26,707 (9,411)	8,860 (4,963)	22,589 (14,114)	14,022 (7,442)	26,707 (9,415)	8,860 (4,964)
Mar 16-31	15,799 (7,409)	11,128 (6,244)	20,420 (8,561)	17,712 (7,365)	15,799 (7,411)	11,128 (6,247)	19,664 (8,387)	17,712 (7,964)
Apr 1-15	5,239 (4,913)	1,237 (1,265)	0 (0)	12,541 (6,272)	5,643 (4,945)	1,226 (1,265)	0 (18)	12,172 (6,195)
Apr 16-30	0 (0)	3,932 (3,255)	0 (0)	9,712 (5,466)	0 (82)	3,926 (3,261)	0 (639)	9,712 (5,478)
May 1-15	0 (0)	0 (0)	0 (0)	0 (0)	0 (182)	0 (297)	0 (318)	0 (888)
May 16-31	0 (0)	0 (0)	0 (0)	0 (0)	0 (34)	0 (214)	0 (213)	0 (356)
Jun 1-15	0 (0)	0 (0)	0 (0)	0 (0)	0 (18)	0 (11)	0 (63)	0 (302)
Jun 16-30	0 (0)	0 (0)	0 (0)	0 (0)	0 (12)	0 (141)	0 (172)	0 (195)
Jul 1-15	0 (0)	0 (0)	0 (0)		0 (0)	0 (2)	0 (424)	
Jul 16-31	0 (0)	0 (0)	0 (0)		0 (0)	0 (0)	0 (145)	
Total	44,540	50,659	64,199	60,420	44,943	51,228	63,442	60,051
	(16,705)	(13,825)	(14,682)	(13,646)	(16,719)	(13,877)	(14,884)	(13,987)

Table 18. Annual abundance estimates for juvenile Chinook salmon by run and sample year based on observed and corrected DNA assignments. Annual abundances are shown for four alternative estimates of Chipps Island trawl efficiency (Jersey Point releases, paired-release tests, Pittsburg releases, and the fish-flux method). Standard errors are shown in parentheses. Year 2008 is defined as August 1st, 2007 – July 31st, 2008 and similarly for 2009, 2010 and 2011.

		Annual abundance based on observed assignments (thousands)				Annual abundance based on corrected assignments (thousands)			
Run	Year	Jersey Point	Paired release	Pittsburg	Fish flux	Jersey Point	Paired release	Pittsburg	Fish flux
Fall	2008	1392.6 (275.5)	1914.8 (327.7)	988.3 (173.5)	306.4 (48.8)	1400.3 (294.2)	1925.5 (355.0)	993.8 (187.5)	308.1 (53.3)
	2009	2333.6 (356.1)	3208.7 (347.2)	1656.1 (192.6)	513.4 (43.2)	2382.5 (399.8)	3276.0 (416.6)	1690.8 (227.2)	524.2 (55.9)
	2010	5024.0 (836.0)	6908.0 (913.6)	3565.4 (492.6)	1105.3 (128.0)	5166.8 (924.3)	7104.3 (1044.8)	3666.8 (559.2)	1136.7 (150.3)
	2011	7319.9 (1131.6)	10064.9 (1224.0)	5194.8 (661.6)	1610.4 (170.0)	7542.8 (1256.9)	10371.3 (1409.5)	5352.9 (755.7)	1659.4 (201.5)
Late-fall	2008	77.6 (21.4)	106.7 (28.3)	55.1 (14.7)	17.1 (4.5)	70.8 (84.2)	97.3 (115.6)	50.2 (59.7)	15.6 (18.5)
	2009	155.3 (29.9)	213.6 (38.1)	110.2 (19.9)	34.2 (5.9)	100.9 (145.1)	138.7 (199.4)	71.6 (102.9)	22.2 (31.9)
	2010	230.6 (44.0)	317.0 (54.9)	163.6 (28.8)	50.7 (8.4)	111.7 (304.8)	153.6 (418.9)	79.3 (216.2)	24.6 (67.0)
	2011	369.9 (60.0)	508.6 (71.0)	262.5 (37.7)	81.4 (10.5)	186.4 (416.0)	256.2 (571.6)	132.3 (295.0)	41.0 (91.4)
Spring	2008	65.7 (19.3)	90.3 (25.0)	46.6 (13.0)	14.4 (3.9)	66.7 (20.3)	91.8 (26.4)	47.4 (13.7)	14.7 (4.1)
Butte	2009	224.8 (44.8)	309.1 (53.9)	159.5 (28.5)	49.5 (8.1)	256.3 (55.5)	352.4 (68.2)	181.9 (35.9)	56.4 (10.4)
	2010	299.2 (62.6)	411.4 (74.1)	212.3 (39.3)	65.8 (11.0)	330.8 (73.9)	454.8 (89.1)	234.7 (47.0)	72.8 (13.4)
	2011	285.0 (62.7)	391.9 (74.0)	202.3 (39.3)	62.7 (11.0)	317.1 (74.5)	436.1 (89.6)	225.1 (47.3)	69.8 (13.4)
Spring	2008	38.2 (14.4)	52.5 (19.2)	27.1 (9.9)	8.4 (3.0)	35.8 (26.9)	49.2 (36.7)	25.4 (18.9)	7.9 (5.8)
Mill-Deer	2009	73.6 (21.5)	101.2 (28.0)	52.3 (14.6)	16.2 (4.4)	47.1 (43.4)	64.7 (59.4)	33.4 (30.7)	10.4 (9.5)
	2010	146.5 (38.5)	201.4 (47.5)	103.9 (25.0)	32.2 (7.2)	91.8 (87.2)	126.2 (119.1)	65.1 (61.5)	20.2 (19.0)
	2011	97.2 (24.2)	133.7 (30.6)	69.0 (16.0)	21.4 (4.7)	26.2 (115.1)	36.0 (158.2)	18.6 (81.7)	5.8 (25.3)
Winter	2008	44.5 (16.7)	61.2 (22.0)	31.6 (11.4)	9.8 (3.5)	44.9 (16.7)	61.8 (22.0)	31.9 (11.4)	9.9 (3.5)
	2009	50.7 (13.8)	69.7 (18.1)	36.0 (9.4)	11.1 (2.8)	51.2 (13.9)	70.4 (18.1)	36.4 (9.4)	11.3 (2.8)
	2010	64.2 (14.7)	88.3 (18.4)	45.6 (9.6)	14.1 (2.8)	63.4 (14.9)	87.2 (18.7)	45.0 (9.8)	14.0 (2.9)
	2011	60.4 (13.6)	83.1 (17.7)	42.9 (9.2)	13.3 (2.8)	60.1 (14.0)	82.6 (18.3)	42.6 (9.5)	13.2 (2.9)

Table 19. Percent difference between annual abundance estimates for juvenile Chinook salmon by run and sample year based on observed versus corrected DNA assignments. Differences in abundance estimates were computed relative to abundances based on observed assignments (i.e., % difference = 100*[corrected – observed]/observed).

Sampling year	Fall	Late-fall	Spring Butte	Spring Mill-Deer	Winter
2008	0.6	-8.8	1.6	-6.3	0.9
2009	2.1	-35.1	14.0	-36.1	1.1
2010	2.8	-51.6	10.5	-37.3	-1.2
2011	3.0	-49.6	11.3	-73.0	-0.6

Table 20. Coefficient of variation (CV) and components of variance (as a percentage of total variance) by run and sample year for annual abundance estimates based on corrected assignments and the Jersey Point (proximal release) estimate of Chipps Island trawl efficiency.

			Components of variance in annual abundance (% of total variance)			
Run	Year	CV (%)	Assignment corrections	Sampling error (Poison)	Missing days (catch)	Efficiency estimate
Fall	2008	21.0	8.8	7.1	52.0	32.2
	2009	16.8	14.9	8.3	17.2	59.6
	2010	17.9	12.2	3.3	39.2	45.4
	2011	16.7	12.2	1.7	39.2	46.9
Late-fall	2008	118.9	95.5	2.9	1.2	0.4
	2009	143.8	98.3	1.1	0.3	0.2
	2010	272.9	99.5	0.2	0.1	0.1
	2011	223.2	99.4	0.3	0.1	0.2
Spring Butte	2008	30.4	8.8	58.0	18.2	15.0
	2009	21.7	20.1	39.7	12.1	28.1
	2010	22.3	14.3	26.4	26.8	32.5
	2011	23.5	12.8	14.7	39.5	33.0
Spring Mill-Deer	2008	75.1	73.0	23.7	0.8	2.4
	2009	92.1	86.9	10.9	0.9	1.2
	2010	95.0	91.0	5.7	1.4	1.9
	2011	439.3	99.4	0.5	0.0	0.0
Winter	2008	37.2	0.1	83.9	4.1	11.9
	2009	27.1	0.3	61.8	24.3	13.7
	2010	23.5	4.3	49.9	23.0	22.8
	2011	23.3	6.1	55.8	23.2	14.9

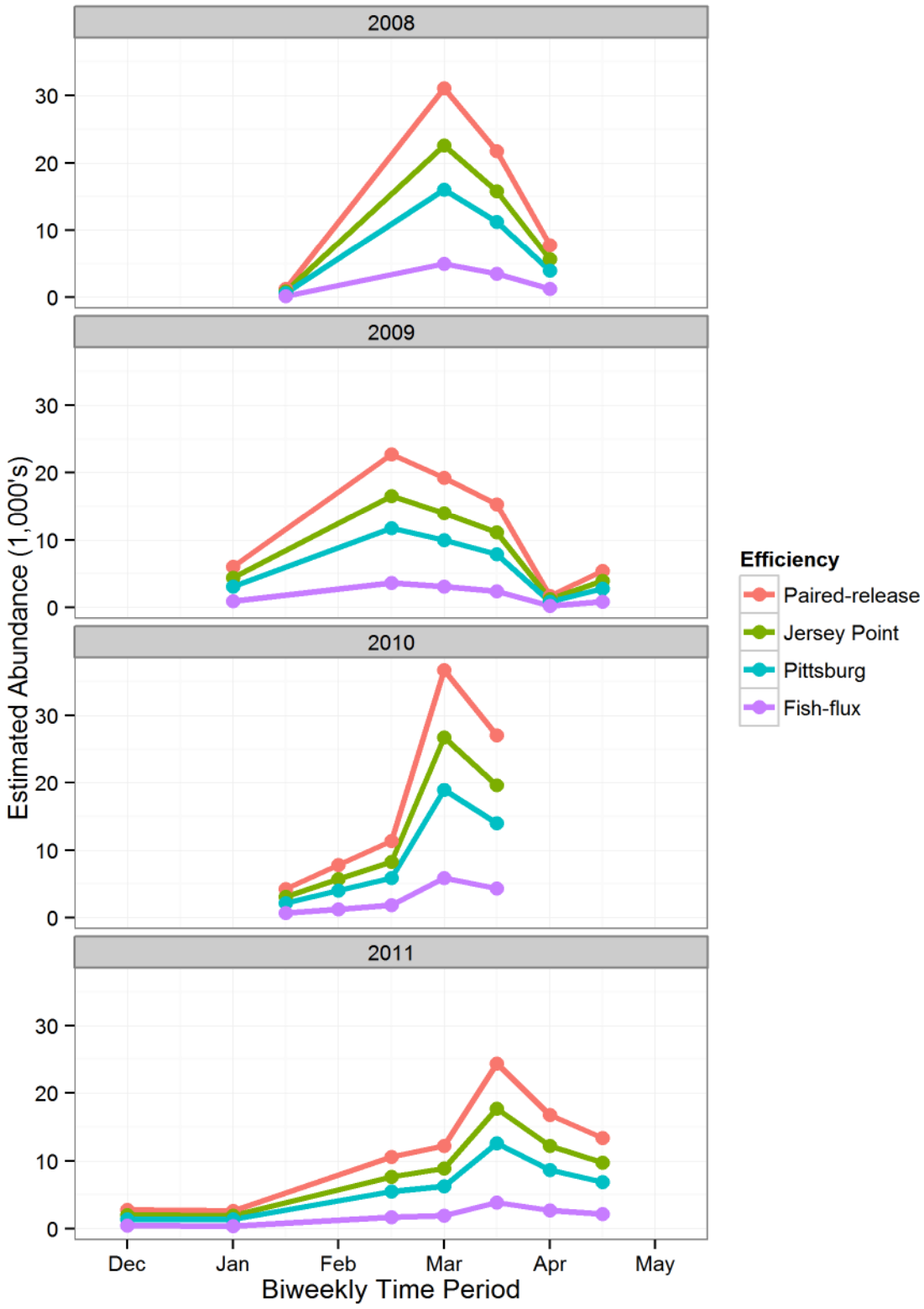

Figure 8. Abundance estimates of winter-run juvenile Chinook salmon at Chipps Island by sample year for four different estimates of trawl efficiency (abundance estimates based on corrected DNA assignments).

Figure 9. Pie chart depicting the run composition of juvenile Chinook salmon abundance at Chipps Island by sample year. Abundance estimates were based on corrected DNA assignments using the Jersey Point estimate of trawl efficiency. Run abbreviations are fall (F), lafe-fall(LF), spring Butte (SB), spring Mill-Deer (SMD), and winter (W).

Discussion

In this study, we developed and applied an analytical framework for estimating juvenile abundances of genetically distinct Chinook salmon populations captured in trawl samples near Chipps Island. The results of four years of juvenile sampling indicate that DNA assignments are likely to be much more accurate than length-at-date criteria (the historical method) for distinguishing winter and spring-run Chinook salmon, which are both ESA-listed. However, there were two critical sources of uncertainty in DNA-based estimates. First, there is a lack of blind-test data to reliably determine DNA assignment errors and corrections for spring run, and assignment corrections for Mill-Deer creek spring run were highly uncertain. Second, estimates of total juvenile abundance (i.e., juveniles emigrating past Chipps Island) were strongly influenced by estimates of trawl efficiency. It is currently unclear which of the efficiency estimates we examined is most accurate, and to what extent trawl efficiency may vary seasonally or among years.

Comparison to length-at-date criteria

A key limitation of the use of length-at-date criteria for run classification is that juveniles of the fall and late-fall runs may overlap with, and potentially dominate, those categories designated for spring and winter runs. Our results indicate that such overlap occurred in all four years examined, and when compared to length criteria, use of DNA assignments provided much more accurate, and reduced, estimates of run composition for the spring and winter runs (see Figure 6 and Figure 7 for results relevant to this discussion). Note that although we did not estimate total abundances based on length criteria, the raw assignments provide a good proxy for comparing relative differences in run compositions between methods.

In general, most fall run migrate to sea as subyearling juveniles in April and May, with small percentages migrating in other months or as yearlings in their second spring. Late-fall-run juveniles, as classified by their DNA, showed a life-history diversity and length-at-date distribution similar to fall run. These runs overlapped considerably with the length-at-date criteria for spring and winter runs. As a result, estimates of spring- and winter-run composition based on length-at-date assignments were roughly 2 to 6 times greater (i.e., overestimates) than compared to DNA assignments. In contrast, late-fall compositions were strongly underestimated in most years based on length criteria (i.e., relatively few fish were captured in the length criteria for late-fall run, while most DNA assignments of late-fall run occurred within the length criteria for other runs).

These findings have important implications. First, given the broad overlap in length-at-date distributions observed among runs (based on DNA assignments), it is clear that the length-at-date method cannot be substantively improved to better allocate runs. In short, the use of mutually exclusive run criteria is inappropriate, in particular given the low relative abundances of spring and winter run. Winter run was the only run for which the length-at-date criteria was accurate, but relatively high numbers of fall and late-fall DNA assignments were also present within the

winter length-at-date criteria. The length-at-date range for spring run was incomplete and included large numbers of fall-run DNA assignments in most years. Given the numerical dominance of fall run (e.g., 84% to 93% of the total abundance across years; Figure 9), it is inevitable that overlaps of fall run will inflate estimates of spring and winter run based on length criteria.

Second, the consistent and substantial overestimates in spring and winter-run compositions, when determined by length criteria, indicates that past estimates for these runs (all based on length criteria) were likely biased high. This conclusion should be applicable to all Delta sampling programs that have employed length criteria to estimate run compositions. The same tendency for length criteria to overestimate the number of winter run has been found through genetic sampling of juvenile salmon salvaged at the Delta Fish Facilities (Hedgecock 2002; B. Harvey, California Department of Water Resources, pers. comm.). Because length criteria consistently overestimated spring and winter assignments in the four years we examined, it is tempting to consider the development of possible correction factors to apply to length-based estimates in previous years. However, there was considerable variation in the overestimates (e.g., 2- to 6-fold changes), and we might expect much greater variation across years due to changes in the true relative compositions of the various runs. At a minimum, it is reasonable to conclude that past estimates based on length criteria would tend to strongly overestimate the spring run and winter-run components.

Corrections to DNA assignments based on blind-test data

The methodology we used to generate "corrected" estimates of DNA run assignments appears intuitive and appropriate; however, it was beyond the scope of this project to conduct a thorough review of the relevant statistical literature. The premise of the approach is sound, that is, there will be assignment errors using DNA methods, and blind-test data provide estimates of those error rates that can be used to adjust or "correct" new samples of observed assignments. In our application, the correction method had important effects on estimates for some runs, but there were also limitations of the blind-test data and methodology that warrant further investigation.

To review, we divided the available blind-test data (Tables 1-3) into two ONCOR assignment probability categories ($P = 1$ and $P < 1$) to account for differing error rates between these categories. Due to a lack of true spring-run subjects, we combined subjects for Butte Creek ($n = 13$) and Mill-Deer creek ($n = 2$), and applied these data to both runs and both probability categories. Application of the blind-test data had the largest effects on assignments for late-fall run and Mill-Deer creek spring run; the corrected estimates for these runs were often considerably lower than the observed assignments, and were highly uncertain.

Obviously, there is a pressing need for additional blind-test data for true spring run. The corrected spring-run estimates reported in this study should be interpreted cautiously because they are based on very limited blind-test data and arbitrary assumptions (i.e., we used predominantly Butte Creek subjects with $P = 1$ to represent Mill-Deer creek run and the $P < 1$

categories). However, it is instructive to understand the different results found for the Butte Creek and Mill-Deer creek runs. Even though the same blind-test data were used to represent the "true" subjects for both runs, their run corrections differed greatly. Compared to observed assignments, corrections for Butte Creek were slightly larger and reasonably precise, while corrections for Mill-Deer creek were often much lower than observed and very imprecise. These differences were due entirely to the false-negative error rates observed for true fall run in the P < 1 category, in which two of 46 fish (4.3%) were incorrectly assigned to Mill-Deer creek but none to Butte Creek. Consequently, when observed assignments of Mill-Deer creek run were present with large numbers of fall run (a frequent scenario), the correction algorithm reallocated Mill-Deer creek assignments to the fall run. Because these reallocations were based on a small and uncertain binomial probability (2 of 46), variances for the Mill-Deer creek corrections were very large. A similar explanation underlies the results for late-fall run.

These results contain an important insight. Because of the numerical dominance of fall run, its false-negative error rates were the key determinants of change and uncertainty in the corrected estimates (and abundance estimates) for late-fall run and Mill-Deer creek spring run. Thus, while obtaining additional blind-test data for true spring run is important, it is more important (if possible) to eliminate false-negative error rates in assignments of true fall run.

In contrast, results for winter run were very encouraging. In blind tests, true winter-run were correctly identified 98.2% of the time when ONCOR P = 1, and roughly 98% of observed field assignments of winter run fell into this category. More importantly, true fall run were never incorrectly identified as winter run in blind tests. As a result, assignment corrections for winter-run (after rounding) always equaled the number of observed assignments, and were very precise.

Unfortunately, we omitted a potentially important source of variance in estimates of corrected DNA assignments (K.Newman, U.S. Fish and Wildlife Service, pers. comm.), which should be accounted for in future applications. Specifically, our Equation (8) accounts for uncertainty in estimates of assignment probabilities (error rates) derived from blind-test data, but ignores the multinomial variation or "sampling error" associated with each new sample of observed assignments. As a result, our reported variances for total abundance estimates were underestimated to some extent. However, we expect that this omission would have little effect on variance estimates for winter run and Butte Creek spring run, in particular for their annual abundance estimates, for two reasons: (1) multinomial sampling variation would be minimal when key error rates are close to 0, which was the case winter run and Butte Creek spring run; and (2) the relative importance of multinomial sampling variation, which is specific to each sample, would diminish when summing abundances across multiple periods and length strata, whereas variances in estimated assignment probabilities (blind-test data) apply to all samples and accumulative across strata via covariance terms. Larger implications would be expected for late-fall run and Mill-Deer creek spring run (due to false-negative error rates in assignments of true fall run), but variances in the abundance estimates for these runs are already dominated by uncertainty in corrected DNA assignments, so our general conclusions would not change.

Other improvements to our methodology could be explored. First, additional stratification of ONCOR assignment probabilities may be useful, in particular if more blind-test data are collected. While there were clear differences in error rates between the $P = 1$ and $P < 1$ categories, we only cursorily examined other subcategories (e.g., $P < 0.9$ or $P < 0.8$) before concluding that there were insufficient data to warrant further stratification. Second, we used a bootstrap procedure to estimate variances for assignment corrections. However, if an analytical variance estimator could be developed, it would greatly simplify computations and make variance estimation possible in a spreadsheet, for example. Third, the correction algorithm often produced negative estimates of corrected assignments. As detailed above, we dealt with this using a simple procedure in which negative estimates were set to zero and the remaining estimates were scaled so their sum equaled the total observed assignments. A more sophisticated approach would involve bounded likelihood or Bayesian models that explicitly incorporate the blind-test data, observed assignments, and parameter constraints (i.e., $\hat{x}_i \geq 0$) to estimate corrected assignments. However, such nonlinear models can be a challenge to fit, and separate fits would be required for each stratification that resulted in negative estimates (more than 100 cases in our application). It seems doubtful that such an approach would lead to substantively different estimates worthy of the effort.

Estimates of total abundance and trawl efficiency

The accuracy and precision of abundance estimates depend critically on estimates of trawl efficiency. For a given efficiency estimate, annual abundances were reasonably precise (e.g., CV = 20% to 30%) for the fall, Butte-Creek spring, and winter runs. While these precision estimates are encouraging, they should be interpreted cautiously for three reasons, which we discuss in turn: (1) abundances were sensitive to the choice of efficiency estimate; (2) efficiency was assumed to be constant over time; and (3) sampling error in catch assignments may be greater than assumed.

We used three efficiency estimates that were independently derived using CWT-release data (Pyper et al. 2013). The lowest efficiency (0.0064 for paired-release tests) produced abundances that were roughly two times greater than those based on the highest efficiency (0.0124 for Pittsburg releases). This two-fold difference implies considerably greater uncertainty than indicated by the standard errors for abundances based on any single efficiency estimate. Thus, determining the most appropriate data and methodology for estimating Chipps Island trawl efficiency is of high priority. As discussed in Pyper et al. (2013), there were advantages and disadvantages to the data and methods used to develop each efficiency estimate. Speculatively, they suggest that the paired-release estimate is biased low, while the Jersey Point estimate appears most defensible (the Pittsburg estimate was based on only three releases). In any case, additional releases and analyses such as those recommended in Pyper et al. (2013) may help to resolve these uncertainties.

By comparison, the fish-flux method (Kimmerer 2008) produced by far the lowest abundance estimates. We have little confidence in these estimates. The fish-flux method, which had an implied efficiency (0.04) that was roughly four times greater than the empirical estimates, is a simple conceptual model that relies on several key assumptions (e.g., a fixed migration speed and random trawl and/or fish distributions). Most critically, the method does not account for avoidance behaviors that would likely reduce fish vulnerability to trawl capture (see Pyper et al. 2013 for further discussion). For Chipps Island trawl, it is clear that the fish-flux method likely produces substantial underestimates of abundance, and we would expect similar biases to occur at other trawl-sampling locations.

The second key source of uncertainty relates to possible temporal variation in trawl efficiency. In our application, we assumed that efficiency was constant across years, and the variance terms we used for efficiency (Table 4) reflected only statistical error in estimates of "mean efficiency." However, additional temporal variation is expected, and hence, the standard errors we reported for abundance estimates (and variance components due to efficiency) are likely biased low.

Temporal variation in efficiency may occur at short time scales (e.g., daily) and longer time scales (e.g., seasonal or annual differences). For example, daily fluctuations in efficiency could result from daily differences in trawl operation (e.g., time of day and location of tows). As noted below, additional analyses could be pursued to better characterize variation in daily catch and efficiency. However, the relative importance of short-term variation would be diminished or "averaged out" to a large extent when estimating annual abundances across numerous days.

Seasonal or annual variation in efficiency is of greater concern. For example, a 30% difference in annual efficiency (relative to the assumed constant value) would result in a roughly 30% bias in the abundance estimate, and such variation would not be adequately captured in the variance estimator we used. Seasonal or annual changes in efficiency could result from seasonal/annual variation in conditions affecting fish behavior (e.g., fish size, water flow, temperature, turbidity, etc.). Although Pyper et al. (2013) found little evidence of such relationships, the paired-release data they examined were highly variable. Furthermore, it is very difficult to quantify temporal variation in efficiency using available CWT-release data because of the confounding effects of variation in survival rates. As discussed in Pyper et al. (2013), further efforts should be considered to either develop reliable, year-specific estimates of efficiency, or better quantify potential inter-annual variation in efficiencies from past data.

The third source of uncertainty relates to sampling error. We accounted for sampling error in abundance estimates by assuming catch assignments followed Poisson distributions. However, daily trawl catches are likely "overdispersed" (i.e., have more patchy or clumpy distributions with higher variances than assumed under the Poisson model). Numerous factors could result in overdispersion, including spatial and temporal patchiness in daily fish migration, and daily differences in trawl operation (i.e., analogous to short-term variation in efficiency noted above). It should be possible to quantify (or approximate) levels of overdispersion in daily catches by

analyzing tow-specific catch data (and simultaneously assess potential covariates such as time of day, channel location, trawl direction, etc., that may affect trawl efficiency). Catch assignments could then be modeled as overdispersed Poisson variables, for example, in the variance estimator for abundance. The implications of overdispersion could be large for the spring and winter runs because these runs had low numbers of catch assignments. A low number of assignments translates into high sampling error (e.g., see results in Table 20 for winter run). Thus, if sampling-error variances increased considerably due to overdispersion, we would expect potentially large reductions in the precision of abundance estimates for Butte Creek spring run and winter run (Mill-Deer creek precisions were largely driven by assignment errors). In sum, the potential for overdispersion in daily catch warrants further investigation.

Independent estimates of winter run abundance

Noble Hendrix of R2 Resources Consultants, Inc., developed the *Oncorhynchus* Bayesian ANalysis (OBAN) model, which is a statistical life-cycle model for winter-run salmon in the Sacramento River. The OBAN model was developed to evaluate factors influencing the returning numbers of winter-run salmon to the upper Sacramento River. It contains two estimates of survival: 1) the survival from adults on the spawning grounds to juveniles at Red Bluff Diverson Dam (RBDD) and 2) the survival from juveniles at RBDD to adults on the spawning ground. In order to identify the survival rate in the Delta, Hendrix concluded that an index of abundance was needed at Chipps Island to separate the survival in the Delta from survival in the ocean (N.Hendrix, R2 Resources Consultants, Inc., pers. comm.). Estimates of survival to age 2 could also be obtained by using run reconstruction information for age 3 and age 4 winter-run Chinook salmon (e.g. O'Farrell et al. 2012). Hendrix also concluded that the data obtained at Chipps Island, although imprecise, could be quite influential on the results of the OBAN model (N.Hendrix, R2 Resources Consultants, Inc., pers. comm.).

When Hendrix initially used the Chipps Island estimates of winter-run abundance based on the length-at-date criteria, the OBAN model consistently under-estimated these abundances (N.Hendrix, R2 Resources Consultants, Inc., pers. comm.). Hendrix then re-ran the OBAN model to determine the expected abundance of winter run at Chipps Island, and he estimated abundances of winter run between 33,506 and 37,398 for the years between 2008 and 2011, although these abundances were confounded by the inability to differentiate survival in the Delta from survival in the ocean (N. Hendrix, R2 Resources Consultants, Inc., pers. comm.). Results from our study, using corrected DNA assignments and the Jersey Point efficiency estimate, suggest winter-run abundance at Chipps Island ranged from 45 thousand to 63 thousand between 2008 and 2011. Although the OBAN abundance estimates incorporate mortality after Chipps Island, they are within the relative magnitude of our abundance estimates (using DNA and Jersey Point efficiency), but much lower than winter- run estimates at Chipps Island obtained using the length-at-date criteria (~200,000 for all four years; Speegle et al. 2013). The results from re-running the OBAN model appear to support the relative magnitude of the estimates of winter-run

abundances we obtained using corrected DNA assignments and the Jersey Point efficiency estimate.

Implications for past and future sampling

Tissue samples of juvenile Chinook salmon captured in Chipps Island trawl were collected from 1996 to 2002, but not all samples were DNA analyzed. We reviewed these data to determine if reliable DNA-based estimates of abundance could be obtained for the winter and/or spring runs. Tissue sampling was sparse and sporadic from 1996 to 2000 (e.g., annual sample sizes ranged from 15 to 272), with negligible sample numbers and/or poor temporal coverage within the length criteria for the winter and spring runs. However, useful estimates for winter-run may be obtained for 2001 and 2002, with minimal effort, assuming that most migrants were within the winter-run length-at-date criteria (consistent with observed assignments for sample years 2008-2011). In 2001, tissue was collected from all 102 juvenile salmon caught in the winter-run length criteria. Although only five of these were DNA analyzed, they were all assigned to winter run. Speculatively, genetic analysis of the remaining tissue samples could provide enough DNA assignments of winter-run (e.g., > 30) to achieve precisions for 2001 abundance estimates similar to those for 2010 and 2011. In 2002, there were 71 juvenile salmon caught in the winter-run length criteria, of which 63 were tissue sampled, 48 were DNA analyzed, and 13 were assigned to winter run. Thus, genetic analysis of the remaining 15 tissue samples would likely yield only a few more winter-run assignments. With or without additional genetic analysis, we would expect precisions for 2002 abundance estimates to be somewhere between those for 2008 and 2009.

The methods used in this study could be readily applied (or adapted) to the DNA assignments of juveniles collected in Sacramento trawl sampling from 2008 to 2011. At a minimum, expansions could be estimated to account for sampling fractions and trawl effort, thereby providing estimates of run composition. However, it is unclear if trawl efficiency at Sacramento can be reliably estimated to provide meaningful abundance estimates. In addition, genetic sampling and analysis could be used in similar ways to estimate run compositions of migrating juvenile Chinook salmon at other locations in the Central Valley. Future DNA sampling could be particularly advantageous at Sacramento trawl or at the Knights Landing screw traps, which are intended to monitor juvenile Chinook produced in the Sacramento Basin as they enter the Sacramento Delta. As demonstrated for Chipps Island trawl, location-specific estimates of winter and spring-run compositions (relative abundances) based on DNA would likely be much more accurate than estimates based on length criteria.

The results of this study can also be used to improve the sampling design for tissue collection and DNA analysis at Chipps Island trawl in future years. Presumably, there will be numerous constraints, objectives, and alternative sampling designs to consider. Constraints may include trawl restrictions to reduce take of Delta smelt, and budget restrictions that limit trawl effort and/or tissue sampling for DNA analysis. Key objectives may include the run types to target

(e.g., winter and/or spring run) and the desired precision of estimates. Given such objectives and constraints, alternative sampling designs could be explored to best allocate trawl effort and tissue sampling across discrete time periods and fish-length strata. The original sampling plan for this study (Attachment A) was based on analyses of optimal sample allocations; however, the statistical framework and assignment data in this report would provide a much stronger basis for determining optimal sampling designs.

Obviously, from a sampling perspective, the key to improving estimates for winter and spring run is to increase the number of true juveniles of these runs that are DNA analyzed. This will be most easily achieved for winter run because of the relatively constrained time and length distribution of juvenile migrants. To improve estimates, trawl sampling would be maximized during the peak winter-run period, with tissue collection targeting the larger length classes in which winter run are predominantly found. Speculatively, trawl effort would be directed toward more days of sampling, which would increase winter-run catches as well as reduce uncertainty due to missing trawl days, as opposed to increasing minutes fished on selected days (also useful, of course). By comparison, it would likely be much more costly to increase observed DNA-assignments of Butte Creek spring run due to their broad overlap with fall run. Nevertheless, the same principles would generally apply: target trawl sampling and tissue collection at the periods and length strata of peak juvenile migration.

Related management implications

Improved estimates of juvenile run composition and abundance at Chipps Island, as provided by DNA sampling, would improve our understanding of the population dynamics of the ESA-listed Chinook runs. In the case of winter run, the estimates of fry passing Red Bluff Diversion Dam (RBDD) can be compared to the abundance estimates of juveniles passing Chipps Island to estimate juvenile survival in freshwater. RBDD is located near the lower limit of winter-run spawning, and most winter-run juveniles pass RBDD as fry less than 45 mm in length during September through November, while winter-run juveniles pass Chipps Island from mid-February to mid-April at 100 to 125 mm in length. Thus, the abundance estimates for winter run at RBDD and Chipps Island trawl provide meaningful bookends for the freshwater rearing of the population. Accurate estimates of freshwater survival derived from these two sampling locations would greatly enhance assessments of effects of water management actions and other human activities on the freshwater production of winter run. The reduced estimate of winter run juvenile production that results from DNA-based run assignments means that freshwater survival is less than would have been calculated by methods employed before the 2008 sample year; however, such estimates were rarely used because of the low reliability of distinguishing winter-run juveniles based on length criteria.

The lack of reliable abundance estimates for Chinook salmon juveniles reaching San Francisco Bay each year has been an obstacle to resolving debate over management actions that should be taken to restore runs of ESA-listed winter and spring-run Chinook salmon. For example, there has been much speculation about the magnitude of mortality that water project operations impose

on these runs. In particular, the number of juvenile Chinook captured at the Delta Fish Facilities (DFF) has been used as the basis for calculating direct loss due to the water project pumps, and increases in this index of loss have been assumed to indicate increases in mortality rather than increases in abundance of juveniles passing through the Delta. Modeling studies are underway to estimate the influence of water project operations on juvenile survival through the Delta, and accurate estimates of juvenile numbers arriving at and leaving the Delta would be of great value for developing and validating such models.

Summary of recommendations

1. Past estimates of juvenile abundance in the Delta for winter and spring runs of Chinook salmon based on length criteria should be regarded as unreliable and biased substantially high. Given the broad overlap in length-at-date distributions observed among runs (based on DNA assignments), it is clear that the length-at-date method will consistently produce high rates of error in non-fall-run assignments.
2. Determining the most appropriate data and methodology for estimating Chipps Island trawl efficiency is of high priority. Efforts should be made to better quantify mean trawl efficiency, as well as potential seasonal/annual variation in efficiency and overdispersion in trawl catch. Additional releases and analyses such as those recommended in Pyper et al. (2013) may help to resolve these uncertainties.
3. There will be assignment errors using DNA methods, and the use of blind-test data can provide estimates of those error rates to adjust or "correct" new samples of observed assignments. Application of the blind-test data had the largest effects on assignments for late-fall run and Mill-Deer creek spring run. Because of the numerical dominance of fall run, its false-negative error rates were the key determinants of change and uncertainty in the corrected estimates (and abundance estimates) for late-fall run and Mill-Deer creek spring run. Thus, while obtaining additional blind-test data for true spring run is important, it would be more valuable to develop genetic markers that could eliminate false-negative error rates in assignments of true fall run.
4. We omitted a component of variance (multinomial sample variation) for estimates of corrected DNA assignments that should be included in future applications (see Equation (8) and related text). Other improvements to our methods for handling assignment error rates could be explored, including stratification of ONCOR assignment probabilities, development of an analytical estimator for variances, and a better method for handling negative estimates of corrected DNA assignments.
5. The statistical framework and assignment data in this report would provide a strong basis for determining optimal designs for collecting genetic samples in future years. To improve estimates of non-fall runs, trawl effort and tissue sampling would focus on the peak periods of migration and length classes for the target run.
6. Future DNA sampling could be particularly advantageous at Sacramento trawl or at the Knights Landing screw traps, which are intended to monitor juvenile Chinook produced in the Sacramento Basin as they enter the Sacramento Delta. Comparison of size, time,

and abundance of juveniles entering the Delta to those leaving the Delta would be valuable for elucidating mechanisms that relate to through-Delta survival.

7. Future analysis could assess the utility of using DNA run assignments at the Delta Fish Facilities (DFF) as surrogate for estimating past run composition at the Chipps Island trawl. DNA sampling has been more extensive at salvage prior to this study, and may be useful for expanding past years of trawl catch at Chipps Island.
8. We recommend a comparison between abundance of winter run at Chipps Island relative to abundance at the Delta Fish Facilities to help determine if the direct loss estimated at the facilities is a function of higher mortality at the pumps or higher abundance using years where genetic composition at both locations was estimated with HMSC16 set of microsatellites.

References

Banks M.A., Rashbrook V.K., Calavetta M.J., Dean C.A. & Hedgecock D. 2000. Analysis of microsatellite DNA resolves genetic structure and diversity of Chinook salmon (*Oncorhynchus tshawytscha*) in California's Central Valley. Canadian Journal of Fisheries and Aquatic Sciences 57, 915-927.

Banks M.A. & Jacobson. D.P. 2004. Which genetic markers and GSI methods are more appropriate for defining marine distribution and migration of salmon? North Pacific Anadromous Fish Commission Technical Note 5, 39-42.

Banks, MA. 2005. Stock identification for the conservation of threatened or endangered species. In: Stock identification methods, eds: Cadrin, S. X., K. D. Friedland and J. R. Waldman. Elsevier Press. pp 609-629.

Banks, MA., D. Jacobson, I. Meusnier, C. Greig, V. Rashbrook, W. Arden, J. Bernier-Latmani, J. Van Sickle, K. O'Malley. In review. Testing Advances of Molecular Discrimination among Chinook salmon Life Histories: Evidence from a Blind Test. Submitted to Animal Genetics. 5/31/13.

Brandes, P. and J. McLain. 2001. Juvenile Chinook salmon abundance and distribution, and survival in the Sacramento-San Joaquin Estuary. In: Brown RL, editor. Fish Bulletin 179: Contributions to the Biology of Central Valley Salmonids. Volume 2. Sacramento (CA): California Department of Fish and Game.

Cramer, S.P., M. Daigneault, and M. Teply. 2004. Integrated Modeling Framework User's Guide. S.P. Cramer & Associates prepared for California Urban Water Agencies and State Water Contractors, Sacramento, CA 105 pp.

Fisher, F. W. 1992. Chinook salmon, *Oncorhynchus tshawytscha*, growth and occurrence in the Sacramento-San Joaquin River system. California Department Fish and Game.

Fisher, F.W. 1994. Past and present status of Central Valley Chinook salmon. Conservation Biology 8(3):970-873.

Greig C.A. & Banks. M.A. 1999. Five multiplexed microsatellite loci for rapid response run identification of California's endangered winter Chinook salmon. Animal Genetics 30, 318-320.

Greig C.A. & Banks. M.A. 2003. New tetranucleotide microsatellites for fine-scale discrimination among endangered Chinook salmon (*Oncorhynchus tshawytscha*). Molecular Ecology Notes 3, 376-379.

Harvey, B. and C. Stroble (in press). Comparison of genetic versus Delta Model Length-at-Date run assignments for juvenile Chinook salmon at state and federal south Delta salvage facilities.

California Deparment of Water Resources. Submitted to Interagency Ecological Program for the San Francisco Estuary as a technical report. March 2013.

Hedgecock D., Banks M.A., Rashbrook V.K., Dean C.A. & Blankenship. S.M. 2001. Applications of population genetics to conservation of Chinook salmon diversity in the Central Valley In: *Contributions to the Biology of Central Valley Salmonids* (ed. By R.L. Brown) State of California Resources Agency Department of Fish and Game. *Fishery Bulletin* 179, 45-70.

Hedgecock D. 2002. Microsatellite DNA for the management and protection of California's Central Valley Chinook salmon (Oncorhynchus tshawytscha). Final Report for the Amendment to Agreement No. B-59638. University of California Davis, Bodega Marine Laboratory. 2099 Westside Road, Bodega Bay, CA 94923-0247.

Kalinowski S.T. 2008. ONCOR software for genetic stock identification. http://www.montana.edu/kalinowski/Software/ONCOR.htm

Kimmerer, W.J. 2008. Losses of Sacramento River Chinook salmon and delta smelt to entrainment in water diversions in the Sacramento-San JoaquinDelta. San Francisco Estuary Watershed Science. Available from: http://escholarship.org/uc/item/7v92h6fs

Kormos, B., M. Palmer-Zwahlen and A. Low. 2012. Recovery of Coded-Wire Tags from Chinook salmon in California's Central Valley Escapement and Ocean Harvest in 2010. California Department of Fish and Game. Fisheries Branch Administrative Report 20120-02. March 2012. 41pp.

Mood, A.M, Graybill, F.A and D.C. Boes. Introduction to the Theory of Statistics, 3rd Edition. New York: McGraw-Hill, 1974.

Naish K.A. & Park L.K. 2002. Linkage relationships for 35 new microsatellite loci in Chinook salmon *Oncorhynchus tshawytscha*. Animal Genetics 33, 316–318.

National Marine Fisheries Service. (NMFS) 1994. Endangered and threatened species; threatened status for two Chinook salmon Evolutionarily Significant Units (ESu's) in California; final rune Federal Register 50393.64 (179). 16 September, 1999.

Nelson R.J. & Beacham. T.D. 1999. Isolation and cross species amplification of microsatellite loci useful for study of Pacific salmon. *Animal Genetics* 30, 228–229.

O'Farrell, M.R., Mohr, M.S., Grover, A.M., Satterthwaite, W.H., 2012. Sacramento River winter Chinook cohort reconstruction: analysis of ocean fishery impacts. U.S. Department of Commerce, NOAA Technical Memorandum NMFS- SWFSC-491. Available from http://swfsc.noaa.gov/publications/TM/SWFSC/ NOAA-TM-NMFS-SWFSC-491.pdf

O'Malley K., McClelland E.K. & Naish K.A. 2010. Clock genes localize to stage-specific quantitative trait loci for growth in juvenile coho salmon, *Oncorhynchus kisutch*. Journal of Heredity 101, 628-632.

Pyper, B., T. Garrison, and S. Cramer. 2013. Analysis of trawl efficiency at Chipps Island using coded-wire-tagged releases of juvenile Chinook salmon. Cramer Fish Sciences Technical Report for U.S. Fish and Wildlife Service, Lodi, CA. 97 pp.

Rannala, B., and Mountain, J.L. 1997. Detecting immigration by using multilocus genotypes. Proc. Natl. Acad. Sci. USA. 94: 9197–9201.

Speegle, J., J. Kirsch, and J. Ingram. 2013. Annual report: juvenile fish monitoring during the 2010 and 2011 field seasons within the San Francisco Estuary, California. Stockton Fish and Wildlife Office, United States Fish and Wildlife Service, Lodi, California.

U.S. Fish and Wildlife Service (USFWS). 1994. 1993 annual progress report: "Abundance and survival of juvenile Chinook salmon in the Sacramento-San Joaquin Estuary". Stockton, CA.

U.S. Fish and Wildlife Service (USFWS) 1997. 1994 annual progress report: "Abundance and survival of juvenile Chinook salmon in the Sacramento-San Joaquin Estuary". Stockton, CA.

U.S. Fish and Wildlife Service. (USFWS) 2006. 2000 annual progress report: "Abundance and survival of juvenile Chinook salmon in the Sacramento-San Joaquin Estuary". Stockton, CA.

U.S. Fish and Wildlife Service. (USFWS) 2011. Biological Assessment of Artificial Propagation at Coleman National fish hatchery and Livingston Stone National Fish Hatchery: program description and incidental take of Chinook salmon and steelhead. Prepared by U.S. Fish and Wildlife Service, Red Bluff Fish and Wildlife Office, Red Bluff, CA 96080 and U.S. Fish and Wildlife Service Coleman National Fish Hatchery Complex, Anderson, CA 96007. 372 p.

Williamson K.S., Cordes J.F. & May. B. (2002) Characterization of microsatellite loci in Chinook salmon (*Oncorhynchus tshawytscha*) and cross-species amplification in other salmonids. *Molecular Ecology Notes* 2, 17-19.

Appendix A: Derivation of selected estimators

Estimates of total catch by run

The following derivation applies to an estimate of total catch, X_{itk}, for a given run i, biweekly period t, and length stratum k. For simplicity, all subscripts are omitted until the final estimates of interest are obtained.

When deriving estimators for total catch (X) and its variance, two processes are considered: (1) the sampling of catch (C), which determines the distribution of true abundance, x, in the sample (S); and (2) the estimation of x given the observed DNA-run assignments $\{y\}$ and blind-test data. Let f (= S/C) be the fraction of catch that is sampled and assigned to run. Assuming all fish C have an equal probability (f) of being sampled, the sampling of catch is "sampling without replacement" and thus x follows a hypergeometric distribution conditional on the values of C, X, and S (e.g., Mood et al. 1974, p. 91). Formally, $x \sim$ Hypergeometric(C, X, S) with expectation

$$E[x] = X\left(\frac{S}{C}\right) = Xf \tag{A1}$$

and variance

$$\begin{aligned} V[x] &= X\left(\frac{S}{C}\right)\left(\frac{C-S}{C}\right)\left(\frac{C-X}{C-1}\right) \\ &= Xf(1-f)\left(\frac{C-X}{C-1}\right). \end{aligned} \tag{A2}$$

We do not observe the true abundance x (unless DNA assignments are 100% accurate). Rather, we have an estimator $\hat{x}$ that is conditional on x (as well as all other true run-specific abundances and the true error rates associated with DNA assignments). Assuming $\hat{x}$ and x are jointly distributed random variables, we can express the expectation and variance of $\hat{x}$ as (e.g., Mood et al. 1974, p. 158-159):

$$E[\hat{x}] = E_x[E[\hat{x} \mid x]] \tag{A3}$$

$$V[\hat{x}] = E_x[V[\hat{x} \mid x]] + V_x[E[\hat{x} \mid x]], \tag{A4}$$

where $E[\hat{x} \mid x]$ and $V[\hat{x} \mid x]$ denote the conditional expectation and variance of $\hat{x}$, respectively. Further assuming that $E[\hat{x} \mid x] = x$ (i.e., $\hat{x}$ is an unbiased estimate of x) and $E_x[V[\hat{x} \mid x]] = V[\hat{x} \mid x]$, Equations (A3) and (A4) become:

$$E[\hat{x}] = E[x] \tag{A5}$$

(A6) $$V[\hat{x}] = V[\hat{x} \mid x] + V[x].$$

Combining the definitions for Equations (A5) and (A2) and solving for X gives:

(A7) $$X = \frac{E[\hat{x}]}{f}$$

with variance

(A8)
$$\begin{aligned} V[X] &= \frac{V[\hat{x}]}{f^2} \\ &= \frac{1}{f^2}\left(V[\hat{x} \mid x] + V[x]\right) \\ &= \frac{1}{f^2}\left(V[\hat{x} \mid x] + Xf(1-f)\left(\frac{C-X}{C-1}\right)\right). \end{aligned}$$

Finally, to obtain estimators, we substitute $E[\hat{x}]$, X, and $V[\hat{x} \mid x]$ in Equations (A7) and (A8) with the observed estimates $\hat{x}$, $\hat{X}$, and $\hat{\sigma}^2_{\hat{x}}$, respectively. Returning subscripts, the final estimator of total catch by run is given by

(A9) $$\hat{X}_{itk} = \frac{\hat{x}_{itk}}{f_{tk}}$$

with approximate variance

(A10) $$\hat{\sigma}^2_{\hat{X}_{itk}} = \frac{1}{f_{tk}^2}\left(\hat{\sigma}^2_{\hat{x}_{itk}} + \hat{X}_{itk} f_{tk}(1-f_{tk})\frac{C_{tk} - \hat{X}_{itk}}{C_{tk} - 1}\right).$$

Estimates of total abundance by run

The derivation of abundance estimates proceeds stepwise from a simple conceptual model to the final variations used here. We first construct estimators that account for sampling variation and measurement error in corrected run assignments ($\hat{x}$). We then account for uncertainty due to missing days of trawl sampling, followed by uncertainty in trawl efficiency estimates.

To begin, we ignore length stratification and assume that a known number (x_i) of fish of a given run i are identified in a sample (S) of trawl catch (C) collected during a discrete time period. Let f (= S/C) be the fraction of catch that is sampled and assigned to run. We want to estimate the total abundance of juveniles N_i given the observation x_i. It is assumed that all fish are independent have the same probability (E) of capture, where E is the trawl efficiency, and the

same probability (f) of being sampled if caught. Given these assumptions, we could specify $x_i \sim$ Binomial(N_i, Ef); however, because E is expected to be very low (e.g., 0.01 or 1%), we can simplify the model by specifying $x_i \sim$ Poisson($N_i Ef$).

The trawl does not operate continuously; rather, it is further assumed that trawl sampling provides a representative sample of the migration (N_i) passing Chipps Island during a given period (e.g., a day). Let p denote the proportion of the period trawled. Assuming fish passage is random throughout the period, we can now specify:

(A11) $x_i \sim \text{Poisson}(N_i Epf)$; $E[x_i] = N_i Epf$; $V[x_i] = N_i Epf$

where Ep is the probability of capture across the full period.

In our application, we have an estimator $\hat{x}_i$ (assignment correction) rather than a direct observation of the true abundance x_i. Given Equation (A11), and following the same steps outlined for total catch estimates (see Equations (A3)-(A8)), we obtain the following expression for N_i:

(A12) $$N_i = \frac{E[\hat{x}_i]}{Epf}$$

and its variance

(A13) $$\begin{aligned} V[N_i] &= \frac{1}{(Epf)^2}\left(V[\hat{x}_i \mid x_i] + V[x_i]\right) \\ &= \frac{1}{(Epf)^2}\left(V[\hat{x}_i \mid x_i] + N_i Epf\right). \end{aligned}$$

To obtain estimators from Equations (A12) and (A13), we substitute $E[\hat{x}_i]$ and $V[\hat{x}_i \mid x_i]$ with the observed estimates $\hat{x}_i$ and $\hat{\sigma}^2_{\hat{x}_i}$, and $N_i Epf$ (= $E[x_i]$) with $\hat{x}_i$ as well. This gives

(A14) $$\hat{N}_i = \frac{\hat{x}_i}{Epf}$$

with variance estimator

(A15) $$\hat{\sigma}^2_{\hat{N}_i} = \frac{\left(\hat{\sigma}^2_{\hat{x}_i} + \hat{x}_i\right)}{(Epf)^2}.$$

In summary, this simple variance estimator accounts for measurement error ($\hat{\sigma}^2_{\hat{x}_i}$) in DNA assignment corrections and sampling variation in captures (i.e., assuming captures x_i follow a Poisson distribution).

In our application, we computed assignment corrections $\hat{x}_{itk}$ for samples of catch that were stratified into biweekly periods (*t*) and length strata (*k*). Moreover, we were primarily interested in biweekly totals across length strata. We can modify Equation (A14) accordingly:

$$\hat{N}_{it.} = \frac{1}{Ep_t} \sum_k \frac{\hat{x}_{itk}}{f_{tk}} = \frac{\hat{X}_{it.}}{Ep_t} \quad , \tag{A16}$$

where $\hat{N}_{it.}$ is the biweekly estimate of total abundance, $\hat{X}_{it.}$ is the total catch estimate for run *i*, and p_t is a measure of the proportion of the period that was trawled. However, a potential problem with this formulation lies in the definition of p_t. In previous applications (e.g., USFWS 2006), p_t has been computed as an aggregate across days (e.g., the sum of minutes trawled in a month divided by the total minutes in a month). Such an approach will be biased when effort and catch per unit effort vary across days (a reasonable expectation). In addition, there were numerous missing days (i.e., days of no trawl sampling) in most of the biweekly periods we examined, and we wanted to account for uncertainty in catch when expanding observed catches to missing days.

To better account for missing days and variation in daily effort and catch, we estimated biweekly abundances by run (across length strata) as

$$\hat{N}_{it.} = \frac{\hat{\rho}_{it}\hat{\gamma}_t}{E}, \tag{A17}$$

where $\hat{\rho}_{it}$ is the estimated proportion of migrating juveniles composed of run *i* in period *t*, and $\hat{\gamma}_t$ is an estimate of the expected total catch of juveniles (all runs) that would have been observed had the trawl operated *continuously* throughout the period. The estimate $\hat{\rho}_{it}$ was given by

$$\hat{\rho}_{it} = \frac{\hat{X}_{it.}}{C_{t.}} = \frac{1}{C_{t.}} \sum_k \frac{\hat{x}_{itk}}{f_{tk}}, \tag{A18}$$

where $C_{t.}$ is the total observed catch of all juveniles (summed across length strata). The variance of $\hat{\rho}_{it}$ can be expressed as

$$\sigma^2_{\hat{\rho}_{it}} = \left(\frac{1}{C_{t.}}\right)^2 \hat{\sigma}^2 \left[\sum_k \frac{\hat{x}_{itk}}{f_{tk}}\right]$$

$$= \frac{1}{C_{t.}^2}\left(\sum_k \frac{1}{f_{tk}^2}\left(\hat{\sigma}^2_{\hat{x}_{itk}} + \hat{x}_{itk}\right) + 2\sum_k \sum_{l \neq k} \frac{1}{f_{tk}} \frac{1}{f_{tl}} \mathrm{cov}[\hat{x}_{itk}, \hat{x}_{itl}]\right) \quad , \tag{A19}$$

$$= \frac{1}{C_{t.}^2}\left(\sum_k \sum_l \frac{1}{f_{tk}} \frac{1}{f_{tl}}\left(\mathbf{y}'_{\mathrm{A}tk} \hat{\mathbf{Q}}_{\mathrm{A}i} \mathbf{y}_{\mathrm{A}tl} + \mathbf{y}'_{\mathrm{B}tk} \hat{\mathbf{Q}}_{\mathrm{B}i} \mathbf{y}_{\mathrm{B}tl}\right) + \sum_k \frac{\hat{x}_{itk}}{f_{tk}^2}\right).$$

Here, the variance of $\hat{\rho}_{it}$ is computed with respect to total abundance, where the variance of each assignment correction $\hat{x}_{itk}$ comprises sampling variation and measurement error (see Equation A15). Thus, in the final expression of Equation (A19), the first (double) summation is a compact expression for the sum of variances and covariances in assignment corrections (measurement error), while the second summation accounts for sampling variation (assumed to be a Poisson process).

The estimate $\hat{\gamma}_t$ accounted for missing days (i.e., days with no trawling) as well as variation in catch per unit effort among days. Let subscript *d* denote day, let D_t be the total days in biweekly period *t*, and let M_t be the number of missing days (where $M_t < D_t$). For each day of trawling, there is an observed total catch, C_{td} (across all runs and length strata), and a computed proportion of the day trawled, p_{td}. Assuming the days sampled ($D_t - M_t$) represent a random sample within the period, we estimated $\hat{\gamma}_t$ as

$$\hat{\gamma}_t = \sum_d^{D_t - M_t} \frac{C_{td}}{p_{td}} + M_t \bar{c}_t = D_t \bar{c}_t \tag{A20}$$

with variance given by

$$\hat{\sigma}^2_{\hat{\gamma}_t} = M_t^2 \left(\frac{s^2_{ct}}{D_t - M_t}\right) + M_t s^2_{ct} \ , \tag{A21}$$

where $\bar{c}_t$ and s^2_{ct} denote the sample estimates of mean and variance, respectively, of the set of ($D_t - M_t$) daily observations $\{C_{td} / p_{td}\}$, which are analogous to catch-per-unit-effort data.

In our application, we estimated *p* as a standardized proportion of water volume trawled, which matched the definition for trawl efficiencies as estimated by Pyper et al. (2013). Specifically, we computed *p* for a given day *d* as:

(A22) $$p_d = \frac{V_d}{1440 * v},$$

where V_d was the total daily volume of water sampled and v was an arbitrary scalar defining a "standard" rate of volume sampled. As in Pyper et al. (2013), v was set equal to 1000 m^3/minute, such that the "standardized" daily volume sampled (i.e., for continuous 24-hour trawl operation) was 1440 minutes/day * 1000 m^3/minute = 1,440,000 m^3/day.

In summary, in our use of Equation (A17), we computed the total number of fish ($\hat{\gamma}_t$) that would have been caught had the trawl operated continuously throughout a biweekly period, and multiplied this amount by the estimated proportion of fish composed of run i during that period ($\hat{\rho}_{it}$). This provided an estimate of catch for run i, expanded to account for trawl effort (i.e., $\hat{\rho}_{it}$ $\hat{\gamma}_t$). Abundance was estimated by dividing this expanded catch by the trawl efficiency. Note that for certain conditions, such as constant effort (p_{td}) across days, it is easy to show that Equations (A16) and (A17) provide equivalent expressions for abundance.

From Equation (A17), the variance of $\hat{N}_{it.}$ is given by approximate variance of a product of two independent random variables (Mood et al. 1974, p. 180):

(A23) $$\hat{\sigma}^2_{\hat{N}_{it.}} \cong \frac{\hat{\rho}_{it}^2\hat{\sigma}^2_{\hat{\gamma}_t} + \hat{\gamma}_t^2\hat{\sigma}^2_{\hat{\rho}_{it}}}{E^2},$$

which now incorporates potential error due to missing days of trawl sampling.

To obtain our final estimator for biweekly abundance, we substitute E with an estimate of E:

(A24) $$\hat{N}_{it.} = \frac{\hat{\rho}_{it}\hat{\gamma}_t}{\hat{E}}.$$

The variance estimator is given by the approximate variance of a ratio (Mood et al. 1974, p. 181), where the numerator variance follows from Equation (A23):

$$\begin{aligned}\hat{\sigma}^2_{\hat{N}_{it.}} &\cong \frac{(\hat{\rho}_{it}\hat{\gamma}_t)^2}{\hat{E}^2}\left[\frac{\hat{\sigma}^2[\hat{\rho}_{it}\hat{\gamma}_t]}{(\hat{\rho}_{it}\hat{\gamma}_t)^2} + \frac{\hat{\sigma}^2_{\hat{E}}}{\hat{E}^2}\right] \\ &\cong \frac{(\hat{\rho}_{it}\hat{\gamma}_t)^2}{\hat{E}^2}\left[\frac{\hat{\gamma}_t^2\hat{\sigma}^2_{\hat{\rho}_{it}} + \hat{\rho}_{it}^2\hat{\sigma}^2_{\hat{\gamma}_t}}{(\hat{\rho}_{it}\hat{\gamma}_t)^2} + \frac{\hat{\sigma}^2_{\hat{E}}}{\hat{E}^2}\right] \\ &\cong \frac{\hat{\gamma}_t^2}{\hat{E}^2}\hat{\sigma}^2_{\hat{\rho}_{it}} + \frac{\hat{\rho}_{it}^2}{\hat{E}^2}\hat{\sigma}^2_{\hat{\gamma}_t} + \frac{\hat{\rho}_{it}^2\hat{\gamma}_t^2}{\hat{E}^4}\hat{\sigma}^2_{\hat{E}}.\end{aligned} \quad \text{(A25)}$$

It is useful to decompose Equation (A25) further with respect to the variance of $\hat{\rho}_{it}$ (Equation A19) to isolate each component of variation:

$$\hat{\sigma}^2_{\hat{N}_{it\cdot}} \cong \frac{\hat{\gamma}_t^2}{\hat{E}^2 C_{t\cdot}^2}\left(\sum_k\sum_l \frac{1}{f_{tk}}\frac{1}{f_{tl}}\left(\mathbf{y}'_{\mathrm{A}tk}\hat{\mathbf{Q}}_{\mathrm{A}i}\mathbf{y}_{\mathrm{A}tl} + \mathbf{y}'_{\mathrm{B}tk}\hat{\mathbf{Q}}_{\mathrm{B}i}\mathbf{y}_{\mathrm{B}tl}\right) + \sum_k \frac{\hat{x}_{itk}}{f_{tk}^2}\right) + \frac{\hat{\rho}_{it}^2}{\hat{E}^2}\hat{\sigma}^2_{\hat{\gamma}_t} + \frac{\hat{\rho}_{it}^2\hat{\gamma}_t^2}{\hat{E}^4}\hat{\sigma}^2_{\hat{E}} \,. \tag{A26}$$

The four additive terms in Equation (A26) correspond respectively to (1) measurement error in DNA assignment corrections; (2) sampling variation in trawl captures; (3) estimation variance in catch (extrapolation of missing days); and (4) variation in the estimate of trawl efficiency. Potentially large components of variation have been omitted, specifically, temporal variation in efficiency and/or catch (e.g., overdispersion due to clumpy spatial and/or temporal patterns of fish migration).

Last, we estimated annual abundances by sample year as sums across n_t biweekly estimates:

$$\hat{N}_{i\cdot\cdot} = \sum_{t=1}^{n_t}\hat{N}_{it\cdot} = \frac{1}{\hat{E}}\sum_{t=1}^{n_t}\hat{\rho}_{it}\hat{\gamma}_t \;, \tag{A27}$$

with an approximate variance estimator given by

(A28)

$$\hat{\sigma}^2_{\hat{N}_{i\cdot\cdot}} \cong \frac{1}{\hat{E}^2}\sum_{t=1}^{n_t}\sum_{u=1}^{n_t}\left(\frac{\hat{\gamma}_t}{C_{t\cdot}}\frac{\hat{\gamma}_u}{C_{u\cdot}}\sum_{k=1}^{n_k}\sum_{l=1}^{n_k}\frac{1}{f_{tk}}\frac{1}{f_{ul}}\left(\mathbf{y}'_{\mathrm{A}tk}\hat{\mathbf{Q}}_{\mathrm{A}i}\mathbf{y}_{\mathrm{A}ul} + \mathbf{y}'_{\mathrm{B}tk}\hat{\mathbf{Q}}_{\mathrm{B}i}\mathbf{y}_{\mathrm{B}ul}\right)\right) + \frac{1}{\hat{E}^2}\sum_{t=1}^{n_t}\left(\frac{\hat{\gamma}_t^2}{C_{t\cdot}^2}\sum_{k=1}^{n_k}\frac{\hat{x}_{itk}}{f_{kt}^2}\right)$$
$$+ \frac{1}{\hat{E}^2}\sum_{t=1}^{n_t}\hat{\rho}_{it}^2\hat{\sigma}^2_{\hat{\gamma}_t} + \frac{\hat{\sigma}^2_{\hat{E}}}{\hat{E}^4}\sum_{t=1}^{n_t}\sum_{u=1}^{n_t}\hat{\rho}_{it}\hat{\gamma}_t\hat{\rho}_{iu}\hat{\gamma}_u \,.$$

In Equation (A28), variances as well as covariances are computed across all combinations of biweekly strata (*t* and *u*) to account for dependencies due to blind-test data (used in all assignment corrections) and the estimate of trawl efficiency.

Appendix B: Second most likely run assignments

For DNA-run assignments with ONCOR probabilities less than one, a second most likely run assignment was usually provided (Table B1). These data provide an alternative measure to the blind-test data of the direction of run-assignment uncertainty. Most fish that were assigned to fall-run (with assignment probabilities < 1) had a second most likely run assignment of late-fall-run, followed by spring Mill-Deer creek. A similar pattern existed for late-fall-run. Fish first assigned to spring Butte Creek had approximately the same second most likely run assignments belonging to fall and spring Mill-Deer creek, and again a similar pattern existed for fish first assigned to Spring Mill-Deer. There were only two winter-run assignments with probabilities < 1, and neither was assigned to a second run.

Table B1. Number of fish assigned to run by ONCOR first mostly likely run assignment and second most likely run assignment.

		ONCOR 1st Most Likely Assignment				
		Fall	Late-fall	Spring Butte	Spring Mill-Deer	Winter
ONCOR 2nd Most Likely Assignment	Fall	-	181	11	43	0
	Late-fall	409	-	1	3	0
	Spring Butte	11	1	-	15	0
	Spring Mill and Deer	96	9	13	-	0
	Winter	1	0	0	0	-
	Total	517	191	25	61	0

Attachment A:

CRAMER
FISH SCIENCES
600 NW Fariss Road, Gresham, OR 97030
503.491.9577 • www.fishsciences.net

TECHNICAL BREIF

TO: Pat Brandes, USFWS

FROM: Brian Pyper, Casey Justice, and Steve Cramer

DATE: January 30, 2008

SUBJECT:Sample size allocation for DNA analysis of juvenile Chinook salmon captured in Chipps Island midwater trawl

Summary

The following provides a summary of the statistical background, analyses, and recommendations for the 2008 DNA sampling plan for Chipps Island trawl. This memo synthesizes the key findings discussed in the two previous memos (dated January 18, 2008 and January 24, 2008).

Objective

The goal of the DNA analysis is to identify juveniles that are either winter-run or spring-run Chinook salmon, such that the total juvenile abundance of each race passing Chipps Island can be estimated. The objective here is to allocate DNA samples over time to maximize the precision of total abundance estimates. We consider both winter-run and spring-run abundance estimates, bi-weekly sampling periods, length criteria for stratifying catches and samples, and a total sample size for DNA analysis of 3000 juvenile Chinook salmon.

Statistical Framework for Optimal Sample Allocation

First, we consider estimates pertaining to a single race and time period, denoting variables as follows:

Variable	Description
T	Total abundance of Chinook juveniles passing Chipps Island
N	Abundance of the race of interest (e.g., winter-run or spring-run)
C	Trawl catch
S	Total number of juveniles sampled from the catch for DNA analysis
X	Number of juveniles in the sample identified as the race of interest
$p = N/T$	The proportion of total juveniles composed of the race of interest
$e = C/T$	Trawl efficiency
$f = S/C$	Fraction of catch that is sampled

Assuming that all juveniles have an equal probability of capture (*e*), an equal probability of being sampled if caught (*f*), and are sampled without replacement, then the number (*X*) of juveniles of the race of interest identified in the sample follows the hypergeometric distribution with expectation

(1) $$E[X] = N * e * f$$

and variance

(2) $$\text{var}[X] = \frac{S * N * (T - N) * (T - S)}{T^2 * (T - 1)} .$$

With a little algebra, and replacing (*T* - 1) with *T*, the variance can be expressed as:

(3) $$\begin{aligned} \text{var}[X] &\cong S * p * (1 - p) * (1 - e * f) \\ &\cong S * p * (1 - p) \end{aligned} .$$

The term (1 - *e*f*) can be ignored because trawl efficiencies are extremely low (e.g., 0.1%). Hence, the expected variance of *X* is essentially the same as assuming that *X* follows a binomial distribution with sample size *S* and binomial probability *p*.

From equation (1), it follows that an estimate of the total abundance (*N*) of the race of interest is given by:

(4) $$\hat{N} = \frac{X}{e * f} .$$

For simplicity, we assume that both the trawl efficiency (*e*) and the sampling fraction (*f*) are known. From equations (3) and (4), the variance of the abundance estimate can be approximated by:

(5) $$\hat{\sigma}^2_{\hat{N}} = \left(\frac{1}{e * f} \right)^2 \text{var}[X] = \frac{S * \hat{p} * (1 - \hat{p})}{(e * f)^2} = \frac{C^2 * \hat{p} * (1 - \hat{p})}{e^2 * S} .$$

where *p* is replaced by the proportion estimated from the DNA sample $(\hat{p} = X / S)$.

Multiple Time Periods, Length Classes and Races

Catches may be stratified by time and length criteria. For example, length-at-date criteria have been developed to provide rough designations of Chinook juveniles as winter-run, spring-run, fall-run, etc. (e.g., Figures 1 and 2). For a given race, the total abundance estimate across *K* discrete time periods *t*, and across *L* length classes *i*, is the sum:

(6) $$\hat{N} = \sum_{t=1}^{K}\sum_{i=1}^{L}\hat{N}_{t,i} = \frac{1}{e}\sum_{t=1}^{K}\sum_{i=1}^{L}\frac{X_{t,i}}{f_{t,i}} \ ,$$

with variance

(7) $$\hat{\sigma}^2_{\hat{N}} = \frac{1}{e^2}\sum_{t=1}^{K}\sum_{i=1}^{L}\frac{C^2_{t,i} * \hat{p}_{t,i} * (1-\hat{p}_{t,i})}{S_{t,i}} \ .$$

Here, we assume that trawl efficiency (*e*) is constant across time periods and length classes within a given season, which is consistent with current methods used to expand Chipps Island trawl estimates (USFWS 2000 and 2003). To determine the optimal allocation of sample sizes $\{S_{t,i}\}$ that minimizes the variance, we take the derivative of equation (7) with respect to *S*, set the result equal to zero, and solve for $S_{t,i}$. The following "optimal" allocation results:

(8) $$S_{t,i} = \frac{Y * C_{t,i} * \sqrt{p_{t,i} * (1-p_{t,i})}}{\sum_{t=1}^{K}\sum_{i=1}^{L} C_{t,i} * \sqrt{p_{t,i} * (1-p_{t,i})}},$$

where *Y* denotes the total sample-size constraint:

(9) $$Y = \sum_{t=1}^{K}\sum_{i=1}^{L} S_{t,i} \ .$$

In addition, sample size ($S_{t,i}$) must be less than or equal to the catch ($C_{t,i}$) for each combination of time period (*t*) and length class (*i*).

We are interested in maximizing the precision of two estimates of total juvenile abundance (winter-run and spring-run Chinook salmon). Given the objective of minimizing the overall variance of the abundance estimates (i.e., the sum of their variances), the following allocation results:

(10) $$S_{t,i} = \frac{Y * C_{t,i} * \sqrt{p_{1,t,i} * (1-p_{1,t,i}) + p_{2,t,i} * (1-p_{2,t,i})}}{\sum_{t=1}^{K}\sum_{i=1}^{L} C_{t,i} * \sqrt{p_{1,t,i} * (1-p_{1,t,i}) + p_{2,t,i} * (1-p_{2,t,i})}},$$

where the subscripts "1" and "2" distinguish the two races.

Application to Chipps Island trawl

To provide a rough guide for allocating DNA samples, we examined catch data for Chipps Island trawl for 11 sampling seasons (the 1996 season through the 2007 season). Specifically, we used daily catches by

length category (1 mm intervals for fork length) as provided by Pat Brandes ("CHN Forked.xls"). Across years, length measurements were taken for approximately 92% of the total juvenile catch.

We used the catch-by-length data and daily length criteria (provided by Sheila Green) to determine catches for bi-weekly periods (e.g., March 1-15, March 16-31, April 1-15, April 16-30, May 1-15, etc.) for three length classes (winter length or greater; spring length; and fall length or less). The winter-length class we used was based on the length criteria for the salvage data (e.g., Figure 1) rather than Chipps, but this likely does not matter because the optimal sampling designs suggest that all winter-run length fish should be sampled (we don't expect that to change because even with the lower length criteria, the expected number of captures will still be low, e.g. 400 or less). In any case, the analysis has been setup so that it can be quickly updated for different length criteria.

Table 1 shows the average Chipps Island trawl catches by length class across 1996-2007 for December through June. Refer to Figure 1 for length class designations.

TABLE 1. Average catch (1996-2007) by length class of juvenile Chinook in Chipps Island trawl.

		Catch by Length Class		
	BiWeek	Winter +	Spring	Fall
Dec	1-15	20	0	0
	16-31	16	0	0
Jan	1-15	10	0	1
	16-31	10	0	26
Feb	1-15	6	0	111
	16-28	15	1	44
Mar	1-15	23	15	25
	16-31	16	223	33
Apr	1-15	3	503	246
	16-30	1	1151	3132
May	1-15	0	287	4764
	16-31	0	80	2885
Jun	1-15	0	3	691
	16-30	0	0	126
	Total	**121**	**2263**	**12084**

Note that the average for "fall length" in the first half of February (111, shaded cell) was driven by catches for one year (1996). Thus, the total catch for all length classes through the end of March is expected to be low (roughly 600), with roughly 400 of these being "spring length" or larger. Only two years had considerably higher catches through the end of March (1996 and 1998).

Catches of "spring length" fish peak in April, particularly the second half of April. Catches of "fall length" are expected to be high from mid-April through the end of May.

As discussed below, we computed optimal sample-size allocations based on the catch-by-length data and additional assumptions regarding proportions of winter-run and spring-run juveniles in the catch. Analyses were conducted separately for each year (1996-2007), as well as for the average catches across years. We found that sample allocations based on average catches provided a reasonable summary and generalization of the year-specific results; hence, we only report the allocation results for the average catches (Table 1). These analyses are contained in the attached spreadsheet ("Chipps_DNA_sample_size.xls").

Sample sizes

The optimal sample sizes by length class and period depend critically on assumptions about the proportions of catch composed of either winter-run or spring-run juveniles (see equation 10). While additional data/analyses could be conducted in an attempt to better estimate such proportions, we have arbitrarily selected values as an example; these are shown in Table 2. The DNA analysis completed for salvage (e.g., Figure 1) suggests winter-run are largely found within the "winter" length class, and to a lesser extent in the "spring" length class, with few winter-run expected after April. Spring-run are expected as both yearlings and sub-yearlings, and show a variety of length/timing patterns across years for the DNA analysis completed for salvage (e.g., Figure 2). The implications of the proportions we selected (Table 2) in terms of the distributions of length classes and migration timing within a given race are computed and displayed within the spreadsheet provided ("Chipps_DNA_sample_size.xls").

Given the catches in Table 1, the proportions in Table 2, and a total sample size of 3,000 fish, we computed optimal sample sizes for each period and length class (winter, spring, and fall) (see equation 10). Sample sizes are shown in Table 3, and implied fractions of the catch sampled are shown in Table 4.

The optimal allocation suggests sampling 100% of winter-length fish throughout the season (expected sample size = 121). For spring-length fish, the allocation implied 100% sampling through mid-March (expected sample size = 16), 74% in late March (sample = 165), and roughly 50% of spring-length fish beginning in April onward. Although a much lower fraction of fall-length fish should be sampled, most of the samples are allocated to this length class. Because we assumed that the relative proportion of spring-run juveniles in the fall-length class would decline in late April, May and June (Table 2), a lower proportion of these catches were sampled (Table 4) compared to early April.

TABLE 2. Assumed proportions of Chipps Island trawl catch by length class composed of winter-run and spring-run Chinook.

		Proportion of Length Class Composed of Winter-run			Proportion of Length Class Composed of Spring-run		
	BiWeek	Winter +	Spring	Fall	Winter +	Spring	Fall
Dec	1-15	75.0%	--	--	10.0%	--	--
	16-31	75.0%	--	--	10.0%	--	--
Jan	1-15	75.0%	--	--	10.0%	--	--
	16-31	75.0%	--	--	10.0%	--	--
Feb	1-15	75.0%	--	1.0%	10.0%	--	1.0%
	16-28	75.0%	25.0%	1.0%	10.0%	10.0%	1.0%
Mar	1-15	75.0%	25.0%	1.0%	10.0%	10.0%	1.0%
	16-31	75.0%	5.0%	1.0%	10.0%	10.0%	1.0%
Apr	1-15	75.0%	2.0%	1.0%	10.0%	5.0%	1.0%
	16-30	75.0%	0.5%	0.1%	10.0%	5.0%	0.5%
May	1-15	--	0.0%	0.0%	--	5.0%	0.5%
	16-31	--	0.0%	0.0%	--	5.0%	0.5%
Jun	1-15	--	0.0%	0.0%	--	5.0%	0.2%
	16-30	--	0.0%	0.0%	--	5.0%	0.2%

TABLE 3. Optimal sample allocations for DNA analysis by length class.

		Samples by Length Class		
	BiWeek	Winter +	Spring	Fall
Dec	1-15	20	0	0
	16-31	16	0	0
Jan	1-15	10	0	0
	16-31	10	0	0
Feb	1-15	6	0	31
	16-28	15	1	12
Mar	1-15	23	15	7
	16-31	16	165	9
Apr	1-15	3	259	69
	16-30	1	524	481
May	1-15	0	124	668
	16-31	0	35	405
Jun	1-15	0	1	61
	16-30	0	0	11
	Total (All)	**121**	**1124**	**1756 (3000)**

TABLE 4. Fraction of catch sampled under optimal sample allocations.

		Fraction of Catch Sampled		
	BiWeek	winter +	spring	fall
Dec	1-15	100%	0%	0%
	16-31	100%	0%	0%
Jan	1-15	100%	0%	0%
	16-31	100%	0%	0%
Feb	1-15	100%	0%	28%
	16-28	100%	100%	28%
Mar	1-15	100%	100%	28%
	16-31	100%	74%	28%
Apr	1-15	100%	52%	28%
	16-30	100%	46%	15%
May	1-15	0%	43%	14%
	16-31	0%	43%	14%
Jun	1-15	0%	43%	9%
	16-30	0%	43%	9%
	Overall	**100%**	**50%**	**15%**

We examined various (but seemingly reasonable) values for the proportions in Table 2, and the allocation results did not change all that much (can be tested in the spreadsheet provided). Given the expected catches (Table 1) and the sampling results (Tables 3 and 4), we suggest the following guidelines for sampling (Table 5). It seems prudent to simplify the sampling "rules" as much as possible, while recognizing that each year shall present a different distribution of catches, and yet also recognizing that rough approximations to the optimal design should still yield "almost" optimal results.

TABLE 5. Guidelines for Chipps Island trawl DNA sampling plan.

Period	Winter-length (plus)	Spring-length	Fall-length
Dec-March	All	All (max 250)	All (max 100)
April 1-15	All	250	100
April 16-30	All	500	500*
May 1-15	All	150	500*
May 16-31	All	50	500*
June	All	All (expect < 10)	100
Total	**Expect ~120 (up to 200)**	**1,200**	**1,800**

* If possible, collect additional tissue samples (e.g., 1,000 total) for post-season sub-sampling.

Note, the expected numbers of winter-length fish and sample sizes for spring-run assume the salvage winter-length criteria; we've mimicked the Chipps length-criteria and found that the average annual catch of winter-length fish (Table 1) increased from roughly 120 to 215 fish. This has little effect on the optimal design.

Additional Considerations

We want to obtain 3,000 samples, so if numbers of samples are falling short due to lack of spring-length fish, for example, we should update the sampling plan as needed within the sampling season. We recommend reviewing the status of samples every two weeks, beginning at the end of March.

By examining the year-specific sample allocations (1996-2007), we found that catches (and therefore optimal sample sizes) were quite variable for fall-length juveniles across three bi-weekly periods: April 16-30; May 1-15; and May 16-31 (marked with "*" in Table 5). Ideally, a similar fraction or proportion of each of these catches should be sampled (Table 4), but we cannot know the distribution of catches ahead of time. Thus, the sample allocation for these catches would be enhanced if a "surplus" of tissue samples could be collected. For example, if 1000 tissue samples were collected in each period, these could be sub-sampled at the end of the season such that allocation was in proportion to late-April/May catches and in accordance with the overall sample constraint of 3000.

Figure 1. Juvenile Chinook recovered at SWP Delta fish facilities that were identified via DNA analysis as winter-run Chinook (figure provided by Sheila Green, CA Department of Water Resources).

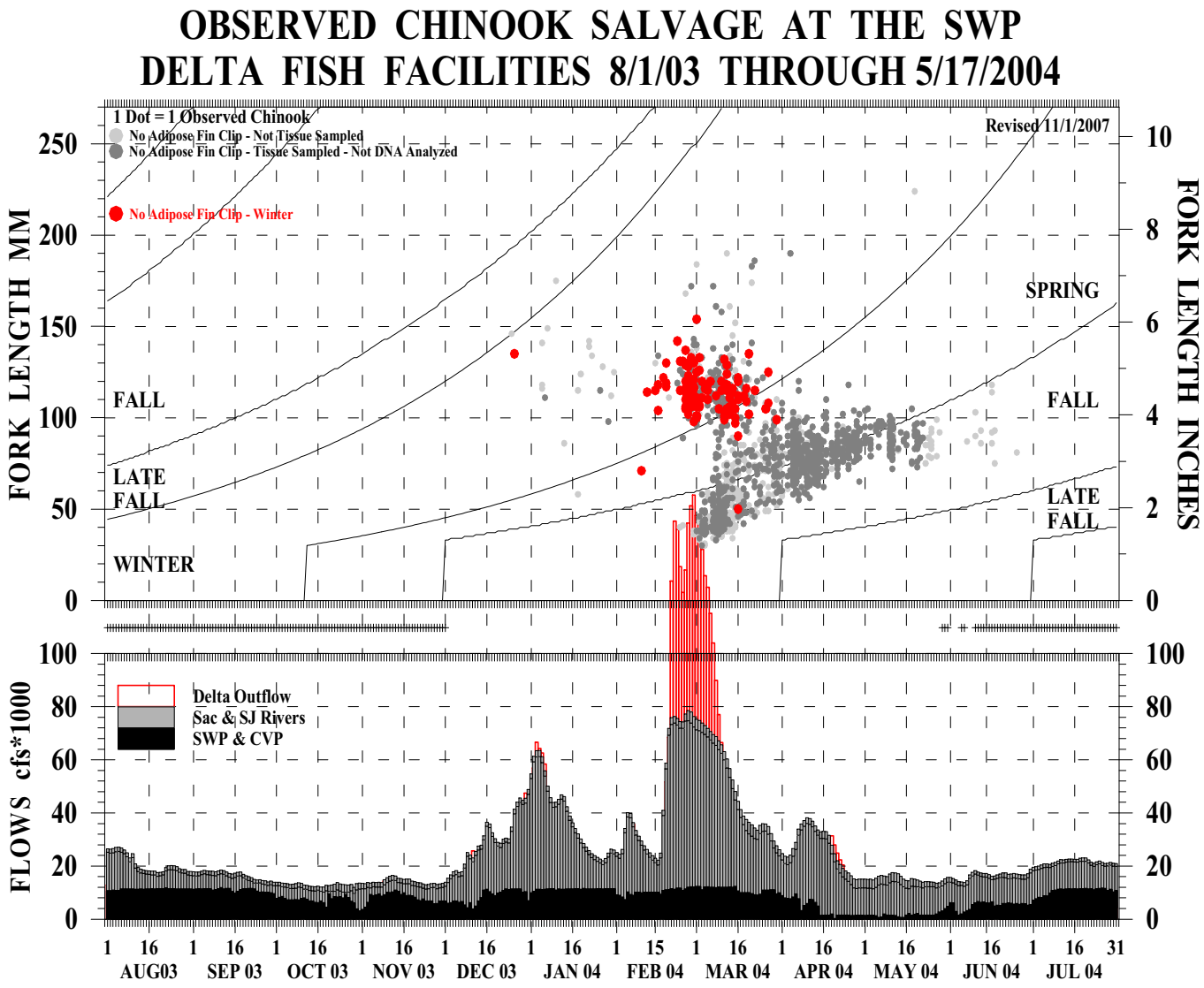

Figure 2. Juvenile Chinook recovered at SWP Delta fish facilities that were identified via DNA analysis as spring-run Chinook (figure provided by Sheila Green, CA Department of Water Resources).